Identification, Analysis, and Control of Power System Events Using Wide-Area Frequency Measurements

Joshua K. Wang

Dissertation submitted to the Faculty of the
Virginia Polytechnic Institute and State University
in partial fulfillment of the requirements for the degree of

Doctor of Philosophy
in
Electrical Engineering

Yilu Liu, Co-Chair
James S. Thorp, Co-Chair
William T. Baumann
Richard Conners
Serkan Gugercin

27 January 2009
Blacksburg, Virginia

Keywords: Power Systems,Wide-Area Monitoring and Control,Pattern Recognition

Copyright 2009, Joshua K. Wang

Identification, Analysis, and Control of Power System Events Using Wide-Area Frequency Measurements

Joshua K. Wang

(ABSTRACT)

The power system has long been operated in a shroud of introspection. Only recently have dynamic, wide-area time synchronized grid measurements brought to light the complex relationships between large machines thousands of miles apart. These measurements are invaluable to understanding the health of the system in real time, for disturbances to the balance between generation and load are manifest in the propagation of electromechanical waves throughout the grid. The global perspective of wide-area measurements provides a platform from which the destructive effects of these disturbances can be avoided. Virginia Tech's distributed network of low voltage frequency monitors, FNET, is able to track these waves as they travel throughout the North American interconnected grids. In contrast to other wide-area measurement systems, the ability to easily measure frequency throughout the grid provides a way to identify, locate, and analyze disturbances with high dynamic accuracy. The unique statistical properties of wide-area measurements require robust tools in order to accurately understand the nature of these events. Expert systems and data conditioning can then be used to quantify the magnitude and location of these disturbances without requiring any knowledge of the system state or topology. Adaptive application of these robust methods form the basis for real-time situational awareness and control. While automated control of the power system rarely utilize wide-area measurements, global insight into grid behavior can only improve disturbance rejection.

Acknowledgments

I am deeply grateful to Dr. Yilu Liu for serving as my advisor. The journey in school is a long and winding road, and she has guided me on that path with a delicate touch. She provides a center from which curiosity can productively abound, and a filter through which ideas transform into reality.

I have had the privilege of studying from exemplary professors throughout my time at Virginia Tech, chief of whom have graciously agreed to serve on my committee. I can only hope to illuminate the path for someone else with the insight you have offered me.

Nothing of consequence is accomplished without the help of others. To those who pioneered the FNET effort - Shu-Jen Tsai, Zhian Zhong, and Jian Zuo, thank you. The list of current colleagues is too numerous to list, but Tao Xia and Jingyuan Dong are deserving of special recognition. Their exemplary work and consistent friendship is an example to us all.

As Goethe said, "A man should hear a little music . . . in order that worldly cares may not obliterate the sense of the beautiful which God has implanted in the human soul." Alan Weinstein, Benedict Goodfriend, Jane Wang, Tim Mauthe, and Terry Tankersley, you have given me clarity in the silence.

There is not much in life worth more than the loyal friendship of Robert M. Gardner and William Cecere. It is no small miracle I can call them my friends.

I cannot begin to appreciate the love my parents, Kai-Jen and Janet Wang, have sacrificially given to me. If I have done anything well, it is thanks to your undying devotion to Godly character and discipline.

Amanda Wang, you are far more than a pearl of great value. You have gone wherever I go, and I cannot imagine going anywhere without you. I am truly undeserving to be able to share my life with you as my wife.

Finally, as the prophet Habakkuk exclaims, "Yet I will exult in the LORD, I will rejoice in the God of my salvation" (Habakkuk 3:18). *Soli Deo Gloria.*

Contents

Abstract . . . . . **ii**

Acknowledgments . . . . . **iii**

Contents . . . . . **iv**

List of Figures . . . . . **vii**

List of Tables . . . . . **xiv**

1 Distributed Measurements of the Electric Power System **1**

1.1 A wide-area frequency monitoring network (FNET) 3

1.2 The value of measuring frequency 6

1.2.1 Global propagation of frequency deviation 6

1.2.2 Voltage level invariance 8

1.3 The statistical nature of wide-area frequency measurements 11

1.3.1 Errors and noise 13

1.3.2 Non-stationary operation of the power system 13

1.4 Fundamentals of robust data conditioning 15

1.5 Organization of study 19

2 Unscheduled Power System Events **20**

2.1 Generation-Load mismatch 20

2.1.1 Types of mismatch events 23

Generator trips 23

Load shedding 28

Islanding 30

2.1.2 Event Detection 32

2.1.3 Mismatch amount 34

2.1.4 Location estimation 35

The least-squares approach 38

Parzen windowing methods . . . 42
2.2 Oscillations . . . 47
2.2.1 Oscillation Detection . . . 47
2.2.2 Oscillation Analysis . . . 51
Damping estimation . . . 51
Windowing effects . . . 52

3 Automated Analysis of Generation Trip Events . . . 56
3.1 Automatic ordering of generation trip events . . . 61
3.1.1 Event time determination . . . 61
3.1.2 Mismatch amount calculation . . . 63
3.1.3 Event threshold determination . . . 64
3.1.4 Crossing time calculations . . . 65
3.2 Pattern recognition and unsupervised learning . . . 66
3.2.1 Supervised learning . . . 67
3.2.2 Unsupervised learning . . . 69
3.2.3 Elimination of false positives . . . 74
3.3 The leverage of event ordering . . . 76

4 Distributed frequency measurements and oscillation control . . . 81
4.1 An example system . . . 81
4.2 Addition of power system stabilizers . . . 83
4.3 Inclusion of a HVDC link . . . 84
4.4 Performance of the modified system . . . 87
4.4.1 Mitigation . . . 88
4.4.2 Robustness . . . 91

5 Conclusions, Contributions, and Future Work . . . 97
5.1 Contributions . . . 97
5.2 Future research opportunities . . . 98

References . . . 101

A FDR Information . . . 109

B 2007 Event Scenario Information . . . 111

C Sample Daily Oscillation Analysis . . . 113

D 2007 Event Analysis Results . . . 145

E Two-area test system parameters **319**

List of Figures

1.1 Reduced Order Schematic of the Eastern U.S. Network[1] . . . 2
1.2 Frequency Monitoring Network Architecture . . . 3
1.3 Current FDR locations . . . 5
1.4 Voltage profiles of the EI before and during a generator trip[1] . . . 7
1.5 Frequency profiles of the EI before and during a generator trip[1] . . . 7
1.6 FDR and PMU locations during 7/25/2006 event . . . 9
1.7 Event recordings from adjacent units . . . 9
1.8 Event recordings from distant units . . . 10
1.9 Typical frequency data . . . 12
1.10 Aggregate frequency distribution for two different days . . . 13
1.11 Inter-FDR frequency distribution comparison . . . 15
1.12 Frequency distribution comparison to the Normal distribution . . . 16
1.13 Cartoon of the Laplacian distribution . . . 16
1.14 Frequency response of various MA filters . . . 18
1.15 Performance of data conditioning techniques on FNET data . . . 18

2.1 Single machine electromechanical diagram . . . 20
2.2 Generalized synchronous interconnection . . . 21
2.3 Aggregate representation of a synchronous electrical interconnection . . . 22
2.4 Typical generator trip signature . . . 24
2.5 NERC frequency response standard[2] . . . 25
2.6 Generator trips in different interconnections[3] . . . 26
2.7 Load shedding in different interconnections[3] . . . 28
2.8 EI islanding map . . . 30
2.9 System performance during islanding . . . 31
2.10 Non-ideal event signature . . . 33
2.11 Example of statistical event detection . . . 34
2.12 Simulated EI generator trip[1] . . . 35
2.13 Simulated event velocities[1] . . . 36
2.14 Electromechanical wave propagation through the grid . . . 37

2.15 Wavefront arrival ordering . . . 38
2.16 Sample LS Event Location Estimate . . . 40
2.17 Velocity-based location errors . . . 41
2.18 A cartoon of a plane containing two points . . . 43
2.19 Cartoons of a plane containing four points . . . 43
2.20 A cartoon of lines representing half-planes in the EUS . . . 44
2.21 Examples of Parzen windowing event location . . . 45
2.22 Power system event with oscillatory behavior . . . 47
2.23 Location of Pacific DC Intertie . . . 48
2.24 Oscillation isolation via normalized frequency . . . 49
2.25 Spectra of raw and normalized frequency . . . 49
2.26 Oscillation isolation via normalized frequency . . . 50
2.27 Threshold oscillation analysis . . . 51
2.28 Illustration of different window sizes during an oscillation . . . 52
2.29 Spectral effects of different window sizes . . . 53
2.30 Windowing effects during an ideal oscillation . . . 53
2.31 Windowing spectral effects during an ideal oscillation . . . 54

3.1 Data flow in the FNET system . . . 56
3.2 Tsunami warning data[4] . . . 57
3.3 Reflections and control effort during an event . . . 58
3.4 Generator trip signature with oscillations . . . 59
3.5 Frequency signature of Belews Creek U1 trip on 6/12/2007 . . . 60
3.6 Frequency and its derivative around trip time . . . 62
3.7 Pre- and Post- disturbance frequencies . . . 63
3.8 Frequency threshold determination . . . 64
3.9 Threshold crossings . . . 65
3.10 Feature space: crossing times . . . 66
3.11 Histogram of crossing times . . . 67
3.12 Supervised class divisions . . . 68
3.13 Unlabeled data set . . . 70
3.14 *k*-means clustering . . . 71
3.15 Failure of *k*-means' distance metric . . . 72
3.16 Division into too many classes . . . 73
3.17 *k*-medians applied to FDR crossing data . . . 74
3.18 Elimination of false positives . . . 75
3.19 Consolidated event ordering calculations . . . 79
3.20 Application of event ordering methods to event location . . . 80

4.1 Sample two-area simulation system . . . 81
4.2 Sample two-area simulation system: Natural oscillation . . . 82
4.3 MATLAB™ simulation diagrams . . . 82
4.4 Simulated and Observed Oscillations . . . 83
4.5 Addition of HVDC inter-area link . . . 85
4.6 Relationship between power mismatch and inter-area frequency difference . . . 85
4.7 Modeling the WECC as a mass-spring system[5] . . . 86
4.8 HVDC oscillation control using wide-area frequency measurements . . . 87
4.9 HVDC oscillation control using wide-area frequency measurements with time delays 88
4.9 HVDC oscillation control using wide-area frequency measurements with time delays 89
4.10 Variable transport delays and oscillation mitigation . . . 89
4.11 Robust HVDC oscillation control . . . 91
4.12 Robust HVDC oscillation control (continued) . . . 92
4.13 Typical noisy frequency . . . 93
4.14 Extraction of noise signal . . . 94
4.15 Extraction of noise signal . . . 94
4.16 Robust HVDC oscillation control (continued) . . . 95

5.1 St. Lawrence, Canada event: 03/29/2006 . . . 99

C.1 Daily oscillation analysis: summary . . . 113
C.2 Daily oscillation analysis: 1 of 31 . . . 114
C.3 Daily oscillation analysis: 2 of 31 . . . 115
C.4 Daily oscillation analysis: 3 of 31 . . . 116
C.5 Daily oscillation analysis: 4 of 31 . . . 117
C.6 Daily oscillation analysis: 5 of 31 . . . 118
C.7 Daily oscillation analysis: 6 of 31 . . . 119
C.8 Daily oscillation analysis: 7 of 31 . . . 120
C.9 Daily oscillation analysis: 8 of 31 . . . 121
C.10 Daily oscillation analysis: 9 of 31 . . . 122
C.11 Daily oscillation analysis: 10 of 31 . . . 123
C.12 Daily oscillation analysis: 11 of 31 . . . 124
C.13 Daily oscillation analysis: 12 of 31 . . . 125
C.14 Daily oscillation analysis: 13 of 31 . . . 126
C.15 Daily oscillation analysis: 14 of 31 . . . 127
C.16 Daily oscillation analysis: 15 of 31 . . . 128
C.17 Daily oscillation analysis: 16 of 31 . . . 129
C.18 Daily oscillation analysis: 17 of 31 . . . 130

C.19 Daily oscillation analysis: 18 of 31 . . . 131
C.20 Daily oscillation analysis: 19 of 31 . . . 132
C.21 Daily oscillation analysis: 20 of 31 . . . 133
C.22 Daily oscillation analysis: 21 of 31 . . . 134
C.23 Daily oscillation analysis: 22 of 31 . . . 135
C.24 Daily oscillation analysis: 23 of 31 . . . 136
C.25 Daily oscillation analysis: 24 of 31 . . . 137
C.26 Daily oscillation analysis: 25 of 31 . . . 138
C.27 Daily oscillation analysis: 26 of 31 . . . 139
C.28 Daily oscillation analysis: 27 of 31 . . . 140
C.29 Daily oscillation analysis: 28 of 31 . . . 141
C.30 Daily oscillation analysis: 29 of 31 . . . 142
C.31 Daily oscillation analysis: 30 of 31 . . . 143
C.32 Daily oscillation analysis: 31 of 31 . . . 144

D.1 Differential LoD solutions: Parzen windowing . . . 146
D.2 Differential LoD solutions: Least-squares . . . 147
D.3 Differential mismatch calculations . . . 148
D.4 Individual LoD solutions: Parzen windowing . . . 149
D.5 Individual LoD solutions: Least-squares . . . 150
D.6 Individual mismatch calculations . . . 151
D.7 Statistical LoD solutions: Parzen windowing . . . 152
D.8 Statistical LoD solutions: Least-squares . . . 153
D.9 Statistical mismatch calculations . . . 153
D.10 Consolidated event ordering calculations: 01/02/2007 . . . 155
D.11 Event location estimates: 01/02/2007 . . . 156
D.12 Consolidated event ordering calculations: 01/03/2007 . . . 158
D.13 Event location estimates: 01/03/2007 . . . 159
D.14 Consolidated event ordering calculations: 01/11/2007 . . . 161
D.15 Event location estimates: 01/11/2007 . . . 162
D.16 Consolidated event ordering calculations: 01/24/2007 . . . 164
D.17 Event location estimates: 01/24/2007 . . . 165
D.18 Consolidated event ordering calculations: 01/25/2007 . . . 167
D.19 Event location estimates: 01/25/2007 . . . 168
D.20 Consolidated event ordering calculations: 02/05/2007 . . . 170
D.21 Event location estimates: 02/05/2007 . . . 171
D.22 Consolidated event ordering calculations: 02/07/2007 . . . 173
D.23 Event location estimates: 02/07/2007 . . . 174

D.24 Consolidated event ordering calculations: 02/15/2007 176
D.25 Event location estimates: 02/15/2007 177
D.26 Consolidated event ordering calculations: 02/28/2007 179
D.27 Event location estimate: 02/28/2007 180
D.28 Consolidated event ordering calculations: 03/13/2007 182
D.29 Event location estimates: 03/13/2007 183
D.30 Consolidated event ordering calculations: 03/16/2007 185
D.31 Event location estimates: 03/16/2007 186
D.32 Consolidated event ordering calculations: 03/20/2007 188
D.33 Event location estimates: 03/20/2007 189
D.34 Consolidated event ordering calculations: 03/21/2007 191
D.35 Event location estimates: 03/21/2007 192
D.36 Consolidated event ordering calculations: 03/24/2007 194
D.37 Event location estimates: 03/24/2007 195
D.38 Consolidated event ordering calculations: 04/06/2007 197
D.39 Event location estimates: 04/06/2007 198
D.40 Consolidated event ordering calculations: 04/23/2007 200
D.41 Event location estimates: 04/23/2007 201
D.42 Consolidated event ordering calculations: 04/30/2007 203
D.43 Event location estimates: 04/30/2007 204
D.44 Consolidated event ordering calculations: 05/03/2007 206
D.45 Event location estimates: 05/03/2007 207
D.46 Consolidated event ordering calculations: 05/06/2007 209
D.47 Event location estimates: 05/06/2007 210
D.48 Consolidated event ordering calculations: 05/08/2007 212
D.49 Event location estimates: 05/08/2007 213
D.50 Consolidated event ordering calculations: 05/10/2007 215
D.51 Event location estimates: 05/10/2007 216
D.52 Consolidated event ordering calculations: 05/14/2007 218
D.53 Event location estimates: 05/14/2007 219
D.54 Consolidated event ordering calculations: 05/19/2007 221
D.55 Event location estimates: 05/19/2007 222
D.56 Consolidated event ordering calculations: 05/24/2007 224
D.57 Event location estimates: 05/24/2007 225
D.58 Consolidated event ordering calculations: 05/25/2007 227
D.59 Event location estimates: 05/25/2007 228
D.60 Consolidated event ordering calculations: 06/09/2007 230

D.61 Event location estimates: 06/09/2007 231
D.62 Consolidated event ordering calculations: 06/09/2007 233
D.63 Event location estimates: 06/09/2007 234
D.64 Consolidated event ordering calculations: 06/09/2007 236
D.65 Event location estimates: 06/09/2007 237
D.66 Consolidated event ordering calculations: 06/12/2007 239
D.67 Event location estimates: 06/12/2007 240
D.68 Consolidated event ordering calculations: 06/19/2007 242
D.69 Event location estimates: 06/19/2007 243
D.70 Consolidated event ordering calculations: 06/27/2007 245
D.71 Event location estimates: 06/27/2007 246
D.72 Consolidated event ordering calculations: 06/27/2007 248
D.73 Event location estimates: 06/27/2007 249
D.74 Consolidated event ordering calculations: 06/29/2007 251
D.75 Event location estimates: 06/29/2007 252
D.76 Consolidated event ordering calculations: 07/01/2007 254
D.77 Event location estimates: 07/01/2007 255
D.78 Consolidated event ordering calculations: 07/02/2007 257
D.79 Event location estimates: 07/02/2007 258
D.80 Consolidated event ordering calculations: 07/03/2007 260
D.81 Event location estimates: 07/03/2007 261
D.82 Consolidated event ordering calculations: 07/04/2007 263
D.83 Event location estimates: 07/04/2007 264
D.84 Consolidated event ordering calculations: 07/07/2007 266
D.85 Event location estimates: 07/07/2007 267
D.86 Consolidated event ordering calculations: 07/25/2007 269
D.87 Event location estimates: 07/25/2007 270
D.88 Consolidated event ordering calculations: 08/04/2007 272
D.89 Event location estimates: 08/04/2007 273
D.90 Consolidated event ordering calculations: 08/06/2007 275
D.91 Event location estimates: 08/06/2007 276
D.92 Consolidated event ordering calculations: 08/06/2007 278
D.93 Event location estimates: 08/06/2007 279
D.94 Consolidated event ordering calculations: 08/18/2007 281
D.95 Event location estimates: 08/18/2007 282
D.96 Consolidated event ordering calculations: 08/20/2007 284
D.97 Event location estimates: 08/20/2007 285

D.98 Consolidated event ordering calculations: 08/24/2007 287
D.99 Event location estimate: 08/24/2007 288
D.100 Consolidated event ordering calculations: 08/28/2007 290
D.101 Event location estimates: 08/28/2007 291
D.102 Consolidated event ordering calculations: 09/01/2007 293
D.103 Event location estimates: 09/01/2007 294
D.104 Consolidated event ordering calculations: 09/04/2007 296
D.105 Event location estimates: 09/04/2007 297
D.106 Consolidated event ordering calculations: 10/03/2007 299
D.107 Event location estimate: 10/03/2007 300
D.108 Consolidated event ordering calculations: 10/03/2007 302
D.109 Event location estimates: 10/03/2007 303
D.110 Consolidated event ordering calculations: 10/12/2007 305
D.111 Event location estimate: 10/12/2007 306
D.112 Consolidated event ordering calculations: 11/04/2007 308
D.113 Event location estimates: 11/04/2007 309
D.114 Consolidated event ordering calculations: 11/04/2007 311
D.115 Event location estimates: 11/04/2007 312
D.116 Consolidated event ordering calculations: 11/09/2007 314
D.117 Event location estimate: 11/09/2007 315
D.118 Consolidated event ordering calculations: 11/14/2007 317
D.119 Event location estimates: 11/14/2007 318

List of Tables

1.1 TDOA for Bull Run trip 11

3.1 Old and new mismatch calculations 64
3.2 Ordering method comparison: base case 78

A.1 FDR names and locations 109

B.1 Scenario Information 111

D.1 Performance summary of new ordering method 145
D.2 Ordering method comparison: 01/02/2007 154
D.3 Ordering method comparison: 01/03/2007 157
D.4 Ordering method comparison: 01/11/2007 160
D.5 Ordering method comparison: 01/24/2007 163
D.6 Ordering method comparison: 01/25/2007 166
D.7 Ordering method comparison: 02/05/2007 169
D.8 Ordering method comparison: 02/07/2007 172
D.9 Ordering method comparison: 02/15/2007 175
D.10 Ordering method comparison: 02/28/2007 178
D.11 Ordering method comparison: 03/13/2007 181
D.12 Ordering method comparison: 03/16/2007 184
D.13 Ordering method comparison: 03/20/2007 187
D.14 Ordering method comparison: 03/21/2007 190
D.15 Ordering method comparison: 03/24/2007 193
D.16 Ordering method comparison: 04/06/2007 196
D.17 Ordering method comparison: 04/23/2007 199
D.18 Ordering method comparison: 04/30/2007 202
D.19 Ordering method comparison: 05/03/2007 205
D.20 Ordering method comparison: 05/06/2007 208
D.21 Ordering method comparison: 05/08/2007 211
D.22 Ordering method comparison: 05/10/2007 214

D.23 Ordering method comparison: 05/14/2007 217
D.24 Ordering method comparison: 05/19/2007 220
D.25 Ordering method comparison: 05/24/2007 223
D.26 Ordering method comparison: 05/25/2007 226
D.27 Ordering method comparison: 06/09/2007 229
D.28 Ordering method comparison: 06/09/2007 232
D.29 Ordering method comparison: 06/09/2007 235
D.30 Ordering method comparison: 06/12/2007 238
D.31 Ordering method comparison: 06/19/2007 241
D.32 Ordering method comparison: 06/27/2007 244
D.33 Ordering method comparison: 06/27/2007 247
D.34 Ordering method comparison: 06/29/2007 250
D.35 Ordering method comparison: 07/01/2007 253
D.36 Ordering method comparison: 07/02/2007 256
D.37 Ordering method comparison: 07/03/2007 259
D.38 Ordering method comparison: 07/04/2007 262
D.39 Ordering method comparison: 07/07/2007 265
D.40 Ordering method comparison: 07/25/2007 268
D.41 Ordering method comparison: 08/04/2007 271
D.42 Ordering method comparison: 08/06/2007 274
D.43 Ordering method comparison: 08/06/2007 277
D.44 Ordering method comparison: 08/18/2007 280
D.45 Ordering method comparison: 08/20/2007 283
D.46 Ordering method comparison: 08/24/2007 286
D.47 Ordering method comparison: 08/28/2007 289
D.48 Ordering method comparison: 09/01/2007 292
D.49 Ordering method comparison: 09/04/2007 295
D.50 Ordering method comparison: 10/03/2007 298
D.51 Ordering method comparison: 10/03/2007 301
D.52 Ordering method comparison: 10/12/2007 304
D.53 Ordering method comparison: 11/04/2007 307
D.54 Ordering method comparison: 11/04/2007 310
D.55 Ordering method comparison: 11/09/2007 313
D.56 Ordering method comparison: 11/14/2007 316

E.1 Simulated system parameters[6] 319

Chapter 1

Distributed Measurements of the Electric Power System

The electric power grid is an amazingly peculiar machine. Charles Steinmetz, the inventor of the phasor,[7] is reputed to have declared the functioning interconnection of the thousands of electrical machines in North America to be "the largest and most complex machine ever devised by man."[6] Recently the National Academy of Engineering declared this system to be the single greatest engineering achievement of the 20th century.[8] This achievement is all the more astounding considering even today the grid is operated without even an approximation of observability. Recent events like the August 14, 2003 blackout underscore the vague understanding regional system operators have of events outside their service area.[9]

In fact, it was only after a similarly catastrophic blackout of the northeast United States in 1965 that the need for real-time system information was realized.[10] Research efforts after this event led to the development of state estimation, whereby a semi-regular scan of a few strategically placed sensors could be extrapolated to guess at the state of any node in the system.[11] Only after the microprocessor and the completion of the satellite-based Global Positioning System (GPS) in 1995[12] were dynamic (high time resolution) time-synchronized system observations possible.

Virginia Tech has led the development of time-synchronized dynamic monitoring of the power system through the work of Dr. Arun Phadke, inventor of the phasor measurement unit or PMU.[11,13] The PMU is capable of measuring all of the significant complex parameters of the grid, namely voltage, $\mathbf{E}_i$, and current, $\mathbf{I}_i$, at the i^{th} node where it is installed. Typically measurements are taken 30 times a second. From voltage and current other parameters can be determined, such as active and reactive power flow. A GPS receiver in each PMU allows for time synchronization of measurements at different nodes. Thus such measurements are called synchrophasors.[11] Additionally the PMU has communications capabilities by which it can send its measurements to a central repository for archival,[9,14] post-event analysis,[15,16] and system planning.[16,17]

The most significant benefit of wide-area time synchronized measurements is the realization of Energy Management Systems (EMSs) that were first envisioned in the aftermath of the 1965 blackout.[11] Ideally, an EMS uses the real-time data gathered from PMUs and like devices to monitor system state and provide early and preventative warnings of potential hazards to the system.[18] Specifically, the EMS uses these distributed measurements to determine[18] and visualize[19] system state, detect disturbances,[20] and suggest avoidance strategies during an event.[21,22] The slow implementation of such applications of dynamic wide-area measurements is in large part due to the legacy equipment still connected to the system. As the availability of such measurements are still very new,[23–25] the control strategies on many older devices are not compatible with available sub-second measurements.[6,26]

Transitioning from state estimation to state observation is not trivial because of the vast electrical size of the system. Even though wide-area studies of the power system generally neglect the localized distribution networks and focus on the higher capacity transmission network, the number of lines and nodes is still prohibitive. As an illustration, consider Figure 1.1,[27] which shows only a portion of the high voltage (> 345 kV) transmission lines in the eastern section of the U.S. grid. The computer model[1] from which this reduced schematic was created includes 2,287 generators, 16,016 busses, 20,093 transmission lines, and 7,221 branches with transformers.[27]

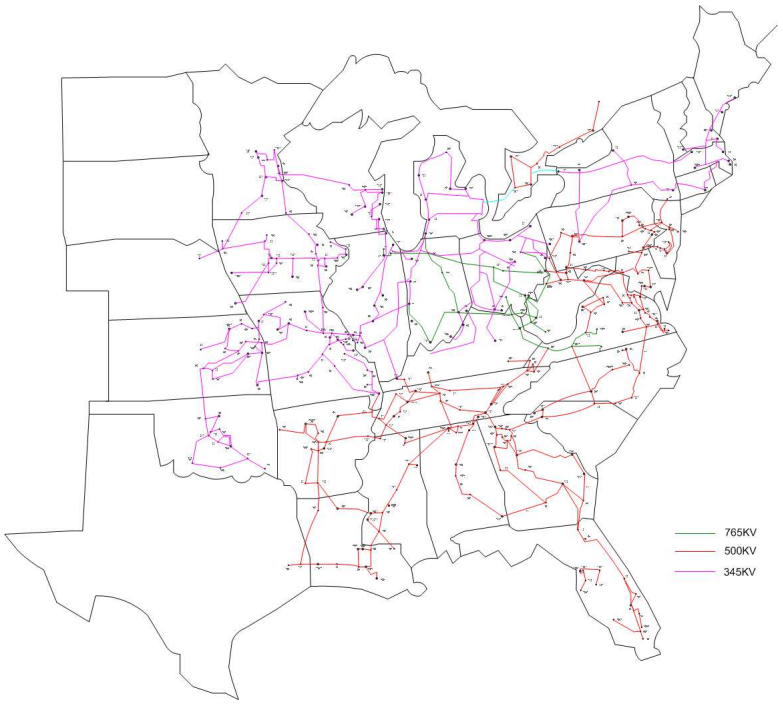


Figure 1.1. Reduced Order Schematic of the Eastern U.S. Network[1]

[1] As of the time of this report, non-disclosure agreements with the provider of this model prohibit the dissemination of further model details.

The overwhelming number of nodes in the network make full observability, at least in the immediate future, impossible. For this reason much of the current synchrophasor research centers on optimal unit placement.[28] The other main impediment to pervasive PMU placement is cost. Most often the PMU requires delicate installation inside a substation since it measures three-phase quantities. Thus the installed cost of one unit is rarely lower than $100,000,[29] making even optimal placement difficult for such a large system. Only through the development of a different kind of sensor are all the benefits of wide-area monitoring realizable.

Ubiquitous, cost-effective placement of sensors throughout the grid necessitate a device that can be easily installed and deployed. Since such a requirement eliminates three-phase installation, is there a useful electrical parameter that can be reliably measured at low-voltage, single-phase (distribution) levels? For reasons that will be detailed in Section 2.1, frequency is such a parameter. Since the speeds of every generator attached to the grid are synchronized, the frequency at any node in the system is directly related to the speed at which these generators are rotating.[30,31] Therefore when a significant disturbance occurs in a power system, the frequency varies in time and space.[32,33] To contrast, voltage and current disturbances are highly localized phenomena which do not give an accurate system-wide perspective. Not only is frequency the most descriptive parameter of the electric grid,[19,34] but it is also voltage level invariant and easily measured from a standard 110 V outlet. The value of monitoring frequency throughout the grid in real time led to Virginia Tech's development of a wide-area frequency monitoring network in 2001.

1.1 A wide-area frequency monitoring network (FNET)

For the past eight years, Virginia Tech has been developing and deploying an internet based, wide-area frequency monitoring system (FNET).[29,35] The objective of the FNET effort is to create an extremely low cost and quickly deployable wide-area frequency measurement system with high dynamic accuracy. The FNET system utilizes data collected from Frequency Disturbance Recorders (FDRs) placed throughout the grid, as shown in Figure 1.2

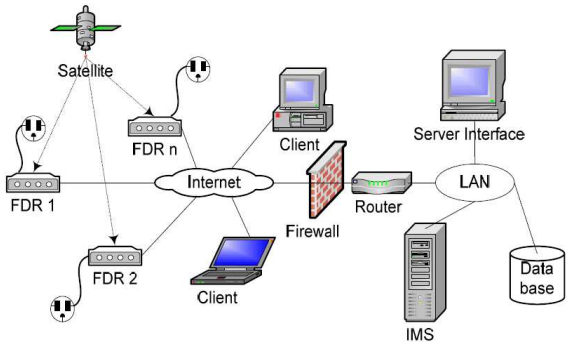


Figure 1.2. Frequency Monitoring Network Architecture

FNET is comprised of more than 30 Frequency Disturbance Recorders and an information management server (IMS) at Virginia Tech. The FDRs are precision measurement instruments that can be installed at low voltage (110V) outlets. Each of these instruments measures voltage magnitude, voltage angle, and computes frequency ten times per second. The measurements are then GPS synchronized and sent to the IMS via the internet. Once the server receives the measurements, it simultaneously stores the measurements in a database and updates the real-time web display.[35] Thus the FDR can be understood as a "reduced-order" PMU, because it lacks the capacity to measure current and current-related quantities like power flow and power factor.

The installed cost of an FDR ($1,000) is negligible compared to that of a PMU, but the FDR has two other significant logistical advantages compared to the PMU. Since the FDR only requires a 110 V receptacle, an internet connection, and a view of the sky, pervasive FDR placement is realistic. Upcoming improvements to the FDR include wireless capabilities[36] and indoor GPS[37] so even these meager constraints will soon be eliminated. Not only can FDRs be placed nearly anywhere, but their location is easily adaptable. While early FDR placement was primarily determined by convenience and personal relationships with an FDR's host, current and future FDR placement is determined by historical data analysis. In fact, it is a trivial matter to place an FDR in the middle of a region with a history of notable events.

While the FDR has many positive attributes, there are also two major drawbacks to its use. The first concern is one of function. The FDR is not a replacement for a PMU; moreover it is not useful for many PMU applications, particularly those in the operations and planning areas. The ability of a PMU to measure current should not be understated. However, there is great benefit to adding the data gathered from a low-cost, pervasive measurement network to that collected from a limited PMU network.

The second drawback is that the particulars of the FDR's construction lead to reliability concerns. Past research[38] and personal experience indicate that on average 50% of the deployed FDRs are reporting data at any given time. This percentage is attributed to both software malfunctions and network errors. Although the current internet is believed to lack the reliability and latency to support real-time communication, many of the applications intended by FNET are not time-critical. These applications include system observation, model validation, and post-mortem analysis. The current network performance has proven to be satisfactory for FNET and its applications. FDR redundancy can more than compensate for data transfer reliability. Furthermore, network providers are moving towards several crucial milestones in network evolution. It is expected that the next generation of the internet should meet many of the real-time communication requirements.

Of additional concern is the fact that the FNET system managers cannot ensure each FDR has consistent, dependable connections to either the grid or the internet. These tasks are the responsibility of the host. However, FNET's goals are not adversely affected by the inability to control

each unit's connections. If a wide-area frequency monitoring network were to be used in the operation of the grid, a utility would eliminate these concerns by reconfiguring an FDR to use its own existing dedicated communications channels, just like a PMU uses. In summary any problem a single device may have is not a systemic one, even though all the devices are essentially the same. Pervasive FDR placement provides the redundancy to mitigate the effects of any disturbance to a unique data stream.

Figure 1.3 shows the present location of each FDR that has been placed in each of the four synchronous interconnections in North America. These interconnections are referred to as the Eastern United States Interconnection System (EI or EUS), the Western Electric Coordinating Council (WECC), the Electric Reliability Council of Texas (ERCOT), and Hydro-Québec. The time average of frequency within each interconnection is a constant 60 Hz, and each interconnection is only connected to the other interconnections via direct-current tie lines, thus isolating each interconnection's frequency from one another. We can thus make the assumption that events originating in one interconnection are not observable in another interconnection.

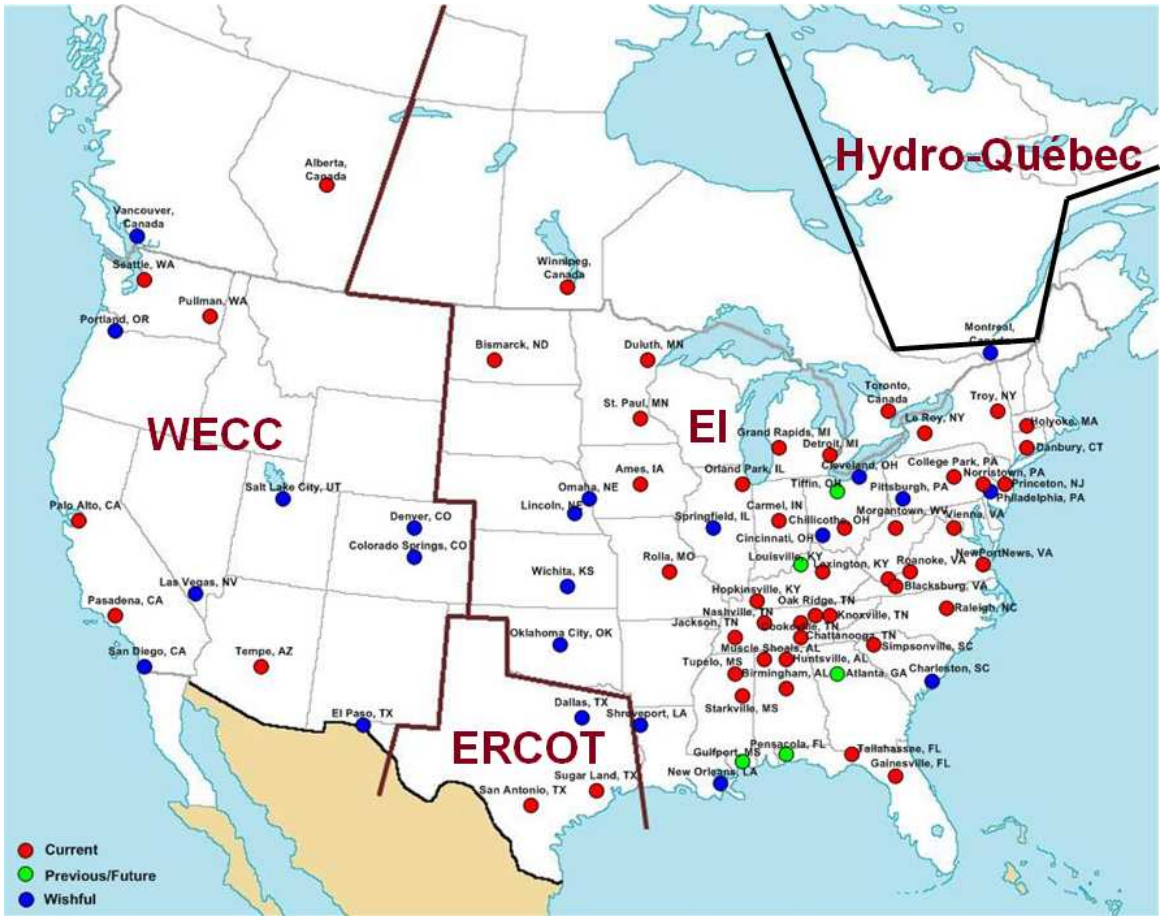


Figure 1.3. Current FDR locations

1.2 The value of measuring frequency

The preeminent value of measuring system-wide frequency is confirmed by both simulations and real data. The following examples underscore the value of frequency as the only parameter that offers global visibility of power system events, even down to the lowest level of the distribution network. Even at the highest levels of the transmission system, quantities such as voltage are not globally perturbed during the course of an event.

1.2.1 Global propagation of frequency deviation

Since the PMUs currently installed in the system are not enough to approximate a ubiquitous sensor network, PSS/E™simulations are most often used to understand system response to an event. The following example, first reported in Gardner [1], confirms the localized extent of voltage perturbation during an event. This simulation monitors the system reaction to the sudden disconnection of the W. H. Zimmer facility near Clermont, Ohio, with capacity of 1300 MW. This generator is in one of the major generating regions in the EI, and there were at least three confirmed reports of this facility tripping during the 2007 calendar year. Whenever a generator is suddenly taken offline, the remaining generators are subjected to an immediate overloading:

$$\Delta P_{\text{system}} = \sum_{\text{All Generators}} P_{\text{mechanical}} - \sum_{\text{All Loads}} P_{\text{electrical}} \approx -1300 \text{ MW}$$

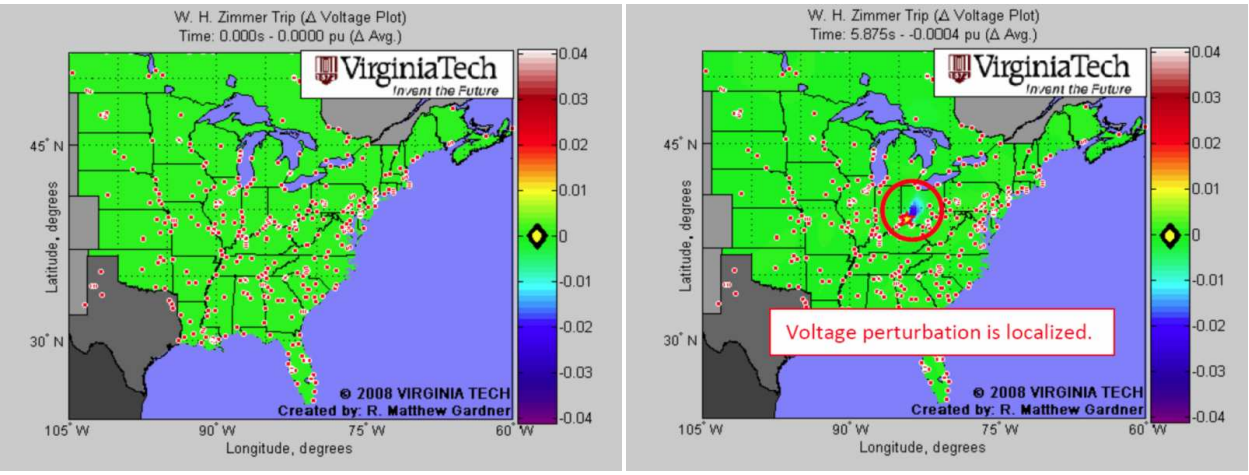
These simulations measure voltage and frequency deviation from nominal as functions of space ($\mathbf{x} = (x, y)$) and time:

$$E_{dev}(\mathbf{x}, t) = E(\mathbf{x}, t) - E(\mathbf{x}, t_0)$$
$$f_{dev}(\mathbf{x}, t) = f(\mathbf{x}, t) - f(\mathbf{x}, t_0)$$

A measure of the global visibility of an event is the interconnection average, measured at each of n PMUs:

$$\overline{E}_{dev}(t) = \frac{1}{n} \sum_{i=1}^{n} E_{dev}(\mathbf{x}_i, t)$$
$$\overline{f}_{dev}(t) = \frac{1}{n} \sum_{i=1}^{n} f_{dev}(\mathbf{x}_i, t)$$

Figures 1.4 and 1.5 show E_{dev} in per unit and f_{dev} in Hz respectively. The small red dots represent PMUs and the diamond in the colorbar is $\overline{E}_{dev}(t)$ and $\overline{f}_{dev}(t)$.

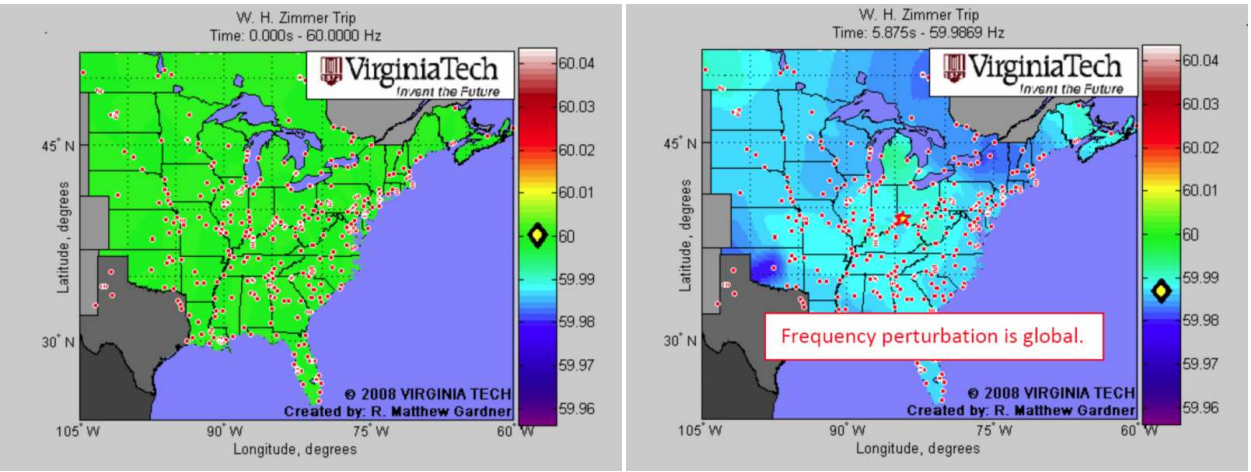


(a) Voltage pre-event[1]

(b) Voltage 4.875s after generator trip[1]

Figure 1.4. Voltage profiles of the EI before and during a generator trip[1]

Even in the overloaded case (Figure 1.4b), the voltage profile remains essentially unchanged from the system state pre-event. The region of voltage depression is so localized around the tripped generator (the star in Figures 1.4b and 1.5b) that fewer than 1% of the PMUs in this system would have even recorded a decreased voltage. To contrast, the frequency profiles in Figure 1.5 are quite different from the voltage profiles. The frequency at every PMU registers a significant drop in frequency after the event, as seen in Figure 1.5b.



(a) Frequency pre-event[1]

(b) Frequency 4.875s after generator trip[1]

Figure 1.5. Frequency profiles of the EI before and during a generator trip[1]

These results are not altogether unexpected. Circuit laws such as Ohm's law determine the voltages at each node of the circuit, so there is no reason to expect the voltage across the system to

decline simply because the voltage at one node in the circuit changes. Similarly current and phase angle experience no such equivalence constraints.

Unlike voltage, however, the laws of physics require the frequency of each generator to drop. In order for the system to be synchronized, the time average of frequency measured at any two points in the interconnection $\mathcal{R}$ must be equal. This constraint reduces to[2]

$$\int_{t-\frac{T}{2}}^{t+\frac{T}{2}} f(\mathbf{x}_i, \tau)\partial\tau = \int_{t-\frac{T}{2}}^{t+\frac{T}{2}} f(\mathbf{x}_j, \tau)\partial\tau \qquad \forall i, j \in \mathcal{R},\ T > \mathcal{T}^2 \tag{1.1}$$

Therefore, just as any rotating machine slows down when its loading is increased, so do the aggregated remaining generators after the generator trip. As each generator participates in picking up the excess load, frequency declines across the system in accordance with Newton's second law of motion.

It is important to note that (1.1) is not a restriction on instantaneous frequency, as it can deviate between units at an arbitrary t_1. These sub-second differences are the reason frequency measurements are so useful in determining the state of the power system.[1,15,27]

1.2.2 Voltage level invariance

While the previous simulation conclusively shows the value of wide-area frequency measurements, there are data quality issues with distribution level measurements. The transition from transmission to distribution levels introduce considerable amounts of noise, phase shifts, and other distortions to distribution-level measurements. Many projects have already shown the quality of transmission level PMU measurements,[39] and preliminary research has shown that in special cases distribution level voltage measurements can cleanly approximate transmission level voltages,[40] but historical analysis of FNET data shows that 110 V voltage measurements are not good predictors of transmission level voltages.[1] Once again, frequency's value is reaffirmed: events appearing in transmission level measurements are equally apparent in distribution level measurements.

The following example provides some empirical justification for this claim. The FNET team was able to obtain transmission level PMU measurements from five units in the American Electric Power (AEP) service area during a trip of the Bull Run generator near Oak Ridge, Tennessee on July 25, 2006. Figure 1.6 shows the locations of each FDR and PMU. The synchronized interconnection, per (1.1), implies that the data recorded by adjacent units should be similar, regardless of voltage level. Figure 1.7 confirms there is no significant difference between PMU and FDR measurements.

[2]The coupling parameter $\mathcal{T}$ is determined by machine inertias and the reactances of the transmission network.

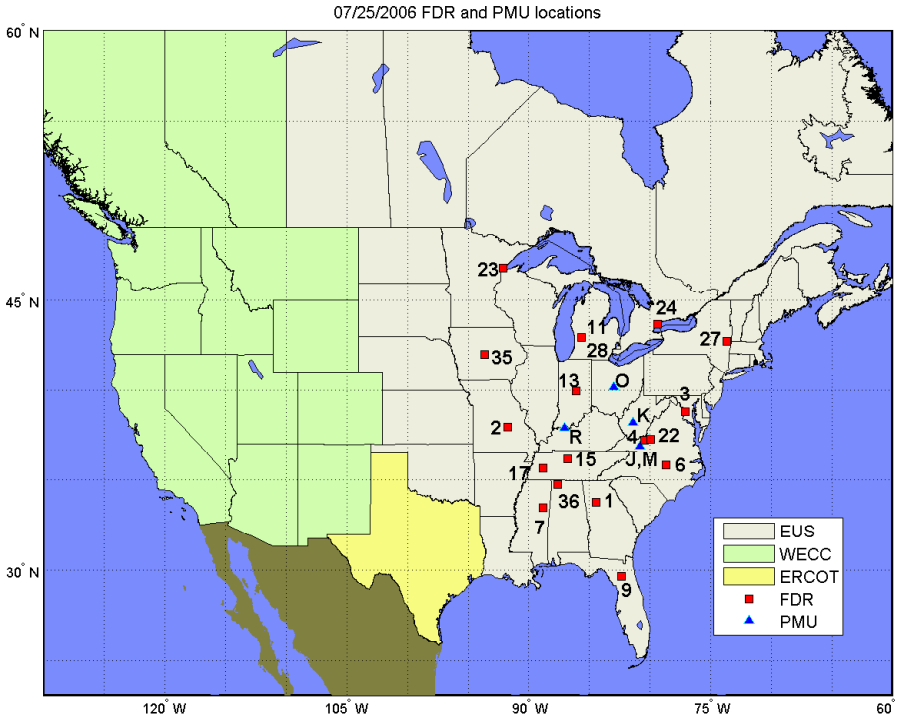


Figure 1.6. FDR and PMU locations during 7/25/2006 event. Numbers identify FDRs and letters identify PMUs.

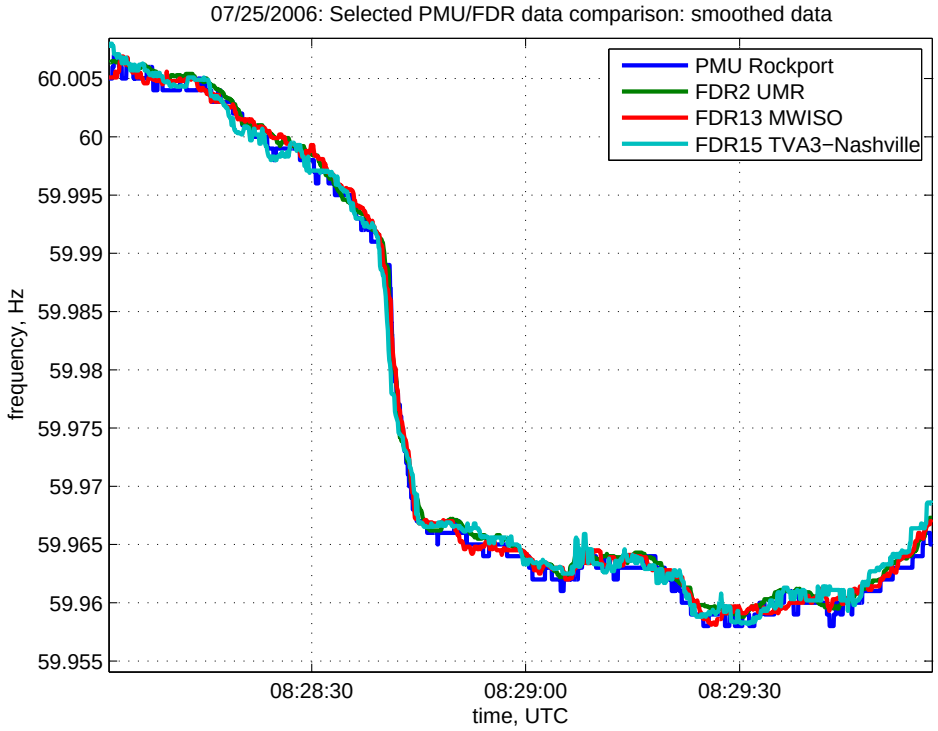


Figure 1.7. Event recordings from adjacent units

Not only does this example show the voltage level invariance of wide-area frequency measurements, but it also gives insight into the importance of sub-second frequency deviations between units. Figure 1.8 shows frequency traces from units geographically far away from one another. While the general shape and slope of the frequency decline remain similar between units, the point at which each unit records its maximum slope is appreciably different. This phenomena is attributed to the propagation of electromechanical waves through the system.[41,42] The sudden step change in the load-generation balance incites an electromechanical disturbance that propagates as a wave throughout the continuum of the power grid.[43]

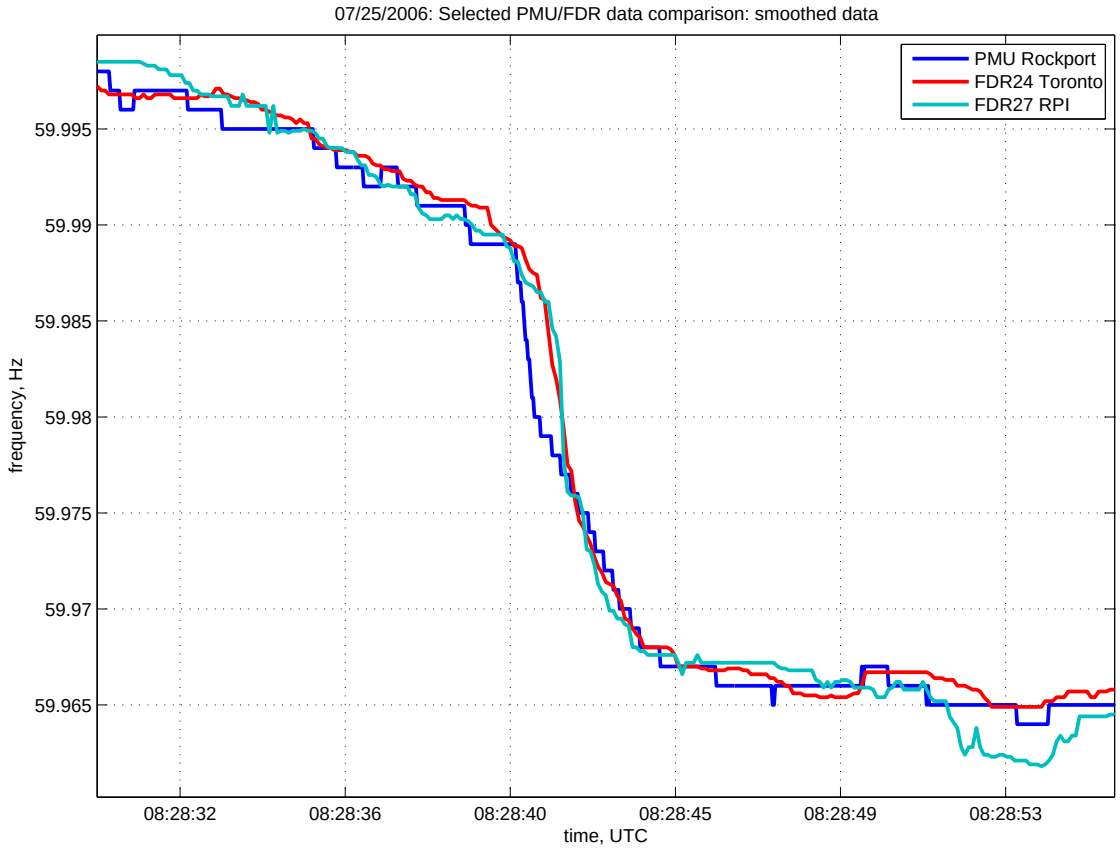


Figure 1.8. Event recordings from distant units

As this wave propagates out from its hypocenter with finite velocity,[34] sensors at different distances from the hypocenter record the presence of the wavefront at different times. This time-delay of arrival (TDOA) marks one of the many indicators of the system's health that can be gleaned from distributed frequency observations. One use of TDOA is in the solution of the Location-of-Disturbance (LoD) problem, where measurement data is used to estimate an event hypocenter. In general, units closer to the event hypocenter will record the passage of the wavefront earlier than units farther away. This is not always the case, as evidenced by Table 1.1, because

of the heterogeneous distribution of generation and load centers and the nonlinearities of the network. However, the use of TDOA has proven[44] to be a good metric for LoD problems, as will be detailed in Chapter 3.

Table 1.1. TDOA for Bull Run trip (7/25/2006, 950 MW, 36.10°,-84.15°)

		Arrival Time (UTC)	Delay (s)	Hypocentral Distance: statute mi (km)
Unit ID: FDRs(numbers), PMUs(letters)	36	8:28:39.20	0.00	217.84 (350.58)
	J	8:28:39.33	0.13	192.24 (309.37)
	7	8:28:39.40	0.20	322.01 (518.22)
	15	8:28:39.50	0.30	147.31 (237.07)
	4	8:28:39.50	0.30	220.45 (354.79)
	9	8:28:39.50	0.30	456.17 (734.14)
	K	8:28:39.53	0.33	209.06 (336.44)
	SO	8:28:39.60	0.40	288.82 (464.81)
	R	8:28:39.63	0.43	203.18 (326.98)
	27	8:28:39.80	0.60	721.91 (1161.8)

1.3 The statistical nature of wide-area frequency measurements

Any measurement of a real system will have imperfections. In the case of FNET data, these imperfections can be broadly classified in three categories: mistakes, errors, and noise. In mathematical terms, a common description[45] of frequency measurements are of the form

$$\hat{f}(t) = f(t) + m(t) + e(t) + n(t)$$

where the measured (or estimated) frequency $\hat{f}(t)$ consists of the true frequency $f(t)$ perturbed by mistakes $m(t)$, errors $e(t)$, and noise $n(t)$. Since the objective of FNET is to study system-wide events, the true frequency $f(t)$ is understood to be the frequency at the point where the distribution feeder supplying the FDR connects to the transmission grid.[46]

Mistakes result from hardware problems, the most common of which are firmware errors and failed interactions with the GPS module. These problems were more prevalent in earlier firmware iterations. Not only are mistakes decreasing in prevalence, but they are typically quite distinct (different from typical data patterns) and therefore easily filtered out. Figure 1.9 shows 30 minutes of data surrounding a generator trip that illustrates mistakes, errors, and noise.

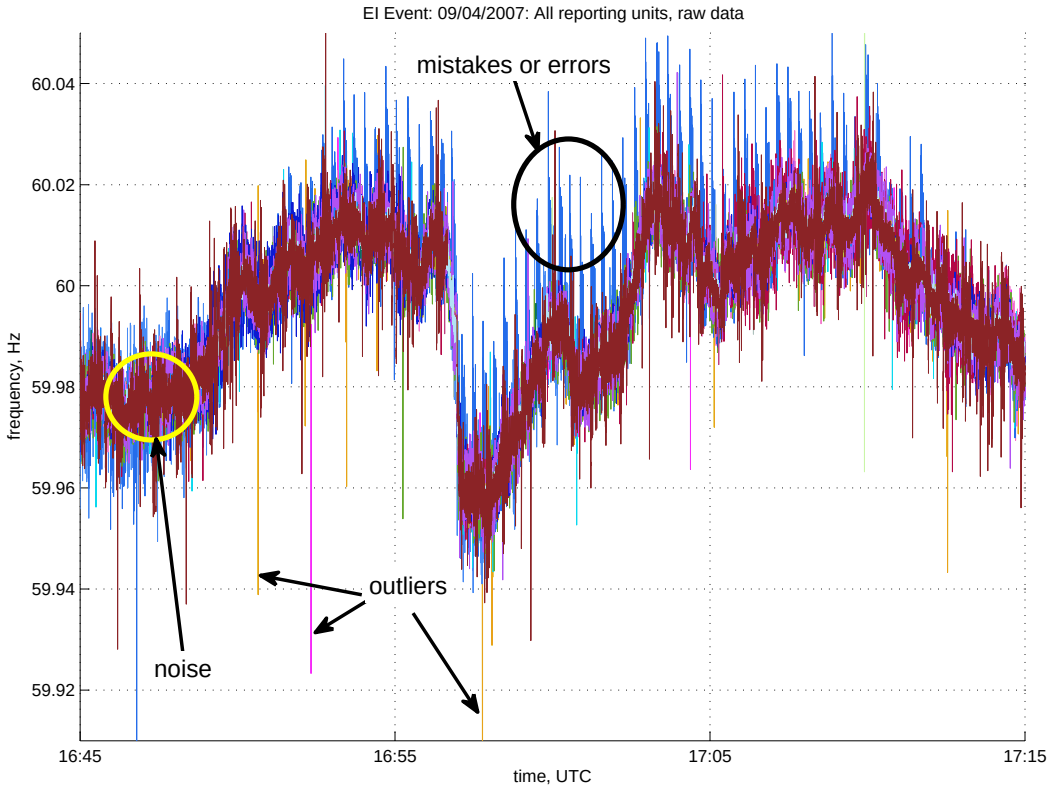


Figure 1.9. Typical frequency data

Typically mistakes manifest themselves as outliers - single point spikes that deviate significantly from the frequency trend. These outliers are most often attributed to old firmware that has yet to be upgraded. Non-outlier mistakes, such as the loss of GPS satellite visibility, result in non-existent or dropped data points. In either case, these mistakes are simple to eliminate with elementary smoothing techniques. Thus without loss of generality, frequency data can be expressed as

$$\hat{f}(t) = f(t) + e(t) + n(t)$$

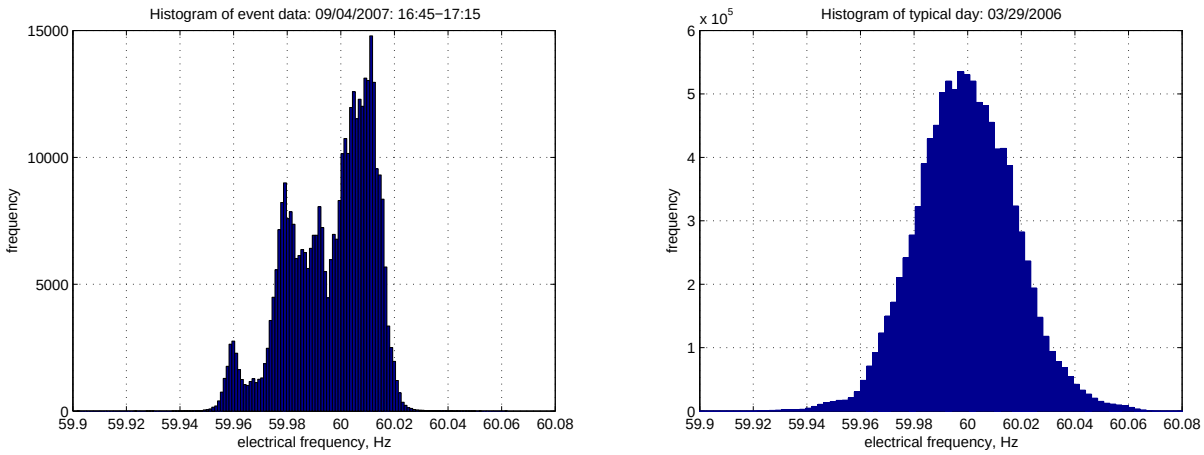
1.3.1 Errors and noise

The difference between noise and errors in frequency is the physical phenomena causing the distortion. Noise, assumed to be additive white Gaussian noise (AWGN), is the combination of minuscule (but ever-present) measurement error, solar wind, and astrological phenomena. Conversely errors are a result of the FDR's direct connection to the distribution network. The kind of power quality issues that propagate through the distribution network are well documented[31,33] and understood to be strictly local in scope. Hence these errors, while being an accurate description of the physics of the electric grid, are not relevant in the wide-area perspective.[47]

Just as Figure 1.9 illustrates, such errors also manifest themselves as outliers. These outliers, however, typically consist of multiple adjacent outliers, in contrast with the single-point outliers indicative of mistakes. Often local loading phenomena is periodic, so the blue trace in Figure 1.9 is most likely a power quality issue. There is a slight possibility, however, these excursions are the product of a corrupted hardware setting. In either case, robust data conditioning can largely ignore these kinds of outliers.

1.3.2 Non-stationary operation of the power system

Proper data conditioning cannot be performed without a more thorough description of the stochastic properties of FNET data. Figure 1.10a is a histogram of the aggregated frequency data from Figure 1.9, and Figure 1.10b is the aggregate frequency distribution of a typical day in the EI. These two distributions are quite different, and the properties of the event do not fully explain all of these differences.



(a) Aggregate frequency distribution, 9/4/2007

(b) Aggregate frequency distribution, 3/29/2006

Figure 1.10. Aggregate frequency distribution for two different days

The signature of the generator trip (occurring approximately at 16:57) from Figure 1.9 shows that the instantaneous overloading of the system causes the frequency to drop to a "minimum" value around 59.96 Hz, which explains the small mode apparent in the histogram at that same frequency. While some of the multi-mode behavior in Figure 1.10a, particularly the mode greater than 60 Hz, can be attributed to the aforementioned error outliers, it cannot explain the lack of a mode at 60 Hz like in Figure 1.10b. These differences are explained by the concept of stationarity, which is defined by the relationship

$$\mathbf{E}\left[\hat{f}(t)\right] = \hat{\mu}_f(t) = \hat{\mu}_f(t+\tau) \qquad \forall \tau \in \mathbb{R}$$

Since the distribution of frequency data does not remain constant in time, it is not stationary. This lack of stationarity is a function of the operation of the system, as system operators act in a precautionary manner. For example, operators bring generators online prior to the early morning run on demand as customers begin their day to ensure reliability. This anticipatory action has the result of the system speeding up as net loading decreases until the morning load brings the frequency back to nominal. These daily variations are referred to as the daily load curve. On a broader scale, variations in system operation also manifest themselves between peak (summer and winter) and shoulder seasons, primarily in accordance with the maintenance schedules.

Not only does the frequency distribution at one node vary with time, but the frequency distributions at two disparate locations varies as well. Taking into account the non-stationarity of the data, the frequency at two nodes i and j can be described as

$$\hat{f}_i(t) = \mu_i(t) + s_i(t) + e_i(t) + n_i(t)$$
$$\hat{f}_j(t) = \mu_j(t) + s_j(t) + e_j(t) + n_j(t)$$

where the the true frequency $f(\mathbf{x}, t) = \mu(t) + s(t)$. $\mu(t)$ describes the trend of data, including the daily load curve, and $s(t)$ is the seasonal component. There is no clear quantitative description of $s(t)$, so any seasonal variation (which is incredibly slow compared to the sub-second time resolution) is sublimated into the daily trend:

$$s_i(t) = s_j(t) = 0$$

Since the trend $\mu(t)$ describes long-term (daily) variations, the general behavior of a synchronous grid per (1.1) is

$$\mu_i(t) \approx \mu_j(t)$$

In the absence of a contingency,

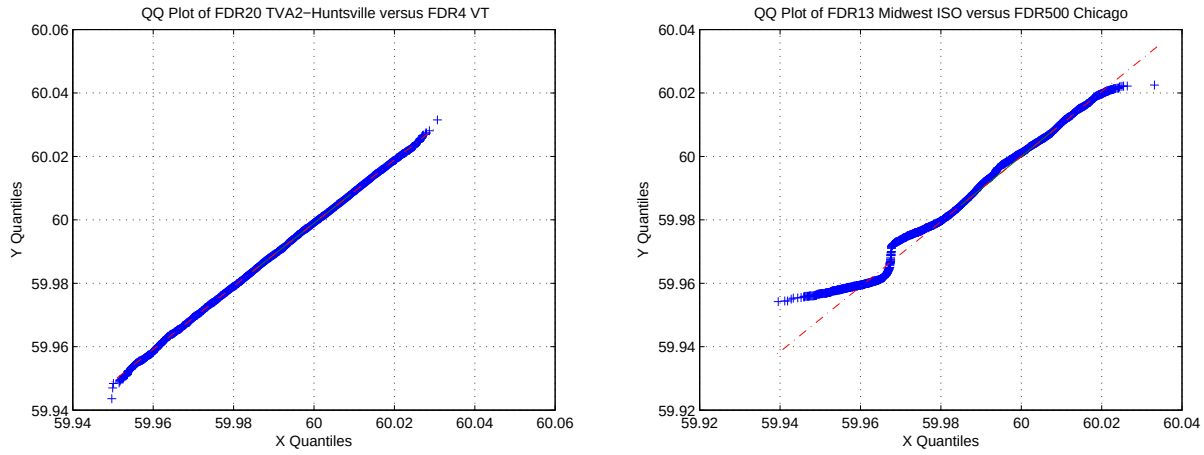
$$\mu_i(t) \approx \mu_j(t) \approx 60 \text{ Hz}$$

Thus the inter-sensor variations are primarily a function of the local effects described by $e(t)$.

Quantitative description of these effects are accomplished by the use of quantile-quantile (Q-Q) plots. A β-quantile of a data set $\mathbf{X}$ is any value x such that

$$\mathrm{P}(\mathbf{X} \leq x) = \beta \tag{1.2}$$

The Q-Q plot is simply the quantiles of the first data set on the abscissa versus the quantiles of the second data set on the ordinate. If both data sets come from the same distribution, the Q-Q plot will result in a straight line (Figure 1.11a), even if the two data sets have different parameters, like the mean and variance[48]. If the Q-Q plot is not a line, the two data sets are not from the same distribution. The non-linear Q-Q plot can have either heavy or light tails. A heavy-tailed Q-Q plot diverges below on the left and above on the right from the straight line, while the light-tailed Q-Q plot diverges above on the left and below on the right (Figure 1.11b).



(a) Q-Q plot for two FDRs approximately 388 miles apart (b) Q-Q plot for two FDRs approximately 144 miles apart

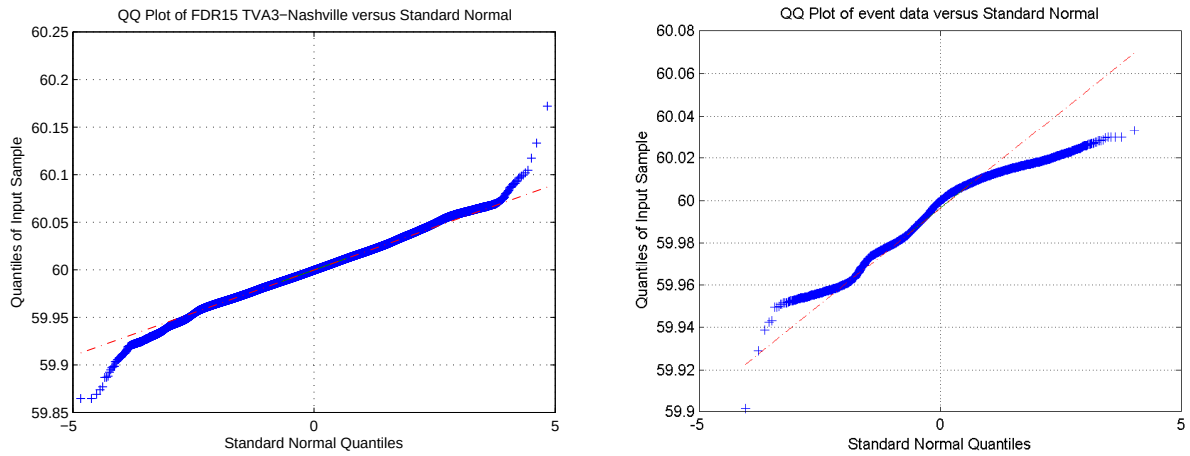
Figure 1.11. Inter-FDR frequency distribution comparison

As Figure 1.11 illustrates, the data of some FDRs is very similar to that of other FDRs (Figure 1.11a), while sometimes the distributions of two FDRs are very different (Figure 1.11b). Moreover, as each FDR's distribution varies with time, the groups of FDRs which share similar distributions also change.

1.4 Fundamentals of robust data conditioning

Not only can Q-Q plots be used to compare the statistical properties of different FDRs, but they can be used to describe how a single unit's distribution compares to that of the Standard Normal distribution. If FNET data were to be similar to the Normal distribution, many convenient statistical assumptions could be made about the data thanks to the Central Limit Theorem.[48] If the Q-Q plot

is heavy- or light- tailed, then care must be taken in data conditioning. Figure 1.12 shows the Q-Q plot of typical FNET data compared with the standard Normal distribution.



(a) Q-Q plot for data recorded during normal operation

(b) Q-Q plot for data recorded during an event

Figure 1.12. Frequency distribution comparison to the Normal distribution

If a Q-Q plot is heavy-tailed, it indicates that the data set of the ordinate axis has thicker tails than those of the data set on the abscissa. Since the Q-Q plot of the FNET data is heavy-tailed, as in Figure 1.12a, its distribution can be understood to have thicker tails than the tails of the Gaussian distribution. A distribution that fits FNET data quite well is the Laplacian, or double-exponential distribution, because of the Laplacian's thick tails. The density function of the Laplacian distribution is given by:

$$f(x) = \frac{1}{2a}\, e^{-\frac{|x-b|}{a}} \tag{1.3}$$

A graphical interpretation of the parameters of the Laplacian distribution is presented in Figure 1.13.

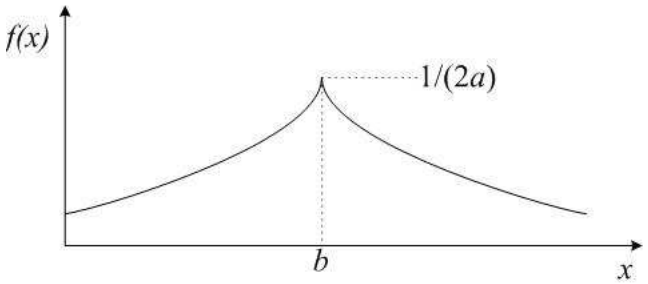


Figure 1.13: Cartoon of the Laplacian distribution

The statistical nature of FNET measurements requires robust statistical conditioning instead of classical statistical methods because of its heavy tails.[49–51] One robust technique for extracting the true frequency $f(t)$ from $\hat{f}(t)$ is the moving median. Given a discrete sequence of frequency measurements $\left\{\hat{f}[k]\right\}_{k=1}^{N}$, application of an n-point moving median yields a sequence[3] $\left\{\tilde{f}[k]\right\}_{k=n}^{N}$ where the median is defined as[53,54]

$$\tilde{f}[k] = \text{median}\left[\hat{f}[k-n+1],\, \hat{f}[k-n+2], \ldots,\, \hat{f}[k-1],\, \hat{f}[k]\right]$$

Use of the moving median is optimal for FNET data because it is the Maximum-Likelihood (ML) estimator of the Laplacian distribution, which minimizes the L_1 norm:[55]

$$\phi(f) = \sum_{k=1}^{n} |f[k]|$$

Colloquially the moving median's "ride-through" capabilities are necessary for proper treatment of FNET data and its many outliers. Contrast this robustness with that of an n-point moving mean:

$$\overline{f}[k] = \frac{1}{n} \sum_{i=k-n+1}^{k} \hat{f}[k]$$

The moving average (MA filter) is perturbed by a single outlier, while the moving median requires $\frac{n+1}{2}$ outliers to be disrupted.[55] The moving mean's performance is is explained by the fact that as a least squares estimator, it is the ML estimator of the Normal, or Gaussian, distribution which minimizes the objective function[56,57]

$$\phi(f) = \sum_{k=1}^{n} r_k^2 = \sum_{k=1}^{n} \left(\hat{f}[k] - f[k]\right)^2$$

As both the moving mean and moving median are understood to be "smoothing" techniques, both techniques behave as low-pass filters.[58] While median filtering is not a linear process, and therefore does not have a "frequency response" in the usual sense, the moving mean is a linear process and its frequency response for various windowing methods is shown in Figure 1.14. Median filtering requires empirical determination of window size and as such is application dependent. Chapter 2 will detail some window sizing criteria.

[3] The index declaration of this sequence is somewhat arbitrary. For real-time applications, $\tilde{f}[k]$ must only rely on past measurements. However, post-mortem analysis can make use of a centered moving median, where $\tilde{f}[k]$ is the median of an n point window centered around k. To accomplish this centering in real-time, a time delay of $\frac{n+1}{2}$ is used.[52]

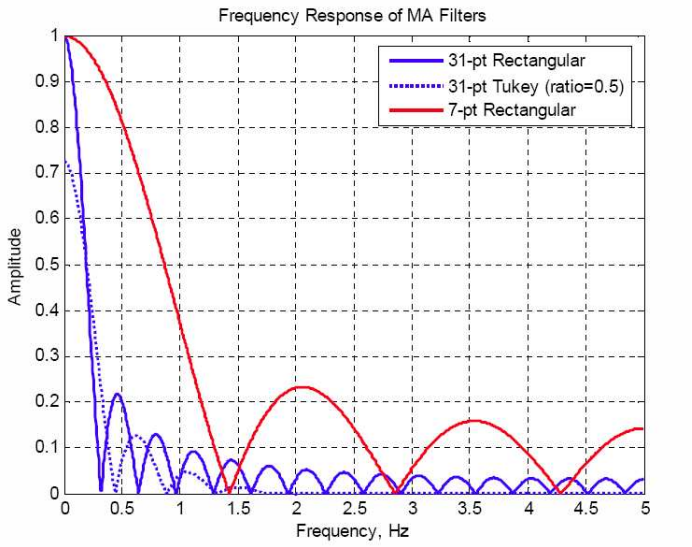
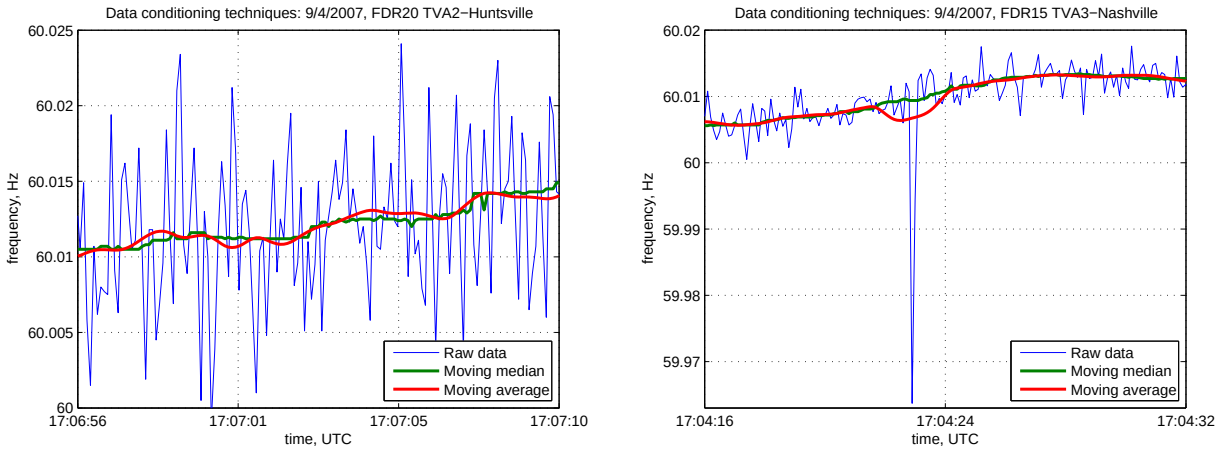


Figure 1.14: Frequency response of various MA filters

Figure 1.15 revisits the data of Figure 1.9 to illustrate the robustness of the moving median in the presence of outliers. As expected, the moving median shows exceptional robustness in the presence of extreme outliers, as illustrated in Figure 1.15b. Additionally the moving median outperforms the moving average in ignoring the local errors and noise shown in Figure 1.15a during normal grid operation. The value of MA filtering to wide-area frequency measurements lies in its computational efficiency. Some real-time applications may not be able to afford the cost of resorting the window every time step, especially as sampling rates increase and applications become more complex.



(a) Normal operation

(b) Outlier rejection

Figure 1.15. Performance of data conditioning techniques on FNET data

In summary, the properties of FNET measurements require proper statistical handling to accurately understand the electromechanical phenomena captured in frequency measurements. As the FNET system is the first and only research group to have collected such a vast and detailed sample set of system data, the rest of this report is highly data-centric. First access to real-life data yields many solutions of the "low-hanging fruit" variety - straightforward to conceptualize, but quite difficult to materialize.

1.5 Organization of study

Chapter 2 will begin by discussing the basic mechanics that describe the nature and propagation of electromechanical events in an interconnection. These events are of two major forms: generator-load mismatch and oscillations. Methods to detect and analyze both types of events will be discussed. Analysis of these kinds of events are highly dependent on sub-second deviations in sensor recordings.

Chapter 3 details the first comprehensive and automated event ordering methods. These methods are of primary importance to successful determination of generation-load mismatch events. Current methods are first discussed and analyzed, and then followed by a description of the new method. Finally, results of both old and new methods are presented to illustrate the leverage an event ordering method provides existing mismatch analysis algorithms.

Fifty-five confirmed EI generator trip events that occurred during 2007 are presented as base cases in this chapter. The details of each scenario are presented in Appendix B. This list is not comprehensive for several reasons. First, equipment malfunction or missing data may make an event unobservable. Second, the locations of many events have not yet been confirmed with outside data. Lastly, some events may not have been triggered. Events falling in this last category are generally insignificant, as the mismatch is typically less than 500 MW. Moreover, frequency data from each sensor is not available for each event for reasons described in Section 1.1.

Chapter 4 presents simulation work to affirm the value of distributed frequency measurements not only as analysis tools, but control inputs as well.

Chapter 5 concludes the body of the report, provides a summary of the author's contributions, and suggests future research endeavors.

Chapter 2

Unscheduled Power System Events

Having demonstrated the value of distributed frequency measurements and the ability to determine system frequency from distribution level measurements, a basic understanding of machine dynamics further illuminates frequency's ability to determine the instantaneous health of the grid. Description of power system events from frequency data leads to the classification into two major categories: generation-load mismatch and oscillations. Robust techniques have been developed to detect, analyze, and locate these events.

The motivation for detecting and analyzing these events is two-fold: understanding system response and accommodating market demands. First, events often incite subsequent events which may be more destructive than the precipitating event. Analysis and cataloging system-wide response to these events provide base cases for the development of operational responses to an event. Second, the financial consequences of failing to meet generation contracts because of an event are motivation to understand how to operate the system as smoothly as possible during an event.

2.1 Generation-Load mismatch

The mechanical properties of generators provide the theoretical explanation of how power system events manifest themselves in the electrical frequency. Consider the generator in Figure 2.1:

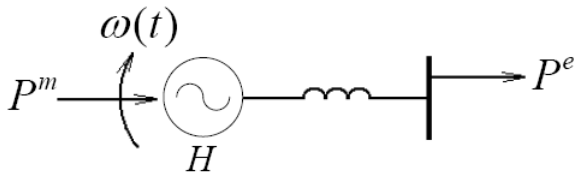


Figure 2.1. Single machine electromechanical diagram

Newton's second law of motion can be applied to rotating masses, yielding the Swing Equation which governs a generator's dynamics:

$$\frac{2H}{\omega_0}\frac{\partial\omega(t)}{\partial t} = P^m - P^e \tag{2.1}$$

where P^m is the mechanical power in megawatts (MW) resulting from the applied torque on the rotor, P^e is the electrical power in MW output by the generator, H is the generator's inertial parameter in seconds ($\frac{\text{J}}{\text{VA}} = s$), and $\omega(t)$ is the machine's rotational velocity in $\frac{\text{rad}}{\text{s}}$. The parameter ω_0 represents the nominal operating frequency of the machine, which in the case of the North American power system is 60 Hz or $2\pi \cdot 60$ $\frac{\text{rad}}{\text{s}}$. Equation (2.1) confirms that any mismatch between the mechanical power input to the generator and the electrical power extracted from the machine manifests itself in the machine's frequency. Moreover the calculation of mismatch amount from frequency measurements is a trivial one *should* all the system parameters be known.

In an interconnection, however, there are many machines supplying many loads through a complex circuit, as illustrated in Figure 2.2:

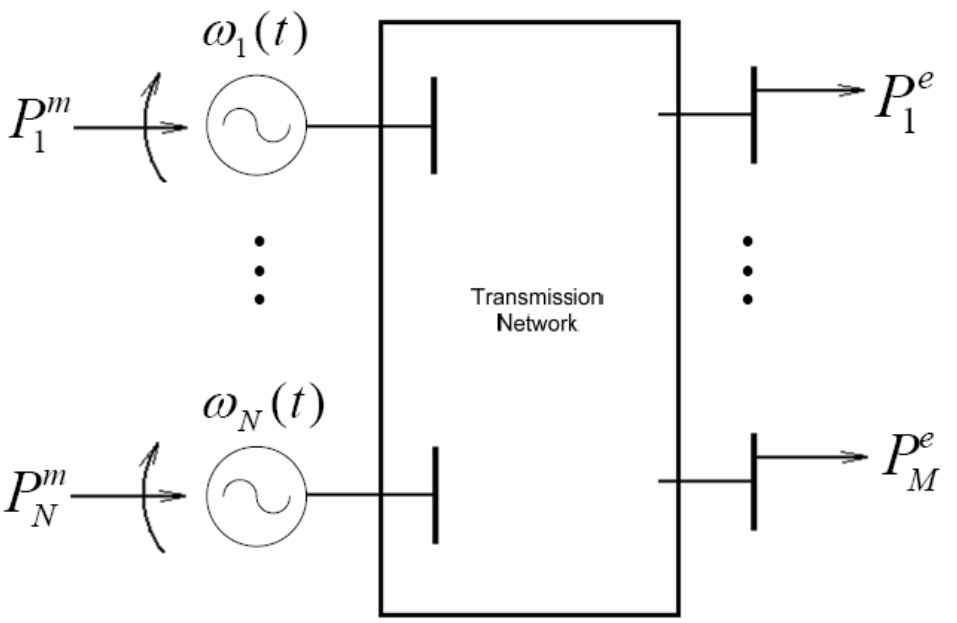


Figure 2.2. Generalized synchronous interconnection

Equation (1.1) can be applied to each and every generator in the interconnection:

$$\int_{t-\frac{T}{2}}^{t+\frac{T}{2}} \omega_1(\tau)\partial\tau = \int_{t-\frac{T}{2}}^{t+\frac{T}{2}} \omega_2(\tau)\partial\tau = \cdots = \int_{t-\frac{T}{2}}^{t+\frac{T}{2}} \omega_N(\tau)\partial\tau$$

In this manner, assuming all parameters are converted to per-unit with consistent MVA base, the system can be aggregated into a single representative machine as shown in Figure 2.3, where

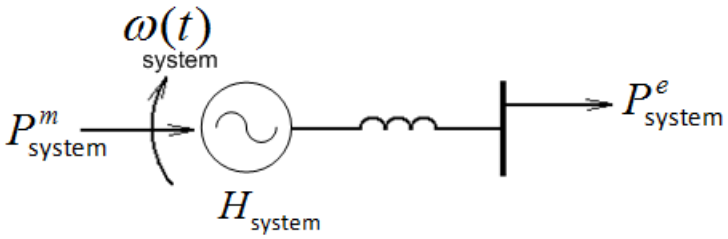


Figure 2.3. Aggregate representation of a synchronous electrical interconnection

$$H_{\text{system}} = \sum_{i=1}^{N} H_i$$

$$P^m_{\text{system}} = \sum_{i=1}^{N} P^m_i$$

$$P^e_{\text{system}} = \sum_{i=1}^{N} P^e_i$$

Finally the Swing Equation for the aggregate system becomes

$$\frac{2H_{\text{system}}}{\omega_0}\frac{\partial\omega_{\text{system}}(t)}{\partial t} = P^m_{\text{system}} - P^e_{\text{system}} \tag{2.2}$$

Once again the observation is made that a disturbance in the balance between mechanical power injected into the system and electrical power delivered to the system's loads will manifest itself in the system frequency, ω_{system}. The sub-second FNET frequency measurements have been previously demonstrated to be the perfect window from which to investigate how these disturbances are actually observed.[6,39,59] The interconnection frequency $\omega_{\text{system}}(t)$ can be determined from the mean of each sensor's frequency recordings $\hat{\omega}_i(t)$:

$$\omega_{\text{system}}(t) = \frac{1}{p}\sum_{i=1}^{p} \hat{\omega}_i(t)$$

2.1.1 Types of mismatch events

During normal system operation generation matches load:

$$P^m_{\text{system}} \approx P^e_{\text{system}} \Longrightarrow \frac{2H_{\text{system}}}{\omega_0}\frac{\partial \omega_{\text{system}}(t)}{\partial t} \approx 0 \tag{2.3}$$

Equation 2.3 is empirically justified by noting that in general, FNET data recorded during normal system operation is flat. Slowly-varying trends, such as the daily and seasonal load curves, are manifest in a time-varying system inertia $H_{\text{system}}(t)$. Instances of generation-load mismatch fall into one of two categories:

$$P^m_{\text{system}} < P^e_{\text{system}} \tag{2.4}$$

$$P^m_{\text{system}} > P^e_{\text{system}} \tag{2.5}$$

These situations result in system deceleration or acceleration, respectively. In the case of a sudden, unscheduled mismatch, there is a step change in either mechanical or electrical power, while the other remains relatively constant.

Generator trips

When a generator trips at $t = t_0$, for example, there is a sudden drop in mechanical power while electrical power remains constant (Equation 2.4):

$$\begin{aligned}
\frac{2H_{\text{system}}}{\omega_0}\frac{\partial \omega_{\text{system}}(t)}{\partial t}\bigg|_{t=t_0^-} &= P^m_{\text{system}}(t_0^-) - P^e_{\text{system}}(t_0^-) \approx 0 \\
P^m_{\text{system}}(t_0^-) &= P^m_{\text{system}}(t_0^+) + \Delta P^m_{\text{system}} \\
P^e_{\text{system}}(t_0^-) &= P^e_{\text{system}}(t_0^+) \\
\frac{2H_{\text{system}}}{\omega_0}\frac{\partial \omega_{\text{system}}(t)}{\partial t}\bigg|_{t=t_0^+} &= P^m_{\text{system}}(t_0^+) - P^e_{\text{system}}(t_0^+) \approx -\Delta P^m_{\text{system}}
\end{aligned} \tag{2.6}$$

Equation 2.6 predicts that frequency sharply declines immediately after the event time t_0, and this is confirmed by FNET data. Figure 2.4 shows a typical generator trip.

The trip signature has three areas: first, the pre-event region is relatively flat indicating consistent generator-load interaction. Second is the time immediately after the trip, where the frequency declines in accordance with Equation 2.6, and last the system settles to a new equilibrium point at a slightly lower frequency to indicate heavier loading conditions upon the remaining interconnected generators.

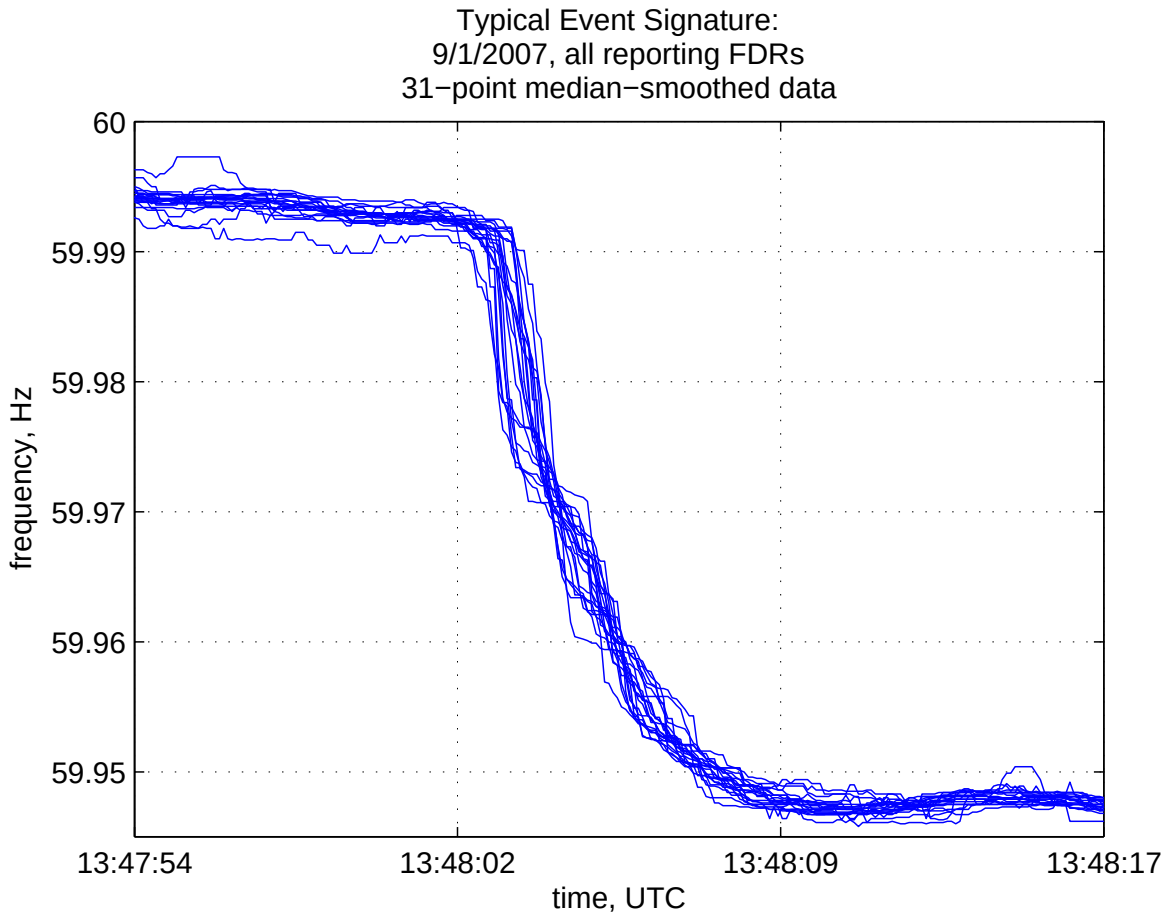


Figure 2.4. Typical generator trip signature

Notably absent from this discussion so far is mention of generator speed controllers. While frequency immediately declines after an event, Figure 2.4 shows it takes roughly 7 seconds for the speed governors to stabilize the frequency. Consequently the sub-second decline at the beginning of an event is effectively decoupled from any control action.[6]

The North American Electric Reliability Corporation (NERC)[2] defines a frequency response standard that identifies the following four important points in the trip signature (Figure 2.5):

A. Interconnection frequency immediately before the disturbance
B. Interconnection frequency at the point immediately after the frequency stabilizes due to generator action but before the contingent control area takes corrective action
C. Interconnection frequency at its maximum deviation due to the loss of rotating kinetic energy from the interconnection
D. Interconnection settling frequency at 60 seconds after point A

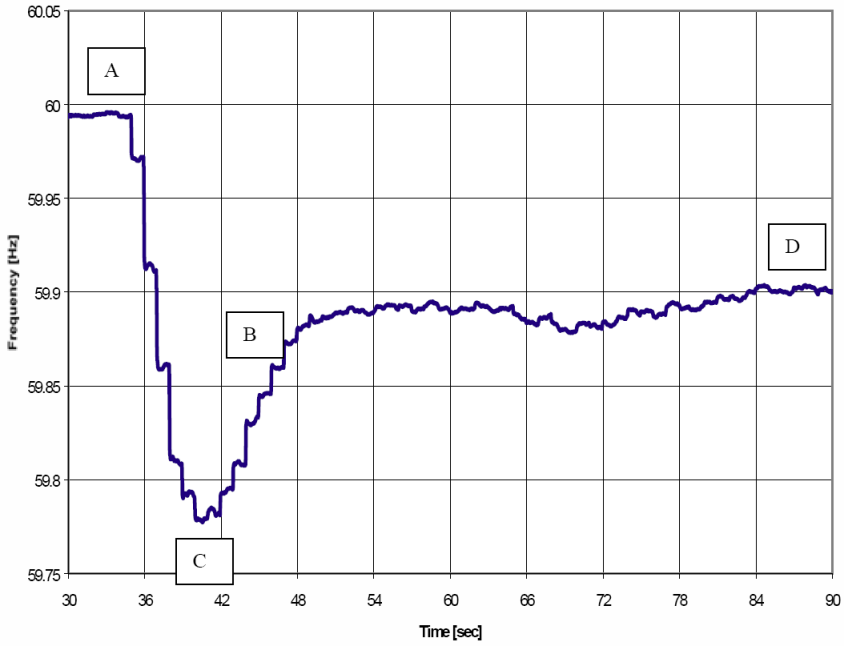
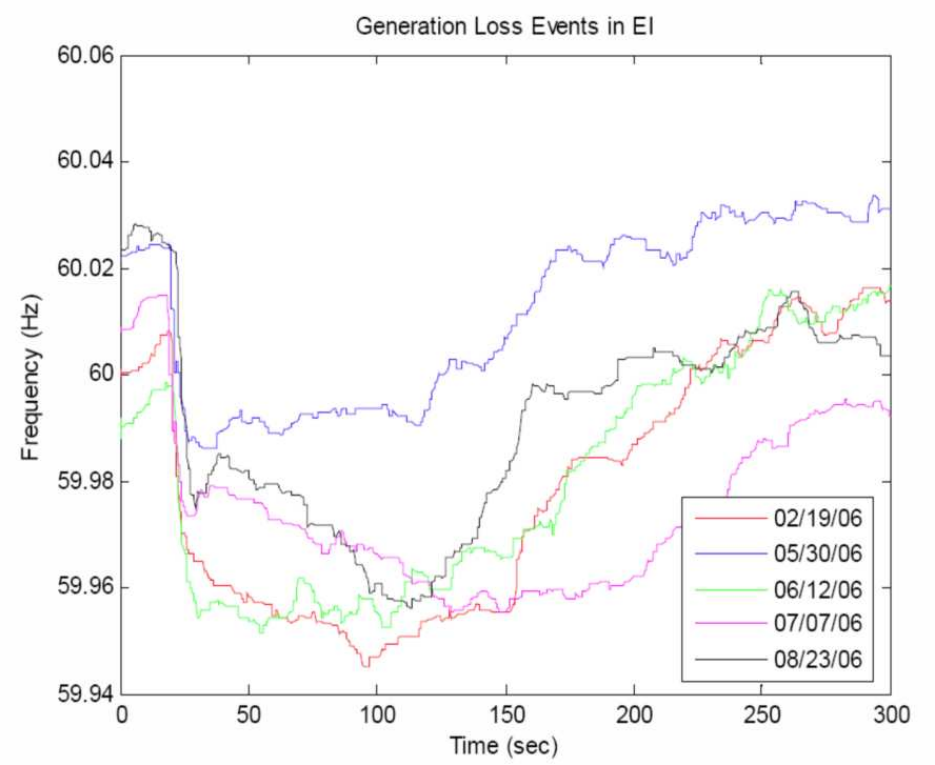


Figure 2.5. NERC frequency response standard[2]

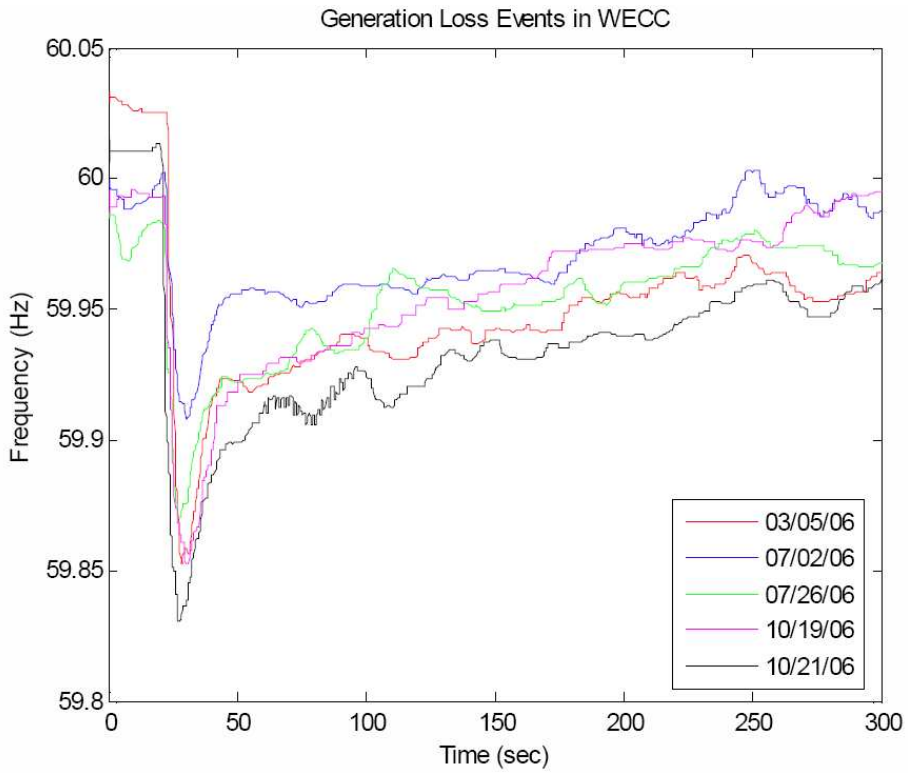
Generator trips, in theory, are visible from every point in the grid.[15] However, the inherent noise and errors in real frequency measurements obscure trips where $\Delta P_{system} < 500$ MW. While each sensor in Figure 2.4 clearly records the trip signature, each frequency trace begins to decline at a slightly different time from other records. This delay is descriptive of the TDOA corresponding to the finite propagation speed of the electromechanical wave.[42,43] These delays, combined with knowledge of the distances between sensors, provide the basis for topology-independent hypocentral location estimation.

Of additional interest is the response of the different North American interconnections to generator trips of similar size, as shown in Figure 2.6.

Evaluating each interconnection's performance with the NERC standards yields three major observations corresponding to points B, C, and D (Figure 2.5). First, the total frequency deviation ($A - B$) is inversely proportional to system size. As a system increases in size (more remaining generators), the system inertia increases according to Equation 2.2, which shrinks the total frequency deviation. For reference the EI system inertia is roughly four times greater than that of the WECC, and even more than that of ERCOT.[60] Second, the delineation between points B and C is more distinct in the WECC and ERCOT. This is most likely due to the structure of each grid. The WECC and ERCOT both have ring-like topologies, with disparate load centers connected via unpopulated corridors, which in combination with their small inertias, allow governor control to have a more pronounced effect. Finally, point D is closest to point A in the WECC (Figure 2.6b). This can be attributed to the unique control strategy each interconnection employs.

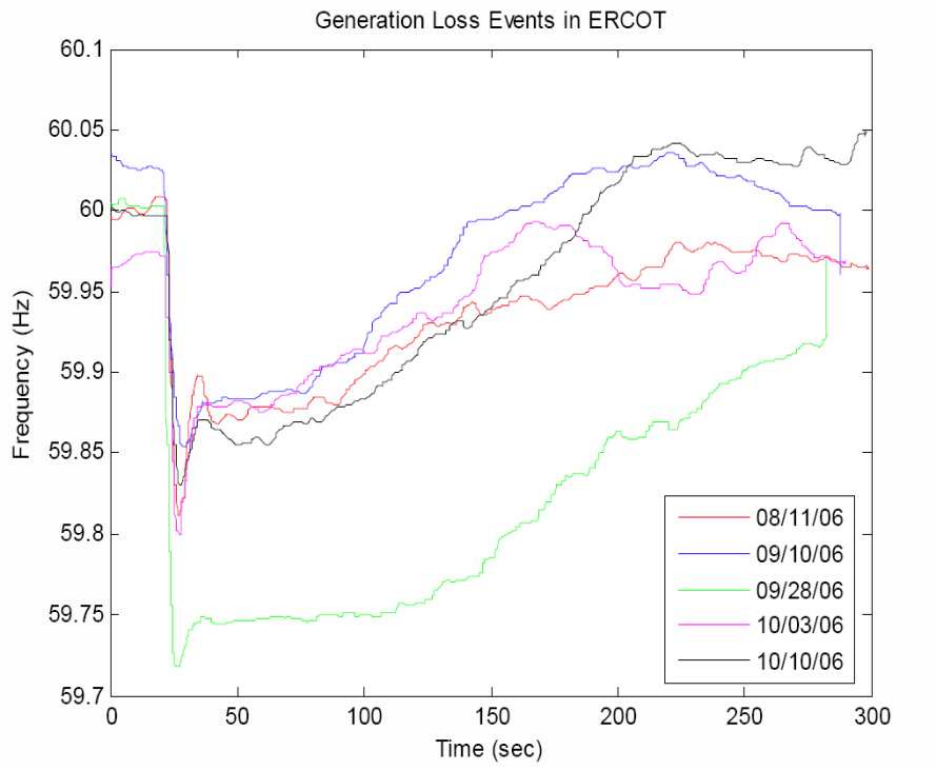


(a) EI



(b) WECC

Figure 2.6. Generator trips in different interconnections[3]



(c) ERCOT

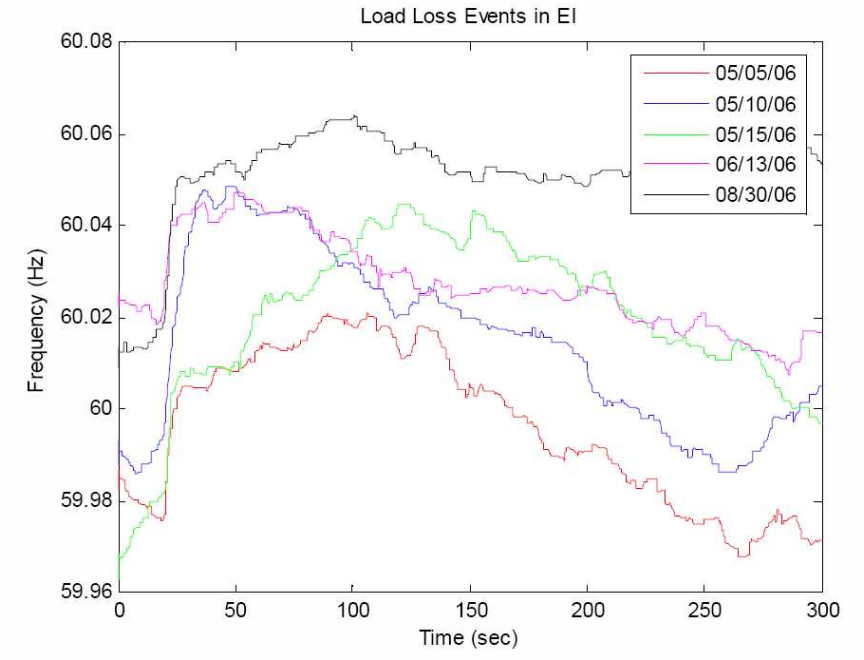
Figure 2.6. Generator trips in different interconnections[3] (continued)

Load shedding

Generator trips are the major focus of this report. However, another kind of mismatch occurs when load is unexpectedly lost, as in Equation 2.5. As the load is suddenly removed from the system, the system accelerates. This causes a frequency perturbation of similar shape to that of a generator trip but with opposite (positive) slope. Formulations along the lines of Equation 2.6 can be developed for the load shedding case:

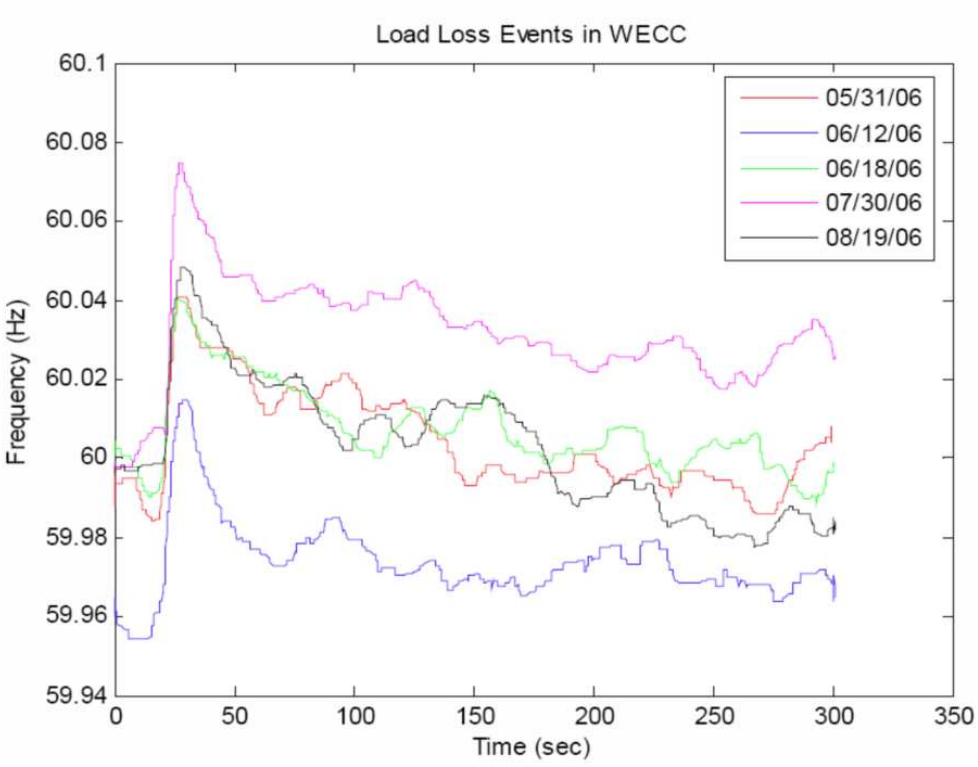
$$\begin{aligned}
\frac{2H_{\text{system}}}{\omega_0}\frac{\partial\omega_{\text{system}}(t)}{\partial t}\bigg|_{t=t_0^-} &= P^m_{\text{system}}(t_0^-) - P^e_{\text{system}}(t_0^-) \approx 0 \\
P^e_{\text{system}}(t_0^-) &= P^e_{\text{system}}(t_0^+) + \Delta P^e_{\text{system}} \\
P^m_{\text{system}}(t_0^-) &= P^m_{\text{system}}(t_0^+) \\
\frac{2H_{\text{system}}}{\omega_0}\frac{\partial\omega_{\text{system}}(t)}{\partial t}\bigg|_{t=t_0^+} &= P^m_{\text{system}}(t_0^+) - P^e_{\text{system}}(t_0^+) \approx \Delta P^e_{\text{system}}
\end{aligned} \tag{2.7}$$

Load shedding events are both less frequent and less harmful than generator trips, and as a result such events are less regulated by the NERC. One side effect of the industry's ambivalence to load shedding is the paucity of utility confirmed load shedding case studies. Despite the smaller sample size, representative load trips from each of the three major interconnections are presented in Figure 2.7.

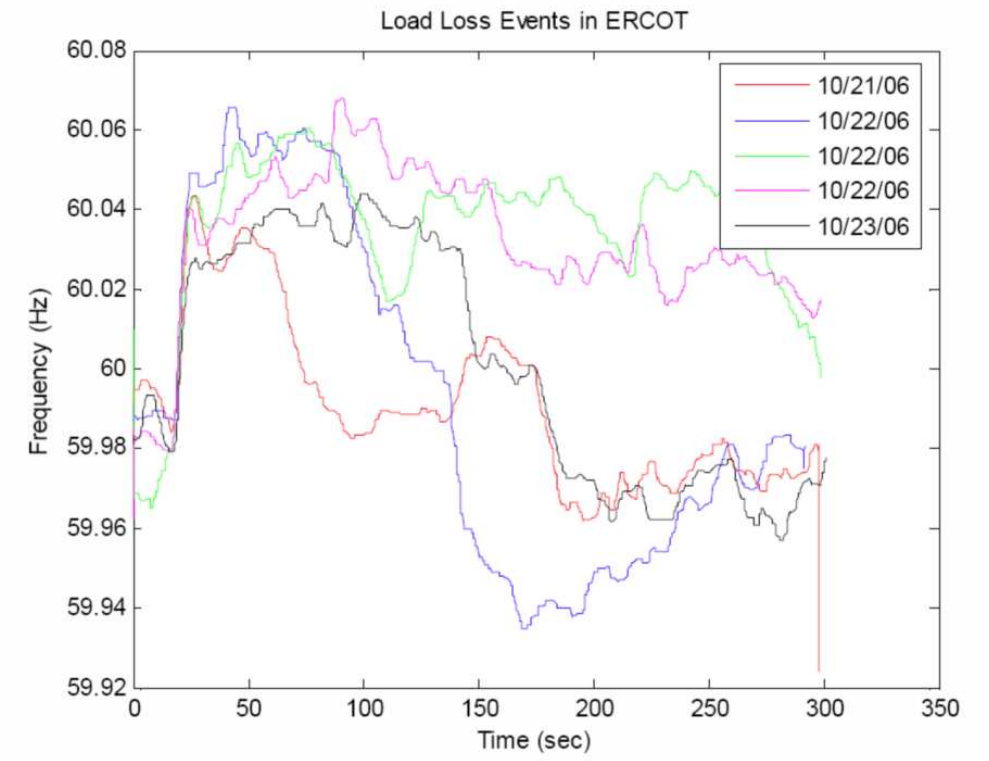


(a) EI

Figure 2.7. Load shedding in different interconnections[3]



(b) WECC



(c) ERCOT

Figure 2.7. Load shedding in different interconnections[3] (continued)

Islanding

There is one final kind of mismatch event - islanding, which occurs when an interconnection subdivides into multiple interconnections. Machines in one island maintain synchronism with all the machines within the island, but islands do not maintain synchronism with one another. Such events are especially rare, as it has happened only once during FNET's existence, in September 2007 (Figure 2.8).

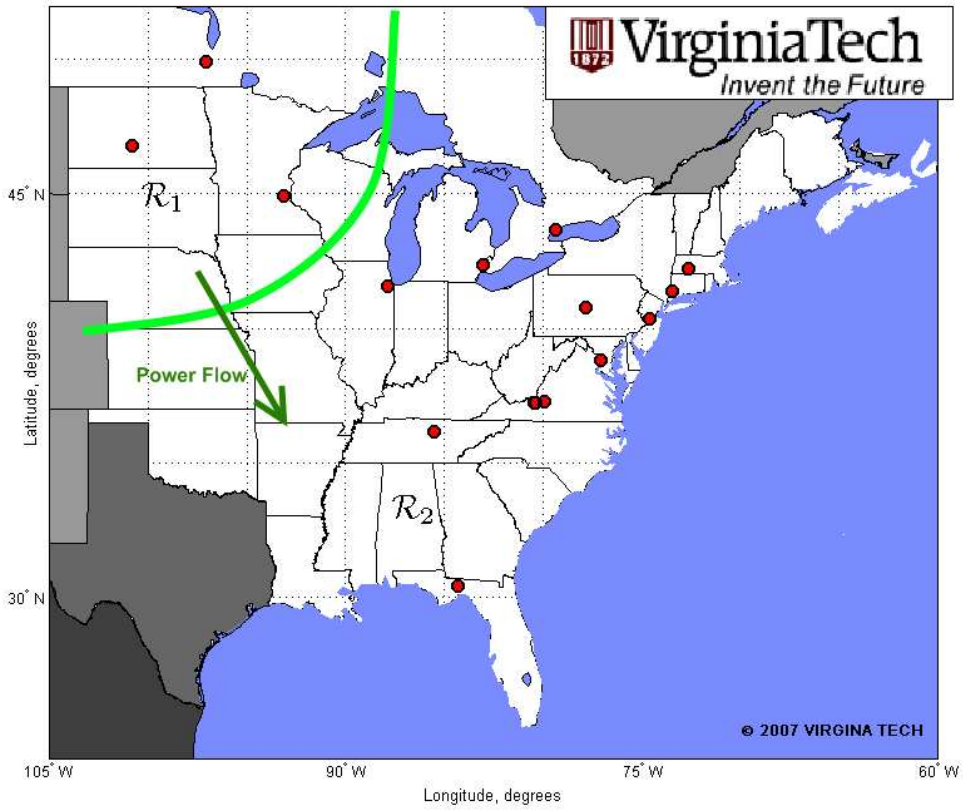


Figure 2.8. EI islanding map

Islanding is not guaranteed to be visible in frequency data, and is determined by the particular generation-load balance in each area. If the interconnection splits into two regions $\mathcal{R}_1$ and $\mathcal{R}_2$, both of which have enough internal generation to meet load, than each area's frequency response during islanding will remain flat and indistinguishable from one another. If, however, one region experiences a lack of generation and the other a lack of load, then each island will accelerate or decelerate accordingly. In the September 2007 event the northwestern region, $\mathcal{R}_1$ of the EI split off from the rest of the grid, $\mathcal{R}_2$. The excess generation within $\mathcal{R}_1$ causes its frequency to rise. As $\mathcal{R}_2$

lacks generation to meet its load its frequency declines.

During normal grid operation pre-event, $\mathcal{R}_1$ is supplying power to $\mathcal{R}_2$ and the amount of transferred power P^t that is effectively lost or gained after separation at t_0 causes each island's respective frequency response. In other words,

$$\left[\sum_{\mathcal{R}_1} P^m - P^e - P^t\right]_{t\leq t_0} \approx 0 \Longrightarrow \left[\sum_{\mathcal{R}_1} P^m - P^e\right]_{t>t_0} \approx P^t$$
$$\left[\sum_{\mathcal{R}_2} P^m - P^e + P^t\right]_{t\leq t_0} \approx 0 \Longrightarrow \left[\sum_{\mathcal{R}_2} P^m - P^e\right]_{t>t_0} \approx -P^t$$

Naturally, as the inertia of each island is different, the frequency excursions experienced in each region are of different magnitudes, per (2.2). Figure 2.9 illustrates the frequency behavior during the islanding event.

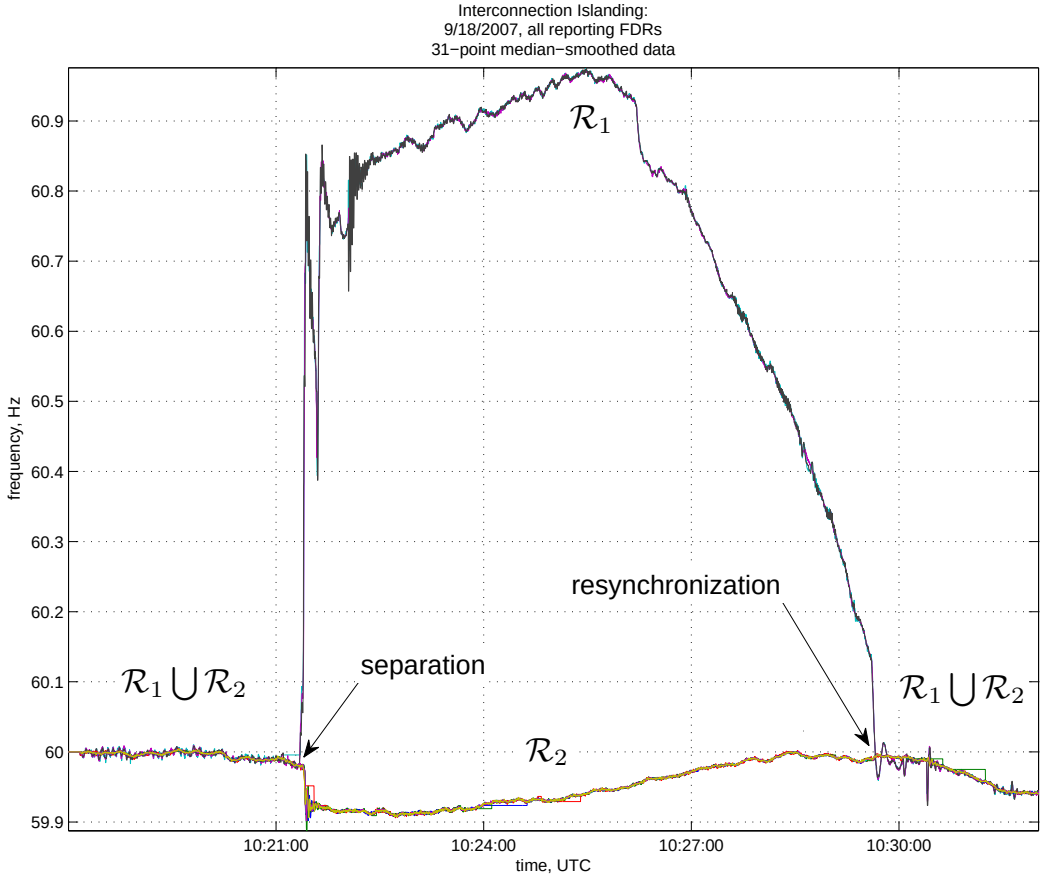


Figure 2.9. System performance during islanding

The following sections of this chapter up to Section 2.2 focus on the detection and analysis of generator trips, because of the scarcity of confirmed load shedding and islanding events. Moreover load shedding events do not always pose an immediate threat to system infrastructure.

The use distributed frequency measurements in event detection and analysis is not a replacement for the existing measurement systems internal to each system operator. Rather, the benefits of FNET data complement utility-specific measurements. The first benefit is one of access. There is no possibility of exposing confidential operational protocols as the FDR has no specialized connection to the grid. Such privacy becomes increasingly important in a deregulated market as wide-area devices are used in closed-loop applications. Second, the goal of the FNET system is topology independence. Thus the detection and analysis of events requires no understanding of the specific system configuration before, during, or after the event. Robust system-wide techniques allow operators the ability to coordinate anticipatory action before an event propagates throughout the system.

2.1.2 Event Detection

As generator trips cause a step decline in frequency per Equation (2.6), trip detection from frequency measurements is a straightforward process. Simply put, an event is determined to have occurred if the frequency has declined past a certain threshold within a certain amount of time. The pseudocode for such a routine is given in EVENT-DETECTION. The frequency data is contained in the vector f, while F represents the frequency deviation threshold and T represents the time threshold.

EVENT-DETECTION(f, T, F)
1 **for** $i \leftarrow T$ **to** *length*[f]
2 **if** $f[i-T] - f[i] > F$
3 **then** Event has occurred

The success of EVENT-DETECTION depends on the shape of the event signature. For typical events that look similar to Figure 2.4, this approach works well. As long as the flat frequency characteristic pre- and post- event are more than F Hertz apart, the event will successfully be triggered. However, there are significant numbers of events that do not have flat characteristics preceding or following an event. Figure 2.10 shows such an event. In this case, EVENT-DETECTION will trigger false positives, or identify regions of normal operation as a generator trip. The number of false positives will be determined by the values of T and F. As each parameter becomes smaller, the number of false positives increases.

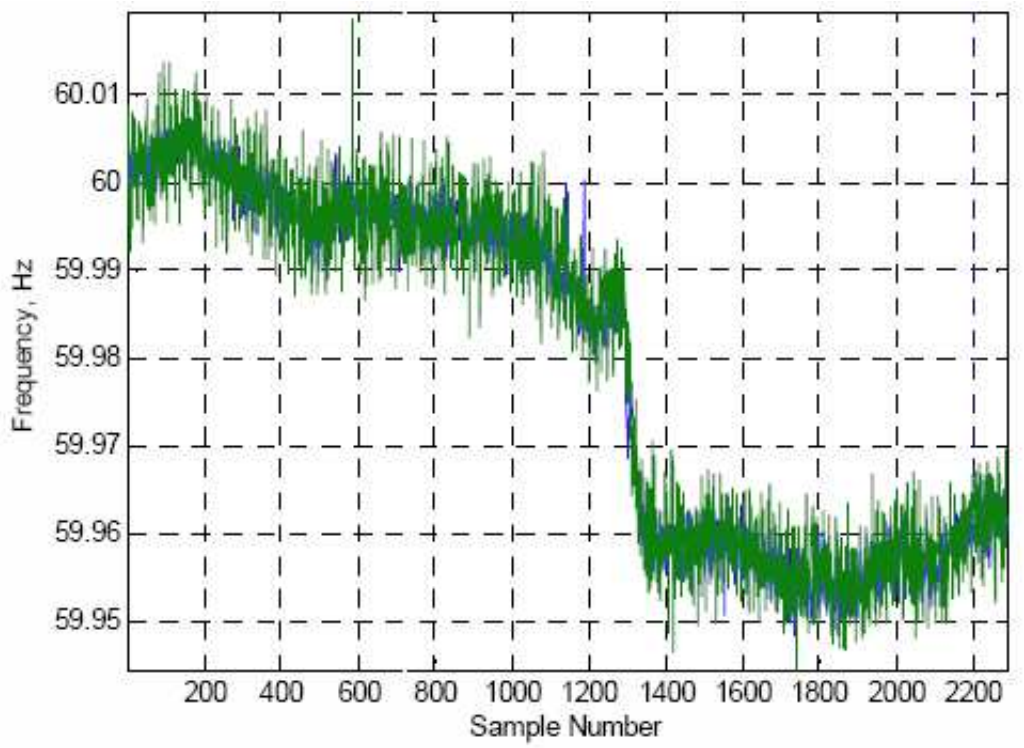


Figure 2.10. Non-ideal event signature

To avoid these kind of errors, statistical event detection algorithms have been developed.[1] Such processes create a parent cluster from the data recorded by two arbitrary FDRs. Since the majority of points in each FDR's trace correspond to normal operation, any small subset of points within the data stream whose statistical parameters differ substantially from those of the parent cluster are determined to correspond to an event. The metric used to calculate the parameters of the parent and test clusters is the Mahalanobis Distance, which is determined from the covariance of the cluster.

Figure 2.11 illustrates this approach. The plot on the right shows the same data streams as in Figure 2.10. On the right graph, the blue dots represent the points which make up the parent cluster, and the pink dots represent the test cluster of points taken from the region indicated by the vertical light green line in the left graph. The axes on the right correspond to the frequencies measured by each FDR - the first FDR's frequencies define the abscissa and the second unit's measurements define the ordinate. Each cluster defines an ellipse, determined by the covariance of the cluster elements. When the centroid of the test cluster lies too far away from the centroid of the parent cluster, as measured by the Mahalanobis Distance, then an event is triggered. Figure 2.11 shows the relationship of the test and parent ellipses during an event.

The statistical approach is preferred to the threshold method of Event-Detection for its robustness. Because there are no implicit restrictions placed upon the pre- and post- event charac-

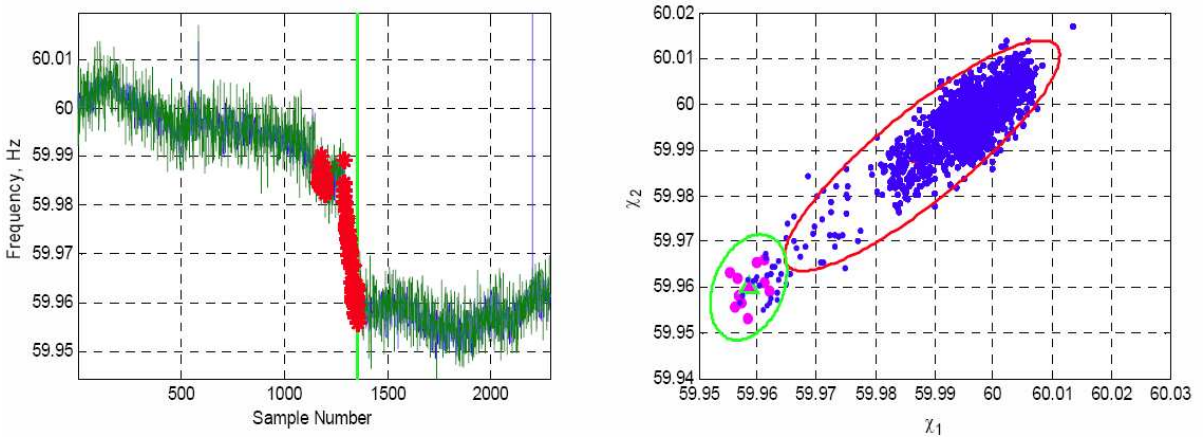


Figure 2.11. Example of statistical event detection

teristics, false positives are far less likely to occur. Moreover, this metric can be repeated for any combination of two reporting FDRs, so any false positive that may arise from one pairing are not guaranteed to occur in another pairing. Thus a voting process can be instituted so an event is only triggered if a certain number of FDR pairs trigger such an event.

2.1.3 Mismatch amount

As the amount of generation lost is directly reflected in the frequency drop, the calculation of the mismatch amount is also easily established. The NERC has defined a load-frequency sensitivity parameter, β, to measure frequency response to loss of generation:[2]

$$\beta = \frac{-\Delta P}{\Delta f}$$

where ΔP is the generation trip amount in MW and Δf is the frequency deviation (the difference between points A and B of the NERC standard in Figure 2.5). Moreover, this parameter can also be determined (with much more difficulty) from the parameters of each of the n generators in operation:

$$\beta = \frac{2\pi}{\frac{1}{R_1} + \frac{1}{R_2} + \cdots + \frac{1}{R_n} + D}$$

where R_i is the governor drooping characteristic of each generator, and D represents the system's load frequency sensitivity.[26] Because of seasonal variations in load and operating schedules, β will vary with the seasons. Monitoring of this parameter over years of operation yields valuable information into the reserve capacity of the interconnection.[61]

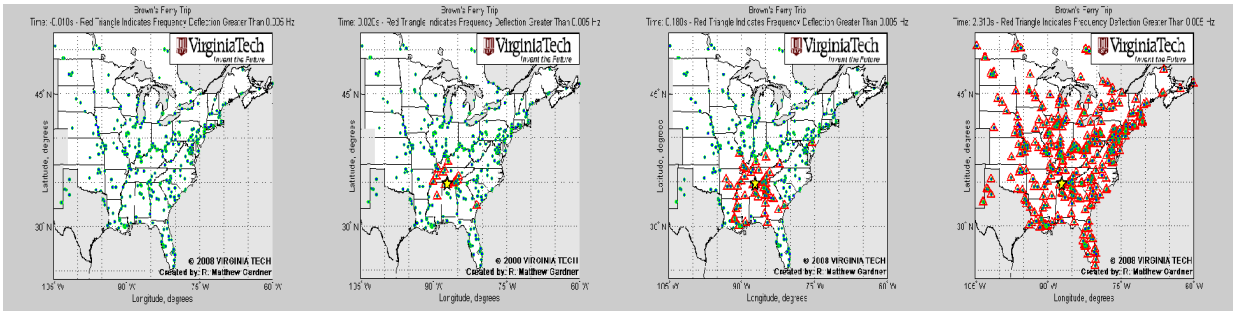
As FNET provides an exhaustive catalog of generator trips in each North American interconnections, its data can easily be used in conjunction with confirmed trips to accurately revise

β estimates. Likewise, with knowledge of the latest β values, the amount of frequency deviation recorded by FDRs is accurately used to identify the quantity of generation lost.[34]

2.1.4 Location estimation

While event detection and mismatch calculation are well-defined tasks, the location of an event hypocenter is not. Moreover, topology independent event location has never been attempted before FNET's first efforts in 2004.[34] Each day, the grid operates in a multitude of unique topographies determined by events such as maintenance schedules, market contracts, and weather. Not only are these individual changes to the system's structure impossible to track in real time, but the base system topology is impossible to know on a global scale. Each utility knows its system down to the last detail, but is unwilling and unable to share all of those intricacies in an efficient manner. Moreover, the amount of equipment connected to the grid makes it computationally impossible to use all of the system data in real time even if it were available. Therefore it is of immense practical and theoretical benefit to understand how events propagate through the system.

As mentioned earlier and illustrated in Figure 2.4, sub-second differences in the frequency decline recorded by different sensors are used to estimate an event's hypocenter. Figure 2.12 shows how a simulated event propagates in time past FDRs located throughout the grid.[1] As expected, the FDRs closest to the hypocenter record the frequency decline first, and units progressively further away from the event record the frequency decline at correspondingly later times. This phenomenon is attributed to the propagation of an electromechanical wave throughout the system.[62,63] Since the wavefront arrival time, or the time at which the frequency begins to decline, can be calculated for each FDR, the sequence of reporting FDRs can be determined. Moreover the amount of delay (TDOA) between successive reporting FDRs can be calculated. Location estimation using TDOA has long been used in the communications[64] and radar[65] industries, among others.



(a) steady-state (b) 20 ms after trip (c) 180 ms after trip (d) 2.31 s after trip

Figure 2.12. Simulated EI generator trip[1]

The use of TDOA makes some key assumptions that have been empirically proven wrong. The first assumption is that the grid is homogeneous, meaning the wave propagates through the system with equal speed in any direction. While accurate in a broad sense, data gathered from any generator trip shows this to be incorrect, as previously shown by the arrival time table for the Bull Run trip (Table 1.1). Figure 2.13 shows the different simulated velocities a wave takes in traveling to an FDR (the yellow dots) for different events.[1]

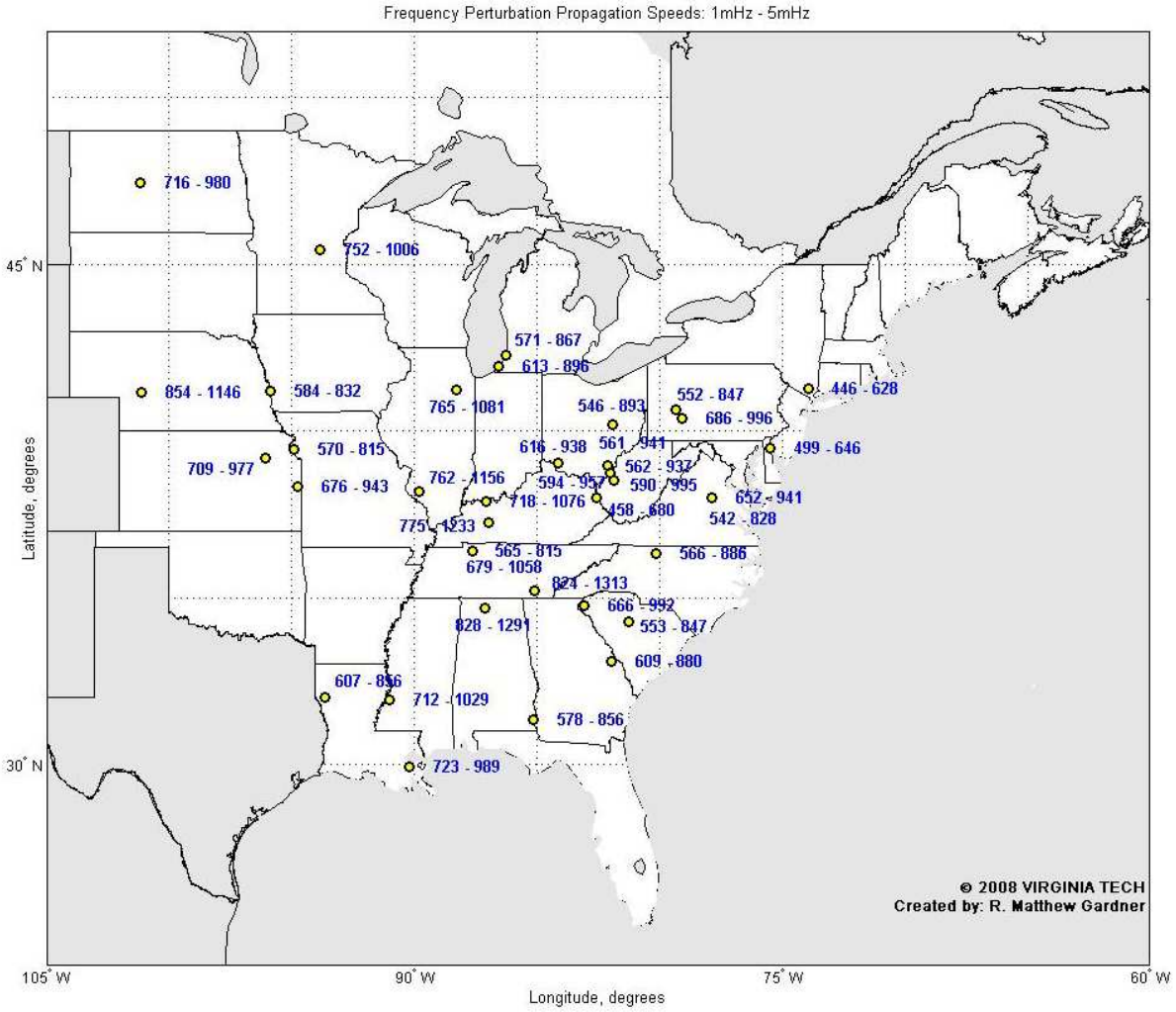


Figure 2.13. Simulated event velocities[1]

Additionally, TDOA expects events with the same hypocenter to record the same response. In other words, any event originating from the loss of a specific generator should produce the same order (and delays) of reporting FDRs. However, actual data reveals that events with the same hypocenter produce wave velocities of differing velocities. The causes for these discrepancies are most likely due to seasonal changes in system loading as well as errant data and outliers.

To further visualize the usefulness of TDOA in event location, imagine throwing a rock into

a pond. Once the rock disturbs the water at impact, waves begin to propagate from the hypocenter all the way out to the edge of the pond. Analogously the generator trip acts as the rock, inciting an electromechanical wave that propagates throughout the grid, as Figure 2.14 suggests.

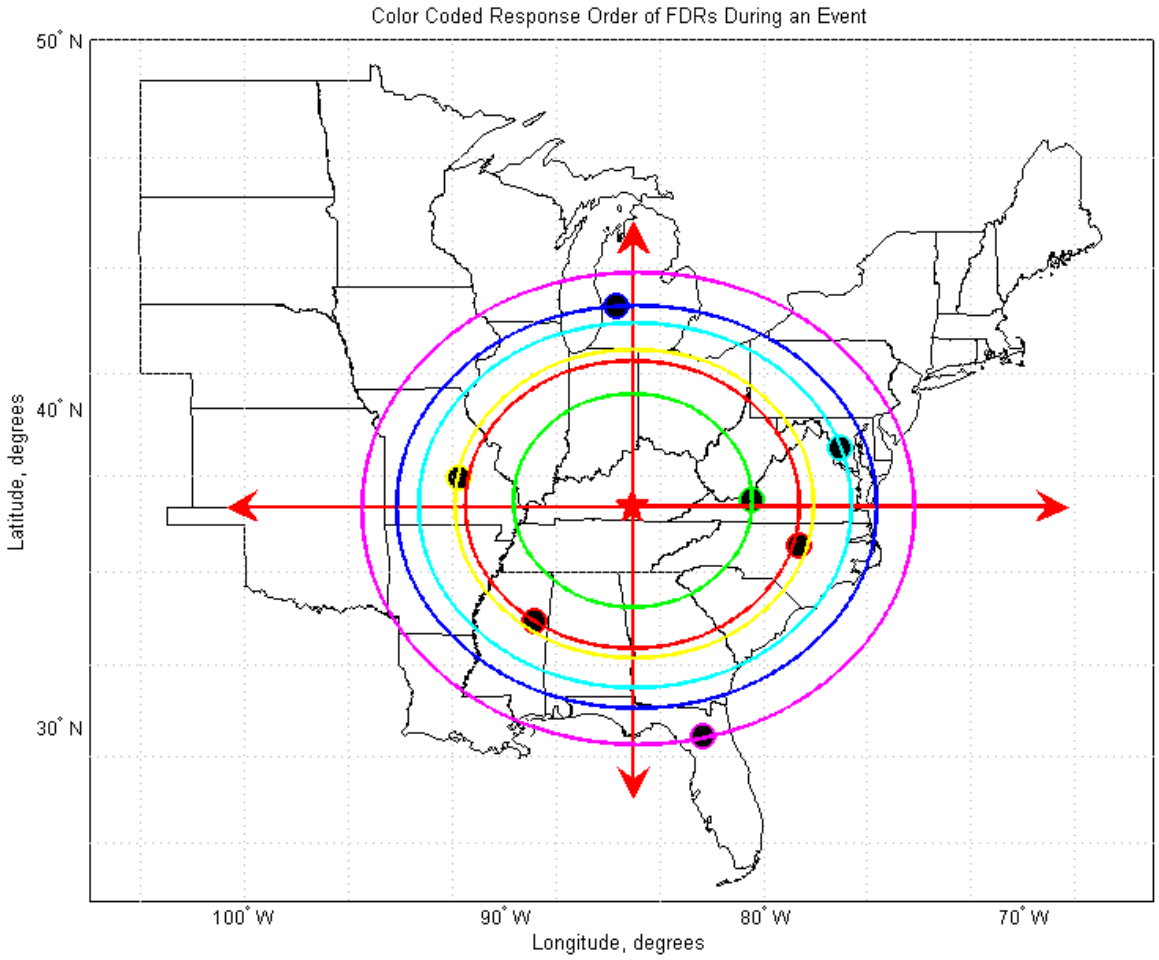


Figure 2.14. Electromechanical wave propagation through the grid

Each FDR is like a buoy in the pond, which begins to rise and fall as the wave passes the point where the buoy is floating. Likewise the frequency at an FDR's location begins to decline as the electromechanical wave passes the sensor's connection point. As closer sensors record the wavefront's arrival before remote sensors, the order of sensor proximity can be determined, as illustrated in Figure 2.15.

The methods that use TDOA information to estimate an event hypocenter fall into two main categories: deterministic and stochastic. Deterministic methods attempt to estimate wave velocity and use that velocity to determine the hypocenter. Stochastic methods attempt to utilize some statistical properties of the event order to robustly identify a likely region of hypocentral points.

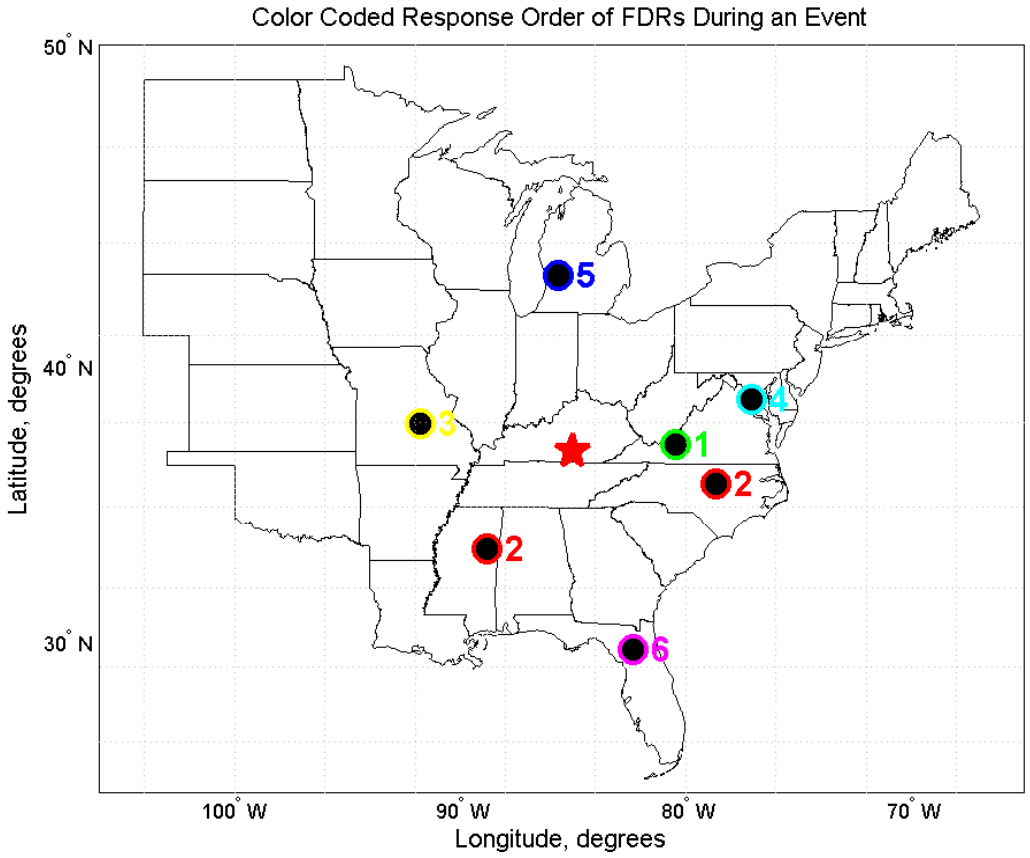


Figure 2.15. Wavefront arrival ordering

The least-squares approach

The deterministic approach uses least-squares (LS) estimation of the wave velocity. This approach is derived in much the same way that geologists develop velocity models of the earth's core and crust to pinpoint the epicenter of an earthquake.[66] Consider the following equation relating mean velocity, time of travel, and distance traveled:

$$Distance = Velocity \times Time \tag{2.8}$$

Applying this concept to electromechanical waves with the assumption that such waves travel throughout the electric grid as a continuum, (2.8) can be developed using the Pythagorean relation written in terms of TDOA data as:

$$(x_i - x_h)^2 + (y_i - y_h)^2 = V^2 (t_i - t_h)^2 \tag{2.9}$$

For each responding FDR,

$$\begin{aligned}(x_1 - x_h)^2 + (y_1 - y_h)^2 &= V^2 (t_1 - t_h)^2 \\ (x_2 - x_h)^2 + (y_2 - y_h)^2 &= V^2 (t_2 - t_h)^2 \\ &\vdots \\ (x_n - x_h)^2 + (y_n - y_h)^2 &= V^2 (t_n - t_h)^2\end{aligned}$$

where (x_n, y_n) are the (x, y) coordinates of the n^{th} FDR to respond; (x_h, y_h) are the (x, y) coordinates of the hypocenter (origin of disturbance); t_n is the time at which the n^{th} FDR measures the electromechanical wave; t_h is the time at which the event occurred; and V is the mean velocity at which the frequency perturbation travels. The unknowns in the above equation set are the hypocentral coordinates, (x_h, y_h), and the time at which the event occurred, t_h. A set of assumed mean velocities, $\{V_1, V_2, \ldots, V_k\}$, generate a set of hypocentral coordinates, $\{(x_{h_1}, y_{h_1}), (x_{h_2}, y_{h_2}), \ldots, (x_{h_k}, y_{h_k})\}$, in the solution of the system.

To find a set of solutions, a linear system in terms of the hypocentral coordinates is developed such that the LS method of solving an over-constrained system of equations can be used. In general, this system of equations will be over-constrained since many more FDRs typically respond than there are variables. By subtracting successive pairs of equations, a linear equation in terms of the hypocentral coordinates is produced:

$$(x_{i+1} - x_i)\, x_h - (y_{i+1} - y_i)\, y_h - V^2 (t_{i+1} - t_i)\, t_h = C_i \tag{2.10}$$

Where C_i is defined as:

$$C_i = \frac{1}{2}\left[V^2 (t_{i+1} - t_i) + x_{i+1}^2 + y_{i+1}^2 - x_i - y_i\right] \tag{2.11}$$

Hence, (2.10) can be written for every unit that responds forming a system of equations that can be placed in a matrix to form:

$$\mathbf{C} = \mathbf{H}\mathbf{x} \tag{2.12}$$

with matrix variables defined as:

$$\mathbf{C} = \begin{bmatrix} C_1 \\ C_2 \\ \vdots \\ C_n \end{bmatrix} \qquad \mathbf{x} = \begin{bmatrix} x_h \\ y_h \\ t_h \end{bmatrix}$$

$$\mathbf{H} = \begin{bmatrix} x_2 - x_1 & y_2 - y_1 & V^2(t_2 - t_1) \\ x_3 - x_2 & y_3 - y_2 & V^2(t_3 - t_2) \\ \vdots & \vdots & \vdots \\ x_n - x_{n-1} & y_n - y_{n-1} & V^2(t_n - t_{n-1}) \\ x_1 - x_n & y_1 - y_n & V^2(t_1 - t_n) \end{bmatrix}$$

There are many well-defined ways to solve (2.12) for **x**.[67,68]

A disadvantage of using the LS method to find the hypocentral coordinates is that one must assume that the electromechanical waves are traveling in a continuum at a constant velocity in each direction. Therefore, the velocity set, $\{V_1, V_2, \ldots, V_k\}$, must be assumed before solving. To date, there is no accepted velocity model for the travel of electromechanical waves in the EUS. Figure 2.16 shows the results of the LS method, plotted with red asterisks, using velocities, $V_j \in \{V_1, V_2, \ldots, V_k\}$, that vary from 100 mi/s to 1000 mi/s. This range for V_j was chosen based upon past observations of disturbances traveling between 350 mi/s and 660 mi/s in the EUS[34]. In Figures 2.16 and 2.17 , the closest solution location is enlarged and pointed out with an arrow. The base case location (true value) being estimated is plotted with a square and the FDR locations are shown using blue dots.

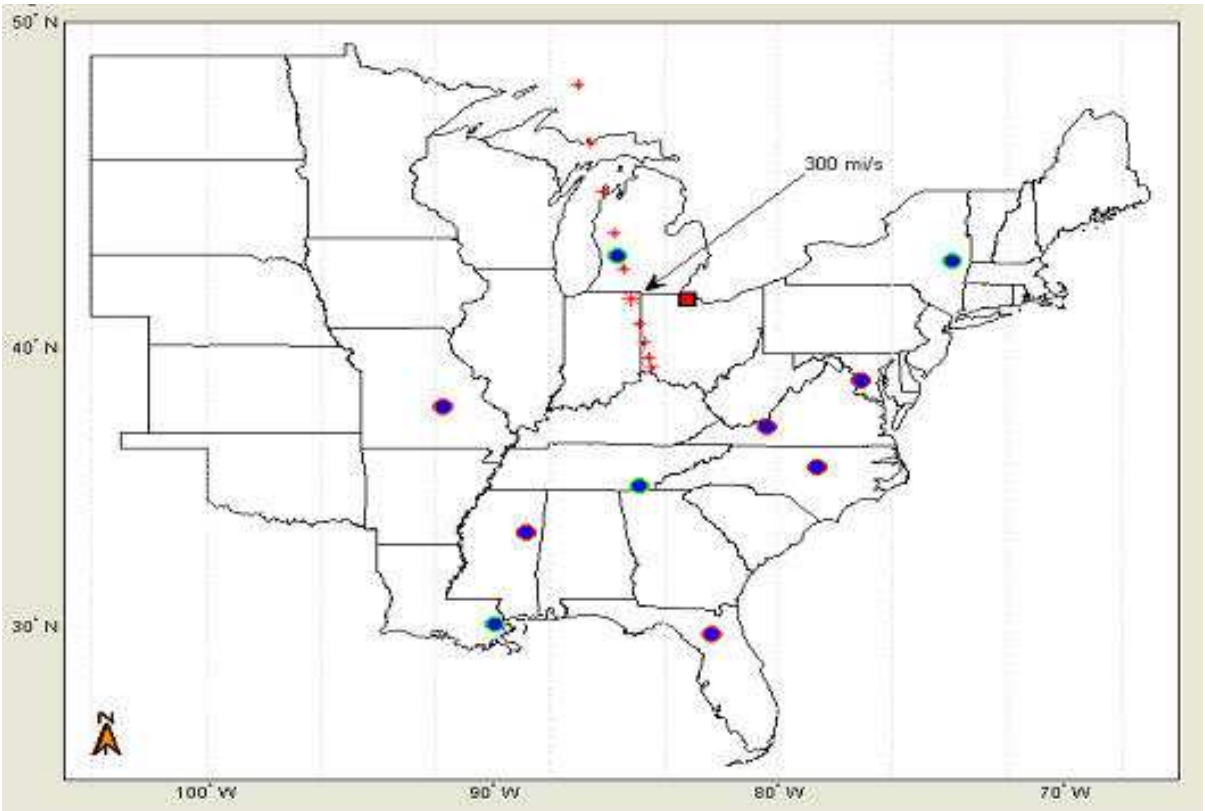


Figure 2.16. Sample LS Event Location Estimate

These assumptions about wave velocity in the grid are detrimental to the process. In addition to the aforementioned problems with velocity estimates (see Figure 2.13), this kind of approach is ambiguous because it only chooses a single point in the grid as the event location. In the likely case that this specific point is incorrect, even if the estimated location is "close" to the actual location, there exists no suitable metric with which to determine whether the process was actually successful because of the arbitrary nature of the velocity estimates. In fact, while a certain mean velocity may produce an estimated hypocenter close to the actual location, an incremental change in the velocity estimate can cause the hypocentral estimate to vary wildly, as Figure 2.17 illustrates.

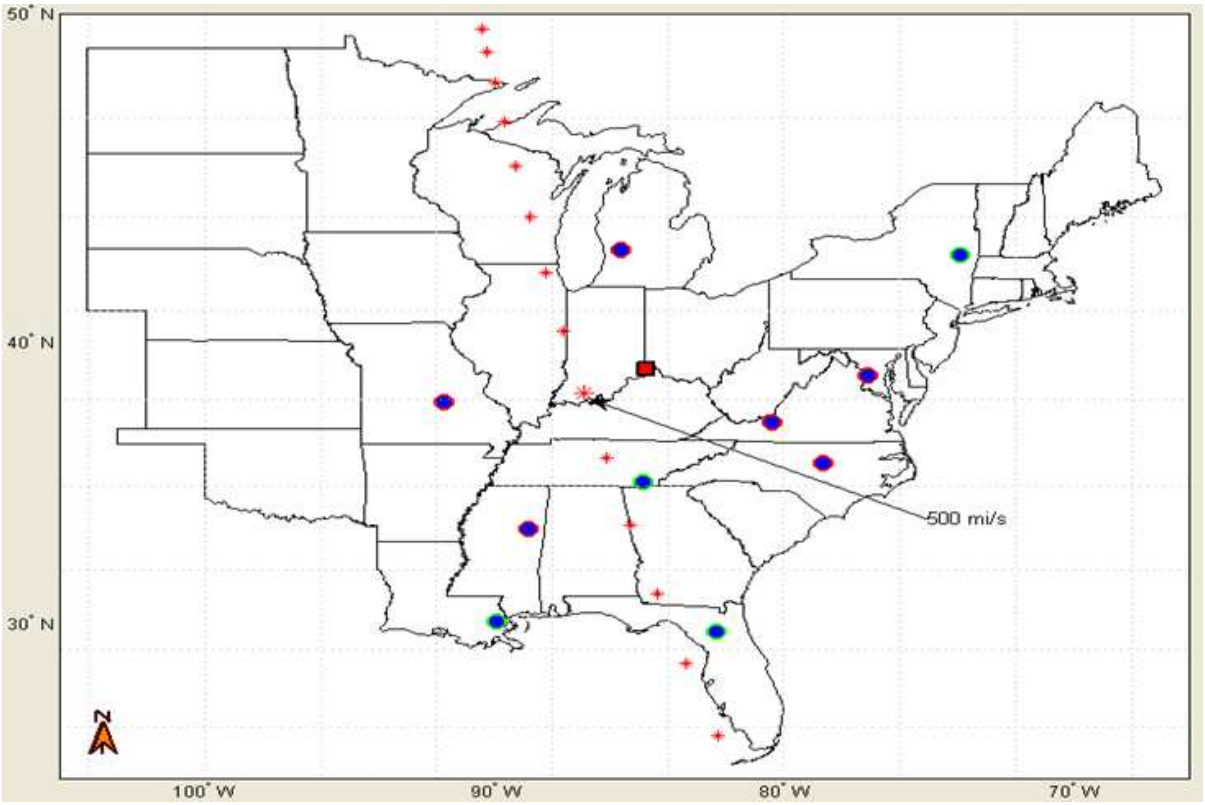


Figure 2.17. Velocity-based location errors

A much better location estimate would be to assign every point in the grid a probability of being the event hypocenter. This approach would quantify the success or failure of a location estimate. If the estimates assigns a small region $\mathcal{R}$ centered around the hypocenter $\mathbf{x}_h$ a probability of 0.75, that estimator is more successful than one which assigns $\mathcal{R}$ a probability of of 0.2.

Probabilistic location estimates take on many different forms, including decision trees[69] and naïve Bayes classifiers, to name a few. The most successful approach to date is the use of Parzen windowing techniques to identify the region $\mathcal{R}$ most likely to contain the hypocenter $\mathbf{x}_h$

Parzen windowing methods

Stochastic location estimates operate on the assumption that there exists a probability density function $p(\mathbf{x})$ where the probability P that the event hypocenter $\mathbf{x}_h = \{x_h, y_h\}$ is located within a region $\mathcal{R}$ can be found by

$$P = \int_{\mathcal{R}} p(\mathbf{x}')\partial\mathbf{x}'$$

Since P is simply a smoothed version of $p(\mathbf{x})$, a set of independently and identically distributed samples $[\mathbf{x}_1, \mathbf{x}_2, \ldots, \mathbf{x}_n]$ can be used to estimate the probability P. As n increases, P will converge to the actual probability $p(\mathbf{x})$ due to the properties of the binomial distribution.[70] In the case of wide-area frequency measurements, each FDR represents a sample $\mathbf{x}_i$. Parzen windowing techniques are one of the most common ways to estimate the parameters of a distribution from samples distributed throughout the sample space.

The Parzen window is defined by creating a window function $\phi(\mathbf{u})$, which acts as a binary operator. If $\mathbf{u}$ lies within a d-dimensional hypercube with edge length h_n and volume V_n centered at the origin, then $\phi(\mathbf{u}) = 1$. Otherwise the candidate point $\mathbf{u}$ is assigned a zero. The hypocentral probability based upon n sensors, $p_n(\mathbf{x})$ is calculated by determining the number of sample points k_n that lie within this hypercube:

$$k_n = \sum_{i=1}^{n} \phi\left(\frac{\mathbf{x} - \mathbf{x}_i}{h_n}\right)$$

$$p_n(\mathbf{x}) = \frac{1}{n}\sum_{i=1}^{n} \frac{1}{V_n}\phi\left(\frac{\mathbf{x} - \mathbf{x}_i}{h_n}\right)$$

As the number of samples increases, h_n decreases, which decreases the size of the hypercube.[70]

To generate such a windowing function, first consider a plane containing two points as shown in Figure 2.18. Suppose a wave, symmetrical in both directions on the level of the plane is observed by sensors at points $\{x_1, y_1\}$ and $\{x_n, y_n\}$ where the subscript of each point indicates the order in which the wave was detected. If the spread of the wave is indeed uniform in speed and propagation, then the origin of the wave must lie in the half-plane containing the sensor that first detected the wave. This region is shaded in the picture. With just two sensors, the locus of all possible points of origin is reduced by half.

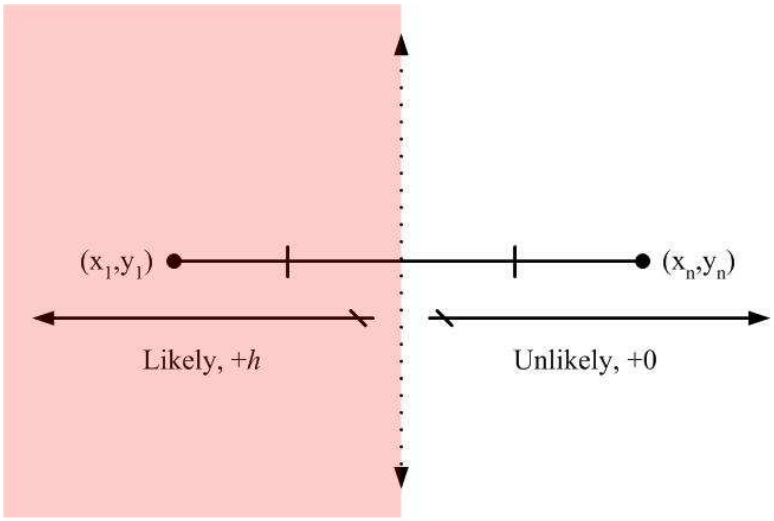
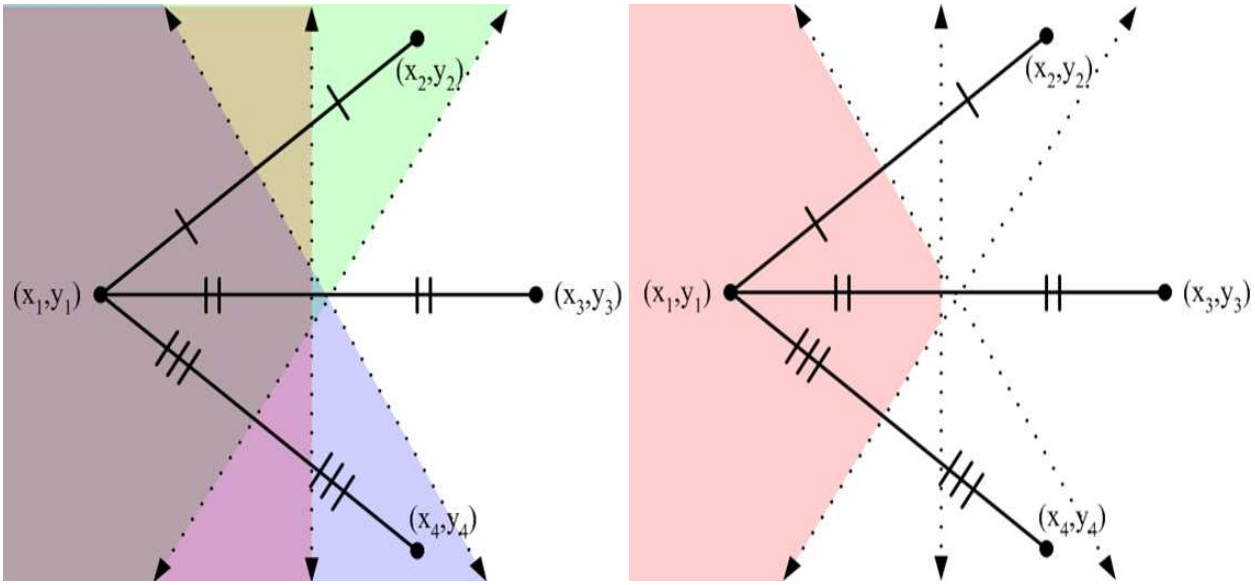


Figure 2.18: A cartoon of a plane containing two points

Perhaps there are more than just two sensors. Say, for example, four sensors are in operation as shown in Figure 2.19a. In this case three half-planes can be constructed, the union of which becomes the most likely region to contain the hypocenter. If these half-planes are labeled $\mathcal{R}_1$, $\mathcal{R}_2$, and $\mathcal{R}_3$, then the region of overlap can be described mathematically as:

$$\mathcal{R}_{\text{overlap}} = \mathcal{R}_1 \bigcap \mathcal{R}_2 \bigcap \mathcal{R}_3$$



(a) Creation of four half-planes

(b) Region of highest hypocentral probability

Figure 2.19. Cartoons of a plane containing four points

Continuing this logic, there exists a confidence region (again assuming that the wave travels with even propagation) that the origin of the wave is in the overlapping portions of the planes of Figure 2.19a. This overlapping region, $\mathcal{R}_{\text{overlap}}$, is shaded separately in Figure 2.19b.

One can imagine that, as the number of sensors increases, $\mathcal{R}_{\text{overlap}}$ tends to get smaller. Therefore, the higher the number of FDRs that respond to any arbitrary event in the EUS, the smaller the region of the supposed origin. Referring back to an EUS example, Figure 2.20 shows the lines needed to construct the half-planes for the event ordering shown in Figure 2.15. The red star shows the actual location of the EUS disturbance, but the green dot corresponding to the FDR at Virginia Tech was the first to measure the disturbance in this example.

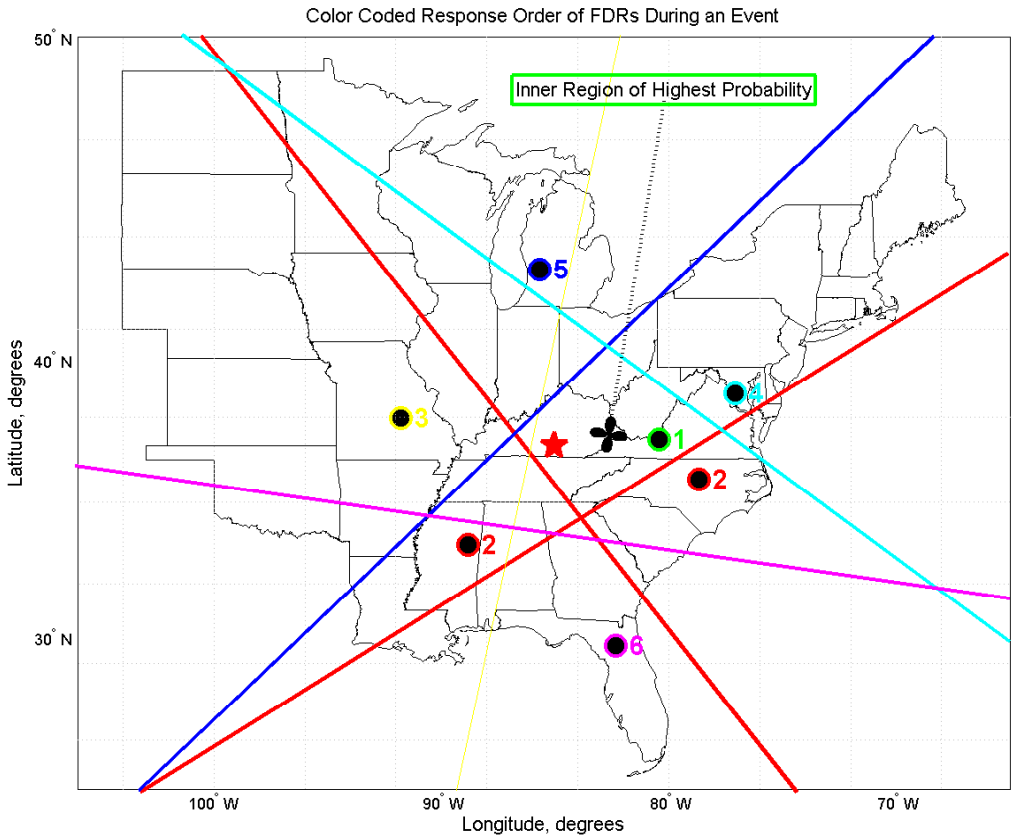
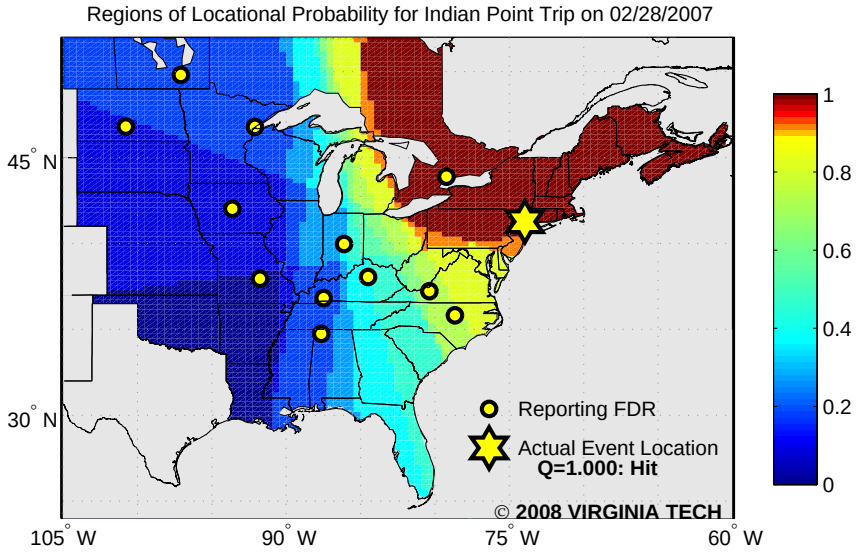


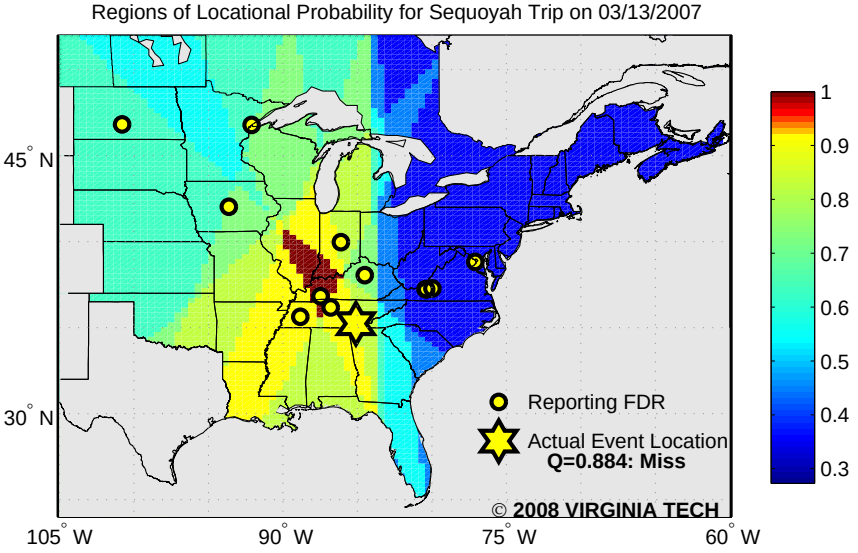
Figure 2.20. A cartoon of lines representing half-planes in the EUS

Now, instead of using half-planes to eliminate regions of the map, the half-planes are used to assign lower probabilities to areas that lie outside the intersection of every half-plane, such as the light green or brown areas of Figure 2.19b. In such manner every point in the grid can be assigned a score corresponding to the number of sensors the half-plane windowing function determines to

be closest to the first responding unit. As expected, $\mathcal{R}_{overlap}$ remains the area of highest probability (and therefore the estimated location of the event), but other areas of the grid are assigned lower probability based upon the order and location of responding FDRs. Figure 2.21 illustrates three examples (success, approximate success, and failure) of such an approach.

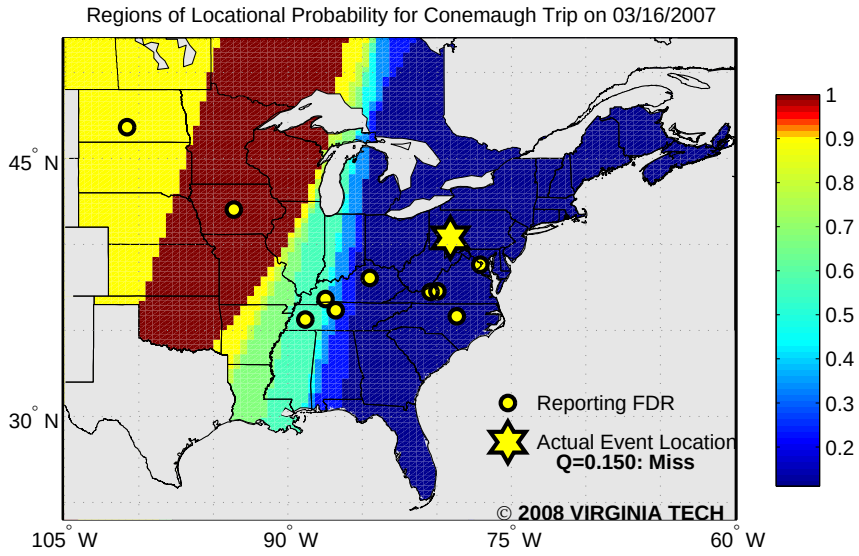


(a) Success



(b) Approximate success

Figure 2.21. Examples of Parzen windowing event location



(c) Failure

Figure 2.21. Examples of Parzen windowing event location (continued)

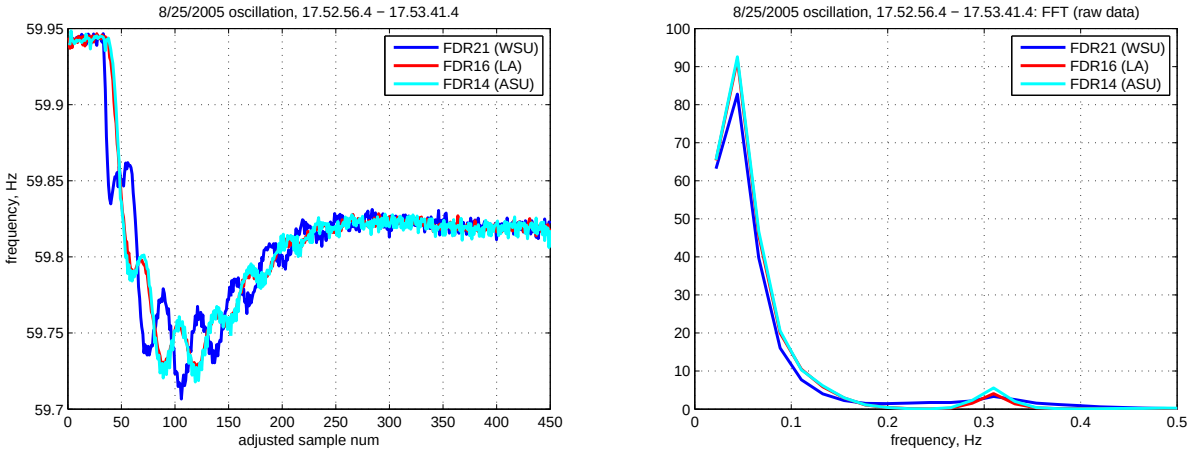
Not only does this method attempt to accurately estimate an event's hypocenter, but it also provides a simple metric by which the success or failure of the location estimate can be measured. If the actual event location lies in the upper quantiles of the generated probability density, the location estimate can be considered a success. Figure 2.21a shows that the actual event location lies in the 1.000th quantile, thus indicating success. For the purposes of this report, quantiles exceeding 0.9 are defined as a success, so the trip of the Sequoyah plant in Tennessee on 3/13/2007 is considered a failure with Q = 0.884. To contrast, the Parzen technique was far more successful locating the Sequoyah trip than the Conemaugh trip in Pennsylvania of 3/16/2007 with Q = 0.15. This relative accuracy metric is important for future revisions and improvements to these methods. Appendix D will summarize the performance of both the LS and Parzen windowing event location techniques.

2.2 Oscillations

The other main type of power system event is an oscillation. Oscillations are a unique kind of incident, because they can not only be incited by another event but they can spontaneously arise as well. While some oscillations are locally observed, FNET has the unique blessing of observing inter-area oscillations that local system operators may or may not be able to detect and locate. Because frequency corresponds to power mismatch, an oscillation in frequency indicates two generators (or more generally, regions) are oscillating against one another. These kind of power oscillations pose a great threat to any generators currently in operation. Moreover inter-area oscillations reduce the effective capability of the system to provide loads with the energy they require. Current and previous research has focused on the detection and post-mortem analysis of oscillations, and there is hope that wide-area frequency measurements may soon be used to mitigate the duration and effect of undesired oscillations.

2.2.1 Oscillation Detection

Historically, the detection and analysis of oscillatory data has utilized the Fourier Transform to identify the spectral content of a signal. The detection of oscillations in FNET data is a slightly more complex task that a simple application of the Discrete Fourier Transform (DFT). Consider a by now well-known example of a generator trip with subsequent oscillatory response, and its corresponding spectra, shown in Figure 2.22.



(a) Recorded frequency data

(b) Frequency content of data

Figure 2.22. Power system event with oscillatory behavior

This example is particularly interesting because of the anti-phase 0.3 Hz oscillations recorded by different FDRs. A quick geographical inspection of the three units' location shows that this os-

cillation is actually a North-South inter-area oscillation. The northern unit (Pullman, Washington) records anti-phase oscillations compared to the southern units (Los Angeles, California and Tempe, Arizona). These oscillations are most likely due to oscillations on the Pacific Direct-Current Intertie, a high-voltage DC (HVDC) line linking the Pacific Northwest and Southern California, as shown in Figure 2.23. For context, all of the installed FDRs (by a blue 'F') and PMUs (by a green 'P') in the WECC are also highlighted.

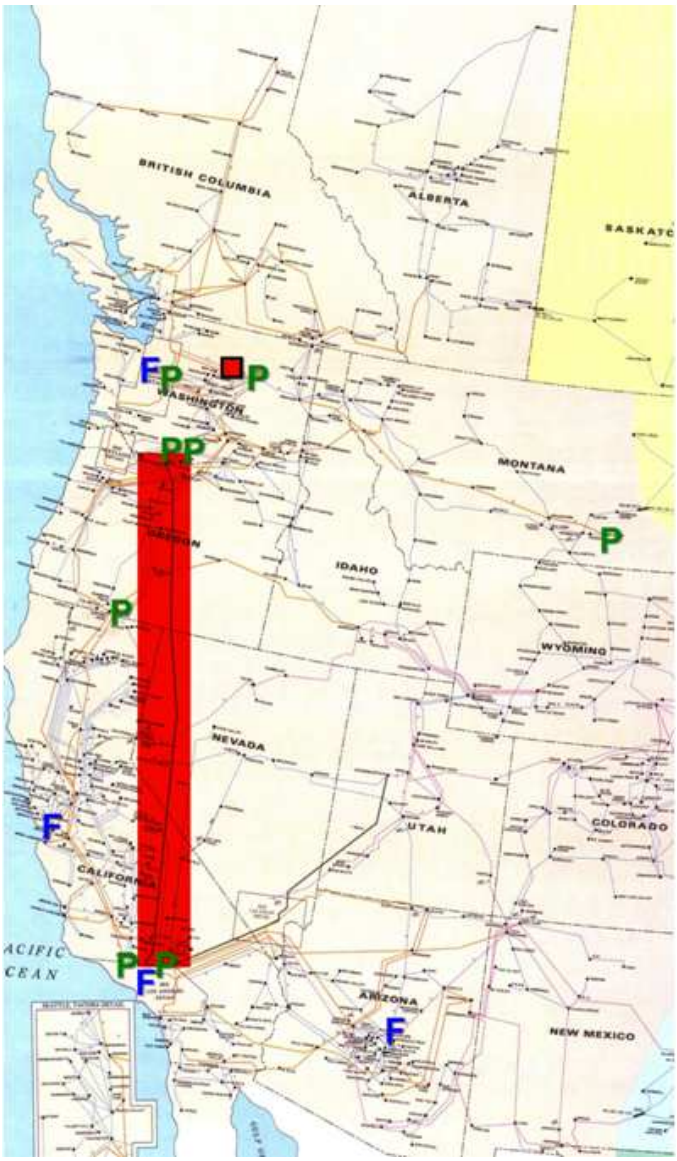
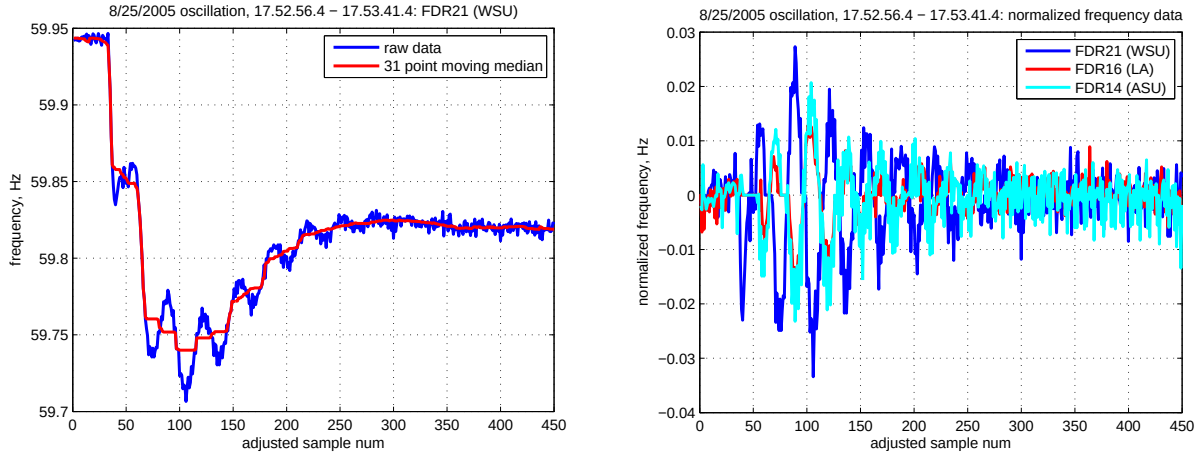


Figure 2.23. Location of Pacific DC Intertie

While the oscillatory component of interest is visible in Figure 2.22b, it appears insignificant compared to the large low-frequency components of the event signature. The sharp frequency decline due to the loss of generation is not of interest in oscillation studies, so it must be filtered out in order to isolate the oscillatory components of interest. Trend removal is accomplished by

subtracting the trend from the raw data, leaving a residual signal that still contains the spectral content of interest. The trend is robustly calculated using a centered 31-point moving median, and is shown in Figure 2.24a. Figure 2.24b shows the detrended, or normalized data.

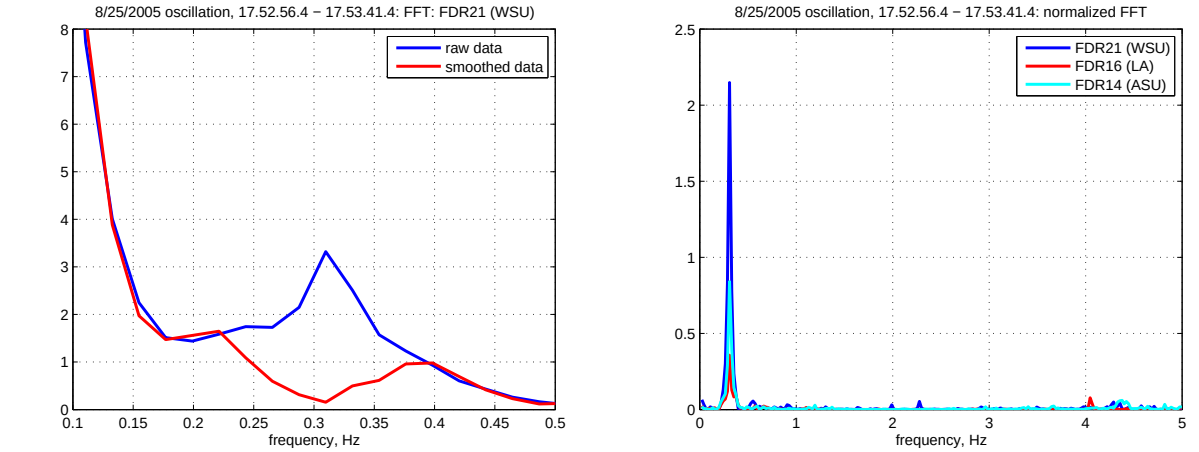


(a) Recorded frequency data

(b) Normalized frequency data

Figure 2.24. Oscillation isolation via normalized frequency

Figure 2.25a illustrates the difference between the spectra of the raw and normalized data. The trend clearly contains the low-frequency components that comprise the event signature and need to be eliminated.



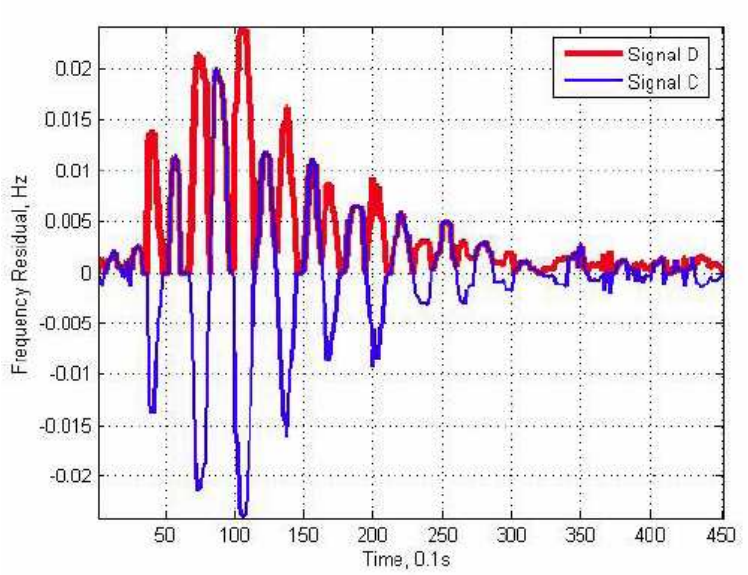
(a) Differences between raw and normalized frequency

(b) Spectra of normalized frequency data

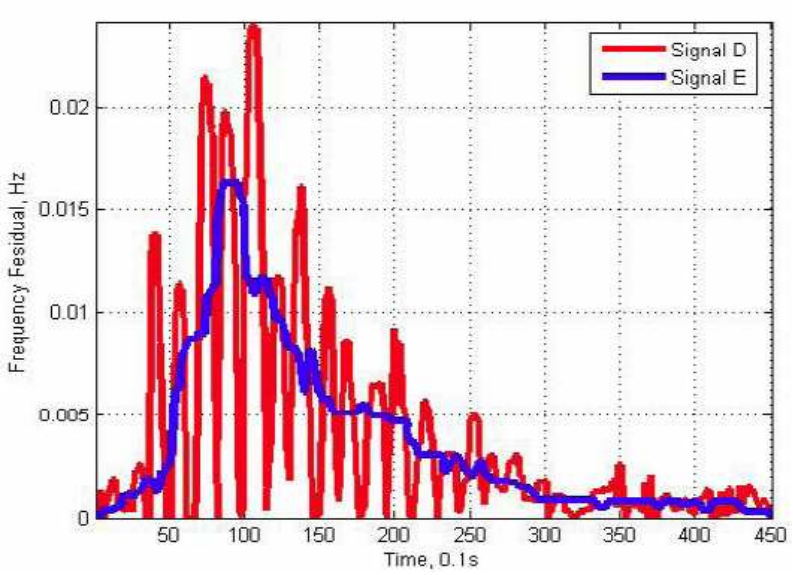
Figure 2.25. Spectra of raw and normalized frequency

Now that the trend has been removed, the 0.3 Hz oscillation is clearly visible as shown in Figure 2.25b, a distinct contrast from the spectra of the raw data shown in Figure 2.22b.

While the FFT has many valuable uses, there are more computationally efficient methods of oscillation detection for real-time applications, such as the use of a simple envelope detector common to many communications systems.[71] Once the normalized frequency has been calculated (Signal C, Figure 2.26a), the signal is rectified (Signal D, Figure 2.26a). Next the rectified signal (Signal D, Figure 2.26b) is smoothed using the moving median to create the final oscillation trigger signal (Signal E, Figure 2.26b). If this signal rises above a threshold for a certain amount of time, an oscillation is said to have occurred.



(a) Normalized and rectified frequency data



(b) Oscillation envelope signal

Figure 2.26. Oscillation isolation via normalized frequency

2.2.2 *Oscillation Analysis*

Similar threshold methods can be used to quantify significant spectral components of an oscillation. Figure 2.27 shows a screenshot from FNET's automated oscillation analysis tool. The frequency recorded by the FDR located in Troy, New York (RPI), in red, recorded an oscillation with significant oscillatory component around 0.5 Hz. The panel at the bottom of the figure shows the FFT of the normalized version of the raw frequency trace in the upper left panel.

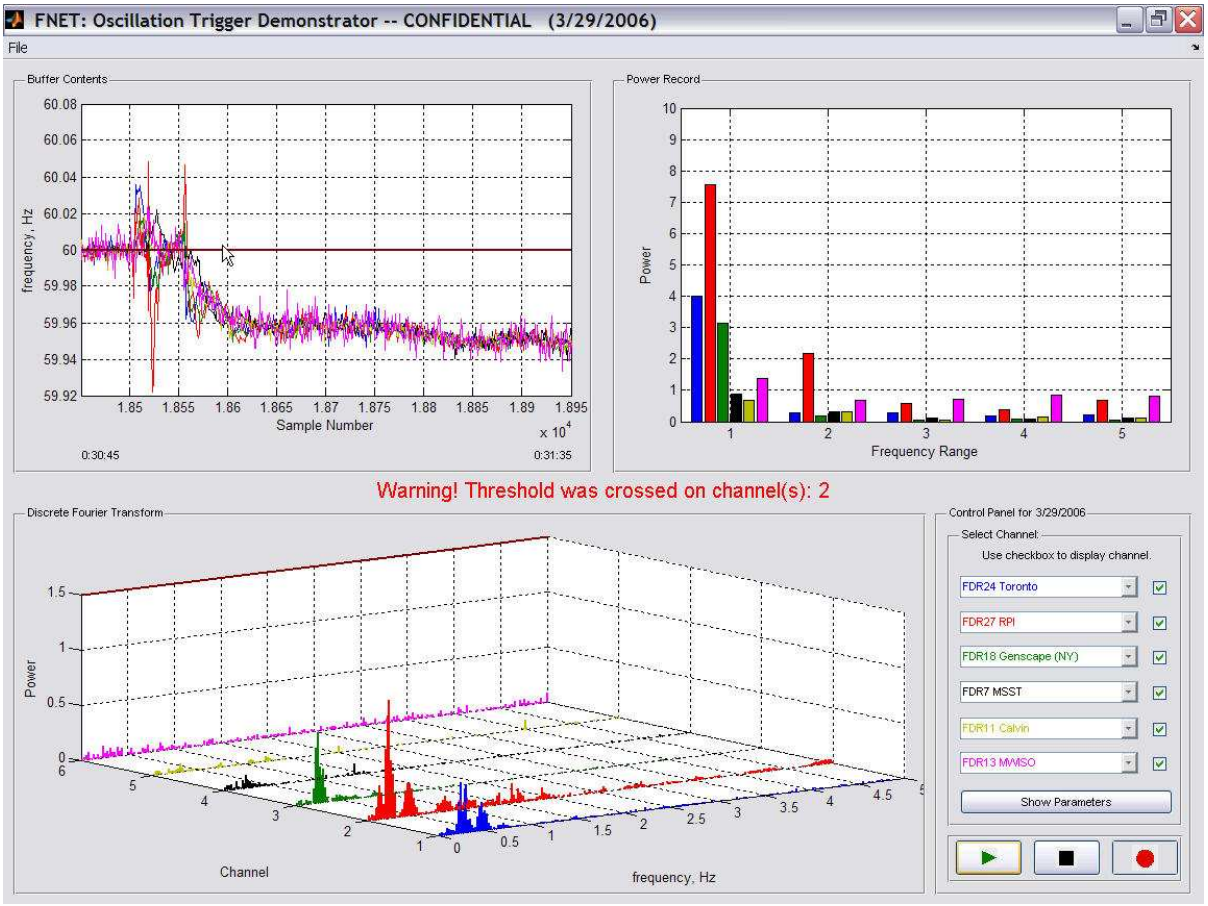


Figure 2.27. Threshold oscillation analysis

Damping estimation

Further oscillation analysis beyond the magnitude and frequency has great benefit in the determination of system stability. As undamped oscillations are representative of system instability,[72] estimation of system pole locations from wide-area frequency measurements is a valuable situational awareness tool. Such estimations are not new, as Prony's method (or polynomial method) has long been used for these purposes, both in theory[73] and in direct power system applications.[52,74–78]

This method has been shown to be deficient in the presence of noise,[79] where pencil-of-functions techniques like the Matrix Pencil are preferred.[80–82] Specific application of these methods to FNET data have already been documented,[1] but it is necessary to make brief mention of these techniques here for completeness.

Windowing effects

While these detrending techniques are essential to proper identification and analysis of oscillatory events, there is a cost associated with the smoothing properties of the moving median. It is quite possible to completely eliminate an oscillation from appearing in the normalized frequency if the moving median window is too small. Consider the oscillation pictured in Figure 2.28. As expected, the moving median data more closely tracks the raw data as the window size decreases. In the context of normalized frequency, the more exactly the median-smoothed data approximates the raw data, the less information will be contained in the difference between the raw and smoothed traces. Figure 2.29 illustrates the same effect in the spectra of the raw and smoothed data.

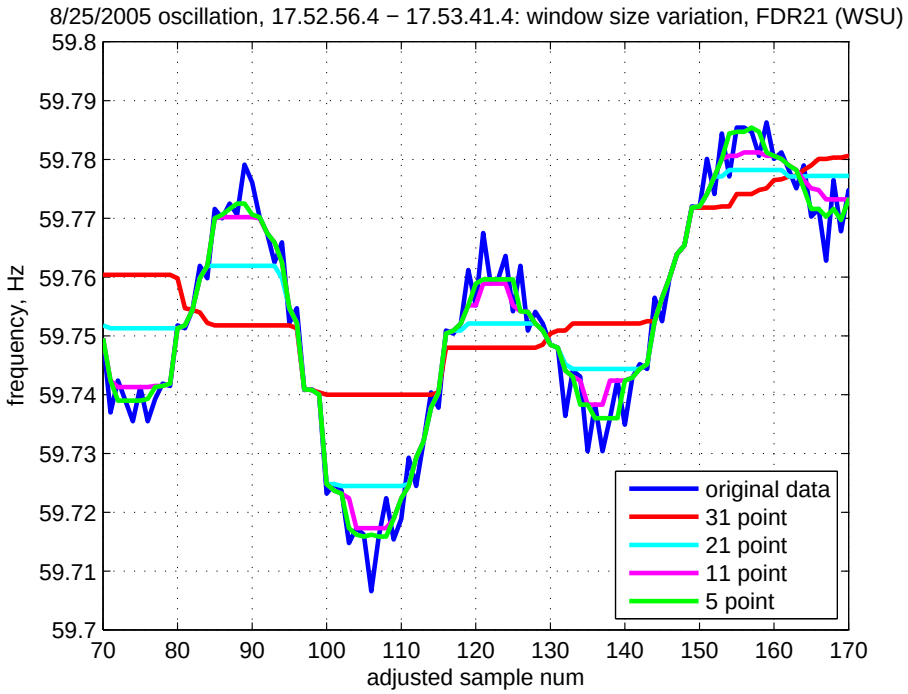


Figure 2.28. Illustration of different window sizes during an oscillation

Thus to accurately detect oscillations using robust detrending techniques, the proper window size must be chosen. This choice is a function of the frequencies which need to be identified. Consider the case where there is a pure oscillation, as shown in the top panel of Figure 2.30. The raw data, shown in blue, is an ideal 0.3 Hz oscillation.

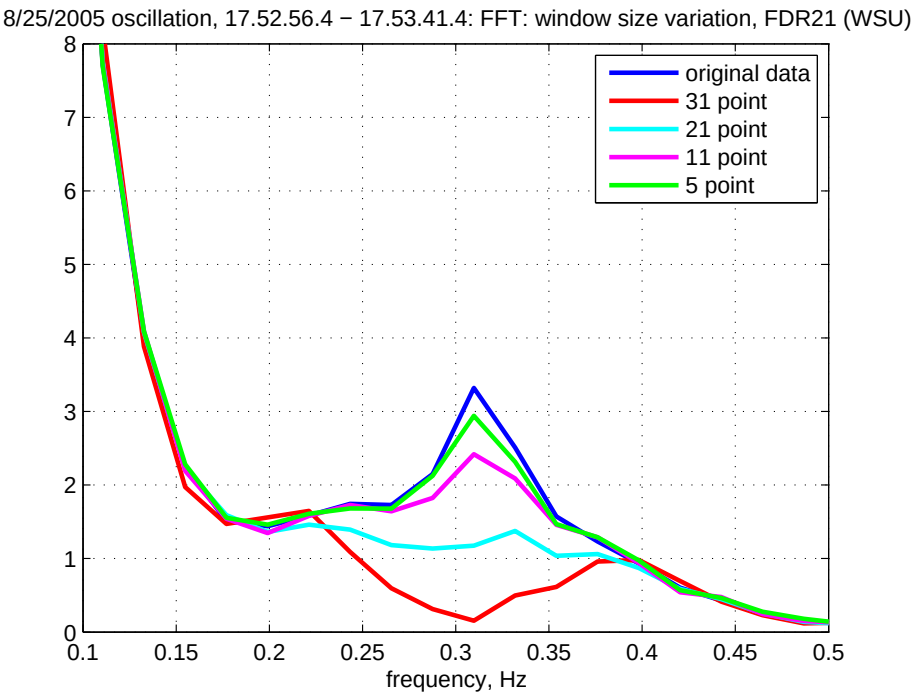


Figure 2.29. Spectral effects of different window sizes

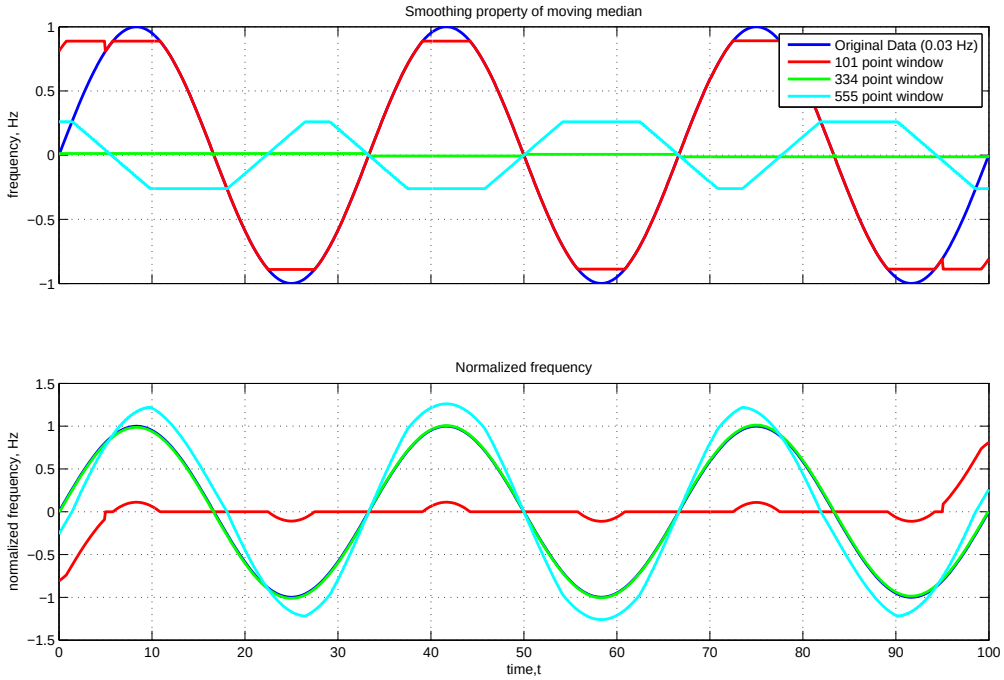


Figure 2.30. Windowing effects during an ideal oscillation

For small window sizes, like the red trace, the moving median stalks the original data closely enough that the oscillation does not appear in the normalized frequency, shown in the bottom pane of Figure 2.30. Large window sizes have the opposite effect: the moving median oscillates out of phase from the raw data, which when subtracted, results in a normalized frequency with an oscillation of the same frequency but larger amplitude and slight delay. There is also a "perfect" window size, where the moving median remains at zero throughout, which results in the normalized frequency trace exactly matching the raw data. Figure 2.31 illustrates the effect each window size has on the spectral content of the normalized frequency.

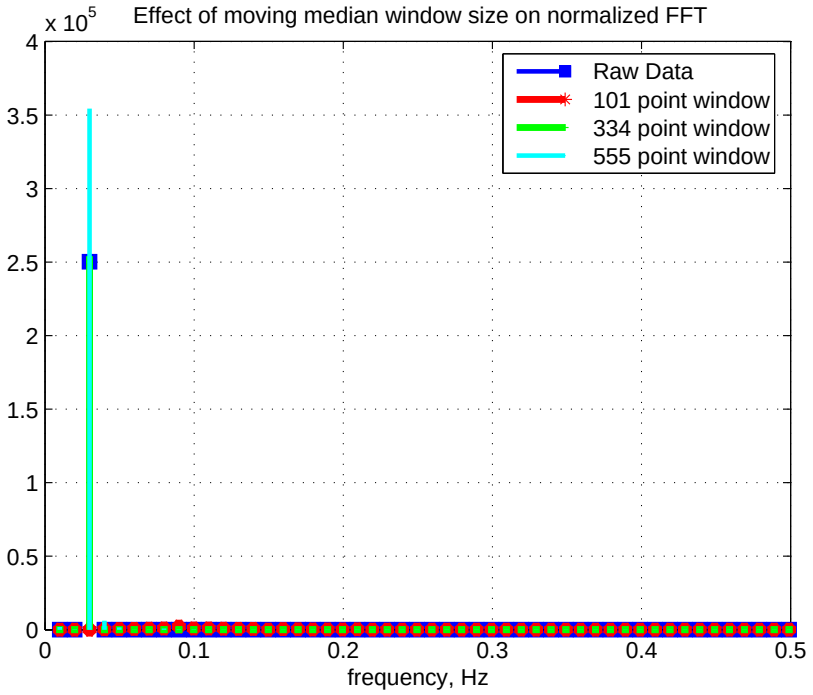


Figure 2.31. Windowing spectral effects during an ideal oscillation

It can be easily deduced this perfect window size is related to the frequency of oscillation. Moreover, since the objective is to detect all oscillations within a certain range of frequencies based upon oscillation magnitude, the behavior of large window sizes is also acceptable. If the oscillation is significant enough to trigger an alarm, the increase in oscillation magnitude from a too large window size will not undermine the triggering mechanism. Given an oscillation with frequency of f Hertz and period T seconds, there are $N = 10T$ samples per period since the FDR sampling rate is 10 Hz. Obviously the perfect window size is when the number of points in the window, W, is precisely equal to the number of samples in the period:

$$W = 10T$$

When $W < N$, the moving median window is smaller than the period of the oscillation and the smoothed data closely tracks the actual data like the red trace in Figure 2.30. For $W > N$, the oscillation amplitude will be amplified, like the light blue trace. Since W is a parameter that is established *a priori*, the window size can be considered fixed. Thus detrending using a moving median with this fixed window size W can only detect frequencies greater than some minimum frequency f_{min}. The relationship between W and f_{min} can be summarized by

$$W \geq \frac{10}{f_{min}} \tag{2.13}$$

By now a vast number of threshold methods have been presented as a means of detecting and analyzing both major types of power system events. The maintenance and automation of these methods are not trivial tasks, thanks in large part to the non-stationarity of FNET data. Furthermore, the dependence of event location estimates on wavefront detection order and TDOA necessitates a comprehensive and robust automated strategy for the ordering of mismatch events.

Chapter 3

Automated Analysis of Generation Trip Events

Distributed frequency measurements are immensely valuable for a variety of real-time and post-mortem applications. Many of these applications utilize sub-second differences between units to detect, analyze, and locate events. To date an automated, adaptable, and robust mechanism to quantify these differences has not been developed. Current methods involve static threshold that are highly irregular and require constant attention and tweaking. This chapter presents the first unified approach for wavefront detection, which utilizes common pattern recognition and robust statistical tools. To refine the goals of this approach, consider the current FNET data handling procedure, shown in Figure 3.1.

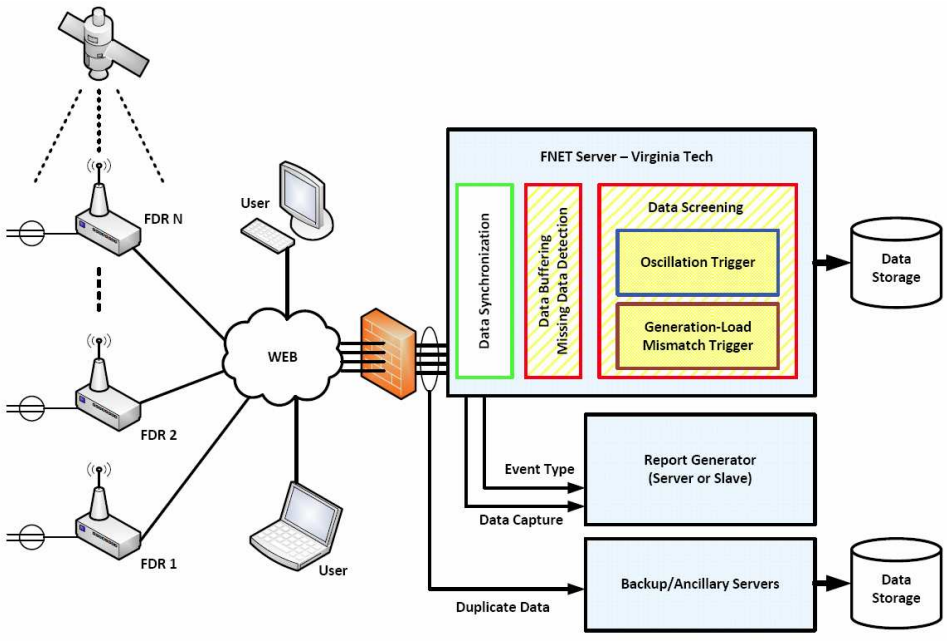


Figure 3.1. Data flow in the FNET system

Streaming data received from each FDR is consolidated, checked for errors, and archived. Well-conditioned data is then subjected to a series of triggers, most notably the event detection and oscillation triggers described in Chapter 2. Should an event be identified, all of the data that contains the event is saved in the proper format and sent to the appropriate analysis routine, such as mismatch calculations or oscillation damping analysis. In the case of a generation-load mismatch event, the amount of mismatch is determined and an event hypocenter is estimated. Both of these routines require robust data analysis - the mismatch calculations require determination of the pre- and post- event frequencies (points A and B/C in the NERC standard), and the LoD solution (the event hypocenter) requires some sort of wavefront detection algorithm that is capable of calculating TDOA.

Both of these calculations operate after an event has been detected, so they operate on a small window (< 10 minutes) of data that surrounds the event data that triggered the system in the first place. The pre- and post- event frequencies are calculated by determining the mean of the data before and after the event data respectively. The difference between these two frequencies is then used to estimate the amount of generation lost. The TDOA calculations are based upon calculating the time each frequency trace crosses threshold 14 mHz below the pre-event frequency.

The rationale for choosing a static frequency deviation threshold is self-evident. To expand the pond analogy, consider a tsunami warning system. Buoys are distributed throughout the ocean to measure pressure, or water height. If a tidal wave passes through the buoy location, the water height will change drastically. So any deviation in pressure beyond some static threshold (to accommodate steady-state wave action) will trigger an alarm, as shown in Figure 3.2.

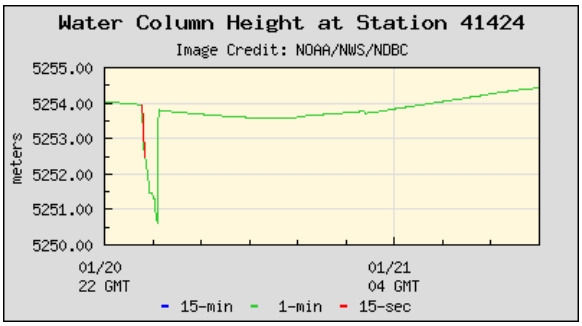


Figure 3.2. Tsunami warning data[4]

As with any warning system, early detection is critical, so the pressure threshold is made as low as reasonably possible. A number of false positives (tsunami alerts when there is no wave) is acceptable provided false negatives (missing a tidal wave) are eliminated. The equivalent is especially true in the power system. From a physical standpoint, the power system is operated according to the $N-1$ contingency constraints, so that the system is always able to withstand one catastrophic event from its current state. If that state changes in the case of a generator trip, the

$N-1$ criterion needs to be recalculated again. Moreover the financial constraints of equipment repair and the energy markets make early warning imperative.

From a data standpoint, early detection is essential for accurate LoD solutions. Unlike the ocean, where a tsunami can eventually wash up on shore, the electric grid has fixed endpoints. Consequently, electromechanical perturbations travel to the edges of the network and reflect back through the system. Instead of violently cascading up the coast, severe power mismatch will destroy machines. Additionally, control actions to arrest the frequency decline take place at different rates in different regions of the system. Figure 3.3 show how both reflections and control actions manifest themselves in the generator trip signature. The changing slopes approximately midway through the frequency decline are indicators of such nonlinearities.

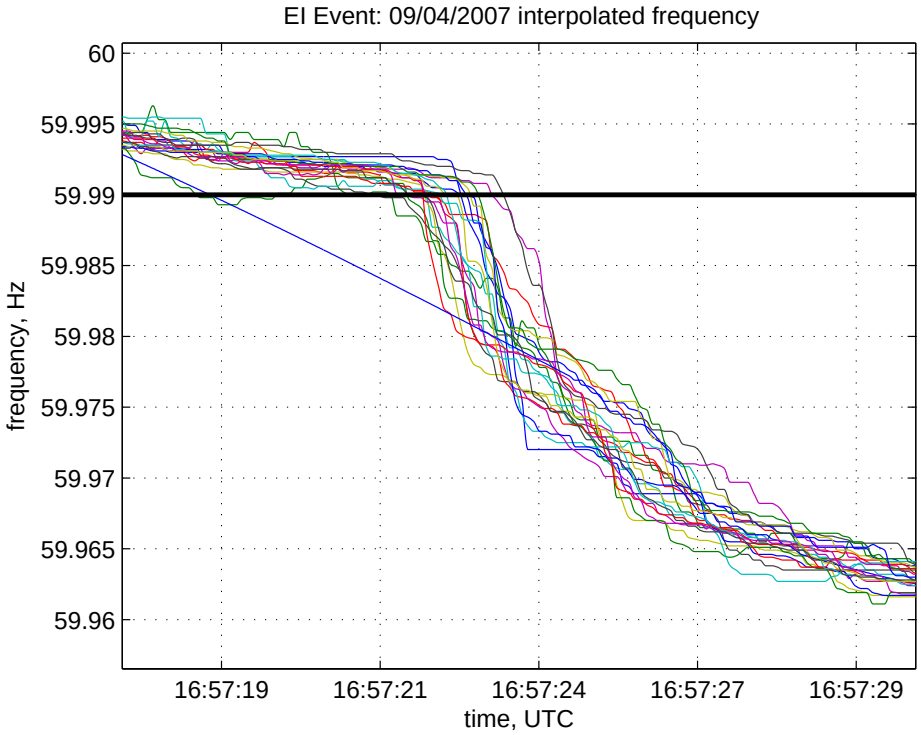


Figure 3.3. Reflections and control effort during an event

Assuming the pre-event frequency for this event is (quite generously) assigned to 59.995 Hz, the static deviation threshold 14 mHz (59.981 Hz) places the TDOA determination exactly during these reflections. It would be far more desirable for the threshold to be as close as possible to the beginning of the frequency decline to avoid any reflections or control actions. In the case of this specific event, the desired threshold would be at 59.99 Hz, as shown by the black line in Figure 3.3. To summarize, a static frequency deviation threshold does not work well because of the variety of event magnitudes in the grid. Large events with large frequency excursions may accommodate a

14 mHz deviation before the rate of decline is restrained, but smaller events may be completely misrepresented with the same threshold.

Even if the threshold were chosen in a proportional manner to the size of the event, such as a certain percentage of the total frequency deviation, the method would still fail. Consider the Chief Joseph generator trip on 8/25/2008 (also shown in Figure 2.22a):

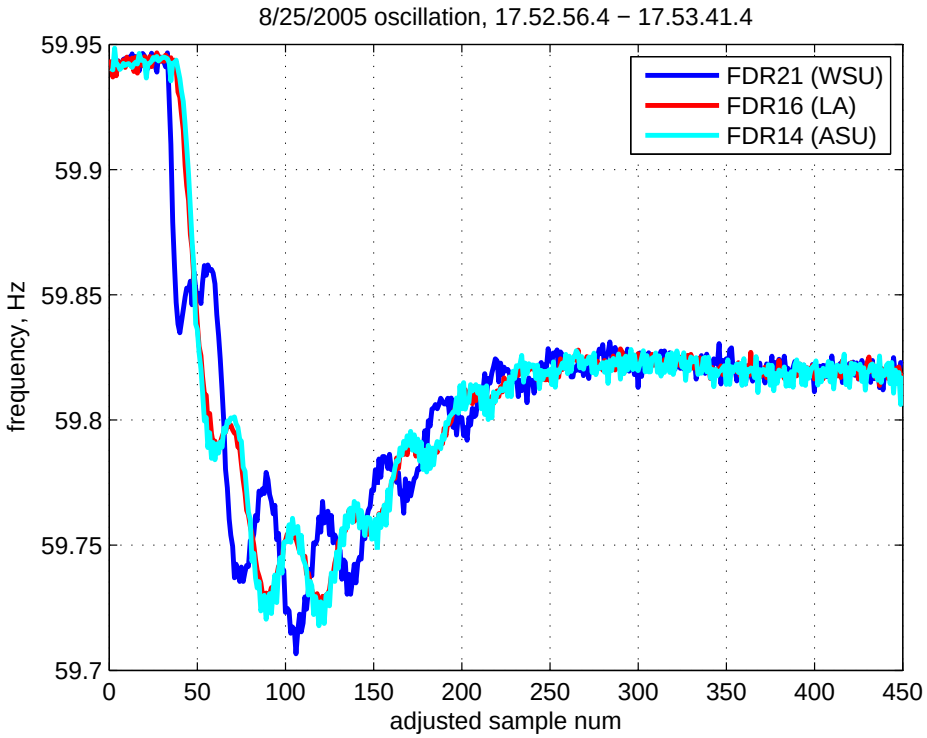


Figure 3.4. Generator trip signature with oscillations

If a 40% percentage threshold or a 10 mHz deviation threshold was chosen, the threshold value of 59.85 Hz would cut directly through the oscillatory behavior recorded by FDR 21 in Pullman, Washington. Therefore, any static deviation threshold method can yield duplicitous arrival times, which can be seen by inspection to drastically alter the ordering of reporting FDRs. There is currently no method in place to robustly determine which of the multiple crossing times is most accurate. In the context of automating the event location process, there is no good method to choose a threshold to guarantee absence of these false positives.

Decreasing a static threshold is also a difficult proposition. The combination of noisy data, outliers, and other mistakes cause multiple threshold crossings for smaller thresholds. There are at least two cases of multiple threshold crossings in Figure 3.3 along with one trace that (due to its extreme non-conforming behavior) should ignored. This trace is of an FDR that lost GPS satellite visibility during the minute or so surrounding the event time. The line is actually an interpola-

tion between the two recorded frequency values immediately before and after the loss of satellite visibility. The precarious balance between more accurate (smaller) thresholds and data problems have caused the static deviation threshold to be altered numerous times throughout FNET's history. In light of these physical and data concerns, any new event ordering routine should be able to accomplish the following tasks:

- Accurately identify pre- and post- event frequencies
- Choose a frequency threshold for TDOA calculations as close as possible to the beginning of the sharp frequency decline (the "knee" of the curve)
- Robustly ignore ill-conditioned data and noise-induced multiple crossings

Figure 3.5 shows the signature from the June 12, 2007 trip of the Belews Creek U1 generator North Carolina. This event will be used as a base case to illustrate each facet of the new event ordering algorithm. It should be noted that because this process is intended to operate on triggered data, the data can be assumed to have already been smoothed using the robust methods discussed in Section 1.4.

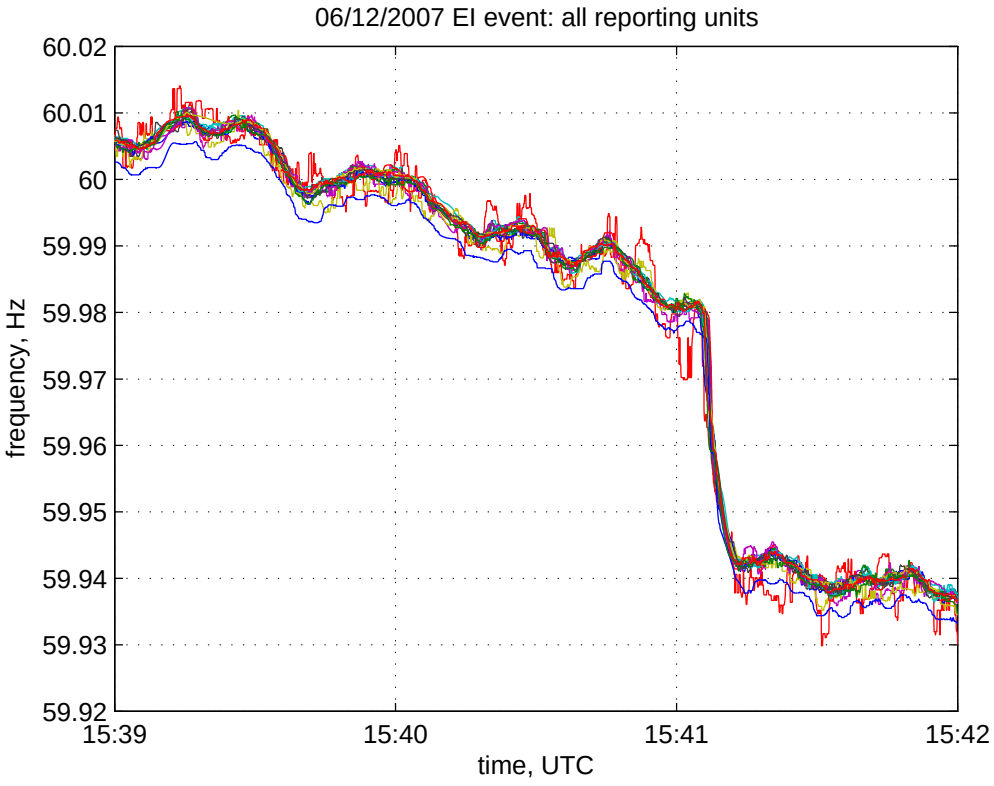


Figure 3.5. Frequency signature of Belews Creek U1 trip on 6/12/2007

3.1 Automatic ordering of generation trip events

Given a small window of data in which an event is known to have occurred, the three major aims of an event ordering scheme reduce to three primary tasks, each of which build upon preceding tasks:

- Identify the time at which the event occurred
- Determine the proper frequency threshold
- Separate false positives

Accurate determination of pre- and post- event frequencies require a precise determination of the event time. Calculation of the proper frequency threshold right at the "knee" of the curve is based upon the frequencies immediately surrounding the event time, and any multiple threshold crossings are a function of the frequency threshold. The event time calculation makes use of the Swing Equation, the threshold is chosen using robust statistics, and the false positives are eliminated using robust outlier detection and pattern recognition.

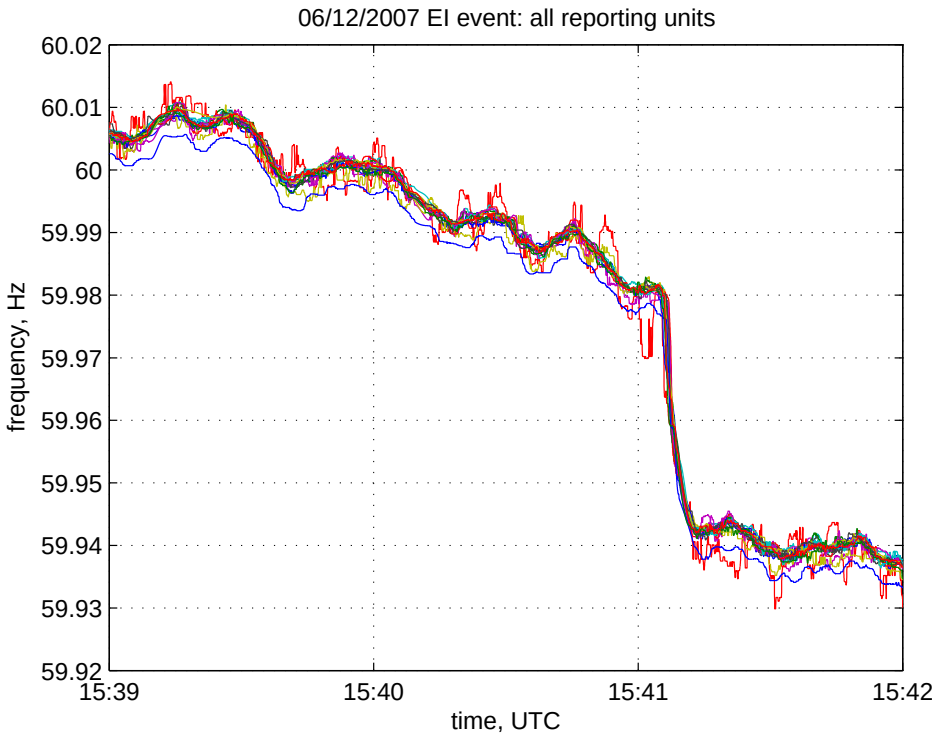
3.1.1 Event time determination

Since the ordering routine receives data that has already triggered an event, the Swing Equation can be applied to identify the event time. Recall Equation 2.2:

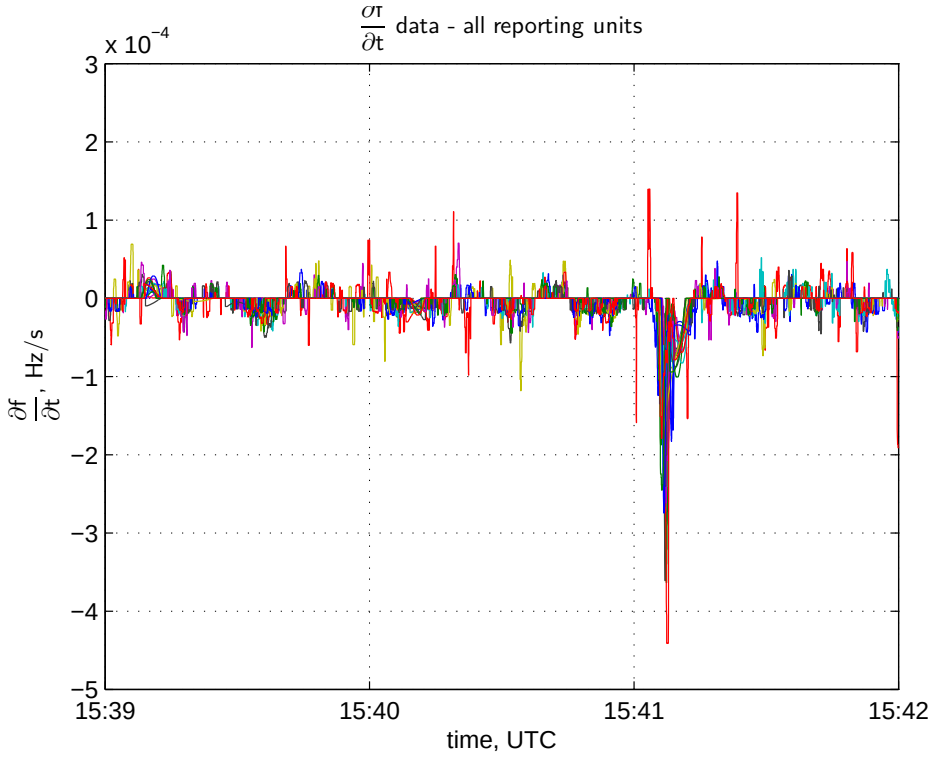
$$\frac{2H_{\text{system}}}{\omega_0}\frac{\partial\omega_{\text{system}}(t)}{\partial t} = P^m_{\text{system}} - P^e_{\text{system}}$$

Thus, the most rigorous way to determine the event time is to use the first derivative of the frequency. Since the rate of change in frequency is proportional to power mismatch, and since the data window is small enough to assume there are not multiple events contained in one window, the time at which $\frac{\partial f}{\partial t}$ is at a minimum can be called the estimated event time, or guess time. Figure 3.6 compares raw data with its derivative for the window containing the base case.

As expected, there is a clear correlation between the minimum of the derivative and the the event signature, just as the Swing Equation predicts. Moreover there is a distinct, easily separable minimum at the event time. The clarity between the minimum value and the rest of the $\frac{\partial f}{\partial t}$ data ensures that the minimum can be robustly determined. In fact, this base case is a comparatively severe test case, as the combination of pre-event oscillatory declining frequency trend skews the derivative closer to the minimum than a typical event (Figure 2.4).



(a) Raw Frequency Data



(b) $\frac{\partial f}{\partial t}$ Data

Figure 3.6. Frequency and its derivative around trip time

3.1.2 Mismatch amount calculation

Once the event time is known, the trip amount is calculated from the total frequency deviation. To calculate the pre- and post- event frequencies, the median is used. The robustness of the median allows the calculations to be unencumbered by any oscillatory or noisy data. Thus the pre-event frequency is determined by calculating the median of 10 seconds worth of data immediately before the event time. Likewise the post-event frequency is determined by calculating the median of the 10 seconds immediately after the event time. This interval was chosen to avoid the start and end points of the data window. The current event trigger saves 40 seconds worth of data when an event occurs. Estimating the event takes no more than 10 seconds, then a 10 second interval before and after the event leave a 5 second buffer on either side of the event. This buffer is necessary because missing data points (primarily due to loss of GPS and internet latency) are interpolated within the 40 second window, which can lead to absurd frequency values at the boundaries of the window.

Figure 3.7 shows the raw frequency data with the event time in purple and the pre- and post-event frequencies ($\{59.9811, 59.9441\}$ Hz) in brown. Table 3.1 shows the mismatch calculations from each method compared to the actual generation capacity of the unit. Belews Creek U1 has a summer capacity of 1135 MW.[83]

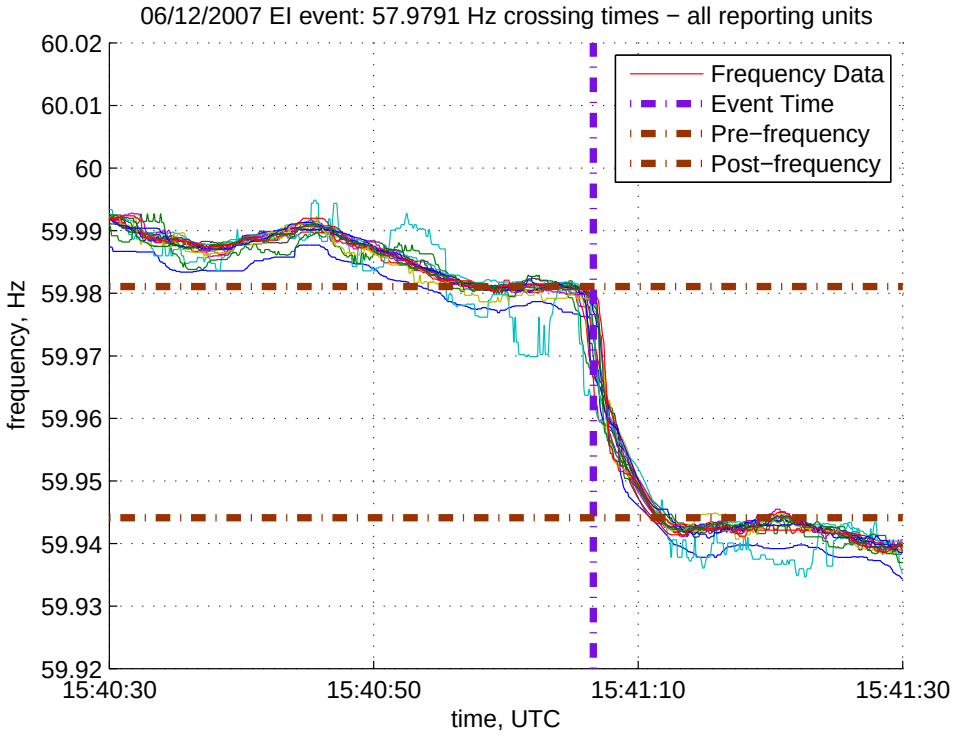


Figure 3.7. Pre- and Post- disturbance frequencies

Table 3.1. Old and new mismatch calculations

Method	Frequency deviation Δf (mHz)	Estimated power lost ΔP_{est} (MW)	Error (MW) $\lvert\Delta P_{actual} - \Delta P_{est}\rvert$	Percent error $\frac{\lvert\Delta P_{actual} - \Delta P_{est}\rvert}{\Delta P_{actual}} \times 100\%$
Current	34.3	870	265	23.35%
Proposed	37.0	938	197	17.36%

3.1.3 Event threshold determination

The first time derivative of the frequency data is also useful in determining precisely where the sharp frequency decline first begins. Visual inspection of Figure 3.5 shows that the desired threshold should be very close to 59.98 Hz. Evaluation of the derivative on each frequency trace yields a set of *n* minimum $\frac{\partial f}{\partial t}$ values, where *n* is the number of reporting FDRs. At the time the first minima occurs, the rest of the frequency traces have not yet reached their maximum decline - in fact, some of them have not yet fallen from the pre-event frequency. Thus the median of each frequency trace at the time the first minimum occurs is determined to be the threshold for all subsequent TDOA calculations.

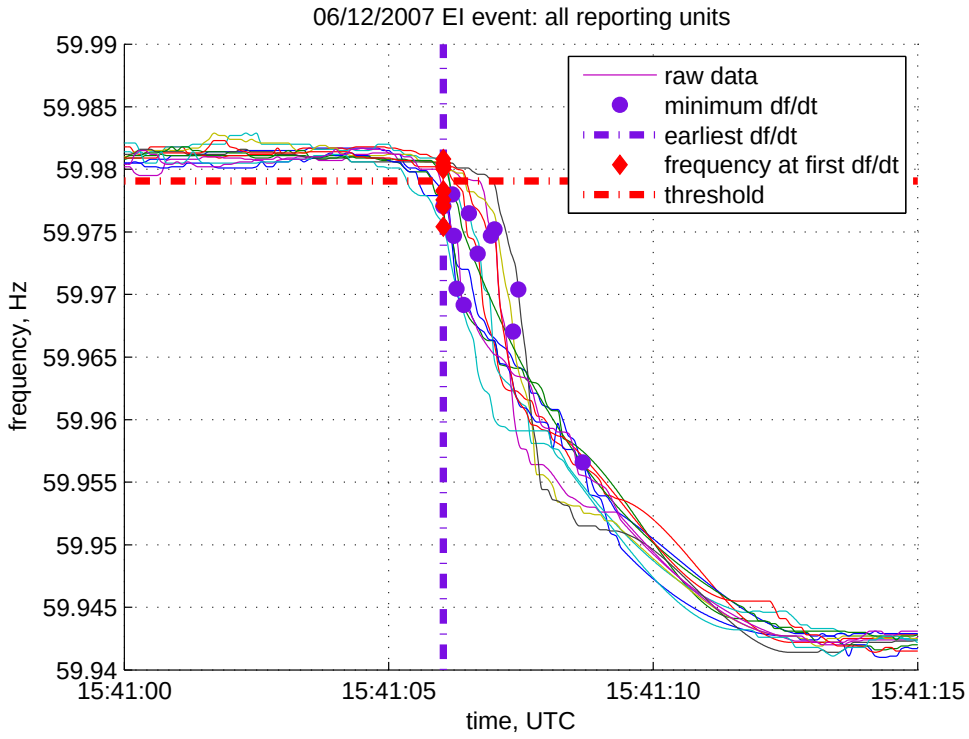


Figure 3.8. Frequency threshold determination

This approach is uniquely adaptable to events of any magnitude and data condition. The frequency decline during an event is always considerably sharper than any other time in grid operation, and as such is a consistent, sure sign of an event. Any traces with interpolated frequency values are ignored to avoid boundary conditions. Consequently the determination of the first occurring $\frac{\partial f}{\partial t}$ minimum is a straightforward calculation and the frequency threshold can be robustly determined at the beginning of the event signature. Figure 3.8 illustrates the threshold calculation for the base case. The process placed the threshold at 59.9791 Hz.

3.1.4 Crossing time calculations

Establishment of the frequency threshold makes threshold crossings trivial. Only downward crossings are considered, since generator trips always induce excess loading. The crossings for this base case are shown in Figure 3.9. Because sub-second differences are very significant in TDOA calculations given the typical wave propagation speeds, the data is interpolated from a sampling rate of 10 Hz up to a sampling rate of 60 Hz to provide more accurate threshold crossing times. Of note is the multiplicity of crossing times for several FDRs. Separation of these false positives will be accomplished using robust pattern recognition techniques.

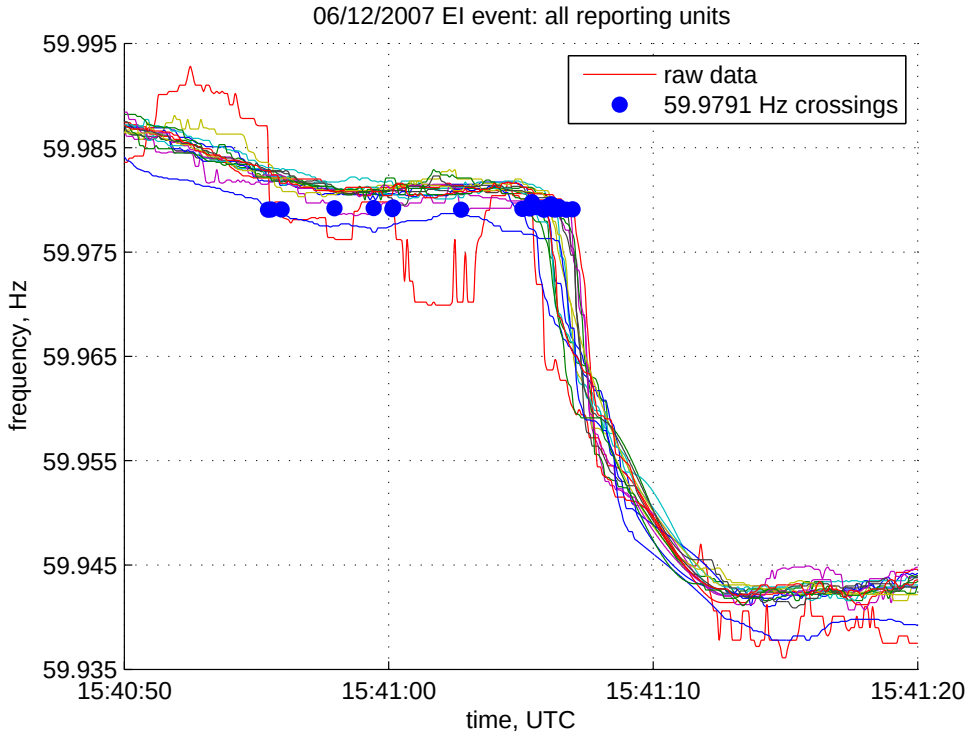


Figure 3.9. Threshold crossings

3.2 Pattern recognition and unsupervised learning

Pattern recognition is an extremely broad field with many different applications. Generally speaking, its beauty lies in its data-driven approach. Any problem can be solved with one system if the right data is supplied to the algorithm. Many times the system trains itself, so very little expert tuning is required. Of course, the beauty of such a system is also its curse. Finding the right combination of inputs, dimensions, and complexity tends towards being an art rather than a science. The case of event ordering can be represented by a one-dimensional problem, so many higher-order problems can be ignored.

With respect to power systems, the most commonly used pattern recognition system is the artificial neural network (ANN). These systems are most often paired with static network models to identify stability metrics such as synchronism,[84,85] Equal-Area Criterion,[86] and fault location.[87] Real-time applications include combinations of fuzzy logic and ANNs as situational awareness tools[88] or alarm triggers.[89] Direct applications of pattern recognition techniques to the scope of this report are extremely peripheral in context. Operators have made some use of expert systems in frequency regulation or Automatic Generation Control (AGC) software, using an ANN and stochastic modeling to determine Area Control Error (ACE) excursions.[90] Some utilities have used local measurements to generate a multi-dimensional feature vector that allows for quicker calculation of generator overvoltages.[91] Real-time (or pseudo-real-time) pattern recognition applications to wide-area frequency data, however, are non-existent.

The event ordering problem, re-phrased in the context of pattern recognition, is a feature extraction or edge detection problem. For each reporting FDR, which of its crossing times is a part of the actual generator trip signature, as opposed to those times created by noise or oscillations? The problem is not as simple as choosing the last crossing time for each FDR, because the presence of oscillations can mean the first crossing time is preferred (see Figure 3.4). Thus the relationship between FDR and its crossing time(s) is not a very useful one. The problem then reduces to a one-dimensional problem: given a set of times, like those from the base case and shown in Figure 3.10, which times are the correct ones?

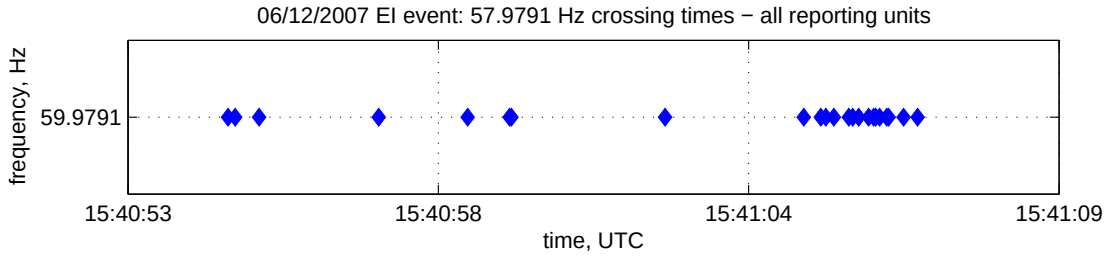


Figure 3.10. Feature space: crossing times

3.2.1 Supervised learning

Most classical pattern recognition techniques utilize probability and statistics to identify patterns in a data set. These techniques take on one of two primary forms: first, given a data set collected from a presumed distribution, estimate the parameters of that distribution. The Maximum-Likelihood approach used in Section 1.4 to justify the use of the moving median falls into this category. The second approach assumes the data is collected from multiple classes, each with its own distribution and known parameters. The goal is to specify criteria that separate the data into its appropriate classes while minimizing identification error. Because both of these methods utilize some *a priori* knowledge or assumptions about the data, they are considered supervised. Consider Figure 3.11, which shows the distribution of the base case's crossing times.

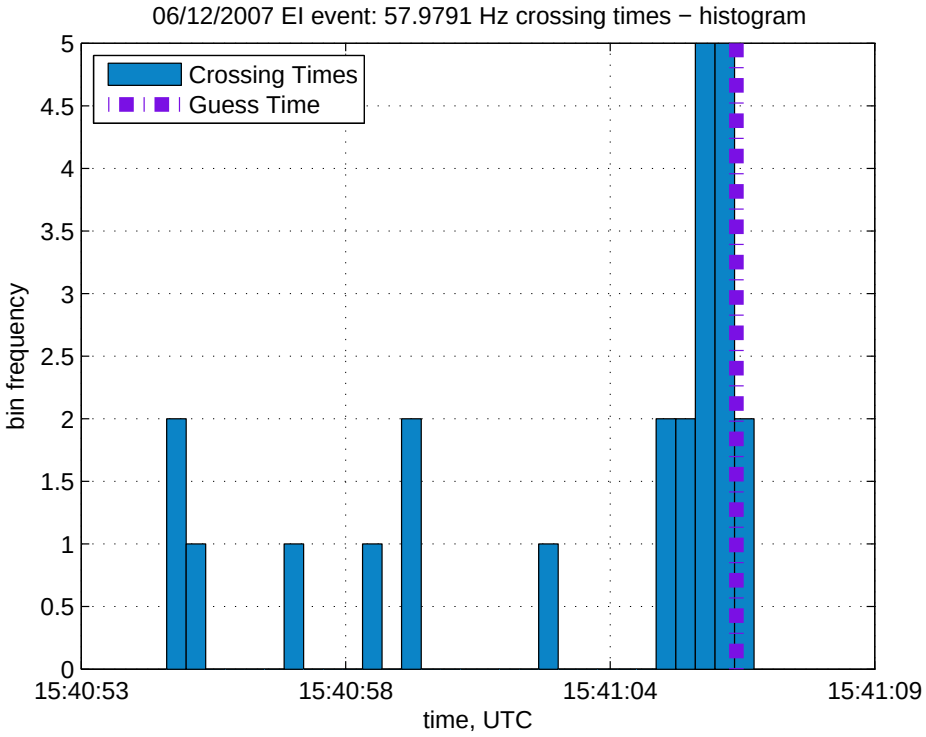


Figure 3.11. Histogram of crossing times

The first kind of supervised approach will not work for intuitive reasons. First, the data is not independently and identically distributed (i.i.d.) since there is no guarantee of multiple crossings. While it is known that each FDR will cross the threshold because frequency perturbations are globally visible, there is no physical constraint requiring multiple crossings to exist, much less take on any prescribed statistical form. Even if there was a way to predict the crossing time distribution, the distribution in and of itself does not provide a robust mechanism by which to ignore the false positives. There are enough outliers in the base case to detract even the median far enough from

the guess time that each FDR's time closest to the sample median would include some of the false positives and ignore some of the true crossings.

The second method suffers from some of the same problems. Consider Figure 3.12, which shows a two-class data set. Both classes are normally distributed with parameters

$$\mu_1 = \begin{bmatrix} 2 \\ 4 \end{bmatrix} \qquad \mu_2 = \begin{bmatrix} 6 \\ 8 \end{bmatrix} \qquad \Sigma_1 = \Sigma_2 = \begin{bmatrix} 4 & 3 \\ 3 & 9 \end{bmatrix}$$

Application of Bayes' Theorem can use the statistical properties of each class's distribution to describe a boundary that minimizes the probability of mistakenly assigning the wrong class to a data point.[92]

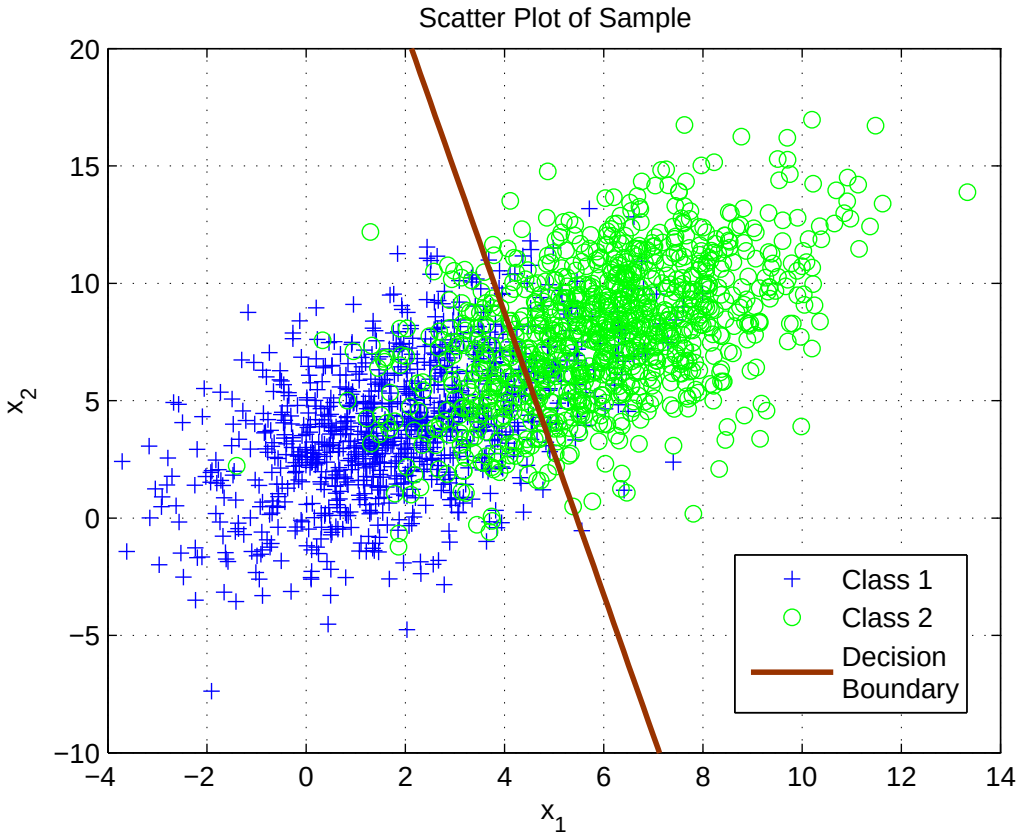


Figure 3.12. Supervised class divisions

While there could be some statistical description of the valid crossing times (normally distributed around the guess time would be a good first try), there is no consistent statistical model of the duplicitous crossing times. Moreover, the ordering algorithm requires a valid time from each reporting FDR. Given there are 17 reporting FDRs and 16 times in the mode surrounding the guess time, there is some overlap between the valid and false positive classes. While the Bayesian model

minimizes the class error, it does not guarantee elimination of false positives. If two crossing times from the same FDR are on the correct side of the boundary, this supervised learning technique does not accomplish the fundamental requirement to eliminate false positives.

To summarize, there is no good way to robustly eliminate false positives while assuming some statistical properties about the crossing time data.

3.2.2 Unsupervised learning

To contrast with supervised learning techniques, unsupervised learning makes no assumptions about a datum's class membership. At first glance, this seems like an impossible problem. Not only is nothing known about the data, but in theory nothing is known about end result! The number of classes and kind of class boundaries are unknown as well. While this approach may appear fruitless, there are reasonable motivations for these techniques. Chief among these reasons is cost. It can be incredibly expensive to record a labeled data set with which to train a supervised routine. In order to approximate the statistical distribution of the valid crossing time data, there needs to be a catalog of events that have been properly ordered. Given that events in the EI happen on average once every other day and only about 1 in 3 are industry confirmed, as well as he seasonal variations in system operation, the task of developing a statistically significant training set takes a lot of time. Moreover the argument could be made that the current event location algorithms are not refined enough to verify an event order is correct. Thus a paralyzing cycle is created where the LoD solutions can only be refined with better data, but not enough is known about the data to assert it should produce good results.

The absence of good data is further motivation for unsupervised learning. Like data mining applications, the amount and kind of information contained in a single trip signature is unknown. Thus the training process acts in reverse - unsupervised learning techniques cluster the data, and those clusters are then expertly refined to extract the most meaningful data.[70] Lastly, unsupervised learning is ideal for non-stationary data, because it allows for "adjust-on-the-fly" performance that adapts to seasonal load variations.

One of the most common types of unsupervised learning processes is *k*-means clustering. Given a set of unlabeled data, this process iteratively minimizes the distance of each point to its closest class center. This process is currently used towards such diverse applications as organization of peer-to-peer networks,[93] image analysis,[94] and protein sequencing.[95]

In this method, a number of classes, *k*, is assumed as well as a conforming number of class centers. Then the distance from each data point to each class center is computed, and each data point is assigned to the class with closest center. The center of each class is then recomputed; the class assignment and class recomputation is repeated until there is no change in the class centers.

K-MEANS provides the pseudocode for a *k*-means algorithm.

K-MEANS$(k, \mu = (\mu_1, \mu_2, \ldots, \mu_k), x)$

```
1  Initialize μ_old                                  ▷ (must be different from μ)
2  repeat
3          μ_old = μ
4          for i ← 1 to n                            ▷ (n=number of data points)
5                  for j ← 1 to k
6                          Compute distance from x_i to μ_j
7                  Assign x_i to closest class center
8          Recalculate μ
9  until μ == μ_old
```

As an example, consider the following set of two-dimensional data shown in Figure 3.13. This data was created from i.i.d. samples from two normal distributions:

$$\mu_1 = \begin{bmatrix} 6 \\ 1 \end{bmatrix} \qquad \mu_2 = \begin{bmatrix} 2 \\ 2 \end{bmatrix} \qquad \mathbf{\Sigma}_1 = \mathbf{\Sigma}_2 = \begin{bmatrix} 1 & 0 \\ 0 & 1 \end{bmatrix}$$

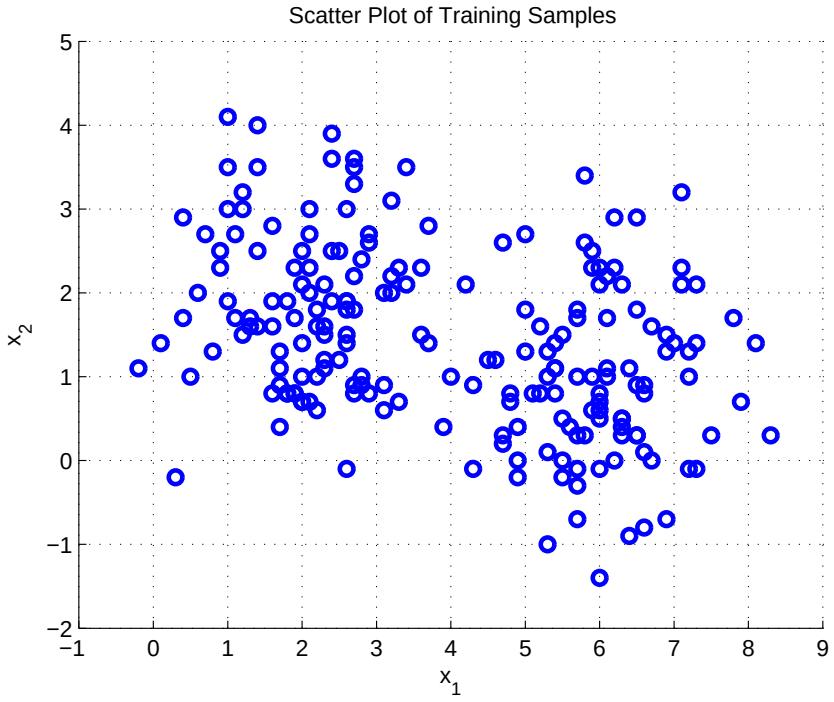


Figure 3.13. Unlabeled data set

The goal is to see if K-MEANS can properly find the class centers. Figure 3.14 shows the final class distribution, as well as each iteration's class center. Both centers started at the origin, and settled on their final locations in 5 iterations. The final locations were quite close the the actual distributions' centers:

$$\hat{\mu}_1 = \begin{bmatrix} 5.9566 \\ 0.9646 \end{bmatrix} \qquad \hat{\mu}_2 = \begin{bmatrix} 2.0604 \\ 1.8871 \end{bmatrix}$$

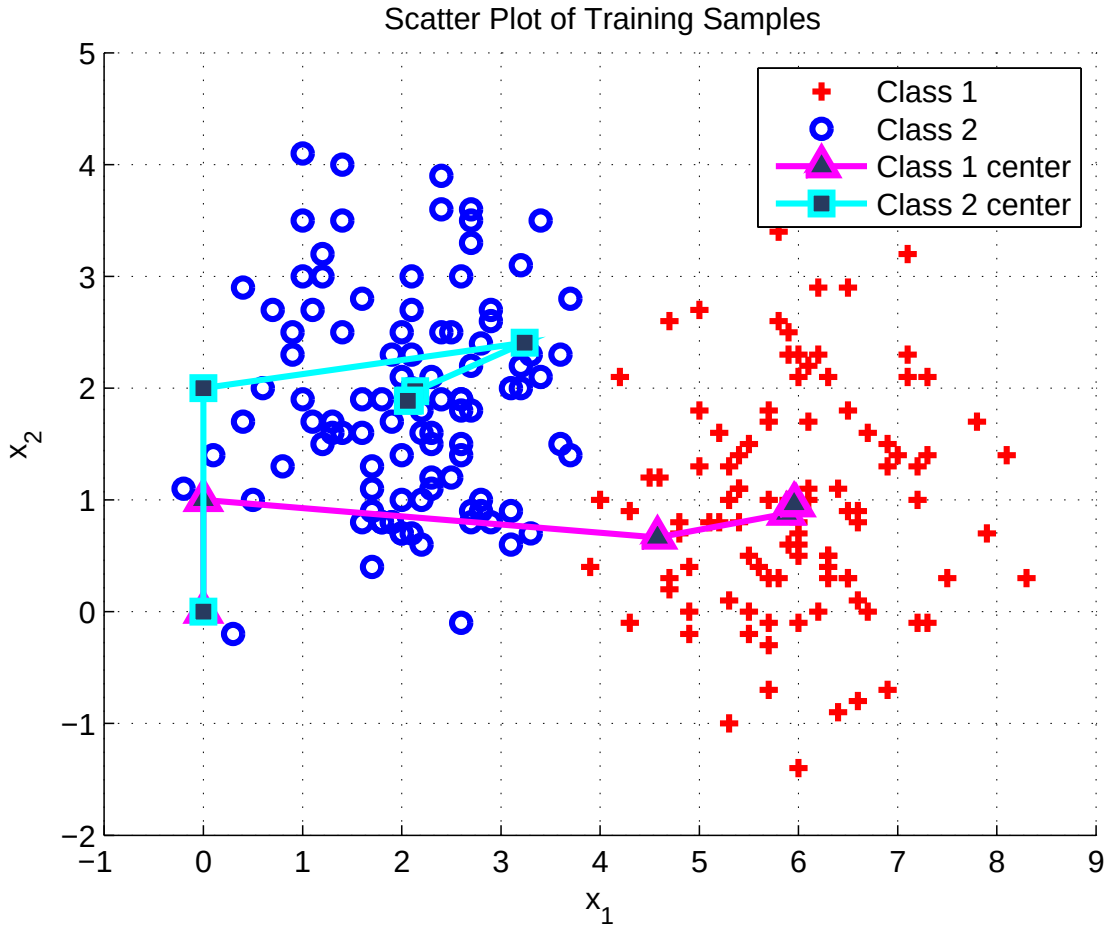
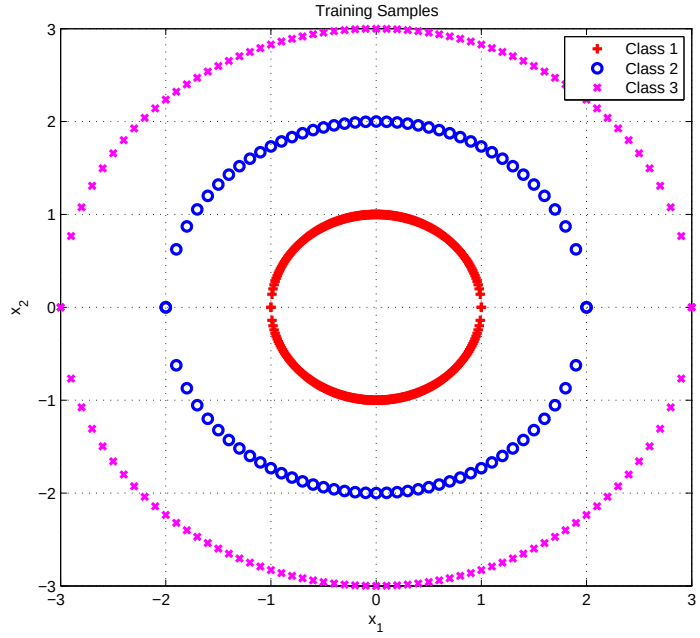


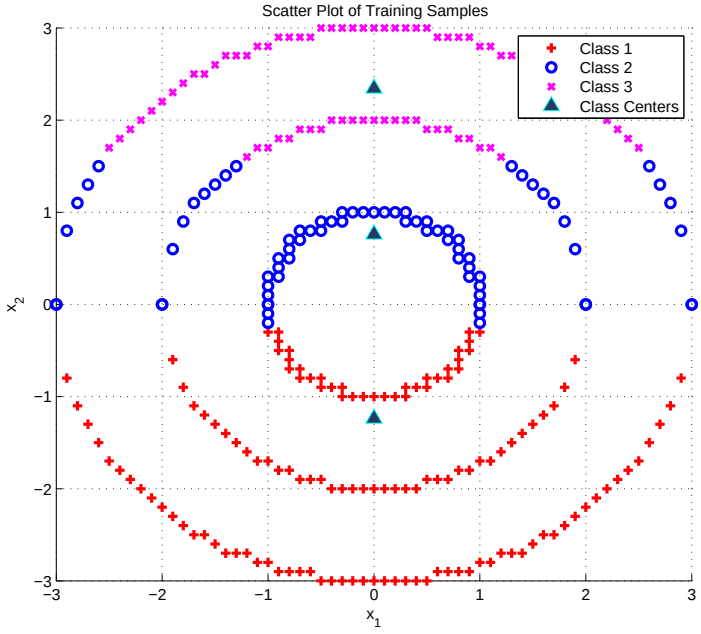
Figure 3.14. *k*-means clustering

Per the No Free Lunch Theorem,[96] there are some caveats to the use of K-MEANS. First is the choice of distance metric. While the name *k*-means implies the use of Euclidean distance since the mean minimizes the 2-norm[55], other distance metrics are able to be used. However the routine is still called K-MEANS for convenience. While the choice of optimal distance can be a difficult choice depending on the application,[97] it should come as no surprise by now that the robust *k*-medians is a preferred routine since it minimizes the L_1 or "city block" norm. Consider the three classes in Figure 3.15a. K-MEANS does not come close to identifying the correct classes (see Figure 3.15b)

because of the distance metric used.



(a) Actual data classes



(b) Calculated classes

Figure 3.15. Failure of *k*-means' distance metric

In addition to the distance metric, K-MEANS is also sensitive to the starting point of the class centers. The example of Figure 3.15 would result in different classes if the starting vectors were

different. The commonly accepted way to properly bias the starting vectors is by choosing the start points upon a preliminary clustering on a small subset of the data.[98] Finally, K-MEANS will force the data into as many classes as it is instructed to do, regardless of the size of the class. Figure 3.16 shows the same K-MEANS routine run on the sample data of Figure 3.13, but with an input of 4 classes instead of 2. As the number of desired classes exceeds the real number of classes, the routine's sensitivity on starting points becomes all the more pronounced.

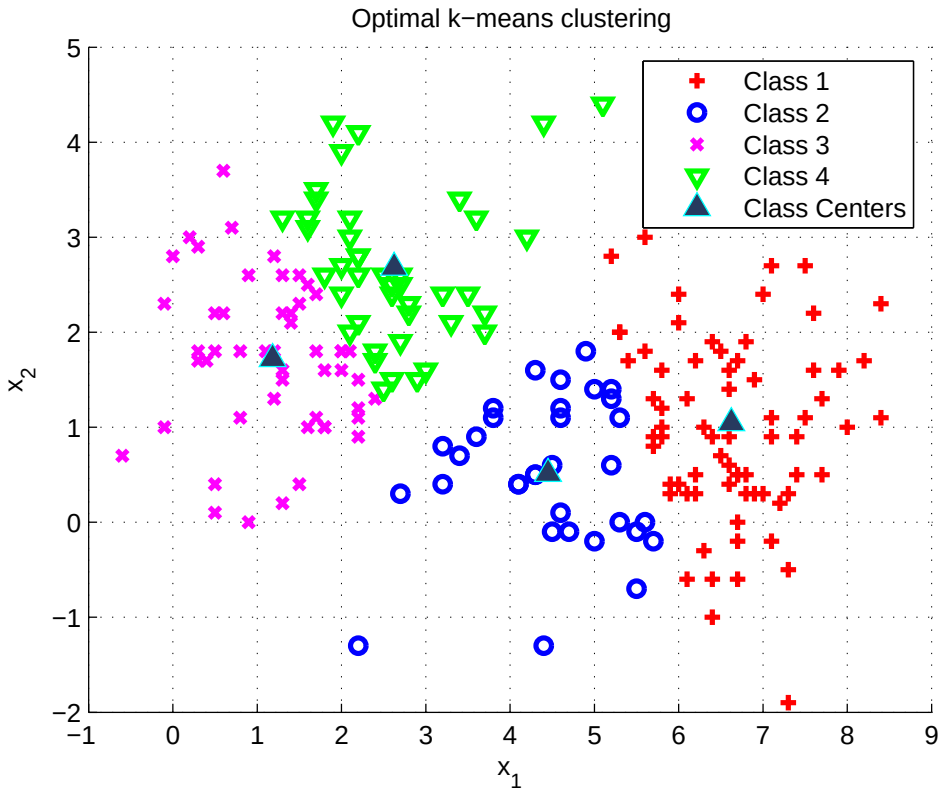


Figure 3.16. Division into too many classes

Figure 3.17 illustrates the application of *k*-means to the base case crossing data. The number of classes is limited to highest number of crossings recorded by a single FDR. The class whose center is closest to the estimated event time is determined to be the class containing at minimum all of the correct crossing times.

Use of K-MEANS to separate false positives from actual crossing data does not in and of itself guarantee one crossing time for each FDR. It merely identifies the time interval that contains all of the correct crossing times. If an FDR records only crossing time, and that time is so far away from the correct class that it is identified as a member of a different class, then that time is rejected as an outlier. Careful inspection of Figure 3.5 will confirm that one of these outliers is present in the base case.

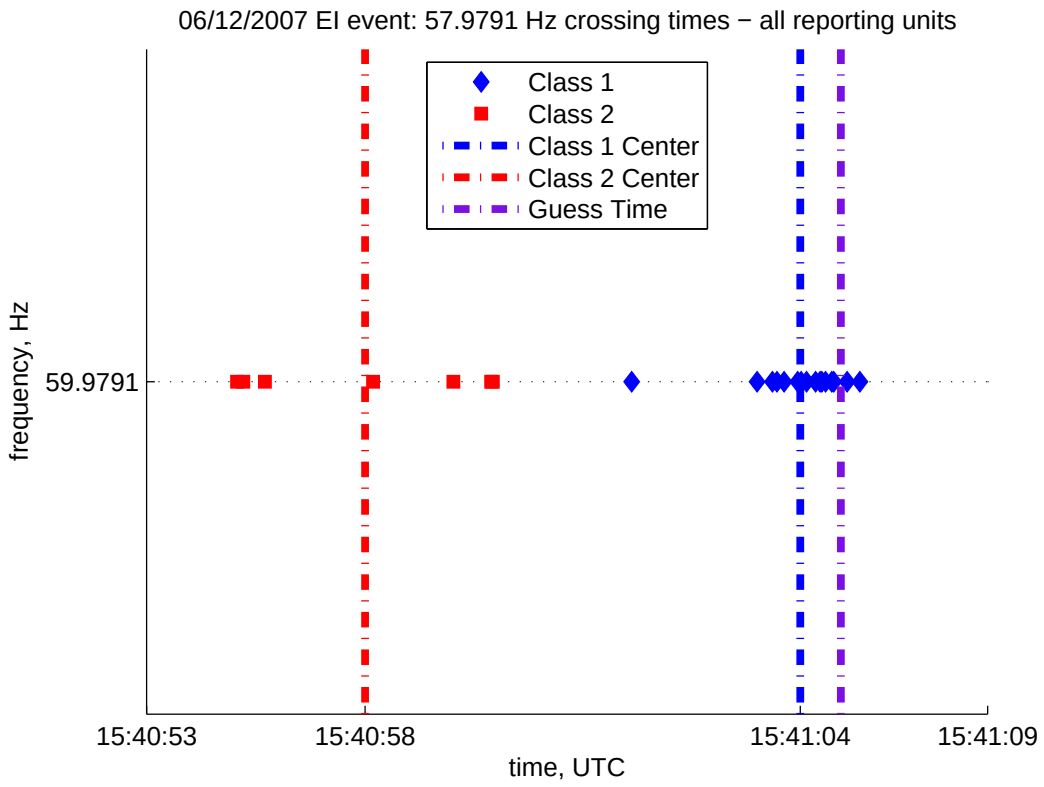


Figure 3.17. *k*-medians applied to FDR crossing data

3.2.3 Elimination of false positives

The elimination of false positives from the correct class is a two-step process:

- Remove duplicitous entries
- Remove outlier times

Selecting the correct crossing time out of several intra-class times from one FDR is determined by each crossing time's proximity to the class centroid and guess time. In general, the majority of FDRs will record one crossing per class. Therefore the centroid of the class will be attracted to those single crossings. In the case of multiple crossings, there is always one crossing time closest to the class center. This time is the correct crossing time, and all others are designated false positives. Figure 3.18 shows all of the members of the correct class sorted along the ordinate by recording FDR. In the base case, FDR 23 records two crossing times in the class. The time marked in blue is certainly farther away from the class center than the red time, so it is discarded.

Since the location of the class center is the determining factor in separating false positives, it is imperative that the class center time is is not attracted to any outlier times. Consider all of the

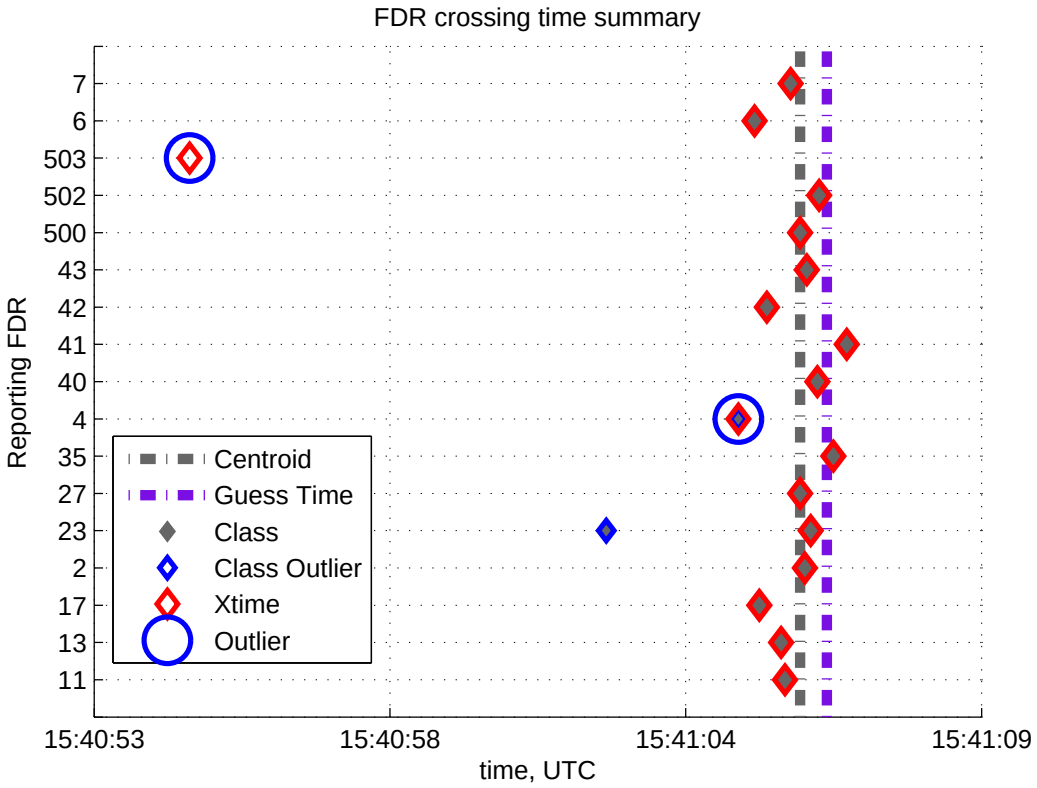


Figure 3.18. Elimination of false positives

class members (in gray) in Figure 3.18. There are two outlier times belonging to FDR 23 and 4, respectively. The crossing time recorded by FDR 503 is actually a member of another class and thus is automatically rejected. If there were a few other outliers, calculating the median of all of the class members would attract the class center towards the outliers, thus making it possible for outlier times like that measured by FDR 23 to be identified as the actual crossing time. Such a mistake would be detrimental to TDOA calculations, so any outlier times are ignored in the determination of the class centroid.

Outliers are identified by the robust median-absolute-deviation, or MAD. The MAD is defined as the median of the residues of each sample in the vector $\mathbf{z}$:

$$\text{MAD} = \text{median}\left(\mathbf{z} - \text{median}(\mathbf{z})\right)$$

The MAD is a predictor of the standard deviation, and since outliers are defined as those points being more than one standard deviation away from the median, a data point z_i is an outlier if it satisfies the following inequality:[55]

$$\frac{|z_i - \text{median } \mathbf{z}|}{\text{MAD}} > 2.57$$

Such outliers, such as the values outlined or circled in Figure 3.18 are not included in either the TDOA or the class centroid calculations.

3.3 The leverage of event ordering

Figure 3.20 shows the results of the event location algorithms when given each ordering method. The yellow hexagram shows the actual event location, and the stars show the old (white) and new (magenta) LS hypocentral estimates. The surface is the approximated hypocentral probability density determined by the Parzen windowing approach. The quantiles of each of the three points of interest are also shown. Obviously the new ordering method works well in this case. An interesting difference between the two maps is number of reporting sensors. While there were only two more (15 compared to 13) sensors used in the new calculations, there are a total of 10 different locations between the two methods. Since only 8 of the 15 sensors used in the new method are also present in the old, it is not surprising that the two hypocentral densities are quite different.

From a heuristic perspective, the old ordering method suffers from the first responder acting as a leverage point. Since the first unit (Jackson, TN) is well west of the true location, the half-planes created by subsequent responding FDRs (which are in fact relatively close to the actual location) pull away from the event location. To contrast, the new ordering method was able to identify one of the closest, most easterly reporting sensors as the first responder. Thus the consequent half-planes are all attracted to the true location instead of away from it.

The analysis on each of the 55 test cases are located in Appendix D. For each event, the order, mismatch, and LS and half-plane event locations were run for both old and new ordering methods. The error for each of these calculations (MW_{error}, LS_{error}, and Q_{actual}), as well as the change in error from one ordering method to the next (ΔMW_{error}, ΔLS_{error}, ΔQ_{actual}) was tabulated and is reported in Table D.1.

There are some common error metrics used in these error calculations. Since these are location estimates, similar results are not discouraged. If, for instance, one ordering method yields a quantile $Q = 0.857$ and the other $Q = 0.803$, the two methods can be said to have equivalent performance. In other words, an event location estimate is considered superior to the other only if its result is considerably better. In the case of the half-plane approach, a difference of $|\Delta Q_{actual} > 0.15|$ was considered significant, while in the least squares case, a difference of 200 miles was considered notable. Since the catalog of 2007 events is limited to generator trips in excess of 500 MW, a superior mismatch calculation must be at least 50 MW better than the other for note. These con-

straints also provide an objective basis from which to define “equivalent or better performance.” Justification for adding a new routine to an already busy server must not only guarantee better performance for some cases, but also ensure that the new method will consistently perform well. In the case of these ordering metrics, the new Parzen location estimate met or exceeded the old estimate in 36 (65.45%) of the time. Likewise in 61.82% of the cases the new LS estimate performed at least as well as the old one. Finally, the new mismatch calculations were at least as accurate as the old 80% of the time. Thus these methods do not only perform better than the old ones, but they do so consistently.

Compared to the LS approach, the Parzen location estimates show considerable robustness for two reasons. First, there are no velocity models with errors to minimize, so there are no convergence problems that result in the common failures in both LS estimates. Second, there are equal numbers of clearly superior and inferior cases, so the method seems to be able to give acceptable results for a wide range of ordering estimates. This is of great benefit since ordering algorithms are still very much in the embryonic stage.

Table 3.2. Ordering method comparison: Belews Creek U1 (1135 MW, 36.3189°, −80.1484°) Trip on 6/12/2007 15:41:06

	Old Ordering Method			New Ordering Method		
Mismatch estimate (MW)	870			938		
FDR Info	Number	Name	Distance (mi)	Number	Name	Distance (mi)
	17	TVA4Jackson	487.4798	6	ABB	89.9991
	6	ABB	89.9991	17	TVA4Jackson	487.4798
	4	VT	65.0139	42	FSU	473.1360
	9	UFL	476.2479	13	MidwestISO	410.3671
	42	FSU	473.1360	11	Calvin	544.2142
	7	MISS	529.6149	7	MISS	529.6149
	13	MidwestISO	410.3671	27	RPI	561.2972
	506	OhioTiffin	366.6413	500	Chicago	550.7249
	11	Calvin	544.2142	2	UMR	649.2997
	500	Chicago	550.7249	43	Bismarck	1283.6
	2	UMR	649.2997	23	Duluth2	949.0917
	503	Danbury	499.6008	40	MISOStPaul	904.5295
	27	RPI	561.2972	502	Toronto	525.7908
				35	ISU	821.1267
				41	Winnipeg	1259.0
LS estimate	Latitude	Longitude	Distance (mi)	Latitude	Longitude	Distance (mi)
	42.0295°	−88.6386°	601.5190	35.4220°	−80.8647°	73.8124
	$Q_{old} = 0.3832$			$Q_{old} = 0.1947$		
	$Q_{new} = 0.0582$			$Q_{old} = 1.0000$		
Parzen windowing results	$Q_{actual} = 0.1139$			$Q_{actual} = 1.0000$		

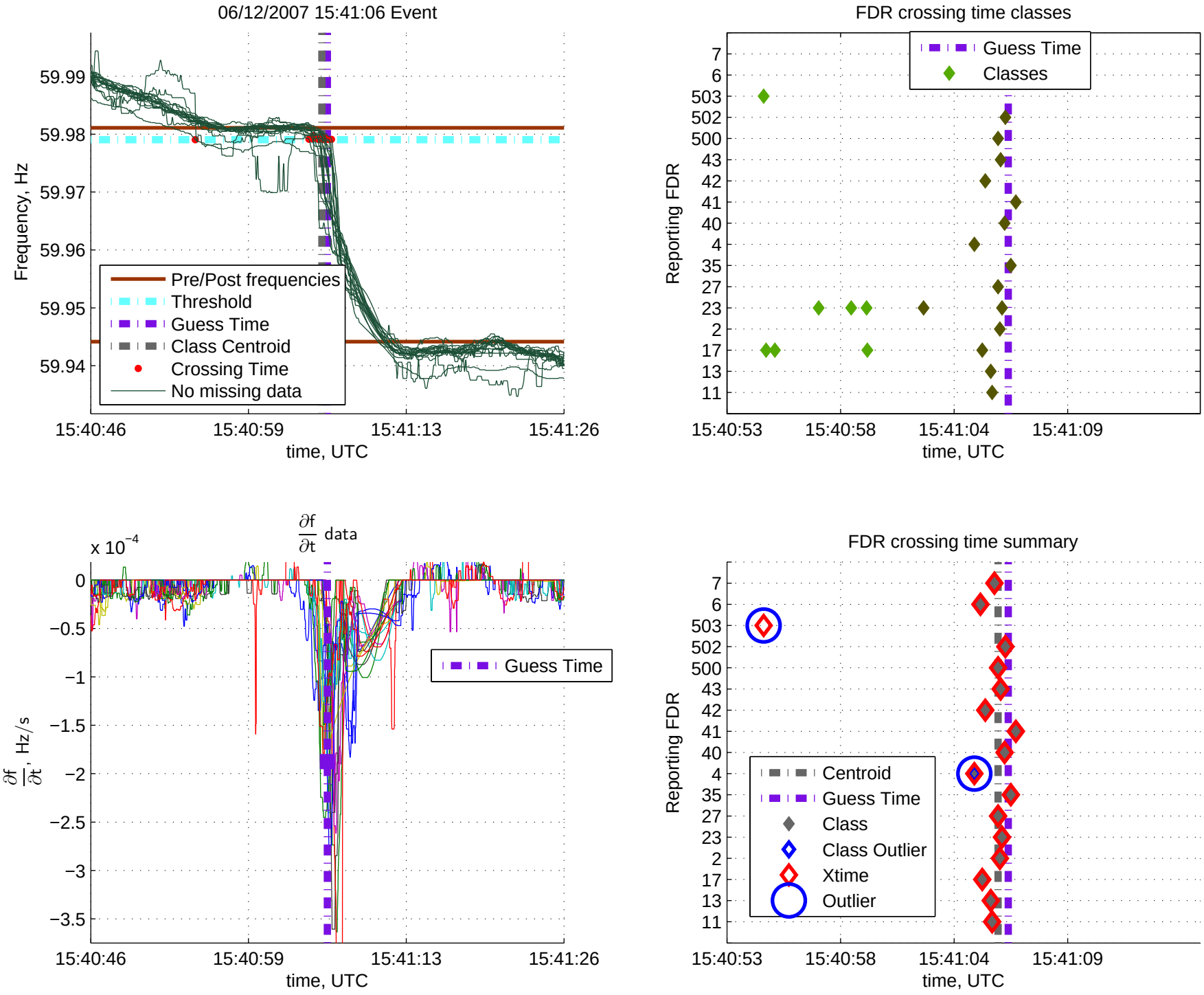
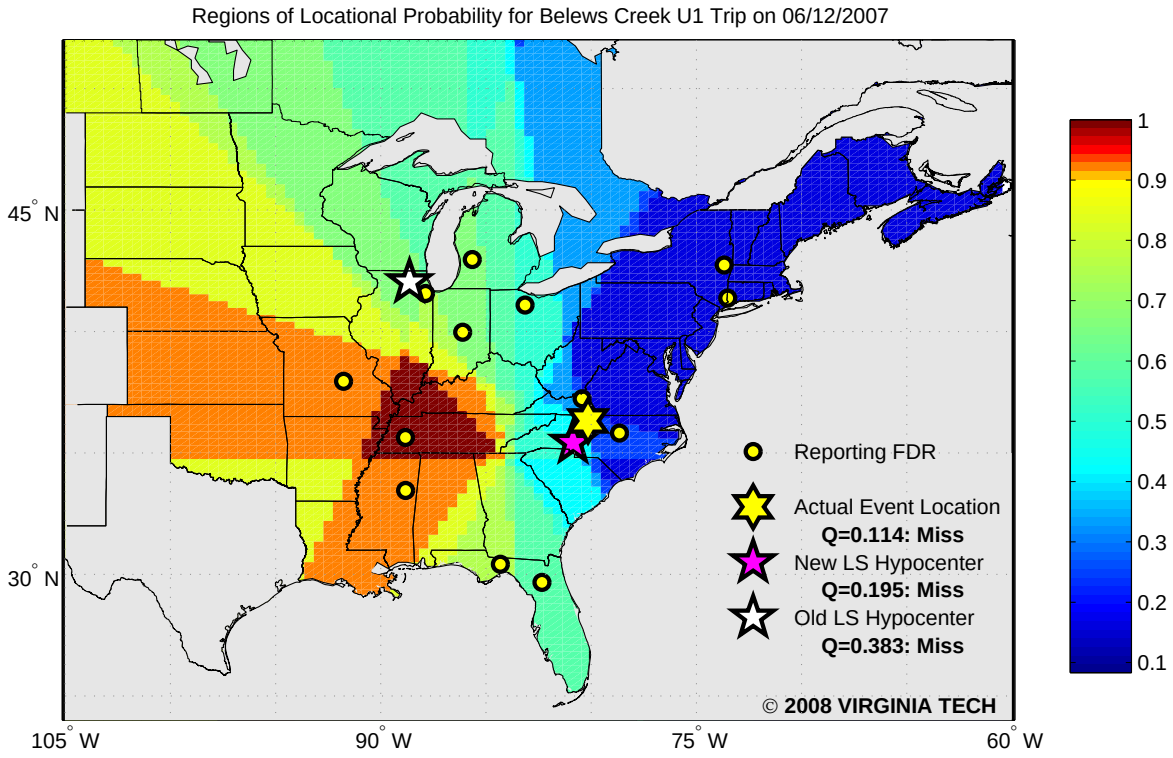
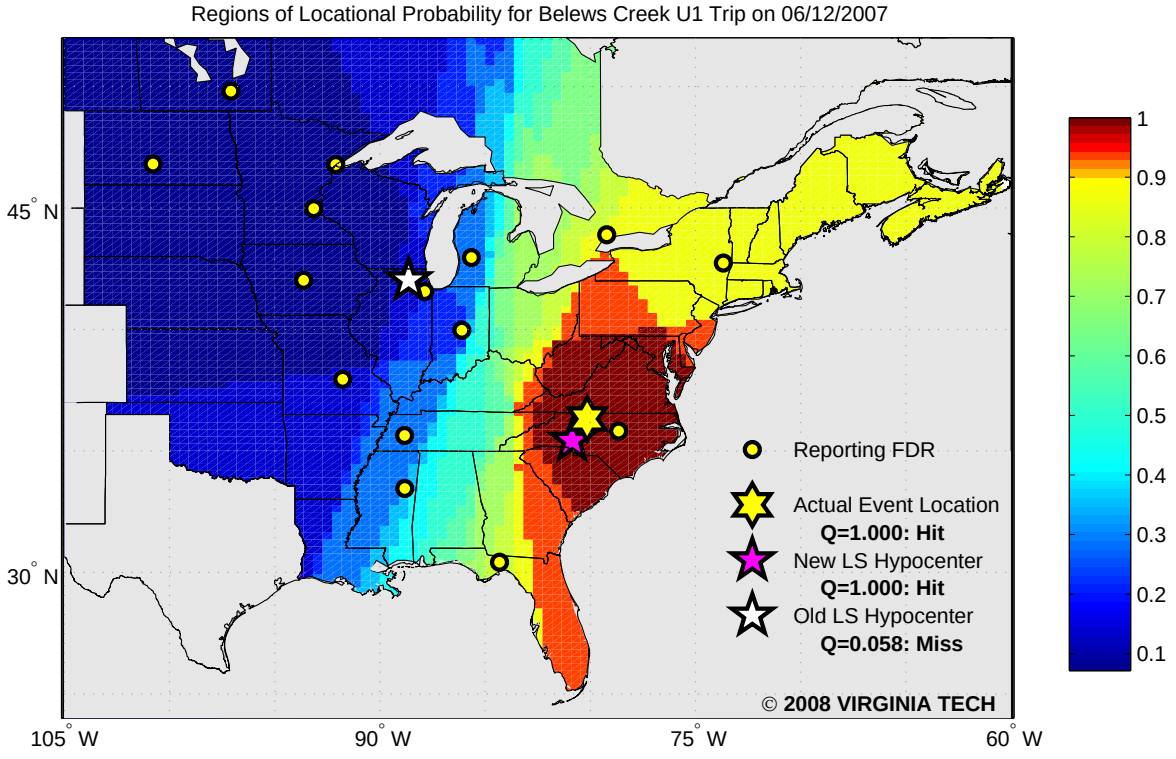


Figure 3.19. Consolidated event ordering calculations



(a) Event location: old ordering method



(b) Event location: new ordering method

Figure 3.20. Application of event ordering methods to event location

Chapter 4

Distributed frequency measurements and oscillation control

The ability to place FDRs at any place throughout the electric grid gives the FNET system an unprecedented vantage point from which to monitor inter-area oscillations. Naturally, the desire is to use wide-area frequency measurements for more the monitoring purposes. Since FNET can see power system events as they develop, can FNET data be successfully used to mitigate oscillations that may arise in the system?

4.1 An example system

To test the efficacy of using FNET measurements to control oscillations, consider a standard four-machine, two-area power system as shown in Figure 4.1. This system is a standard small-signal stability test case.[6,99,100] In steady-state operation, Area 1 (in red) supplies Area 2 (in blue) with 413 MW of power. Appendix E details the specifics of the system.

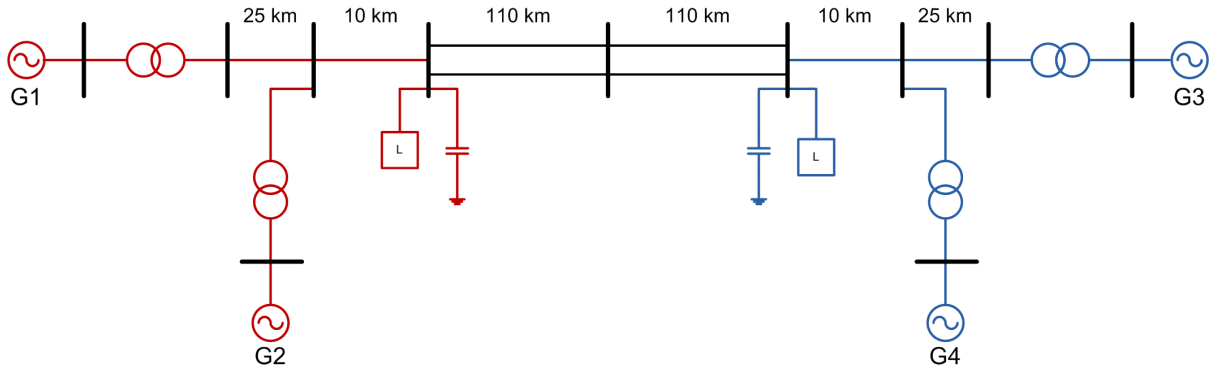


Figure 4.1. Sample two-area simulation system

This system was created[6] to simulate small-signal stability analysis techniques, and so each of the two areas' generator inertias and loads are chosen to cause a naturally undamped inter-area oscillation with natural frequency $f_n = 0.64$ Hz, as shown in Figure 4.2.

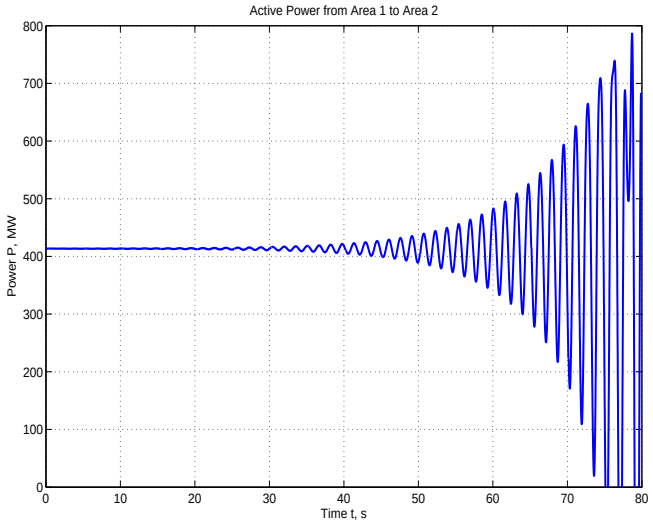
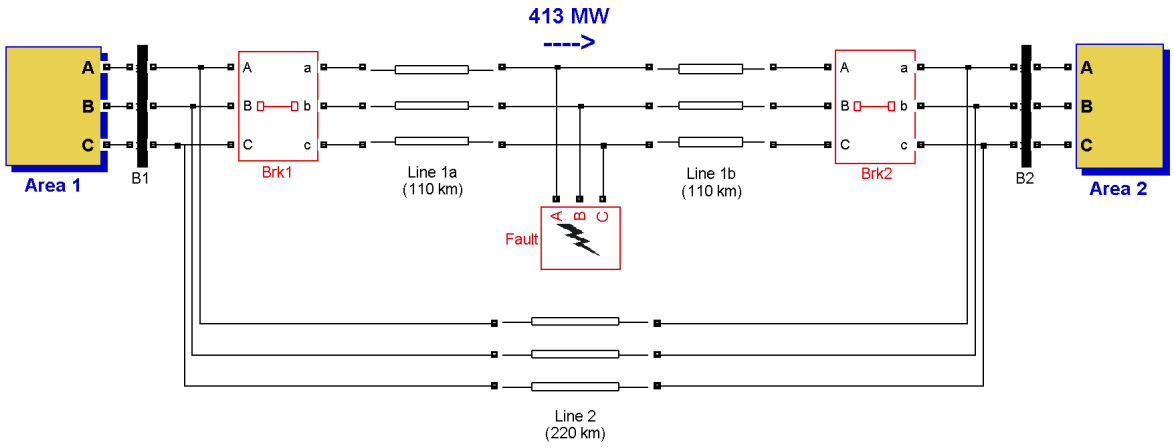


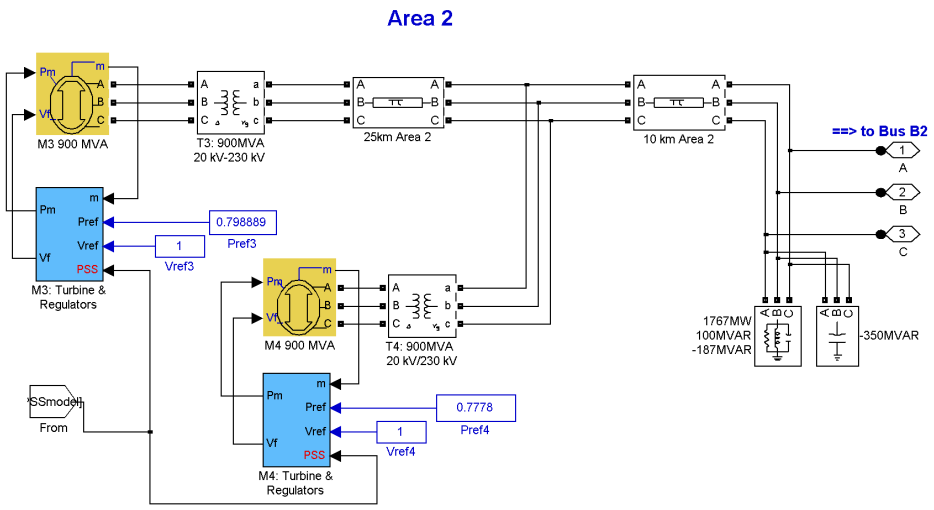
Figure 4.2. Sample two-area simulation system: Natural oscillation

The system was built using the MATLAB™ simulation tool Simulink™ with special library SimPowerSystems™ as shown in Figure 4.3.



(a) Original system

Figure 4.3. MATLAB™ simulation diagrams

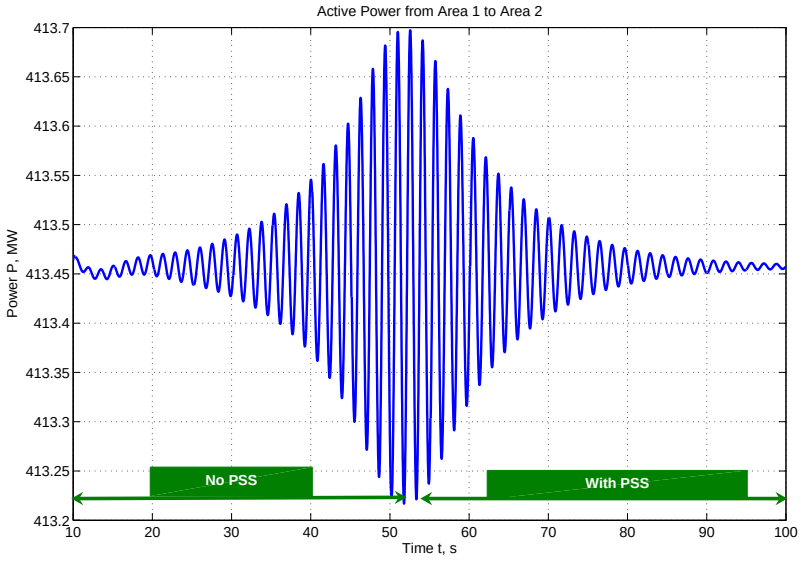


(b) One of the two areas

Figure 4.3. MATLAB™ simulation diagrams (continued)

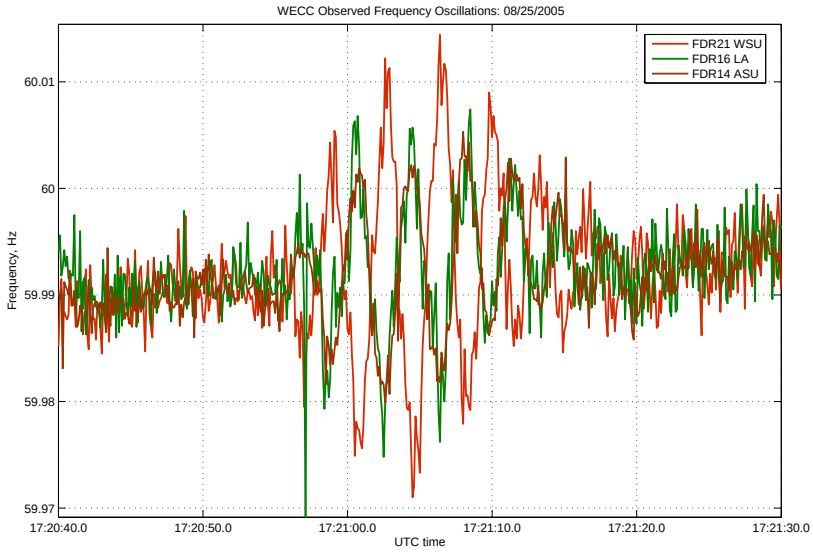
4.2 Addition of power system stabilizers

Undamped oscillations almost never arise in practical operations; to make this example more realistic, the generator controls were modified to create a stable oscillation. In this case, power system stabilizers (PSSs) were used to create an oscillation that grew and then decayed, to mimic recorded data. Figure 4.4a shows the stable simulated oscillation, and Figure 4.4b shows some frequency measurements that illustrate the realistic nature of the simulated oscillation.



(a) Sample two-area simulation system: stable oscillation

Figure 4.4. Simulated and Observed Oscillations



(b) Typical Frequency Data During Oscillation

Figure 4.4. Simulated and Observed Oscillations (continued)

Power system stabilizers modulate the excitation voltage of a generator to damp out oscillations, and have long been used in the damping of local oscillations.[101] In this example, the simulation was started without any PSS active. Once the inter-area power oscillation reached a certain magnitude, the PSS began to act and damp out the system. In this way, the oscillation was allowed to grow before it decayed. This kind of oscillation can be attributed in practice to the incorrect tuning of generators' excitation systems.

4.3 Inclusion of a HVDC link

This system was then modified by adding a model of an HVDC line in parallel with the AC tie line already connecting the two areas, as illustrated in Figure 4.5. In the context of this exercise, an HVDC line is a conceptually straightforward quantity to model. Because of the inverters and rectifiers on each end of the line, the DC tie acts much like a stiff rod in a mechanical system - it can push and pull electrical power at will. Therefore, the HVDC line should in principle be able to damp out the inter-area oscillation by pushing and pulling electrical power between areas.

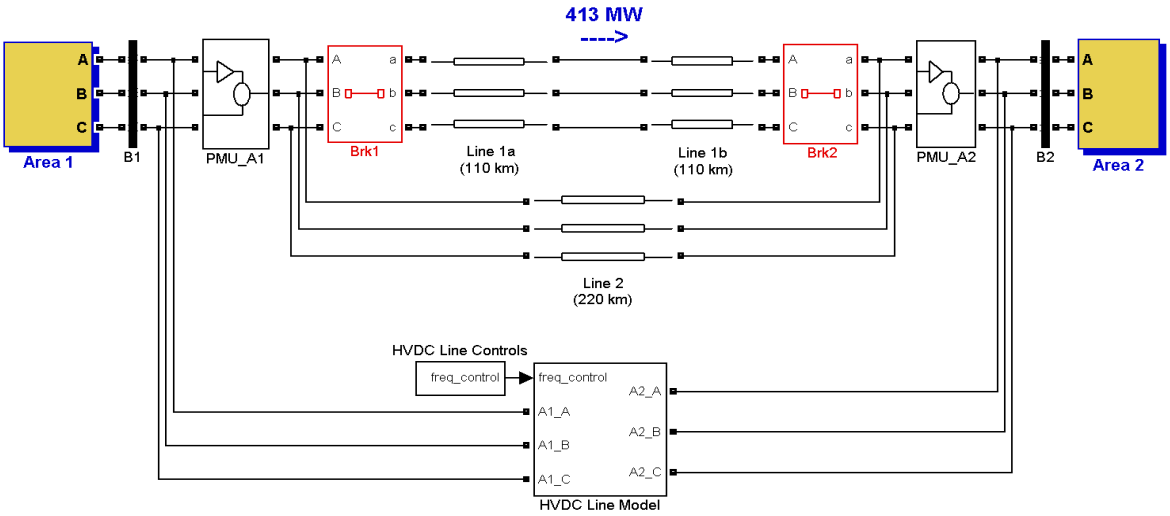


Figure 4.5. Addition of HVDC inter-area link

The HVDC line model took as an input a weighted sum of the frequency measurements in the system. In this case, with only two areas, there were only two frequency measurements, so both measurements were weighted equally but with opposing signs. Therefore, the power flow on the HVDC line was proportional to the difference between the frequency measurements. Since frequency is analogous to power mismatch, the inter-area frequency difference (and consequently the power flow on the DC tie) is proportional to the power mismatch between areas, as shown in Figure 4.6.

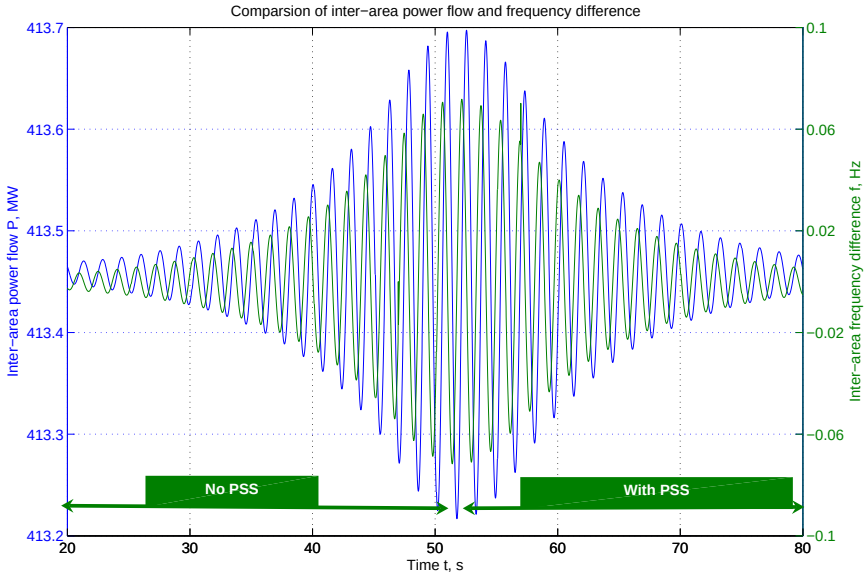


Figure 4.6. Relationship between power mismatch and inter-area frequency difference

This configuration is very similar to the topology of the WECC, where separate areas (located at population centers) are interconnected by AC and DC corridors, like the Pacific DC Intertie connects the Pacific Northwest with Southern California (see Figure 2.23). In fact, this topology, in contrast with the more homogenized EI, behaves much like a mass-spring system, where the corridors act as the springs connecting the load centers, as illustrated in Figure 4.7.[5]

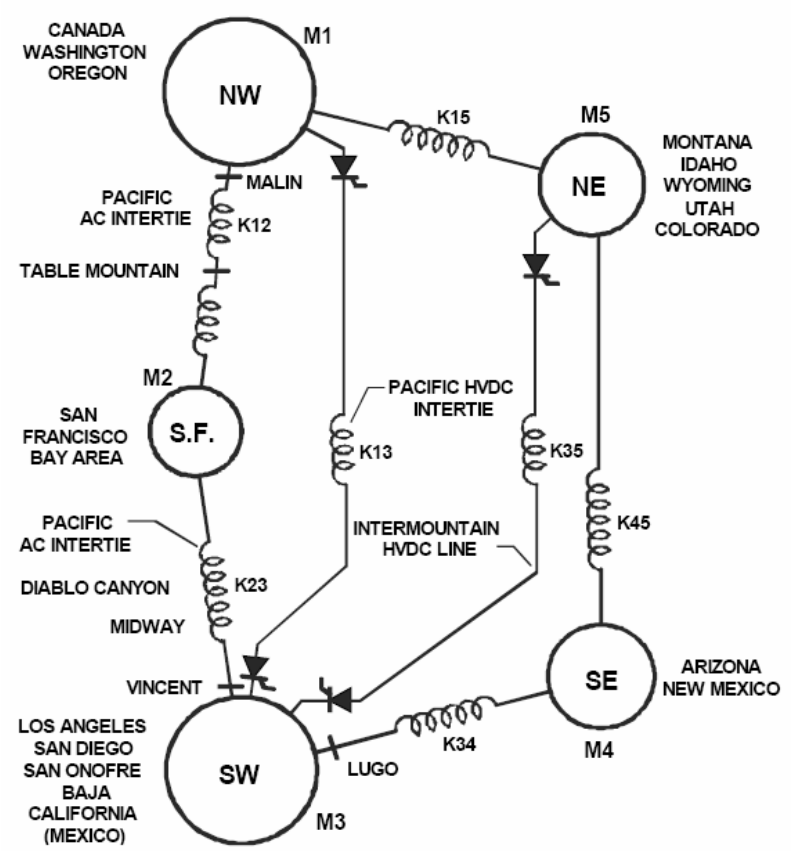
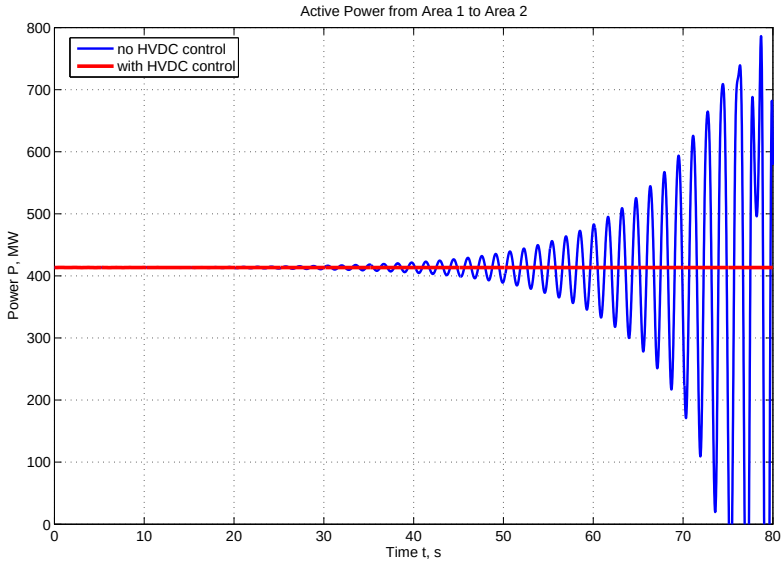


Figure 4.7. Modeling the WECC as a mass-spring system[5]

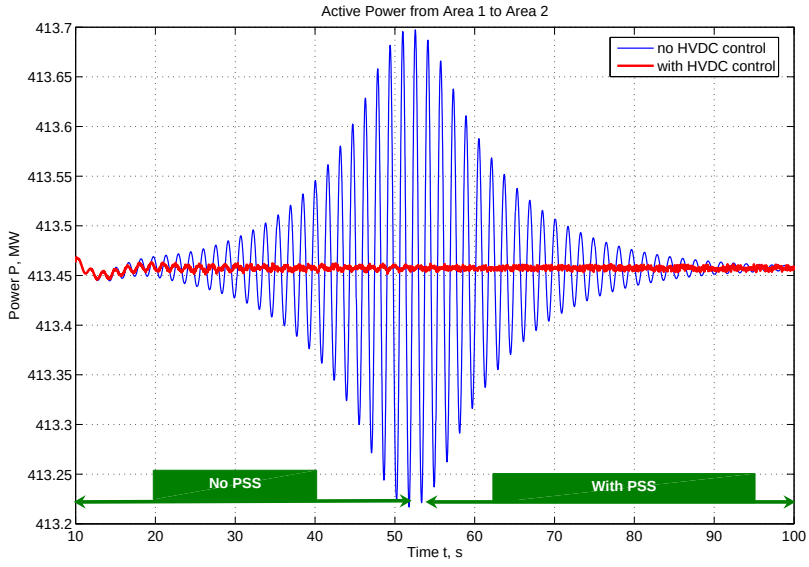
The application of the mass-spring analogy, which is common to many other physical systems, encourages the use of many well-established control strategies used in other fields. The most relevant of these strategies is the use of direct velocity feedback in large space structures, first proposed by Balas in 1979.[102] In the case of power systems, the collocated accelerometer and damper are equivalent to the FDR (which measures angular velocity) and HVDC line. One notable benefit of the construction of a collocated actuator-sensor system is that the control action is guaranteed not to destabilize the system. Much like a physician, the first axiom of managing such a large power system should be "first, do no harm." In like manner, the application of collocated techniques to the power system guarantee continued stability.[103,104]

4.4 Performance of the modified system

The HVDC line proved to be a very effective method to damp out oscillations, as shown in Figure 4.8, eliminating the interaction regardless of PSS action. The DC tie modulated the inter-area power flow to mitigate the power oscillation between area generators. Thus it is possible to use wide-area measurements to mitigate power system oscillations.



(a) HVDC control of undamped oscillation



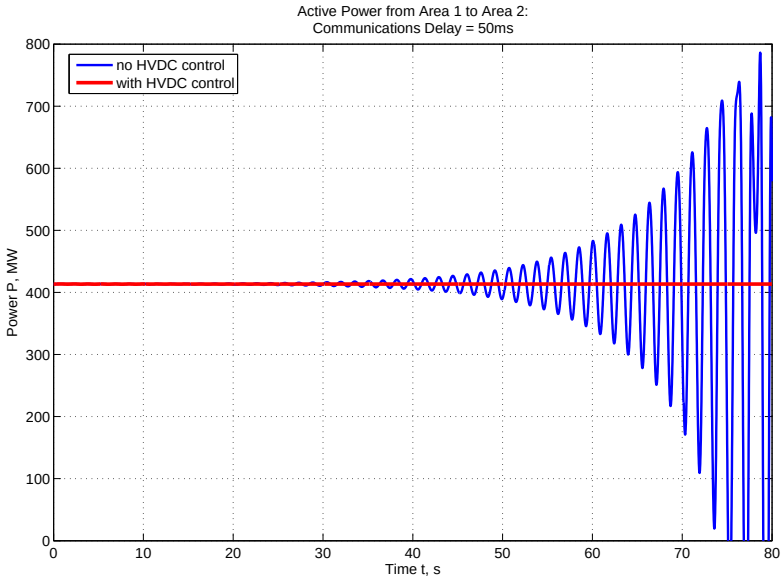
(b) HVDC control of damped oscillation

Figure 4.8. HVDC oscillation control using wide-area frequency measurements

4.4.1 *Mitigation*

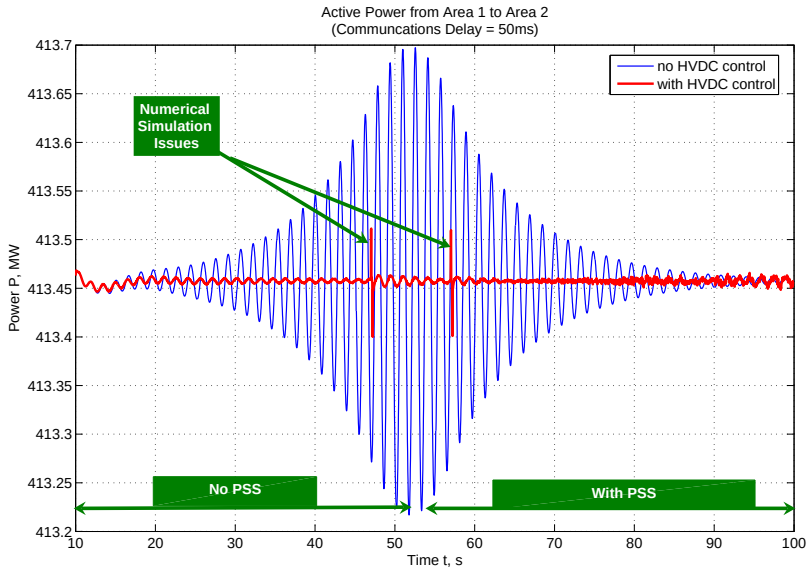
While the internet is a sufficient data transport mechanism in research applications, any control applications of distributed measurements will utilize existing dedicated communications networks. While utilities still maintain microwave (and more broadly analog) networks for legacy and emergency purposes (just like telecom companies still have an order wire), any wide-area measurement systems utilize fiber-optic communications.[105] While local control schemes utilize truly instantaneous feedback signals, the geographic dimensions of the North American interconnections introduce appreciable communication delay. It is commonly accepted that the maximum one-way communications delay does not exceed 50 ms,[105] and the total measurement, calculation, and transport delay in a fiber-optic system is typically 70 ms.[106]

Given the sub-second propagation speeds of power system events, there is concern that orders of this delay are detrimental to the inclusion of wide-area measurements in oscillation control schemes. Thus a variable time delay was introduced to the simulated system. Figure 4.9 shows the successful damping of the same oscillations with the addition of 50 ms communications delay.



(a) HVDC control of undamped oscillation

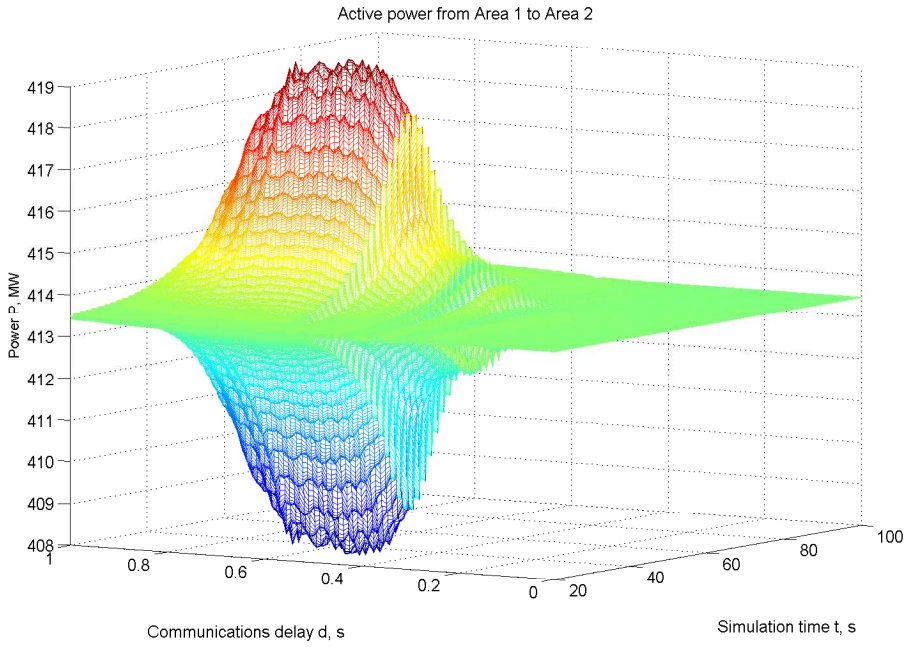
Figure 4.9. HVDC oscillation control using wide-area frequency measurements with time delays



(b) HVDC control of damped oscillation

Figure 4.9. HVDC oscillation control using wide-area frequency measurements with time delays

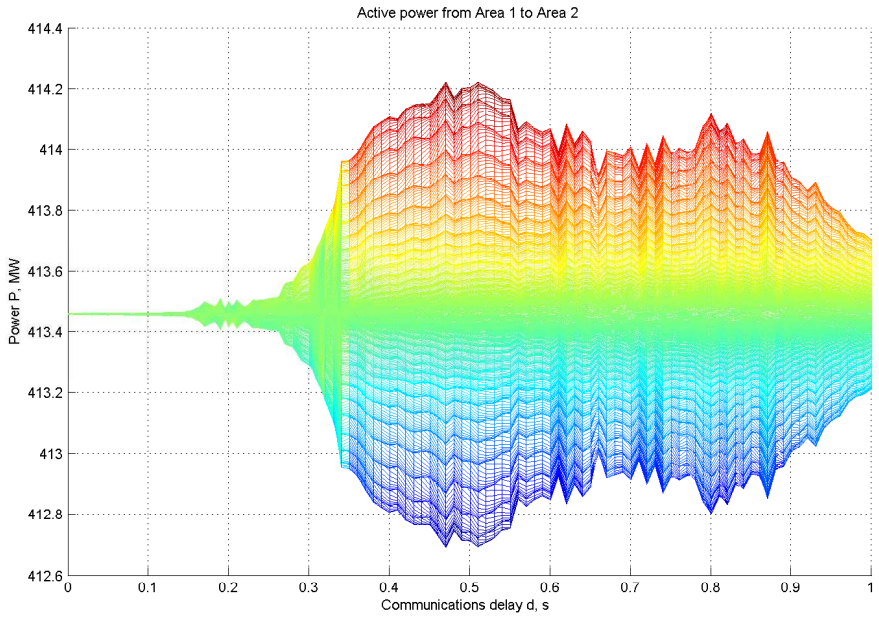
While this delay does not degrade the controller's success, too much delay will cause the control scheme to fail. Figure 4.10 shows the results of simulating the system for each iteration of communications delay from 0 to 1 s.



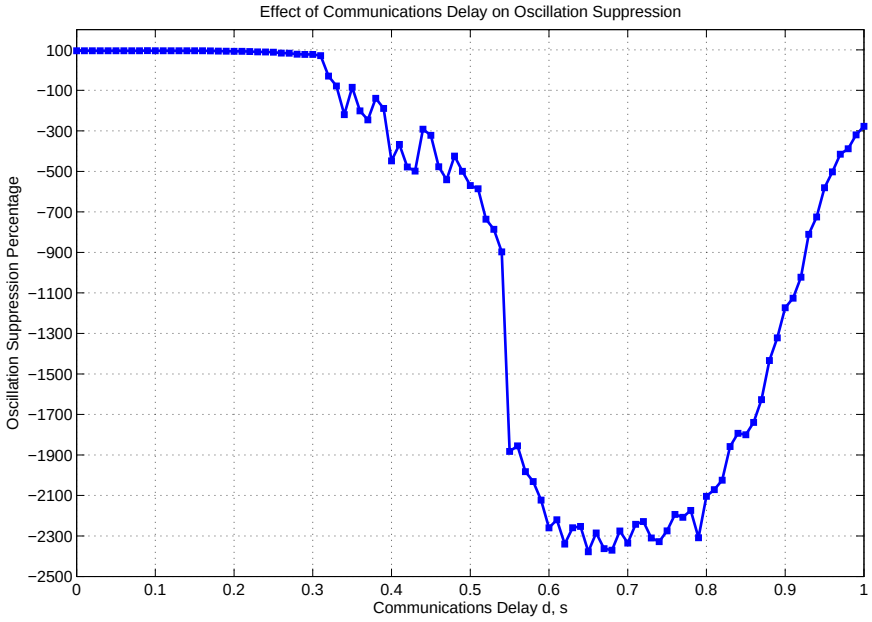
(a) Delay sweep from 0 ⟶ 1 s

Figure 4.10. Variable transport delays and oscillation mitigation

Figure 4.10b shows the maximum oscillation magnitude as a function of the delay time. While small delays do not diminish the damping effect, the oscillation begins to be noticeable at delays around 150 ms and actually exceeds the original oscillation magnitude just past 300 ms.



(b) A second view



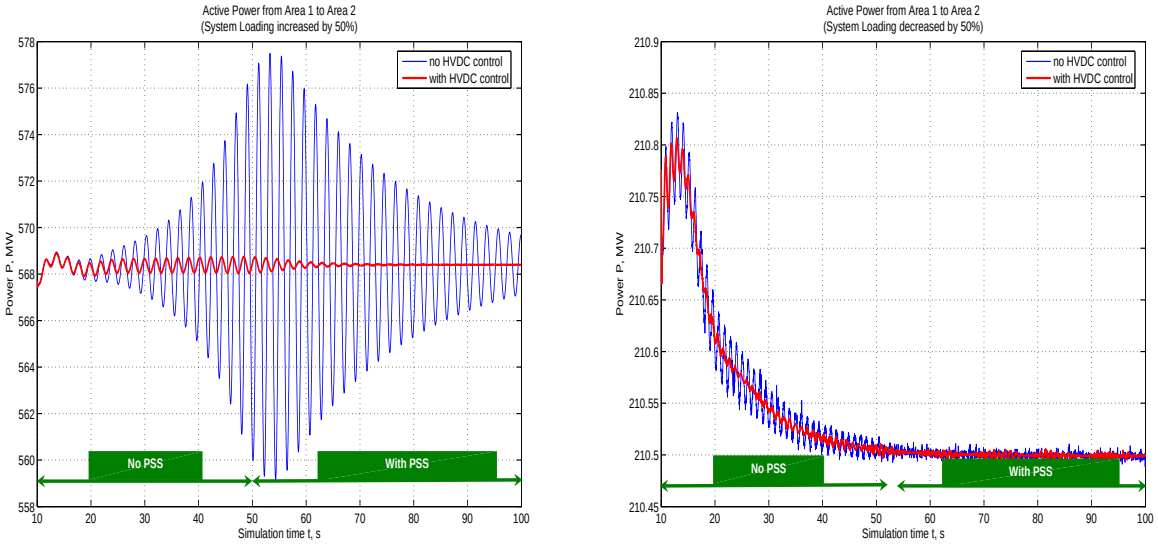
(c) Percentage suppression

Figure 4.10. Variable transport delays and oscillation mitigation (continued)

Figure 4.10c shows the effect of communications delays in terms of damping percentages. As illustrated by the simulations in Figure 4.10, successful suppression lasts until just past 300 ms, and then the suppression turns into amplification. Also of note is that the worst performance occurs around 700 ms, which is nearly one-half of the oscillation period. Thus even better performance with respect to communications delays is expected for oscillations of smaller frequencies, such as the 0.3 Hz oscillation shown in Section 2.2, which is not only measured in the WECC but a known problem frequency in the EI in and around Ontario, Canada.[100]

4.4.2 Robustness

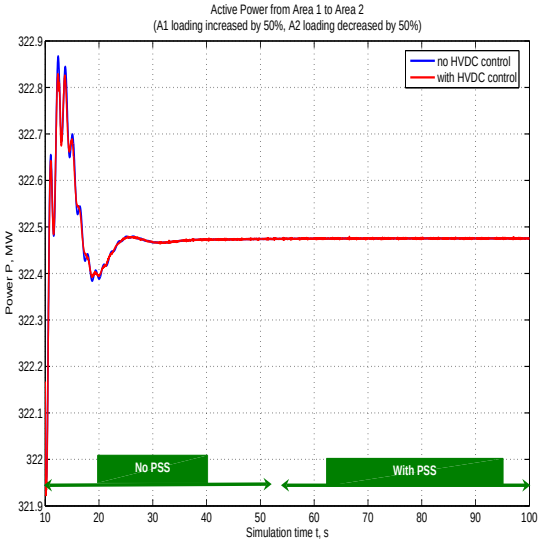
After illustrating the success of wide-area oscillation control, the system was perturbed to test the control strategy's robustness to changes in the plant. Of primary concern was how the system would react when it was loaded differently. Four different cases were tested: the system loading was globally increased and decreased by 50%, and then each area's loading was increased and decreased individually by 50%. The HVDC control scheme was successful in each case, as shown by Figure 4.11. Throughout all of these cases, the communications delay was kept at a constant 50 ms.



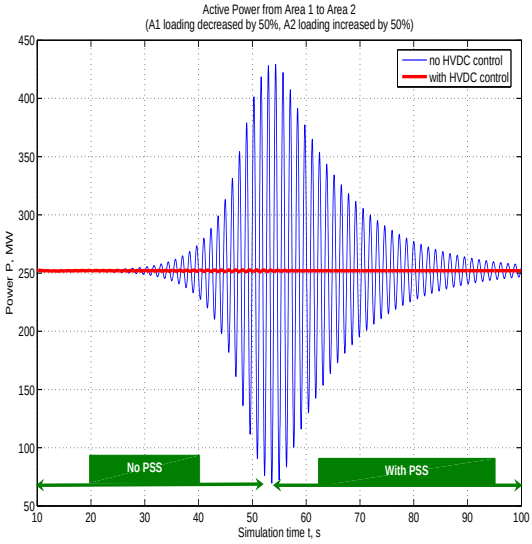
(a) Loading globally increased

(b) Loading globally decreased

Figure 4.11: Robust HVDC oscillation control



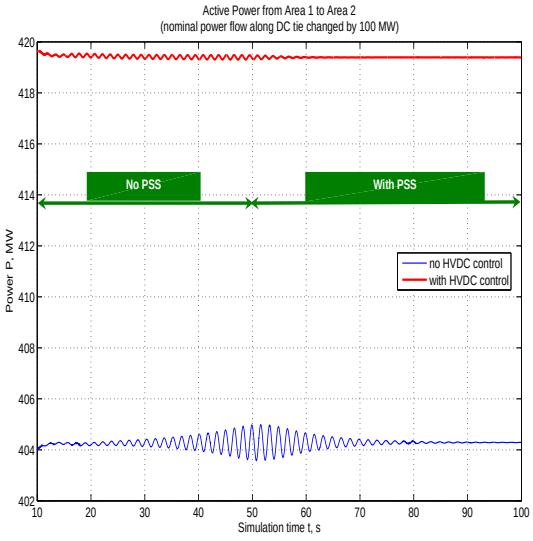
(c) Area 1 loading increased, Area 2 loading decreased



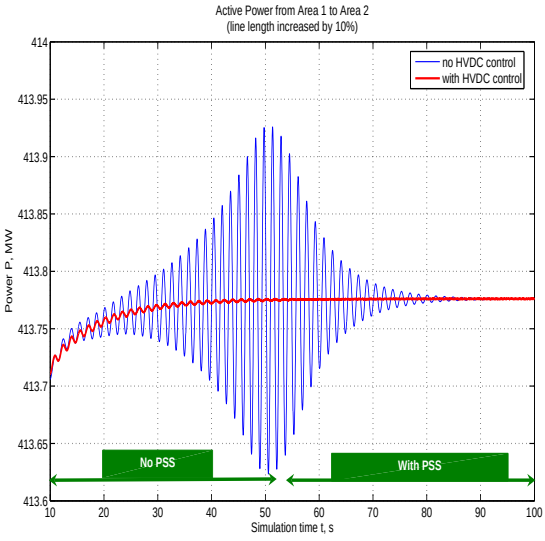
(d) Area 1 loading decreased, Area 2 loading increased

Figure 4.11. Robust HVDC oscillation control (continued)

In addition to the loading parameters, some other steady-state operating parameters of the system were changed. The nominal power flow along the line was increased by 100 MW, the distance between the areas was changed by 10%, and the generator inertias were changed. The communications delay was also kept at 50 ms for these simulations shown in Figure 4.12.

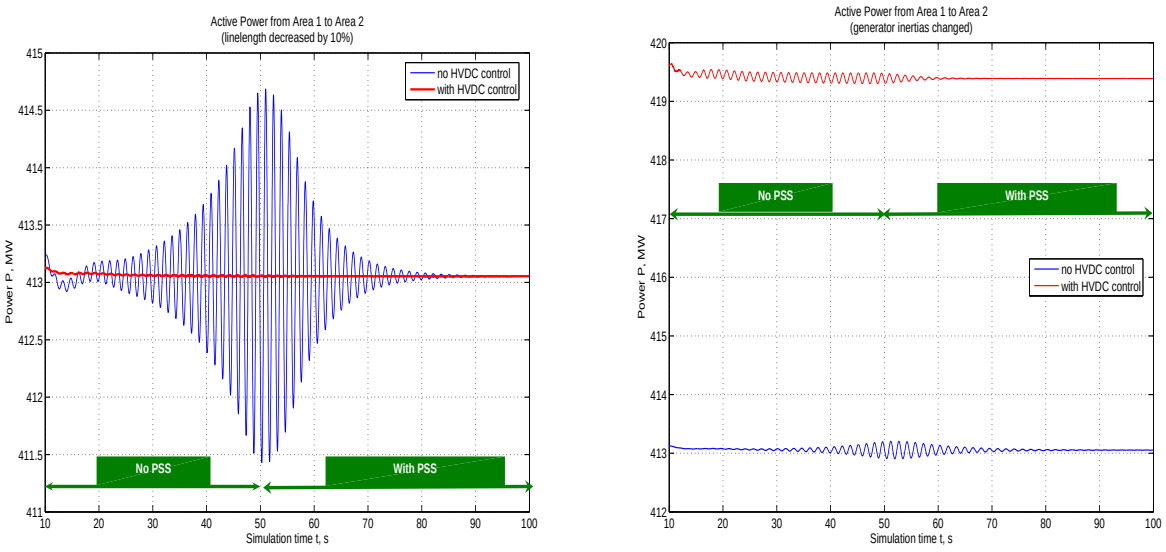


(a) Nominal HVDC power flow increased



(b) Inter-area distance increased by 10%

Figure 4.12. Robust HVDC oscillation control (continued)



(c) Inter-area distance decreased by 10%

(d) Generator inertias changed

Figure 4.12. Robust HVDC oscillation control (continued)

In order to more realistically replicate real-life situations, noise was then added to the frequency measurements. The noise signal was obtained from actual FNET data. Consider a typical interval of FNET data shown in Figure 4.13. Subtraction of the trend from the raw data leaves the noise, shown in Figure 4.14.

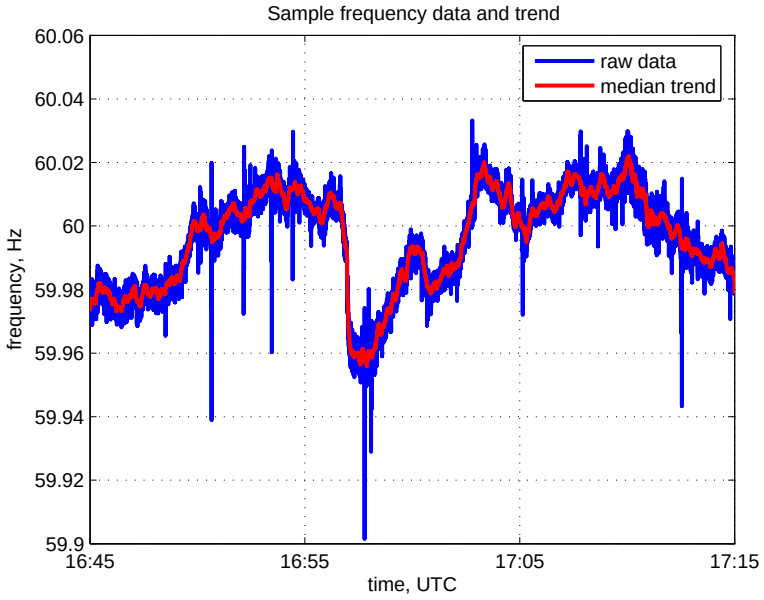


Figure 4.13. Typical noisy frequency

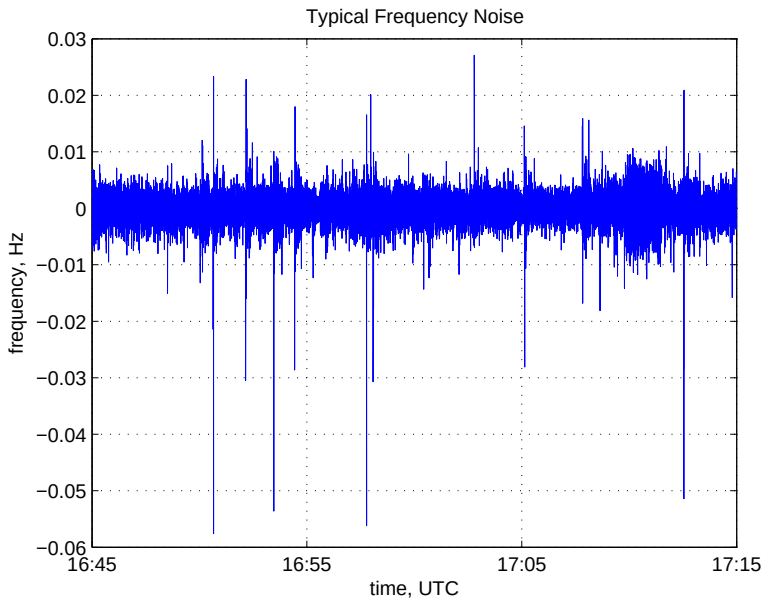


Figure 4.14. Extraction of noise signal

This noise signal was then added to the existing frequency difference calculation to provide a noisy input to the HVDC control system, as illustrated in Figure 4.15.

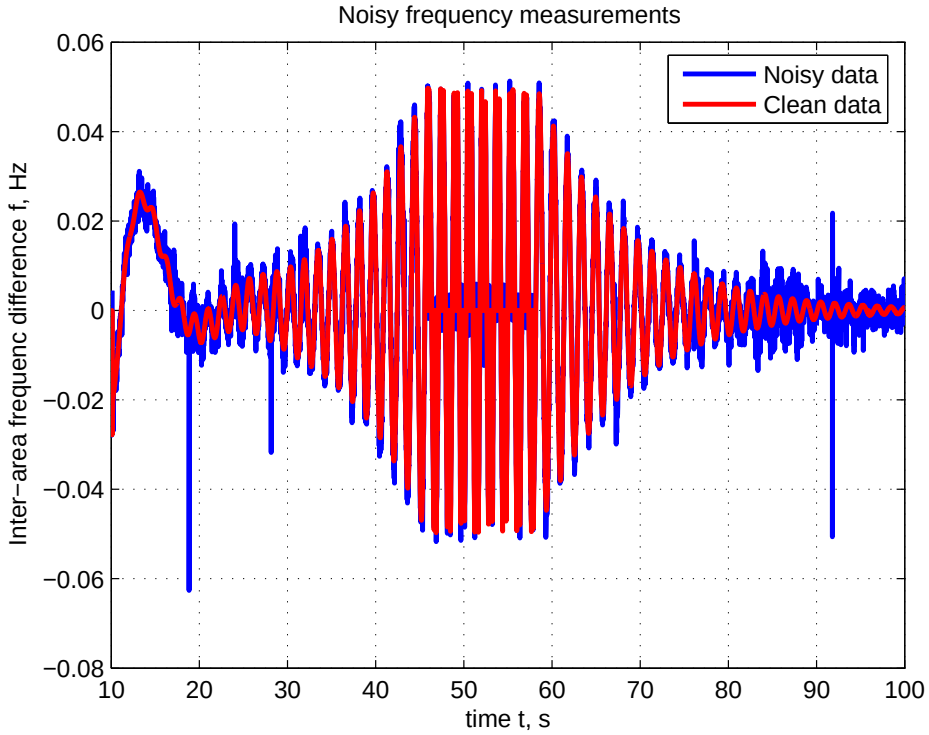
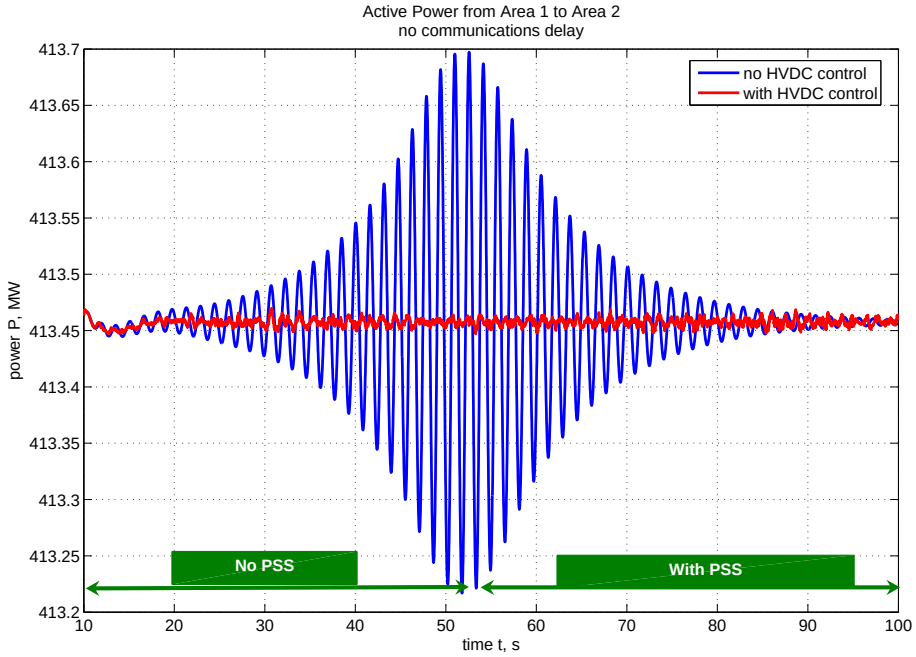
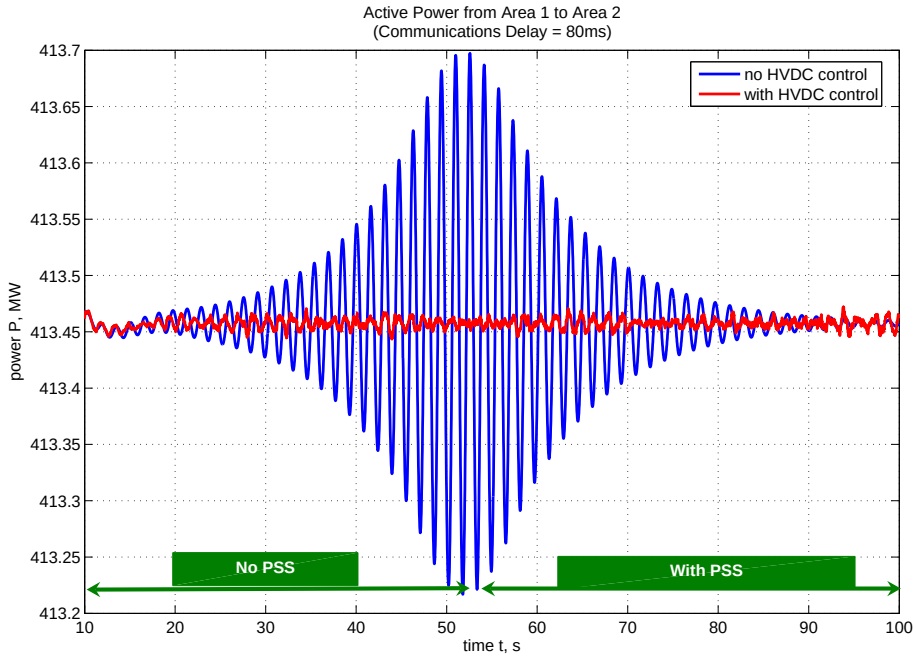


Figure 4.15. Extraction of noise signal

Figure 4.16 shows the performance of the system with noisy control inputs. The control strategy performs quite robustly in the face of a noisy control input, regardless of the communications delay.



(a) No communications delay



(b) 80 ms communications delay

Figure 4.16. Robust HVDC oscillation control (continued)

The results of these simulations provide confirmation that wide-area frequency measurements have great value in the development of closed-loop operations and control schemes for the grid. Not only do such wide-area measurements provide heretofore unavailable grid visibility, but the technical challenges of consolidating data from a wide distribution of sensors does not degrade the performance of the closed-loop system.

Chapter 5

Conclusions, Contributions, and Future Work

This report has detailed the value of distributed network of low-voltage frequency sensors in the measurement, analysis, and control of the electric power grid. The usefulness of such measurements has not always been appreciated as Virginia Tech is the first institution to develop, deploy, and maintain such a system. As new applications that utilize a wide-area perspective of the power grid increase, the data-driven methods in this report will continue to show their value. On a larger scale, the incredible advances in materials have opened up a world of measurement possibilities heretofore unthinkable. Like the power grid, as many other physical systems begin the transition from state estimation to state observation, the robust use of wide-area measurements will continue to grow in importance. Ironically, the real beauty of the methods in this report is its topology independence - the primary reason others thought these methods should fail. However, these methods have shown their value, both in absolute terms and in relation to the system data that has been ignored.

5.1 Contributions

It is in fact this topology independence that is this work's greatest contribution. Not only has simulated data predicted the value of wide-area frequency measurements, but there is empirical data affirming the equivalence of transmission- and distribution- level frequency measurements. The voltage-level invariance of frequency in the power system makes it possible, for the first time, to build a ubiquitous sensor network capable of measuring the entire electrical vastness of North America. The data gathered from this network is not simply of archival, or esoteric future value. Chapter 2 demonstrates the physical phenomena that make frequency the single most informative parameter of the power grid. In other words, frequency provides an accurate snapshot of the health of the entire system in real time. The ability to so easily record, identify, and locate any significant disturbance in the system is unprecedented. Moreover, these events can be accurately analyzed

with the judicious application of the robust statistical tools from Section 1.4.

Chapter 3 presents the first unified robust event ordering method ever developed for FNET. The value of this approach cannot be understated, for virtually every significant event that happens in the grid is visible in the sub-second frequency deviations recorded by sensors at different nodes. These deviations can be used to quantify the exact nature of the event, from the severity of generation lost to the event's originating hypocenter. Never before has an adaptive and robust method for calculating these deviations been developed.

Chapter 4 illustrates the use of wide-area measurements to attempt the long-awaited "closing of the loop" in the power industry. As utilities are better able to visualize what is happening to the system as a whole, they are better able to plan their actions to conform to optimal system operation. The ability to anticipate disturbances allows for far more efficient operation and maintenance of the system. In a broad sense, FNET stands for situational awareness. Real-time data is used to provide a dynamic understanding of the grid that can hopefully be integrated into real-time control actions.

The FNET labs might have the most extensive collection of real-time dynamic data in the world. As such, there are many tasks involved in working with real data that are tedious, time consuming, and hardly repetitive. There is a reason the vast majority of power systems studies utilize simulations alone, and FNET data is a perfect example of the simplicity of simulations. In addition, there have been many contributions to the FNET effort that do not fit within the philosophical scope of this report, which is to detail the principles and applications of robust data techniques to the power system. The tasks required to manipulate the data into a usable form and to accurately visualize the scale of these distributed measurements are significant.

5.2 Future research opportunities

While the scope of the methods in this report is extensive, they simply provide a platform upon which many new applications can be developed. Chief of these is the detection and location of line trips. As confirmed by the 2003 blackout, unscheduled line outages can have a more critical effect on the reliability of the power grid than generator trips. As these events do not create a mismatch between generation and load, the frequency excursions recorded during these events are not as predictable as those experienced during generator trip or load shedding events. The detection and classification of line trips is made even more difficult by the fact that the ability to cross-confirm line trips is virtually non-existent. Should a catalog of line trip events be collected, these events would be an excellent candidate for the application of expert systems such as neural or fuzzy networks.

Along with line trips, FNET data needs to be used to develop a catalog of oscillatory events in the EI. While the WECC has a well-defined set of oscillations and the areas that experience them, such analysis of the EI has yet to be completed. The robust envelope detection of Chapter 2 would be an excellent candidate for this work. Oscillations are often incident to some sort of mismatch event, so a catalog of significant oscillations in the EI would help identify the strange interdependencies in the system. Consider an event from March 2006, shown in Figure 5.1. This event was a line fault followed by a generator trip near Toronto, Canada. While the frequency drop resulting from the trip was categorized correctly, it is interesting to note that this event triggered noticeable oscillations in Tennessee, as evidenced by the spectral information recorded by the Nashville unit (in purple). Unlike the WECC, there is no corridor linking central Tennessee to Ontario, Canada, but there is some kind of "link" between the two. This kind of information is only visible to FNET - the Tennessee Valley Authority (TVA), for example, may see oscillations in its system but have no idea it is connected to a mismatch location in a remote part of the grid.

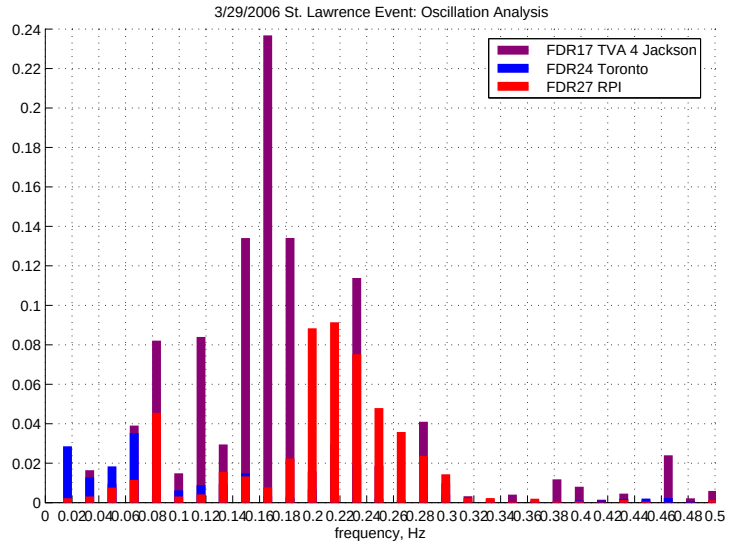


Figure 5.1. St. Lawrence, Canada event: 03/29/2006

Keeping with the data-centricity of the report, there are some aspects of the FNET system that could be improved. As seen in the catalog of 2007 events, it is more difficult to locate events that occur at the edges of the grid. It stands to intuition that the Parzen windowing method will work best when there are similar numbers of sensors on either side of an event. In addition to the simple solution of placing more FDRs everywhere (which is certainly necessary), the use of a common data format makes it possible to easily integrate FNET data with other existing measurement devices like PMUs. The instant access to PMU data that would come with adopting a common format would be a way to instantly increase the effective number of reporting sensors without any hardware costs. Moreover, as the grid continues to see more and more microgrids and smart grids,

which require novel metering and communications infrastructure, the potential exists to tap into another set of pseudo-FDRs. The adoption of the IEEE synchrophasor communications standards should be a priority in future iterations of FDRs.

Specific extensions of the applications developed in this report are numerous. For one, since a routine has been developed to accurately identify false positive crossing times, why limit the ordering algorithm to one threshold? Iterative thresholds with progressive weighting could be a simple way to enhance the accuracy of the Parzen windowing methods. Advanced clustering means, such as kernel *k*-means,[94] provide further refinements to the identification of the proper frequency threshold and crossing time.

The use of an expert system to coordinate multiple locational estimates would also be an excellent improvement. As the catalog of cross-referenced events increases each day, a more thorough classification of the successes and failures of each method would give rise to discriminant functions that could choose an optimal LoD algorithm, based upon some properties of the event. Finally, the use of historical data to determine the inertial properties of the grid would greatly enhance the velocity maps used in the LS approach. The wave velocity is known to vary by direction, and this is most likely caused by the heterogeneous inertial distribution of the EI. Locations with higher inertia will experience frequency deviations much more slowly, with an effect of appearing to the uniform propagation model farther away from the hypocenter than is accurate.

The application of wide-area measurements to control applications is certainly the most exciting line of future work, and it offers the widest variety of applications. The innovative work currently being done in China[106] to implement such a wide-area control scheme will provide much-needed data on the performance of such a scheme. As the power system lags behind other fields (aerospace engineering, for example) in the acceptance of closed-loop control strategies, it has the benefit of selecting proven control schemes, much like the idea of collocated control was first developed in the design of large flexible space structures.[102,103]

References

[1] R. Gardner, "A wide-area perspective on power system operation and dynamics," Ph.D. dissertation, Virginia Polytechnic Institute and State University, March 2008.

[2] NERC, "Frequency response standard whitepaper," April 2004. [Online]. Available: http://www.nerc.com/docs/standards/sar/Frequency_Response_White_Paper.pdf

[3] J. Dong, "Power system disturbance analysis and detection based on wide-area measurements," Ph.D. dissertation, Virginia Polytechnic Institute and State University, Blacksburg, Virginia, December 2008.

[4] National data buoy center. National Oceanic and Atmospheric Administration. Stennis Space Center, Mississippi. [Online]. Available: http://www.ndbc.noaa.gov/dart.shtml

[5] J. Ballance, B. Bhargava *et al.* Use of synchronized phasor measurement system for enhancing AC-DC power system transmission reliability and capability. [Online]. Available: http://phasors.pnl.gov/resources_offline/PMU_ACDC_paper_DOE.pdf

[6] P. Kundur, *Power System Stability and Control*, ser. The EPRI Power System Engineering Series, N. Balu and M. Lauby, Eds. New York: McGraw-Hill, 1994.

[7] *The Magnetic Force of Charles Proteus Steinmetz*, ser. The IEEE Power Engineering Review, vol. 16, no. 9, Institute of Electrical and Electronics Engineers, Sept 1996.

[8] National Academy of Engineering. Washington, D.C. [Online]. Available: http://www.greatachievements.org/

[9] J. P. Stovall, B. J. Kirby *et al.*, "Issues associated with the development of a wide-area analysis and visualization environment," in *Proc. 39th Annual Hawaii International Conference on System Sciences HICSS '06*, vol. 10, 2006, pp. 240a–240a.

[10] A. G. Phadke, "Synchronized phasor measurements-a historical overview," in *Proc. Transmission and Distribution Conference and Exhibition 2002: Asia Pacific. IEEE/PES*, vol. 1, 2002, pp. 476–479 vol.1.

[11] A. G. Phadke and J. S. Thorp, "History and applications of phasor measurements," in *Proc. IEEE PES Power Systems Conference and Exposition PSCE '06*, 2006, pp. 331–335.

[12] S. C. Fisher and K. Ghassemi, "Gps IIF-the next generation," vol. 87, no. 1, pp. 24–47, 1999.

[13] A. G. Phadke, "Synchronized phasor measurements in power systems," vol. 6, no. 2, pp. 10–15, April 1993.

[14] D. Bertagnolli and J. Chow, "Northeastern US oscillation detection and recording project," in *Fault and Disturbance Analysis Conference*, April 2004. [Online]. Available: http://phasors.pnl.gov/Meetings/2004 September/Presentations/WEB-Ingleson Northeastern US Oscillation Detection & Recording Project.pdf

[15] M. W. Baldwin, "Modal analysis techniques in wide-area frequency monitoring systems," Ph.D. dissertation, Virginia Polytechnic Institute and State University, February 2008.

[16] A. R. Phadke, S. K. Bansal *et al.*, "A comparison of voltage stability indices for placing shunt FACTS controllers," in *Proc. First International Conference on Emerging Trends in Engineering and Technology ICETET '08*, 2008, pp. 939–944.

[17] C. L. Chang, A. S. Liu *et al.*, "Oscillatory stability analysis using real-time measured data," vol. 8, no. 3, pp. 823–829, August 1993.

[18] M. G. Adamiak, D. Novosel *et al.*, "Wide area protection and control - today and tomorrow," in *Proc. 2006 IEEE PES Transmission and Distribution Conference and Exhibition*, 2006, pp. 1–7.

[19] S. J. S. Tsai, J. Zuo *et al.*, "Frequency visualization in large electric power systems," in *Proc. IEEE Power Engineering Society General Meeting*, 12–16 June 2005, pp. 1467–1473.

[20] P. Korba, M. Larsson *et al.*, "Detection of oscillations in power systems using Kalman filtering techniques," in *Proc. IEEE Conference on Control Applications CCA 2003*, vol. 1, 2003, pp. 183–188 vol.1.

[21] A. F. Snyder, N. Hadjsaid *et al.*, "Inter-area oscillation damping with power system stabilizers and synchronized phasor measurements," in *Proc. International Conference on Power System Technology POWERCON '98*, vol. 2, 1998, pp. 790–794 vol.2.

[22] J. Yang, "Measurement and improvement of power system low frequency oscillation based on synchronized measurement," NSC 92-2213-E-214-048.

[23] W. Fromm, A. Halinka *et al.*, "Accurate measurement of wide-range power system frequency changes for generator protection," in *Proc. Sixth International Conference on (Conf Developments in Power System Protection Publ. No. 434)*. IEEE, March 1997, pp. 53–57.

[24] A. A. Girgis and W. L. Peterson, "Adaptive estimation of power system frequency deviation and its rate of change for calculating sudden power system overloads," vol. 5, no. 2, pp. 585–594, april 1990.

[25] H. Karimi, M. Karimi-Ghartemani *et al.*, "Estimation of frequency and its rate of change for applications in power systems," vol. 19, no. 2, pp. 472–480, April 2004.

[26] A. Wood and B. Wollenberg, *Power generation, operation, and control*, 2nd ed. Hoboken, New Jersey: John Wiley & Sons, 1996.

[27] S. J. S. Tsai, "Study of global power system frequency behavior based on simulations and FNET measurements," Bradley Department of Electrical and Computer Engineering, Virginia Tech, Blacksburg, Virginia, 2005.

[28] M. Zhou, V. A. Centeno *et al.*, "A preprocessing method for effective pmu placement studies," in *Proc. Third International Conference on Electric Utility Deregulation and Restructuring and Power Technologies DRPT 2008*, 2008, pp. 2862–2867.

[29] B. Qiu, L. Chen *et al.*, "Internet based frequency monitoring network (FNET)," in *Proc. IEEE Power Engineering Society Winter Meeting*, vol. 3, 2001, pp. 1166–1171 vol.3.

[30] S. Chapman, *Electric Machinery and Power system fundamentals*, 1st ed., ser. McGraw-Hill Series in Electrical and Computer Engineering. New York: McGraw-Hill, 2002.

[31] R. Dugan, *Electrical power systems quality*, 2nd ed. New York: McGraw-Hill, 2003.

[32] T. Hashiguchi, M. Yoshimoto *et al.*, "Oscillation mode analysis in power systems based on data acquired by distributed phasor measurement units," in *Proc. International Symposium on Circuits and Systems ISCAS '03*, vol. 3, May 2003, pp. III–367–III–370 vol.3.

[33] Y. Shin, A. C. Parsons *et al.*, "Time-frequency analysis of power system disturbance signals for power quality," in *Proc. IEEE Power Engineering Society Summer Meeting*, vol. 1, 1999, pp. 402–407 vol.1.

[34] S. J. S. Tsai, L. Zhang *et al.*, "Study of global frequency dynamic behavior of large power systems," in *Proc. IEEE PES Power Systems Conference and Exposition*, October 2004, pp. 328–335 vol.1.

[35] Z. Zhong, C. Xu *et al.*, "Power system frequency monitoring network (FNET) implementation," vol. 20, no. 4, pp. 1914–1921, 2005.

[36] Y. C. Zhang, C. Jia *et al.*, "Wireless PMU project phase one final report," January 2009, Confidental Report.

[37] F. van Diggelen, "Indoor GPS theory & implementation," in *Proc. IEEE Position Location and Navigation Symposium*, 2002, pp. 240–247.

[38] J. Bank, "A detailed analysis of missing and erroneous FNET data," December 2006.

[39] J. Hauer, "Use of the WECC WAMs in staged system tests for validation of system performance and modeling," North American SynchroPhasor Initiative, Tech. Rep., 2006. [Online]. Available: http://www.naspi.org/meetings/workgroup/2007_may/presentations/wecc_wams.pdf

[40] O. Samuelsson, M. Hemmingsson *et al.*, "Monitoring of power system events at transmission and distribution level," vol. 21, no. 2, pp. 1007–1008, May 2006.

[41] J. S. Thorp, C. E. Seyler *et al.*, "Electromechanical wave propagation in large electric power systems," vol. 45, no. 6, pp. 614–622, June 1998.

[42] L. Huang, M. Parashar *et al.*, "Impact of electromechanical wave propagation on power system protection and control," in *Proceedings of the 2001 CIGRE conference*. CIGRE, 2001.

[43] M. Parashar, J. S. Thorp *et al.*, "Continuum modeling of electromechanical dynamics in large-scale power systems," vol. 51, no. 9, pp. 1848–1858, September 2004.

[44] Y. Liu, "A US-wide power systems frequency monitoring network," in *Proc. IEEE Power Engineering Society General Meeting*, 2006, pp. 1–8.

[45] A. J. Lyon, *Dealing with data*, 1st ed. Oxford: Pergamon Press, 1970.

[46] J. Bertsch, M. Zima *et al.*, "Experiences with and perspectives of the system for wide area monitoring of power systems," in *Proc. CIGRE/IEEE PES International Symposium Quality and Security of Electric Power Delivery Systems CIGRE/PES 2003*, 2003, pp. 5–9.

[47] D. J. Trudnowski and J. E. Dagle, "Effects of generator and static-load nonlinearities on electromechanical oscillations," vol. 12, no. 3, pp. 1283–1289, 1997.

[48] D. Hoaglin, F. Mosteller *et al.*, *Understanding Robust and Exploratory Data Analysis*. Hoboken, New Jersey: John Wiley & Sons, 1983.

[49] R. G. Staudte and S. J. Sheather, *Robust estimation and testing*, ser. Wiley series in probability and mathematical statistics. New York: Wiley, 1990.

[50] P. J. Rousseeuw and A. M. Leroy, *Robust regression and outlier detection*, ser. Wiley series in probability and mathematical statistics. New York: Wiley, 1987.

[51] P. J. Huber, *Robust statistics*, ser. Wiley series in probability and statistics. New Jersey: Wiley-Interscience, 2004.

[52] J. F. Hauer and F. Vakili, "An oscillation detector used in the bpa power system disturbance monitor," vol. 5, no. 1, pp. 74–79, 1990.

[53] J. S. Milton and J. C. Arnold, *Introduction to probability and statistics: principles and applications for engineering and the computing sciences*, 3rd ed. New York: McGraw-Hill, 1995.

[54] R. E. Walpole and R. H. Myers, *Probability and stochastic processes for engineers*, 5th ed. Toronto, Canada: Macmillan, 1993.

[55] L. M. Mili, *Robust Estimation and Filtering (ECE 5714)*, Virginia Tech, Blacksburg, Virginia, 2005.

[56] C. W. Helstrom, *Probability and stochastic processes for engineers*, 2nd ed. Toronto, Canada: Macmillan, 1991.

[57] J. S. Bendat and A. G. Piersol, *Random data: analysis and measurement procedures*, 2nd ed. New York: Wiley, 1986.

[58] J. G. Proakis and D. G. Manolakis, *Digital signal processing: principles, algorithms, and applications*, 3rd ed. Upper Saddle River, New Jersey: Prentice Hall, 1996.

[59] P. M. Anderson, *Power system protection*, ser. IEEE Press Power Engineering Series. New York: McGraw-Hill, 1999.

[60] Z. Zhong and Y. Liu, "Estimation of event location and tripped generation of generator tripping fault based on FNET frequency information," Virginia Tech, Blacksburg, VA, Final Report submitted to ABB/TVA, 2004.

[61] J. W. Ingleson and D. M. Ellis, "Tracking the eastern interconnection frequency governing characteristic," in *Proc. IEEE Power Engineering Society General Meeting*, 2005, pp. 1461–1466 Vol. 2.

[62] A. Semlyen, "Analysis of disturbance propagation in power systems based on a homogeneoue dynamic model," vol. PAS-93, no. 2, pp. 676–684, 1974.

[63] J. S. Thorp, C. E. Seyler *et al.*, "The large scale electric power system as a distributed continuum," vol. 18, no. 1, pp. 49–50, 1998.

[64] L. Cong and W. Zhuang, "Hybrid TDOA/AOA mobile user location for wideband CDMA cellular systems," vol. 1, no. 3, pp. 439–447, 2002.

[65] G. Huang, Z. Xi *et al.*, "A novel TDOA location algorithm for passive radar," in *Proc. International Conference on Radar CIE '06*, 2006, pp. 1–4.

[66] K. Aki and P. G. Richards, *Quantitative seismology: theory and methods*, 2nd ed. San Francisco: W. H. Freeman, 1980.

[67] P. A. Regalia and M. G. Bellanger, "On the duality between fast qr methods and lattice methods in least squares adaptive filtering," vol. 39, no. 4, pp. 879–891, 1991.

[68] J. Xin, N. Zheng *et al.*, "Simple and efficient nonparametric method for estimating the number of signals without eigendecomposition," vol. 55, no. 4, pp. 1405–1420, 2007.

[69] J. N. Bank, R. M. Gardner *et al.*, "Generator trip identification using wide-area measurements and historical data analysis," in *Proc. IEEE PES Power Systems Conference and Exposition PSCE '06*, 2006, pp. 1677–1681.

[70] R. O. Duda, P. E. Hart *et al.*, *Pattern Classification*, 2nd ed., 2, Ed. New York: John Wiley & Sons, 2001.

[71] A. B. Carlson, P. B. Crilly *et al.*, *Communication Systems: An introduction to signals and noise in electrical communication*, 4th ed., ser. McGraw-Hill Series in Electrical and Computer Engineering, S. W. Director, Ed. New York: McGraw-Hill, 2002.

[72] W. J. Rugh, *Linear System Theory*, 2nd ed. New Jersey: Prentice Hall, 1996.

[73] S. L. Marple, *Digital spectral analysis: with applications*, ser. Prentice-Hall signal processing series. New Jersey: Prentice Hall, 1987.

[74] J. Hauer, D. Trudnowski *et al.*, "Keeping an eye on power system dynamics," vol. 10, no. 4, pp. 50–54, 1997.

[75] J. F. Hauer, "Application of prony analysis to the determination of modal content and equivalent models for measured power system response," vol. 6, no. 3, pp. 1062–1068, 1991.

[76] J. F. Hauer, C. J. Demeure *et al.*, "Initial results in prony analysis of power system response signals," vol. 5, no. 1, pp. 80–89, 1990.

[77] D. J. Trudnowski, M. K. Donnelly *et al.*, "A procedure for oscillatory parameter identification," vol. 9, no. 4, pp. 2049–2055, 1994.

[78] D. J. Trudnowski, J. M. Johnson *et al.*, "Making prony analysis more accurate using multiple signals," vol. 14, no. 1, pp. 226–231, 1999.

[79] R. Kumaresan, D. W. Tufts *et al.*, "A prony method for noisy data: Choosing the signal components and selecting the order in exponential signal models," vol. 72, no. 2, pp. 230–233, 1984.

[80] Y. Hua and T. K. Sarkar, "Matrix pencil method for estimating parameters of exponentially damped/undamped sinusoids in noise," *IEEE Transactions on Acoustics, Speech and Signal Processing*, vol. 38, no. 5, pp. 814–824, 1990.

[81] T. K. Sarkar and O. Pereira, "Using the matrix pencil method to estimate the parameters of a sum of complex exponentials," vol. 37, no. 1, pp. 48–55, 1995.

[82] H. Ouibrahim, "Prony, Pisarenko, and the matrix pencil: a unified presentation," *IEEE Transactions on Acoustics, Speech and Signal Processing*, vol. 37, no. 1, pp. 133–134, 1989.

[83] The energy information administration. United States Department of Energy. Washington, D.C. [Online]. Available: http://www.eia.doe.gov/

[84] G. N. Ramaswamy, G. C. Verghese *et al.*, "Synchrony, aggregation, and multi-area eigenanalysis," vol. 10, no. 4, pp. 1986–1993, 1995.

[85] A. Nuhanovic, M. Glavic *et al.*, "Validation of a clustering algorithm for voltage stability analysis on the bosnian electric power system," *IEE Proceedings-Generation, Transmission and Distribution*, vol. 145, no. 1, pp. 21–26, 1998.

[86] M. Moechtar, T. C. Cheng *et al.*, "Transient stability of power system-a survey," in *Proc. WESCON/'95. Conference record. 'Microelectronics Communications Technology Producing Quality Products Mobile and Portable Power Emerging Technologies'*, 1995, pp. 166–.

[87] J. C. S. Souza, M. A. P. Rodrigues *et al.*, "Fault location in electrical power systems using intelligent systems techniques," vol. 16, no. 1, pp. 59–67, 2001.

[88] C. S. Chang, "Application of pattern recognition techniques for online security-economy and reactive control of power systems," *IEE Proceedings Generation, Transmission and Distribution*, vol. 138, no. 1, pp. 1–10, 1991.

[89] J. C. S. de Souza, E. M. Meza *et al.*, "Alarm processing in electrical power systems through a neuro-fuzzy approach," vol. 19, no. 2, pp. 537–544, 2004.

[90] L. D. Douglas, T. A. Green *et al.*, "New approaches to the agc non-conforming load problem," vol. 9, no. 2, pp. 619–628, 1994.

[91] E. A. Mohamed and G. W. Swift, "Prediction of power system generator self-excitation using pattern recognition," vol. 3, no. 4, pp. 1404–1410, 1988.

[92] L. Abbott, *Pattern Recognition (ECE 5524)*, Virginia Polytechnic Institute and State University, Blacksburg, VA, May 2006.

[93] J. Huang, X. Li *et al.*, "A class-based search system in unstructured P2P networks," in *Proc. 21st International Conference on Advanced Information Networking and Applications AINA '07*, 2007, pp. 76–83.

[94] G. Tzortzis and A. Likas, "The global kernel k-means clustering algorithm," in *Proc. (IEEE World Congress on Computational Intelligence). IEEE International Joint Conference on Neural Networks IJCNN 2008*, 2008, pp. 1977–1984.

[95] W. Zhong, G. Altun *et al.*, "Improved k-means clustering algorithm for exploring local protein sequence motifs representing common structural property," vol. 4, no. 3, pp. 255–265, 2005.

[96] D. H. Wolpert, Ed., *The Mathematics of Generalization*. Reading, MA: Addison-Wesley, 1995.

[97] J. Wu, H. Xiong *et al.*, "A generalization of proximity functions for k-means," in *Proc. Seventh IEEE International Conference on Data Mining ICDM 2007*, 2007, pp. 361–370.

[98] `kmeans` product information. The MathWorks. [Online]. Available: http://www.mathworks.com/

[99] M. Klein, G. J. Rogers *et al.*, "A fundamental study of inter-area oscillations in power systems," vol. 6, no. 3, pp. 914–921, 1991.

[100] ——, "Analytical investigation of factors influencing power system stabilizers performance," vol. 7, no. 3, pp. 382–390, 1992.

[101] F. P. Demello and C. Concordia, "Concepts of synchronous machine stability as affected by excitation control," vol. PAS-88, no. 4, pp. 316–329, 1969.

[102] M. J. Balas, "Direct velociy feedback control of large space structures," *AIAA Journal of Guidance and Control*, vol. 2, no. 3, pp. 252–253, May-June 1979.

[103] J. Lu, J. S. Thorp *et al.*, "Modal control of large flexible space structures using collocated actuators and sensors," vol. 37, no. 1, pp. 143–148, January 1992.

[104] J. Lu, H. D. Chiang *et al.*, "Eigenstructure assignment by decentralized feedback control," vol. 38, no. 4, pp. 587–594, April 1993.

[105] H. Wu, K. S. Tsakalis *et al.*, "Evaluation of time delay effects to wide-area power system stabilizer design," vol. 19, no. 4, pp. 1935–1941, 2004.

[106] J. H. Shi, P. Li *et al.*, "Implementation of an adaptive continuous real-time control system based on WAMs," in *Monitoring of Power System Dynamics Performance*. St. Petersburg, Russia: CIGRE, April 2008.

Appendix A

FDR Information

Table A.1. FDR names and locations

Unit Number	Abbreviated Name	Location	Latitude	Longitude
2	UMR	Rolla, Missouri	37.94873°	−91.76576
3	ARI	Vienna, VA	38.821°	−77.08617
4	VT	FNET Lab, VT	37.23274°	−80.42841
5	Seattle	Seattle, WA	47.6218°	−122.35032
6	ABB	Raleigh, NC	35.82195°	−78.65875
7	MISS	Starkville, MS	33.45672°	−88.82216
8	EPRI	California	37.3992°	−122.13935
9	UFL	Gainesville, FL	29.67415°	−82.33627
11	Calvin	Grand Rapids, MI	42.96125°	−85.65572
12	Houston	Sugar Land, TX	29.61877°	−95.61618
13	MidwestISO	Carmel, IN	39.96931°	−86.1095
14	ASU	Tempe, AZ	33.38835°	−111.93063
15	TVA3Nashville	Nashville TN	36.17155°	−86.78482
16	LA	Pasadena, CA	34.1607°	−118.13872
17	TVA4Jackson	Jackson, TN	35.6337°	−88.82852
20	TVA2Huntsville	Huntsville, AL	34.70704°	−86.62772
21	WSU	Pullman, WA	46.7299°	−117.169
22	ROA2	Roanoke, VA	37.2784°	−79.95839
23	Duluth2	Duluth, MN	46.7872°	−92.099
24	Toronto2	Markham, ON Canada	43.8961°	−79.2252
25	Enernex	Knoxville, TN	35.913482°	−84.092019
27	RPI	Troy, NY	42.73435°	−73.67546
29	Alberta	Alberta, Canada	53.5455°	−113.49
31	UK	Lexington, KY	38.05°	−84.5
32	TVA7Hopkinsville	Hopkinsville, KY	36.8218°	−87.4749

Table A.1. FDR names and locations(continued)

Unit Number	Abbreviated Name	Location	Latitude	Longitude
33	TVA6Chattanooga	Chattanooga, TN	34.26348°	−88.73199
35	ISU	Ames, IA	42.0233°	−93.6256
36	TVA5MuscleShoals	Chattanooga, TN	34.74711°	−87.64203
38	ISONE	Holyoke, MA	42.1859°	−72.6383
40	MISOStPaul	St. Paul, MN	44.9725°	−93.147
41	Winnipeg	Winnipeg, MB Canada	49.8107°	−97.0836
42	FSU	Tallahassee, FL	30.4204°	−84.3181
43	Bismarck	Bismarck, ND	46.8088°	−100.7867
500	Chicago	Orland Park, IL	41.5615°	−87.8779
502	Toronto	Markham, ON Canada	43.8961°	−79.2252
503	Danbury	Danbury, CT	41.377°	−73.5058
504	WayneState	Detroit, MI	42.3562°	−83.0703
506	OhioTiffin	Tiffin, OH	41.0849°	−83.1408
508	ROA	Roanoke, VA	37.2784°	−79.95839
509	WVU	Morgantown, WV	39.646°	−79.9728
510	Blacksburg	Blacksburg, VA	37.2252°	−80.3781
513	PSU	University Park, PA	40.7951°	−77.8639
514	FarrisSabrina	Simpsonville, SC	34.805°	−82.2546
516	LeRoy	LeRoy, NY	43.1511°	−77.713
518	NERC	Princeton, NJ	40.3556°	−74.6728
519	NewportNews	Newport News, VA	37.0823°	−76.4843
520	TTU1	Cookeville, TN	36.1756°	−85.5076
521	Chillicothe	Chilicothe, OH	39.3083°	−82.9132
522	TTU2	Oak Ridge, TN	36.1756°	−85.5076
523	TTU3	Gulfwood, TN	35.9356°	−84.1056
524	TTU	Cookeville, TN	36.1756°	−85.5076
526	SOCO	Birmingham, AL	33.5216°	−86.8151
535	PJM	Gahanna, OH	40.1997°	−75.5229
539	Bangor	Bangor, ME	44.7462°	−68.9051
551	UTSA	San Antonio, TX	29.6615°	−98.4887
553	PlantCity	Plant City, FL	28.0012°	−82.1312
554	Louisville	Louisville, KY	38.2406°	−85.6181
560	Duluth	Duluth, MN	46.7872°	−92.099
562	KansasCity	Kansas City, MO	39.0183°	−94.3698
566	Gulfport	Gulfport, MS	30.4266°	−89.0977
568	Montgomery	Montgomery, AL	32.4088°	−86.2567
569	NewVT	Blacksburg, VA	37.2333°	−80.422
570	Atlanta	Atlanta, GA	33.7808°	−84.3645
572	NewWSU	Pullman, WA	46.7299°	−117.169

Appendix B

2007 Event Scenario Information

Table B.1. Scenario Information

Plant name	Capacity (MW)	Latitude	Longitude	Trip Time (UTC)
Lacygne	840	38.3335	-94.7608	01/02/07 17:16:30
North Anna	910	37.9986	-77.8781	01/03/07 23:03:27
Browns Ferry	1114	34.7055	-87.1173	01/11/07 14:18:45
Paradise	1026	37.2578	-86.9792	01/24/07 14:56:00
W H Zimmer	1300	39.0523	-84.1505	01/25/07 22:07:27
Summer	966	34.2717	-81.2712	02/05/07 08:07:41
McWilliams-Vann	539	31.3999	-86.4749	02/07/07 16:03:44
Oconee U1&U2	1692	34.7538	-83.0674	02/15/07 21:54:12
Indian Point	1025	41.2697	-73.9524	02/28/07 11:33:50
Sequoyah	1127	35.2272	-85.0943	03/13/07 19:27:13
Conemaugh	850	40.3823	-79.0968	03/16/07 07:18:30
Paradise	1000	37.2578	-86.9792	03/20/07 10:06:41
Conemaugh	850	40.3823	-79.0968	03/21/07 20:41:40
W H Zimmer	1300	39.0523	-84.1505	03/24/07 03:13:17
Indian Point Unit3	1025	41.2697	-73.9524	04/06/07 15:09:10
Vogtle Unit 2	1149	33.0894	-81.9780	04/23/07 14:25:33
Salem Unit 1	1174	39.4956	-75.4733	04/30/07 19:02:53
Lacygne	840	38.3335	-94.7608	05/03/07 14:59:01
Coal Creek	598	47.4602	-101.1898	05/06/07 07:54:50
Palisades	778	42.2857	-86.2695	05/08/07 17:23:42
Council Bluffs	690	41.2146	-95.8574	05/10/07 17:54:47
Sherburne	854	45.4365	-93.8410	05/14/07 14:21:06
Grand Gulf	1266	31.9266	-91.0230	05/19/07 16:27:16
Salem U2	1130	39.4956	-75.4733	05/24/07 06:32:56
Dolet Hills	650	32.0037	-93.6731	05/25/07 11:36:41

Table B.1. Scenario Information(continued)

Plant name	Capacity (MW)	Latitude	Longitude	Trip Time (UTC)
Council Bluffs	690	41.2146	-95.8574	06/09/07 05:08:21
Keystone	850	40.6388	-79.3191	06/09/07 05:59:28
Browns Ferry Unit 1	1065	34.7055	-87.1173	06/09/07 16:00:36
Belews Creek U1	1135	36.3189	-80.1484	06/12/07 15:41:06
Belews Creek U2	1135	36.3189	-80.1484	06/19/07 05:09:02
Keystone	850	40.6388	-79.3191	06/27/07 08:50:09
Braidwood	1178	41.2288	-88.2690	06/27/07 14:21:15
North Anna2	924	37.9986	-77.8781	06/29/07 21:53:58
Conemaugh	850	40.3823	-79.0968	07/01/07 23:34:17
Amos U3	800	38.5072	-81.8900	07/02/07 16:49:46
Bull Run U1	879	36.0188	-84.1586	07/03/07 13:55:38
Gavin U1	1300	38.9587	-82.1235	07/04/07 13:27:46
Iatan	651	39.4453	-94.9145	07/07/07 20:37:56
Baldwin	595	38.1764	-89.8265	07/25/07 19:01:42
Rockport	2600	37.8858	-87.0770	08/04/07 21:44:17
Salem U2	1130	39.4956	-75.4733	08/06/07 17:11:24
Amos U3	1300	38.5072	-81.8900	08/06/07 19:39:24
Braidwood Nuclear	1178	41.2288	-88.2690	08/18/07 19:10:22
Nine Mile Point Nuclear	621	29.9137	-90.2078	08/20/07 12:32:15
Sequoyah	1150	35.2272	-85.0943	08/24/07 07:51:02
Donald C. Cook Unit 1	1029	41.9362	-86.5543	08/28/07 17:53:14
Mountaineer U1	1300	38.7292	-82.0223	09/01/07 13:48:03
Rockport Unit2	1300	37.8858	-87.0770	09/04/07 16:57:08
Jeffrey Energy Center U3	1474	39.1987	-96.0683	10/03/07 15:24:29
Farley Unit 2	860	31.3352	-85.1455	10/03/07 19:10:13
Browns Ferry Unit 1	1065	34.7055	-87.1173	10/12/07 13:02:37
Mitchell U2	800	39.9148	-80.7310	11/04/07 09:26:36
Connesville U4	780	40.1804	-81.8951	11/04/07 22:20:30
Big Sandy U2	800	37.9848	-82.5857	11/09/07 13:00:12
W H Zimmer	1300	39.0523	-84.1505	11/14/07 15:57:00

Appendix C

Sample Daily Oscillation Analysis

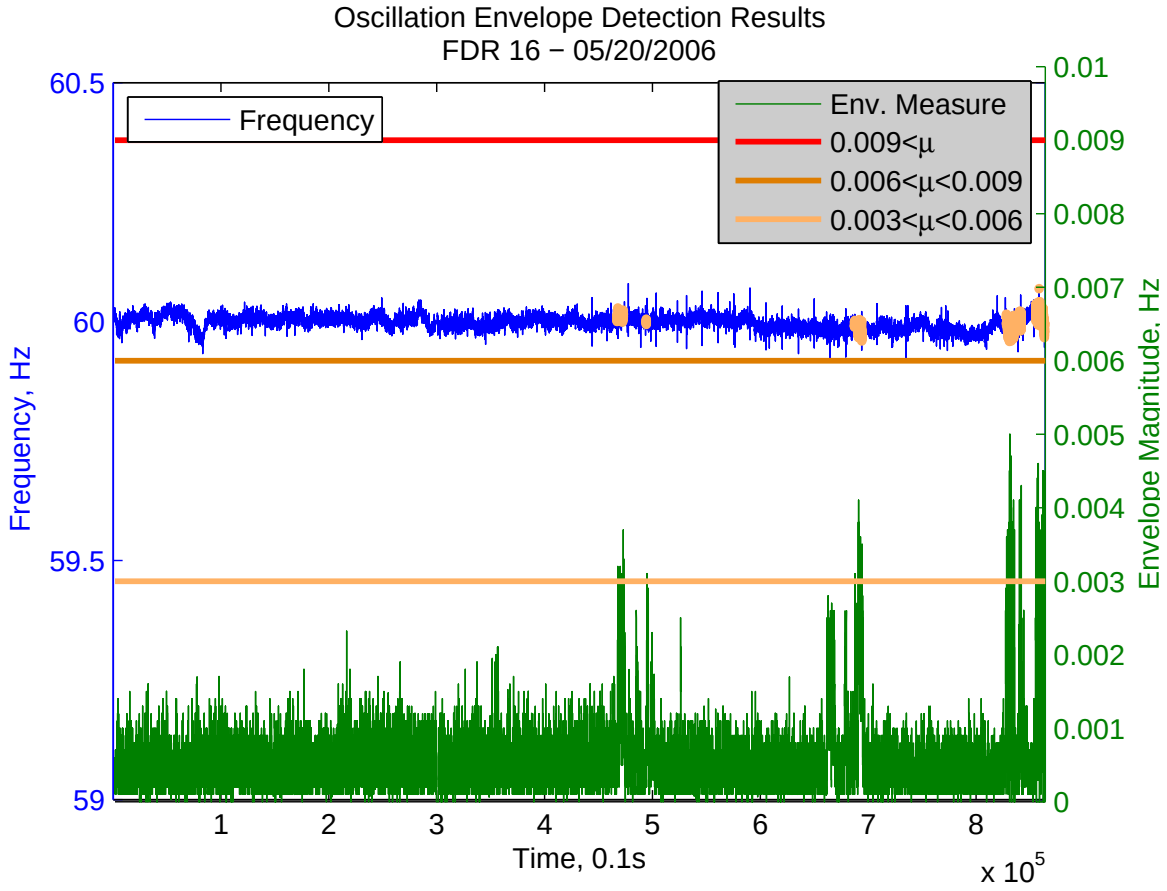


Figure C.1. Daily oscillation analysis: summary

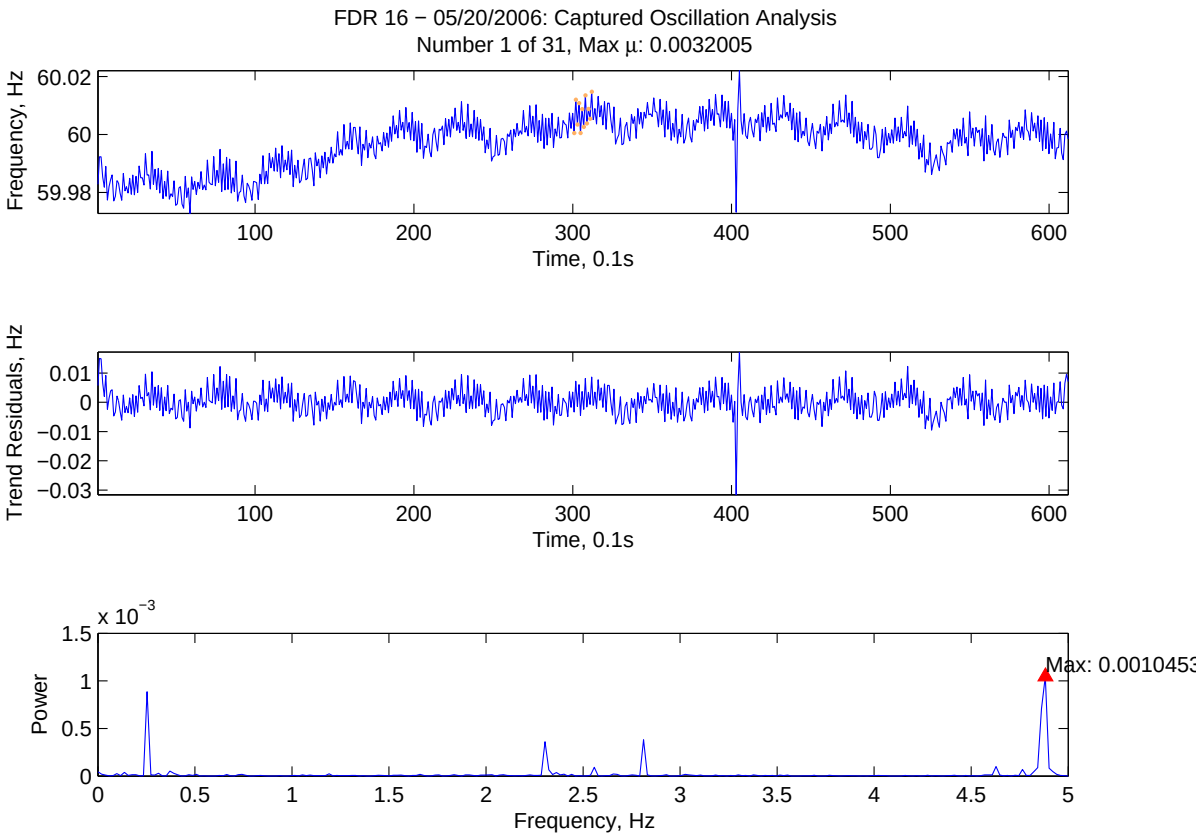


Figure C.2. Daily oscillation analysis: 1 of 31

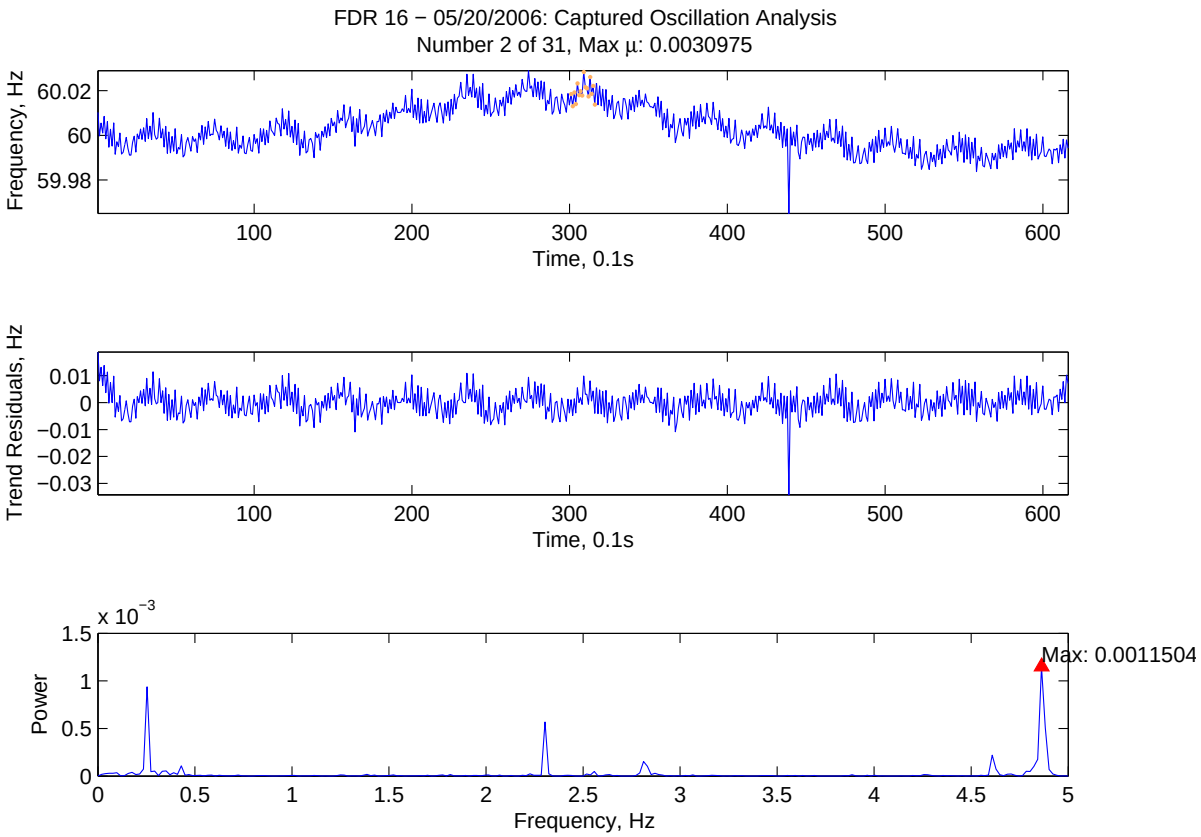


Figure C.3. Daily oscillation analysis: 2 of 31

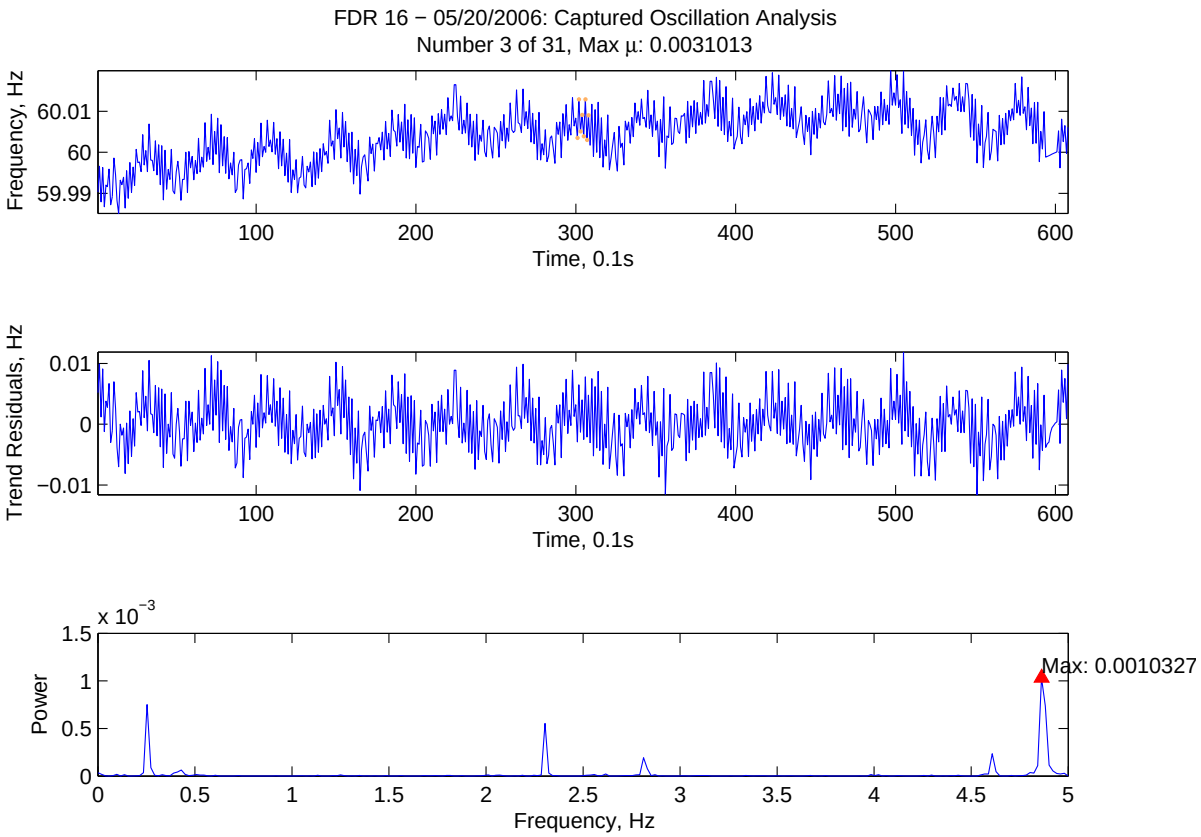


Figure C.4. Daily oscillation analysis: 3 of 31

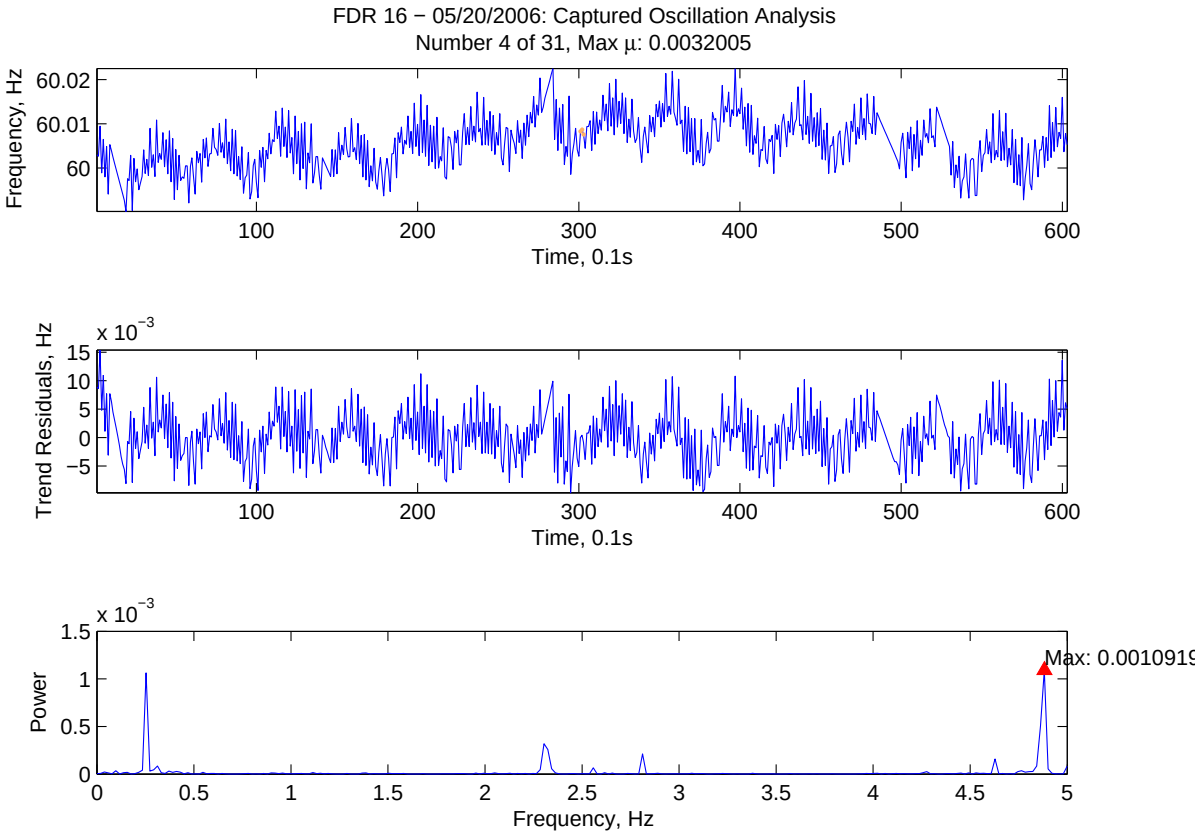


Figure C.5. Daily oscillation analysis: 4 of 31

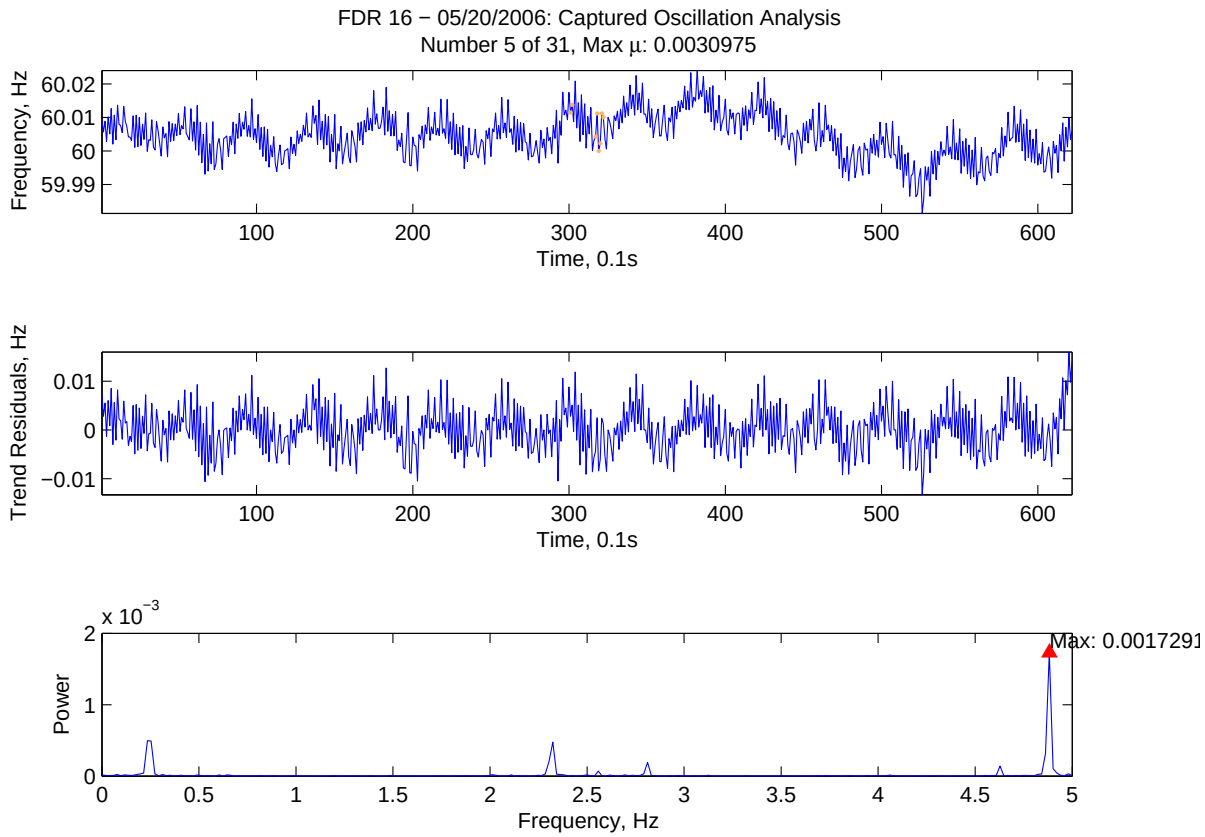


Figure C.6. Daily oscillation analysis: 5 of 31

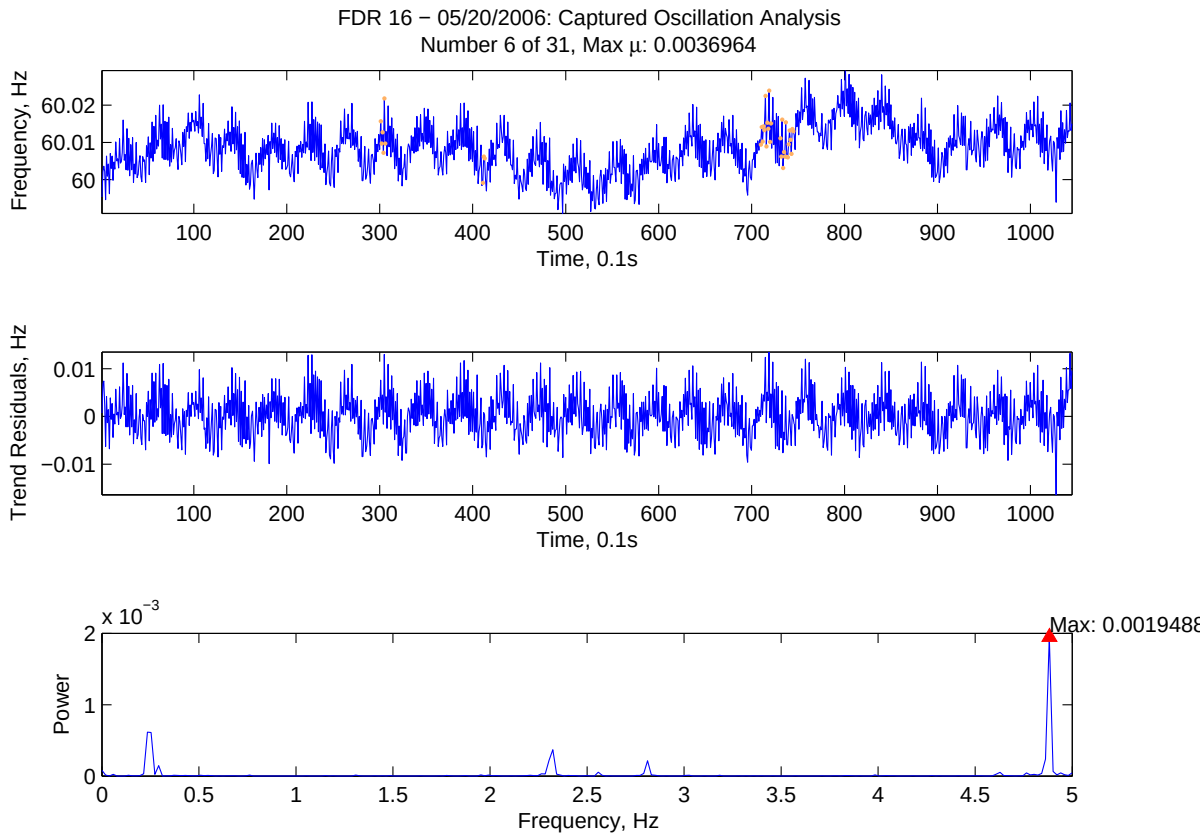


Figure C.7. Daily oscillation analysis: 6 of 31

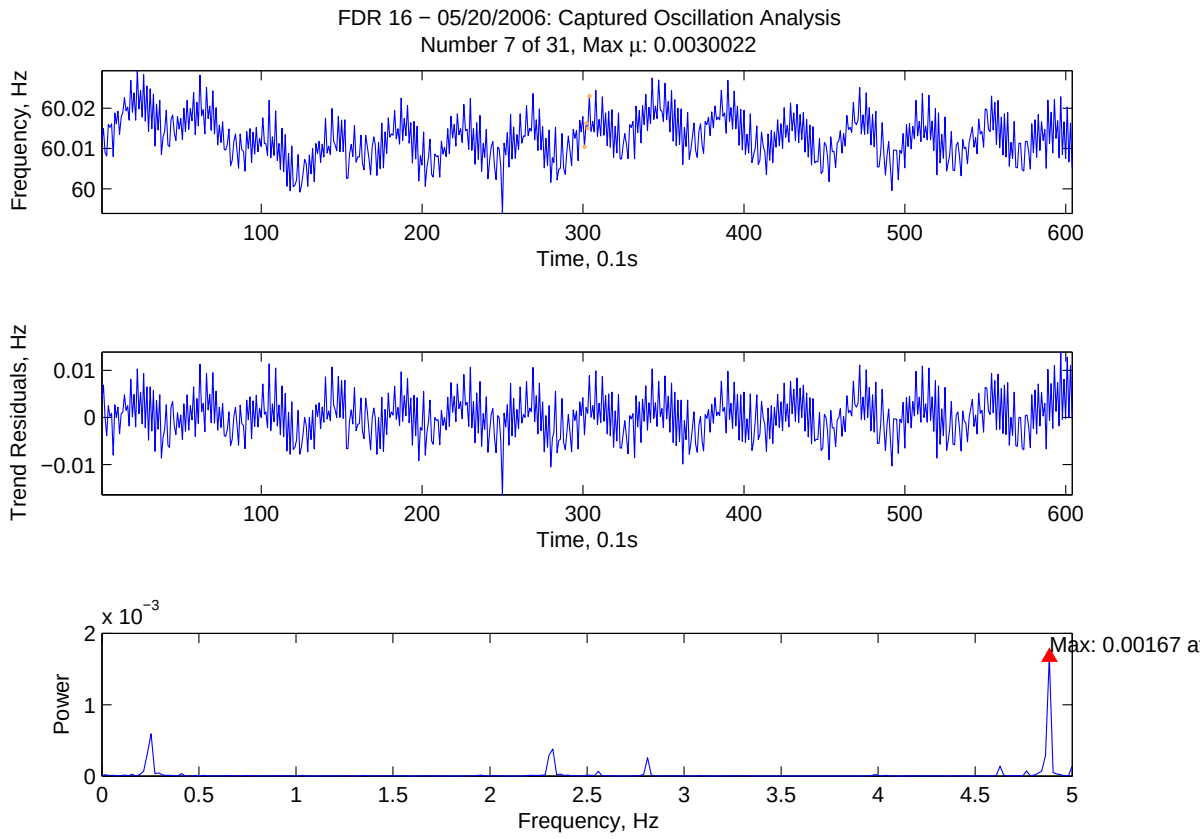


Figure C.8. Daily oscillation analysis: 7 of 31

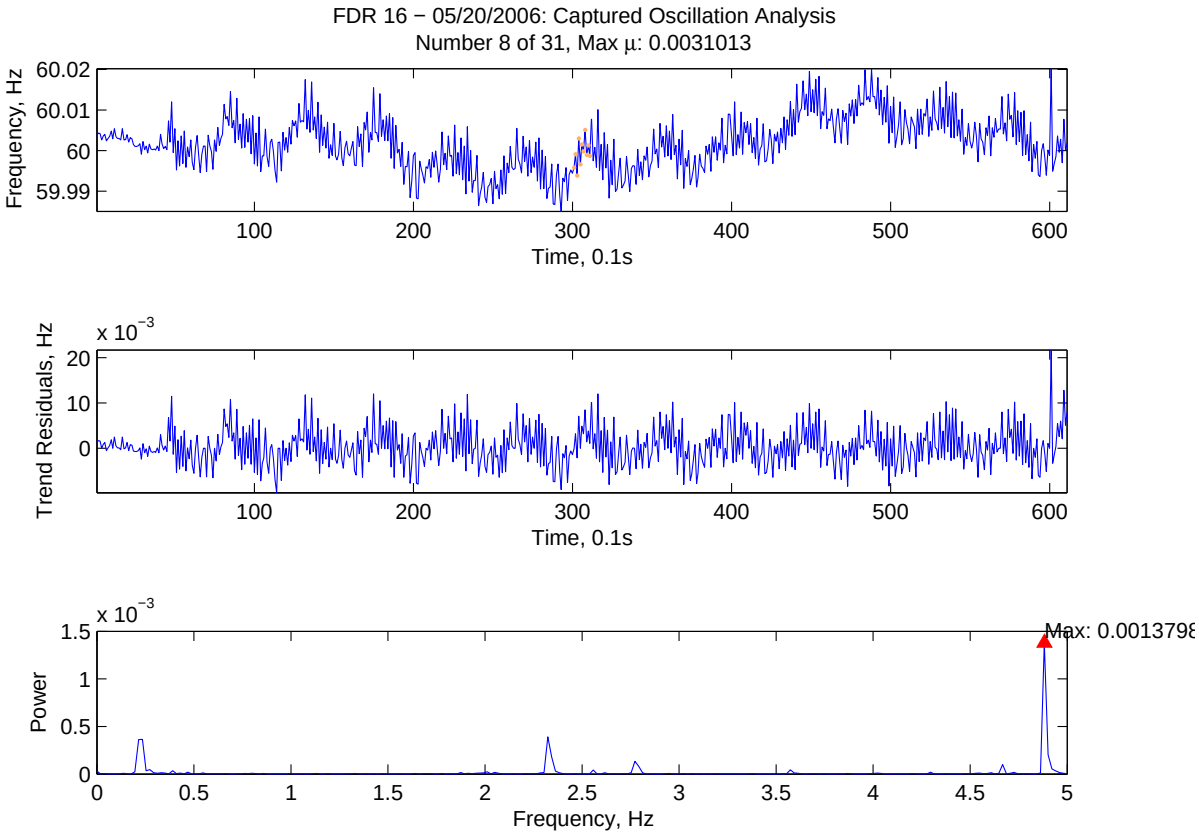


Figure C.9. Daily oscillation analysis: 8 of 31

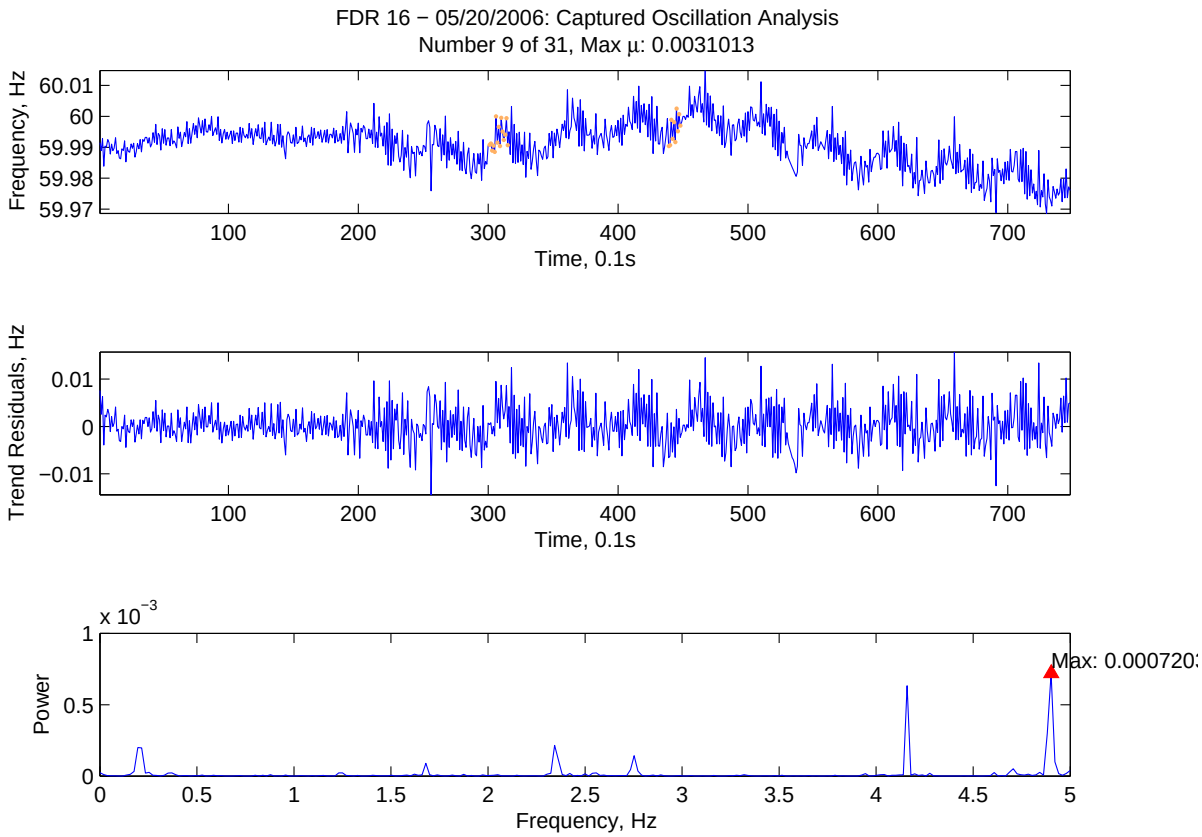


Figure C.10. Daily oscillation analysis: 9 of 31

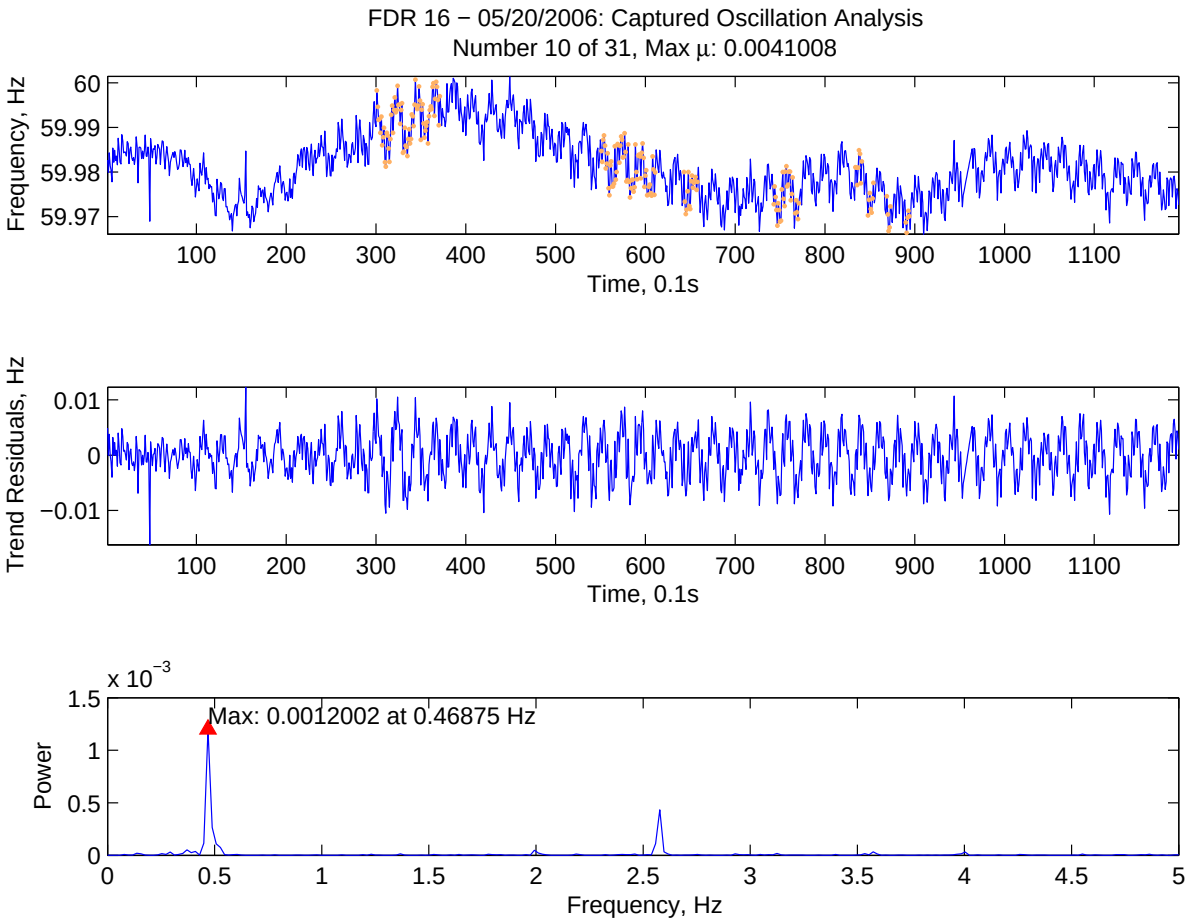


Figure C.11. Daily oscillation analysis: 10 of 31

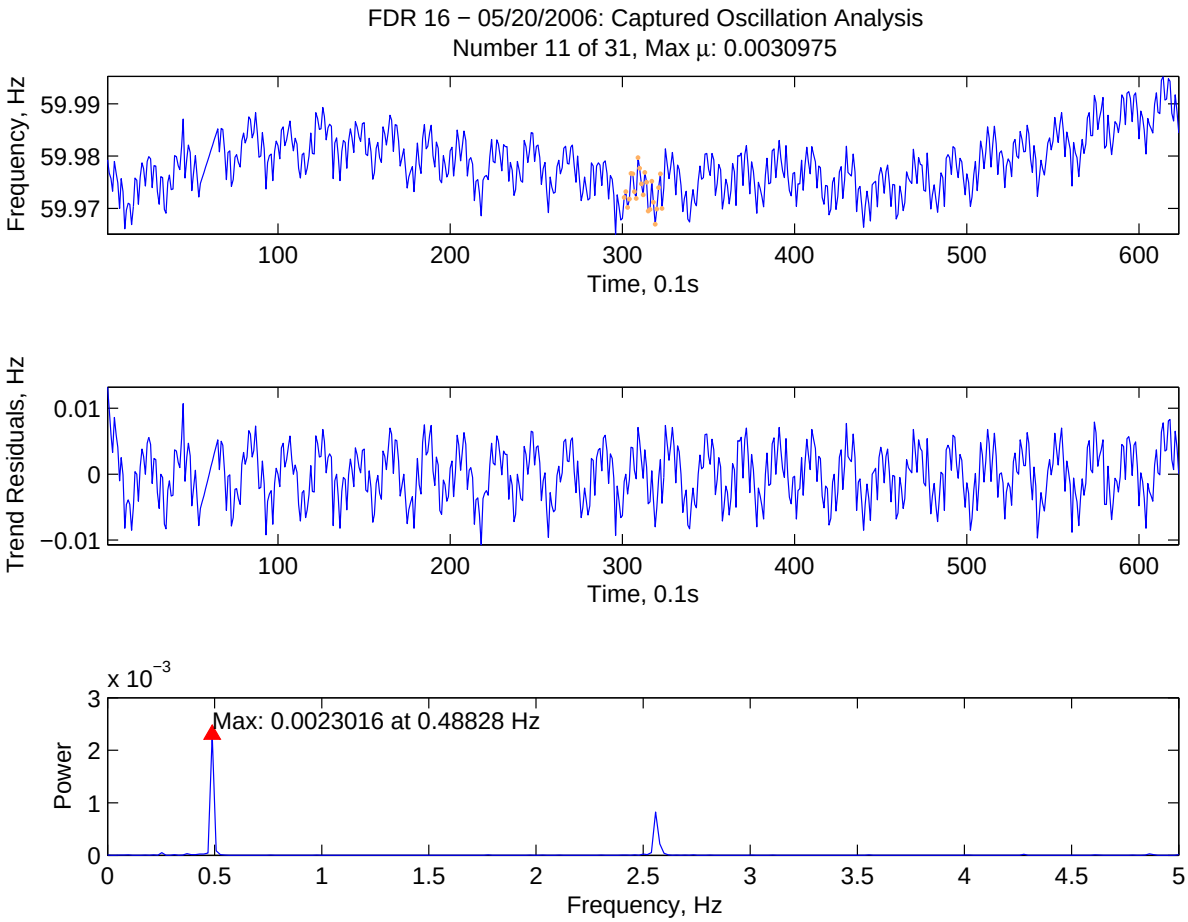


Figure C.12. Daily oscillation analysis: 11 of 31

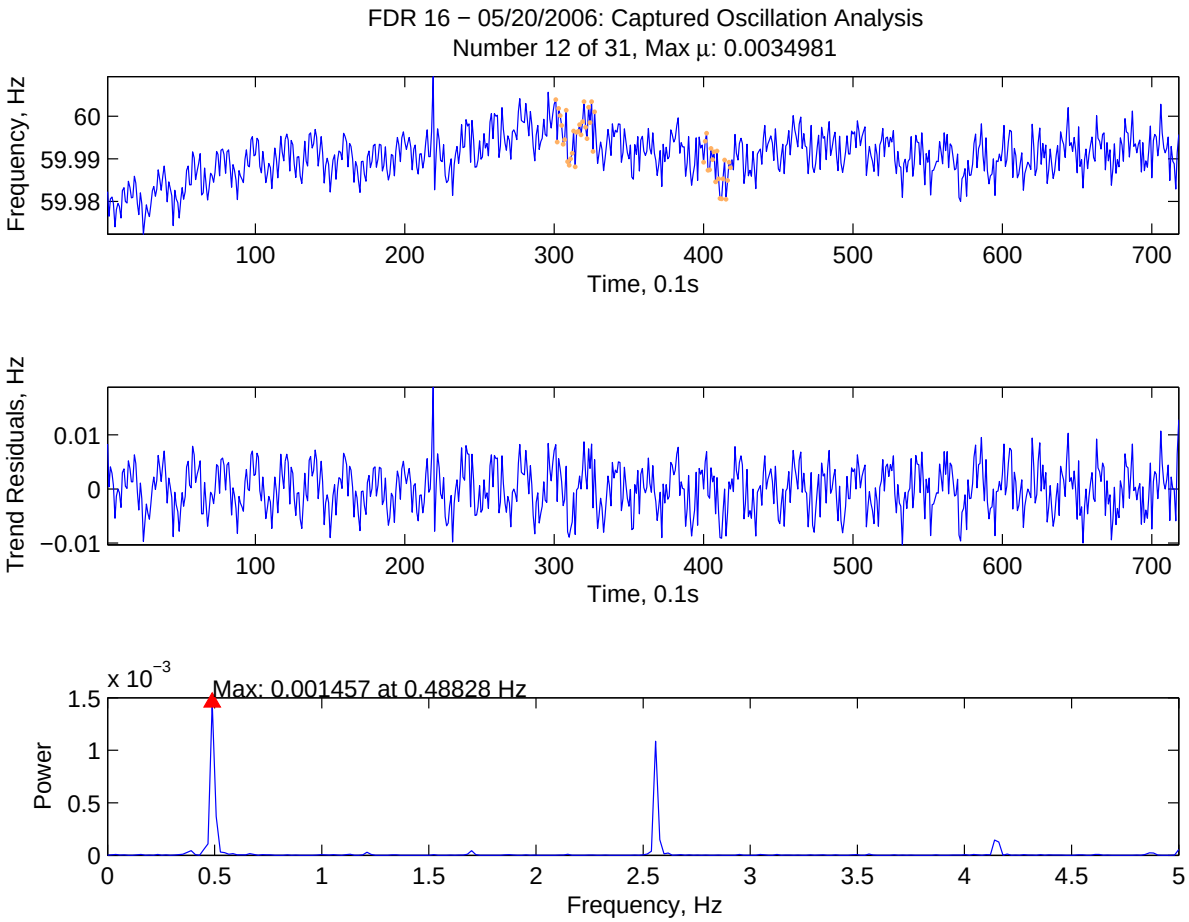


Figure C.13. Daily oscillation analysis: 12 of 31

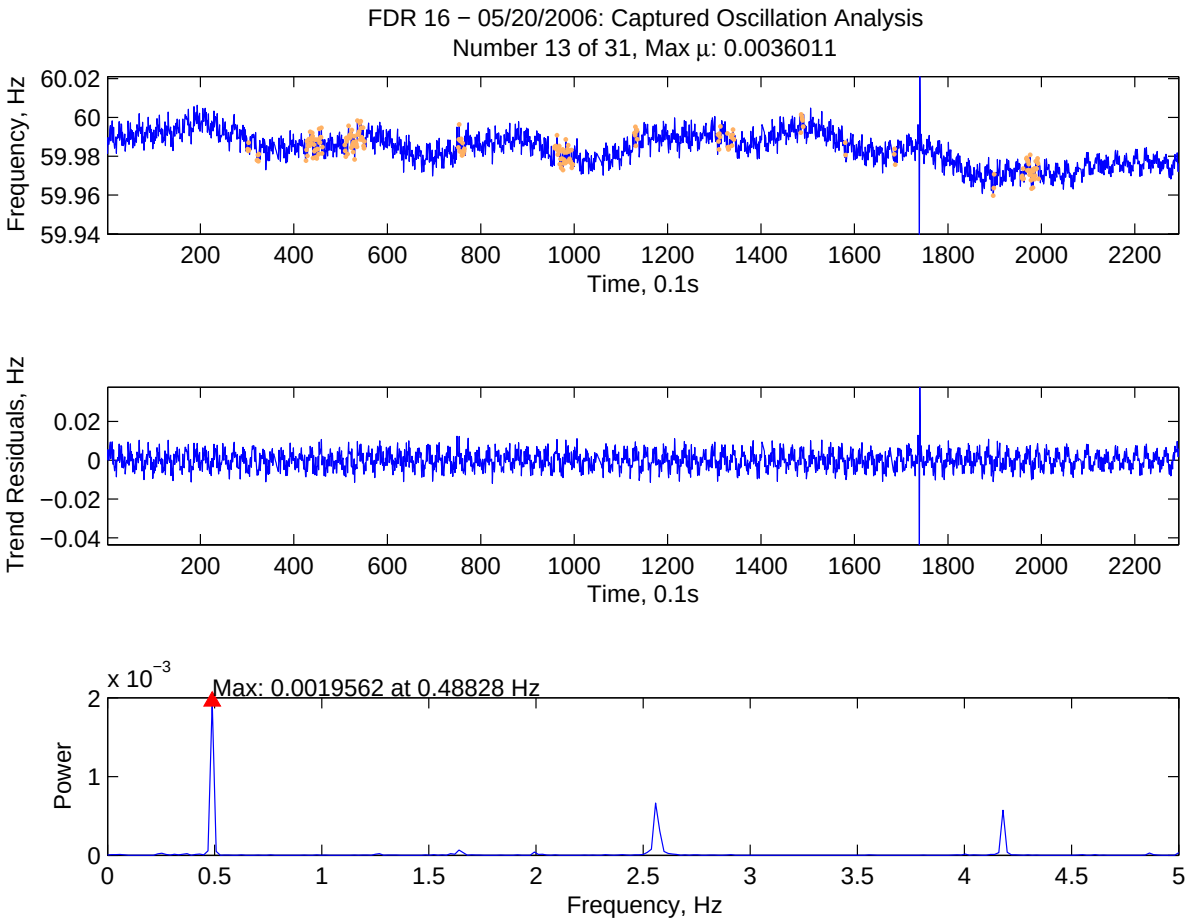


Figure C.14. Daily oscillation analysis: 13 of 31

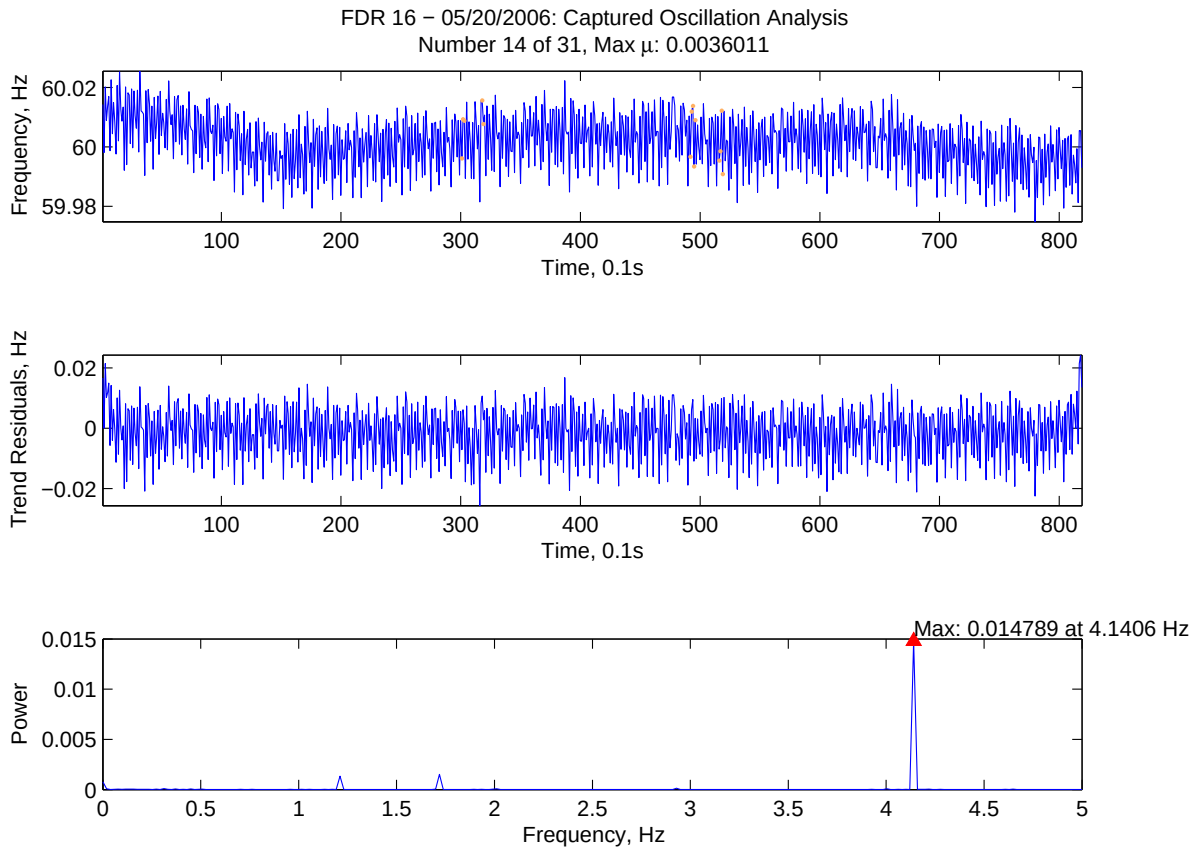


Figure C.15. Daily oscillation analysis: 14 of 31

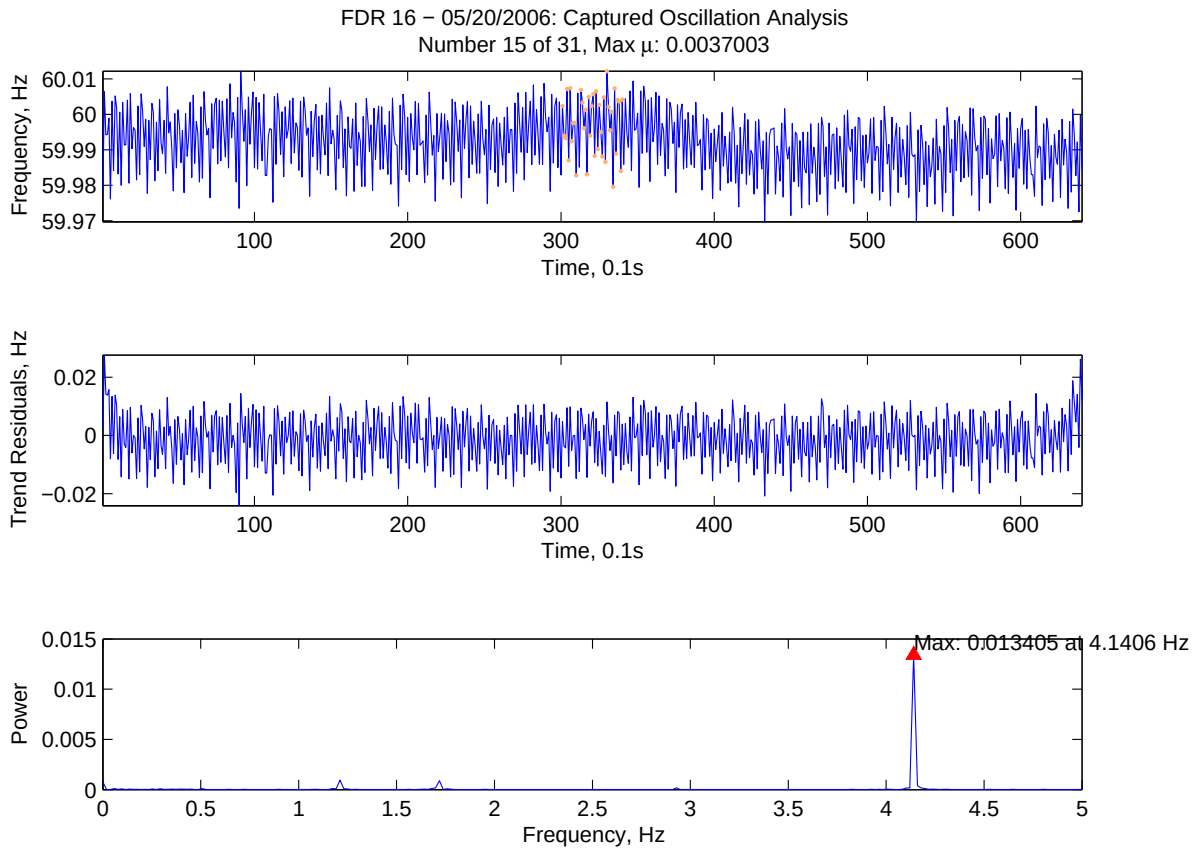


Figure C.16. Daily oscillation analysis: 15 of 31

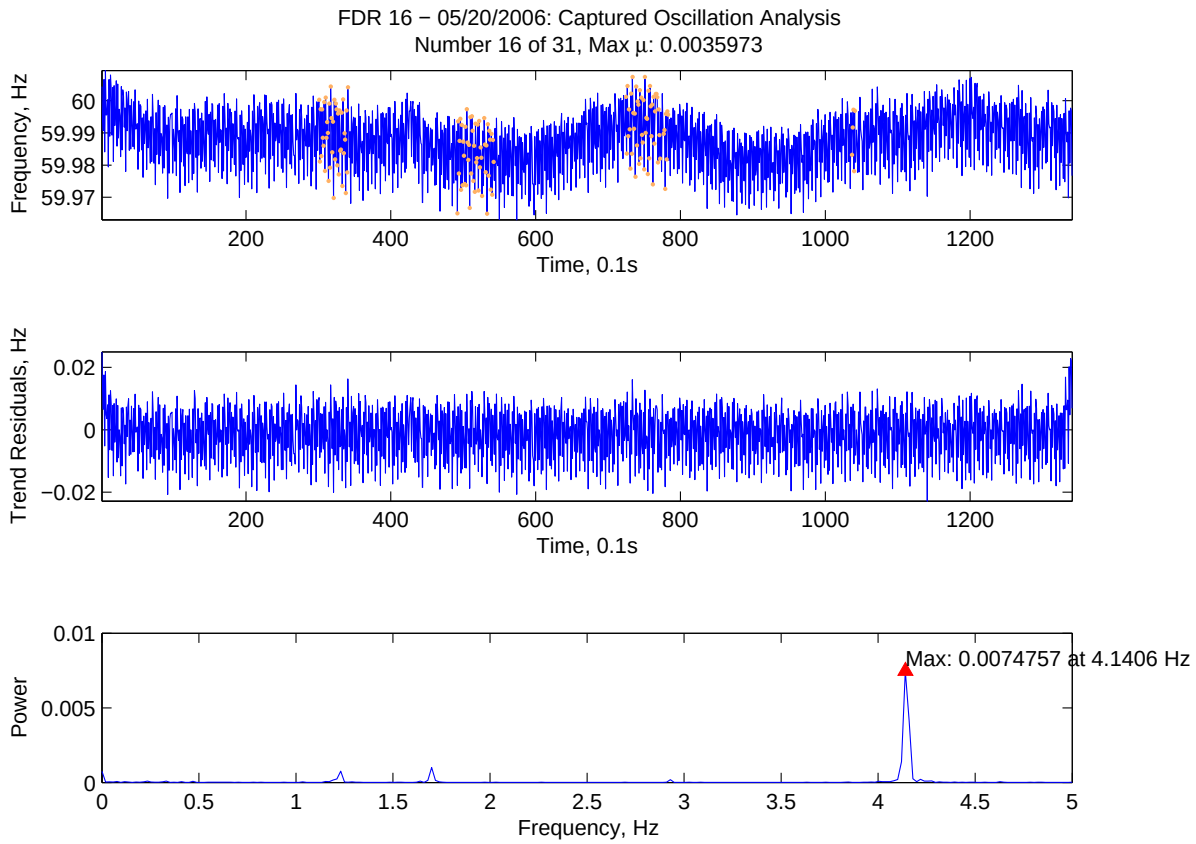


Figure C.17. Daily oscillation analysis: 16 of 31

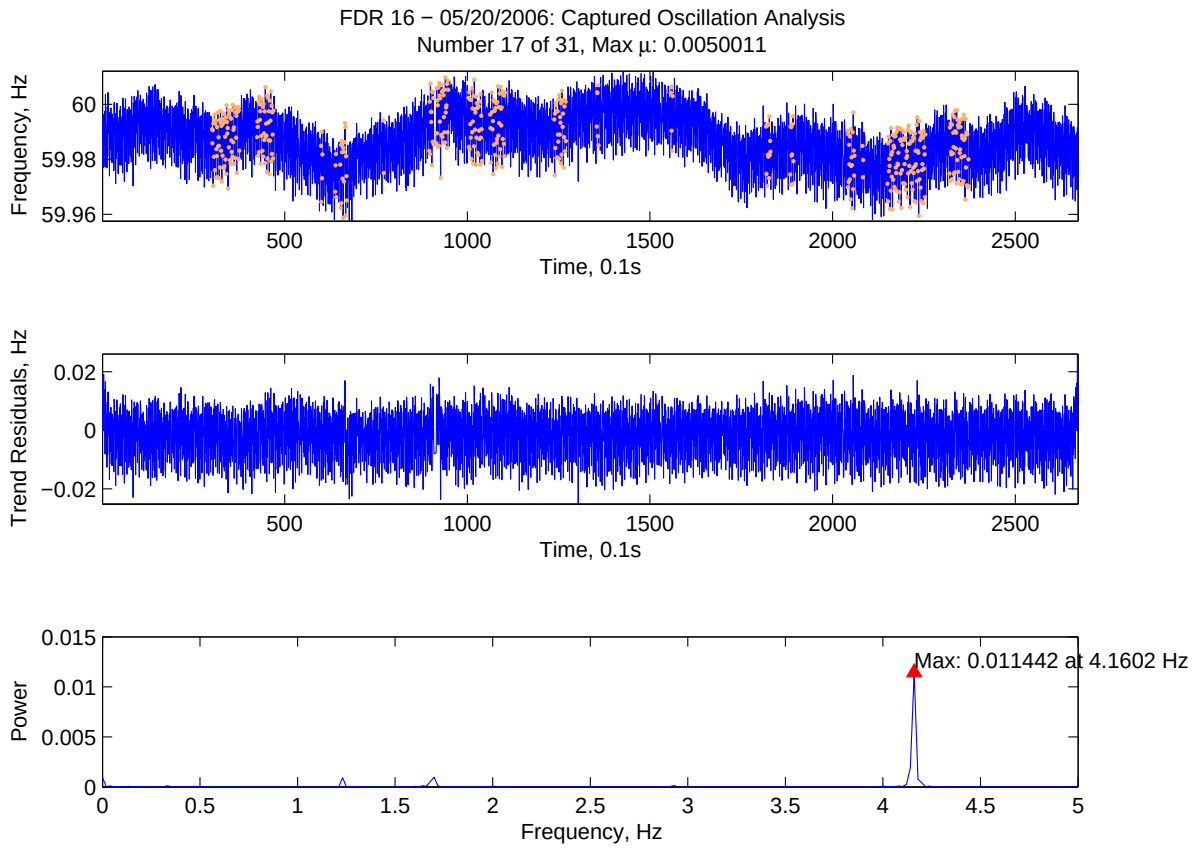


Figure C.18. Daily oscillation analysis: 17 of 31

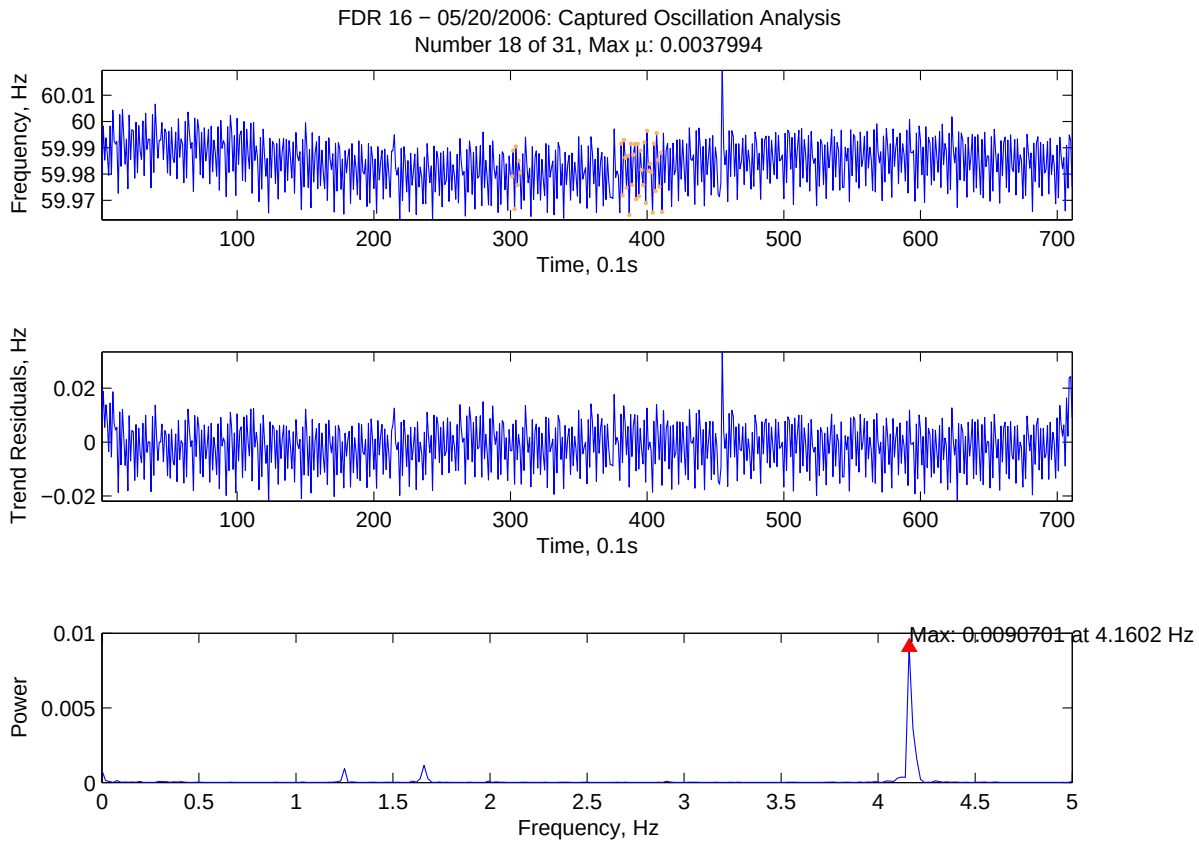


Figure C.19. Daily oscillation analysis: 18 of 31

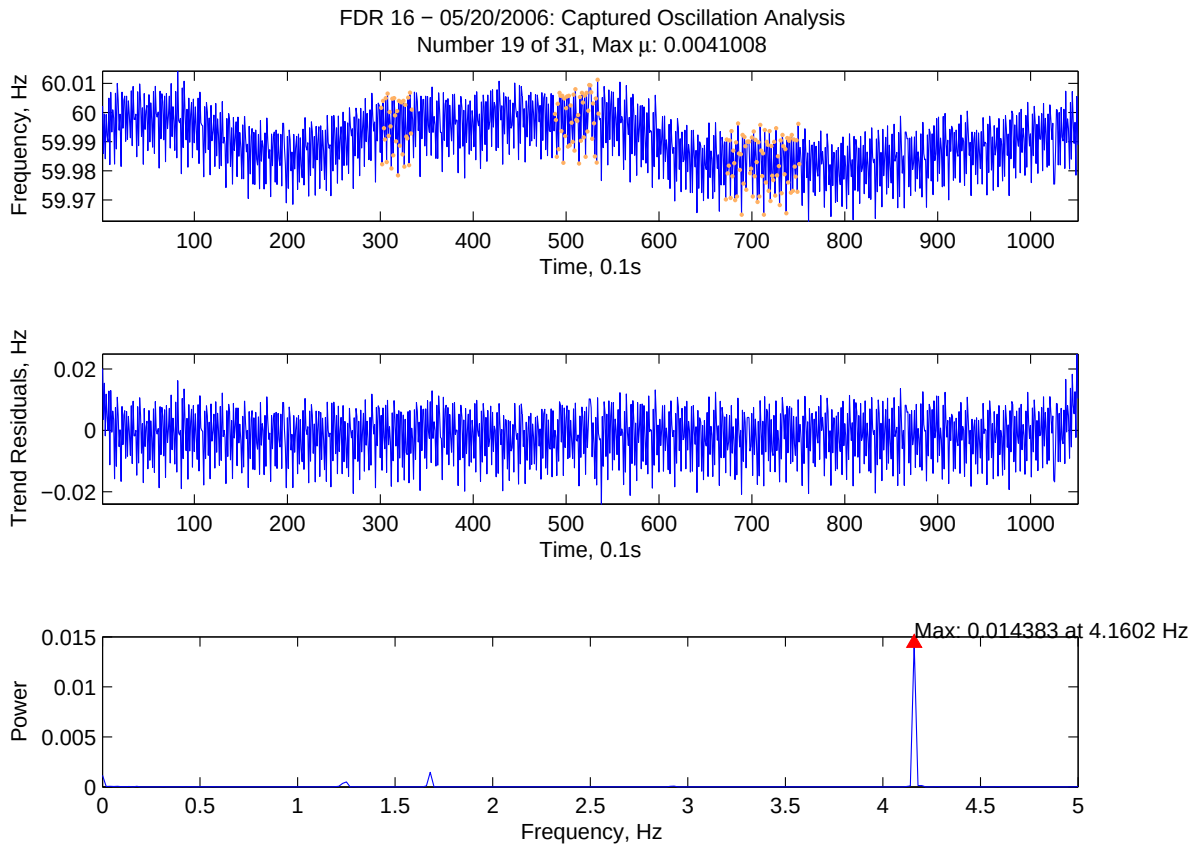


Figure C.20. Daily oscillation analysis: 19 of 31

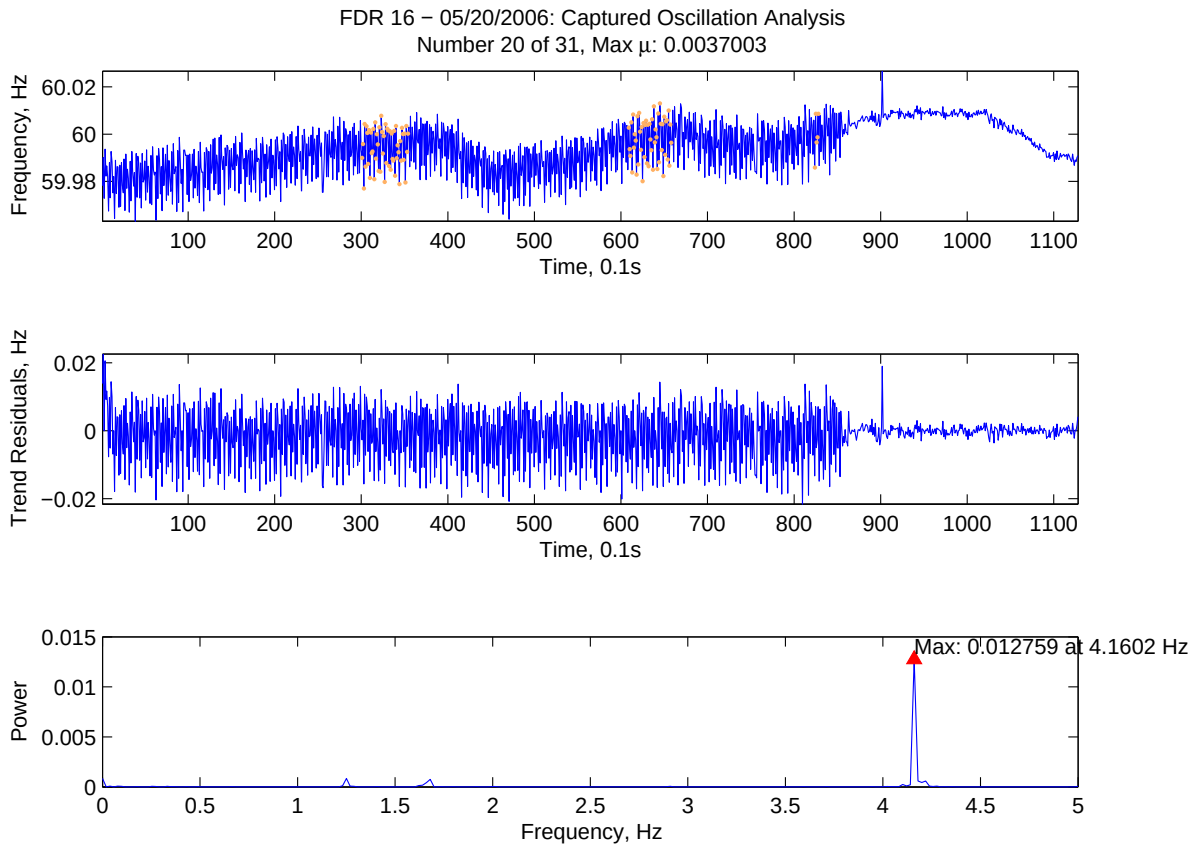


Figure C.21. Daily oscillation analysis: 20 of 31

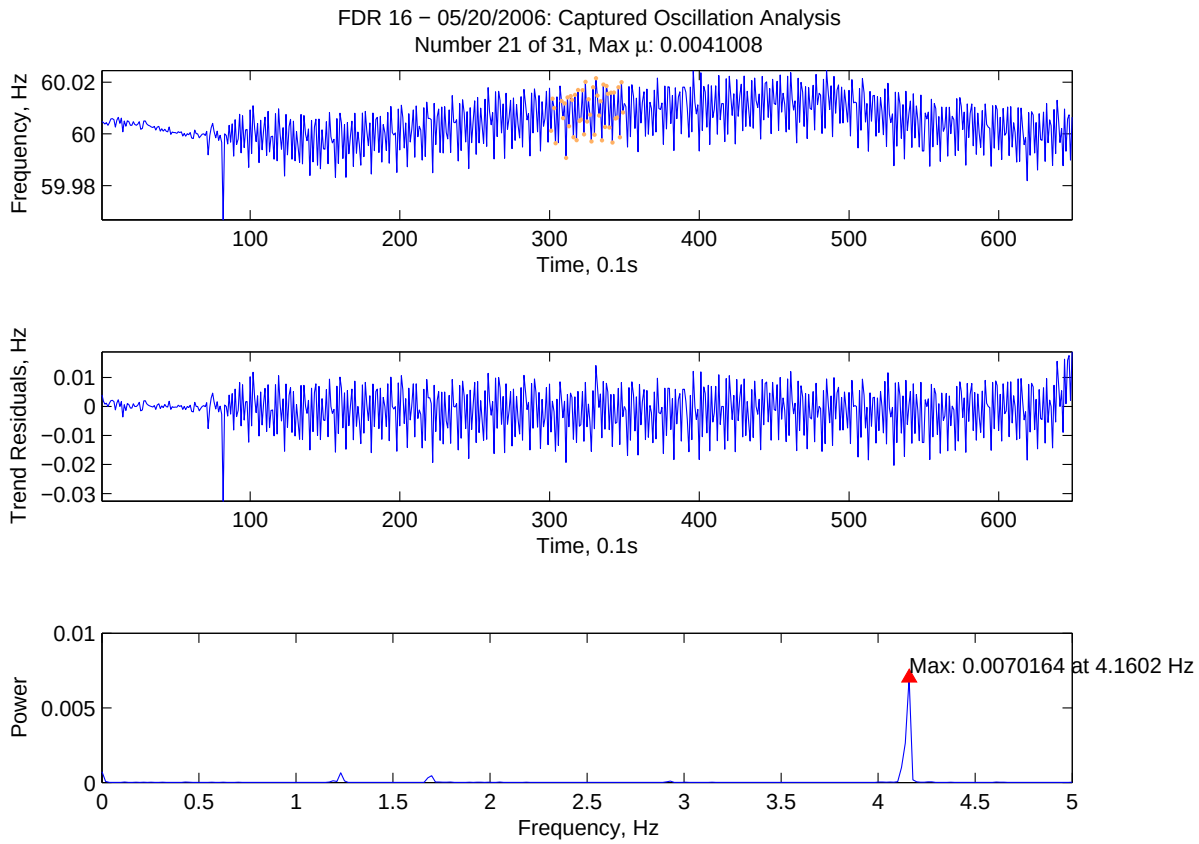


Figure C.22. Daily oscillation analysis: 21 of 31

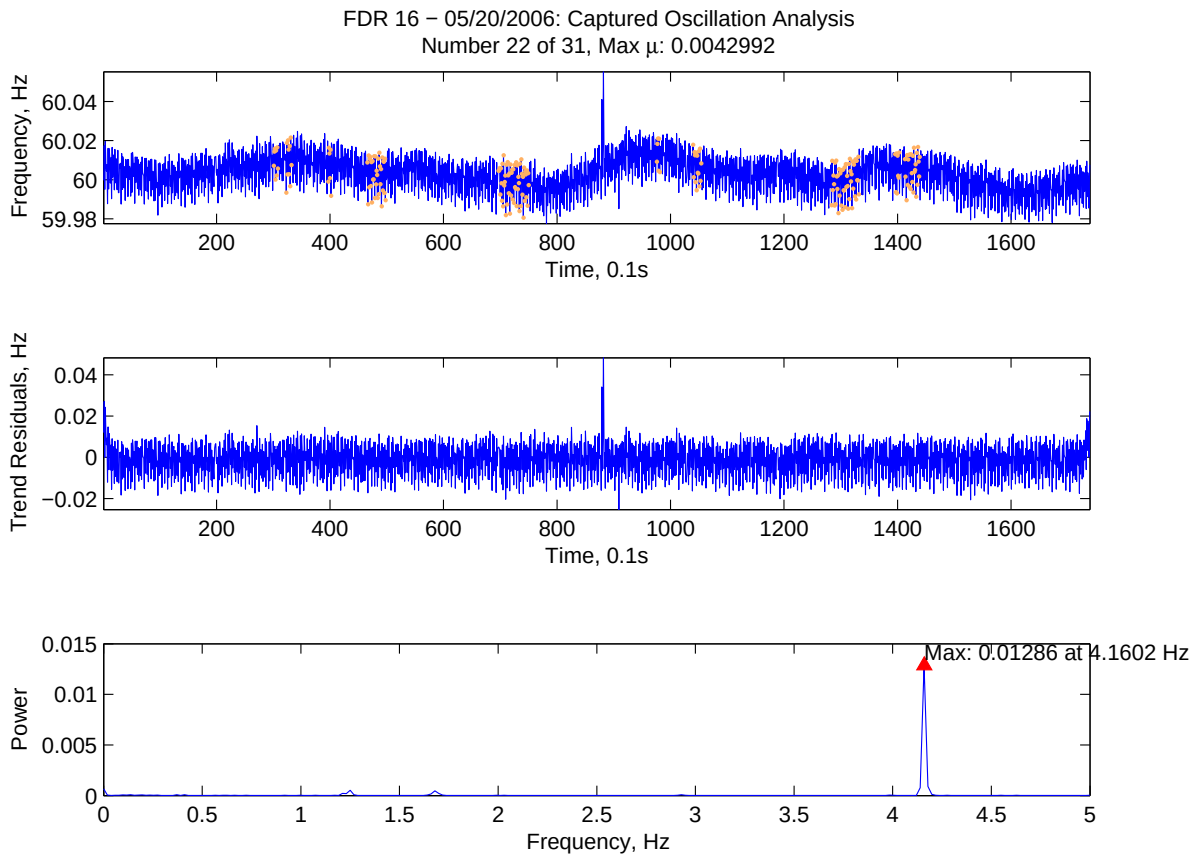


Figure C.23. Daily oscillation analysis: 22 of 31

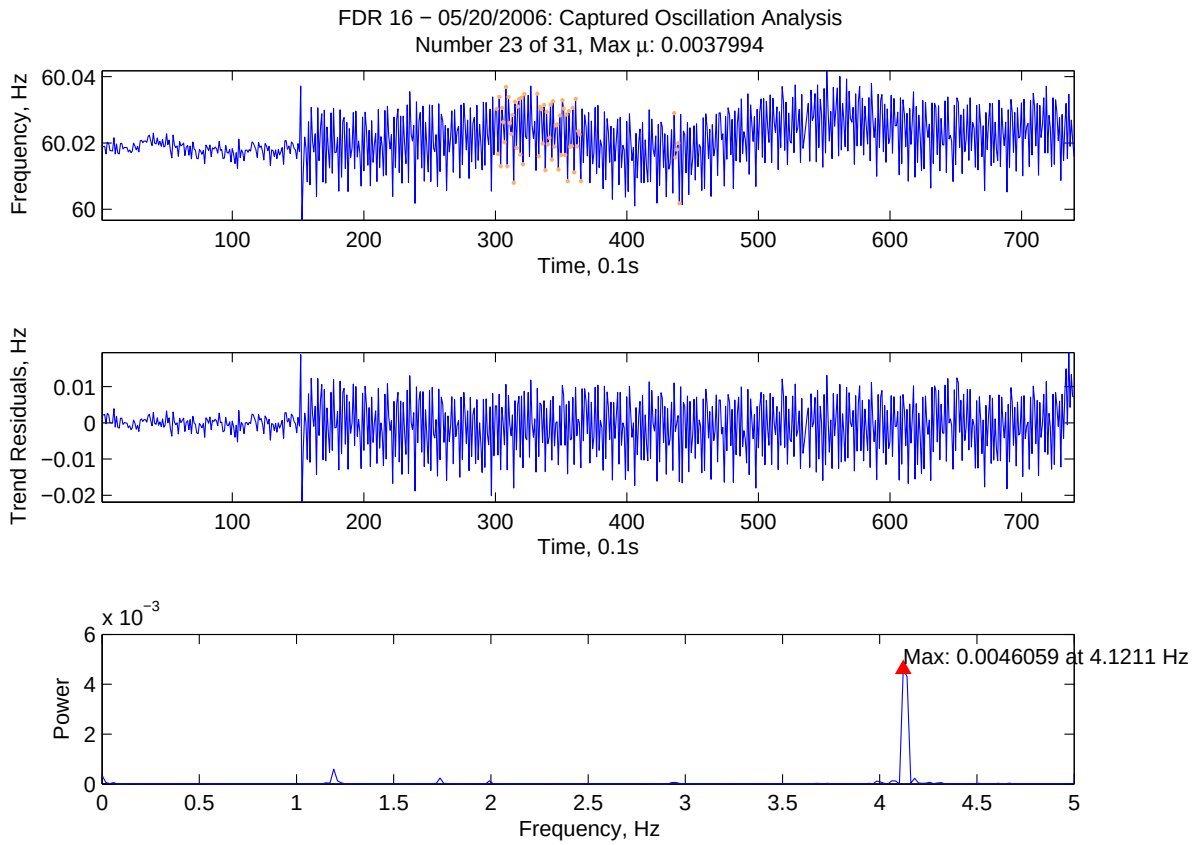


Figure C.24. Daily oscillation analysis: 23 of 31

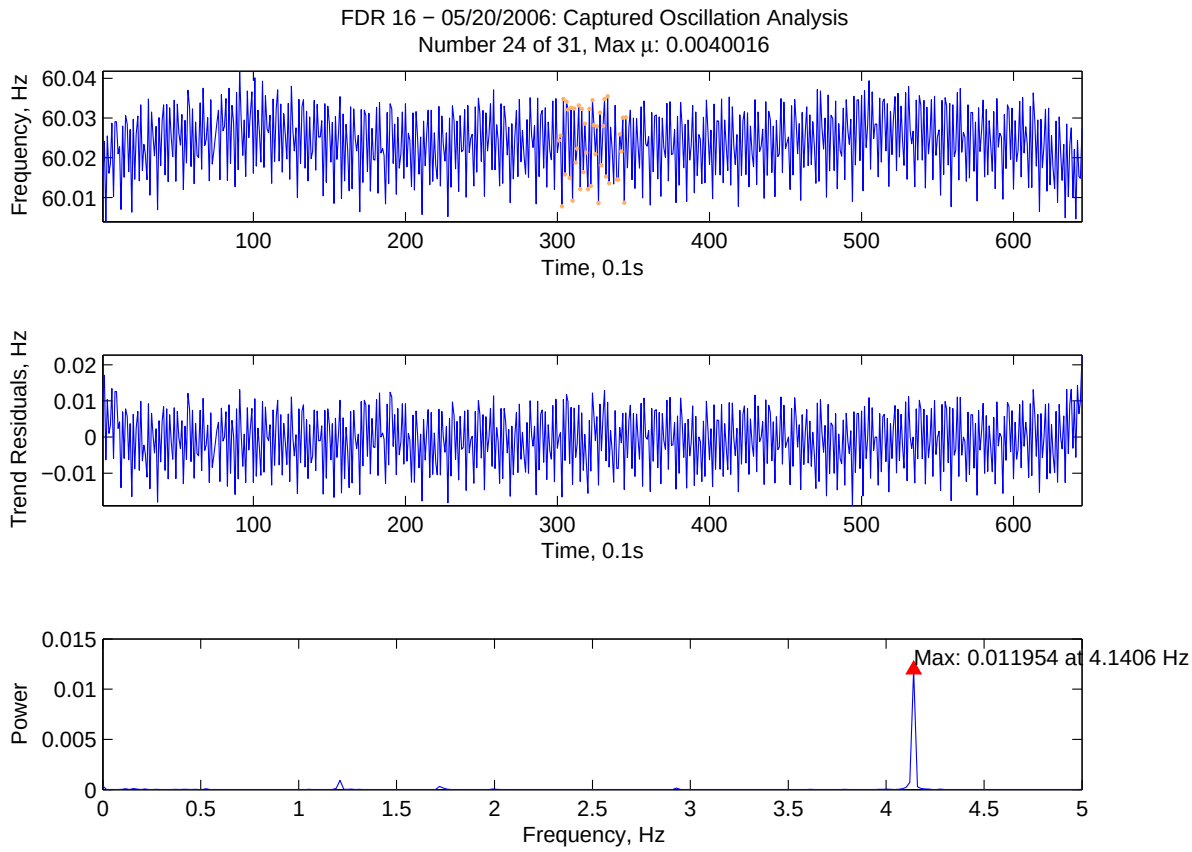


Figure C.25. Daily oscillation analysis: 24 of 31

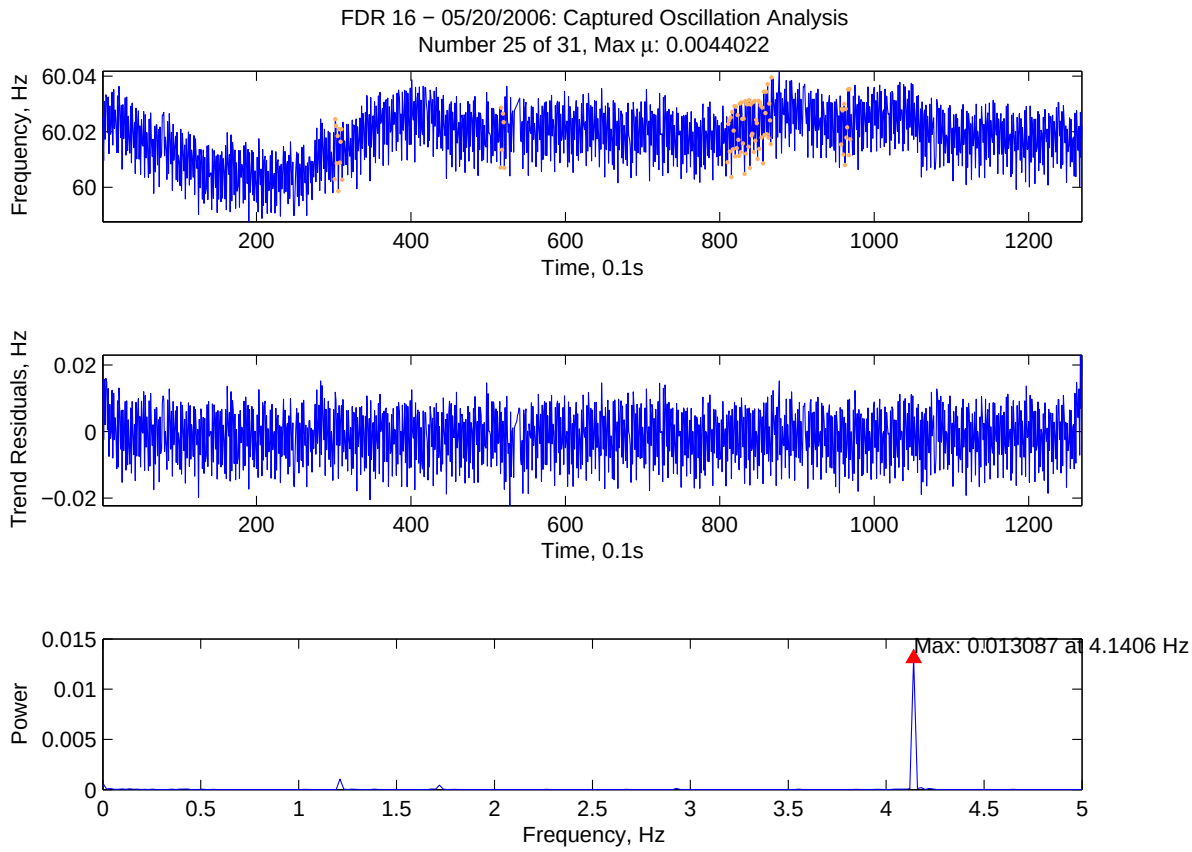


Figure C.26. Daily oscillation analysis: 25 of 31

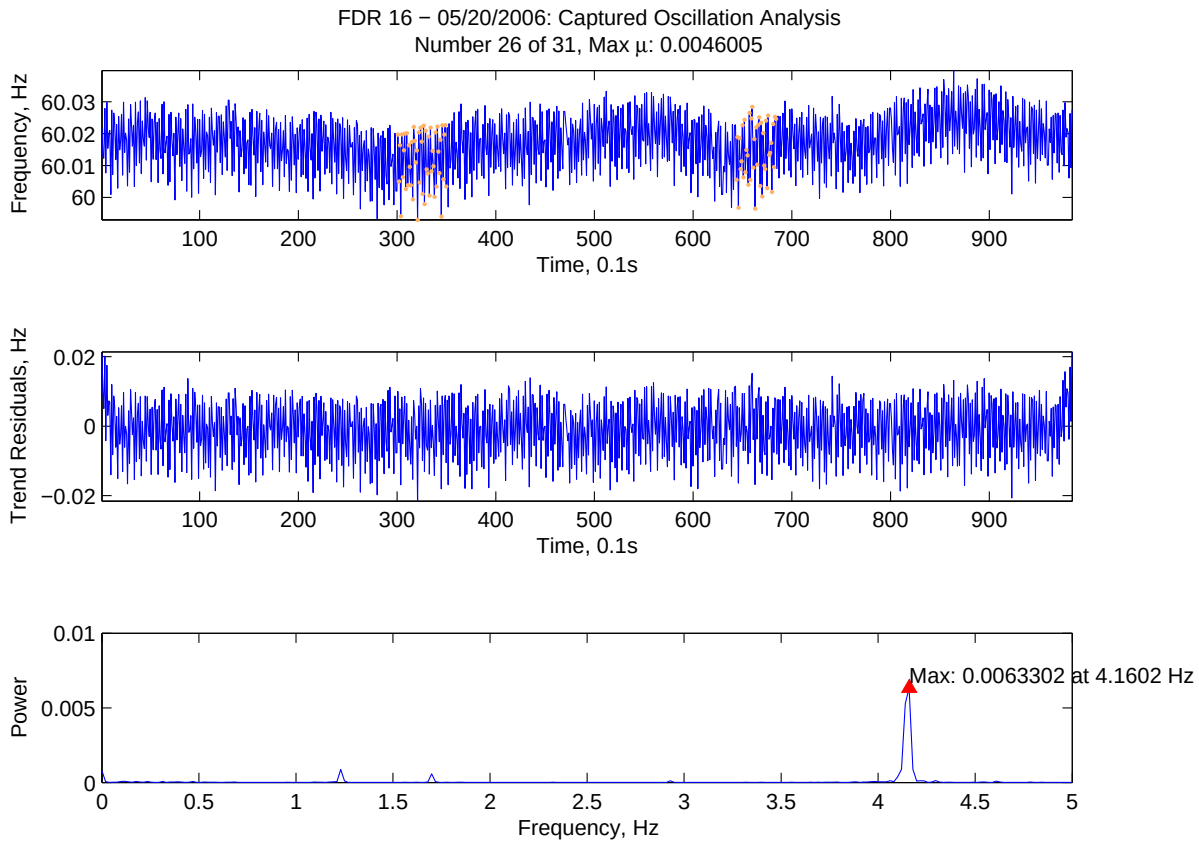


Figure C.27. Daily oscillation analysis: 26 of 31

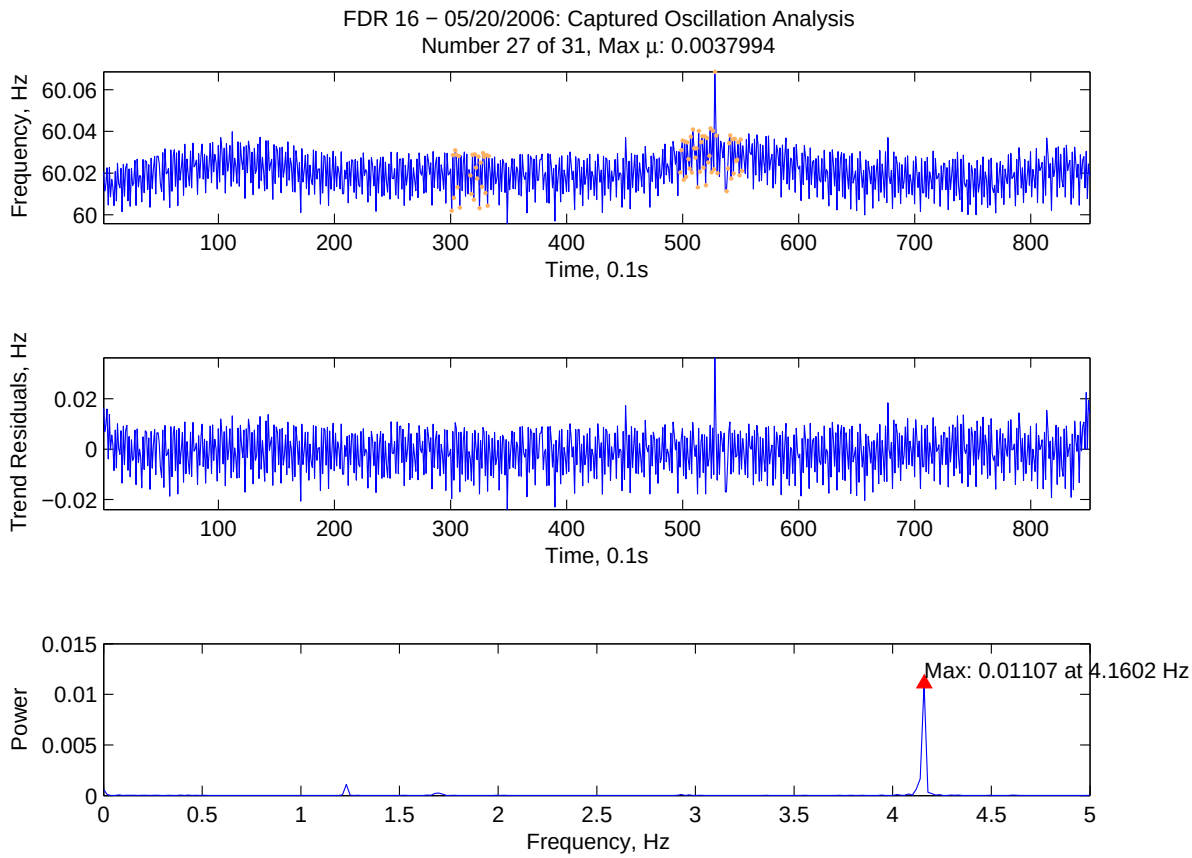


Figure C.28. Daily oscillation analysis: 27 of 31

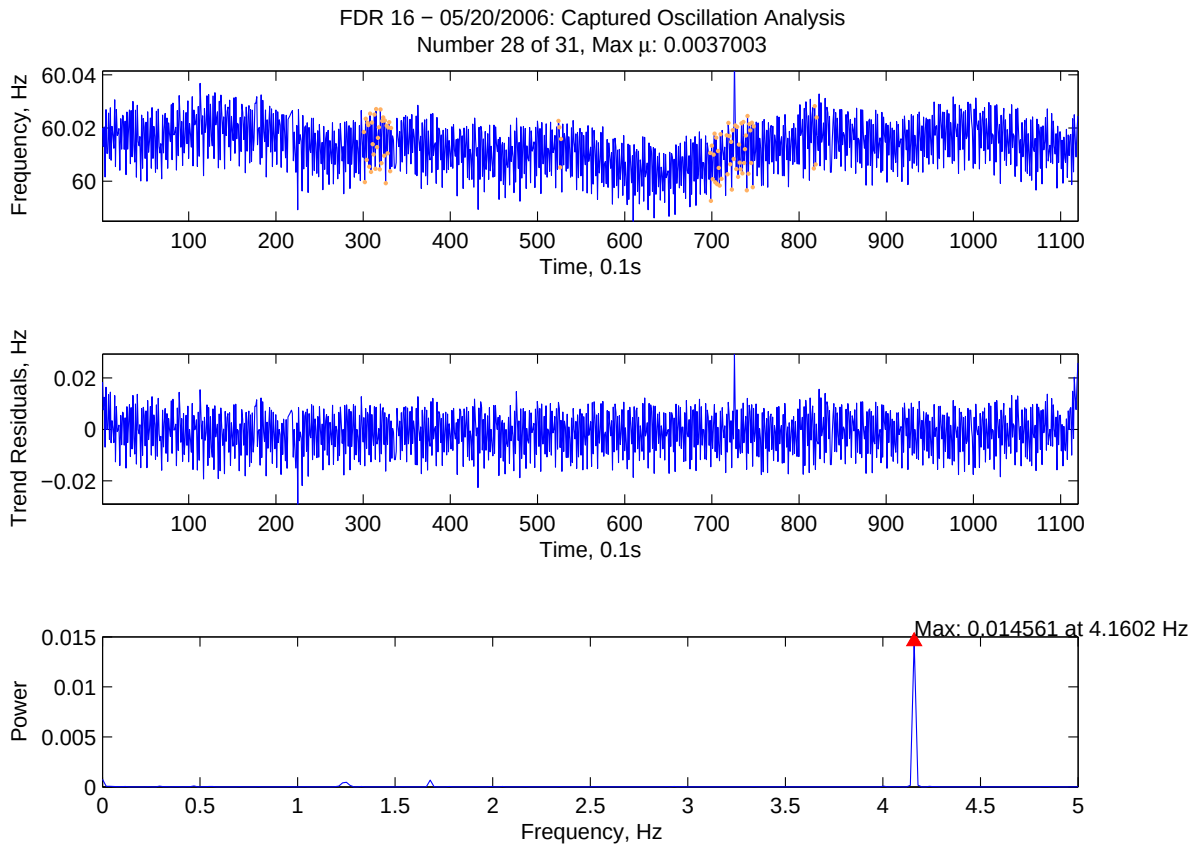


Figure C.29. Daily oscillation analysis: 28 of 31

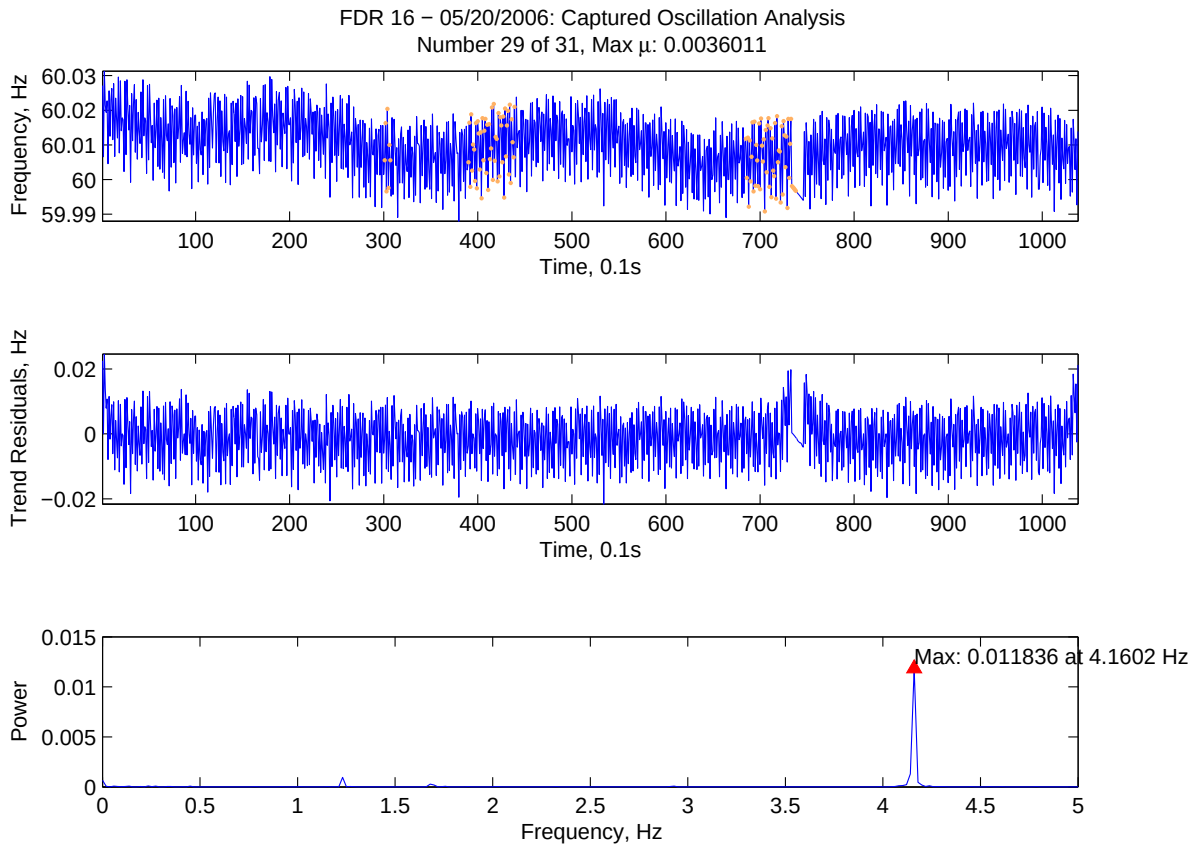


Figure C.30. Daily oscillation analysis: 29 of 31

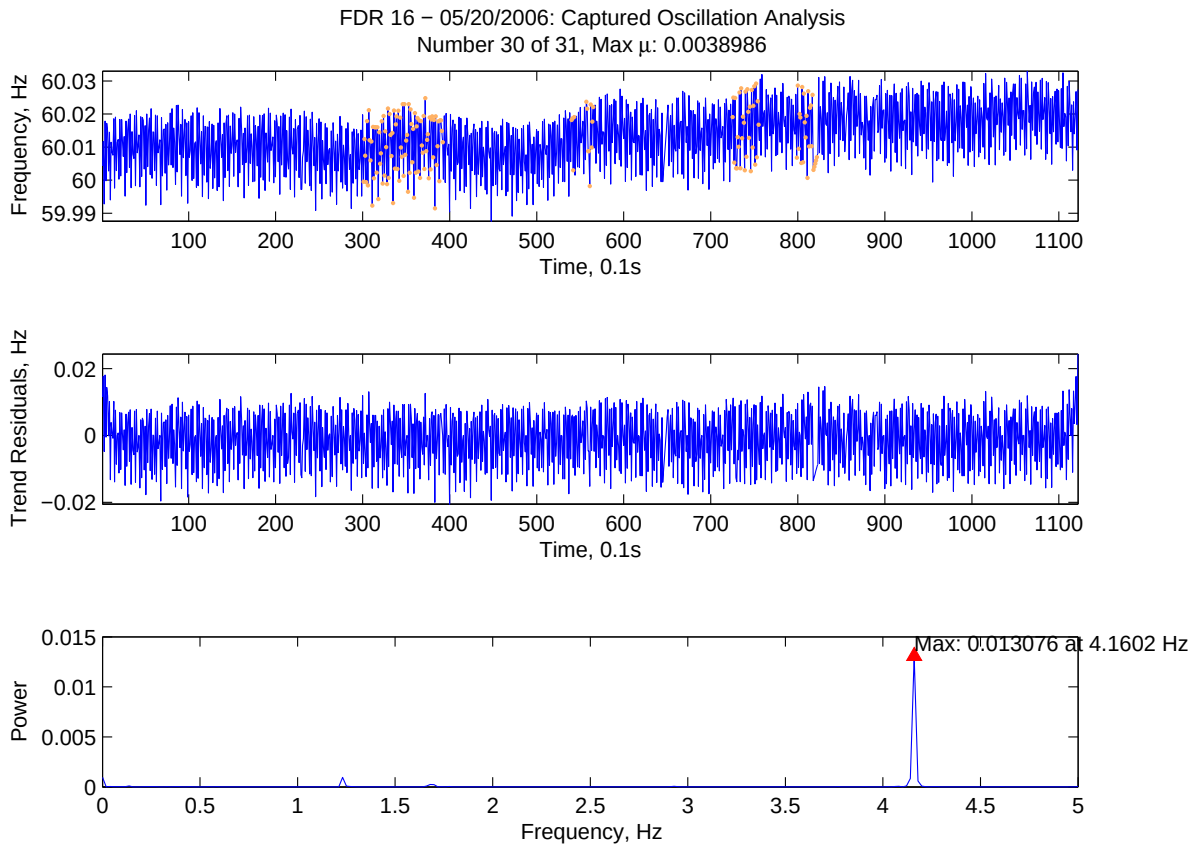


Figure C.31. Daily oscillation analysis: 30 of 31

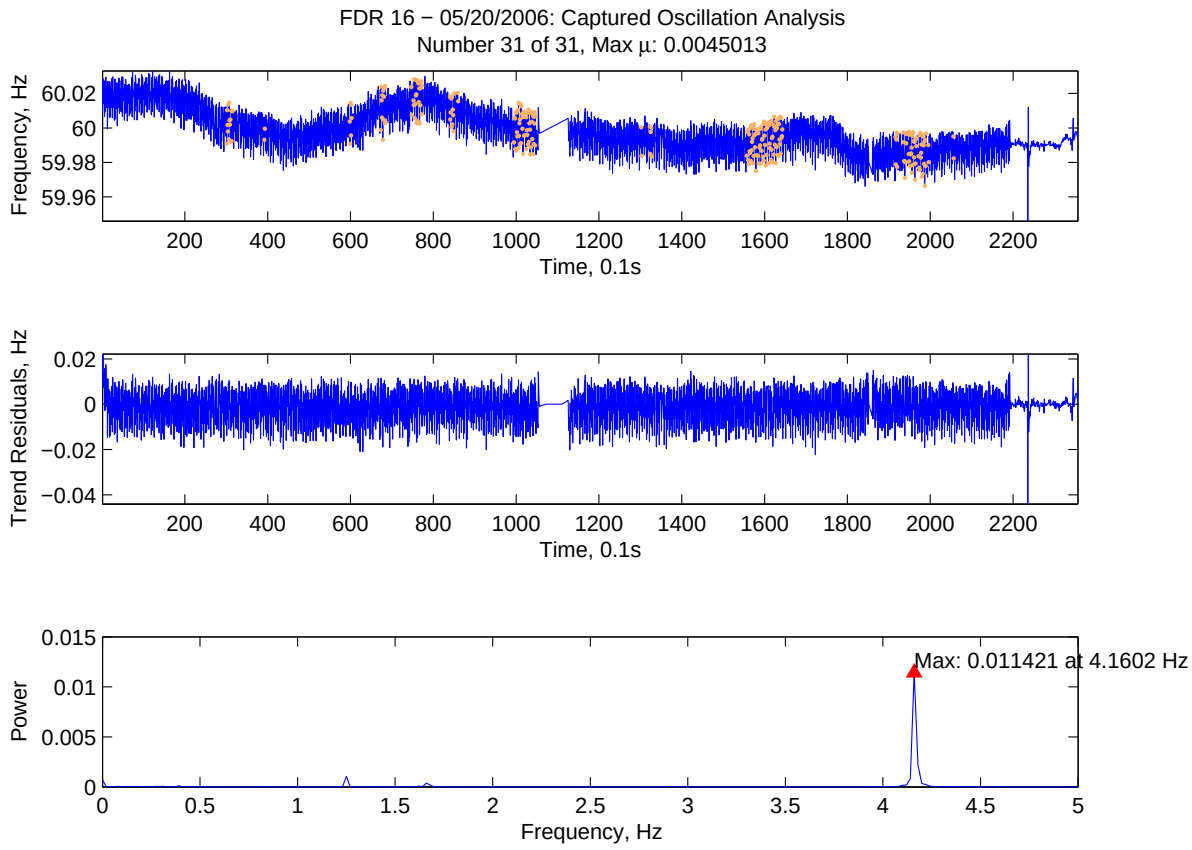


Figure C.32. Daily oscillation analysis: 31 of 31

Appendix D

2007 Event Analysis Results

Table D.1. Performance summary of new ordering method

Parzen windowing method			LS estimate		
Metric (quantile)	Cases	Percentage	Metric (mi)	Cases	Percentage
$\Delta Q_{actual} > 0.15$	19	34.55%	$\Delta LS_{error} > 200$	15	27.27%
$\Delta Q_{actual} > 0.00$	25	45.45%	$\Delta LS_{error} > 0$	28	50.91%
$\Delta Q_{actual} > -0.15$	36	65.45%	$\Delta LS_{error} < 200$	34	61.82%
$\Delta Q_{actual} < 0.00$	30	54.55%	$\Delta LS_{error} < 0$	24	43.64%
$\Delta Q_{actual} < -0.15$	19	34.55%	$\Delta LS_{error} < -200$	9	16.36%
			common failures	3	5.45%

Mismatch estimate		
Metric (MW)	Cases	Percentage
$\Delta MW_{error} > 50$	19	34.55%
$\Delta MW_{error} > 0$	34	61.82%
$\Delta MW_{error} < 50$	44	80.00%
$\Delta MW_{error} < 0$	18	32.73%
$\Delta MW_{error} < -50$	10	18.18%
common failures	3	5.45%

Error distributions			
Method	μ	σ	median
LS: old ordering	267.11 mi	250.34 mi	221.42 mi
LS: new ordering	310.97 mi	246.91 mi	281.22 mi
HP: old ordering	0.7054	0.3641	0.9057
HP: new ordering	0.6691	0.3373	0.7833

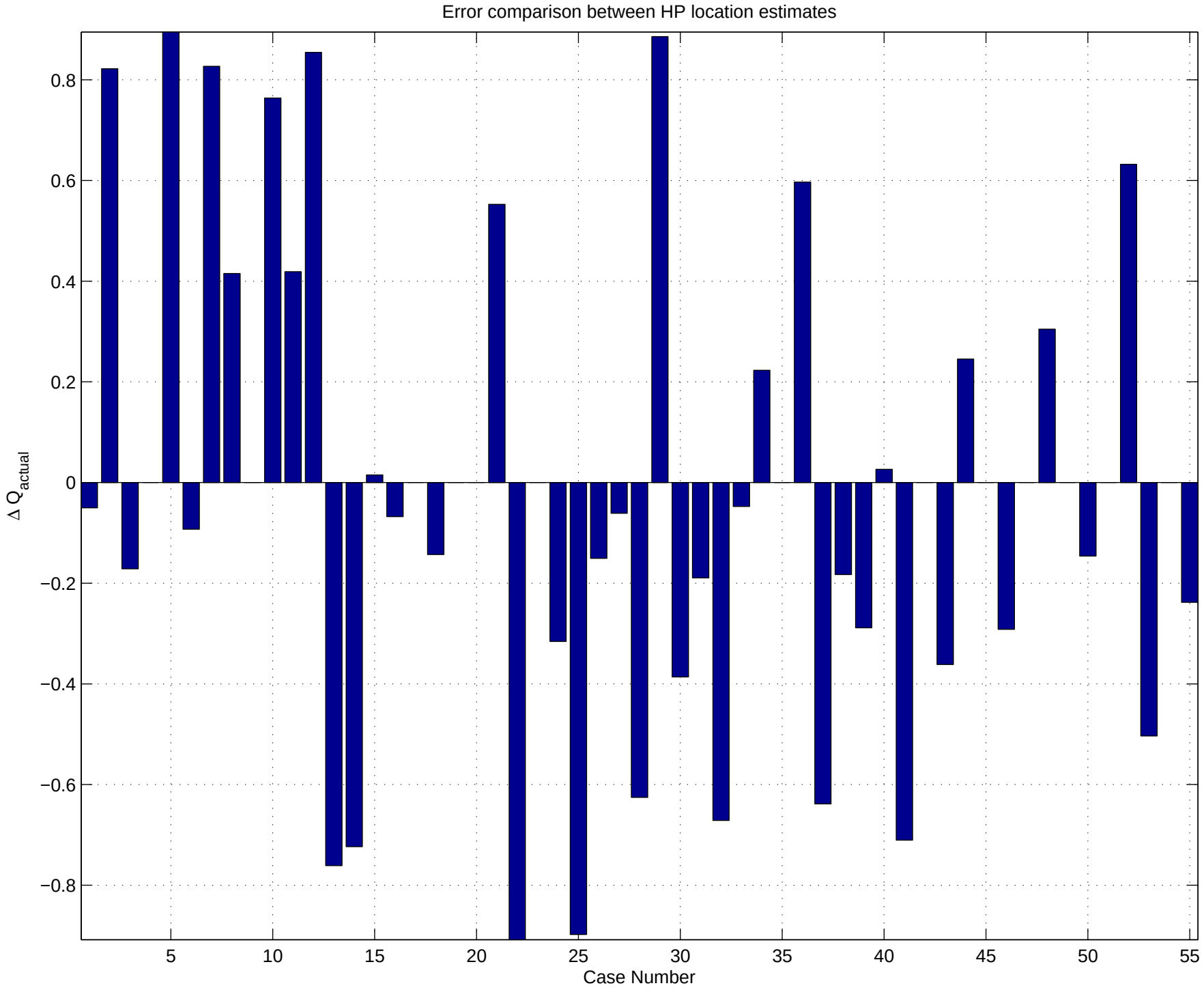


Figure D.1. Differential LoD solutions: Parzen windowing

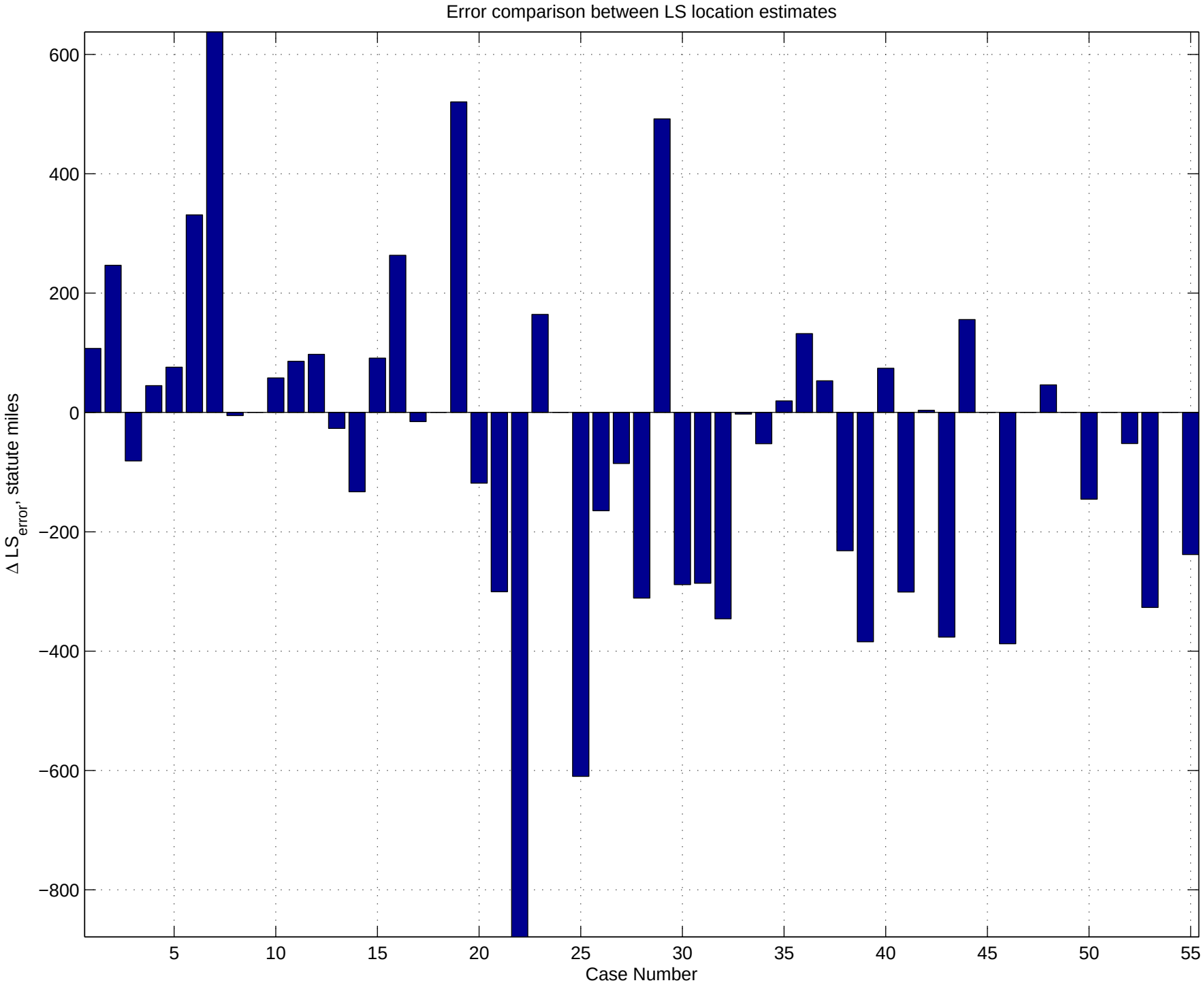


Figure D.2. Differential LoD solutions: Least-squares

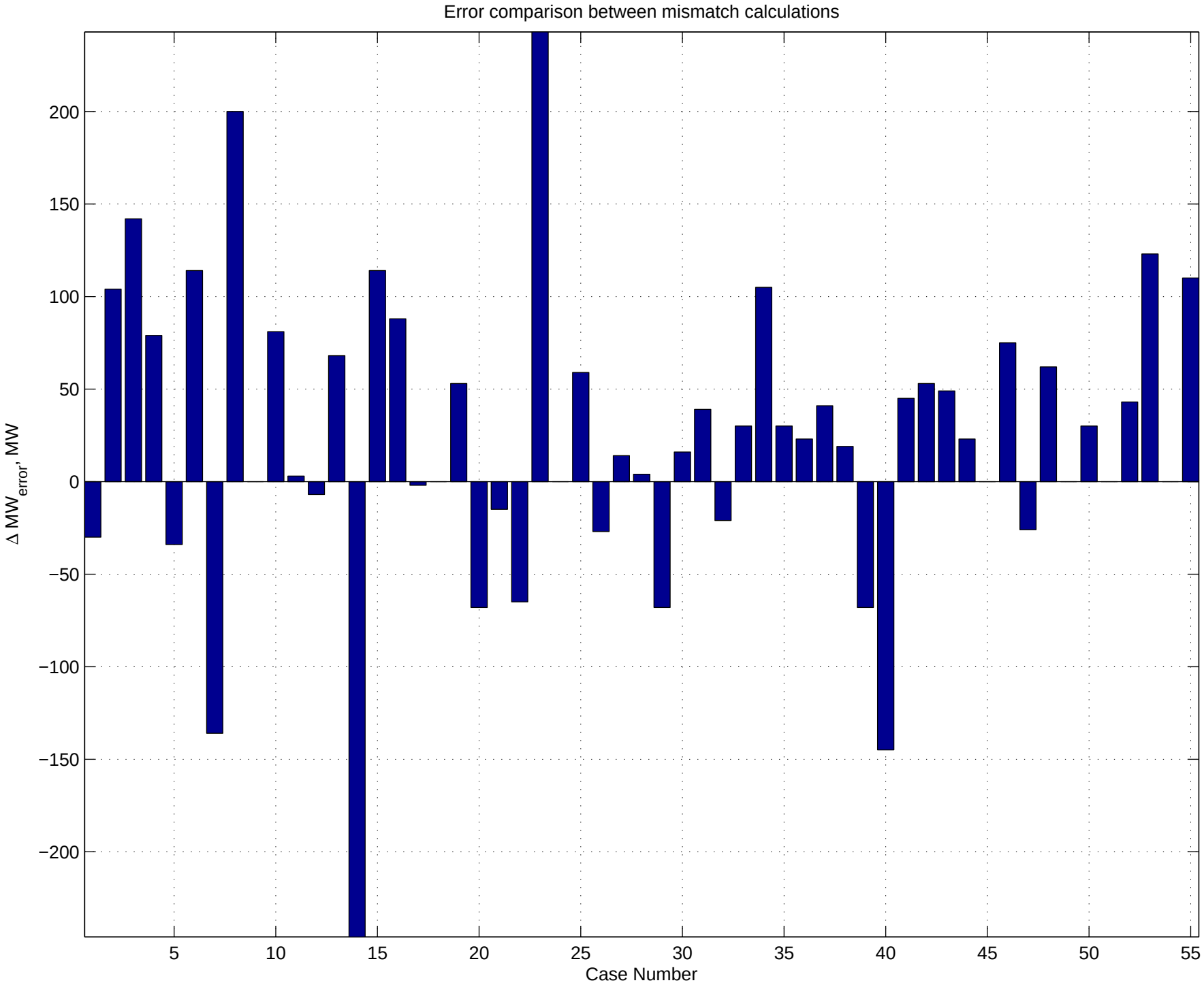


Figure D.3. Differential mismatch calculations

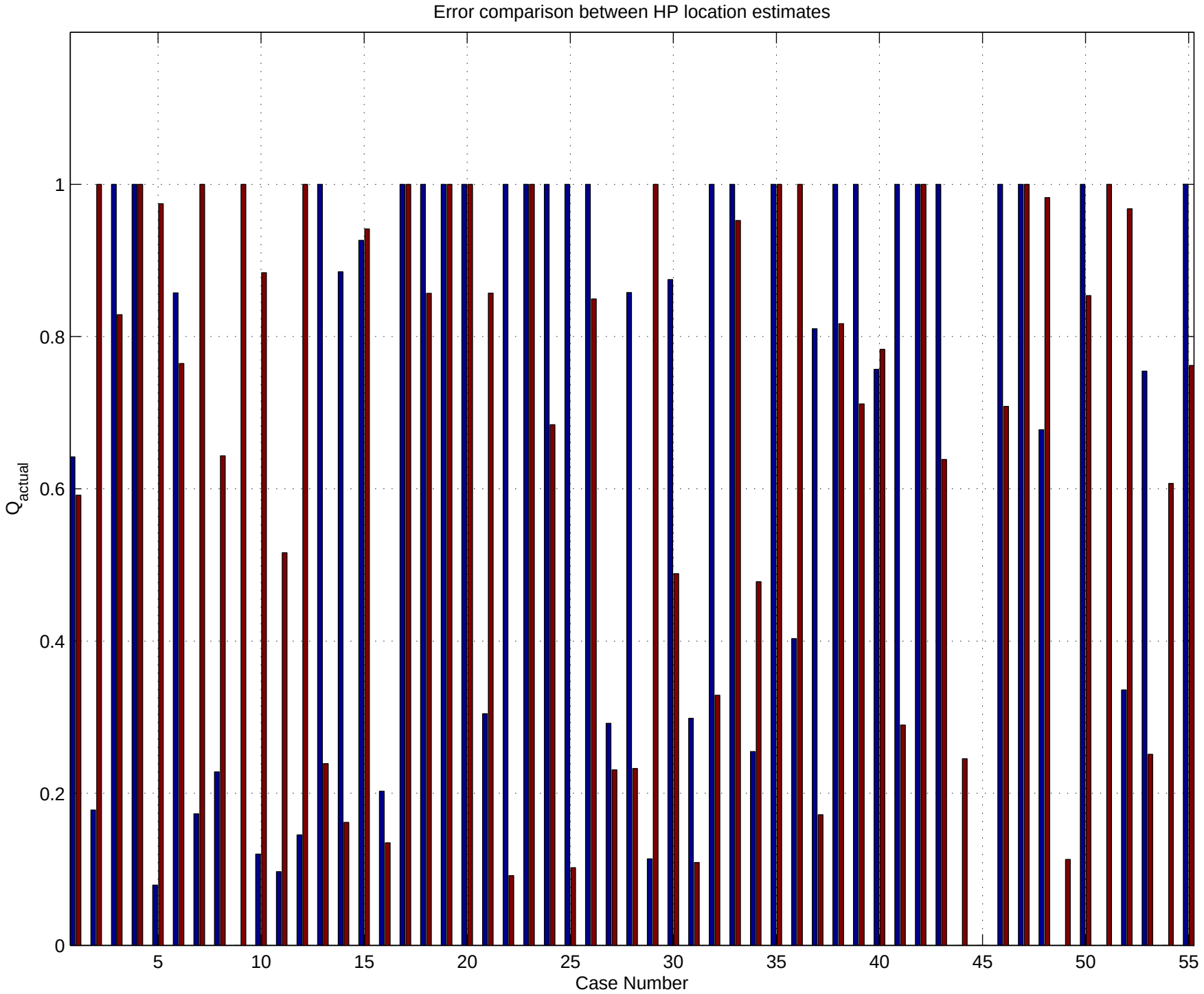


Figure D.4. Individual LoD solutions: Parzen windowing

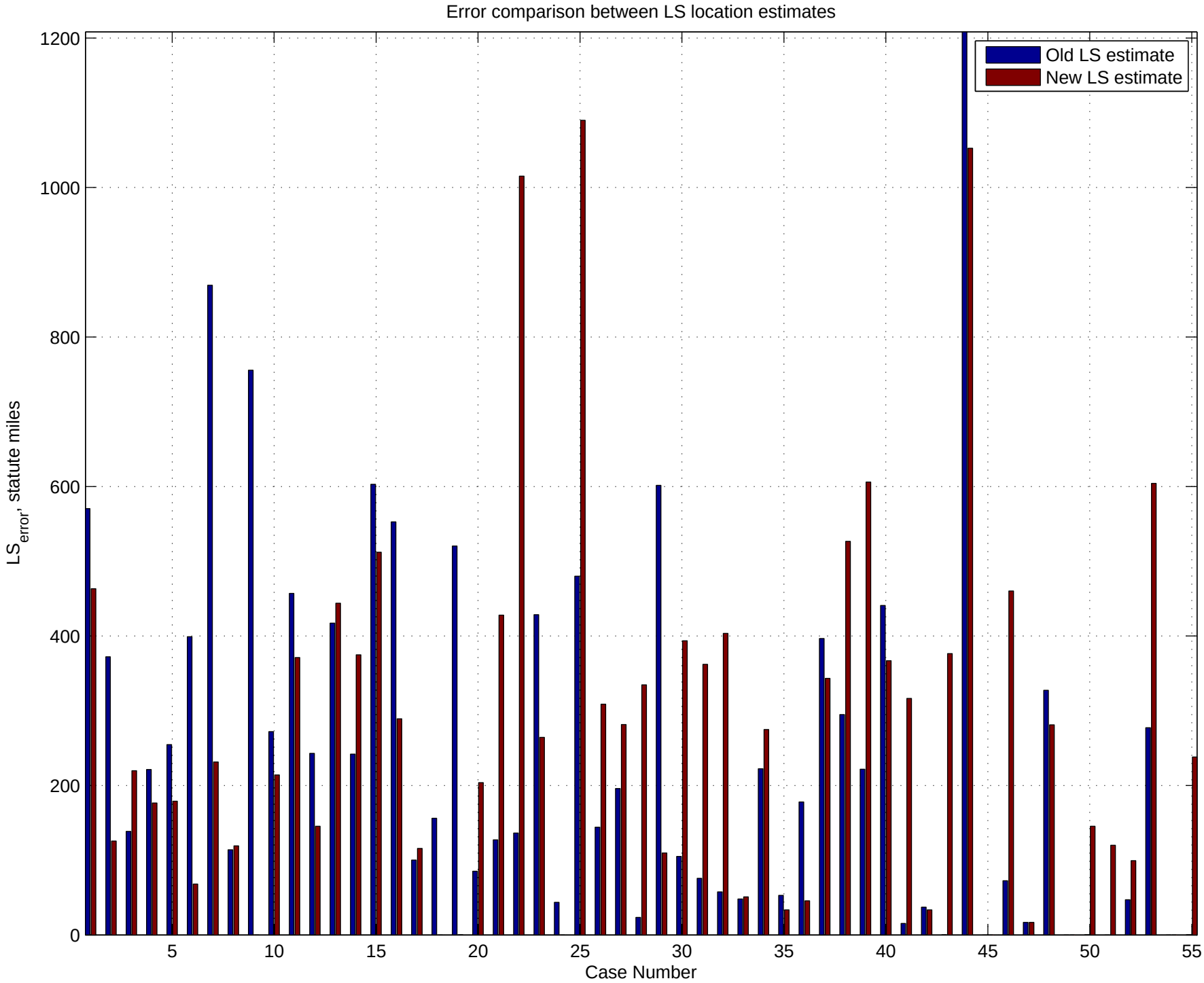


Figure D.5. Individual LoD solutions: Least-squares

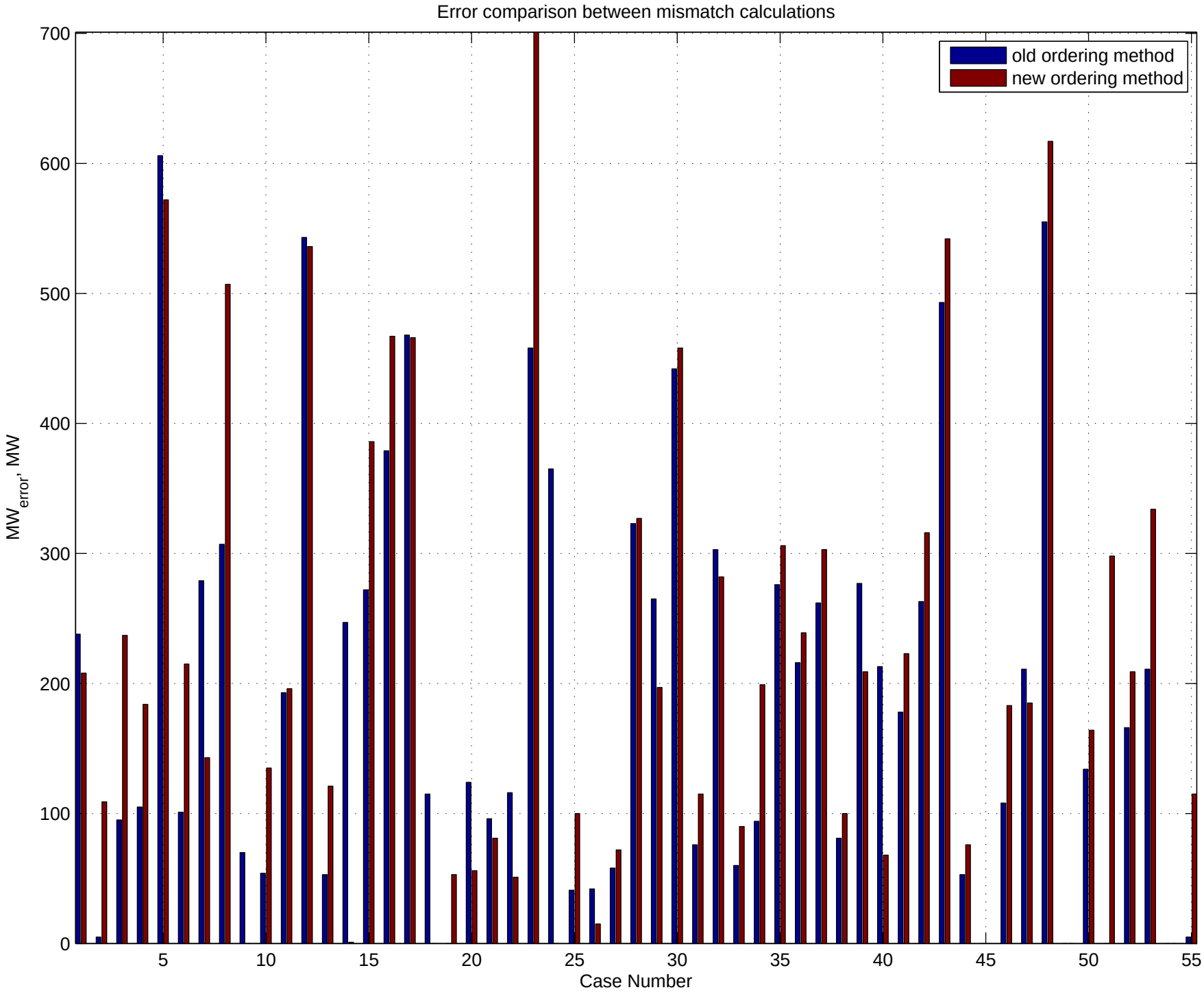


Figure D.6. Individual mismatch calculations

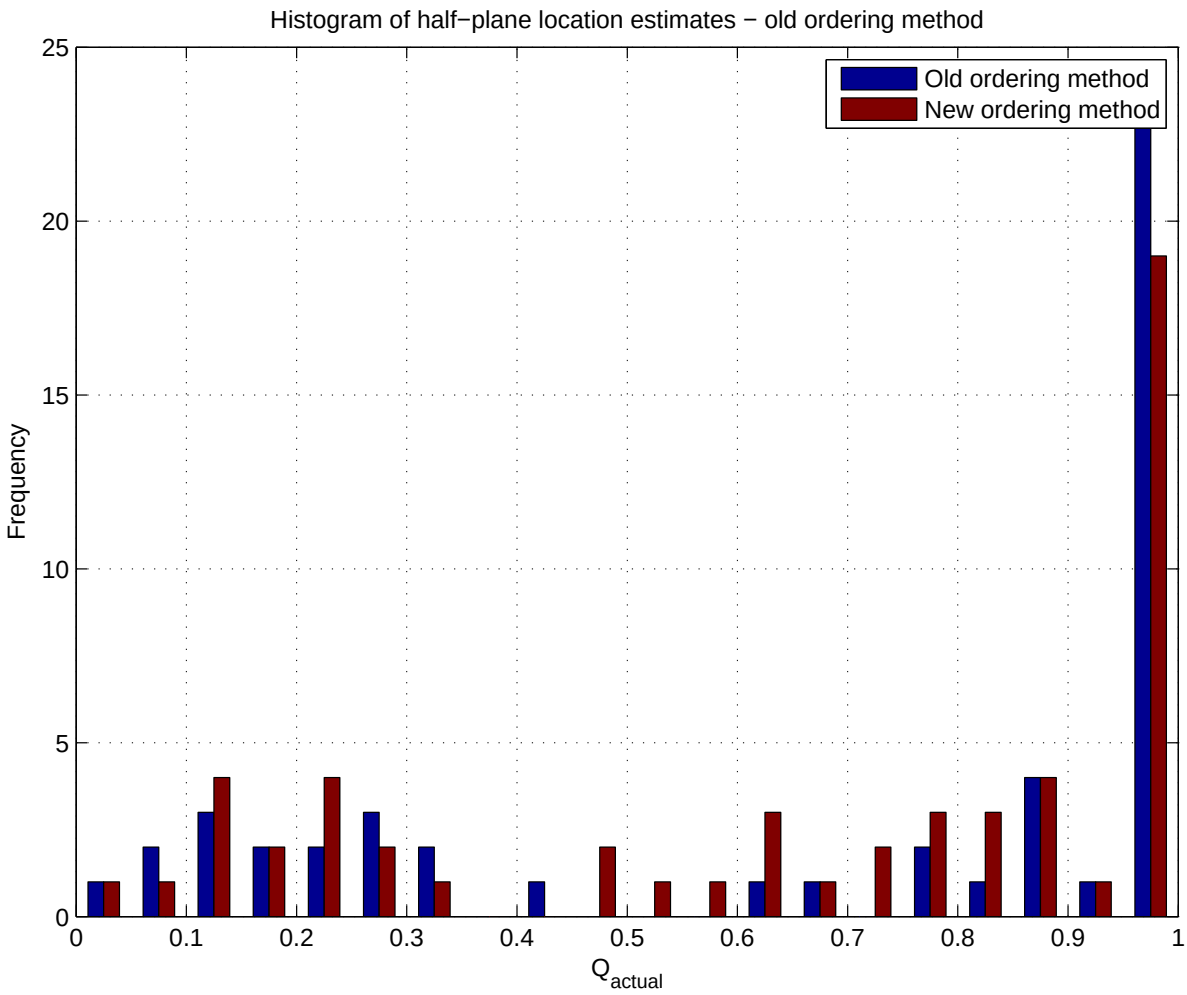


Figure D.7. Statistical LoD solutions: Parzen windowing

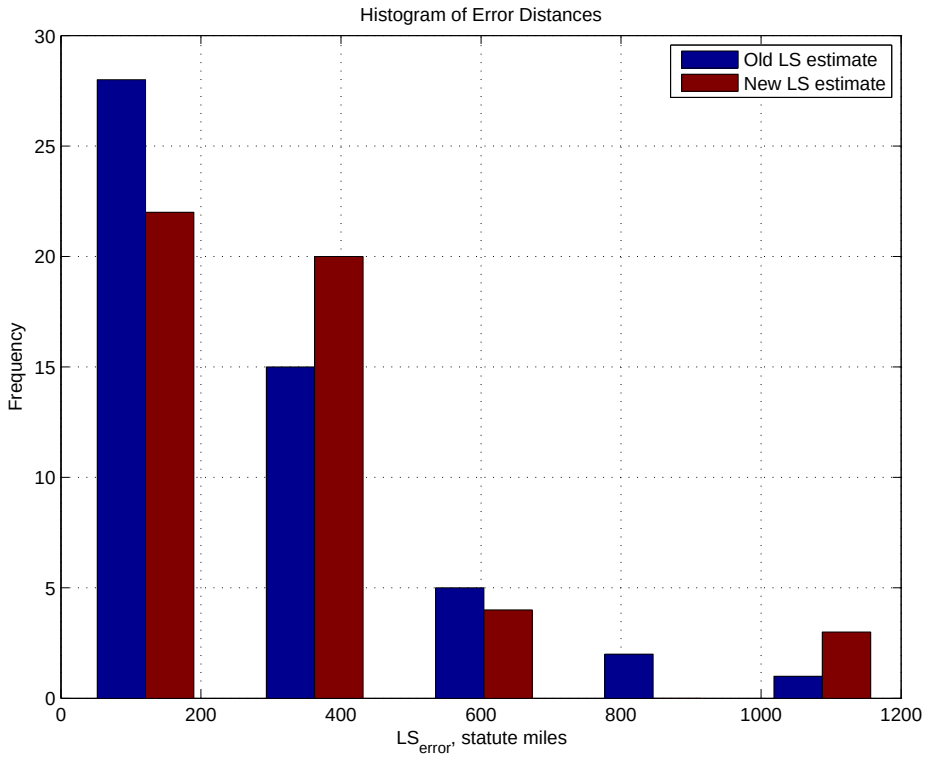


Figure D.8. Statistical LoD solutions: Least-squares

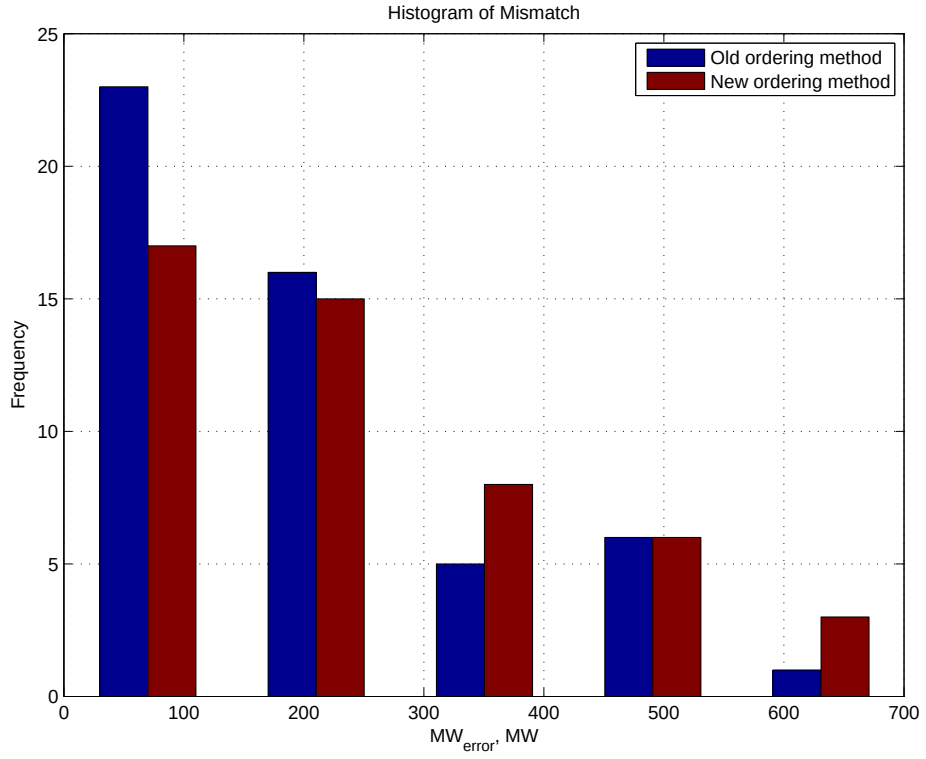


Figure D.9. Statistical mismatch calculations

Table D.2. Ordering method comparison: Lacygne (840 MW, 38.3335°, −94.7608°) Trip on 01/02/2007 17:16:30

	Old Ordering Method			New Ordering Method		
Mismatch estimate (MW)	602			632		
FDR Info	Number	Name	Distance (mi)	Number	Name	Distance (mi)
	35	ISU	261.9	15	TVA3Nashville	463.2
	2	UMR	164.9	35	ISU	261.9
	36	TVA5MuscleShoals	466.2	2	UMR	164.9
	27	RPI	1145	32	TVA7Hopkinsville	412.3
	15	TVA3Nashville	463.2	23	Duluth2	599.5
	9	UFL	928.2	36	TVA5MuscleShoals	466.2
	13	MidwestISO	476.9	4	VT	785.5
	11	Calvin	574	11	Calvin	574
	4	VT	785.5	13	MidwestISO	476.9
	506	OhioTiffin	645.6	6	ABB	903.2
	502	Toronto	893.5	3	ARI	953.8
	3	ARI	953.8	24	Toronto2	893.5
	6	ABB	903.2	27	RPI	1145
	17	TVA4Jackson	376.7			
	32	TVA7Hopkinsville	412.3			
	560	Duluth	599.5			
LS estimate	Latitude	Longitude	Distance (mi)	Latitude	Longitude	Distance (mi)
	40.1099°	−84.3443°	570.5	36.1716°	−86.7848°	463.2
	$Q_{old} = 0.0313$			$Q_{old} = 0.0679$		
	$Q_{new} = 0.8657$			$Q_{new} = 1.0000$		
Parzen windowing results	$Q_{actual} = 0.6420$			$Q_{actual} = 0.5916$		

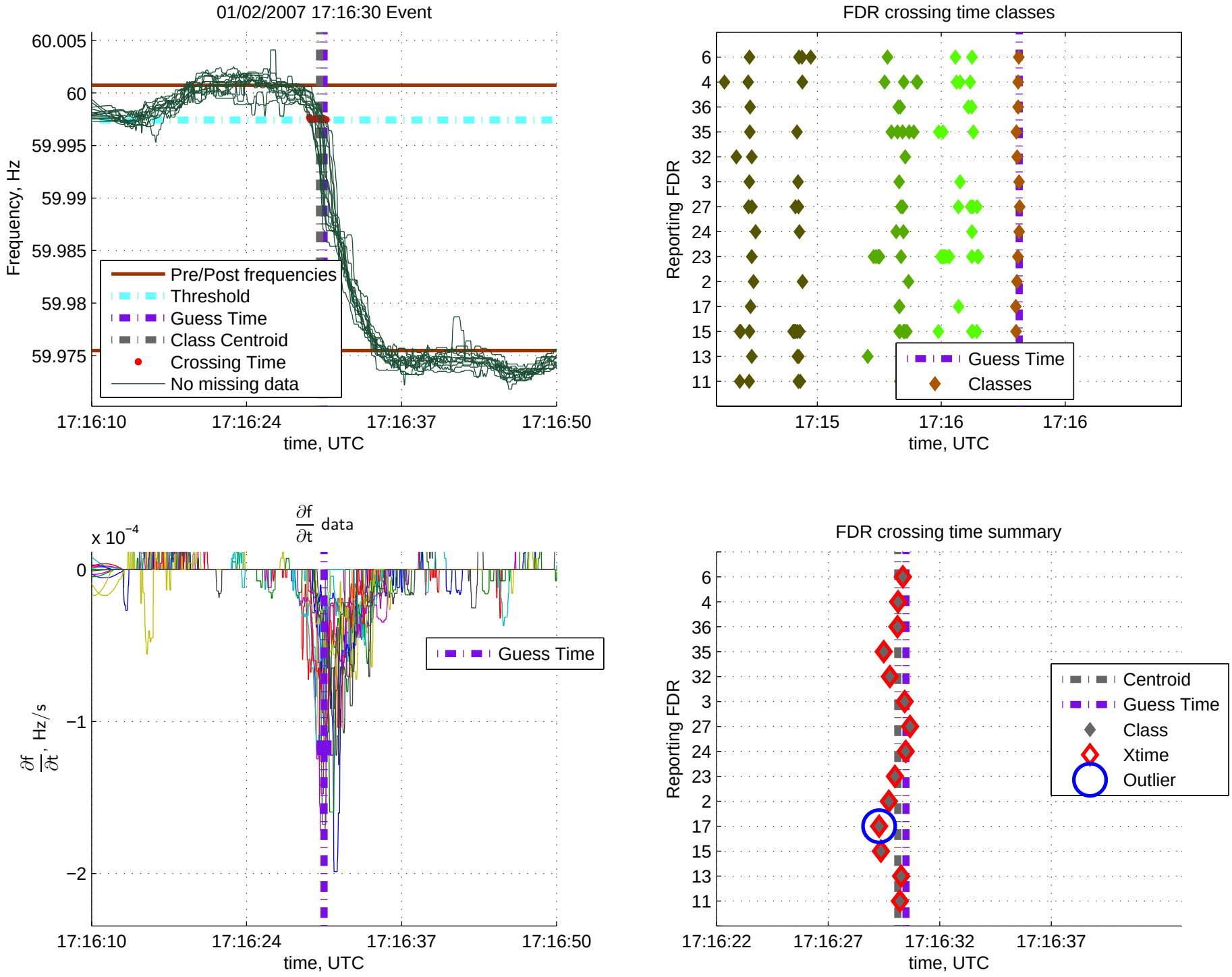
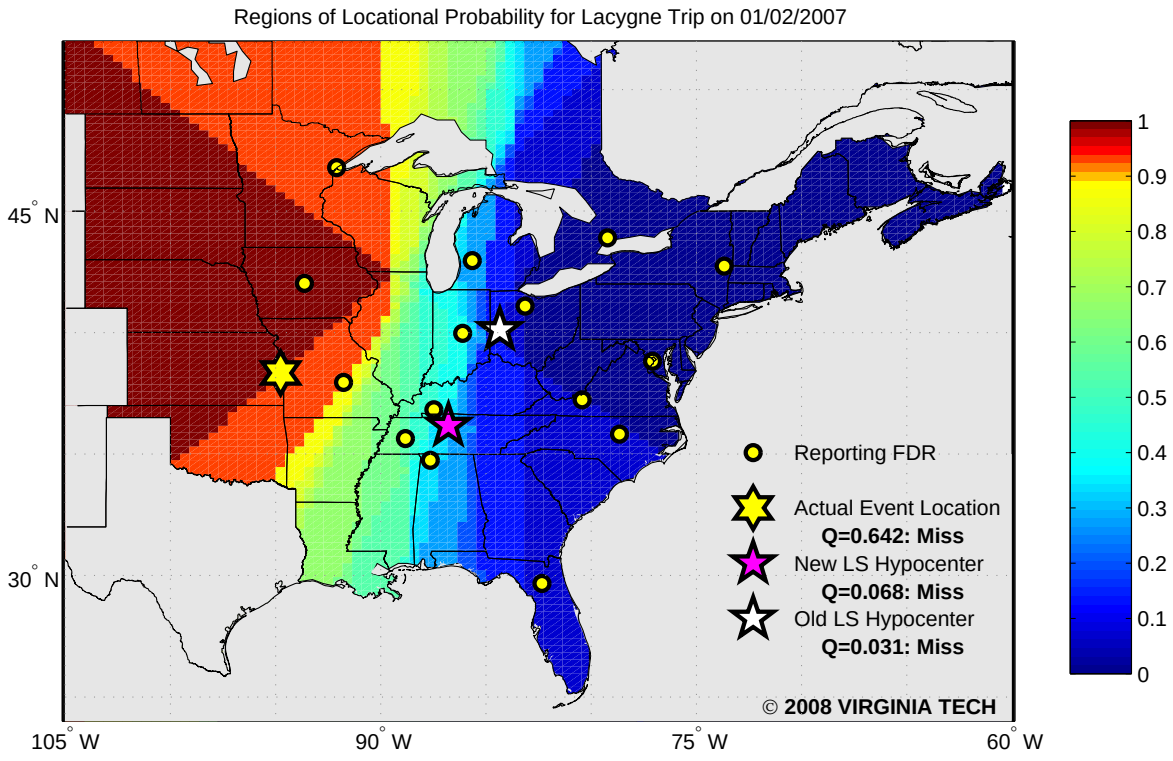
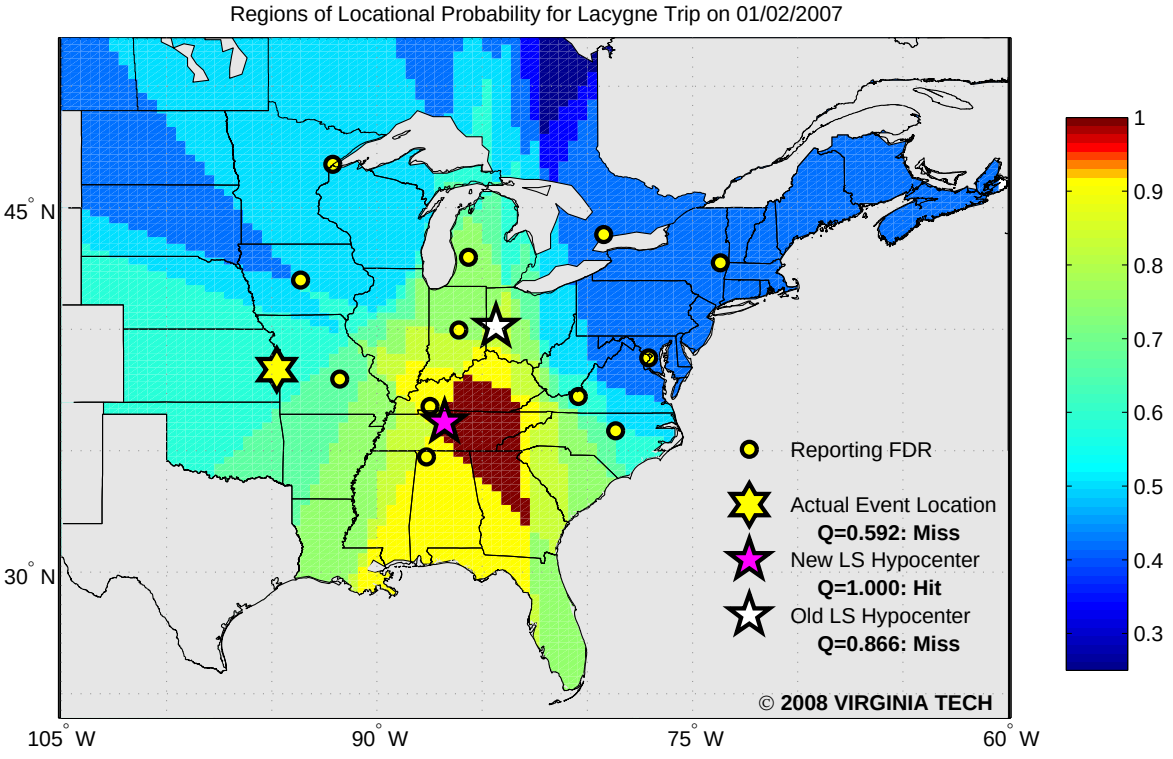


Figure D.10. Consolidated event ordering calculations: Lacygne (840 MW, 38.3335°, −94.7608°) Trip on 01/02/2007 17:16:30



(a) Event location: old ordering method

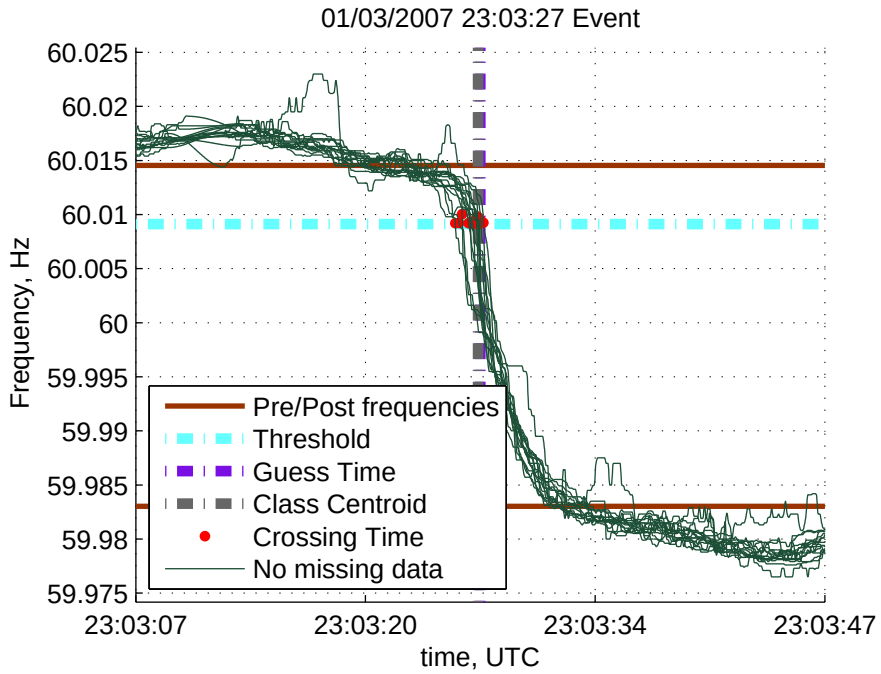


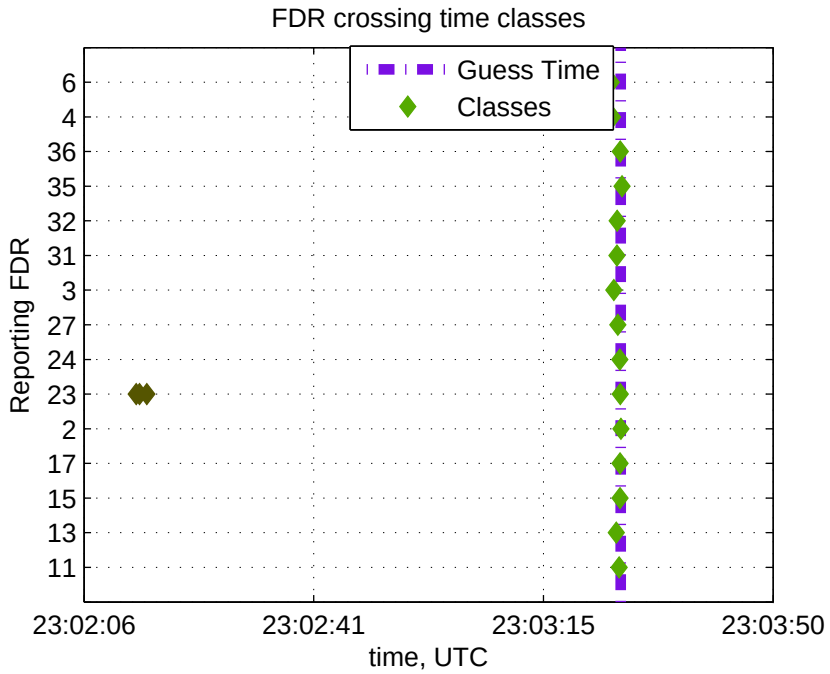
(b) Event location: new ordering method

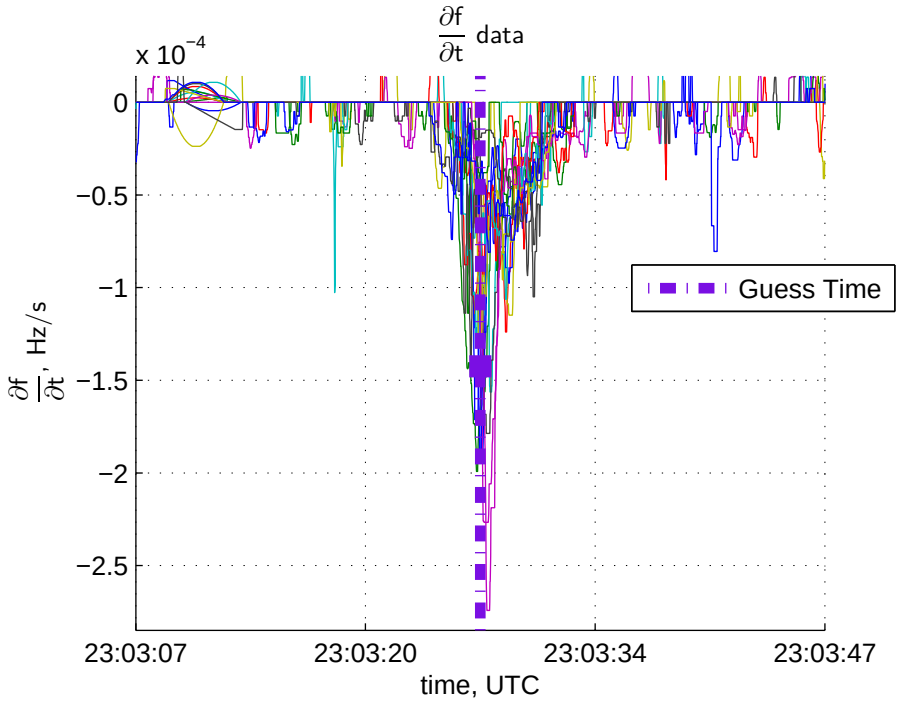
Figure D.11. Event location estimates: Lacygne (840 MW, 38.3335°, −94.7608°) Trip on 01/02/2007 17:16:30

Table D.3. Ordering method comparison: North Anna (910 MW, 37.9986°, −77.8781°) Trip on 01/03/2007 23:03:27

	Old Ordering Method			New Ordering Method		
Mismatch estimate (MW)	905			801		
FDR Info	Number	Name	Distance (mi)	Number	Name	Distance (mi)
	27	RPI	394.9	3	ARI	71.18
	31	UK	360.4	13	MidwestISO	462.4
	506	OhioTiffin	352.2	31	UK	360.4
	11	Calvin	533.1	32	TVA7Hopkinsville	532.7
	13	MidwestISO	462.4	27	RPI	394.9
	32	TVA7Hopkinsville	532.7	11	Calvin	533.1
	4	VT	149.3	24	Toronto2	413.5
	36	TVA5MuscleShoals	587.4	15	TVA3Nashville	506.7
	15	TVA3Nashville	506.7	17	TVA4Jackson	626.9
	502	Toronto	413.5	36	TVA5MuscleShoals	587.4
	2	UMR	755.7	23	Duluth2	943.6
	9	UFL	629.3	2	UMR	755.7
	35	ISU	877	35	ISU	877
	6	ABB	156.5			
	560	Duluth	943.6			
	3	ARI	71.18			
	17	TVA4Jackson	626.9			
LS estimate	Latitude	Longitude	Distance (mi)	Latitude	Longitude	Distance (mi)
	40.6260°	−83.9601°	372.2	36.4067°	−78.9800°	125.6
	Q_{old} = 0.0000			Q_{old} = 0.0794		
	Q_{new} = 0.1003			Q_{new} = 1.0000		
Parzen windowing results	Q_{actual} = 0.1779			Q_{actual} = 1.0000		







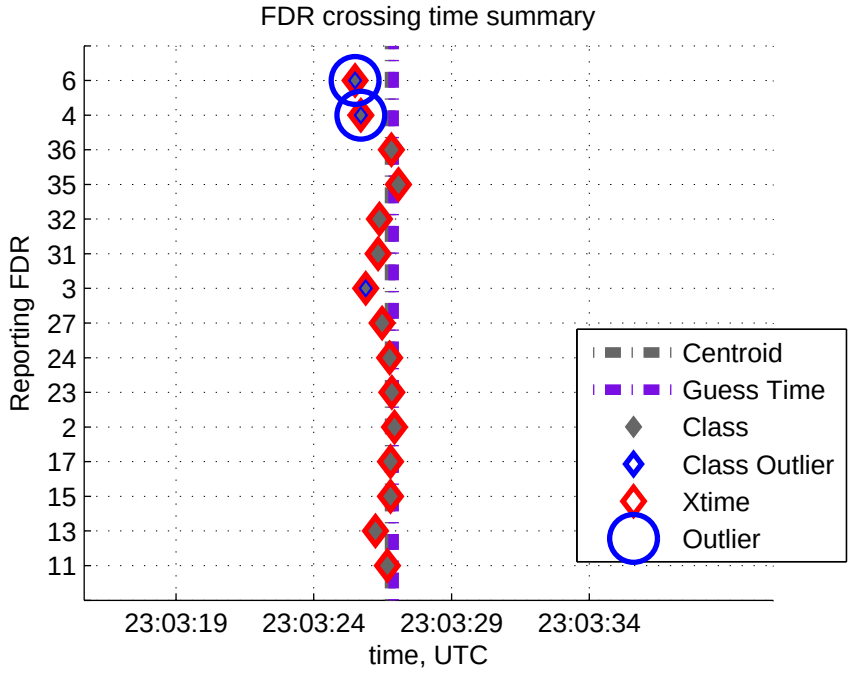
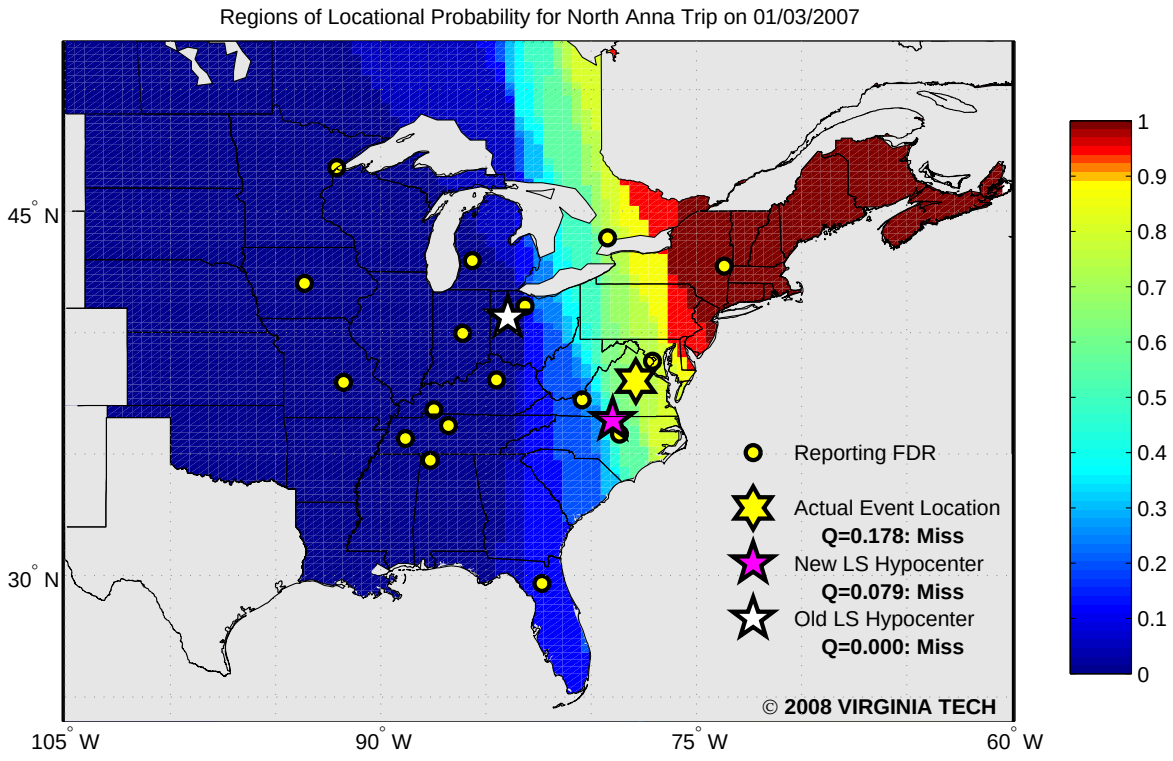
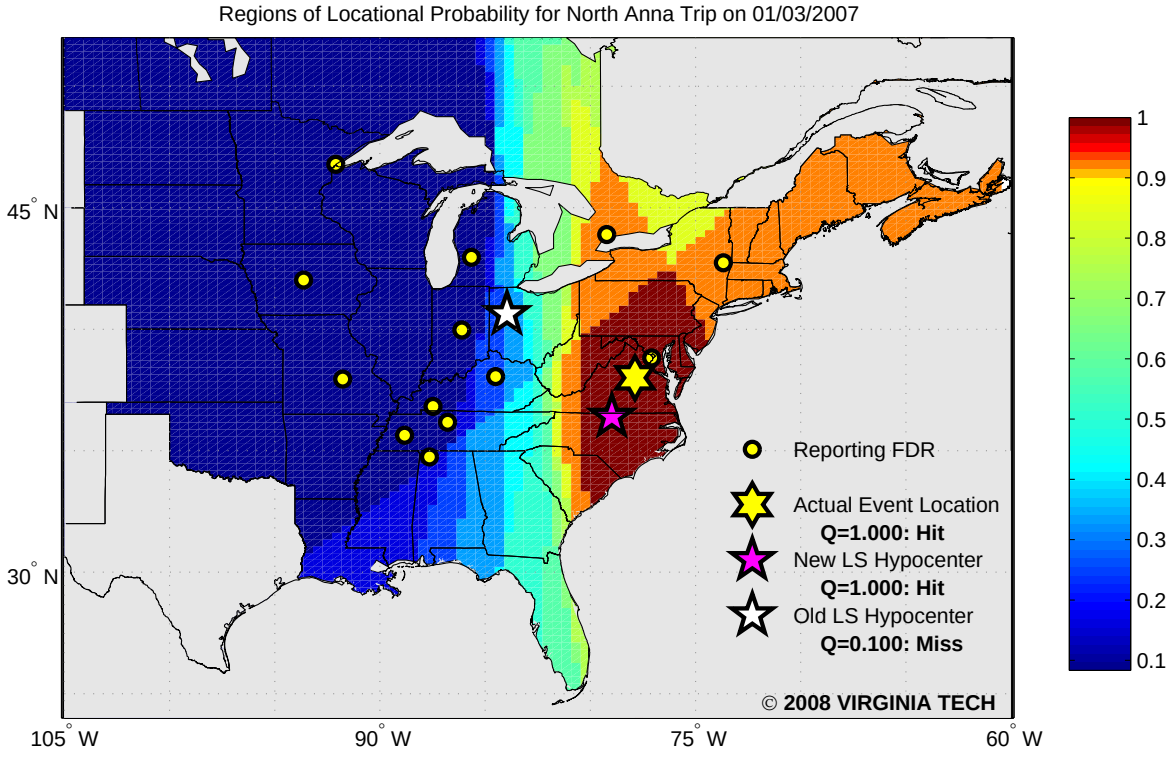


Figure D.12. Consolidated event ordering calculations: North Anna (910 MW, 37.9986°, −77.8781°) Trip on 01/03/2007 23:03:27



(a) Event location: old ordering method



(b) Event location: new ordering method

Figure D.13. Event location estimates: North Anna (910 MW, 37.9986°, −77.8781°) Trip on 01/03/2007 23:03:27

Table D.4. Ordering method comparison: Browns Ferry (1114 MW, 34.7055°, −87.1173°) Trip on 01/11/2007 14:18:45

	Old Ordering Method			New Ordering Method		
Mismatch estimate (MW)	1019			877		
FDR Info	Number	Name	Distance (mi)	Number	Name	Distance (mi)
	15	TVA3Nashville	103	17	TVA4Jackson	116
	32	TVA7Hopkinsville	147.6	32	TVA7Hopkinsville	147.6
	9	UFL	446	31	UK	273.1
	31	UK	273.1	2	UMR	342.2
	2	UMR	342.2	22	ROA2	437.7
	6	ABB	483.2	13	MidwestISO	367.9
	4	VT	412.7	6	ABB	483.2
	508	ROA	437.7	4	VT	412.7
	3	ARI	623.3	11	Calvin	575.8
	13	MidwestISO	367.9	3	ARI	623.3
	17	TVA4Jackson	116	27	RPI	910.7
	35	ISU	616	35	ISU	616
	11	Calvin	575.8	23	Duluth2	874.1
	506	OhioTiffin	491.1			
	560	Duluth	874.1			
	27	RPI	910.7			
	502	Toronto	761.6			
LS estimate	Latitude	Longitude	Distance (mi)	Latitude	Longitude	Distance (mi)
	36.1803°	−85.4494°	138.6	37.8858°	−87.0770°	219.7
	$Q_{old} = 1.0000$			$Q_{old} = 0.9779$		
	$Q_{new} = 0.5893$			$Q_{new} = 0.7184$		
Parzen windowing results	$Q_{actual} = 1.0000$			$Q_{actual} = 0.8287$		

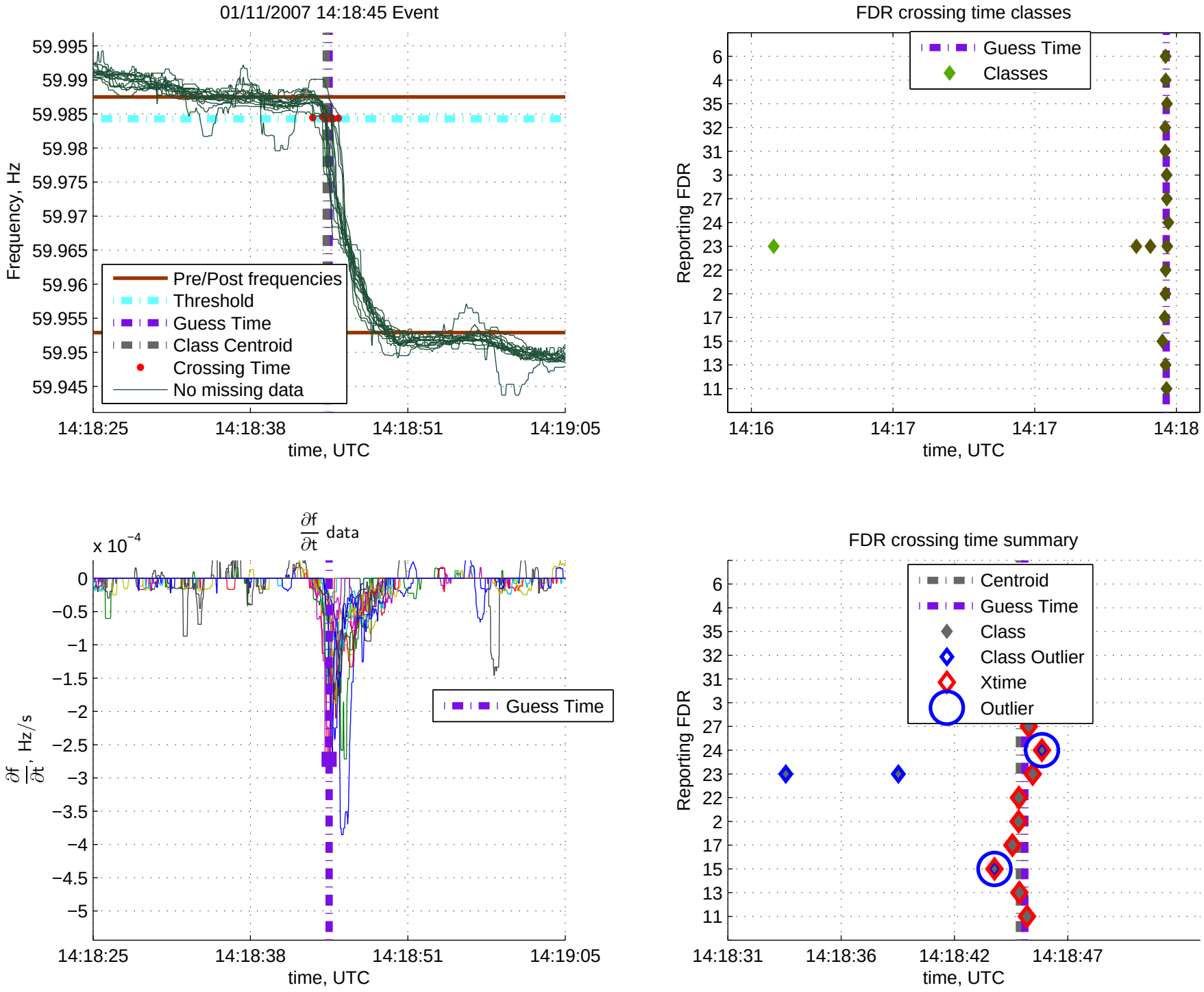
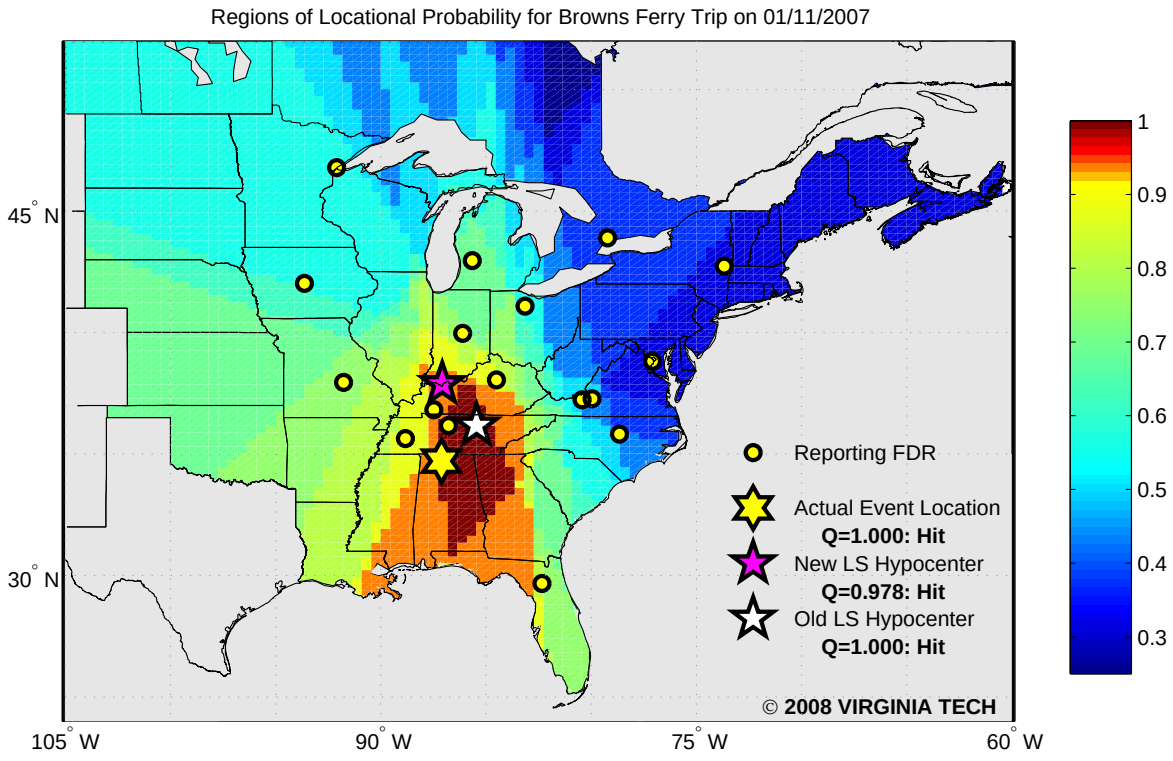
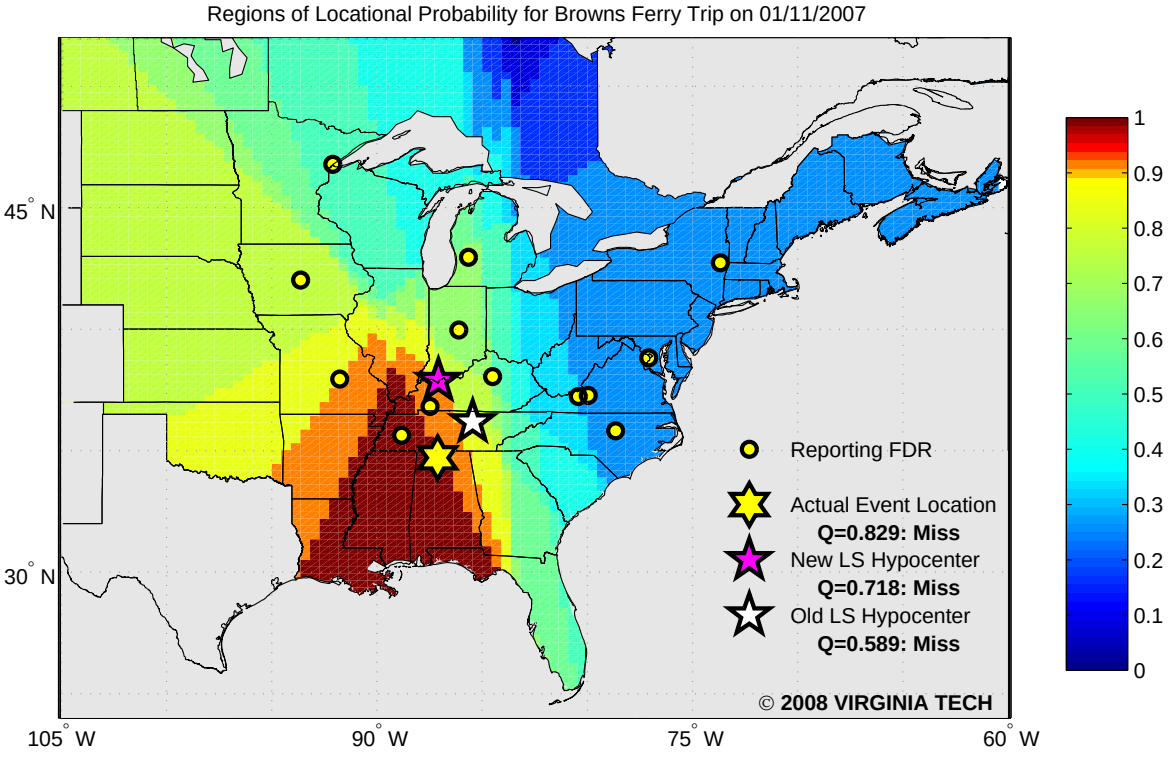


Figure D.14. Consolidated event ordering calculations: Browns Ferry (1114 MW, 34.7055°, −87.1173°) Trip on 01/11/2007 14:18:45



(a) Event location: old ordering method



(b) Event location: new ordering method

Figure D.15. Event location estimates: Browns Ferry (1114 MW, 34.7055°, −87.1173°) Trip on 01/11/2007 14:18:45

Table D.5. Ordering method comparison: Paradise (1026 MW, 37.2578°, −86.9792°) Trip on 01/24/2007 14:56:00

	Old Ordering Method			New Ordering Method		
Mismatch estimate (MW)	921			842		
FDR Info	Number	Name	Distance (mi)	Number	Name	Distance (mi)
	32	TVA7Hopkinsville	40.68	15	TVA3Nashville	75.82
	9	UFL	588.1	17	TVA4Jackson	152.2
	17	TVA4Jackson	152.2	31	UK	146.2
	15	TVA3Nashville	75.82	13	MidwestISO	193.1
	13	MidwestISO	193.1	6	ABB	472.3
	31	UK	146.2	4	VT	360.2
	27	RPI	798.1	11	Calvin	400.2
	502	Toronto	612.6	3	ARI	548.8
	11	Calvin	400.2	35	ISU	482.9
	506	OhioTiffin	334.9	23	Duluth2	708.5
	6	ABB	472.3	502	Toronto	612.6
	4	VT	360.2			
	3	ARI	548.8			
	560	Duluth	708.5			
LS estimate	Latitude	Longitude	Distance (mi)	Latitude	Longitude	Distance (mi)
	38.1407°	−83.0854°	221.4	34.7055°	−87.1173°	176.5
	$Q_{old} = 0.2446$ $Q_{new} = 0.6397$			$Q_{old} = 0.9868$ $Q_{new} = 1.0000$		
Parzen windowing results	$Q_{actual} = 1.0000$			$Q_{actual} = 1.0000$		

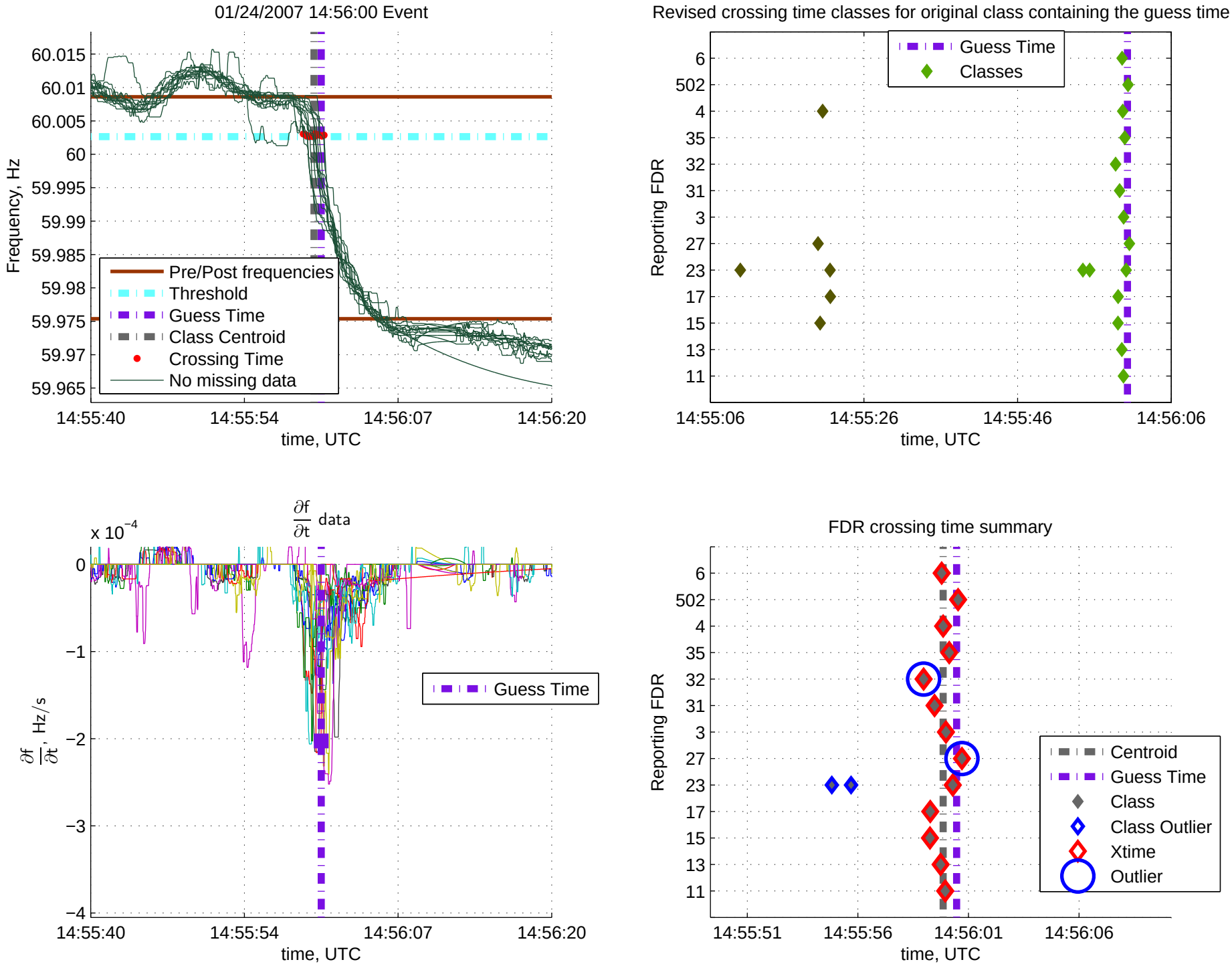
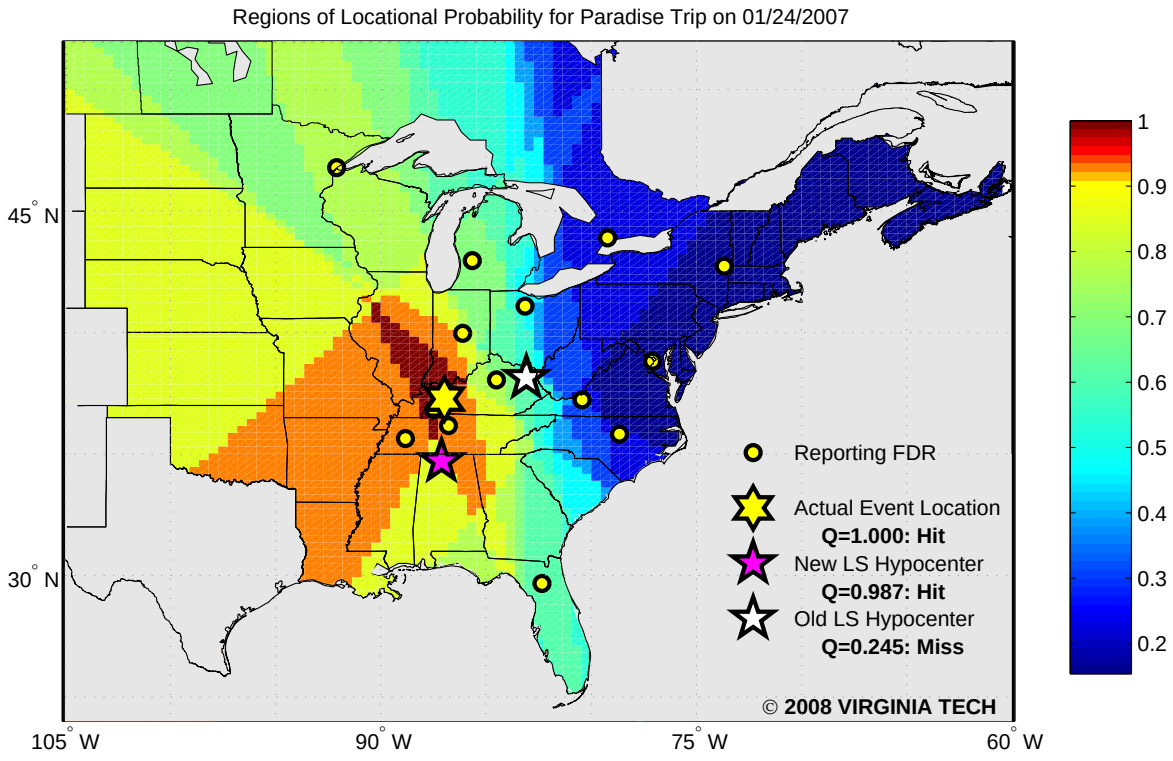
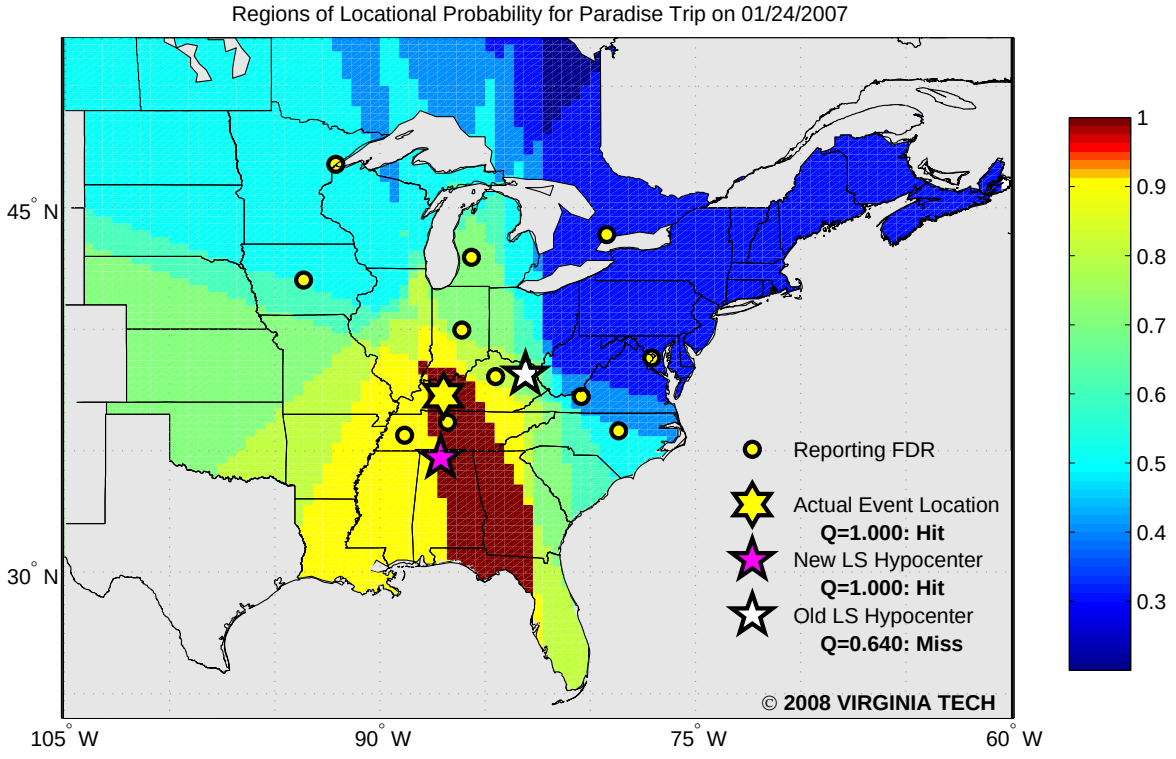


Figure D.16. Consolidated event ordering calculations: Paradise (1026 MW, 37.2578°, −86.9792°) Trip on 01/24/2007 14:56:00



(a) Event location: old ordering method



(b) Event location: new ordering method

Figure D.17. Event location estimates: Paradise (1026 MW, 37.2578°, −86.9792°) Trip on 01/24/2007 14:56:00

Table D.6. Ordering method comparison: W H Zimmer (1300 MW, 39.0523°, −84.1505°) Trip on 01/25/2007 22:07:27

	Old Ordering Method			New Ordering Method		
Mismatch estimate (MW)	694			728		
FDR Info	Number	Name	Distance (mi)	Number	Name	Distance (mi)
	560	Duluth	668.1	13	MidwestISO	122.1
	17	TVA4Jackson	348.9	31	UK	71.78
	11	Calvin	281.2	6	ABB	374.8
	35	ISU	537.8	32	TVA7Hopkinsville	237.8
	4	VT	238.1	15	TVA3Nashville	245.8
	6	ABB	374.8	27	RPI	602.8
	32	TVA7Hopkinsville	237.8	11	Calvin	281.2
	3	ARI	379.9	4	VT	238.1
	31	UK	71.78	17	TVA4Jackson	348.9
	15	TVA3Nashville	245.8			
	13	MidwestISO	122.1			
	506	OhioTiffin	150.2			
	502	Toronto	420.6			
	27	RPI	602.8			
LS estimate	Latitude	Longitude	Distance (mi)	Latitude	Longitude	Distance (mi)
	42.7341°	−84.4239°	254.8	41.5236°	−83.1278°	179
	$Q_{old} = 0.0980$			$Q_{old} = 0.0793$		
	$Q_{new} = 0.9745$			$Q_{new} = 0.7716$		
Parzen windowing results	$Q_{actual} = 0.0793$			$Q_{actual} = 0.9745$		

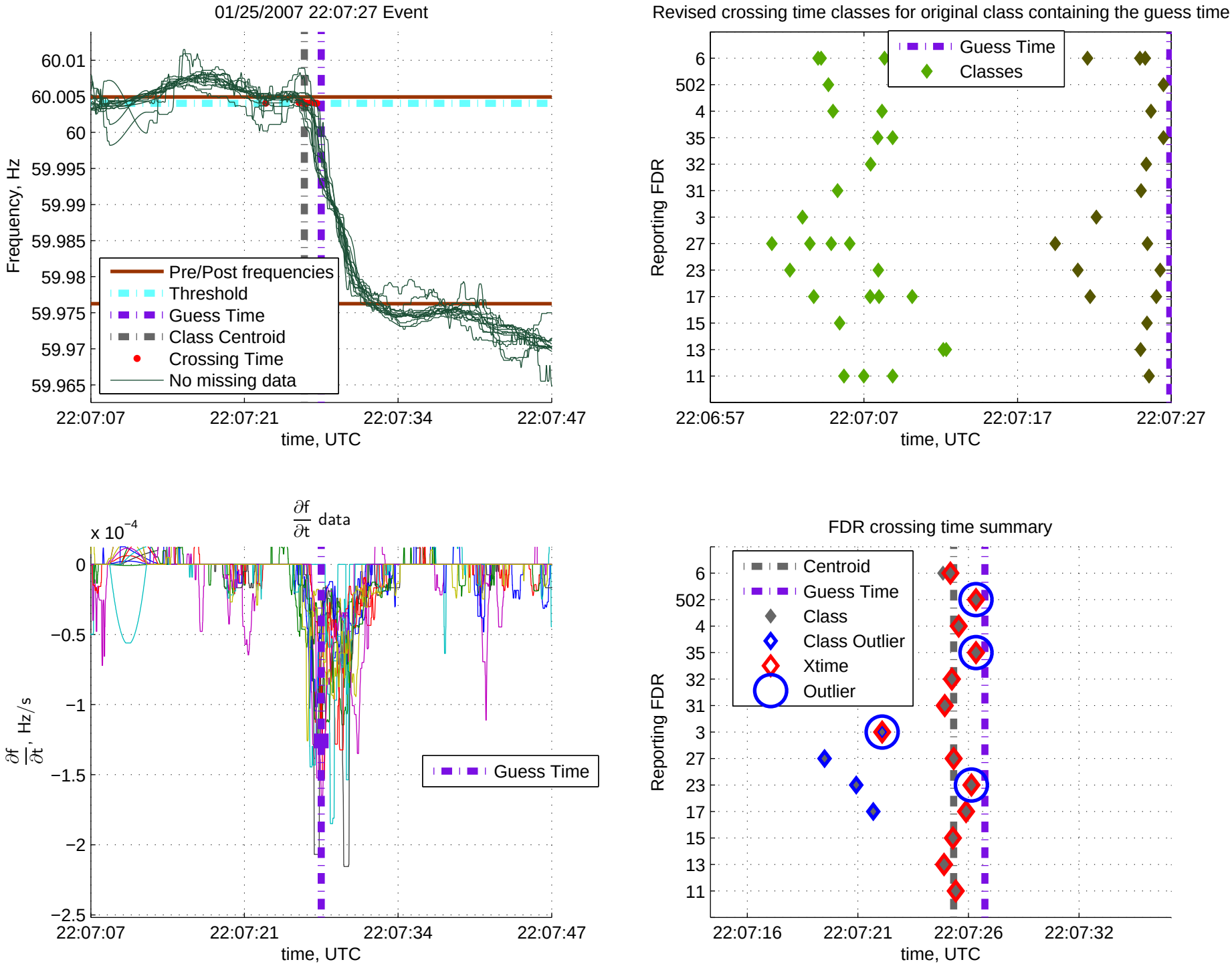
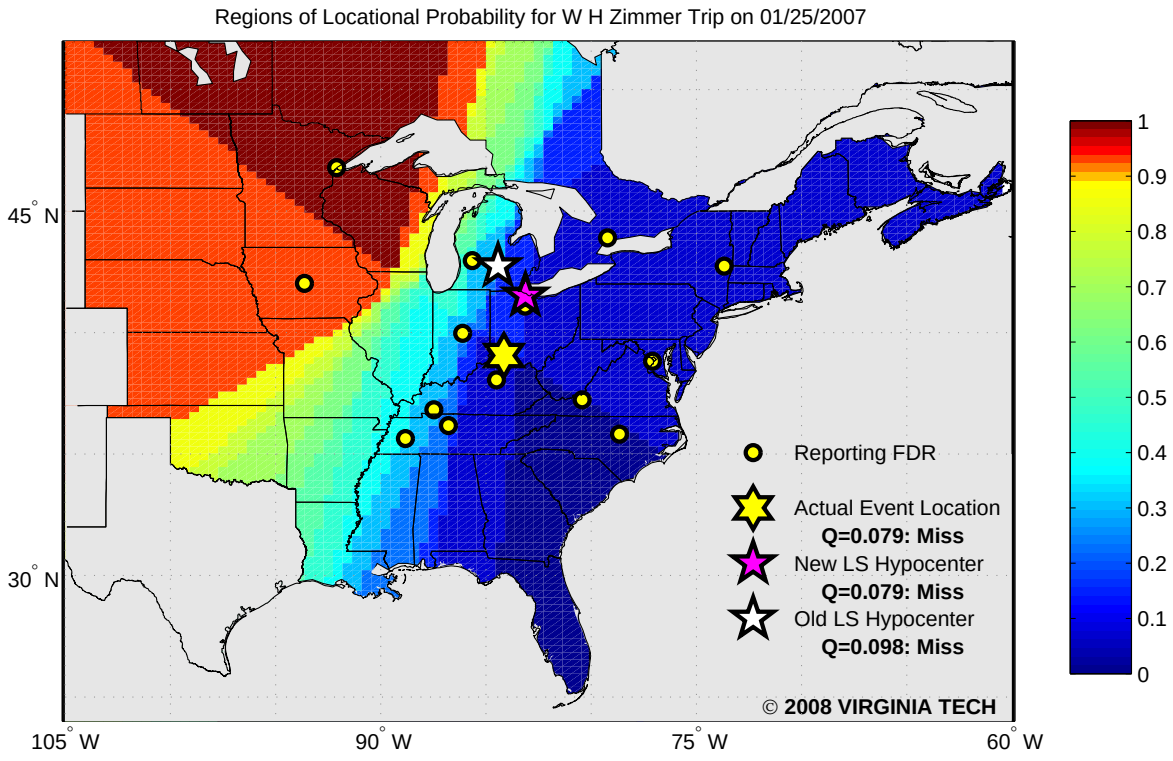
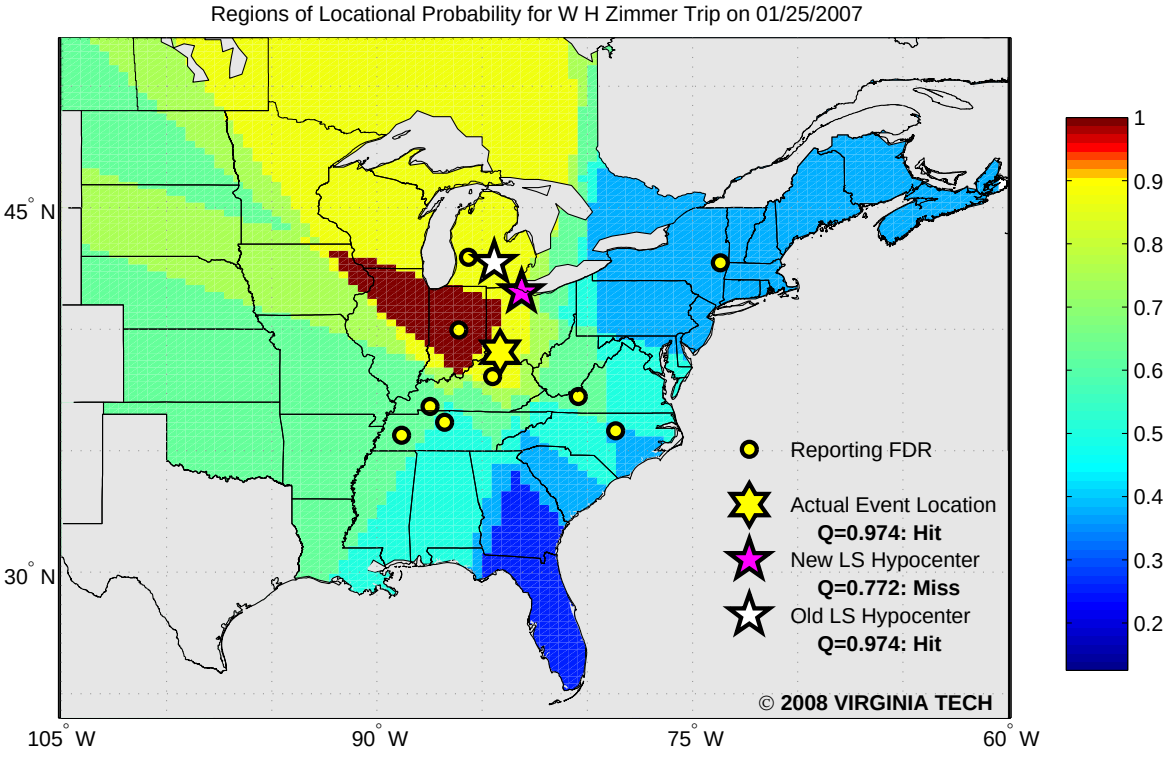


Figure D.18. Consolidated event ordering calculations: W H Zimmer (1300 MW, 39.0523°, −84.1505°) Trip on 01/25/2007 22:07:27



(a) Event location: old ordering method

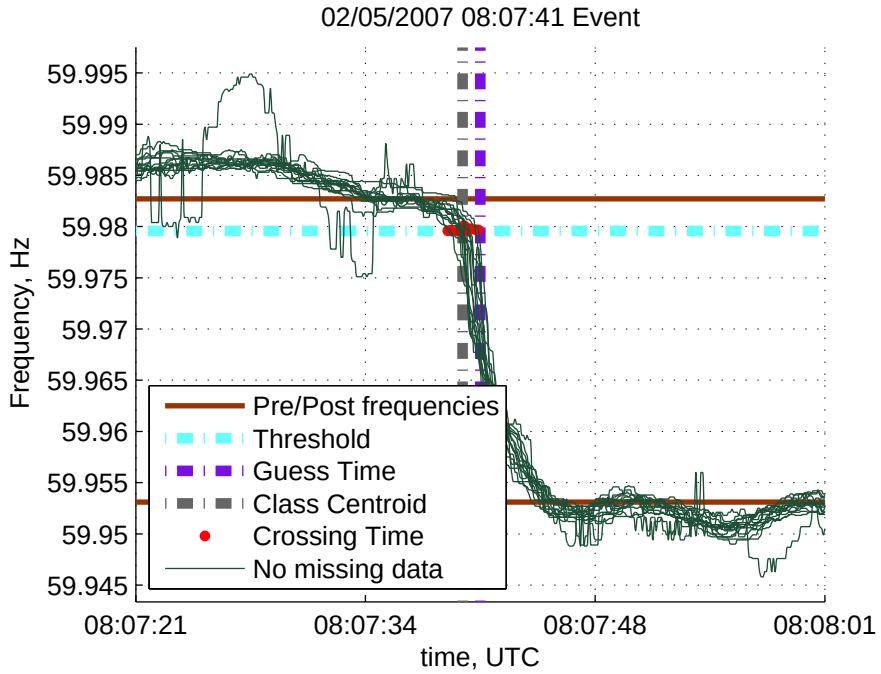


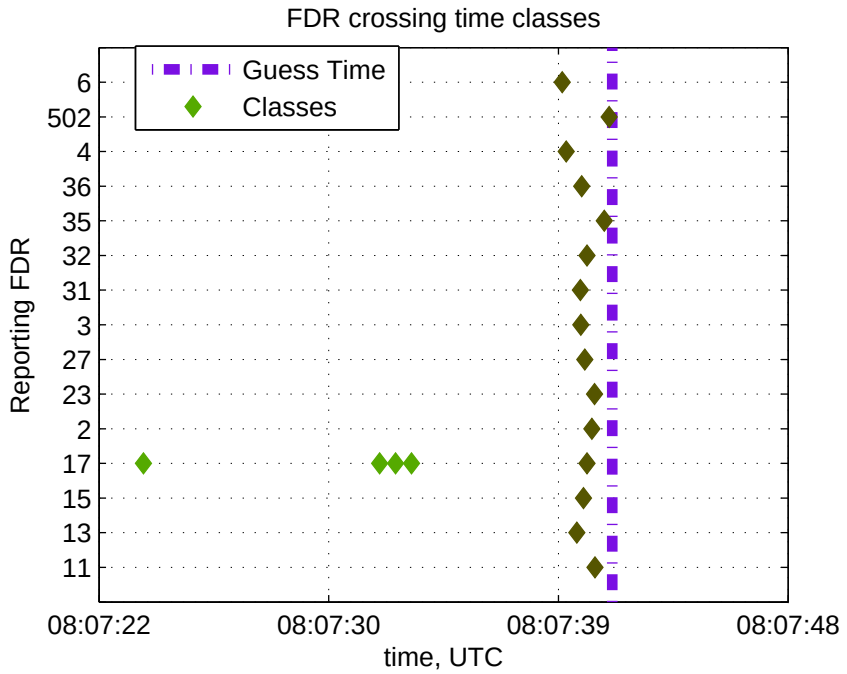
(b) Event location: new ordering method

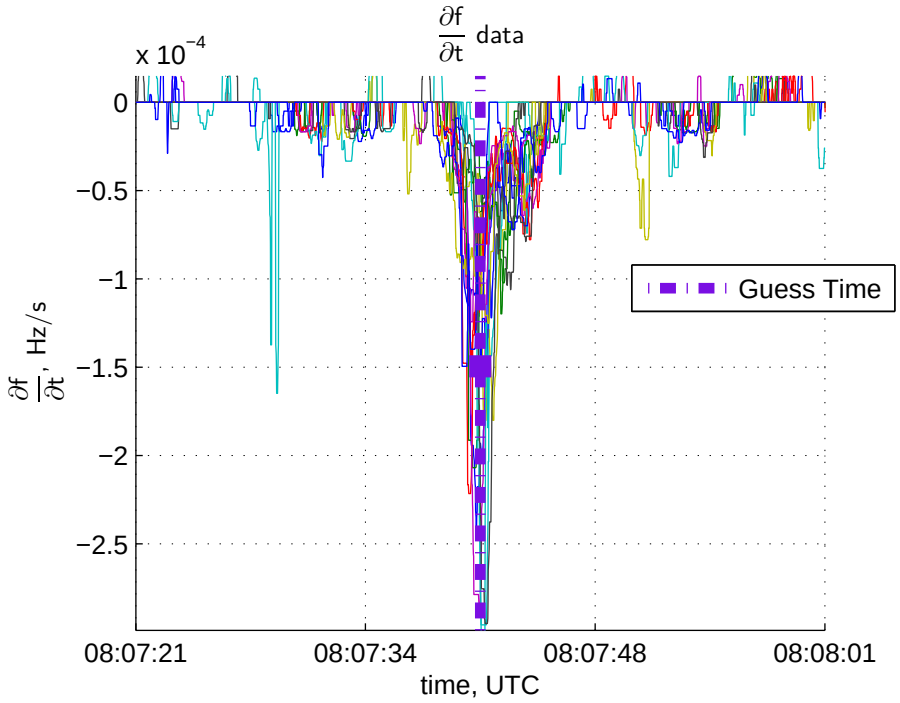
Figure D.19. Event location estimates: W H Zimmer (1300 MW, 39.0523°, −84.1505°) Trip on 01/25/2007 22:07:27

Table D.7. Ordering method comparison: Summer (966 MW, 34.2717°, −81.2712°) Trip on 02/05/2007 08:07:41

	Old Ordering Method			New Ordering Method		
Mismatch estimate (MW)	865			751		
FDR Info	Number	Name	Distance (mi)	Number	Name	Distance (mi)
	6	ABB	182.5	6	ABB	182.5
	9	UFL	323.7	4	VT	210
	3	ARI	390.7	13	MidwestISO	475.2
	36	TVA5MuscleShoals	364.1	31	UK	317.1
	15	TVA3Nashville	337.7	3	ARI	390.7
	32	TVA7Hopkinsville	390.6	36	TVA5MuscleShoals	364.1
	17	TVA4Jackson	438.1	15	TVA3Nashville	337.7
	31	UK	317.1	27	RPI	713.8
	2	UMR	638	17	TVA4Jackson	438.1
	506	OhioTiffin	481.7	32	TVA7Hopkinsville	390.6
	11	Calvin	645.1	2	UMR	638
	4	VT	210	23	Duluth2	1033
	27	RPI	713.8	11	Calvin	645.1
	35	ISU	857.2	35	ISU	857.2
	502	Toronto	673.9	502	Toronto	673.9
	560	Duluth	1033			
	13	MidwestISO	475.2			
LS estimate	Latitude	Longitude	Distance (mi)	Latitude	Longitude	Distance (mi)
	39.6205°	−84.0038°	399.1	34.3756°	−80.0842°	68.11
	$Q_{old} = 0.1463$			$Q_{old} = 1.0000$		
	$Q_{new} = 0.1475$			$Q_{new} = 1.0000$		
Parzen windowing results	$Q_{actual} = 0.8574$			$Q_{actual} = 0.7646$		







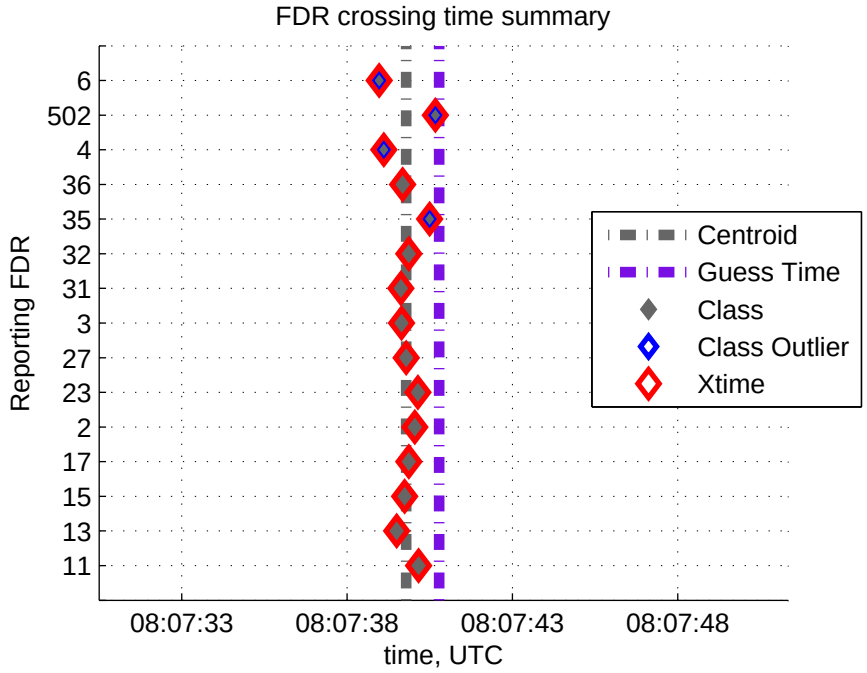
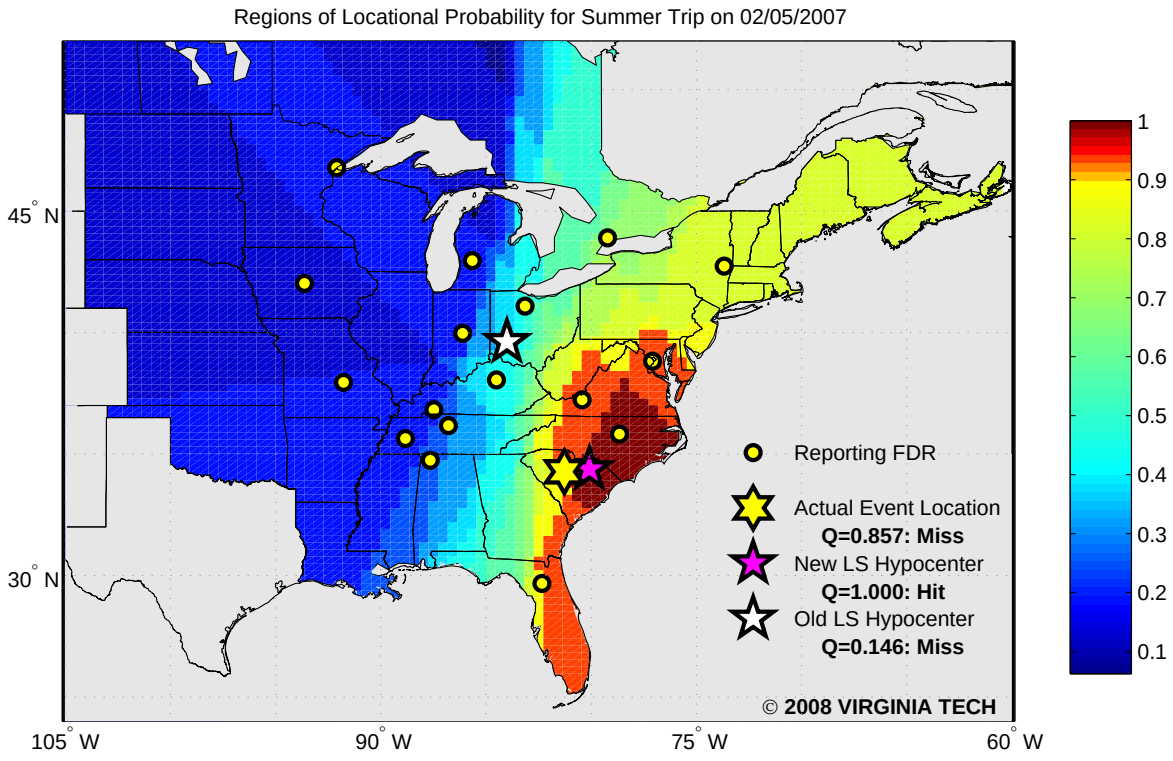
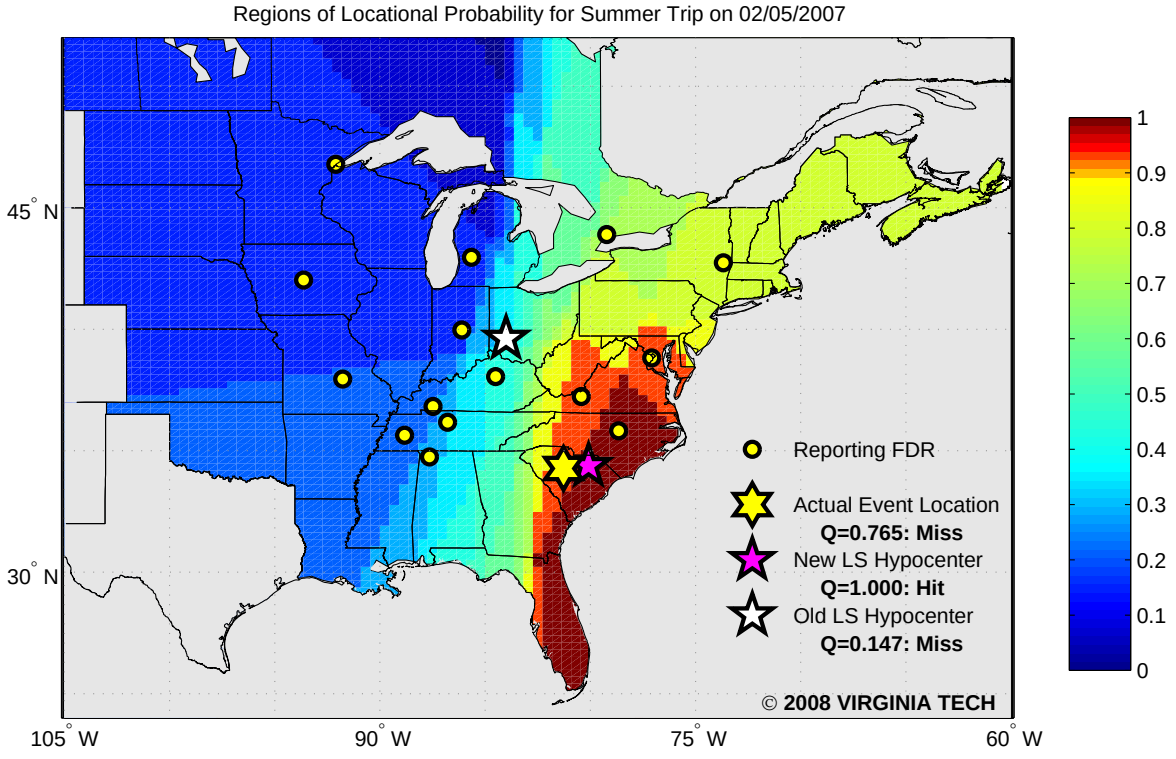


Figure D.20. Consolidated event ordering calculations: Summer (966 MW, 34.2717°, −81.2712°) Trip on 02/05/2007 08:07:41



(a) Event location: old ordering method



(b) Event location: new ordering method

Figure D.21. Event location estimates: Summer (966 MW, 34.2717°, −81.2712°) Trip on 02/05/2007 08:07:41

Table D.8. Ordering method comparison: McWilliams-Vann (539 MW, 31.3999°, −86.4749°) Trip on 02/07/2007 16:03:44

	Old Ordering Method			New Ordering Method		
Mismatch estimate (MW)	818			682		
FDR Info	Number	Name	Distance (mi)	Number	Name	Distance (mi)
	6	ABB	543.4	36	TVA5MuscleShoals	240.9
	3	ARI	737.1	17	TVA4Jackson	322.4
	2	UMR	543	32	TVA7Hopkinsville	378.9
	36	TVA5MuscleShoals	240.9	31	UK	472.9
	31	UK	472.9	2	UMR	543
	17	TVA4Jackson	322.4	4	VT	530.3
	13	MidwestISO	592.4	11	Calvin	800.1
	11	Calvin	800.1	27	RPI	1052
	35	ISU	833.3	13	MidwestISO	592.4
	506	OhioTiffin	694.3	3	ARI	737.1
	32	TVA7Hopkinsville	378.9	23	Duluth2	1104
	560	Duluth	1104	41	Winnipeg	1385
	41	Winnipeg	1385	35	ISU	833.3
	27	RPI	1052			
	502	Toronto	949.2			
	4	VT	530.3			
LS estimate	Latitude	Longitude	Distance (mi)	Latitude	Longitude	Distance (mi)
	43.9604°	−85.5829°	869.2	34.7055°	−87.1173°	231.4
	Q_{old} = 0.0493 Q_{new} = 0.3209			Q_{old} = 0.1343 Q_{new} = 1.0000		
Parzen windowing results	Q_{actual} = 0.1729			Q_{actual} = 1.0000		

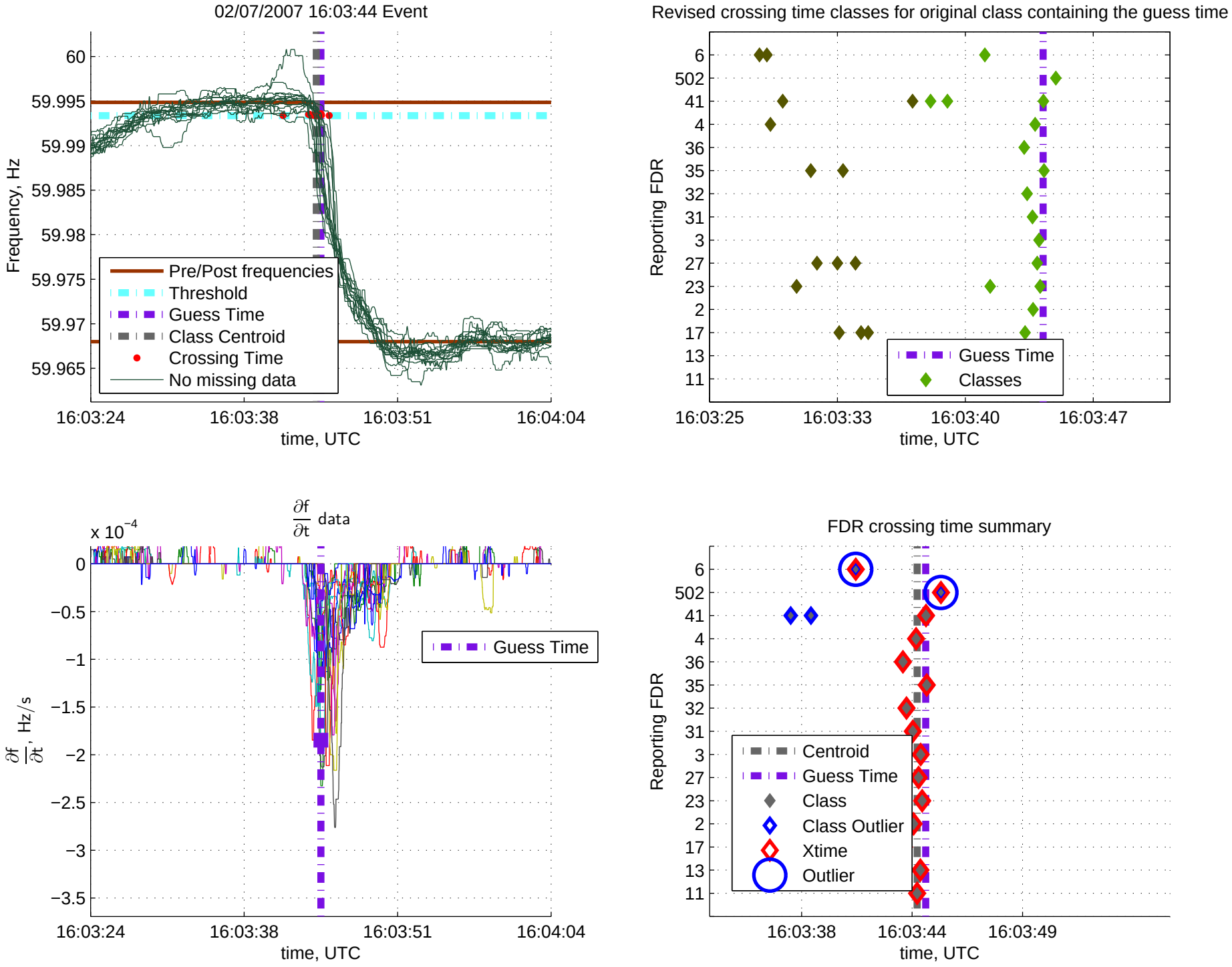
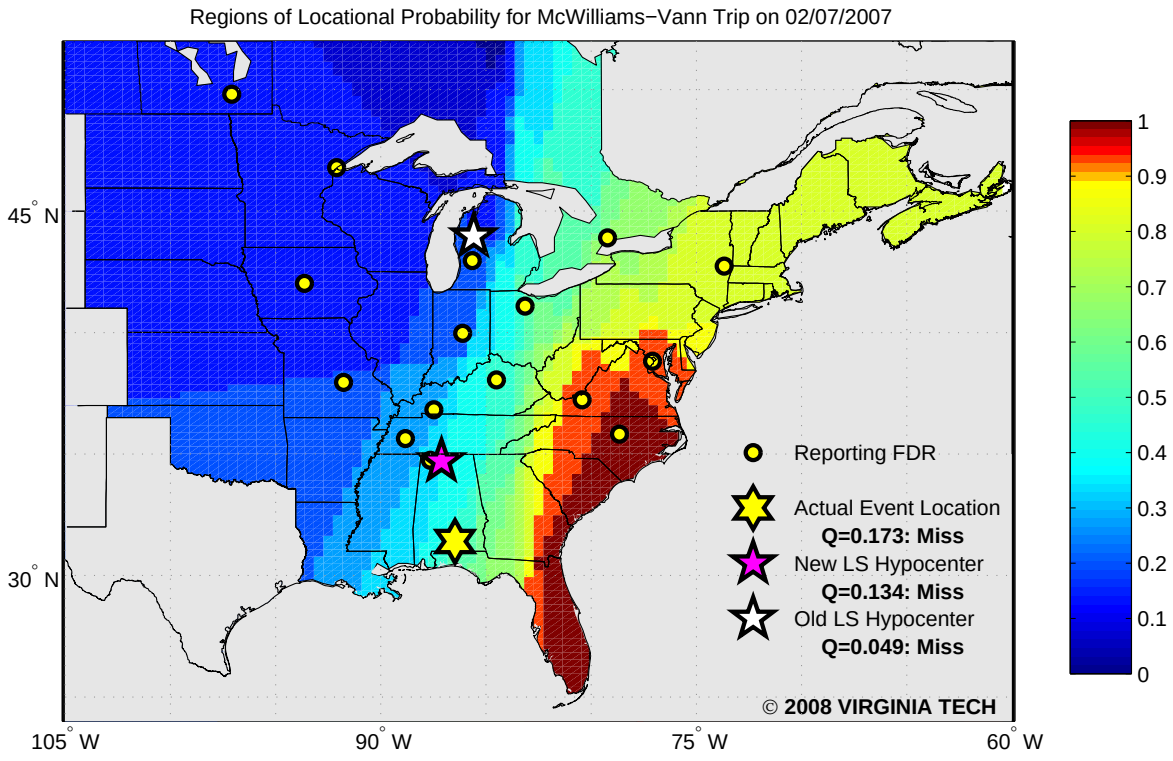
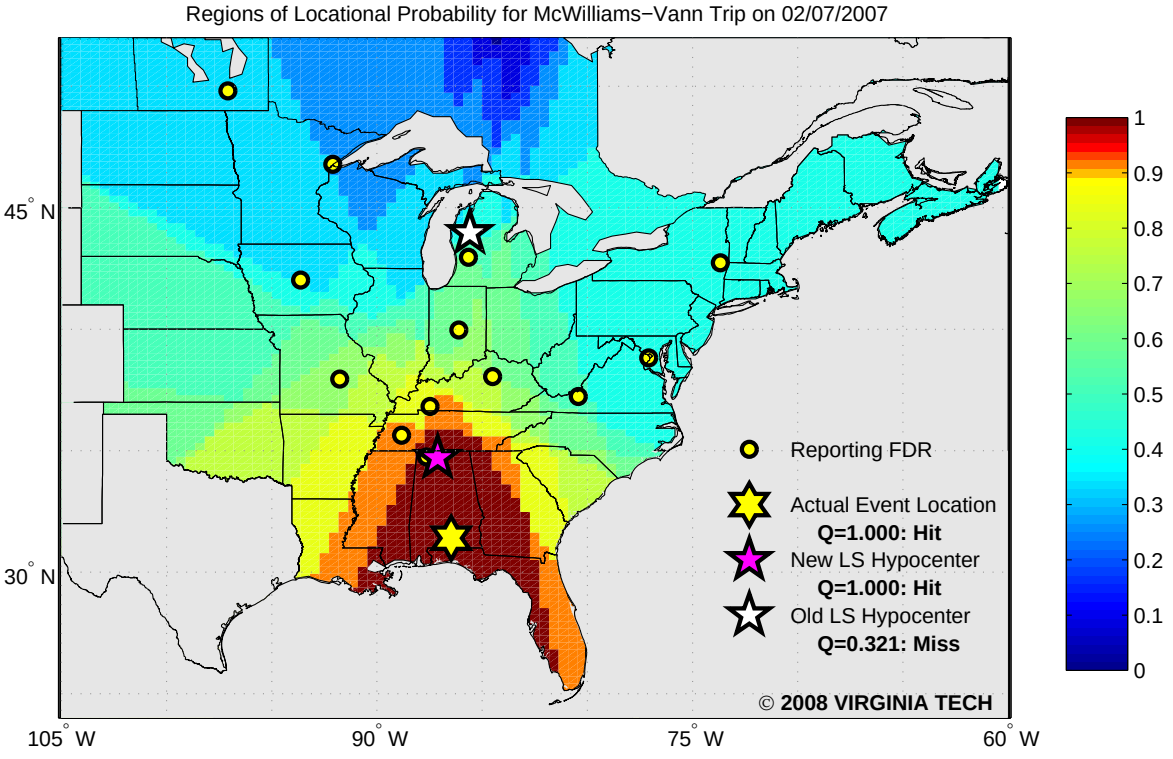


Figure D.22. Consolidated event ordering calculations: McWilliams-Vann (539 MW, 31.3999°, −86.4749°) Trip on 02/07/2007 16:03:44



(a) Event location: old ordering method

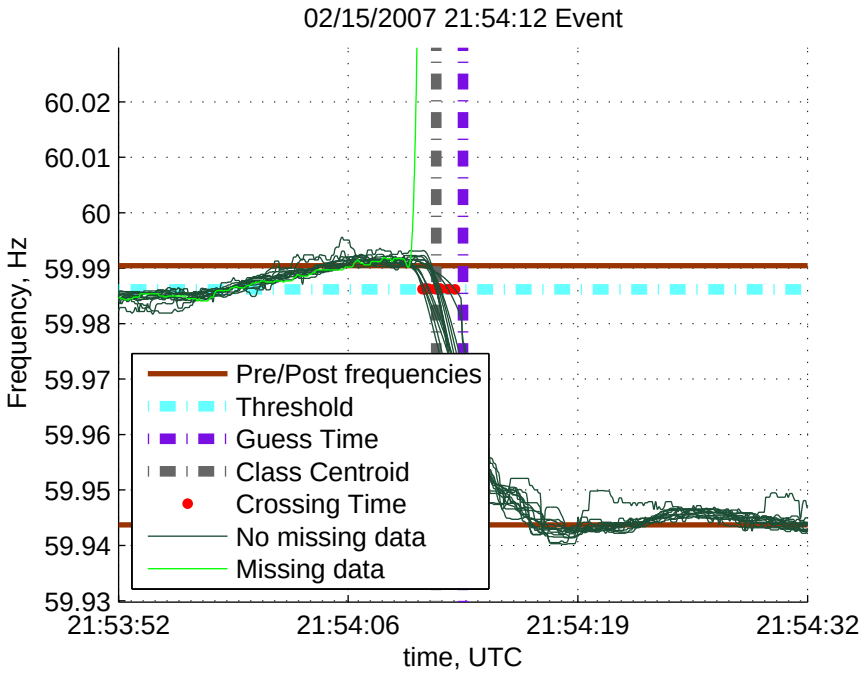


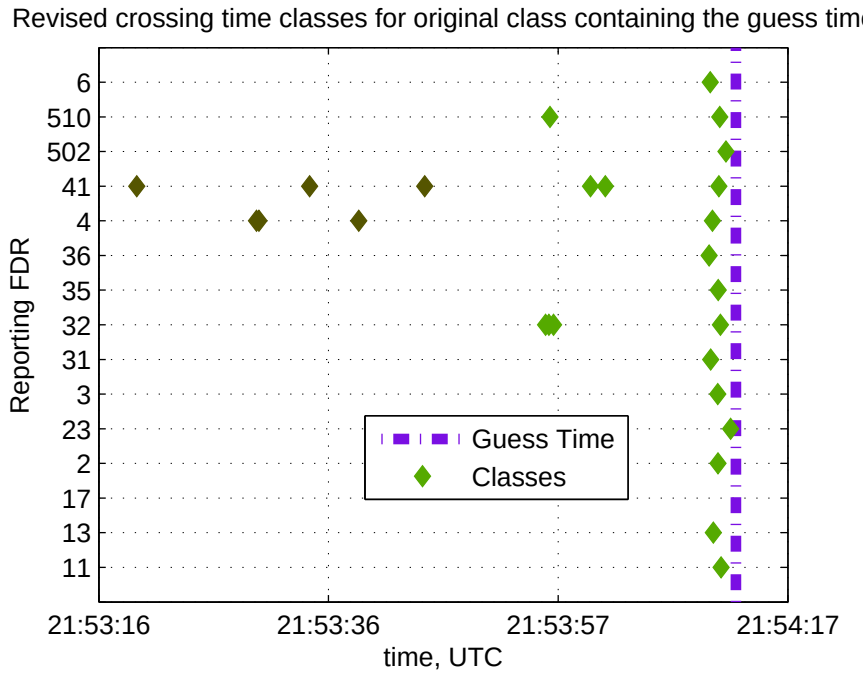
(b) Event location: new ordering method

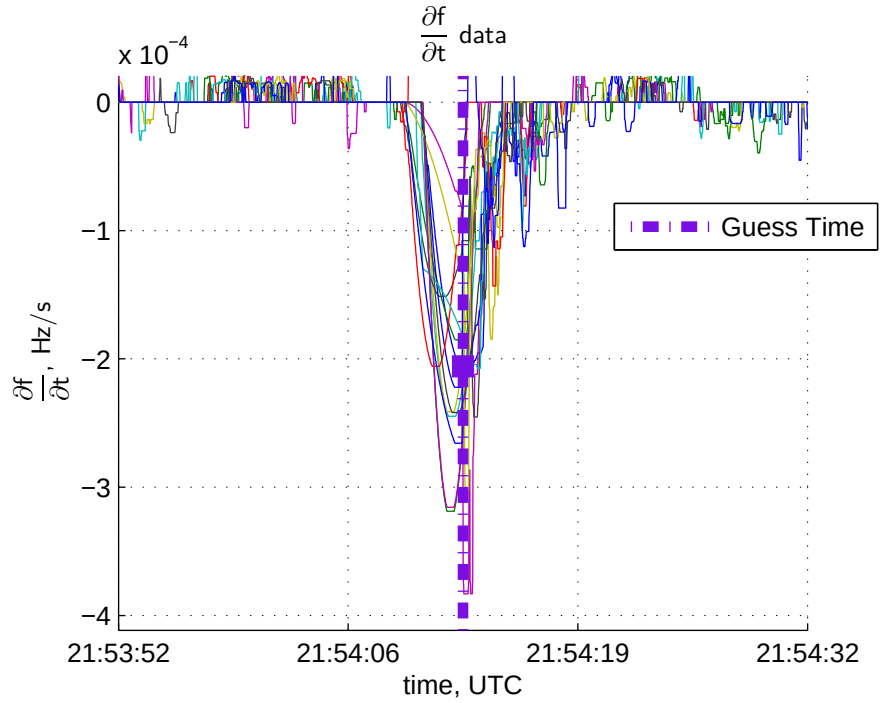
Figure D.23. Event location estimates: McWilliams-Vann (539 MW, 31.3999°, −86.4749°) Trip on 02/07/2007 16:03:44

Table D.9. Ordering method comparison: Oconee U1 & U2 (1692 MW, 34.7538°, −83.0674°) Trip on 02/15/2007 21:54:12

	Old Ordering Method			New Ordering Method		
Mismatch estimate (MW)	1385			1185		
FDR Info	Number	Name	Distance (mi)	Number	Name	Distance (mi)
	6	ABB	259.3	36	TVA5MuscleShoals	259.7
	4	VT	226	6	ABB	259.3
	510	Blacksburg	227.5	31	UK	241.3
	36	TVA5MuscleShoals	259.7	4	VT	226
	9	UFL	353.6	13	MidwestISO	397.1
	3	ARI	434	3	ARI	434
	31	UK	241.3	2	UMR	531.7
	32	TVA7Hopkinsville	285.3	35	ISU	760
	13	MidwestISO	397.1	41	Winnipeg	1259
	506	OhioTiffin	437.5	510	Blacksburg	227.5
	11	Calvin	583.8	32	TVA7Hopkinsville	285.3
	2	UMR	531.7	11	Calvin	583.8
	35	ISU	760	502	Toronto	664
	502	Toronto	664	23	Duluth2	954.9
	560	Duluth	954.9			
	41	Winnipeg	1259			
LS estimate	Latitude	Longitude	Distance (mi)	Latitude	Longitude	Distance (mi)
	35.8087°	−84.6230°	114.1	35.2272°	−85.0943°	119.3
	$Q_{old} = 0.1206$ $Q_{new} = 0.7417$			$Q_{old} = 0.1206$ $Q_{new} = 0.8255$		
Parzen windowing results	$Q_{actual} = 0.2280$			$Q_{actual} = 0.6433$		







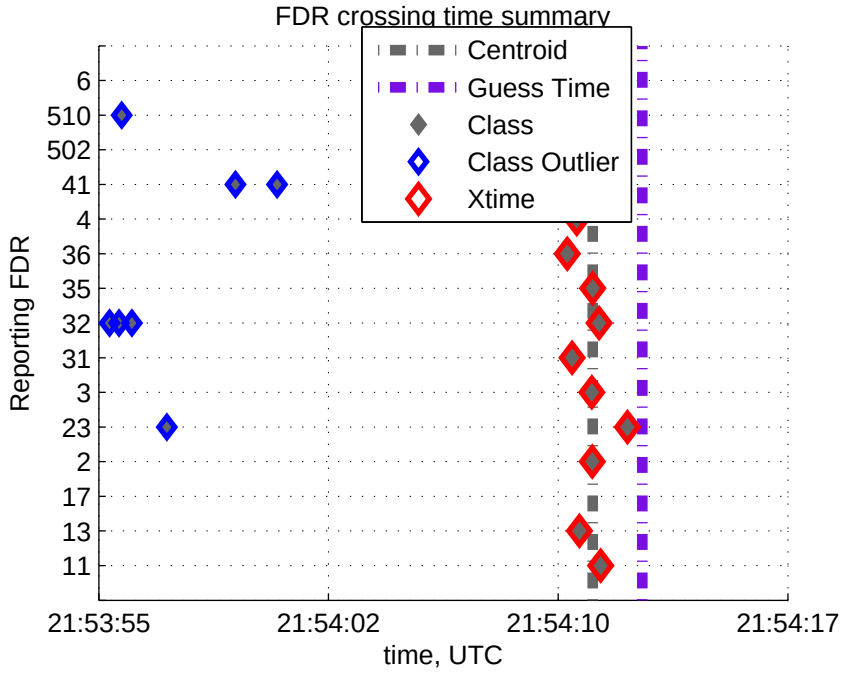
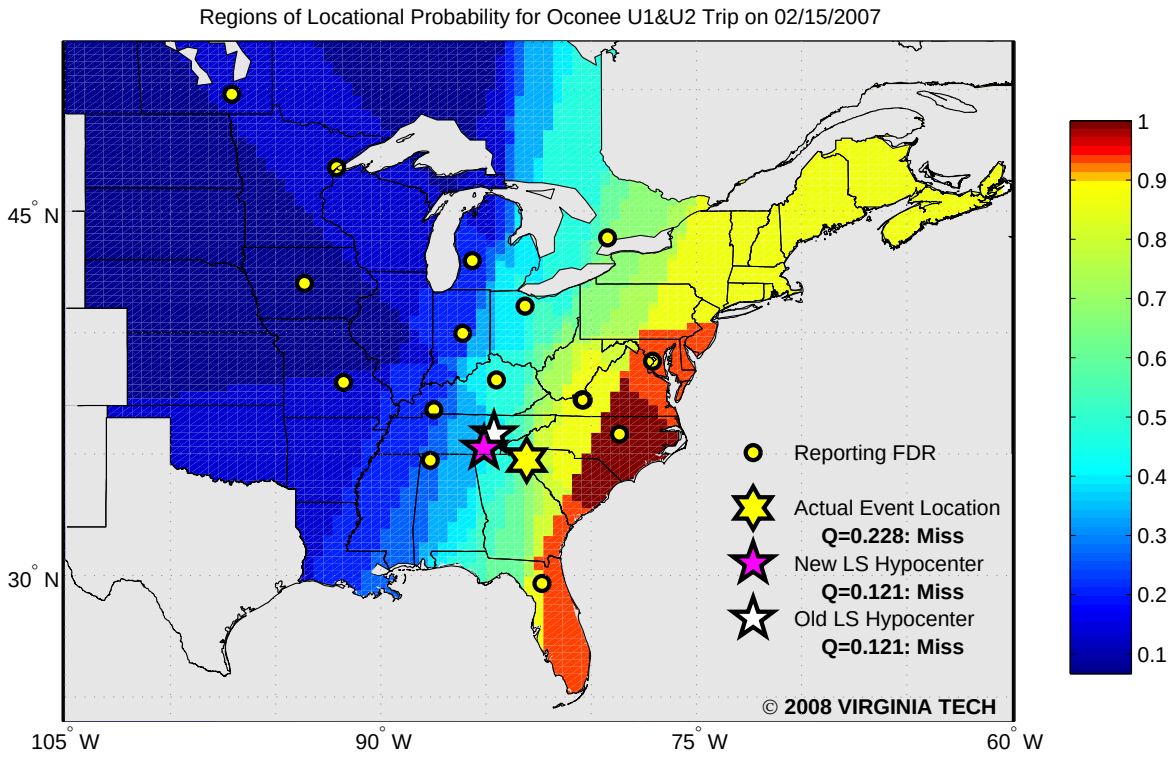
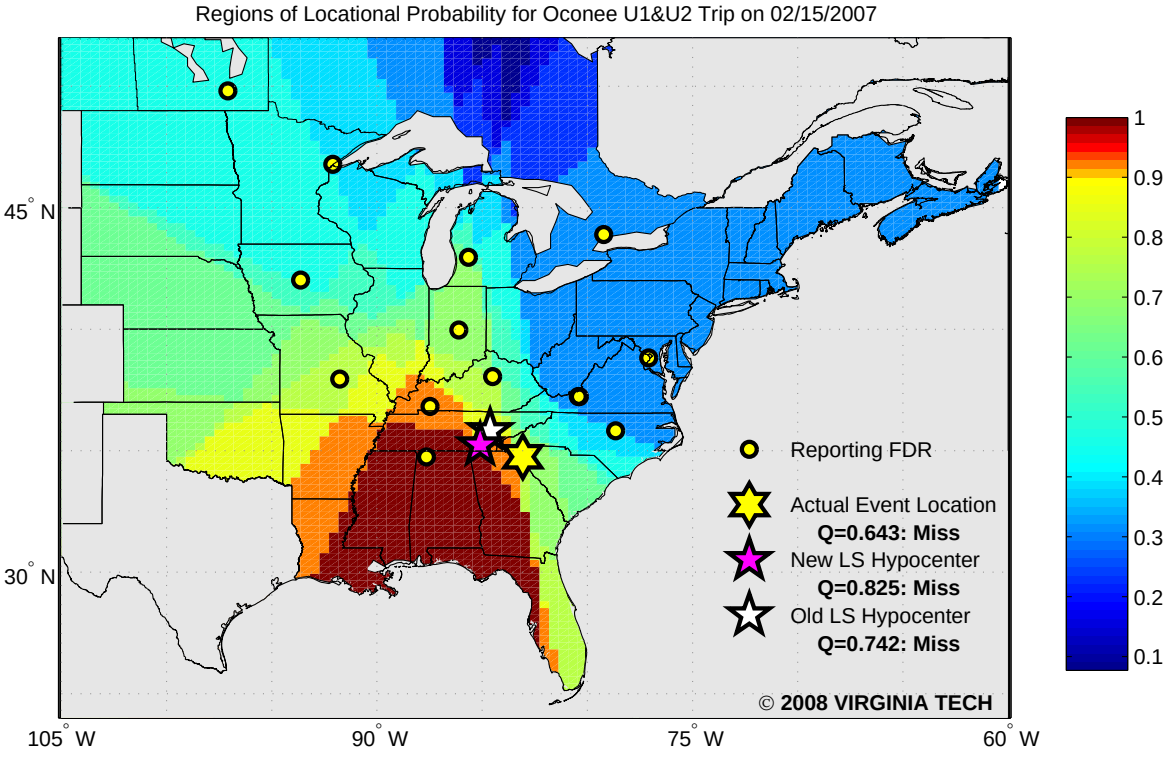


Figure D.24. Consolidated event ordering calculations: Oconee U1 & U2 (1692 MW, 34.7538°, −83.0674°) Trip on 02/15/2007 21:54:12



(a) Event location: old ordering method



(b) Event location: new ordering method

Figure D.25. Event location estimates: Oconee U1& U2 (1692 MW, 34.7538°, −83.0674°) Trip on 02/15/2007 21:54:12

Table D.10. Ordering method comparison: Indian Point (1025 MW, 41.2697°, −73.9524°) Trip on 02/28/2007 11:33:50

	Old Ordering Method			New Ordering Method		
Mismatch estimate (MW)	955			NaN		
FDR Info	Number	Name	Distance (mi)	Number	Name	Distance (mi)
				502	Toronto	323.8
				6	ABB	454.1
				510	Blacksburg	442.8
				31	UK	603
				13	MidwestISO	643.3
				23	Duluth2	975.9
				43	Bismarck	1379
				35	ISU	1015
				36	TVA5MuscleShoals	869.4
				32	TVA7Hopkinsville	786.9
				41	Winnipeg	1258
				2	UMR	973.7
				4	VT	444.6
LS estimate	Latitude	Longitude	Distance (mi)	Latitude	Longitude	Distance (mi)
	41.8869°	−88.5649°	755.5	NaN°	NaN°	NaN
	$Q_{old} = NaN$ $Q_{new} = 0.0805$			$Q_{old} = NaN$ $Q_{new} = NaN$		
Parzen windowing results	$Q_{actual} = NaN$			$Q_{actual} = 1.0000$		

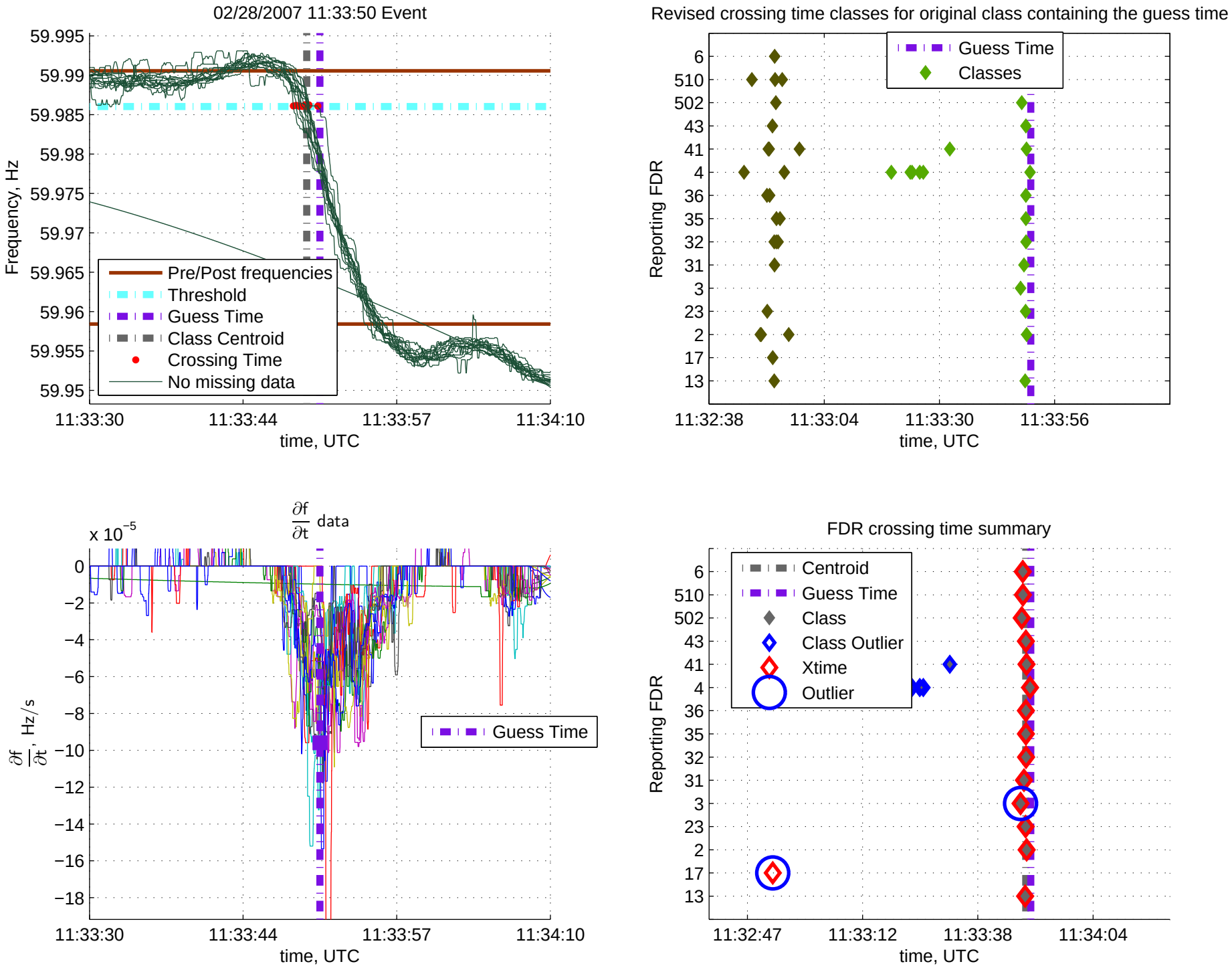


Figure D.26. Consolidated event ordering calculations: Indian Point (1025 MW, 41.2697°, −73.9524°) Trip on 02/28/2007 11:33:50

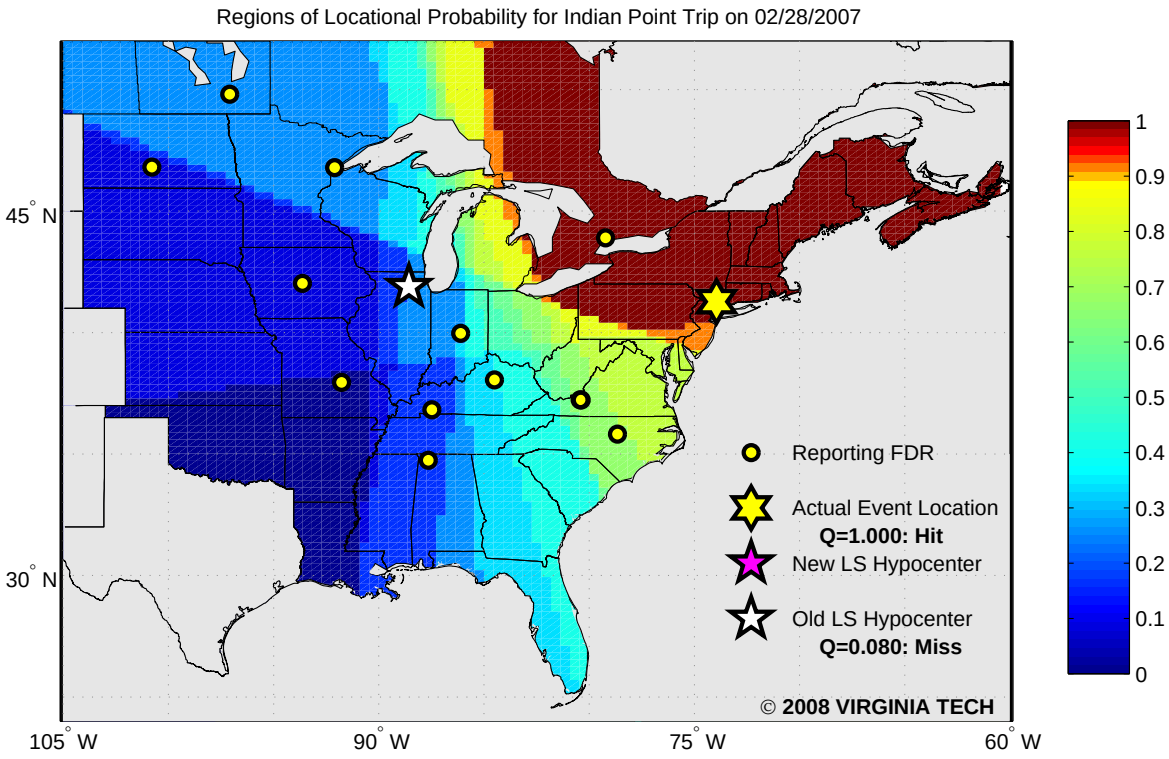


Figure D.27. Event location estimates (new ordering method): Indian Point (1025 MW, 41.2697°, −73.9524°) Trip on 02/28/2007 11:33:50

Table D.11. Ordering method comparison: Sequoyah (1127 MW, 35.2272°, −85.0943°) Trip on 03/13/2007 19:27:13

	Old Ordering Method			New Ordering Method		
Mismatch estimate (MW)	1181			992		
FDR Info	Number	Name	Distance (mi)	Number	Name	Distance (mi)
	6	ABB	364.1	32	TVA7Hopkinsville	172.7
	15	TVA3Nashville	115.1	31	UK	197.8
	32	TVA7Hopkinsville	172.7	510	Blacksburg	296.9
	17	TVA4Jackson	212.1	3	ARI	506.5
	9	UFL	416	35	ISU	657
	31	UK	197.8	4	VT	294.6
	13	MidwestISO	332.3	508	ROA	319.3
	510	Blacksburg	296.9	43	Bismarck	1140
	508	ROA	319.3	15	TVA3Nashville	115.1
	3	ARI	506.5	17	TVA4Jackson	212.1
	506	OhioTiffin	418.4	13	MidwestISO	332.3
	4	VT	294.6	23	Duluth2	877.4
	35	ISU	657			
	560	Duluth	877.4			
	43	Bismarck	1140			
	502	Toronto	675.2			
LS estimate	Latitude	Longitude	Distance (mi)	Latitude	Longitude	Distance (mi)
	37.9184°	−88.6741°	272	37.8858°	−87.0770°	214.1
	$Q_{old} = 0.0874$ $Q_{new} = 1.0000$			$Q_{old} = 0.0874$ $Q_{new} = 1.0000$		
Parzen windowing results	$Q_{actual} = 0.1200$			$Q_{actual} = 0.8840$		

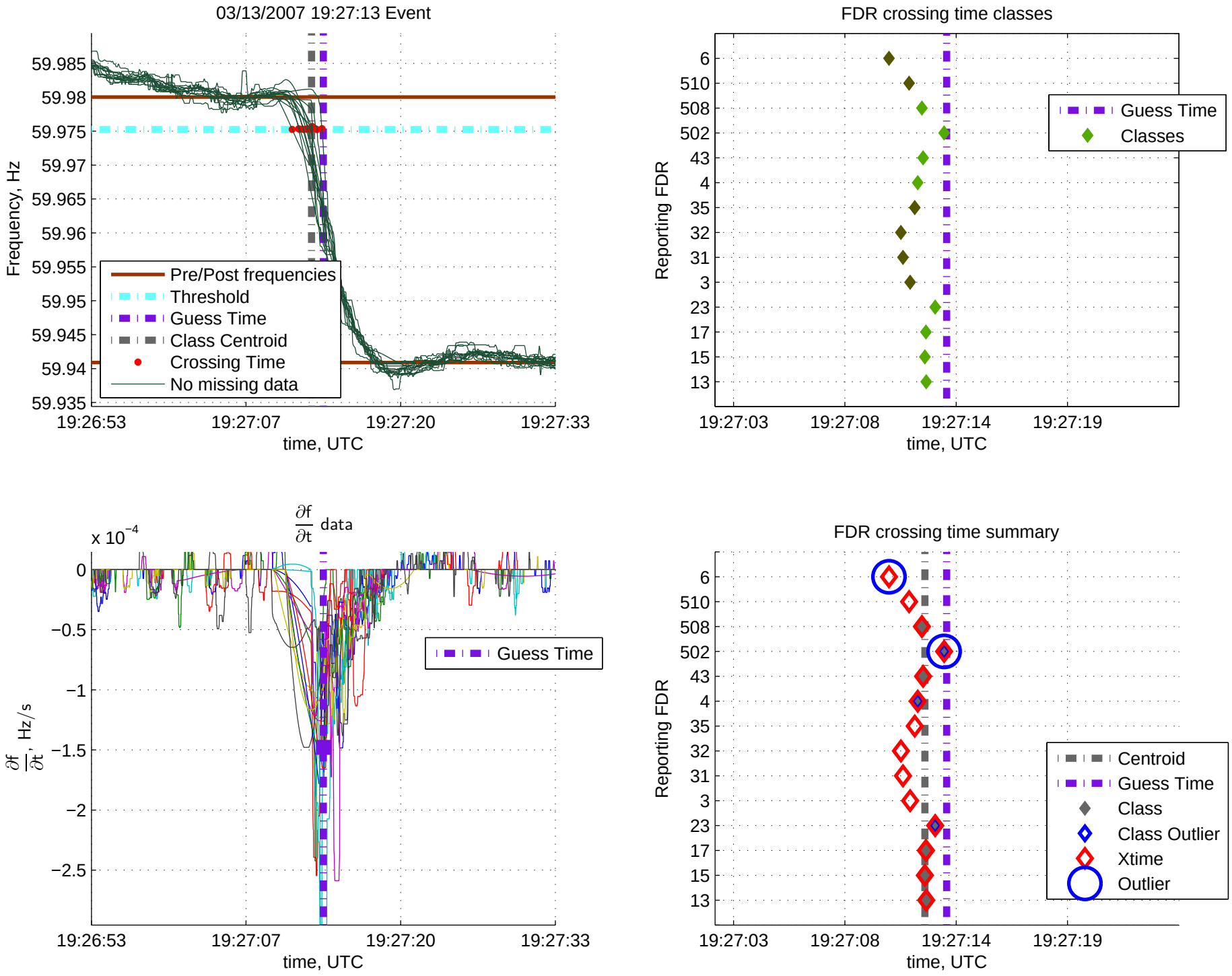
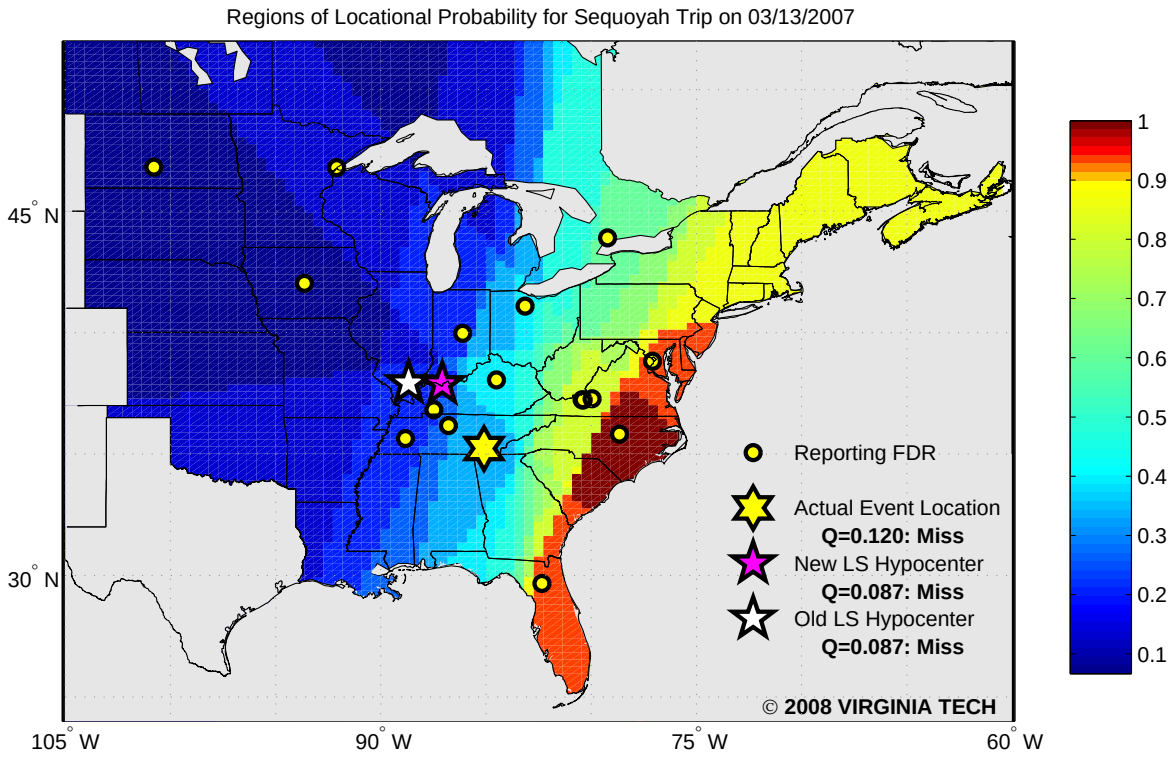
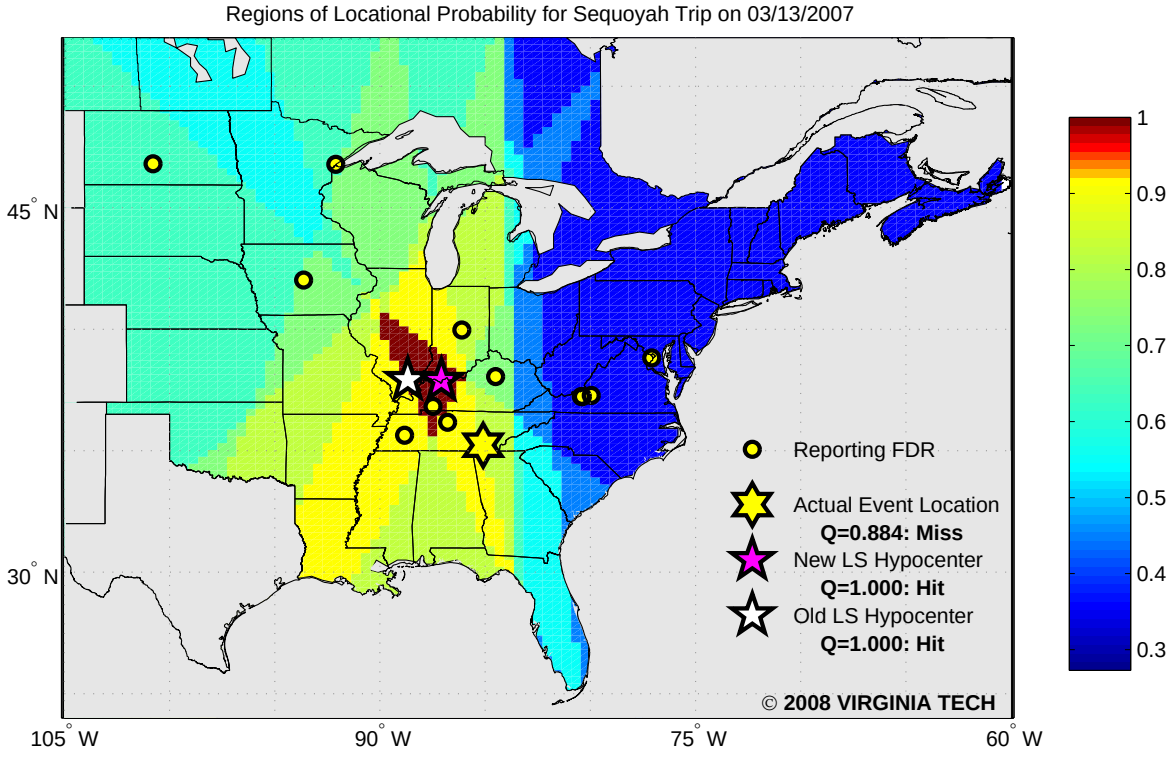


Figure D.28. Consolidated event ordering calculations: Sequoyah (1127 MW, 35.2272°, −85.0943°) Trip on 03/13/2007 19:27:13



(a) Event location: old ordering method

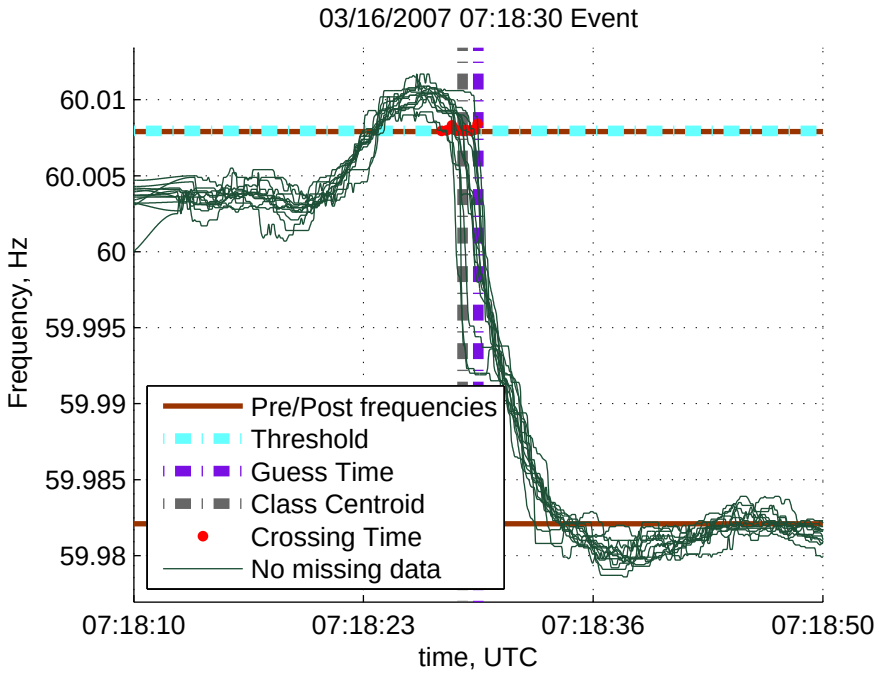


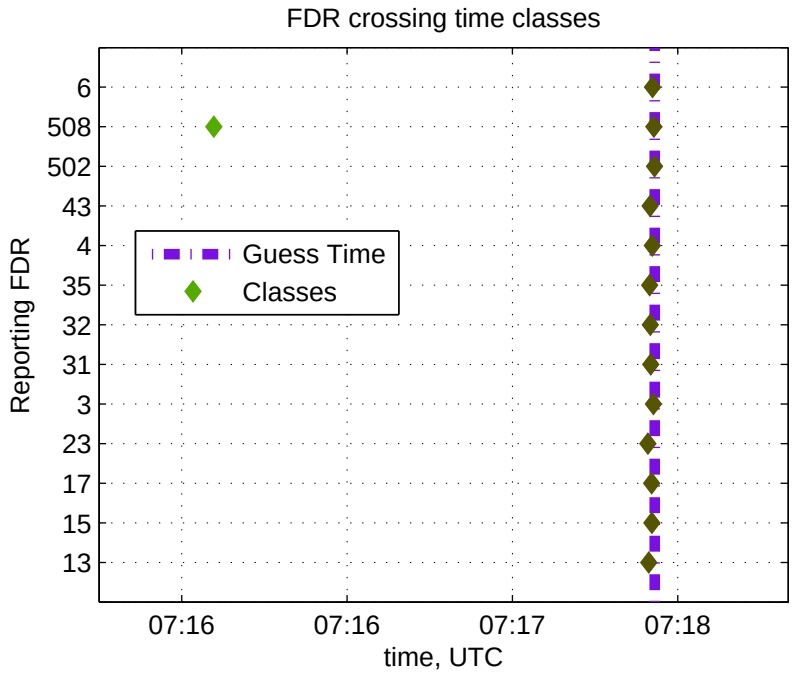
(b) Event location: new ordering method

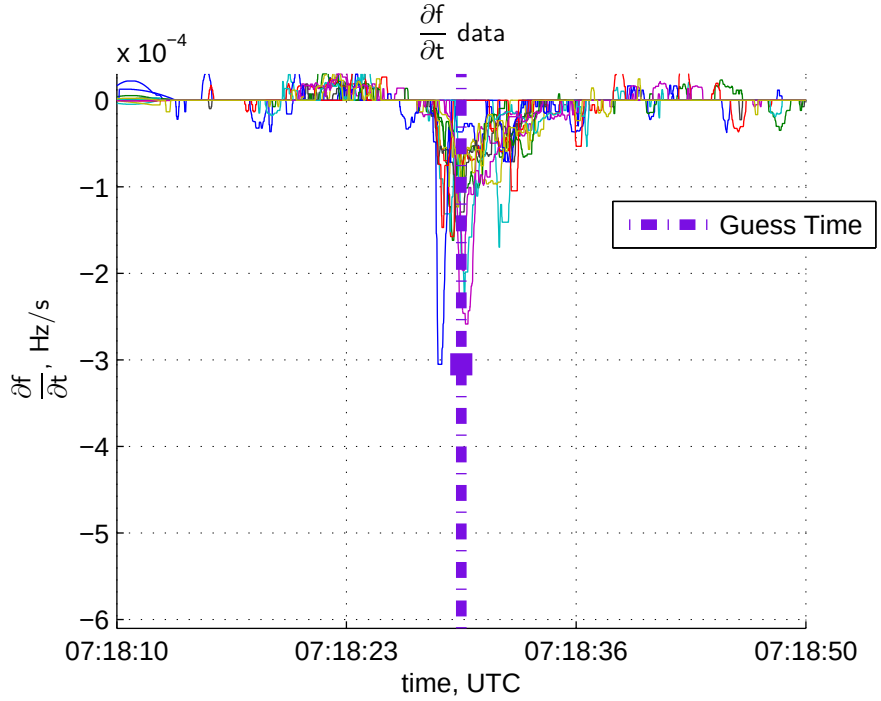
Figure D.29. Event location estimates: Sequoyah (1127 MW, 35.2272°, −85.0943°) Trip on 03/13/2007 19:27:13

Table D.12. Ordering method comparison: Conemaugh (850 MW, 40.3823°, −79.0968°) Trip on 03/16/2007 07:18:30

	Old Ordering Method			New Ordering Method		
Mismatch estimate (MW)	657			654		
FDR Info	Number	Name	Distance (mi)	Number	Name	Distance (mi)
	9	UFL	762.1	13	MidwestISO	371.2
	3	ARI	152	35	ISU	762.8
	6	ABB	316	43	Bismarck	1168
	31	UK	331	32	TVA7Hopkinsville	514.6
	508	ROA	219.4	31	UK	331
	502	Toronto	242.9	17	TVA4Jackson	622.6
	17	TVA4Jackson	622.6	15	TVA3Nashville	508.1
	15	TVA3Nashville	508.1	4	VT	229.1
	506	OhioTiffin	217.2	6	ABB	316
	560	Duluth	785.4	3	ARI	152
	35	ISU	762.8	508	ROA	219.4
	4	VT	229.1			
	32	TVA7Hopkinsville	514.6			
	13	MidwestISO	371.2			
	43	Bismarck	1168			
LS estimate	Latitude	Longitude	Distance (mi)	Latitude	Longitude	Distance (mi)
	40.6194°	−87.7924°	457	39.9693°	−86.1095°	371.2
	$Q_{old} = 0.0391$			$Q_{old} = 0.0109$		
	$Q_{new} = 1.0000$			$Q_{new} = 1.0000$		
Parzen windowing results	$Q_{actual} = 0.0969$			$Q_{actual} = 0.5159$		







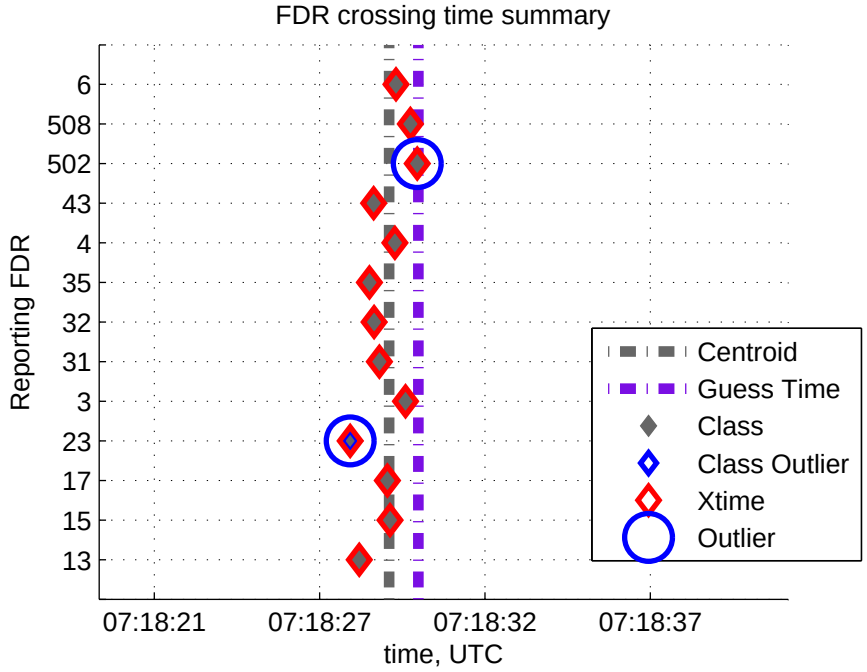
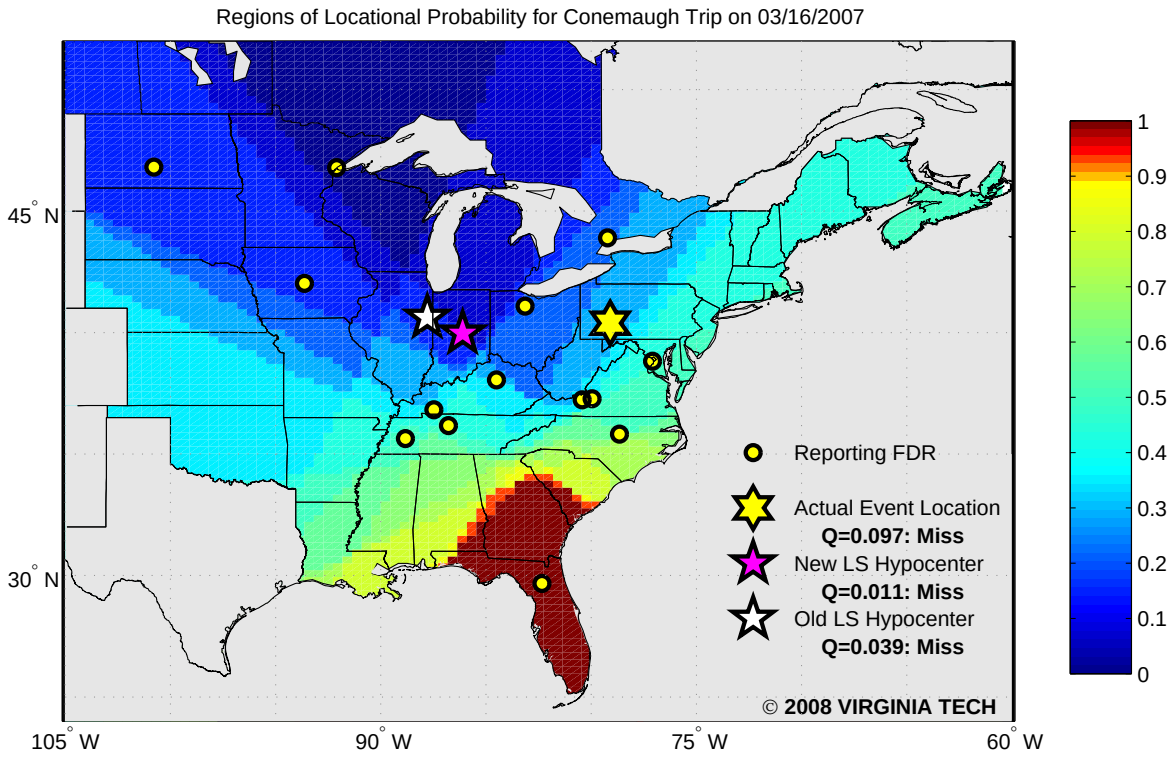
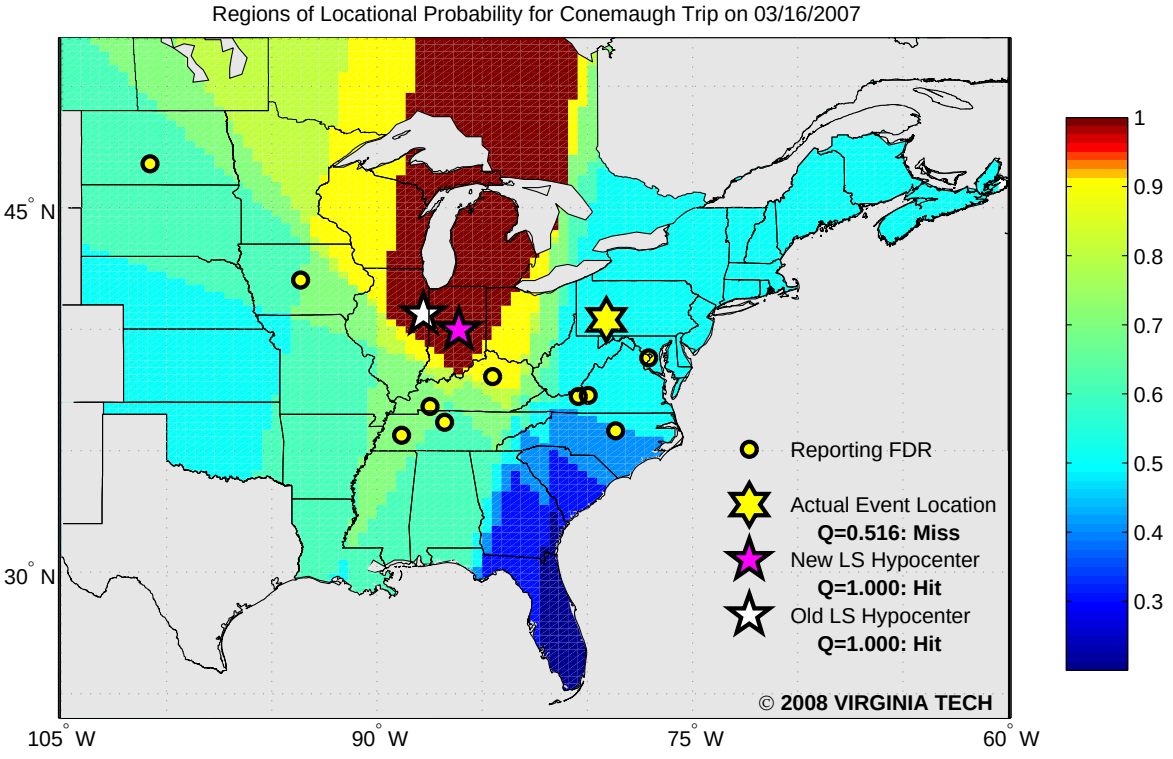


Figure D.30. Consolidated event ordering calculations: Conemaugh (850 MW, 40.3823°, −79.0968°) Trip on 03/16/2007 07:18:30



(a) Event location: old ordering method



(b) Event location: new ordering method

Figure D.31. Event location estimates: Conemaugh (850 MW, 40.3823°, −79.0968°) Trip on 03/16/2007 07:18:30

Table D.13. Ordering method comparison: Paradise (1000 MW, 37.2578°, −86.9792°) Trip on 03/20/2007 10:06:41

	Old Ordering Method			New Ordering Method		
Mismatch estimate (MW)	457			464		
FDR Info	Number	Name	Distance (mi)	Number	Name	Distance (mi)
	560	Duluth	708.5	13	MidwestISO	193.1
	43	Bismarck	965.7	17	TVA4Jackson	152.2
	17	TVA4Jackson	152.2	31	UK	146.2
	31	UK	146.2	4	VT	360.2
	6	ABB	472.3	2	UMR	266.3
	506	OhioTiffin	334.9	6	ABB	472.3
	9	UFL	588.1	510	Blacksburg	363
	502	Toronto	612.6	43	Bismarck	965.7
	13	MidwestISO	193.1	35	ISU	482.9
	4	VT	360.2	23	Duluth2	708.5
	2	UMR	266.3	502	Toronto	612.6
	510	Blacksburg	363			
	35	ISU	482.9			
LS estimate	Latitude	Longitude	Distance (mi)	Latitude	Longitude	Distance (mi)
	40.4696°	−88.8175°	242.9	38.7126°	−85.0472°	145.5
	$Q_{old} = 0.3339$ $Q_{new} = 1.0000$			$Q_{old} = 0.0425$ $Q_{new} = 0.9368$		
Parzen windowing results	$Q_{actual} = 0.1453$			$Q_{actual} = 1.0000$		

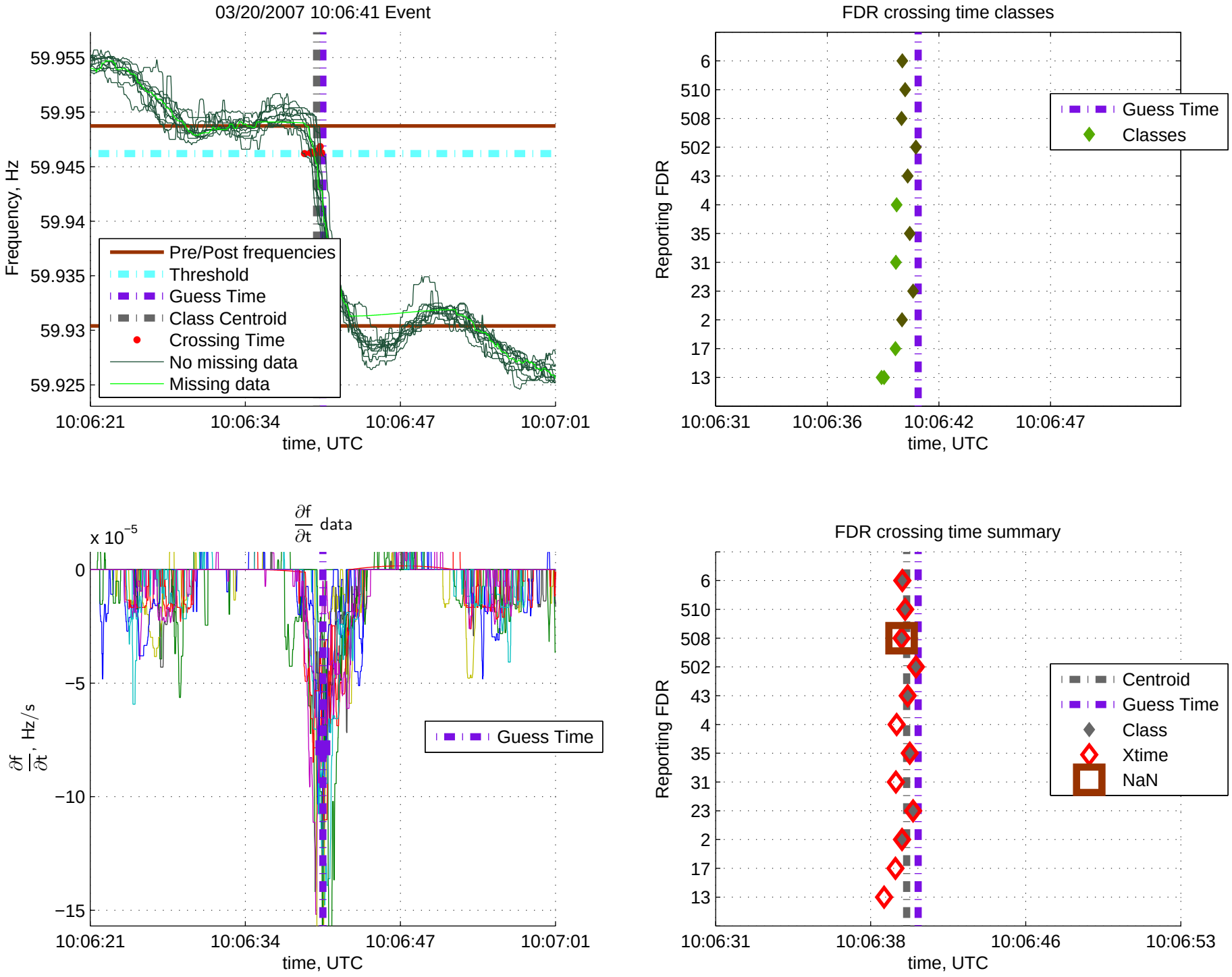
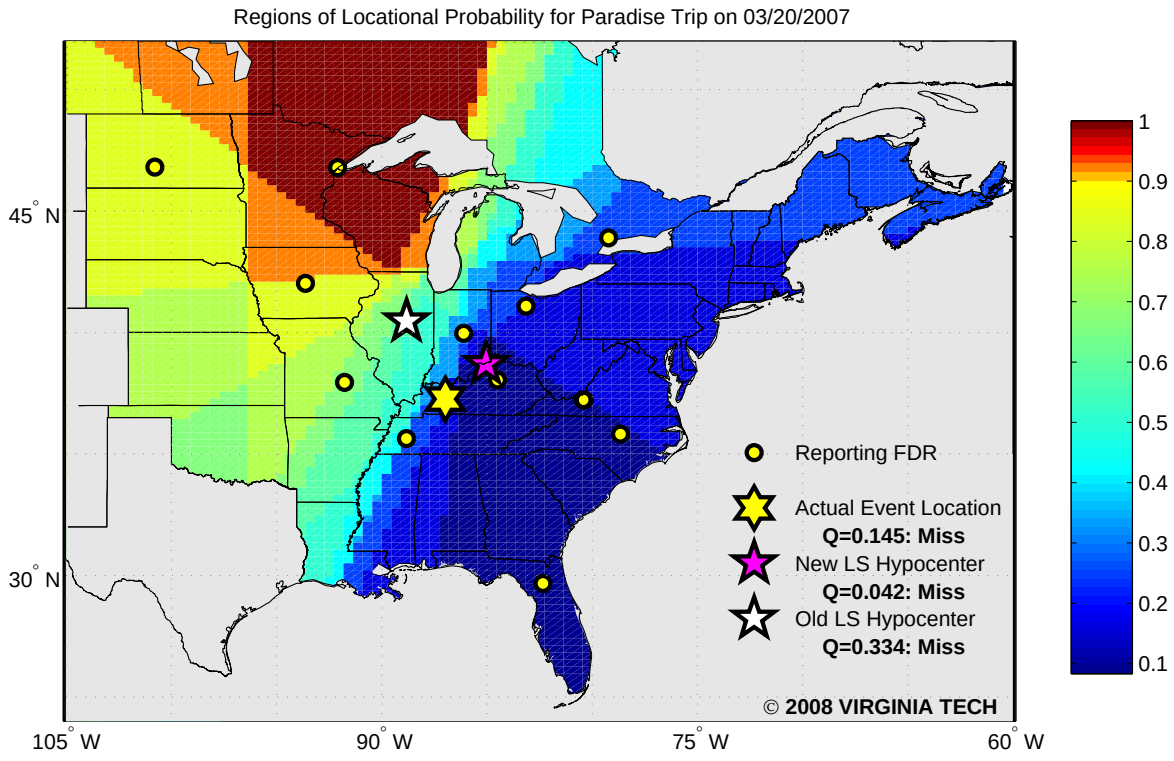
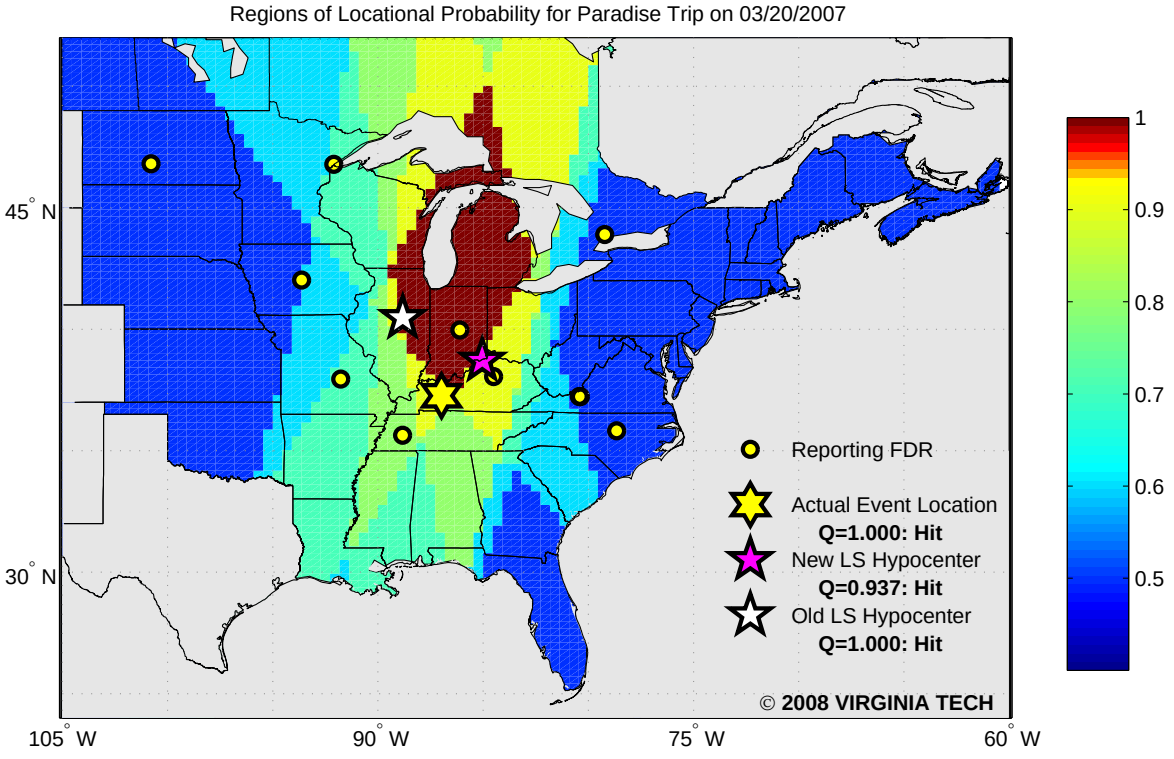


Figure D.32. Consolidated event ordering calculations: Paradise (1000 MW, 37.2578°, −86.9792°) Trip on 03/20/2007 10:06:41



(a) Event location: old ordering method



(b) Event location: new ordering method

Figure D.33. Event location estimates: Paradise (1000 MW, 37.2578°, −86.9792°) Trip on 03/20/2007 10:06:41

Table D.14. Ordering method comparison: Conemaugh (850 MW, 40.3823°, −79.0968°) Trip on 03/21/2007 20:41:40

	Old Ordering Method			New Ordering Method		
Mismatch estimate (MW)	797			729		
FDR Info	Number	Name	Distance (mi)	Number	Name	Distance (mi)
	3	ARI	152	6	ABB	316
	6	ABB	316	13	MidwestISO	371.2
	4	VT	229.1	3	ARI	152
	502	Toronto	242.9	508	ROA	219.4
	508	ROA	219.4	17	TVA4Jackson	622.6
	506	OhioTiffin	217.2	4	VT	229.1
	13	MidwestISO	371.2	502	Toronto	242.9
	560	Duluth	785.4	32	TVA7Hopkinsville	514.6
	43	Bismarck	1168	23	Duluth2	785.4
	35	ISU	762.8	35	ISU	762.8
	9	UFL	762.1	2	UMR	698.5
	32	TVA7Hopkinsville	514.6			
	2	UMR	698.5			
	17	TVA4Jackson	622.6			
LS estimate	Latitude	Longitude	Distance (mi)	Latitude	Longitude	Distance (mi)
	41.5019°	−86.9556°	417.2	34.0121°	−78.0456°	443.9
	$Q_{old} = 0.0282$			$Q_{old} = 0.2226$		
	$Q_{new} = 0.0368$			$Q_{new} = 1.0000$		
Parzen windowing results	$Q_{actual} = 1.0000$			$Q_{actual} = 0.2389$		

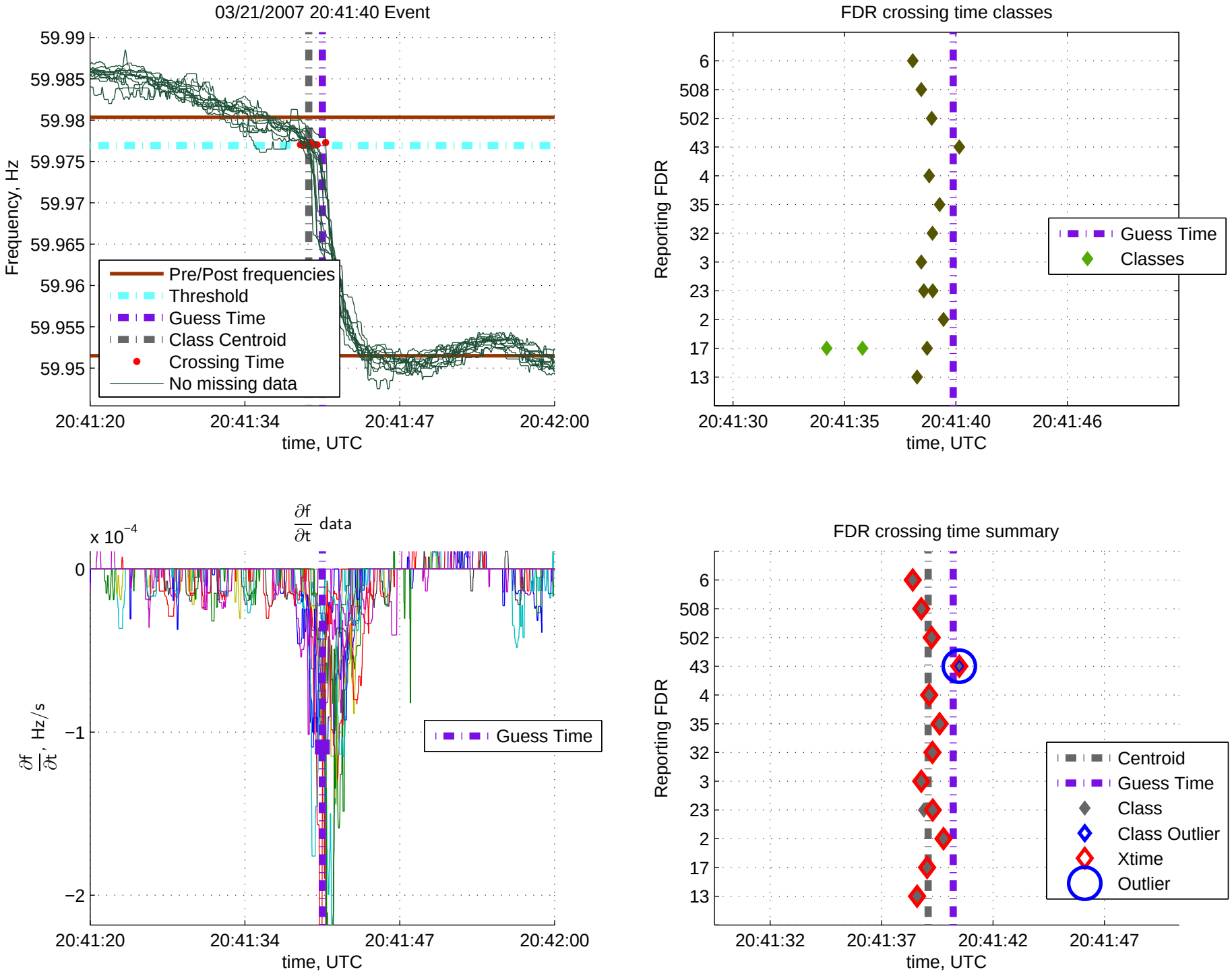
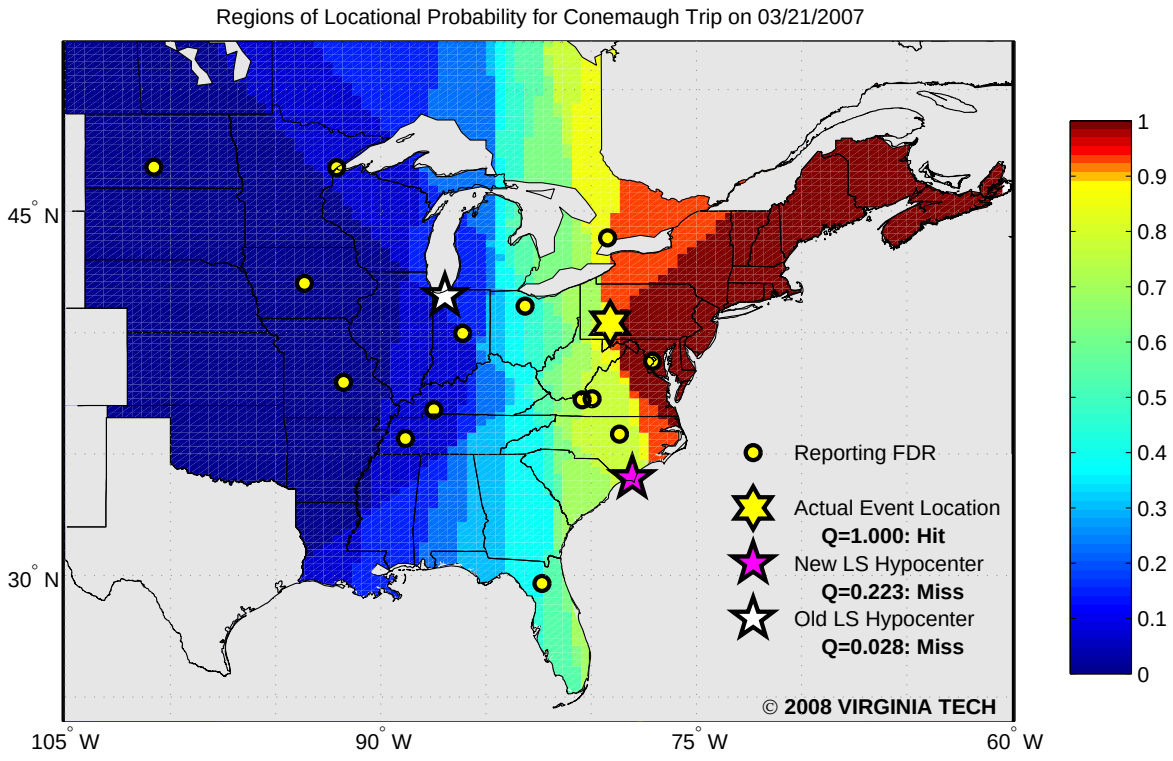
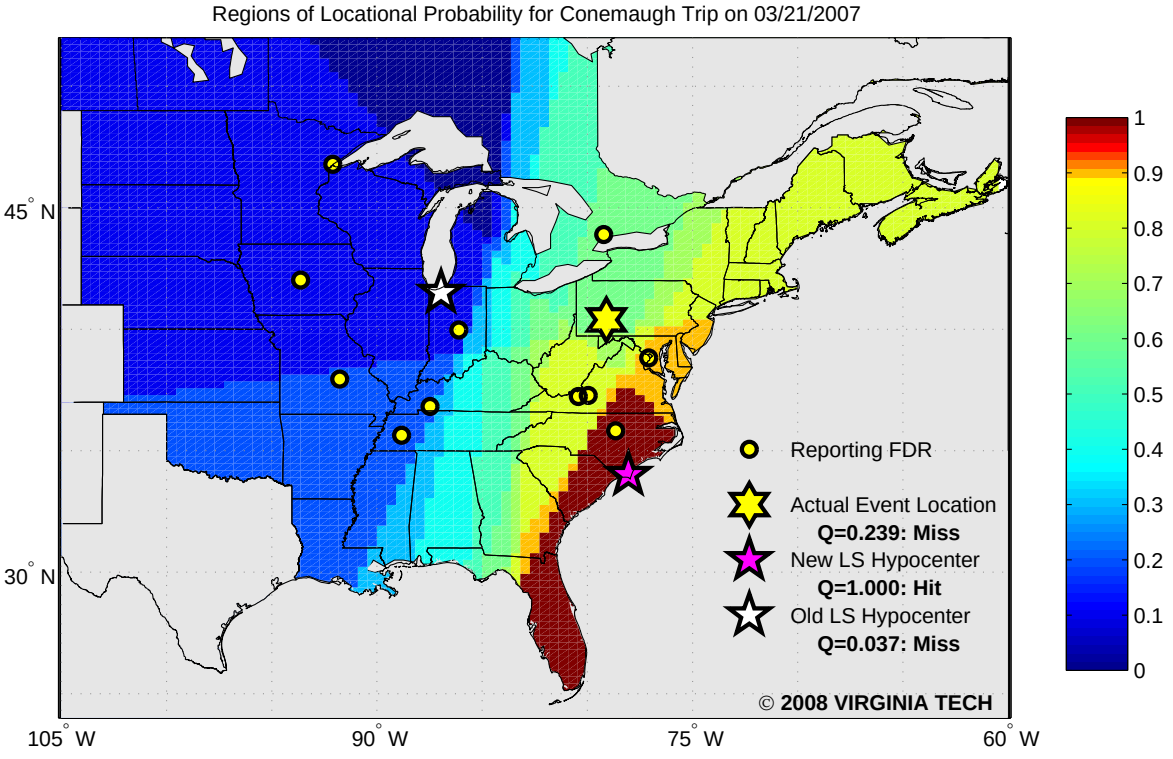


Figure D.34. Consolidated event ordering calculations: Conemaugh (850 MW, 40.3823°, −79.0968°) Trip on 03/21/2007 20:41:40



(a) Event location: old ordering method

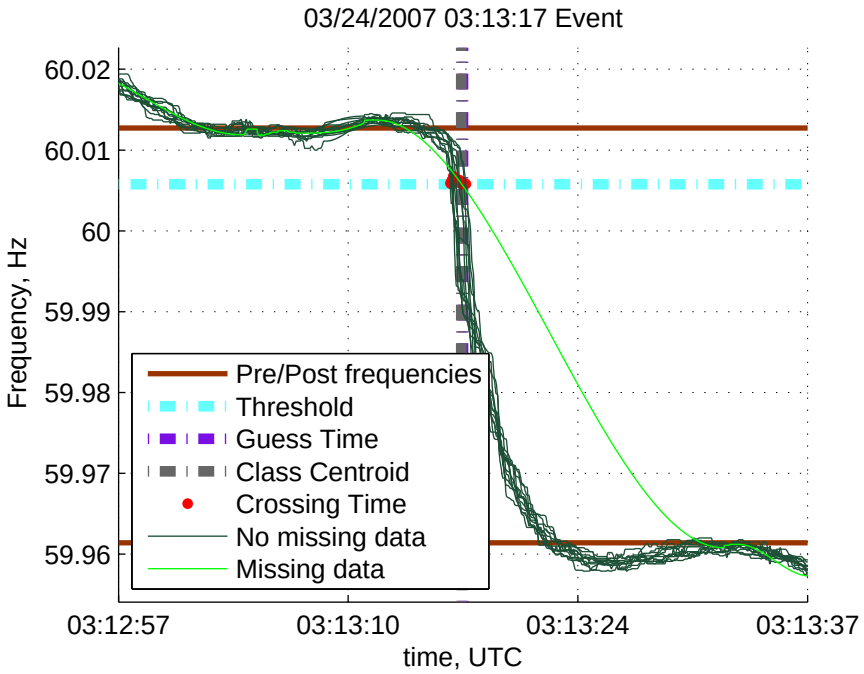


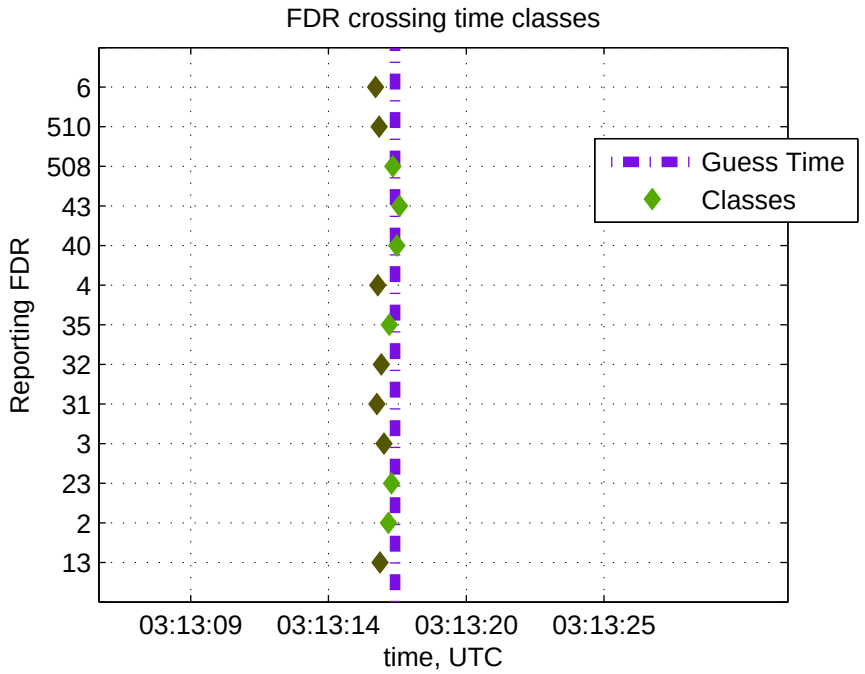
(b) Event location: new ordering method

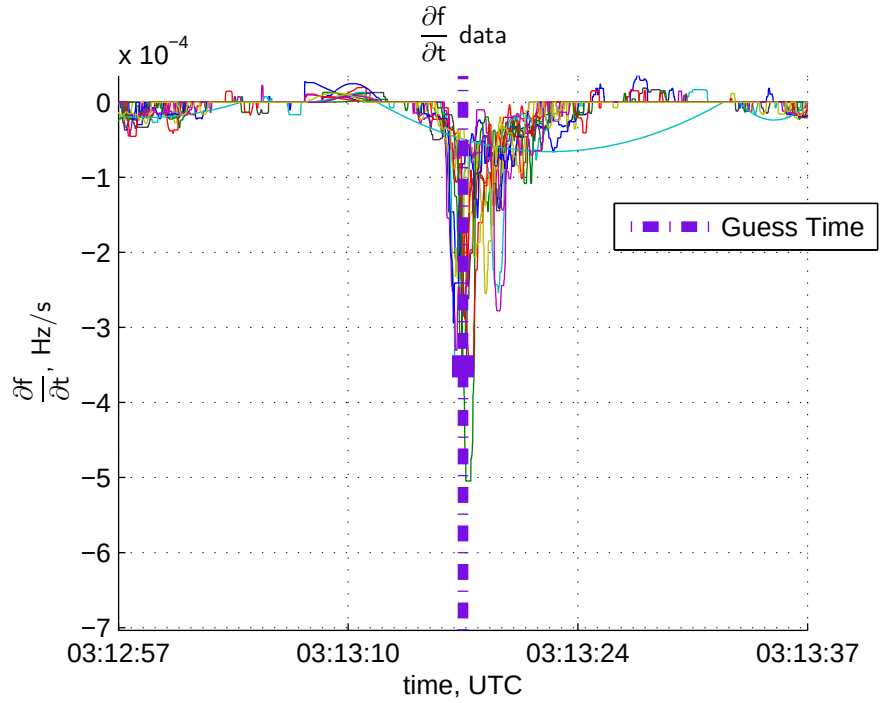
Figure D.35. Event location estimates: Conemaugh (850 MW, 40.3823°, −79.0968°) Trip on 03/21/2007 20:41:40

Table D.15. Ordering method comparison: W H Zimmer (1300 MW, 39.0523°, −84.1505°) Trip on 03/24/2007 03:13:17

	Old Ordering Method			New Ordering Method		
Mismatch estimate (MW)	1547			1301		
FDR Info	Number	Name	Distance (mi)	Number	Name	Distance (mi)
	13	MidwestISO	122.1	6	ABB	374.8
	31	UK	71.78	31	UK	71.78
	508	ROA	258.6	4	VT	238.1
	4	VT	238.1	510	Blacksburg	240.7
	506	OhioTiffin	150.2	13	MidwestISO	122.1
	510	Blacksburg	240.7	32	TVA7Hopkinsville	237.8
	3	ARI	379.9	3	ARI	379.9
	32	TVA7Hopkinsville	237.8	2	UMR	418.6
	6	ABB	374.8	35	ISU	537.8
	2	UMR	418.6	23	Duluth2	668.1
	35	ISU	537.8	40	MISOStPaul	616.3
	40	MISOStPaul	616.3	43	Bismarck	994.6
	560	Duluth	668.1			
	9	UFL	656.1			
	43	Bismarck	994.6			
LS estimate	Latitude	Longitude	Distance (mi)	Latitude	Longitude	Distance (mi)
	41.9440°	−86.7467°	241.9	35.8219°	−78.6588°	374.8
	$Q_{old} = 1.0000$			$Q_{old} = 0.2388$		
	$Q_{new} = 0.0710$			$Q_{new} = 1.0000$		
Parzen windowing results	$Q_{actual} = 0.8851$			$Q_{actual} = 0.1618$		







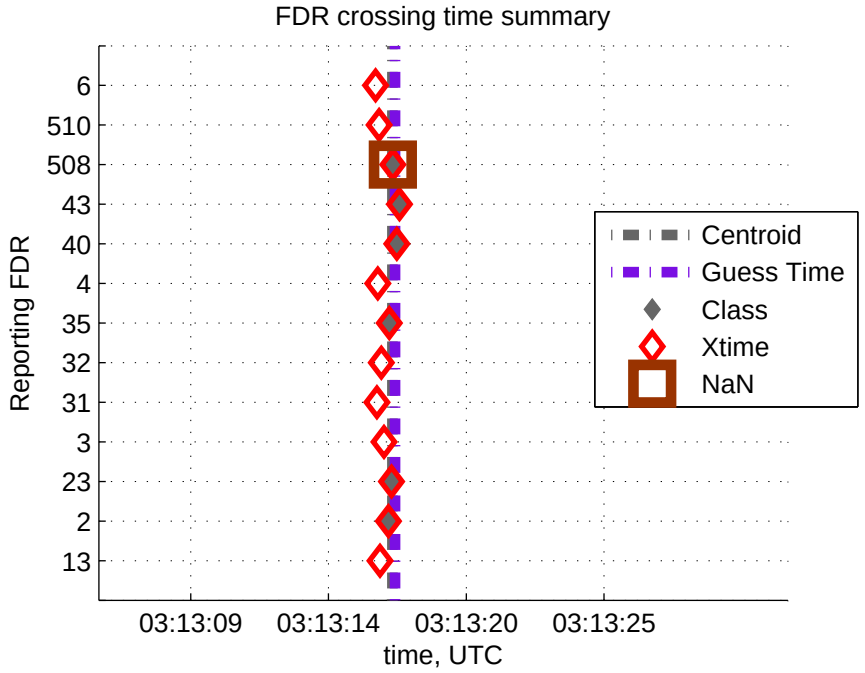
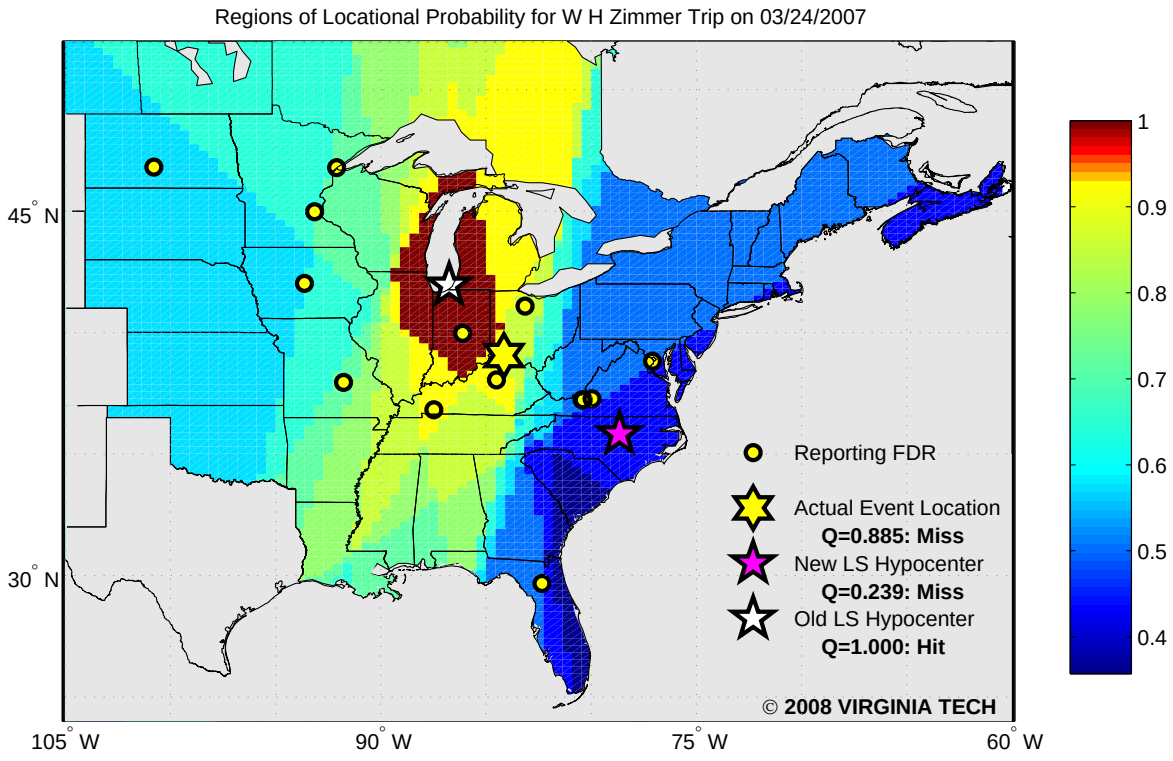
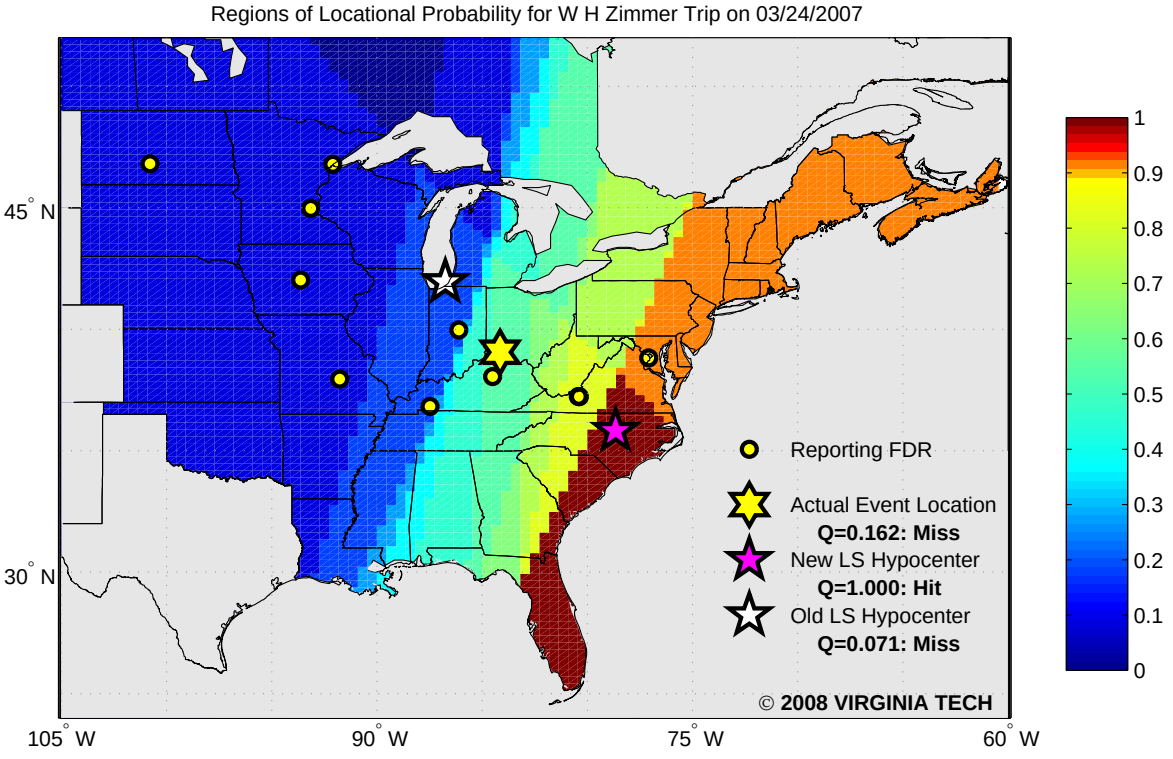


Figure D.36. Consolidated event ordering calculations: W H Zimmer (1300 MW, 39.0523°, −84.1505°) Trip on 03/24/2007 03:13:17



(a) Event location: old ordering method



(b) Event location: new ordering method

Figure D.37. Event location estimates: W H Zimmer (1300 MW, 39.0523°, −84.1505°) Trip on 03/24/2007 03:13:17

Table D.16. Ordering method comparison: Indian Point Unit3 (1025 MW, 41.2697°, −73.9524°) Trip on 04/06/2007 15:09:10

	Old Ordering Method			New Ordering Method		
Mismatch estimate (MW)	753			639		
FDR Info	Number	Name	Distance (mi)	Number	Name	Distance (mi)
	27	RPI	102.2	4	VT	444.6
	503	Danbury	24.33	13	MidwestISO	643.3
	38	ISONE	92.73	23	Duluth2	975.9
	502	Toronto	323.8	510	Blacksburg	442.8
	506	OhioTiffin	477.8	31	UK	603
	13	MidwestISO	643.3	7	MISS	976.7
	500	Chicago	721.1	17	TVA4Jackson	892.5
	31	UK	603	32	TVA7Hopkinsville	786.9
	40	MISOStPaul	998.6	500	Chicago	721.1
	17	TVA4Jackson	892.5	2	UMR	973.7
	4	VT	444.6	40	MISOStPaul	998.6
	7	MISS	976.7	43	Bismarck	1379
	43	Bismarck	1379			
	2	UMR	973.7			
	510	Blacksburg	442.8			
	6	ABB	454.1			
	560	Duluth	975.9			
LS estimate	Latitude	Longitude	Distance (mi)	Latitude	Longitude	Distance (mi)
	46.1560°	−83.9754°	603.1	37.9848°	−82.5857°	512.1
	$Q_{old} = 0.1292$			$Q_{old} = 0.1292$		
	$Q_{new} = 0.1823$			$Q_{new} = 0.9415$		
Parzen windowing results	$Q_{actual} = 0.9263$			$Q_{actual} = 0.9415$		

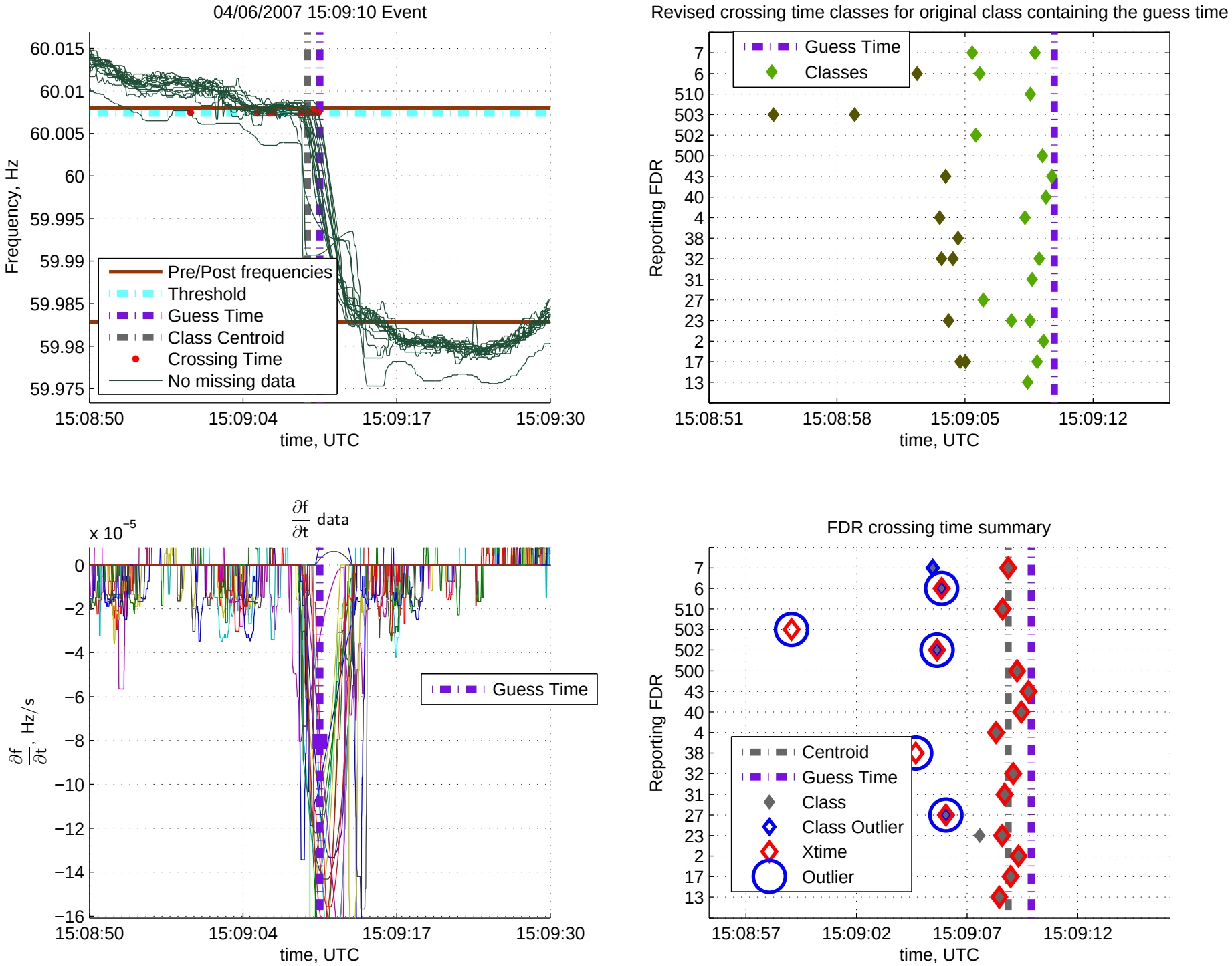
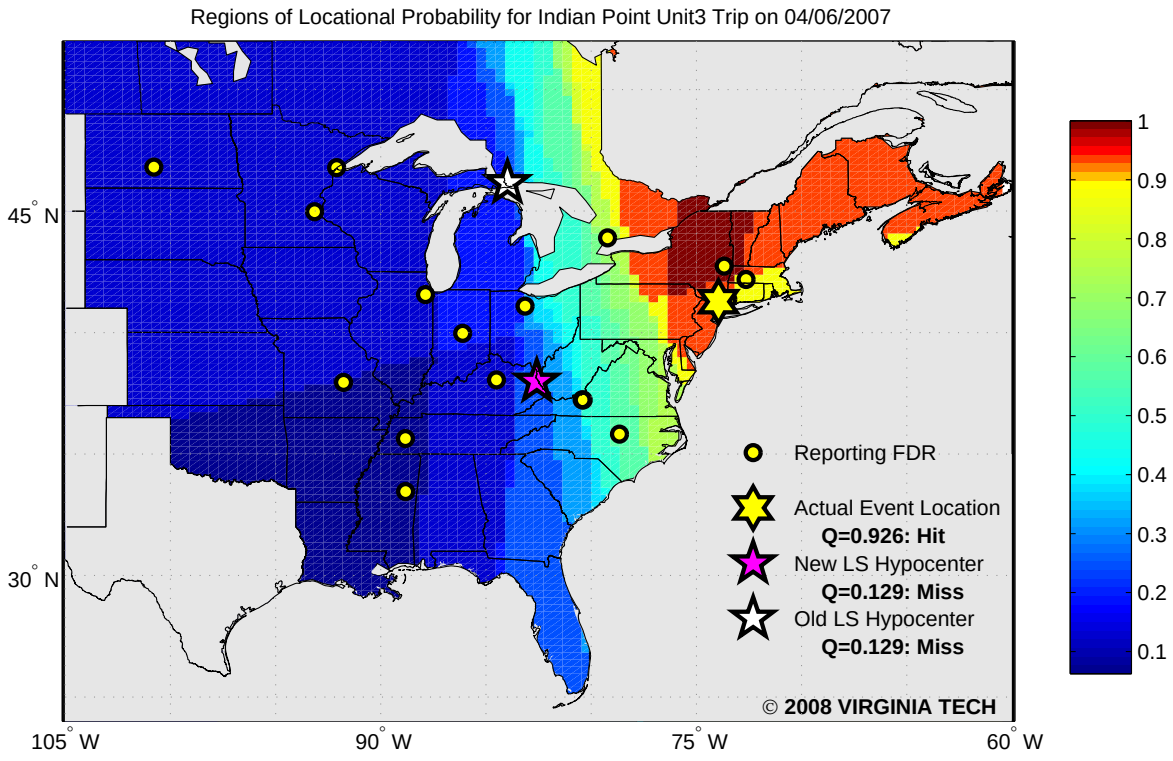
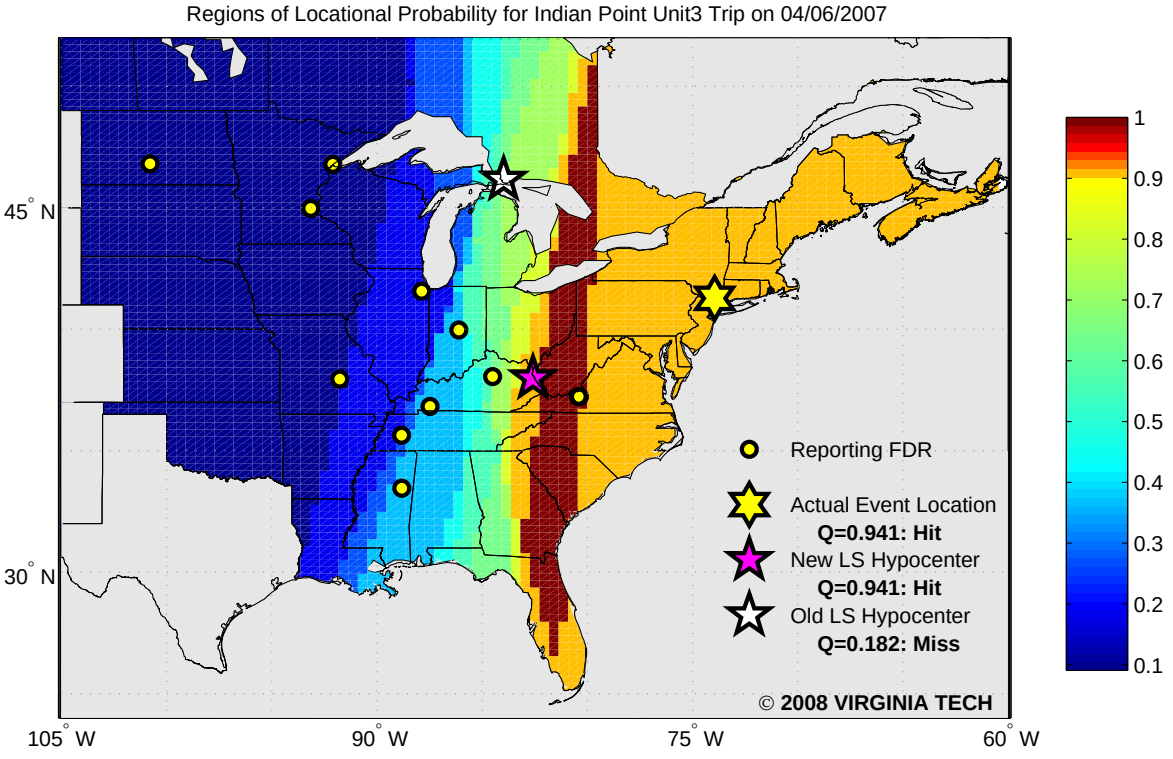


Figure D.38. Consolidated event ordering calculations: Indian Point Unit3 (1025 MW, 41.2697°, −73.9524°) Trip on 04/06/2007 15:09:10



(a) Event location: old ordering method

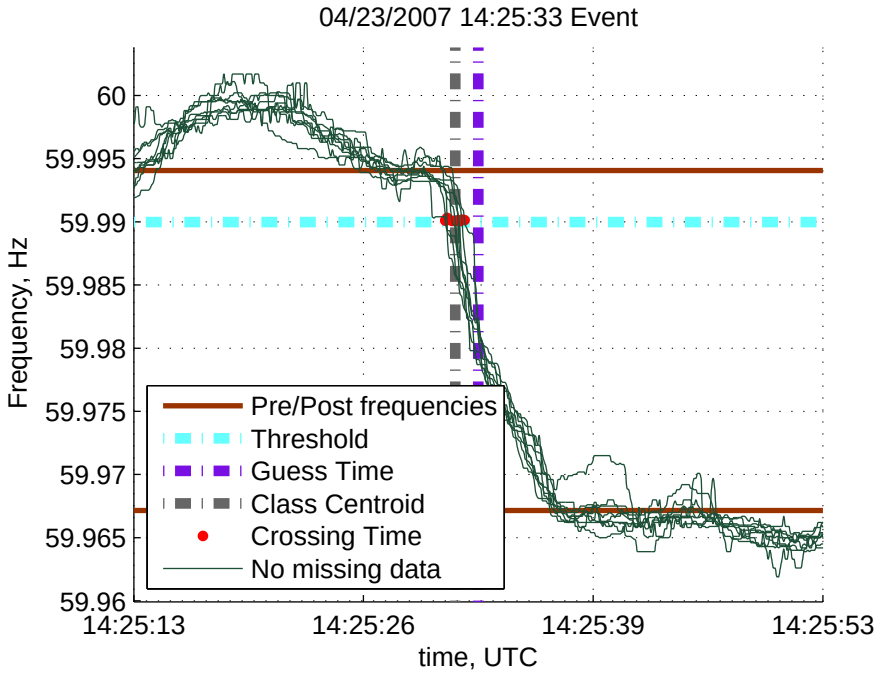


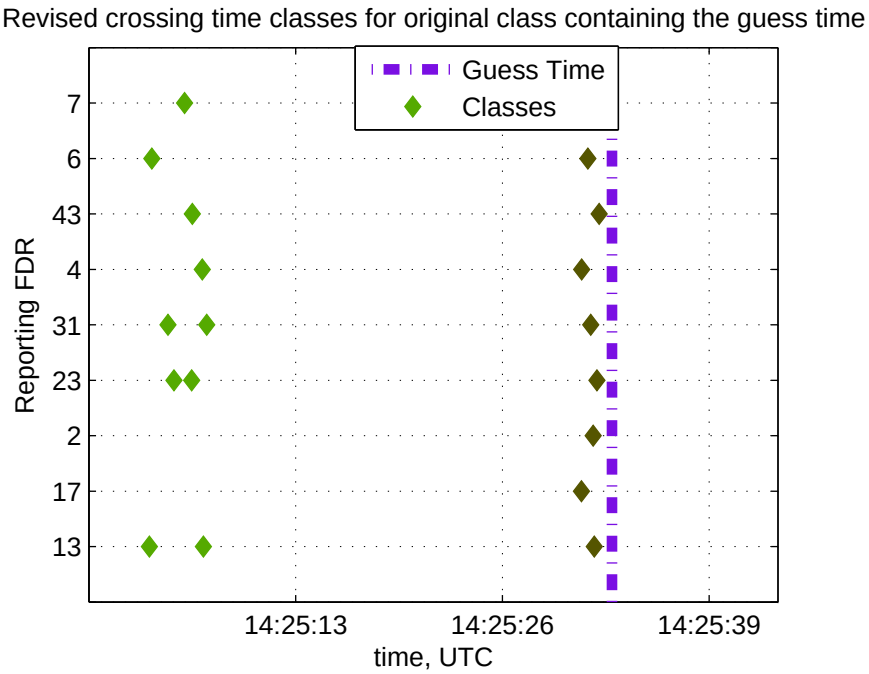
(b) Event location: new ordering method

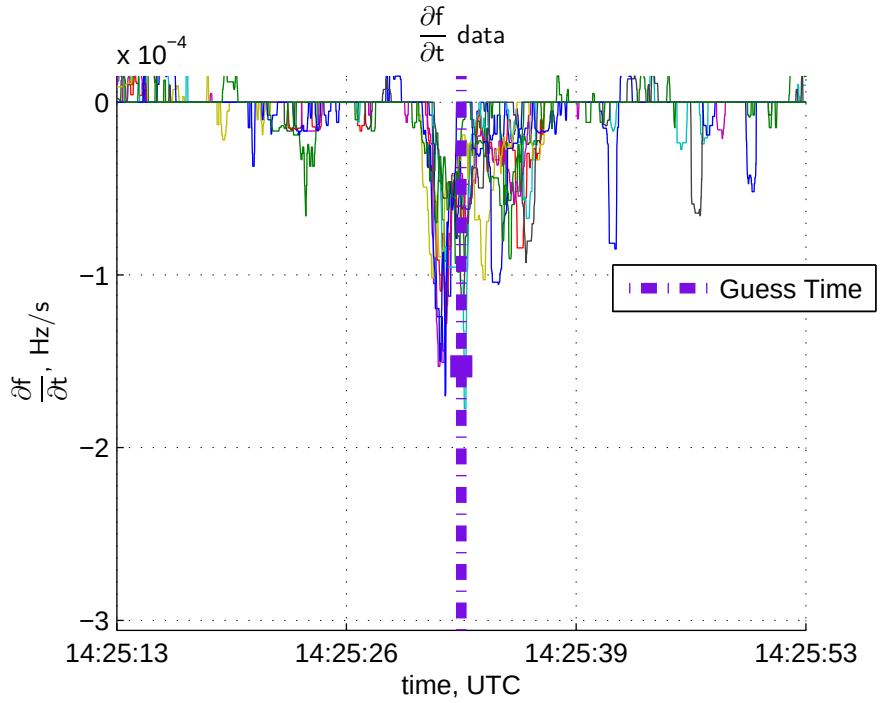
Figure D.39. Event location estimates: Indian Point Unit3 (1025 MW, 41.2697°, −73.9524°) Trip on 04/06/2007 15:09:10

Table D.17. Ordering method comparison: Vogtle Unit 2 (1149 MW, 33.0894°, −81.9780°) Trip on 04/23/2007 14:25:33

	Old Ordering Method			New Ordering Method		
Mismatch estimate (MW)	770			682		
FDR Info	Number	Name	Distance (mi)	Number	Name	Distance (mi)
	6	ABB	267.2	17	TVA4Jackson	428.3
	13	MidwestISO	527.6	4	VT	299.3
	7	MISS	396.1	7	MISS	396.1
	560	Duluth	1086	6	ABB	267.2
	4	VT	299.3	31	UK	370.9
	31	UK	370.9	2	UMR	644.2
	2	UMR	644.2	13	MidwestISO	527.6
	17	TVA4Jackson	428.3	23	Duluth2	1086
				43	Bismarck	1368
LS estimate	Latitude	Longitude	Distance (mi)	Latitude	Longitude	Distance (mi)
	41.0160°	−83.3301°	552.7	33.6336°	−86.9482°	289.2
	$Q_{old} = 0.0855$			$Q_{old} = 0.0173$		
	$Q_{new} = 0.4831$			$Q_{new} = 0.9798$		
Parzen windowing results	$Q_{actual} = 0.2027$			$Q_{actual} = 0.1348$		







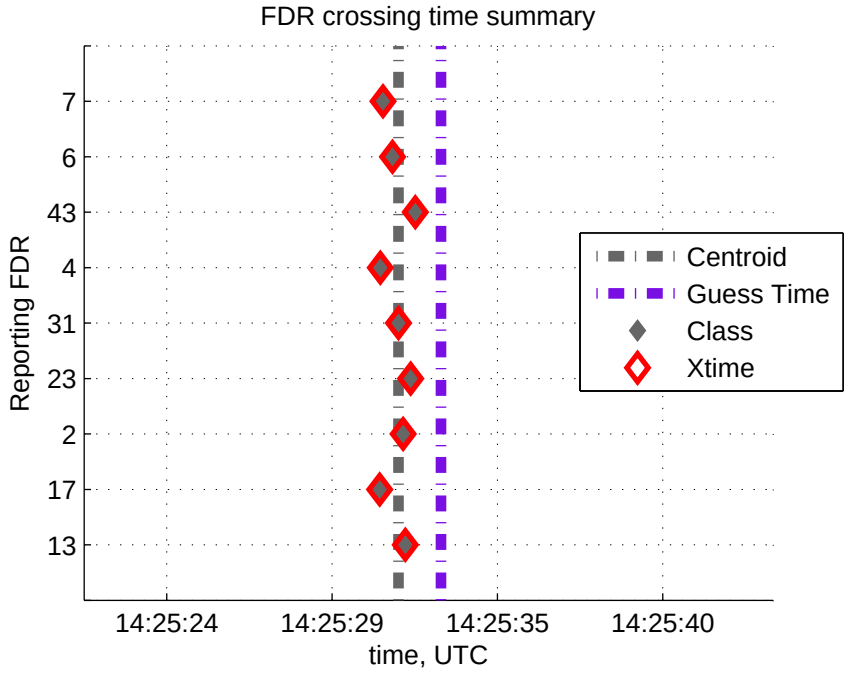
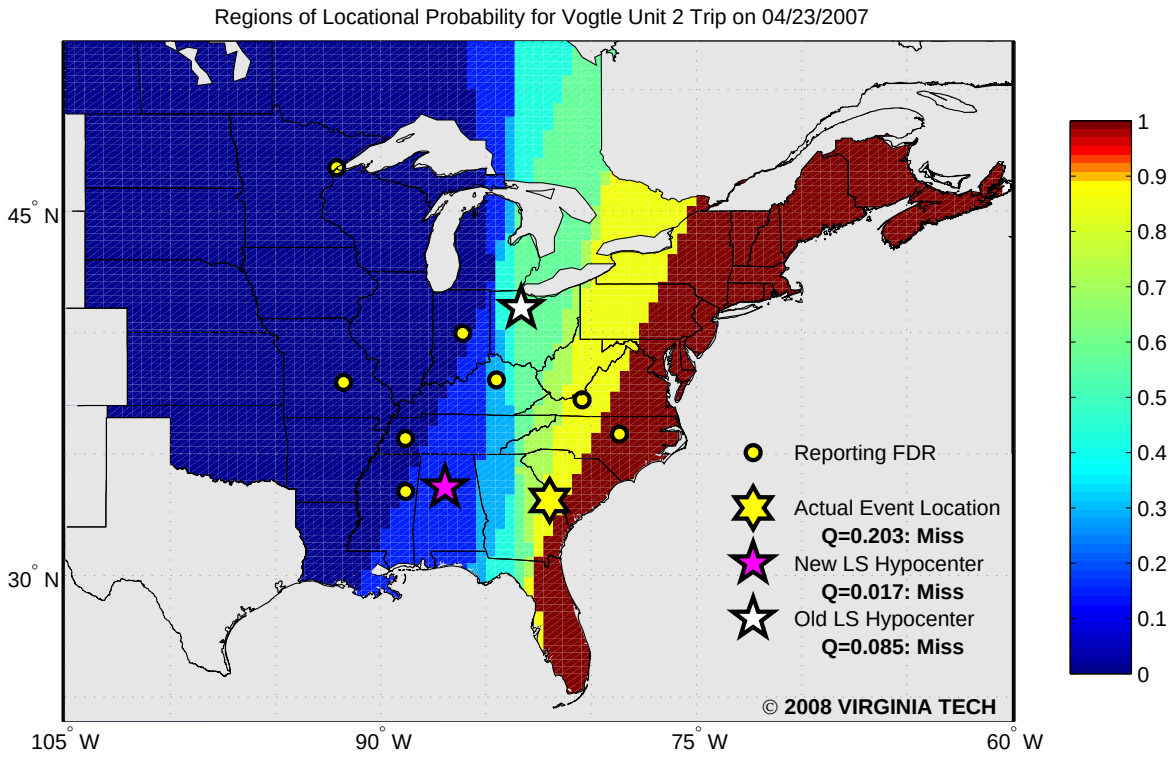
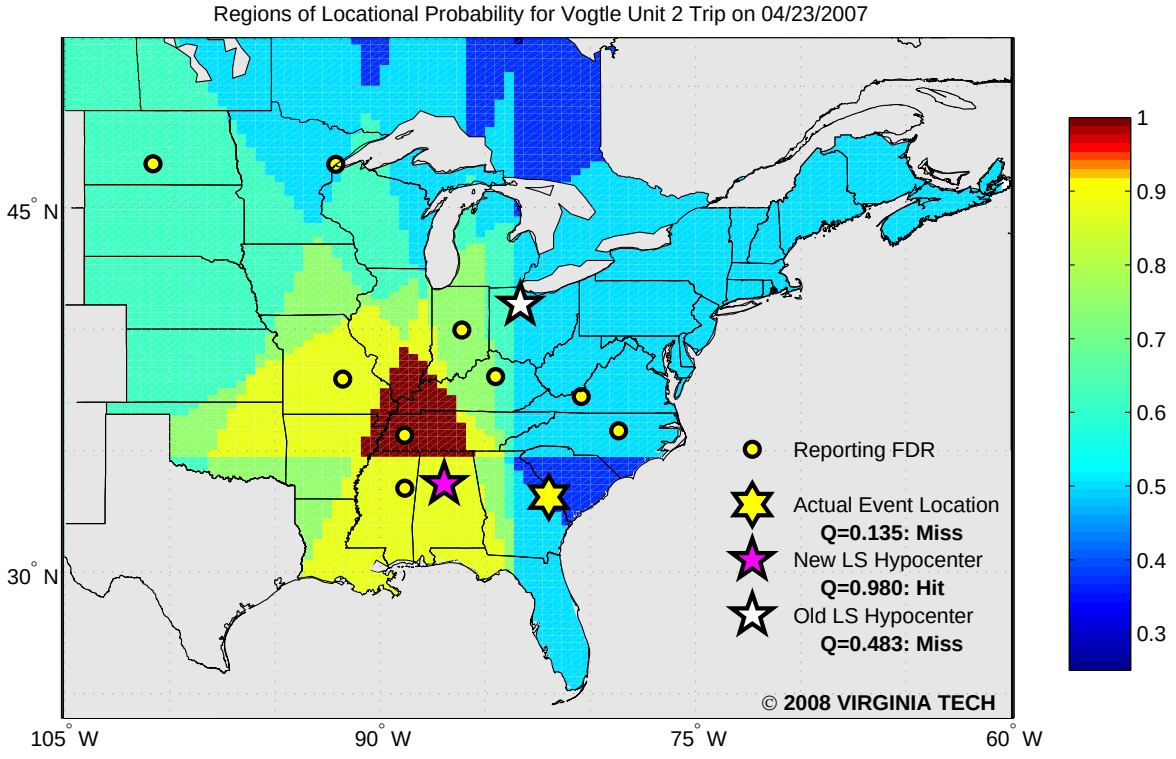


Figure D.40. Consolidated event ordering calculations: Vogtle Unit 2 (1149 MW, 33.0894°, −81.9780°) Trip on 04/23/2007 14:25:33



(a) Event location: old ordering method



(b) Event location: new ordering method

Figure D.41. Event location estimates: Vogtle Unit 2 (1149 MW, 33.0894°, −81.9780°) Trip on 04/23/2007 14:25:33

Table D.18. Ordering method comparison: Salem Unit 1 (1174 MW, 39.4956°, −75.4733°) Trip on 04/30/2007 19:02:53

	Old Ordering Method			New Ordering Method		
Mismatch estimate (MW)	706			708		
FDR Info	Number	Name	Distance (mi)	Number	Name	Distance (mi)
	503	Danbury	166.1	503	Danbury	166.1
	27	RPI	242.5	27	RPI	242.5
	6	ABB	307.8	510	Blacksburg	308.5
	4	VT	310.6	41	Winnipeg	1272
	510	Blacksburg	308.5	6	ABB	307.8
	506	OhioTiffin	418.6	13	MidwestISO	565.8
	13	MidwestISO	565.8	43	Bismarck	1365
	500	Chicago	666.3	500	Chicago	666.3
	17	TVA4Jackson	777.6	7	MISS	849.6
	40	MISOStPaul	977.5	23	Duluth2	975
	7	MISS	849.6	17	TVA4Jackson	777.6
	2	UMR	883.5	2	UMR	883.5
	560	Duluth	975	40	MISOStPaul	977.5
	41	Winnipeg	1272			
	43	Bismarck	1365			
LS estimate	Latitude	Longitude	Distance (mi)	Latitude	Longitude	Distance (mi)
	38.3861°	−74.2686°	100.3	40.9765°	−76.5015°	115.8
	Q_{old} = 1.0000			Q_{old} = 1.0000		
	Q_{new} = 1.0000			Q_{new} = 1.0000		
Parzen windowing results	Q_{actual} = 1.0000			Q_{actual} = 1.0000		

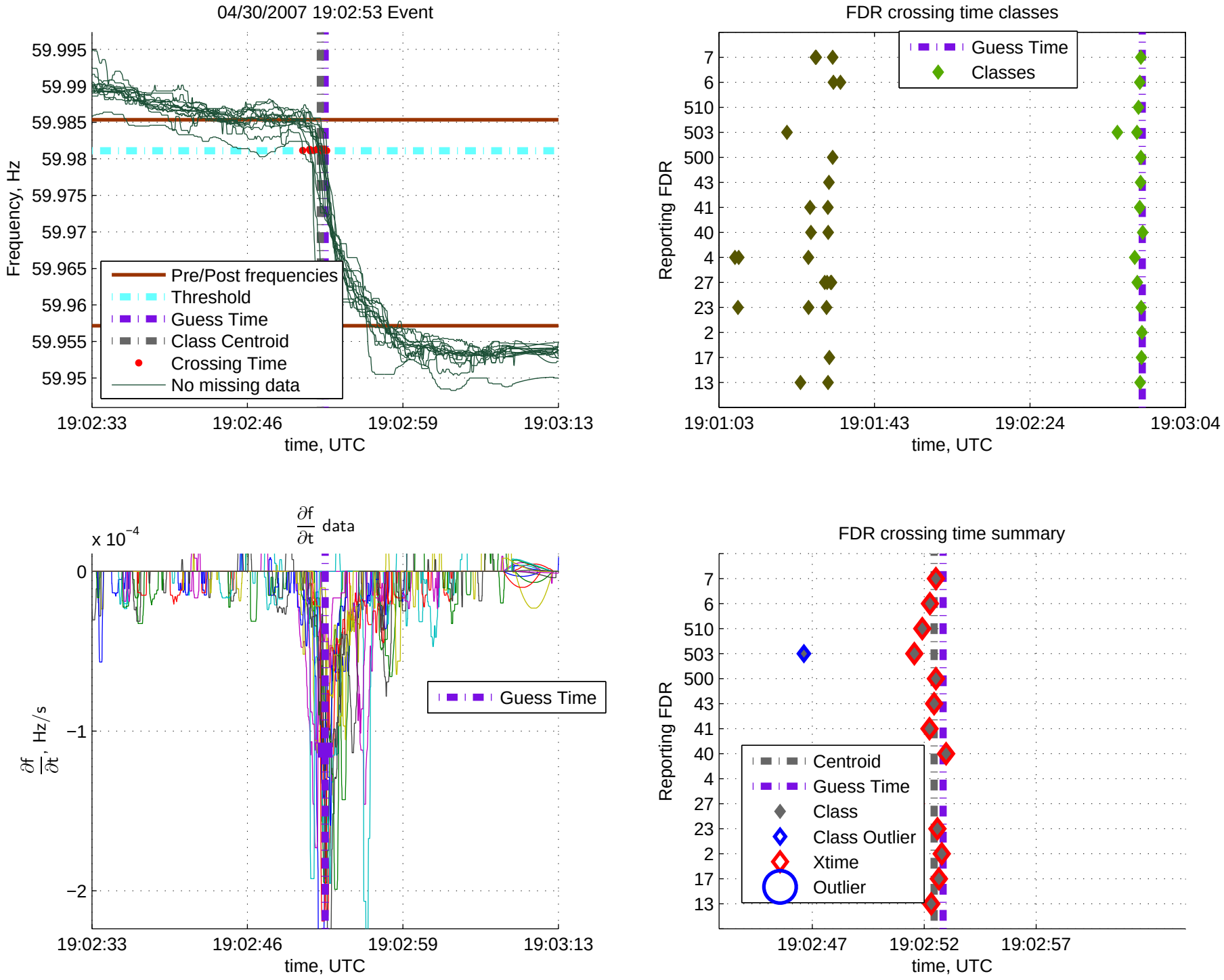
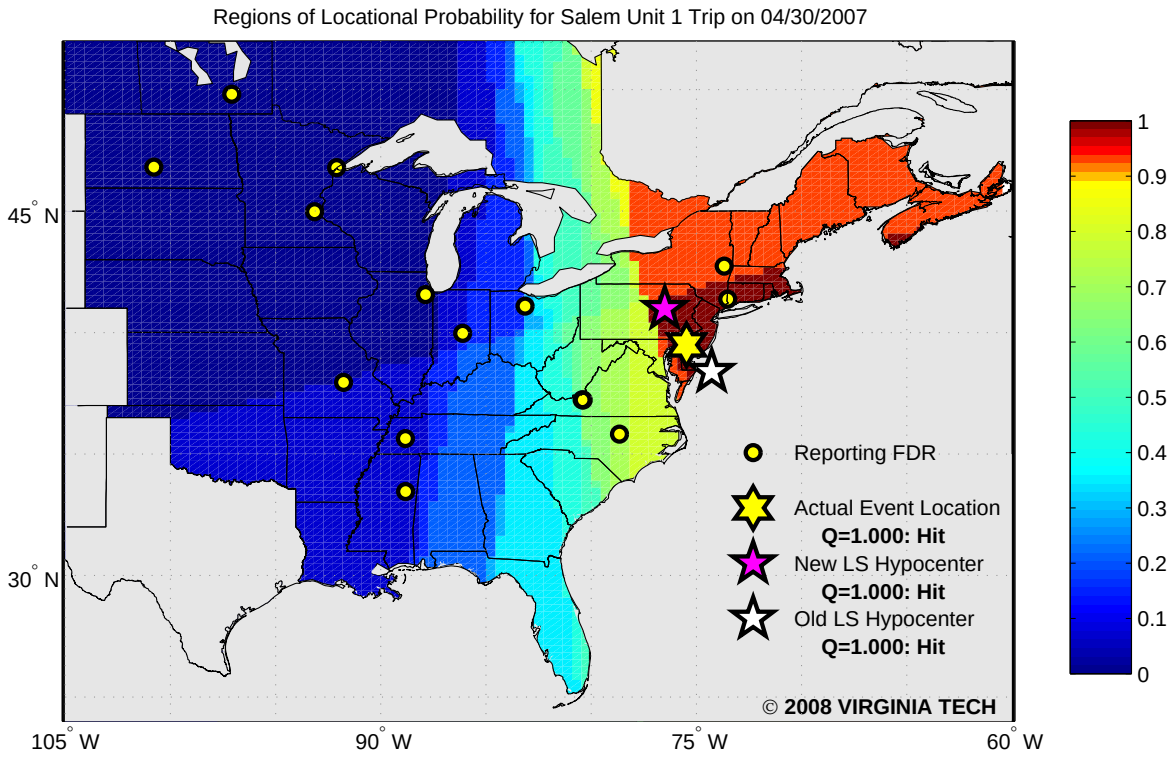
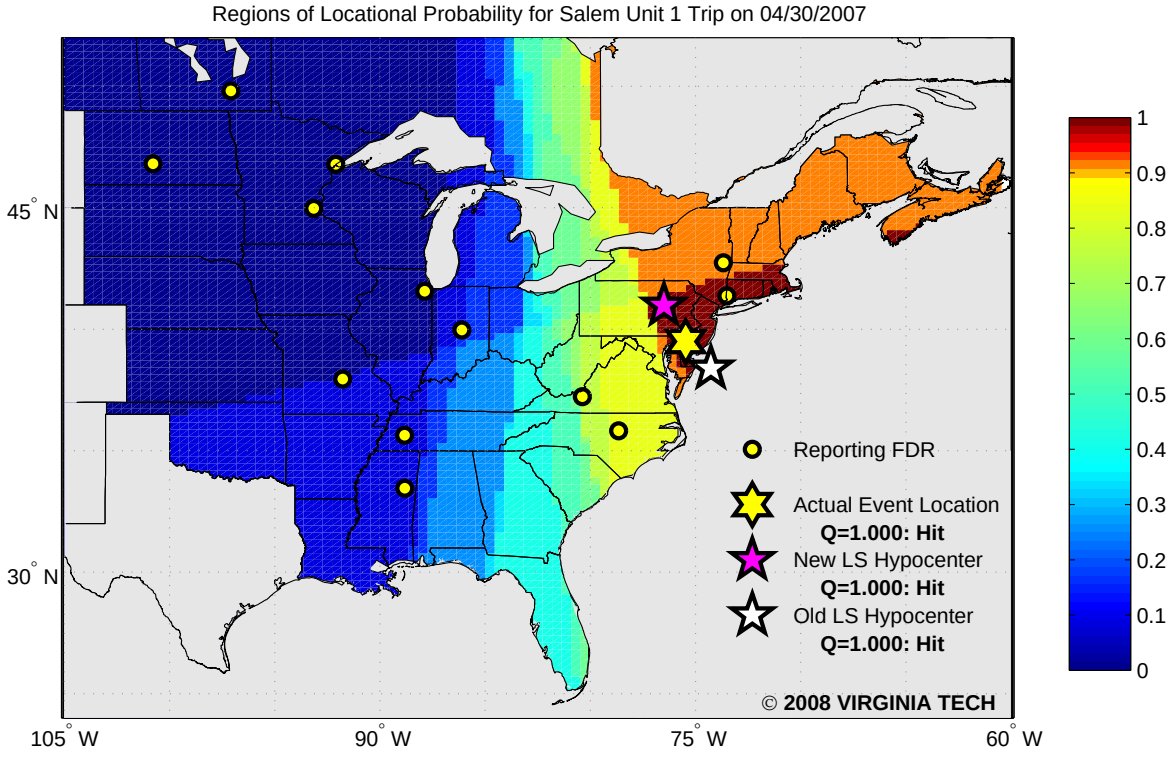


Figure D.42. Consolidated event ordering calculations: Salem Unit 1 (1174 MW, 39.4956°, −75.4733°) Trip on 04/30/2007 19:02:53



(a) Event location: old ordering method



(b) Event location: new ordering method

Figure D.43. Event location estimates: Salem Unit 1 (1174 MW, 39.4956°, −75.4733°) Trip on 04/30/2007 19:02:53

Table D.19. Ordering method comparison: Lacygne (840 MW, 38.3335°, −94.7608°) Trip on 05/03/2007 14:59:01

	Old Ordering Method			New Ordering Method		
Mismatch estimate (MW)	725			NaN		
FDR Info	Number	Name	Distance (mi)	Number	Name	Distance (mi)
	2	UMR	164.9	23	Duluth2	599.5
	43	Bismarck	660.5	13	MidwestISO	476.9
	560	Duluth	599.5	2	UMR	164.9
	40	MISOStPaul	466.2	7	MISS	473.1
	41	Winnipeg	801.2	41	Winnipeg	801.2
	6	ABB	903.2	43	Bismarck	660.5
	7	MISS	473.1	40	MISOStPaul	466.2
	510	Blacksburg	788.4	4	VT	785.5
	4	VT	785.5	500	Chicago	427.2
	27	RPI	1145	27	RPI	1145
	9	UFL	928.2	6	ABB	903.2
	500	Chicago	427.2	510	Blacksburg	788.4
	506	OhioTiffin	645.6			
	503	Danbury	1144			
	13	MidwestISO	476.9			
	38	ISONE	1193			
LS estimate	Latitude	Longitude	Distance (mi)	Latitude	Longitude	Distance (mi)
	39.4462°	−97.2901°	156.2	$NaN°$	$NaN°$	NaN
	Q_{old} = 1.0000 Q_{new} = 0.6454			$Q_{old} = NaN$ $Q_{new} = NaN$		
Parzen windowing results	Q_{actual} = 1.0000			Q_{actual} = 0.8568		

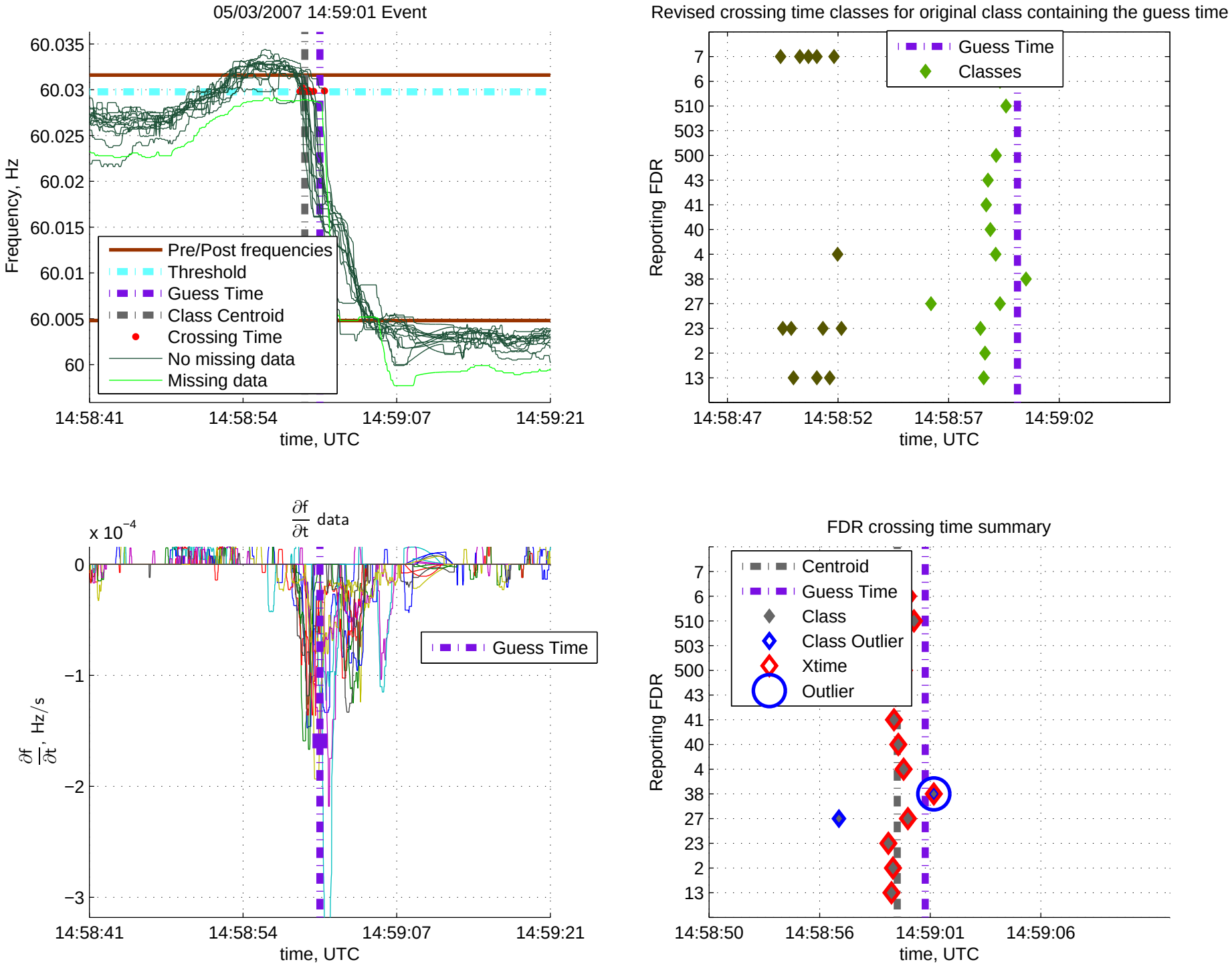
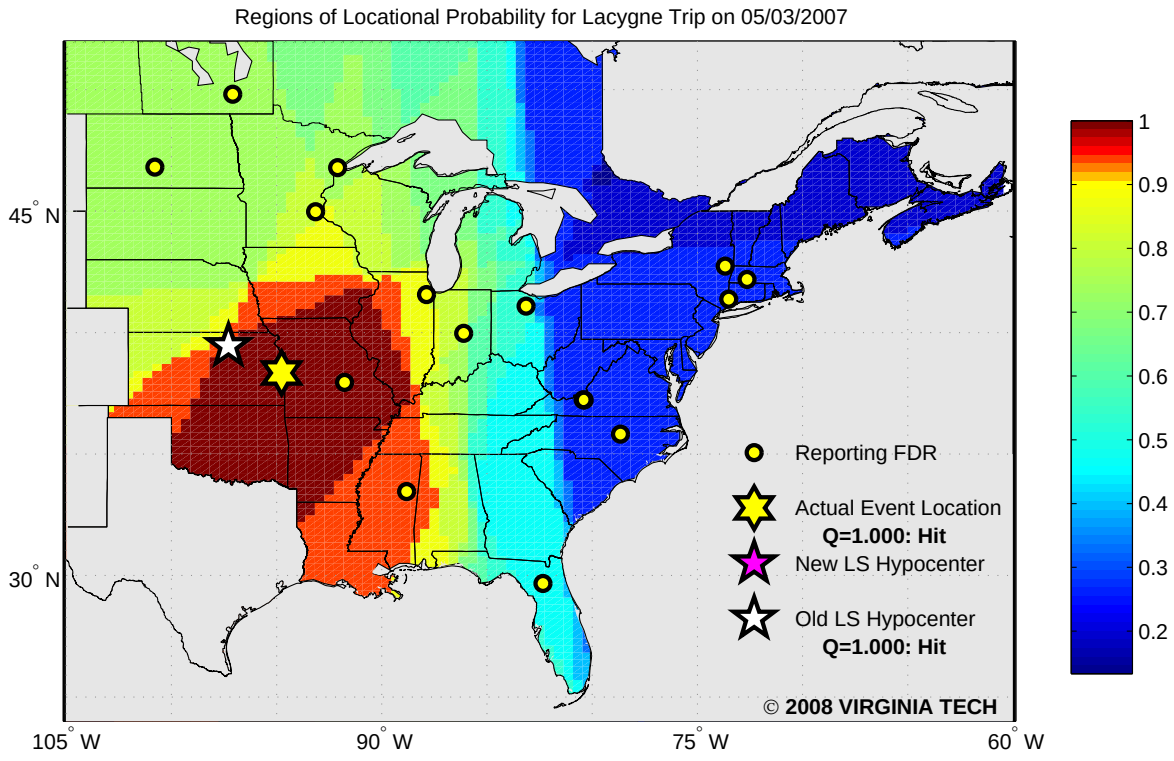
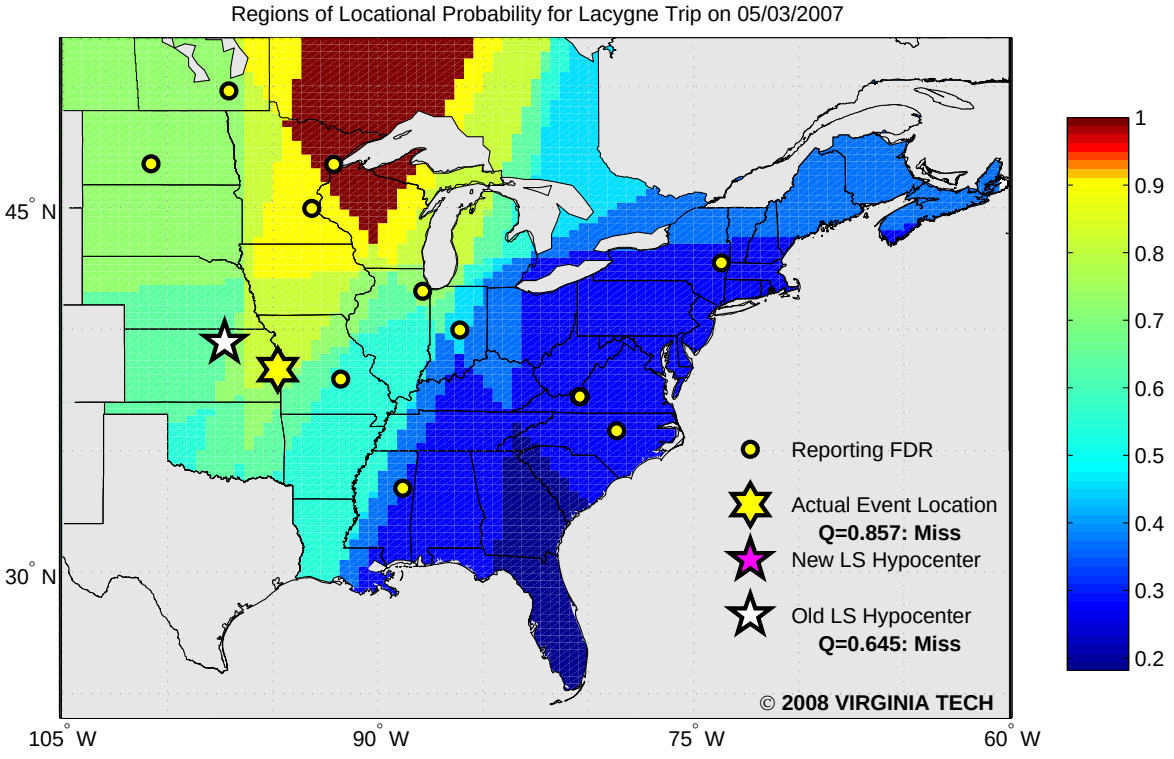


Figure D.44. Consolidated event ordering calculations: Lacygne (840 MW, 38.3335°, −94.7608°) Trip on 05/03/2007 14:59:01



(a) Event location: old ordering method

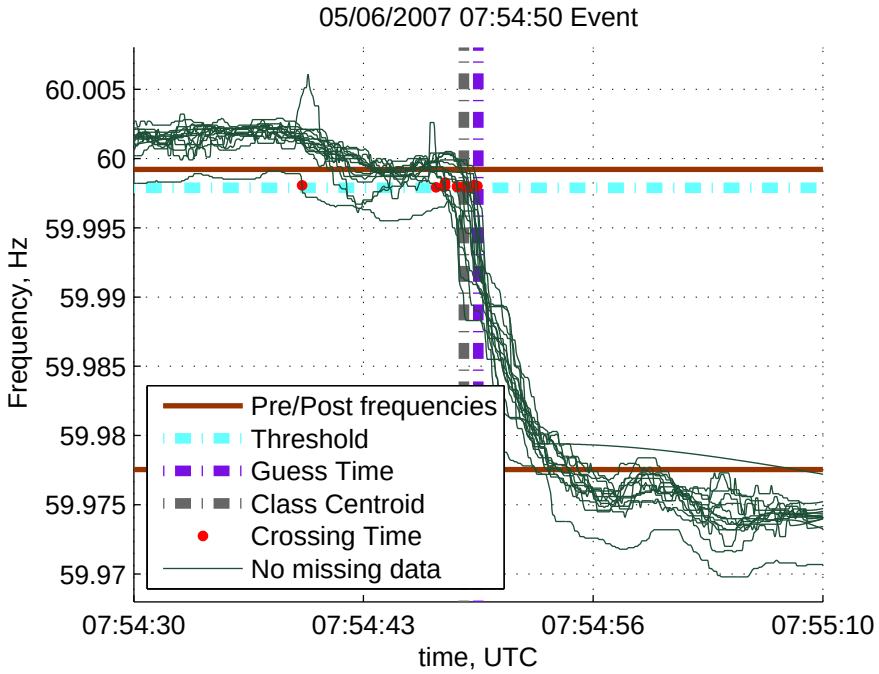


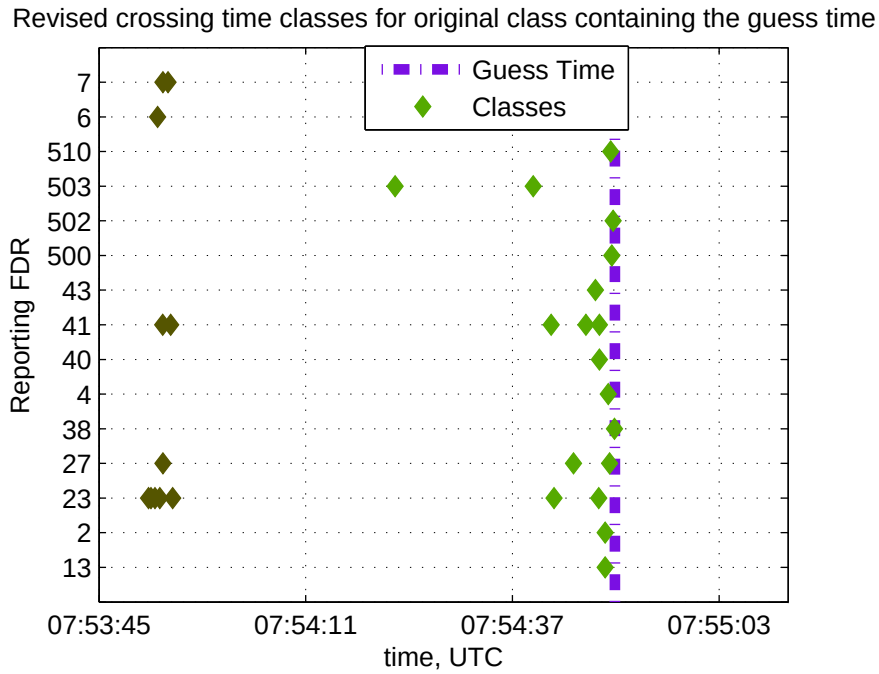
(b) Event location: new ordering method

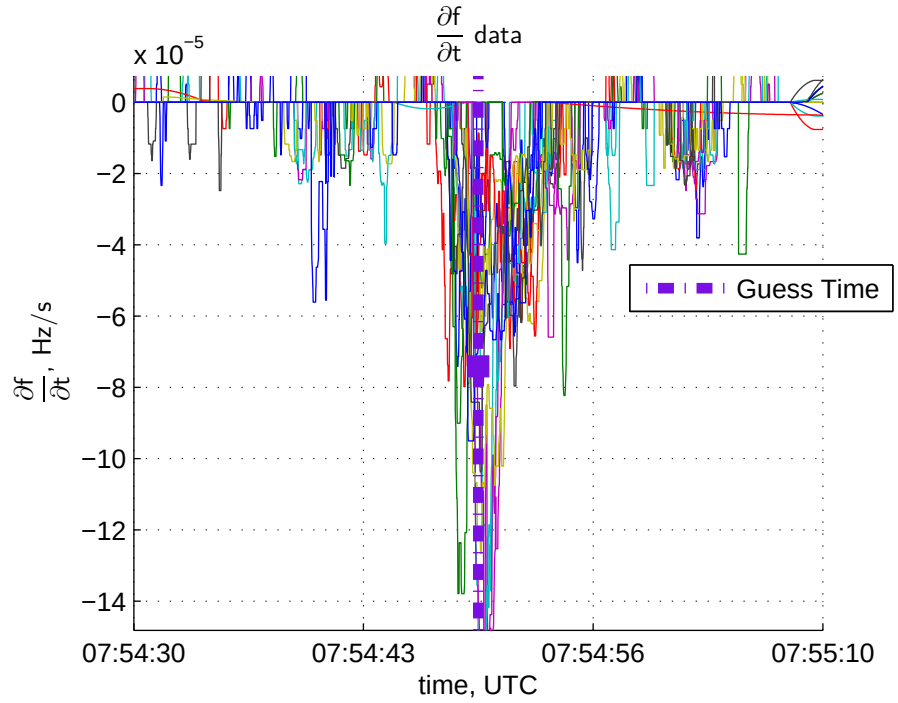
Figure D.45. Event location estimates: Lacygne (840 MW, 38.3335°, −94.7608°) Trip on 05/03/2007 14:59:01

Table D.20. Ordering method comparison: Coal Creek (598 MW, 47.4602°, −101.1898°) Trip on 05/06/2007 07:54:50

	Old Ordering Method			New Ordering Method		
Mismatch estimate (MW)	598			545		
FDR Info	Number	Name	Distance (mi)	Number	Name	Distance (mi)
	43	Bismarck	48.83	43	Bismarck	48.83
	40	MISOStPaul	420.9	23	Duluth2	429.7
	560	Duluth	429.7	40	MISOStPaul	420.9
	41	Winnipeg	248	41	Winnipeg	248
	503	Danbury	1421	2	UMR	811.6
	27	RPI	1373	13	MidwestISO	911.3
	9	UFL	1587	4	VT	1268
	38	ISONE	1437	27	RPI	1373
	502	Toronto	1085	7	MISS	1163
	13	MidwestISO	911.3	6	ABB	1406
	510	Blacksburg	1270	510	Blacksburg	1270
	504	WayneState	951.4	500	Chicago	770.6
	6	ABB	1406	502	Toronto	1085
	4	VT	1268	38	ISONE	1437
	7	MISS	1163			
	2	UMR	811.6			
LS estimate	Latitude	Longitude	Distance (mi)	Latitude	Longitude	Distance (mi)
	43.3874°	−92.1506°	520.4	47.4602°	−101.1898°	0.002577
	$Q_{old} = 0.1917$			$Q_{old} = 1.0000$		
	$Q_{new} = 0.1276$			$Q_{new} = 1.0000$		
Parzen windowing results	$Q_{actual} = 1.0000$			$Q_{actual} = 1.0000$		







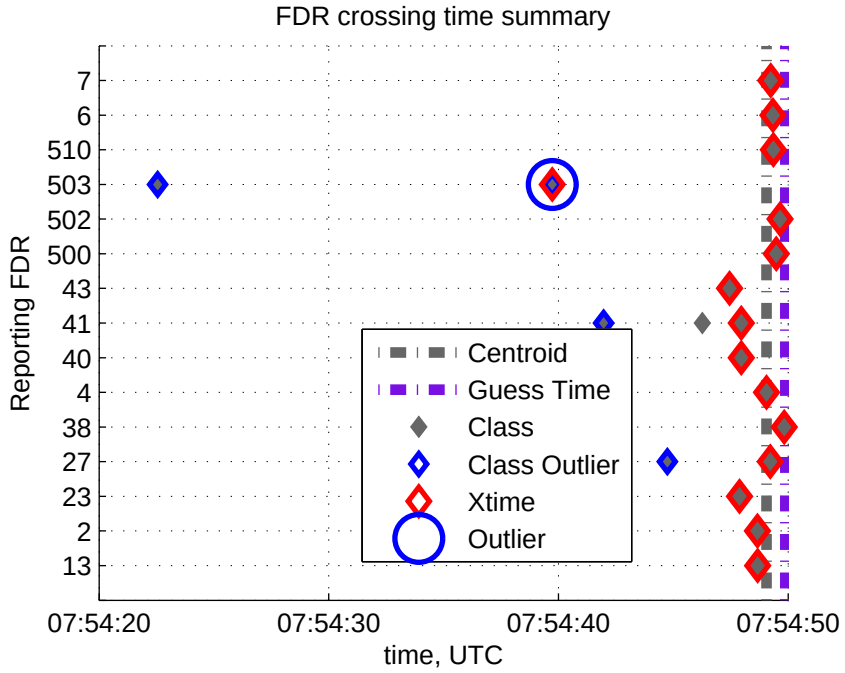
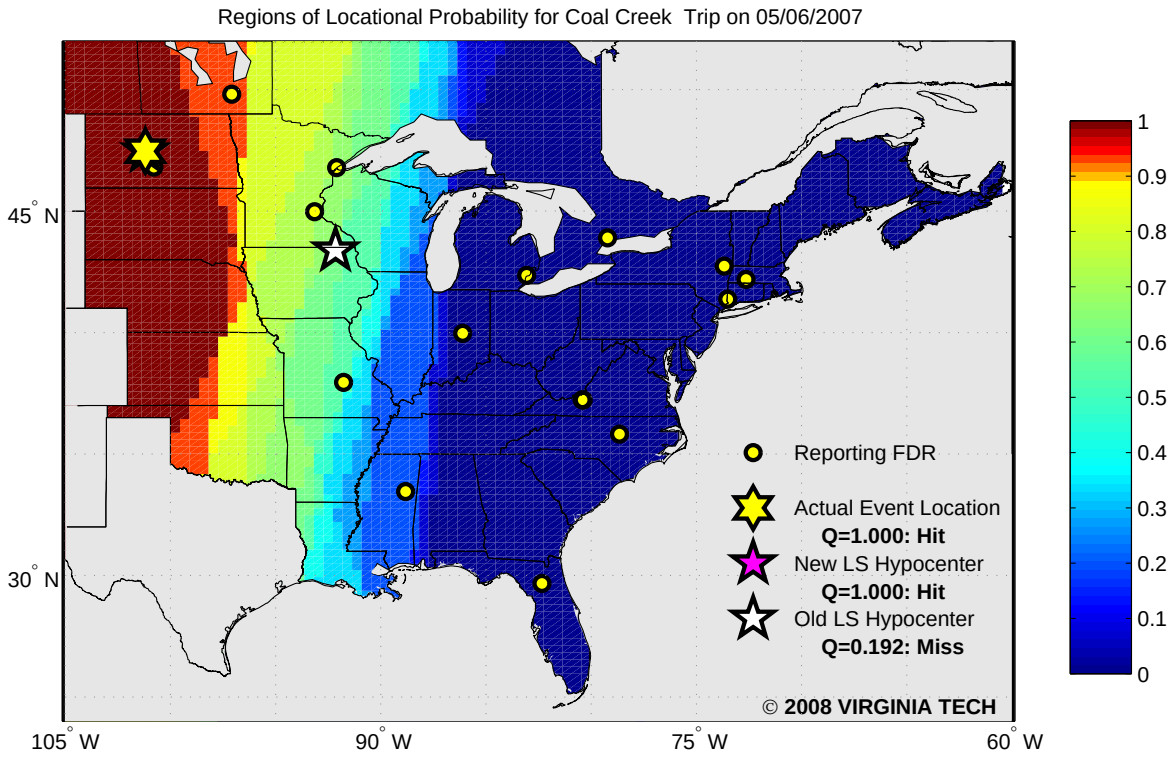
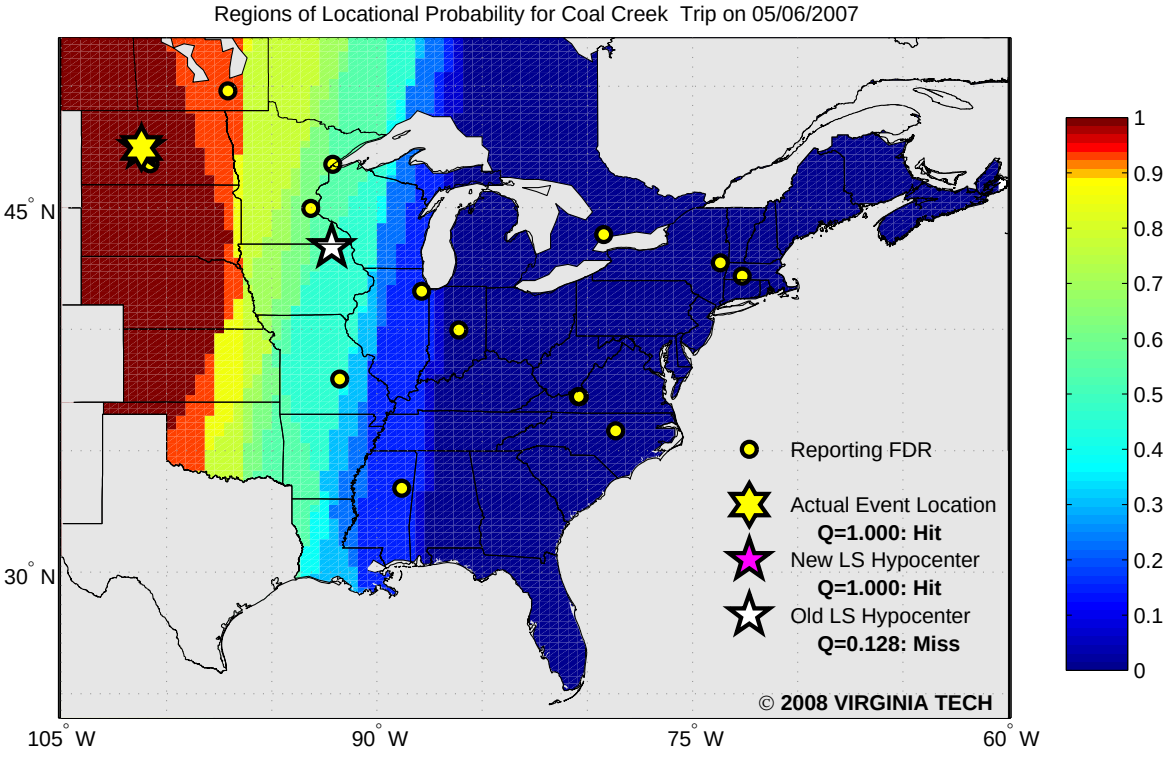


Figure D.46. Consolidated event ordering calculations: Coal Creek (598 MW, 47.4602°, −101.1898°) Trip on 05/06/2007 07:54:50



(a) Event location: old ordering method



(b) Event location: new ordering method

Figure D.47. Event location estimates: Coal Creek (598 MW, 47.4602°, −101.1898°) Trip on 05/06/2007 07:54:50

Table D.21. Ordering method comparison: Palisades (778 MW, 42.2857°, −86.2695°) Trip on 05/08/2007 17:23:42

	Old Ordering Method			New Ordering Method		
Mismatch estimate (MW)	902			834		
FDR Info	Number	Name	Distance (mi)	Number	Name	Distance (mi)
	13	MidwestISO	160.3	13	MidwestISO	160.3
	504	WayneState	163.5	23	Duluth2	423
	4	VT	466.8	4	VT	466.8
	510	Blacksburg	469	510	Blacksburg	469
	560	Duluth	423	2	UMR	417.1
	40	MISOStPaul	390.7	40	MISOStPaul	390.7
	6	ABB	604.6	502	Toronto	372.3
	502	Toronto	372.3	27	RPI	641.6
	503	Danbury	659.5	503	Danbury	659.5
	41	Winnipeg	732.9	6	ABB	604.6
	27	RPI	641.6	41	Winnipeg	732.9
	38	ISONE	696.6	43	Bismarck	778.6
	43	Bismarck	778.6	7	MISS	625.6
	7	MISS	625.6	38	ISONE	696.6
	2	UMR	417.1			
	9	UFL	898.4			
LS estimate	Latitude	Longitude	Distance (mi)	Latitude	Longitude	Distance (mi)
	41.0528°	−86.2027°	85.25	40.1430°	−88.9637°	203.8
	Q_{old} = 1.0000			Q_{old} = 1.0000		
	Q_{new} = 1.0000			Q_{new} = 1.0000		
Parzen windowing results	Q_{actual} = 1.0000			Q_{actual} = 1.0000		

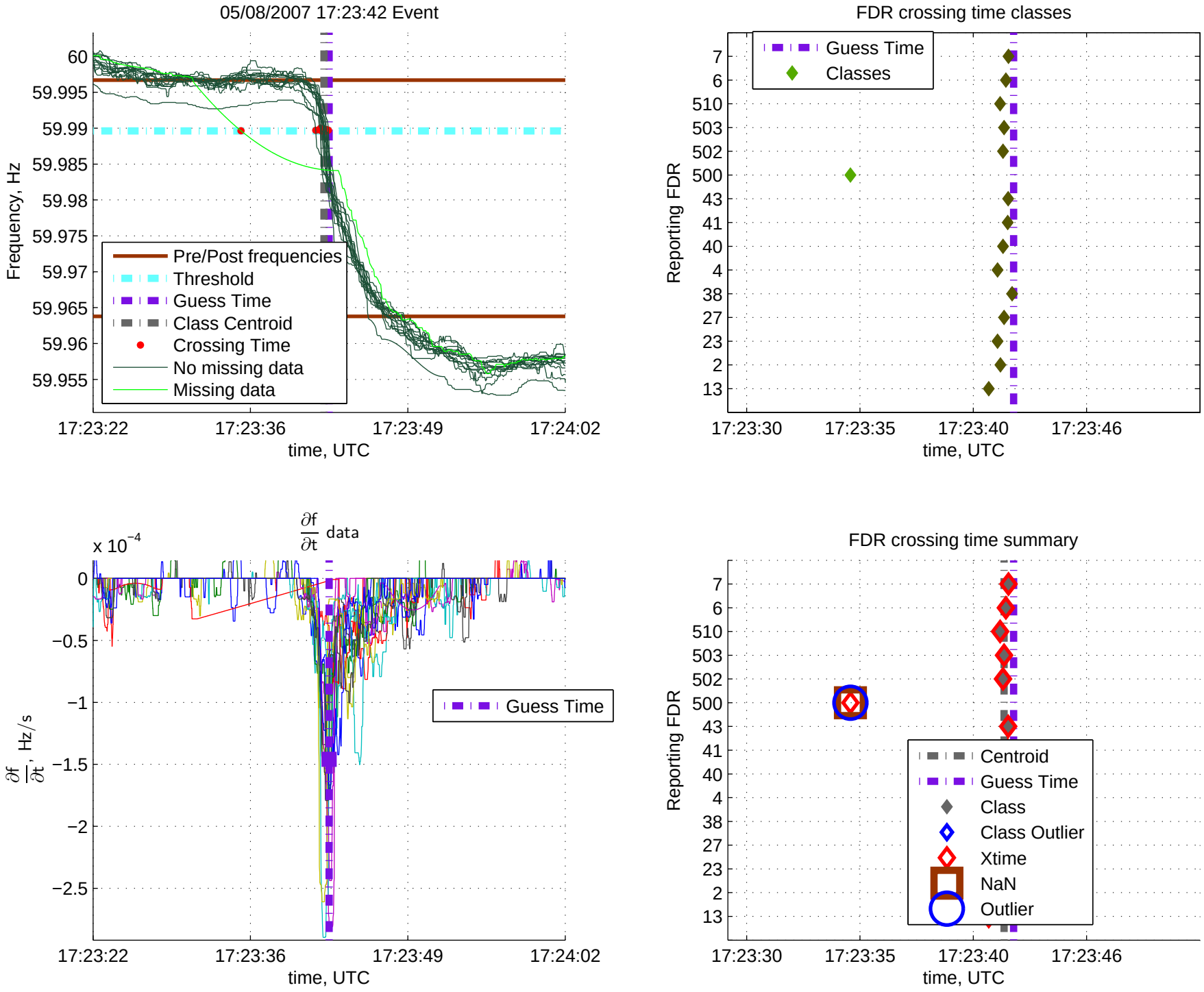
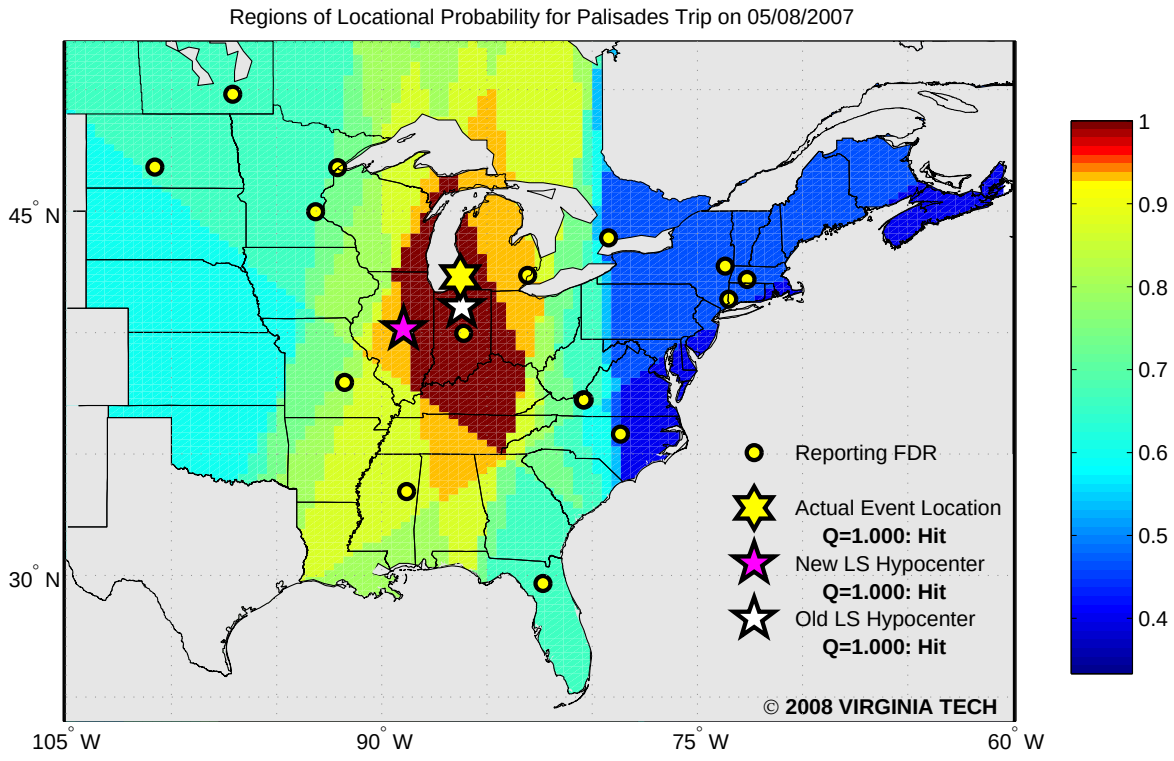
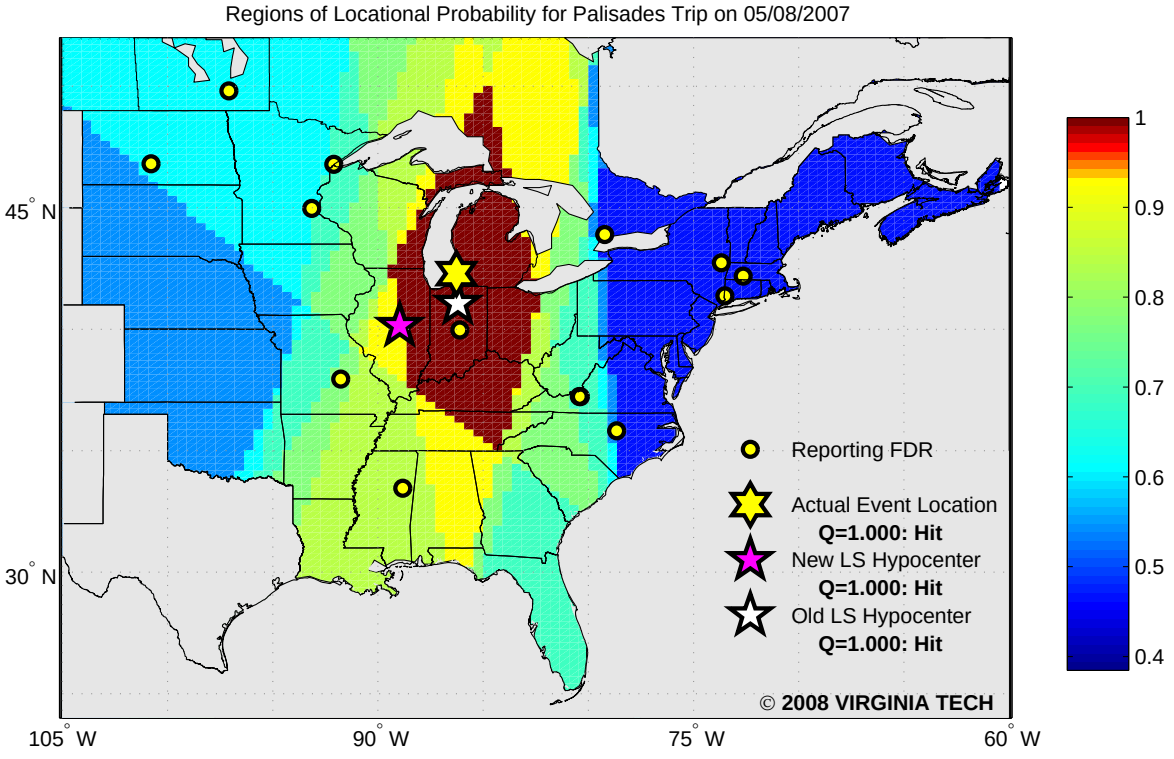


Figure D.48. Consolidated event ordering calculations: Palisades (778 MW, 42.2857°, −86.2695°) Trip on 05/08/2007 17:23:42



(a) Event location: old ordering method



(b) Event location: new ordering method

Figure D.49. Event location estimates: Palisades (778 MW, 42.2857°, –86.2695°) Trip on 05/08/2007 17:23:42

Table D.22. Ordering method comparison: Council Bluffs (690 MW, 41.2146°, −95.8574°) Trip on 05/10/2007 17:54:47

	Old Ordering Method			New Ordering Method		
Mismatch estimate (MW)	786			771		
FDR Info	Number	Name	Distance (mi)	Number	Name	Distance (mi)
	43	Bismarck	457.4	23	Duluth2	427.8
	40	MISOStPaul	293.4	43	Bismarck	457.4
	560	Duluth	427.8	13	MidwestISO	518.3
	41	Winnipeg	596.9	41	Winnipeg	596.9
	2	UMR	313.6	4	VT	869
	500	Chicago	414.2	2	UMR	313.6
	7	MISS	660.3	40	MISOStPaul	293.4
	13	MidwestISO	518.3	6	ABB	999.4
	4	VT	869	27	RPI	1141
	510	Blacksburg	871.8	7	MISS	660.3
	6	ABB	999.4	500	Chicago	414.2
	502	Toronto	864.9	510	Blacksburg	871.8
	9	UFL	1100	38	ISONE	1196
	503	Danbury	1157	502	Toronto	864.9
	38	ISONE	1196			
	27	RPI	1141			
LS estimate	Latitude	Longitude	Distance (mi)	Latitude	Longitude	Distance (mi)
	42.7874°	−97.1506°	127.3	46.7872°	−92.0990°	427.8
	$Q_{old} = 0.6141$			$Q_{old} = 0.2371$		
	$Q_{new} = 0.7956$			$Q_{new} = 1.0000$		
Parzen windowing results	$Q_{actual} = 0.3044$			$Q_{actual} = 0.8571$		

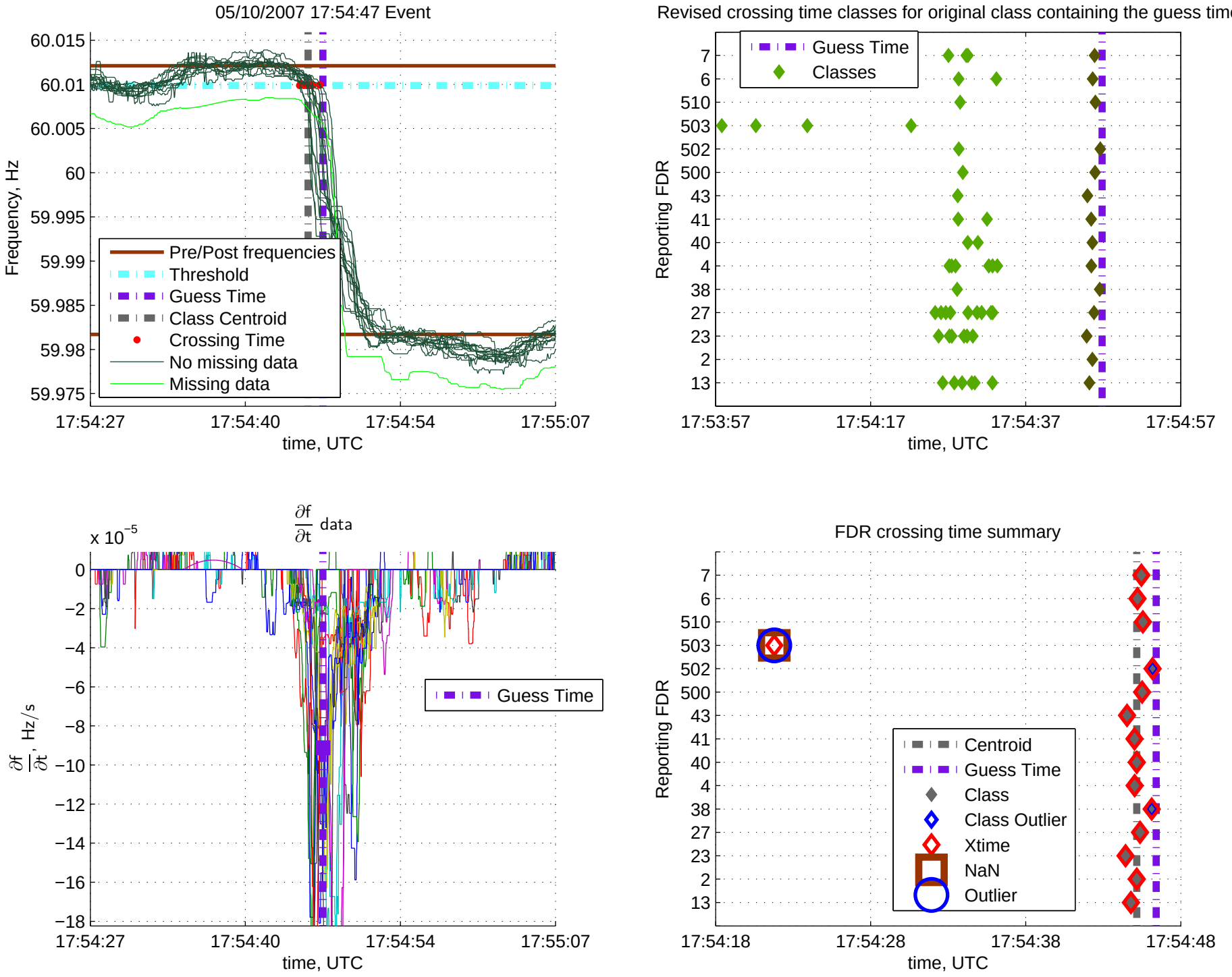
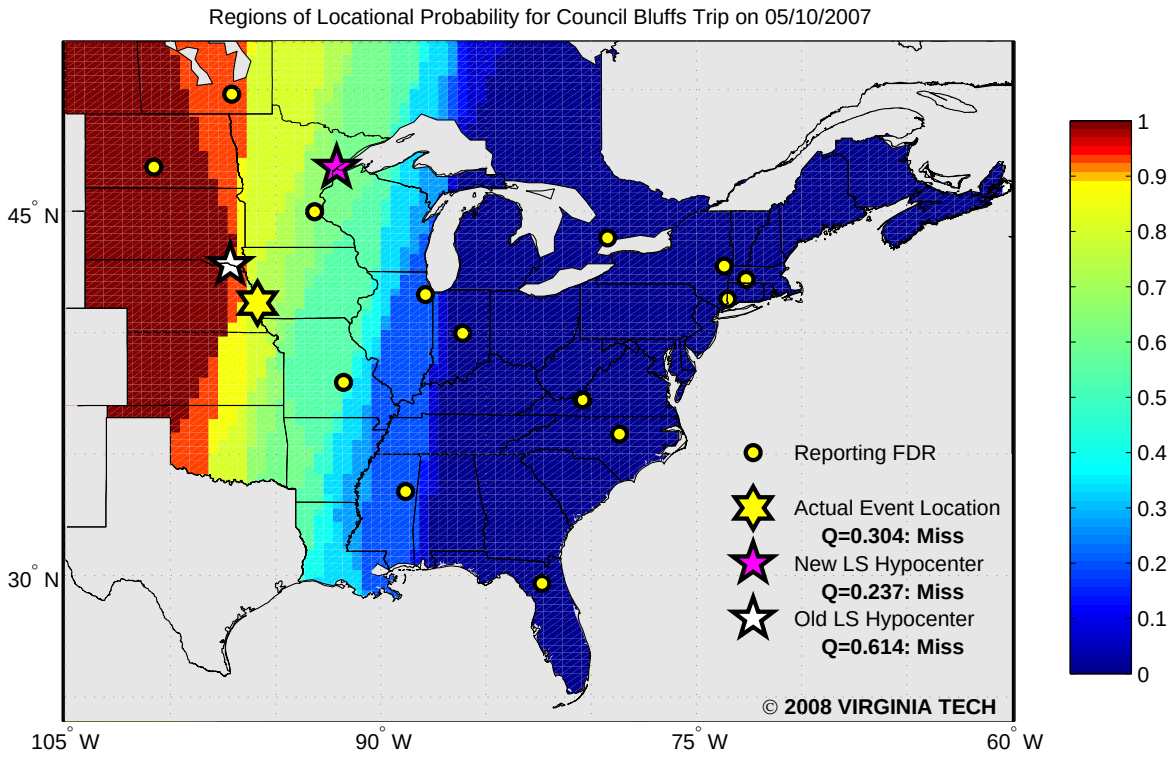
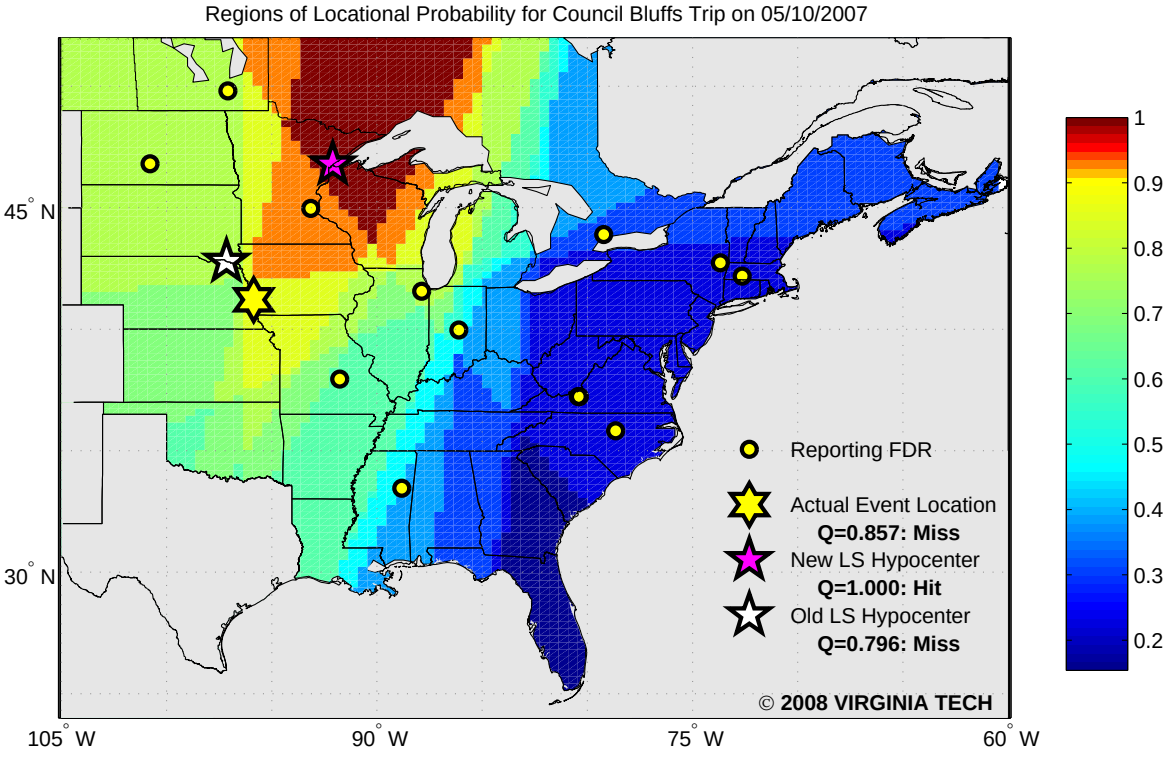


Figure D.50. Consolidated event ordering calculations: Council Bluffs (690 MW, 41.2146°, −95.8574°) Trip on 05/10/2007 17:54:47



(a) Event location: old ordering method

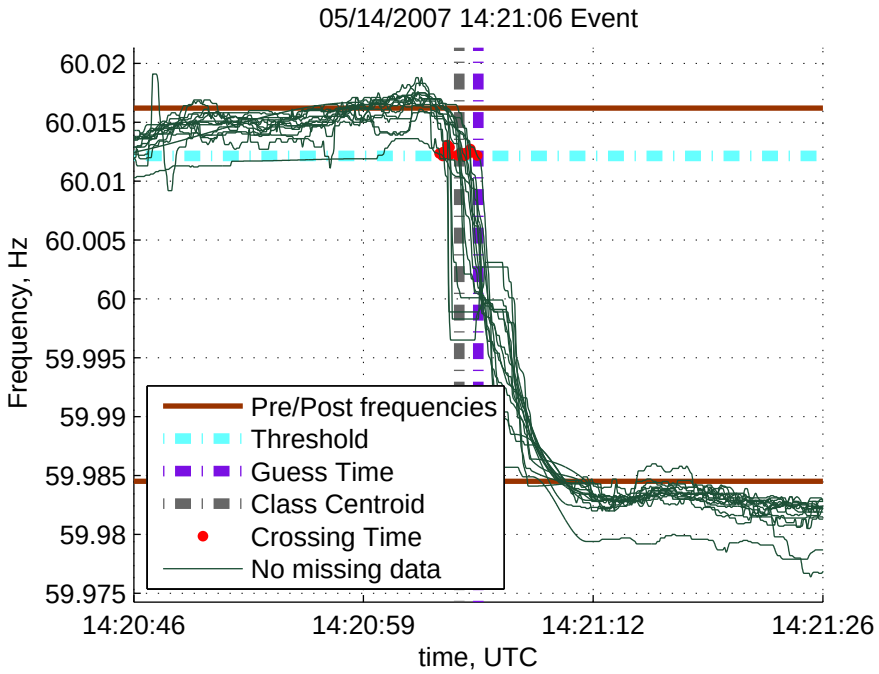


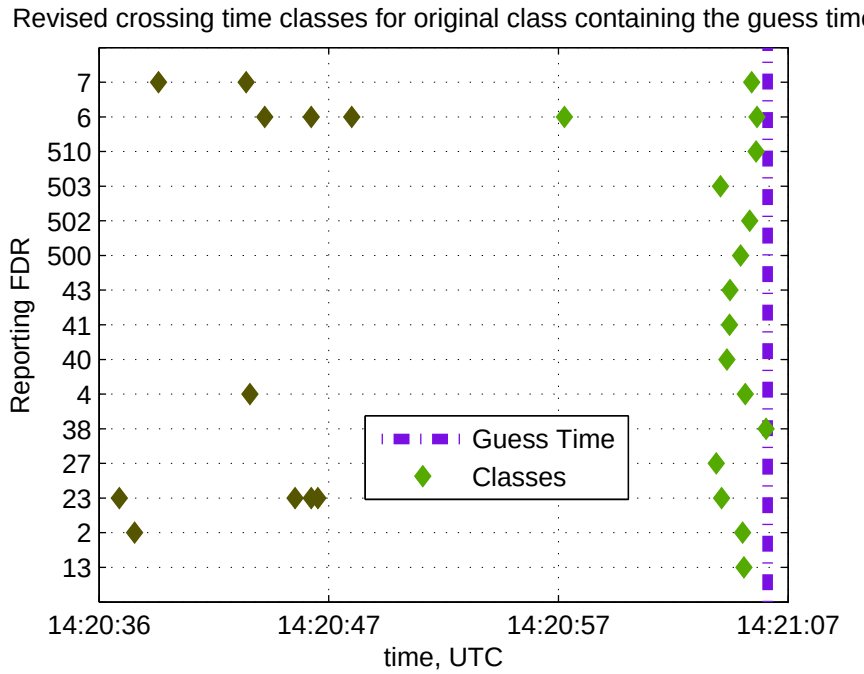
(b) Event location: new ordering method

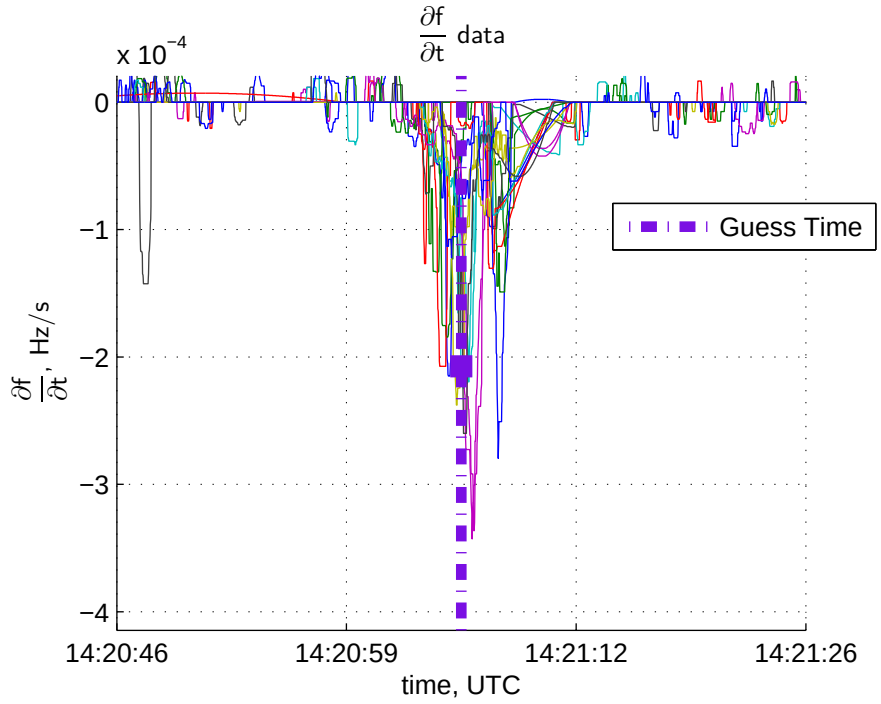
Figure D.51. Event location estimates: Council Bluffs (690 MW, 41.2146°, −95.8574°) Trip on 05/10/2007 17:54:47

Table D.23. Ordering method comparison: Sherburne (854 MW, 45.4365°, −93.8410°) Trip on 05/14/2007 14:21:06

	Old Ordering Method			New Ordering Method		
Mismatch estimate (MW)	738			803		
FDR Info	Number	Name	Distance (mi)	Number	Name	Distance (mi)
	40	MISOStPaul	46.58	27	RPI	1015
	560	Duluth	125.2	503	Danbury	1055
	41	Winnipeg	337.8	23	Duluth2	125.2
	43	Bismarck	345.7	40	MISOStPaul	46.58
	500	Chicago	401	41	Winnipeg	337.8
	2	UMR	528.3	43	Bismarck	345.7
	13	MidwestISO	544.3	500	Chicago	401
				2	UMR	528.3
				13	MidwestISO	544.3
				4	VT	895.4
				502	Toronto	725
				7	MISS	869.5
				510	Blacksburg	897.8
				6	ABB	1034
				38	ISONE	1077
LS estimate	Latitude	Longitude	Distance (mi)	Latitude	Longitude	Distance (mi)
	46.7881°	−95.9162°	136.4	42.7343°	−73.6755°	1015
	$Q_{old} = 0.9469$			$Q_{old} = 0.2846$		
	$Q_{new} = 0.0916$			$Q_{new} = 1.0000$		
Parzen windowing results	$Q_{actual} = 1.0000$			$Q_{actual} = 0.0916$		







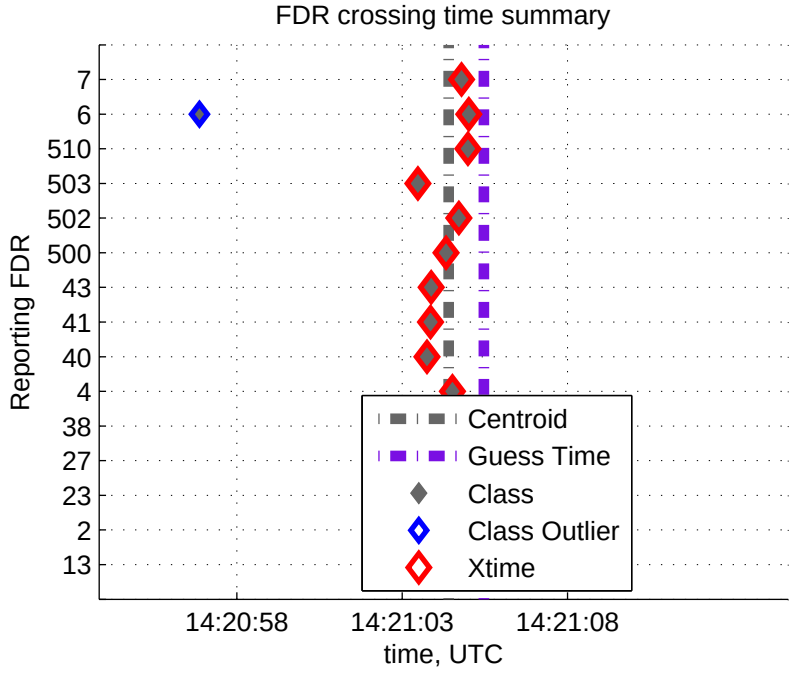
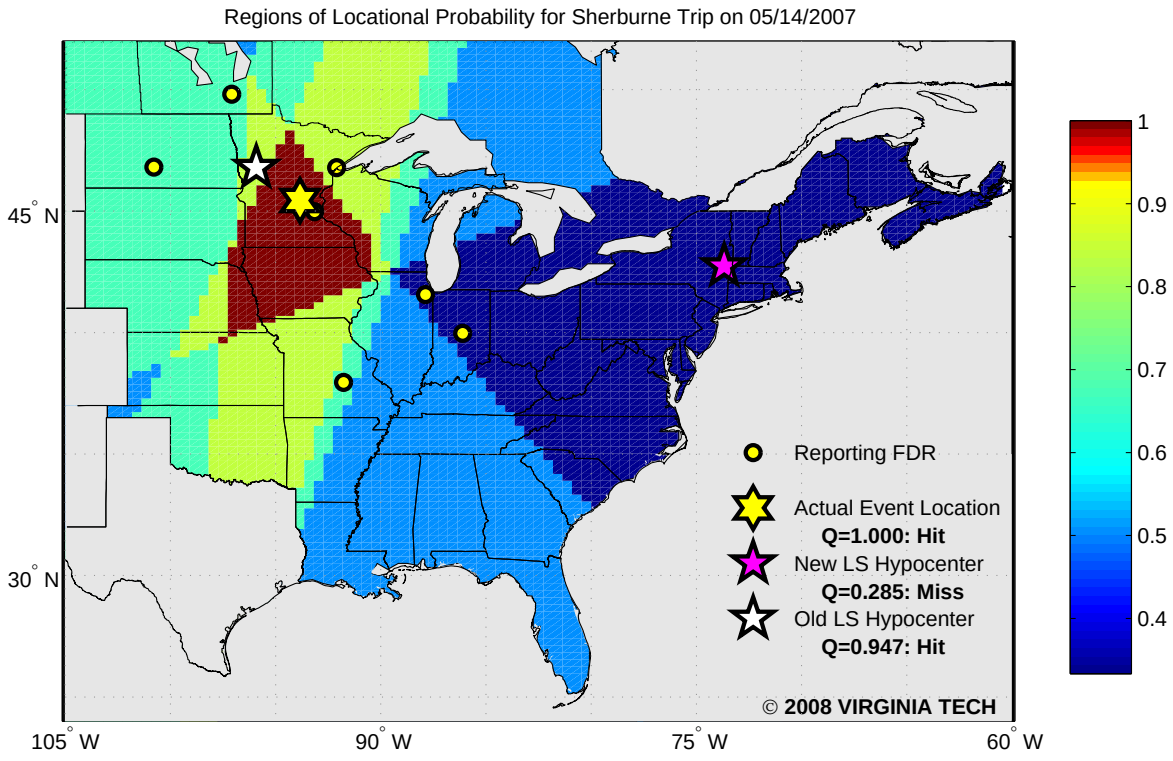
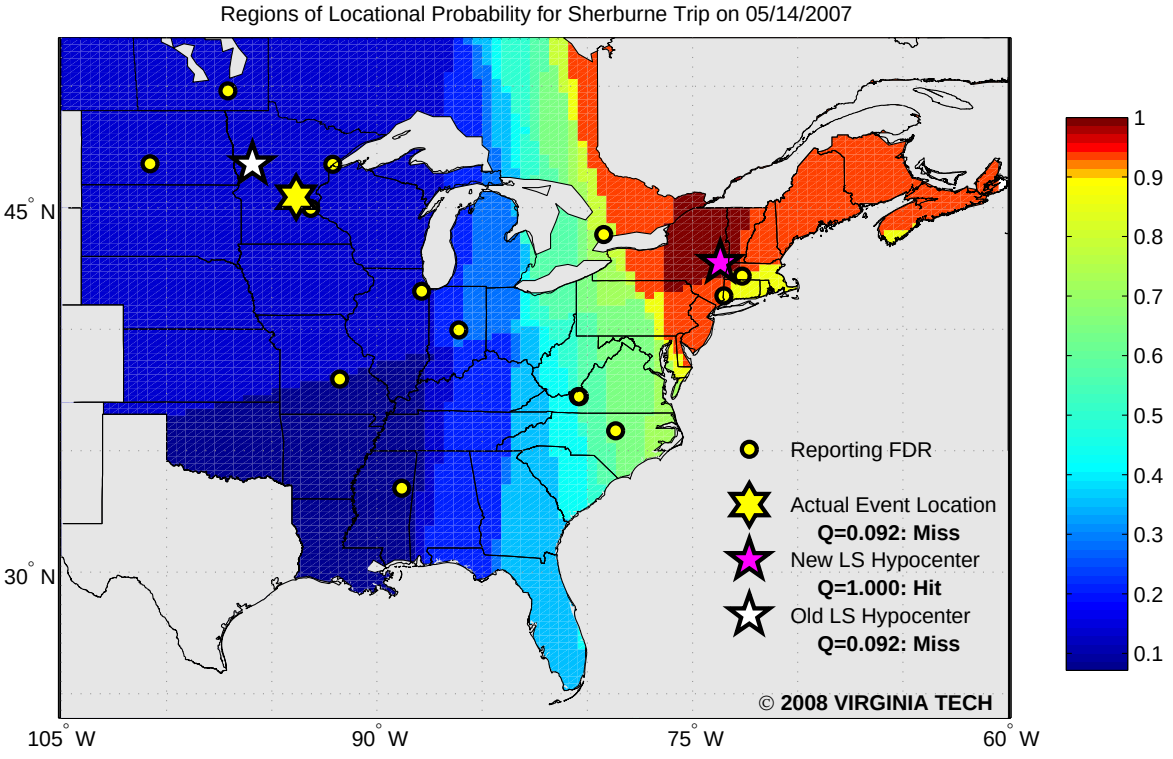


Figure D.52. Consolidated event ordering calculations: Sherburne (854 MW, 45.4365°, −93.8410°) Trip on 05/14/2007 14:21:06



(a) Event location: old ordering method



(b) Event location: new ordering method

Figure D.53. Event location estimates: Sherburne (854 MW, 45.4365°, −93.8410°) Trip on 05/14/2007 14:21:06

Table D.24. Ordering method comparison: Grand Gulf (1266 MW, 31.9266°, −91.0230°) Trip on 05/19/2007 16:27:16

	Old Ordering Method			New Ordering Method		
Mismatch estimate (MW)	808			565		
FDR Info	Number	Name	Distance (mi)	Number	Name	Distance (mi)
	7	MISS	166	7	MISS	166
	42	FSU	409.7	42	FSU	409.7
	504	WayneState	842.4	2	UMR	418.2
	2	UMR	418.2	13	MidwestISO	619.7
	9	UFL	538.3	43	Bismarck	1151
				4	VT	704.8
				41	Winnipeg	1275
				23	Duluth2	1028
				40	MISOStPaul	908.6
				6	ABB	757.9
				510	Blacksburg	707
				27	RPI	1207
				502	Toronto	1045
LS estimate	Latitude	Longitude	Distance (mi)	Latitude	Longitude	Distance (mi)
	36.2111°	−85.6035°	428.6	33.6336°	−86.9482°	264.4
	$Q_{old} = 1.0000$ $Q_{new} = 0.8517$			$Q_{old} = 1.0000$ $Q_{new} = 1.0000$		
Parzen windowing results	$Q_{actual} = 1.0000$			$Q_{actual} = 1.0000$		

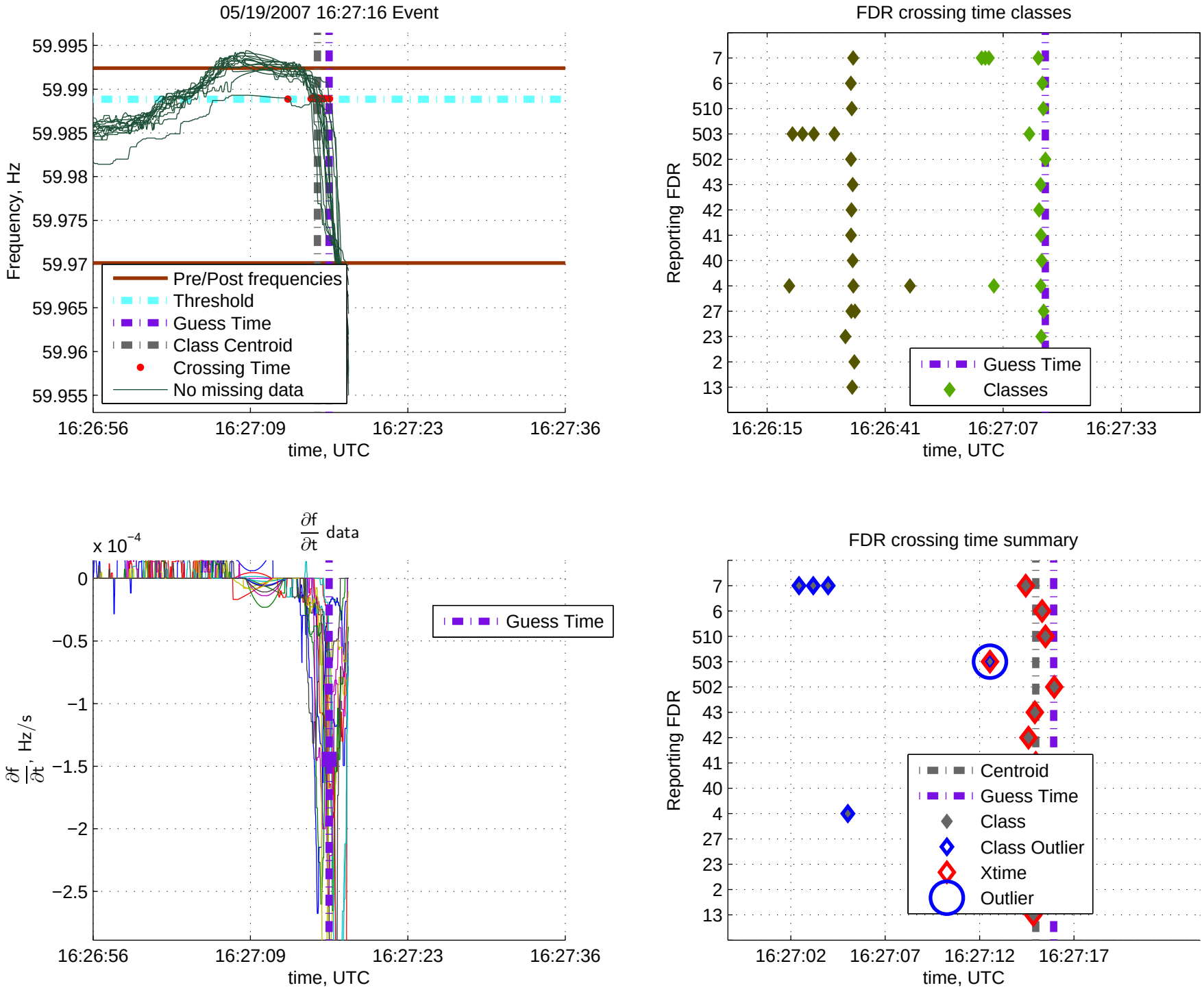
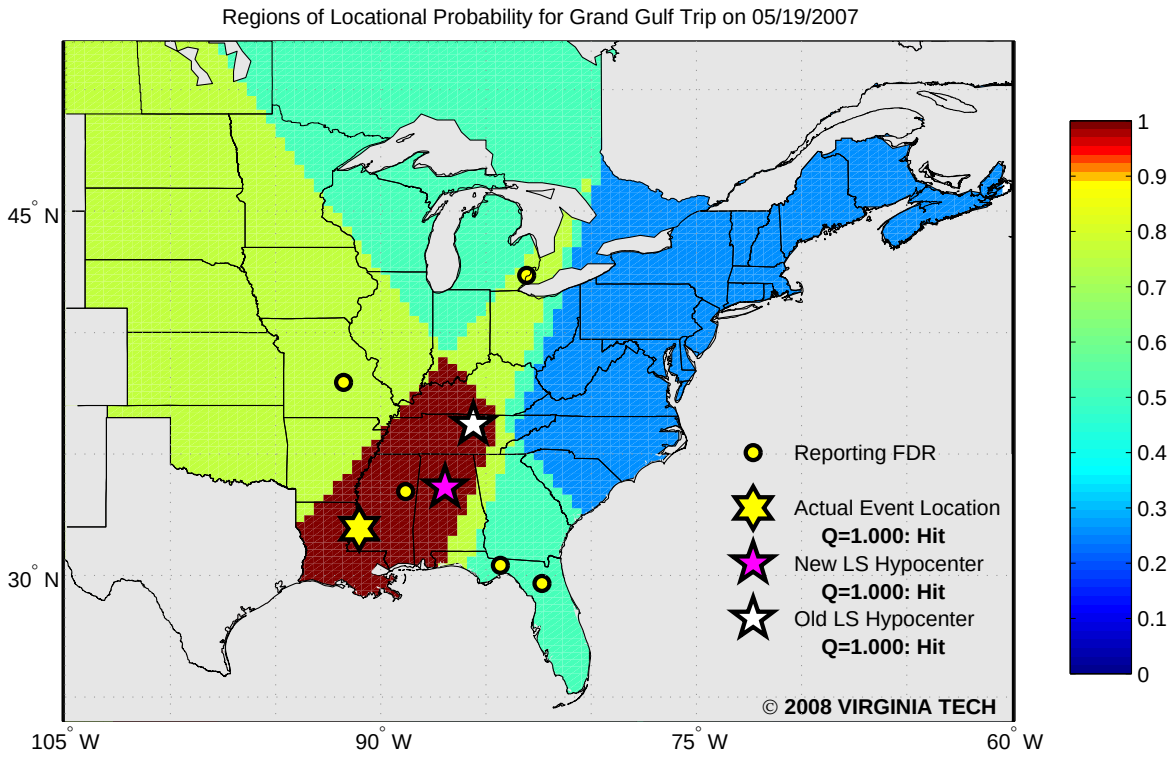
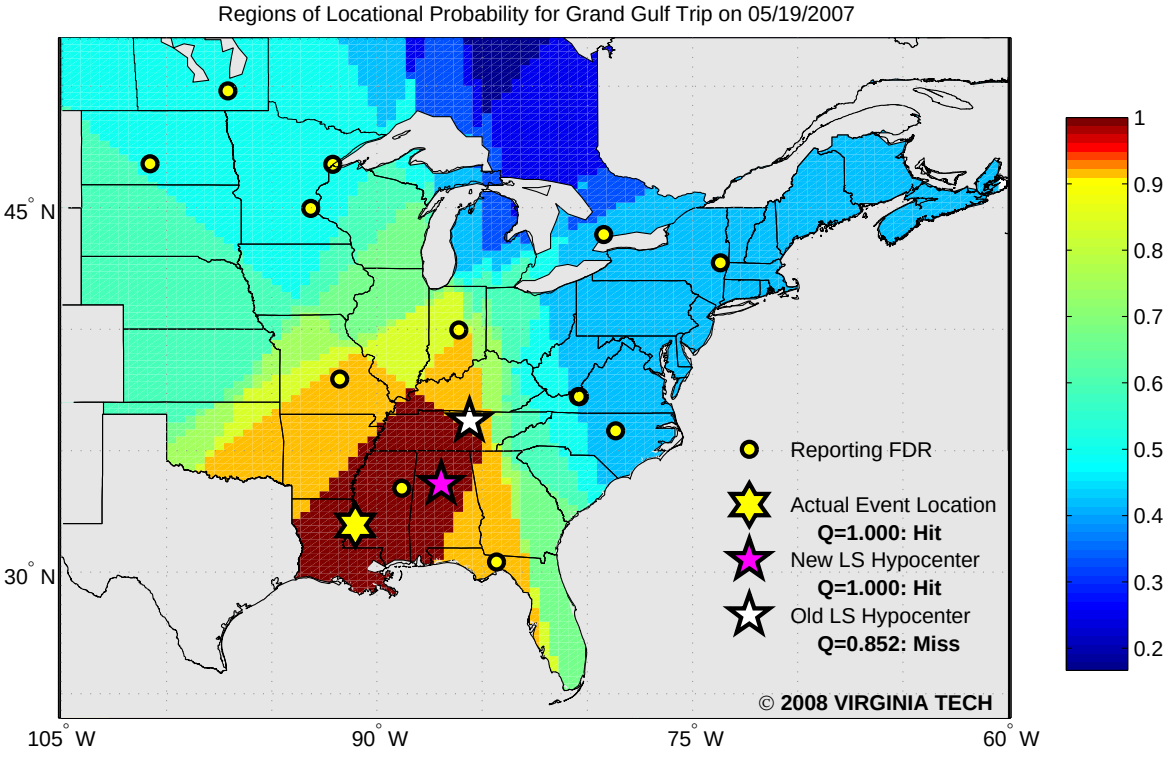


Figure D.54. Consolidated event ordering calculations: Grand Gulf (1266 MW, 31.9266°, −91.0230°) Trip on 05/19/2007 16:27:16



(a) Event location: old ordering method

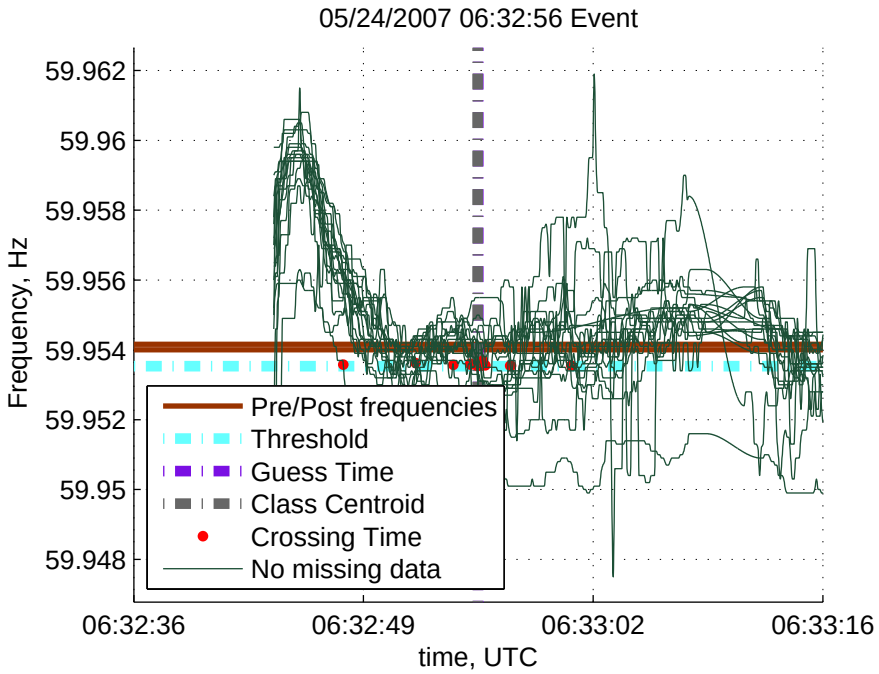


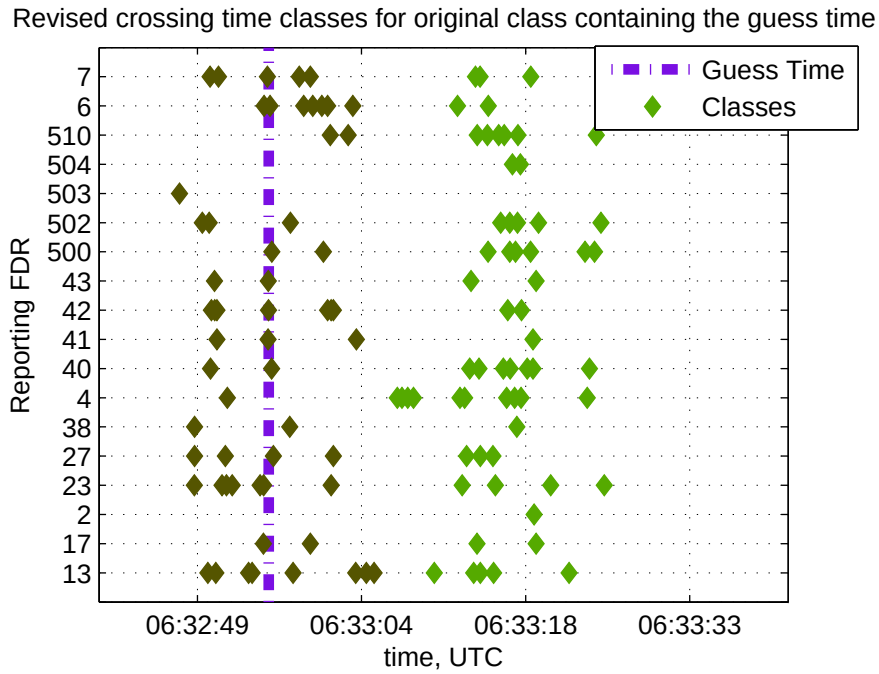
(b) Event location: new ordering method

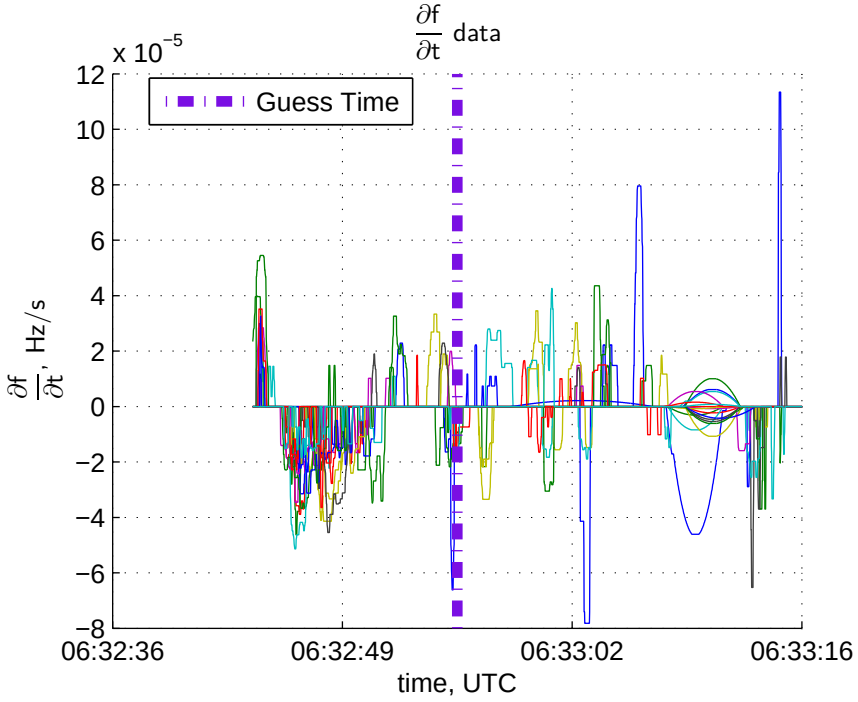
Figure D.55. Event location estimates: Grand Gulf (1266 MW, 31.9266°, −91.0230°) Trip on 05/19/2007 16:27:16

Table D.25. Ordering method comparison: Salem U2 (1130 MW, 39.4956°, −75.4733°) Trip on 05/24/2007 06:32:56

	Old Ordering Method			New Ordering Method		
Mismatch estimate (MW)	765			NaN		
FDR Info	Number	Name	Distance (mi)	Number	Name	Distance (mi)
	503	Danbury	166.1	13	MidwestISO	565.8
	27	RPI	242.5	17	TVA4Jackson	777.6
	38	ISONE	237.7	23	Duluth2	975
	6	ABB	307.8	7	MISS	849.6
	4	VT	310.6	41	Winnipeg	1272
	510	Blacksburg	308.5	43	Bismarck	1365
	504	WayneState	442.9	42	FSU	801.6
	502	Toronto	360.3	6	ABB	307.8
	500	Chicago	666.3	40	MISOStPaul	977.5
	13	MidwestISO	565.8	500	Chicago	666.3
	560	Duluth	975	27	RPI	242.5
	42	FSU	801.6	38	ISONE	237.7
	41	Winnipeg	1272	502	Toronto	360.3
	7	MISS	849.6			
	2	UMR	883.5			
	9	UFL	782.3			
	40	MISOStPaul	977.5			
	43	Bismarck	1365			
	17	TVA4Jackson	777.6			
LS estimate	Latitude	Longitude	Distance (mi)	Latitude	Longitude	Distance (mi)
	40.1074°	−75.2618°	43.74	NaN°	NaN°	NaN
	Q_{old} = 1.0000			$Q_{old} = NaN$		
	Q_{new} = 0.6841			$Q_{new} = NaN$		
Parzen windowing results	Q_{actual} = 1.0000			Q_{actual} = 0.6841		







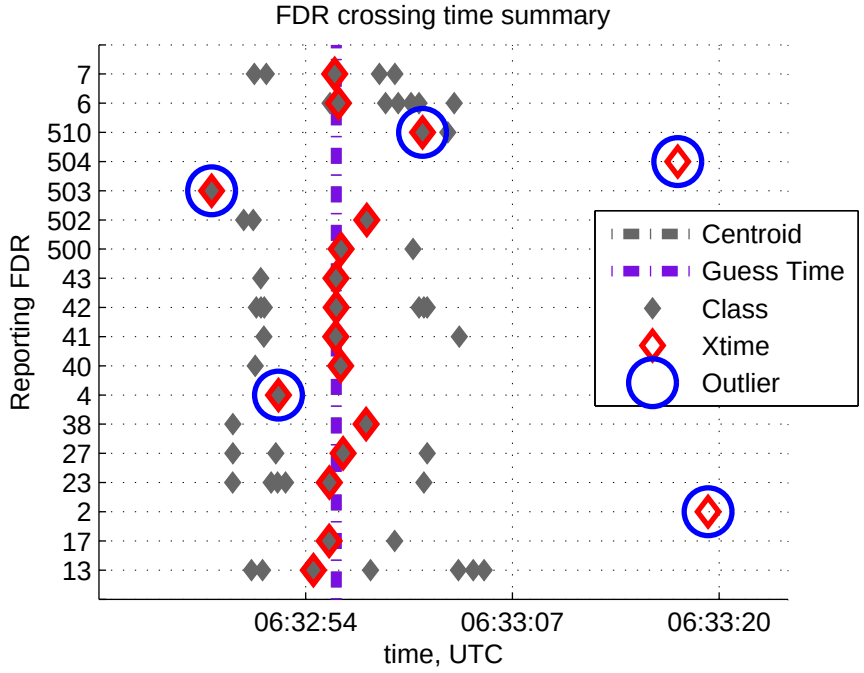
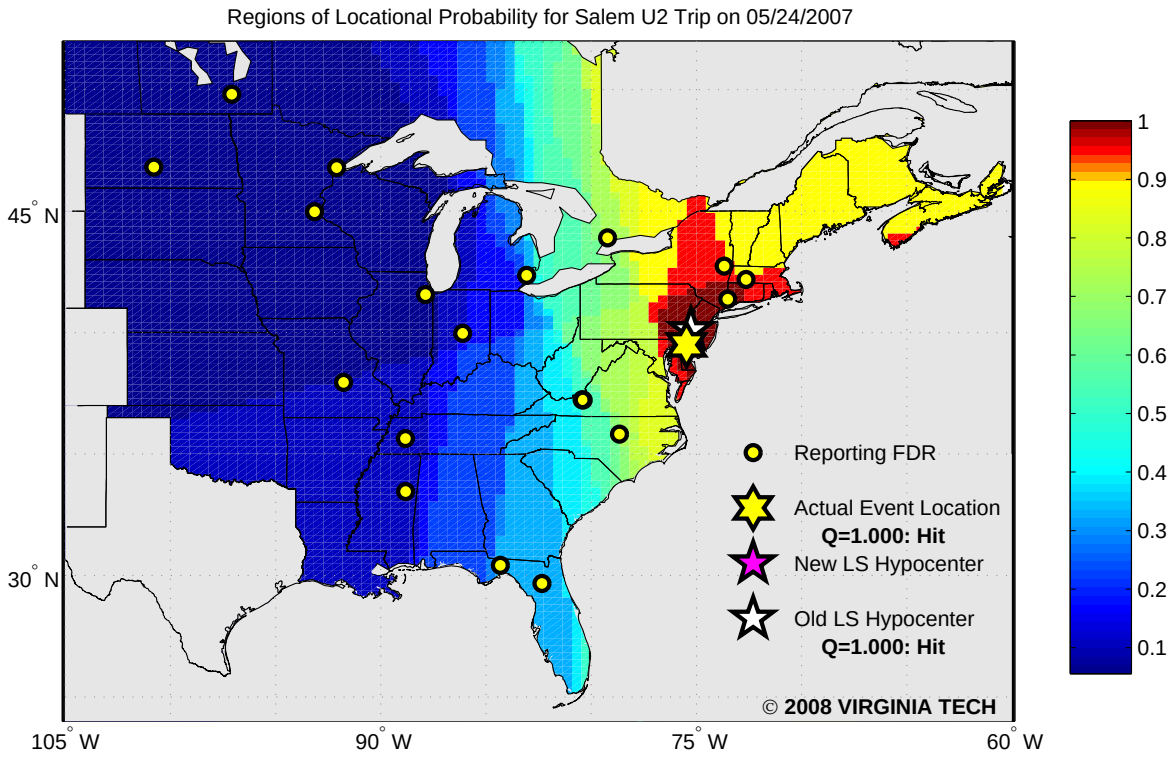
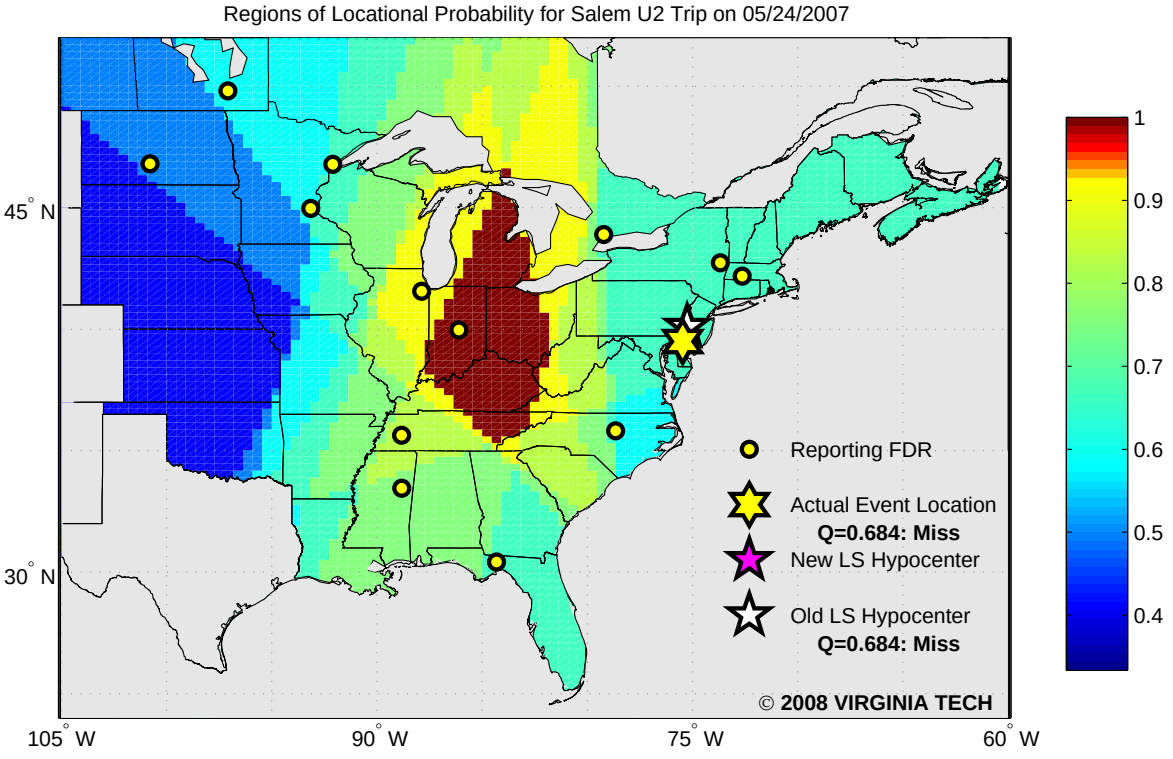


Figure D.56. Consolidated event ordering calculations: Salem U2 (1130 MW, 39.4956°, −75.4733°) Trip on 05/24/2007 06:32:56



(a) Event location: old ordering method



(b) Event location: new ordering method

Figure D.57. Event location estimates: Salem U2 (1130 MW, 39.4956°, −75.4733°) Trip on 05/24/2007 06:32:56

Table D.26. Ordering method comparison: Dolet Hills (650 MW, 32.0037°, −93.6731°) Trip on 05/25/2007 11:36:41

	Old Ordering Method			New Ordering Method		
Mismatch estimate (MW)	609			550		
FDR Info	Number	Name	Distance (mi)	Number	Name	Distance (mi)
	7	MISS	299.3	43	Bismarck	1090
	42	FSU	563.3	17	TVA4Jackson	374.4
	9	UFL	691.2	27	RPI	1320
	6	ABB	899.3	4	VT	834.2
	560	Duluth	1025	7	MISS	299.3
	40	MISOStPaul	896.5	13	MidwestISO	693.5
	41	Winnipeg	1243	23	Duluth2	1025
	13	MidwestISO	693.5	42	FSU	563.3
	500	Chicago	733.7	6	ABB	899.3
	43	Bismarck	1090	2	UMR	424.7
	504	WayneState	921.6	38	ISONE	1350
	503	Danbury	1287	40	MISOStPaul	896.5
	17	TVA4Jackson	374.4	502	Toronto	1135
	502	Toronto	1135	504	WayneState	921.6
	27	RPI	1320	41	Winnipeg	1243
	38	ISONE	1350	500	Chicago	733.7
	510	Blacksburg	836.6	510	Blacksburg	836.6
	4	VT	834.2			
	2	UMR	424.7			
LS estimate	Latitude	Longitude	Distance (mi)	Latitude	Longitude	Distance (mi)
	36.7838°	−87.5588°	480	46.8088°	−100.7867°	1090
	$Q_{old} = 0.8566$			$Q_{old} = 0.4099$		
	$Q_{new} = 0.0026$			$Q_{new} = 1.0000$		
Parzen windowing results	$Q_{actual} = 1.0000$			$Q_{actual} = 0.1021$		

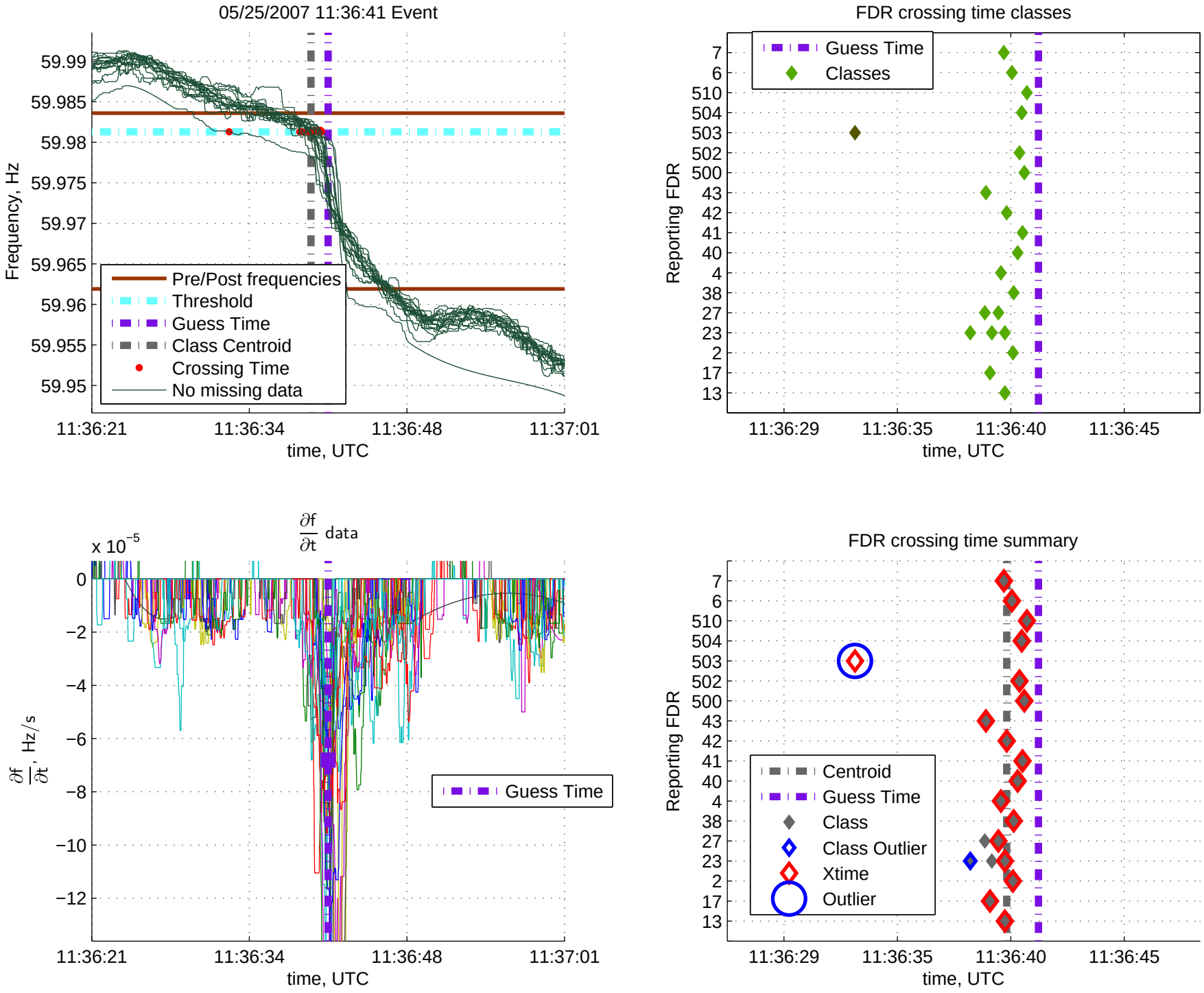
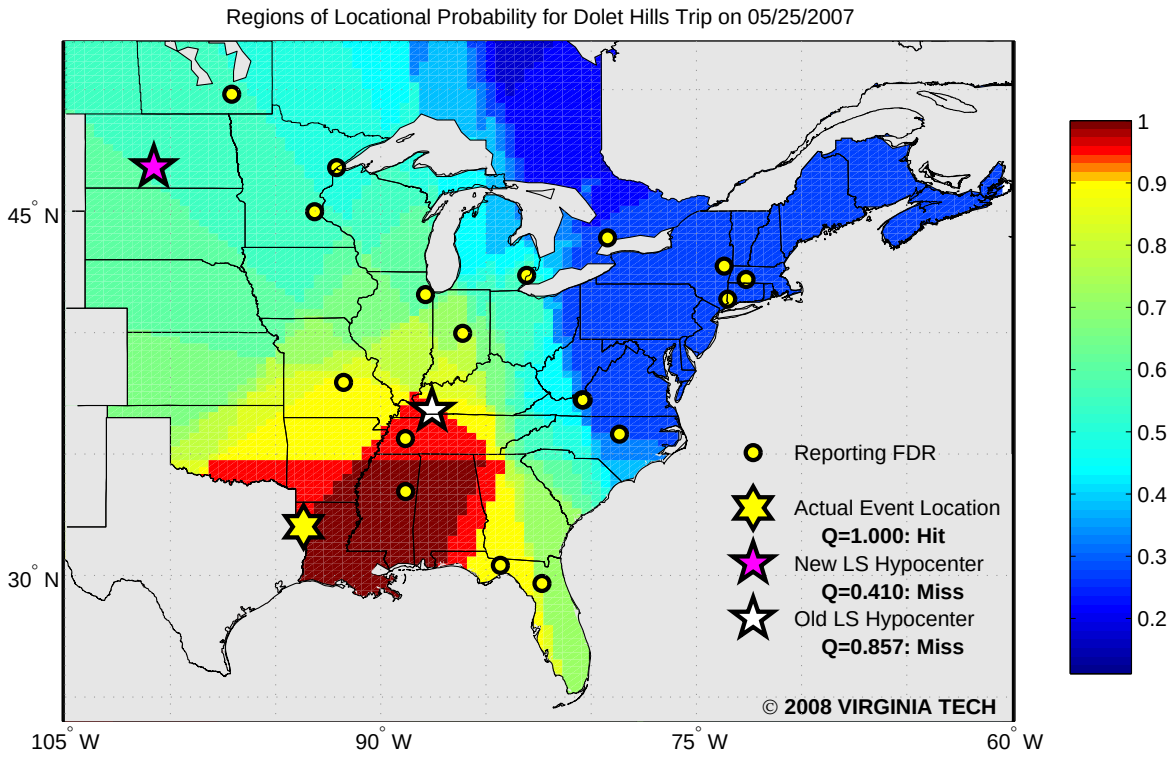
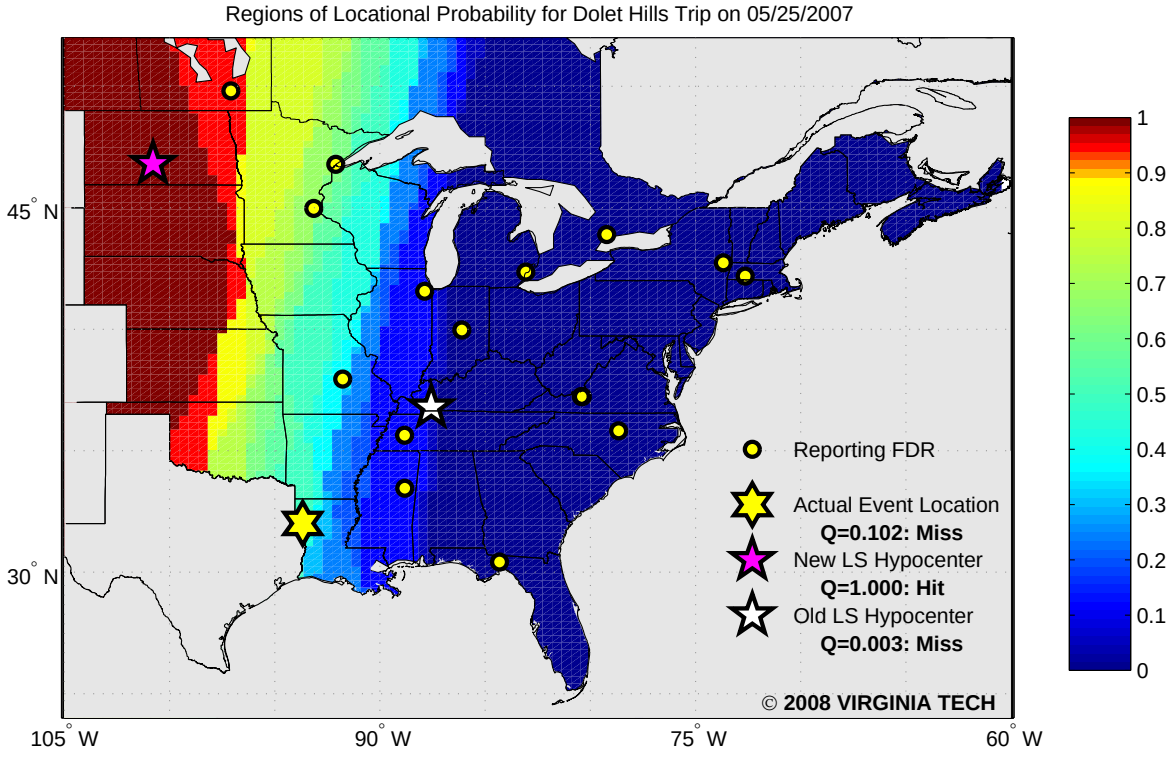


Figure D.58. Consolidated event ordering calculations: Dolet Hills (650 MW, 32.0037°, −93.6731°) Trip on 05/25/2007 11:36:41



(a) Event location: old ordering method

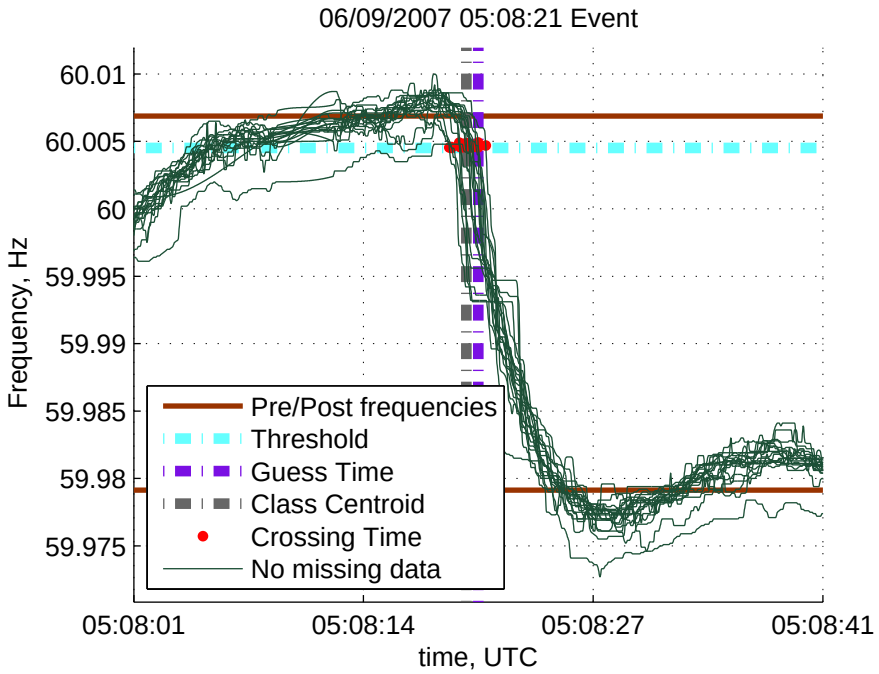


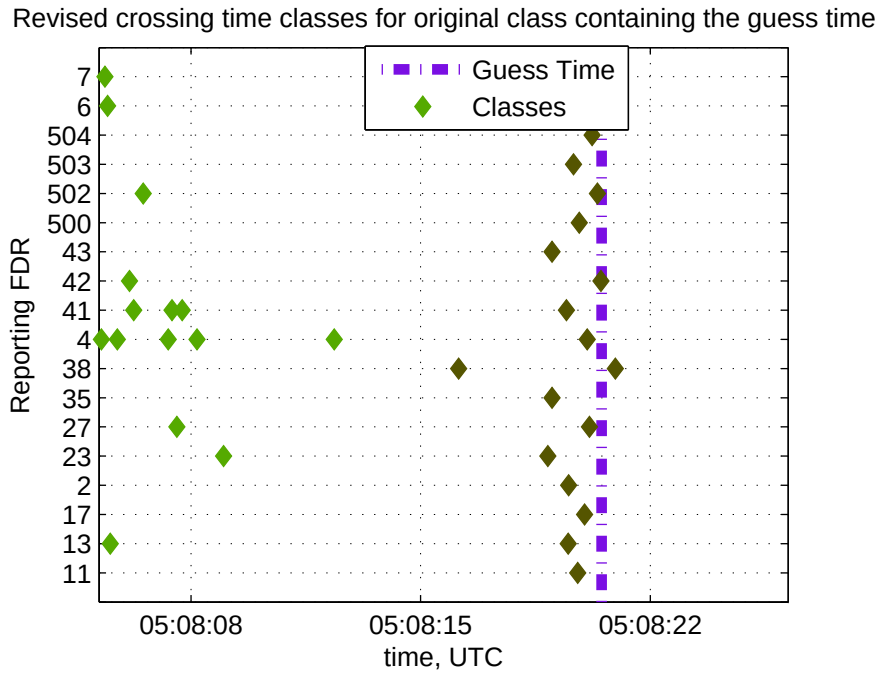
(b) Event location: new ordering method

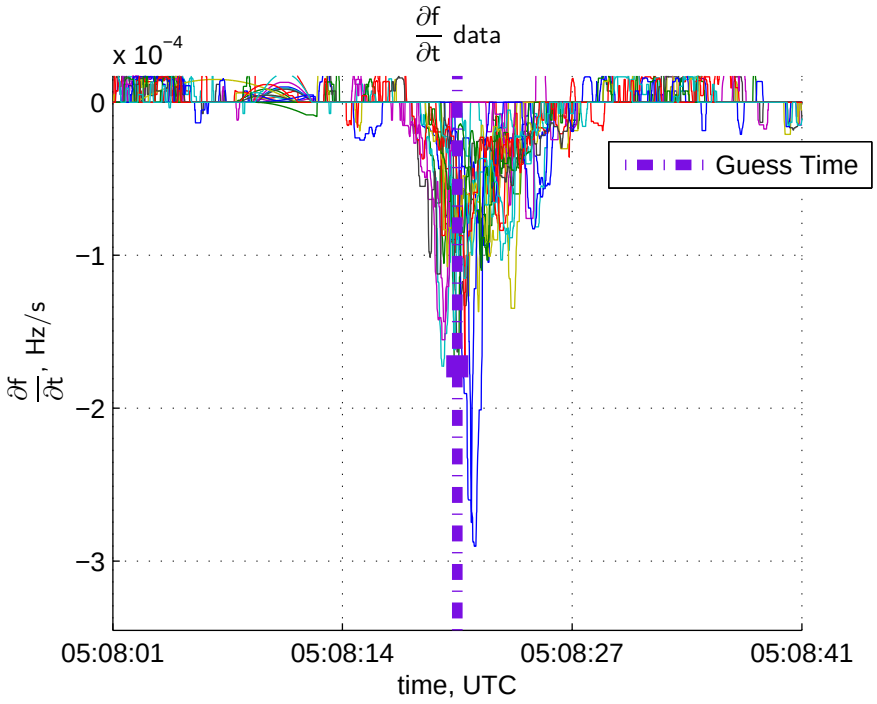
Figure D.59. Event location estimates: Dolet Hills (650 MW, 32.0037°, −93.6731°) Trip on 05/25/2007 11:36:41

Table D.27. Ordering method comparison: Council Bluffs (690 MW, 41.2146°, −95.8574°) Trip on 06/09/2007 05:08:21

	Old Ordering Method			New Ordering Method		
Mismatch estimate (MW)	732			705		
FDR Info	Number	Name	Distance (mi)	Number	Name	Distance (mi)
	35	ISU	128.1	23	Duluth2	427.8
	43	Bismarck	457.4	35	ISU	128.1
	560	Duluth	427.8	43	Bismarck	457.4
	41	Winnipeg	596.9	41	Winnipeg	596.9
	2	UMR	313.6	13	MidwestISO	518.3
	500	Chicago	414.2	2	UMR	313.6
	6	ABB	999.4	503	Danbury	1157
	42	FSU	985.2	11	Calvin	536.5
	504	WayneState	662.8	500	Chicago	414.2
	17	TVA4Jackson	541.3	17	TVA4Jackson	541.3
	9	UFL	1100	7	MISS	660.3
	7	MISS	660.3	4	VT	869
	503	Danbury	1157	27	RPI	1141
	13	MidwestISO	518.3	504	WayneState	662.8
	27	RPI	1141	502	Toronto	864.9
	38	ISONE	1196	42	FSU	985.2
	502	Toronto	864.9	6	ABB	999.4
	4	VT	869	38	ISONE	1196
	11	Calvin	536.5			
LS estimate	Latitude	Longitude	Distance (mi)	Latitude	Longitude	Distance (mi)
	43.2044°	−96.7101°	144.2	45.4365°	−93.8410°	308.8
	Q_{old} = 1.0000			Q_{old} = 0.9099		
	Q_{new} = 0.7761			Q_{new} = 1.0000		
Parzen windowing results	Q_{actual} = 1.0000			Q_{actual} = 0.8494		







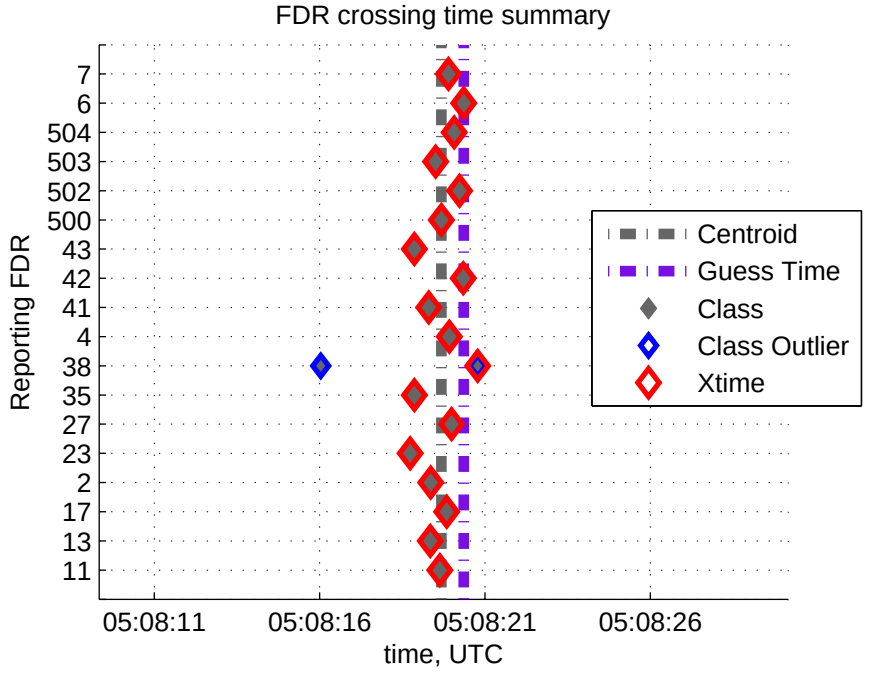
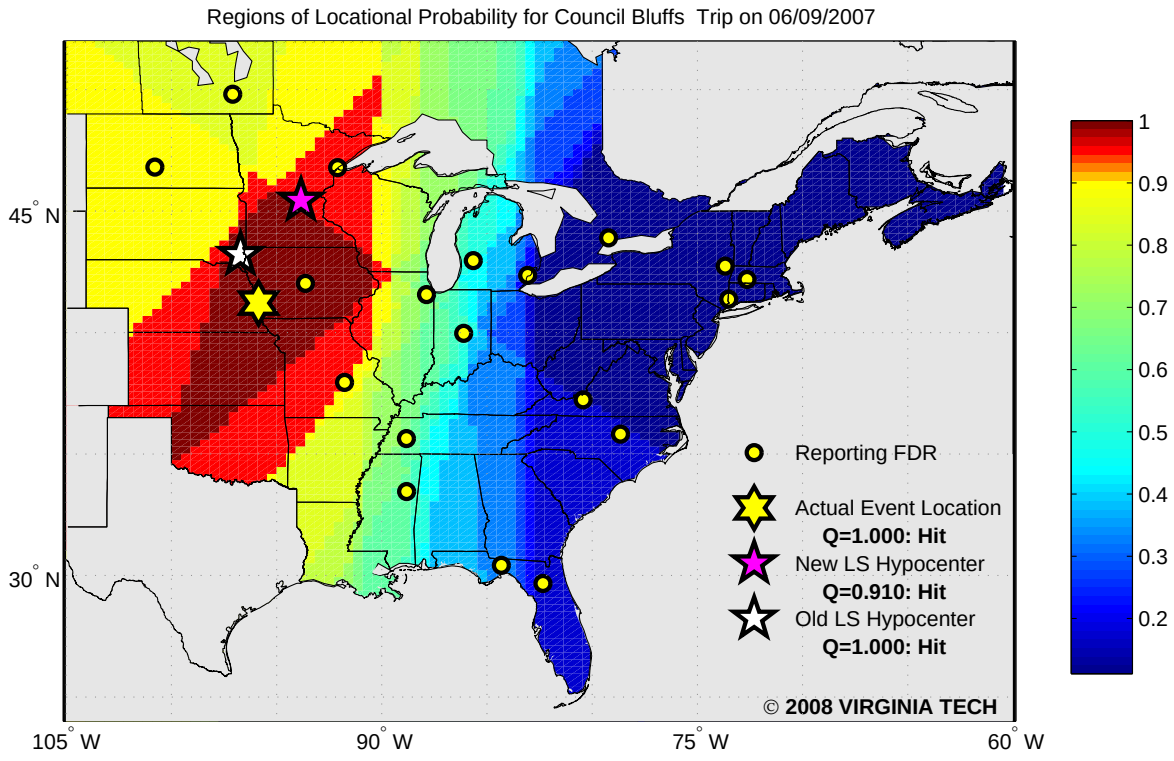
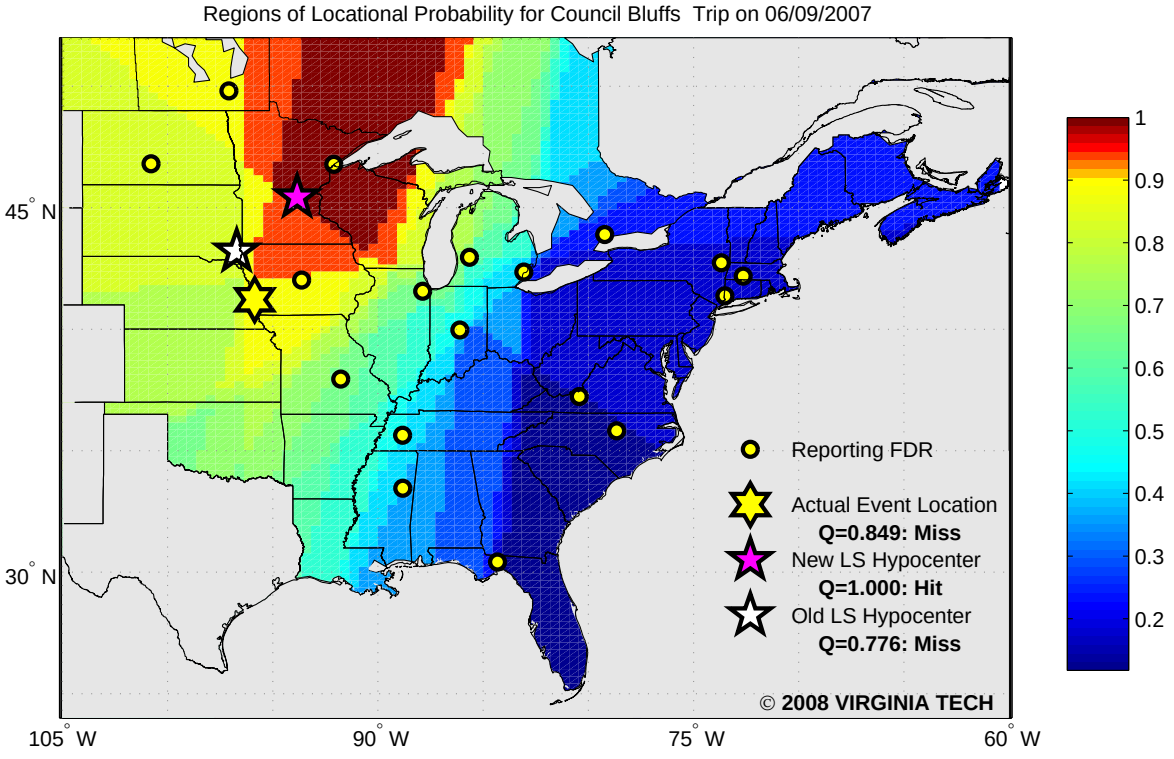


Figure D.60. Consolidated event ordering calculations: Council Bluffs (690 MW, 41.2146°, −95.8574°) Trip on 06/09/2007 05:08:21



(a) Event location: old ordering method



(b) Event location: new ordering method

Figure D.61. Event location estimates: Council Bluffs (690 MW, 41.2146°, −95.8574°) Trip on 06/09/2007 05:08:21

Table D.28. Ordering method comparison: Keystone (850 MW, 40.6388°, −79.3191°) Trip on 06/09/2007 05:59:28

	Old Ordering Method			New Ordering Method		
Mismatch estimate (MW)	908			922		
FDR Info	Number	Name	Distance (mi)	Number	Name	Distance (mi)
	503	Danbury	307.3	503	Danbury	307.3
	38	ISONE	362.2	13	MidwestISO	360.7
	27	RPI	325.1	4	VT	242.8
	502	Toronto	225.1	38	ISONE	362.2
	6	ABB	334.7	27	RPI	325.1
	504	WayneState	227.5	6	ABB	334.7
	17	TVA4Jackson	621.2	504	WayneState	227.5
	11	Calvin	363.6	11	Calvin	363.6
	40	MISOStPaul	761	502	Toronto	225.1
	42	FSU	759.6	40	MISOStPaul	761
	35	ISU	747.5	500	Chicago	450
	9	UFL	776.4	17	TVA4Jackson	621.2
	560	Duluth	765.2	2	UMR	690.3
	4	VT	242.8	42	FSU	759.6
	43	Bismarck	1149	7	MISS	720.9
	2	UMR	690.3	35	ISU	747.5
	7	MISS	720.9	23	Duluth2	765.2
	41	Winnipeg	1067	41	Winnipeg	1067
				43	Bismarck	1149
LS estimate	Latitude	Longitude	Distance (mi)	Latitude	Longitude	Distance (mi)
	40.1074°	−75.6618°	196	40.7597°	−73.9461°	281.5
	Q_{old} = 1.0000			Q_{old} = 1.0000		
	Q_{new} = 1.0000			Q_{new} = 1.0000		
Parzen windowing results	Q_{actual} = 0.2918			Q_{actual} = 0.2307		

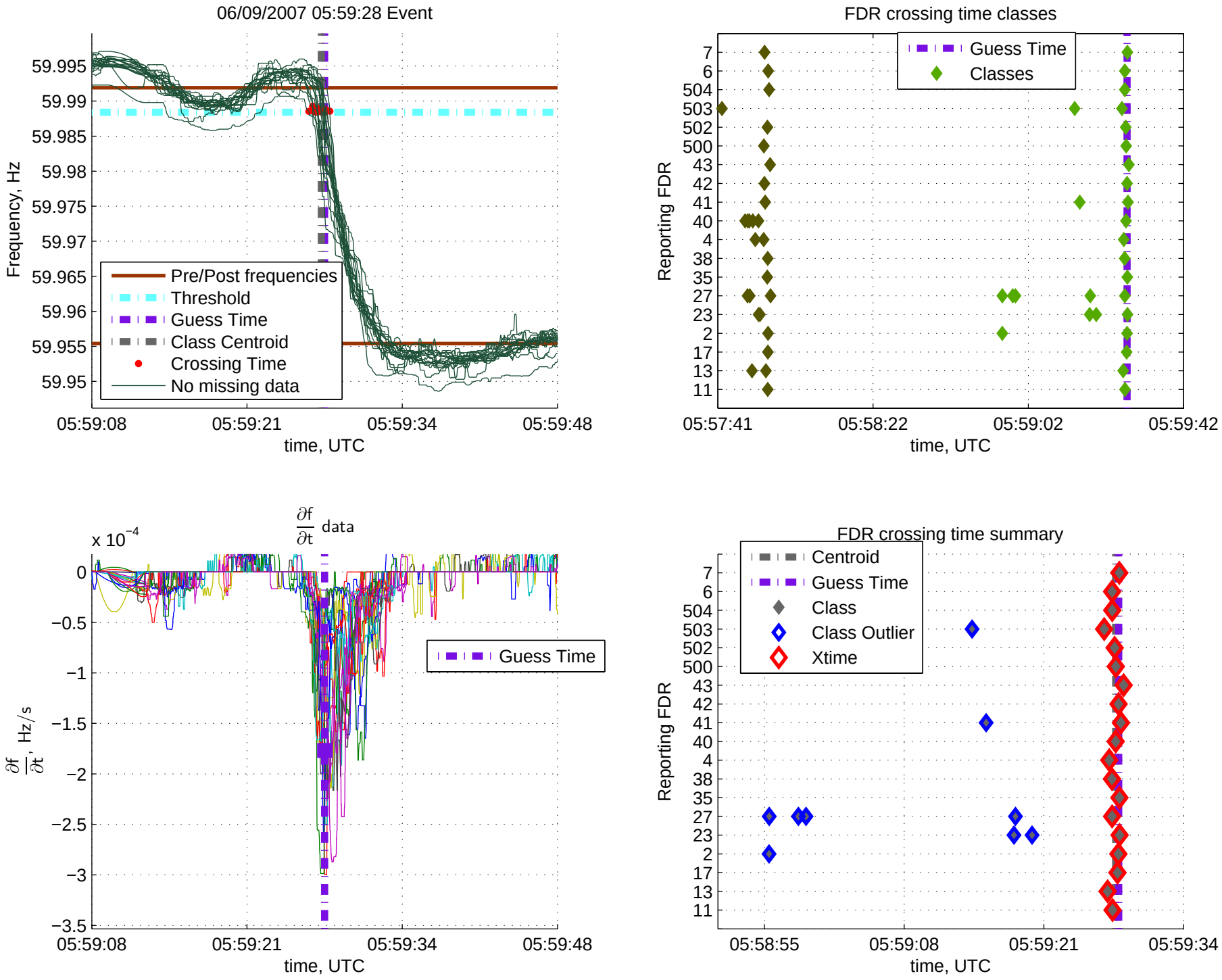
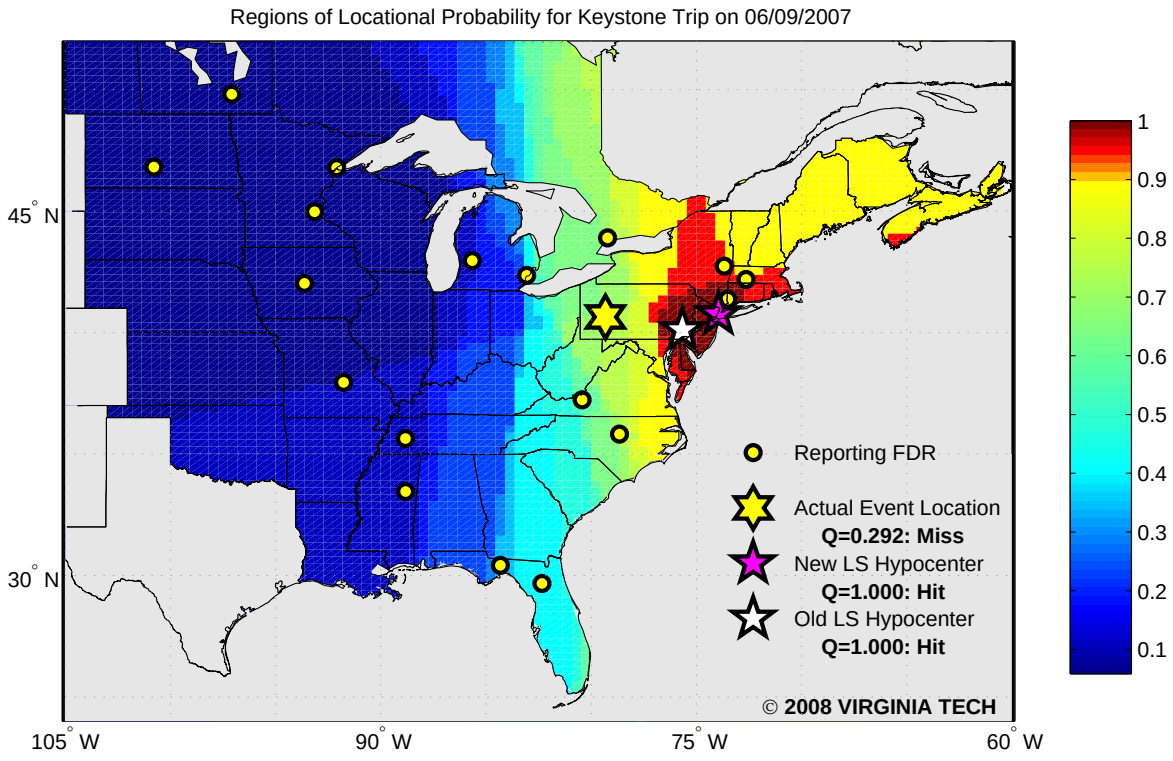
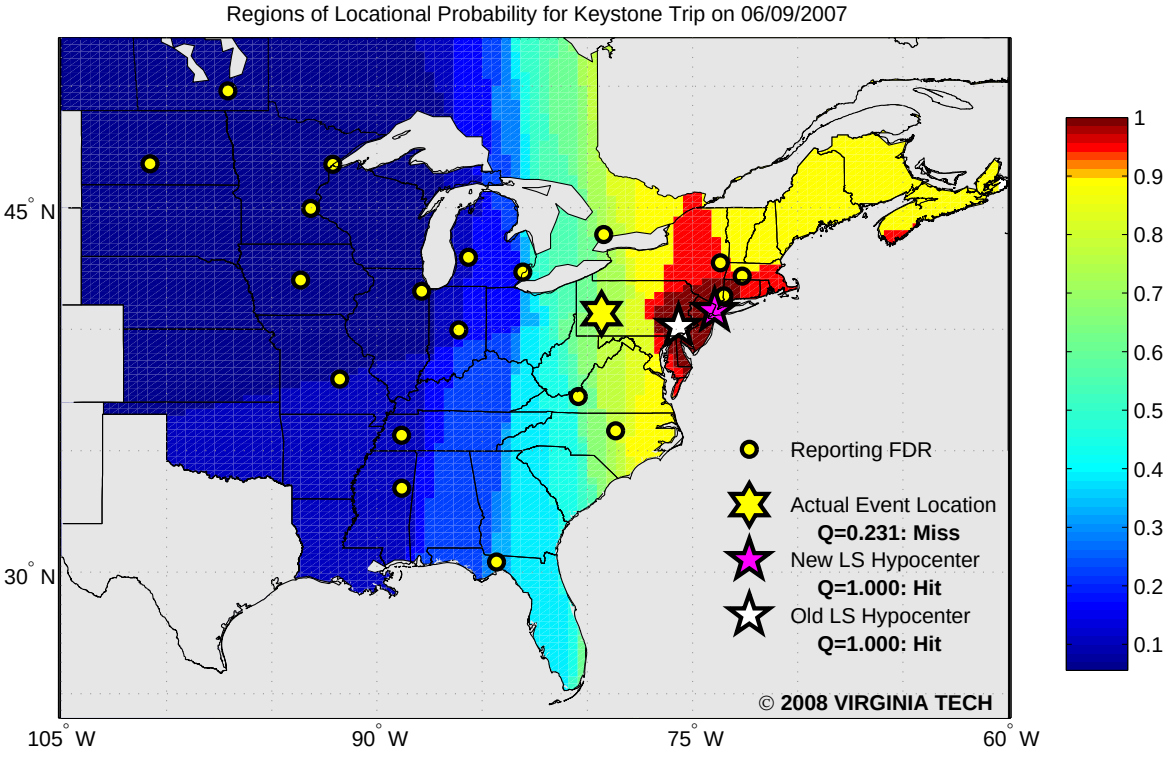


Figure D.62. Consolidated event ordering calculations: Keystone (850 MW, 40.6388°, −79.3191°) Trip on 06/09/2007 05:59:28



(a) Event location: old ordering method



(b) Event location: new ordering method

Figure D.63. Event location estimates: Keystone (850 MW, 40.6388°, −79.3191°) Trip on 06/09/2007 05:59:28

Table D.29. Ordering method comparison: Browns Ferry Unit 1 (1065 MW, 34.7055°, −87.1173°) Trip on 06/09/2007 16:00:36

	Old Ordering Method			New Ordering Method		
Mismatch estimate (MW)	742			738		
FDR Info	Number	Name	Distance (mi)	Number	Name	Distance (mi)
	7	MISS	130.2	4	VT	412.7
	17	TVA4Jackson	116	7	MISS	130.2
	42	FSU	337.9	6	ABB	483.2
	9	UFL	446	42	FSU	337.9
	6	ABB	483.2	11	Calvin	575.8
	4	VT	412.7	27	RPI	910.7
	35	ISU	616	2	UMR	342.2
	560	Duluth	874.1	500	Chicago	475.5
	500	Chicago	475.5	35	ISU	616
	41	Winnipeg	1159	43	Bismarck	1097
	43	Bismarck	1097	38	ISONE	936.6
	11	Calvin	575.8	41	Winnipeg	1159
	503	Danbury	870.8	23	Duluth2	874.1
	2	UMR	342.2	502	Toronto	761.6
	502	Toronto	761.6			
	38	ISONE	936.6			
	13	MidwestISO	367.9			
	27	RPI	910.7			
LS estimate	Latitude	Longitude	Distance (mi)	Latitude	Longitude	Distance (mi)
	34.7703°	−87.5229°	23.46	34.9947°	−81.2245°	334.7
	$Q_{old} = 0.8578$			$Q_{old} = 0.4074$		
	$Q_{new} = 0.2324$			$Q_{new} = 1.0000$		
Parzen windowing results	$Q_{actual} = 0.8578$			$Q_{actual} = 0.2324$		

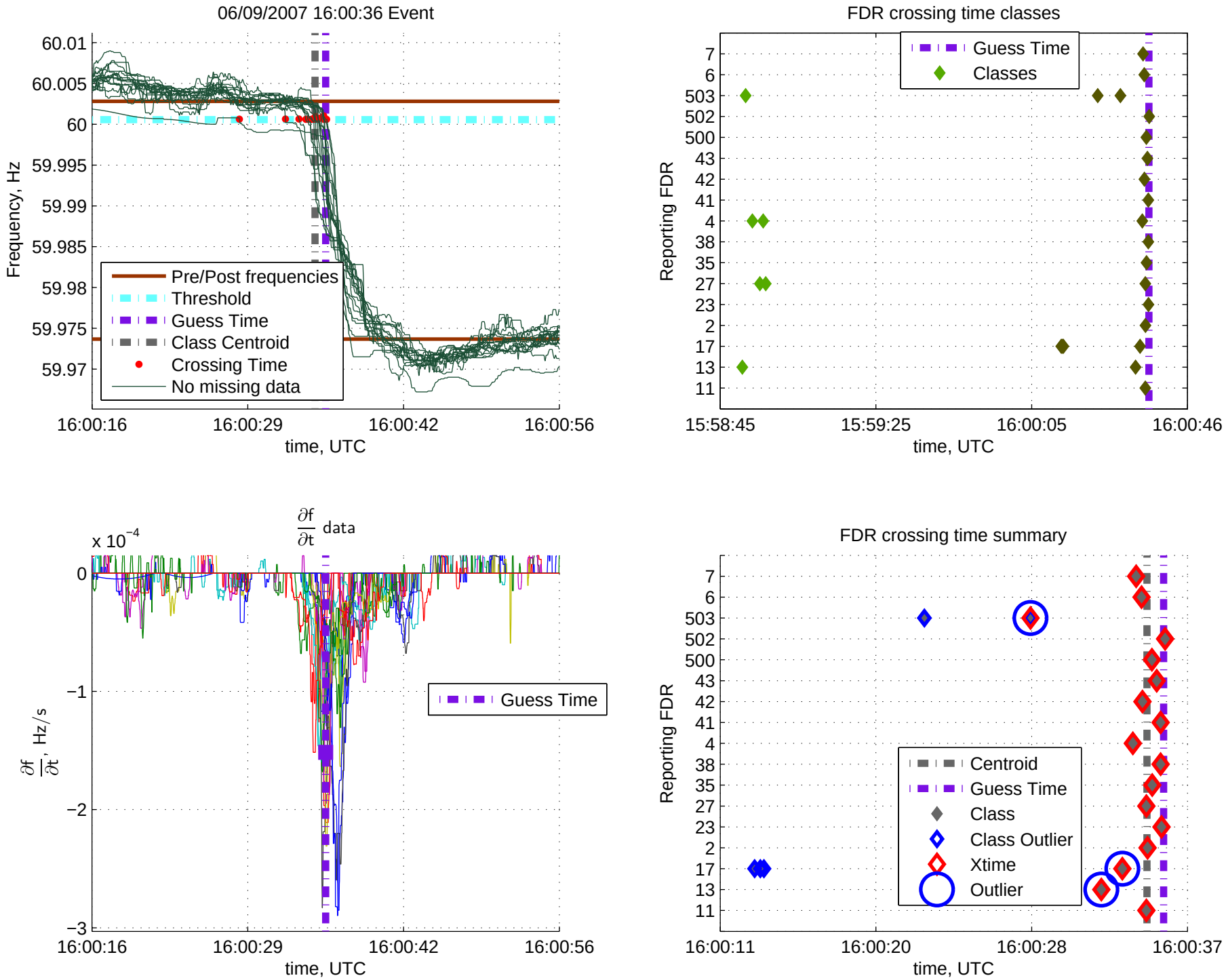
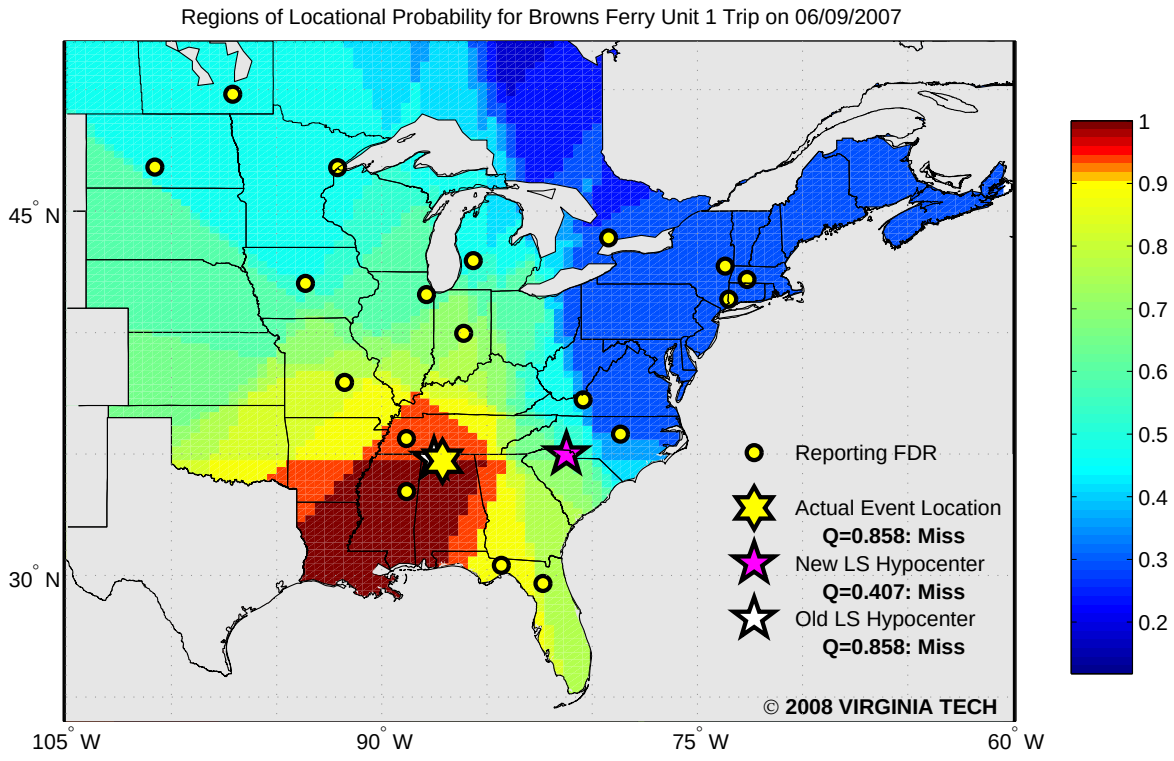
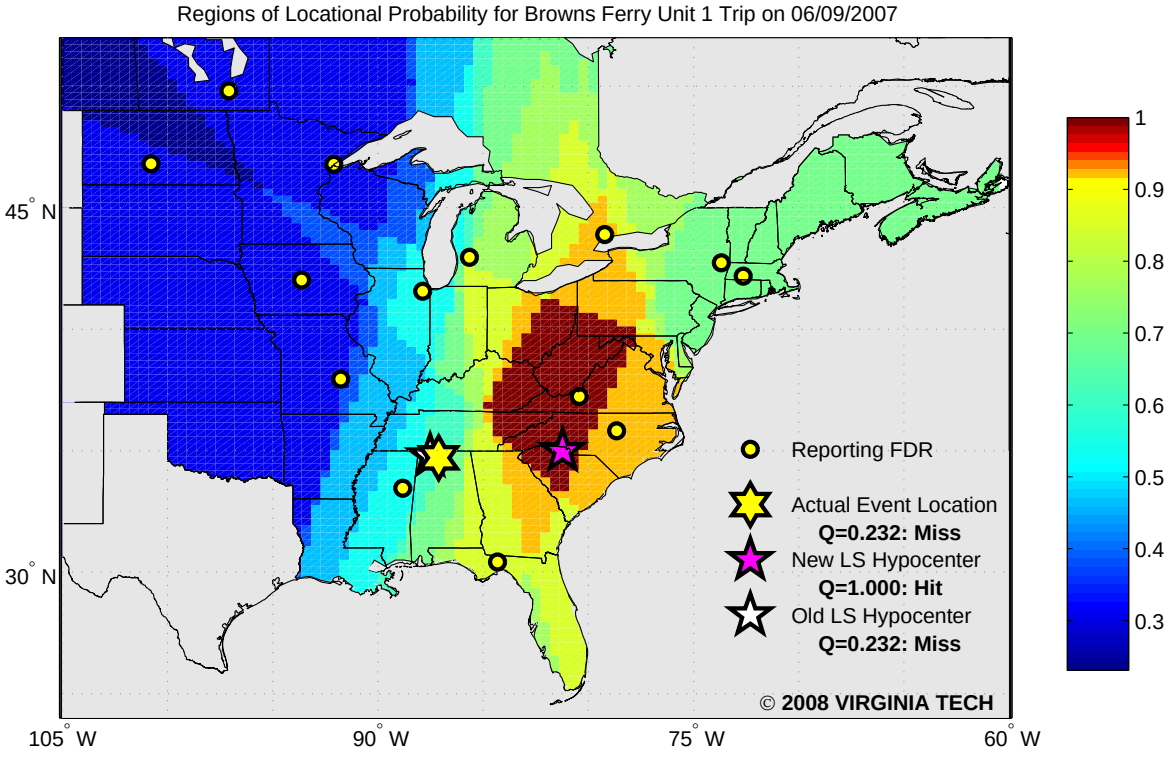


Figure D.64. Consolidated event ordering calculations: Browns Ferry Unit 1 (1065 MW, 34.7055°, −87.1173°) Trip on 06/09/2007 16:00:36



(a) Event location: old ordering method



(b) Event location: new ordering method

Figure D.65. Event location estimates: Browns Ferry Unit 1 (1065 MW, 34.7055°, −87.1173°) Trip on 06/09/2007 16:00:36

Table D.30. Ordering method comparison: Belews Creek U1 (1135 MW, 36.3189°, −80.1484°) Trip on 06/12/2007 15:41:06

	Old Ordering Method			New Ordering Method		
Mismatch estimate (MW)	870			938		
FDR Info	Number	Name	Distance (mi)	Number	Name	Distance (mi)
	17	TVA4Jackson	487.5	4	VT	65.02
	6	ABB	90	6	ABB	90
	4	VT	65.02	17	TVA4Jackson	487.5
	9	UFL	476.2	42	FSU	473.1
	42	FSU	473.1	13	MidwestISO	410.4
	7	MISS	529.6	11	Calvin	544.2
	13	MidwestISO	410.4	7	MISS	529.6
	506	OhioTiffin	366.6	27	RPI	561.3
	11	Calvin	544.2	500	Chicago	550.7
	500	Chicago	550.7	2	UMR	649.3
	2	UMR	649.3	43	Bismarck	1284
	503	Danbury	499.6	23	Duluth2	949.1
	27	RPI	561.3	40	MISOStPaul	904.5
				502	Toronto	525.8
				35	ISU	821.1
				41	Winnipeg	1259
LS estimate	Latitude	Longitude	Distance (mi)	Latitude	Longitude	Distance (mi)
	42.0295°	−88.6386°	601.5	34.9947°	−81.2245°	109.6
	Q_{old} = 0.3832			Q_{old} = 0.2203		
	Q_{new} = 0.1396			Q_{new} = 1.0000		
Parzen windowing results	Q_{actual} = 0.1139			Q_{actual} = 1.0000		

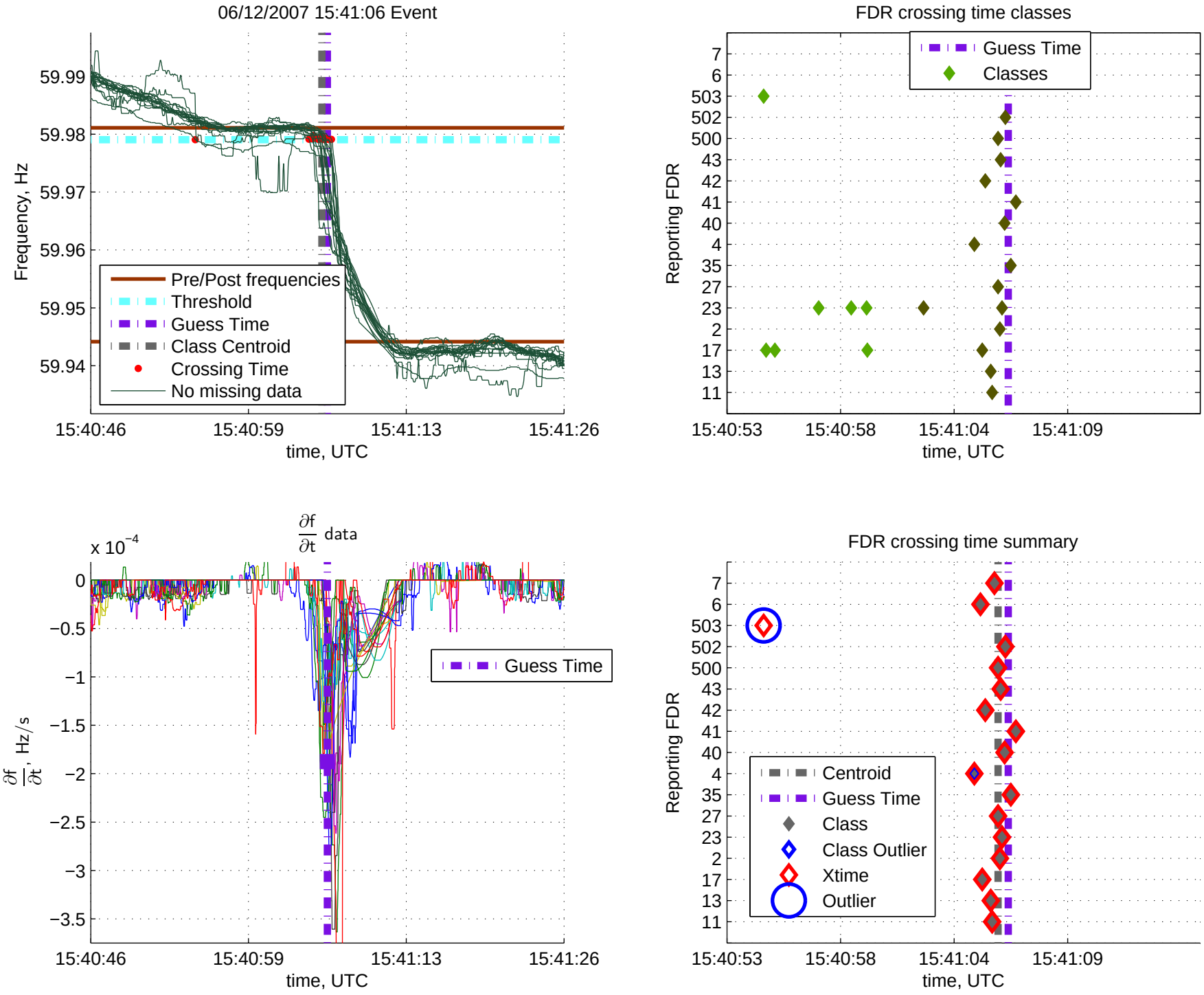
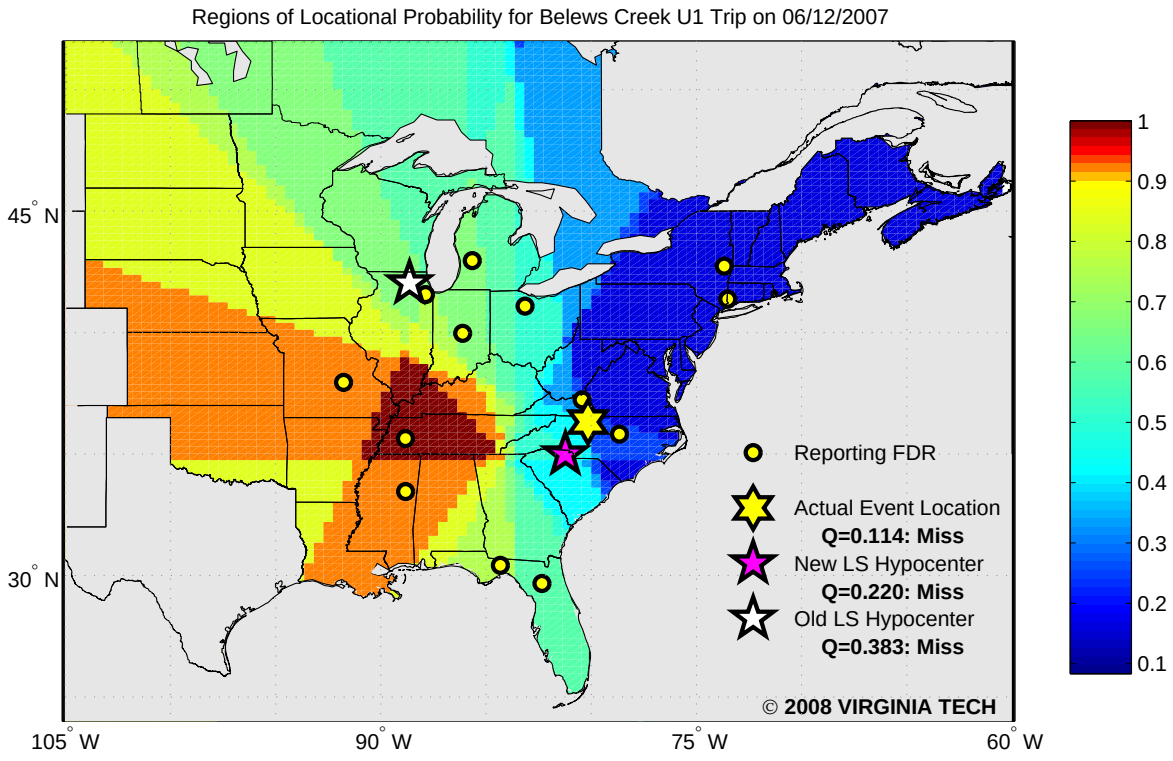
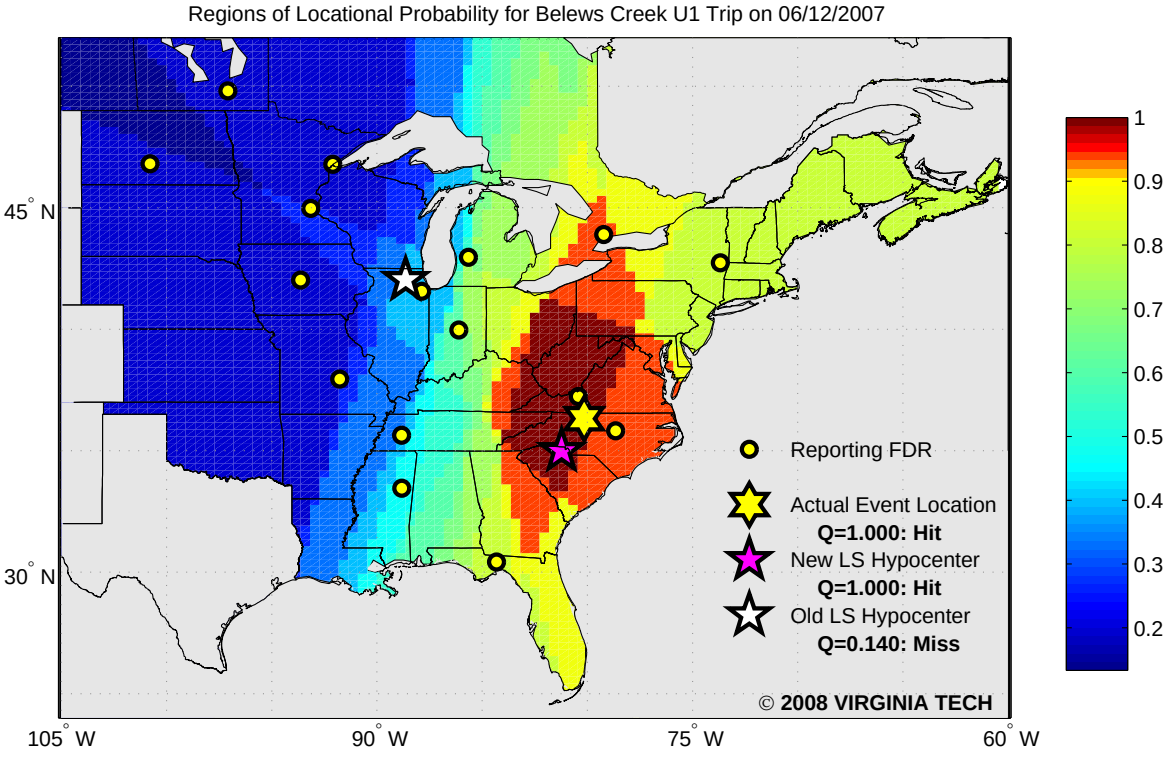


Figure D.66. Consolidated event ordering calculations: Belews Creek U1 (1135 MW, 36.3189°, −80.1484°) Trip on 06/12/2007 15:41:06



(a) Event location: old ordering method

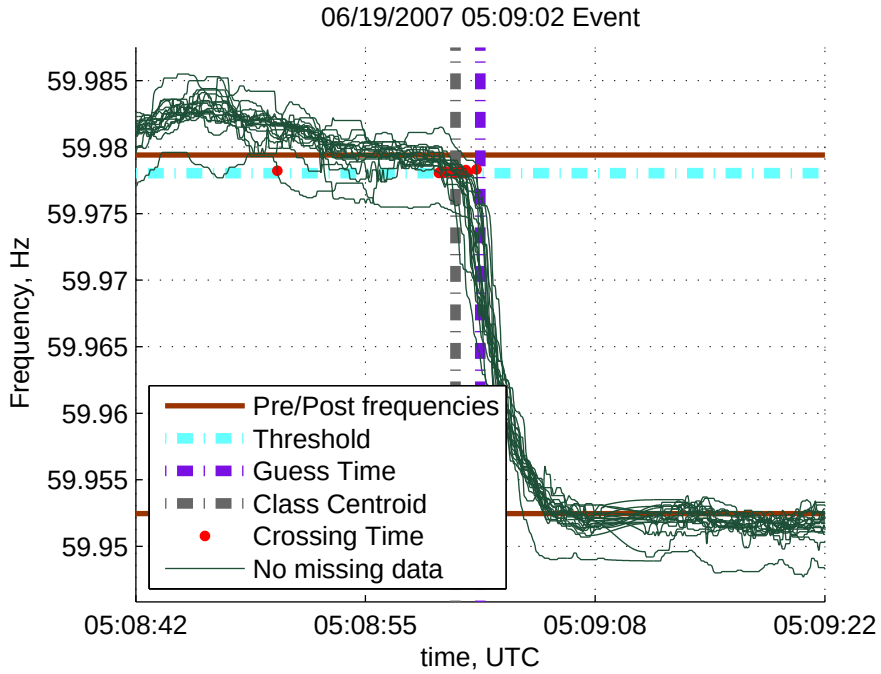


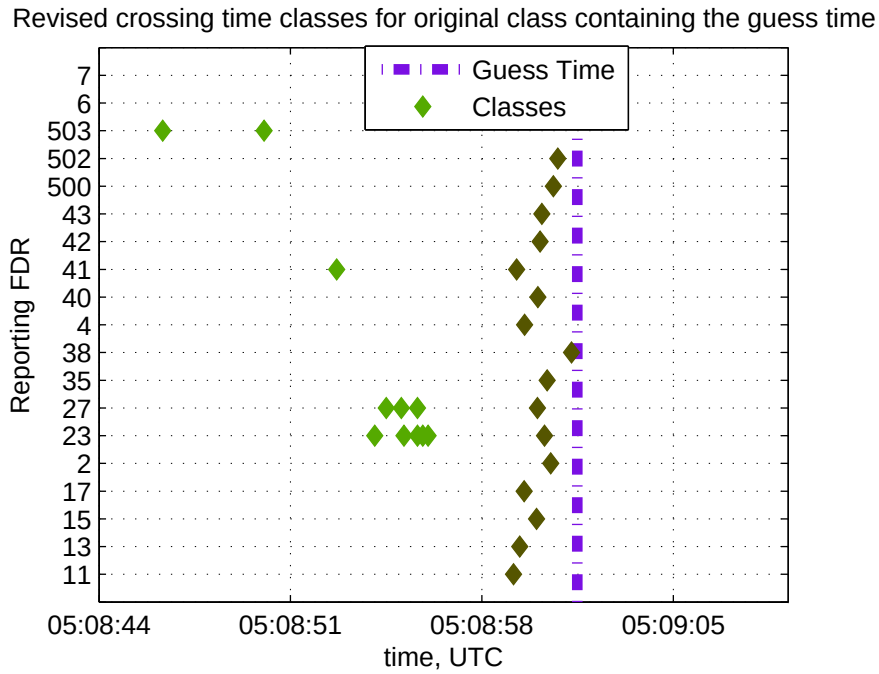
(b) Event location: new ordering method

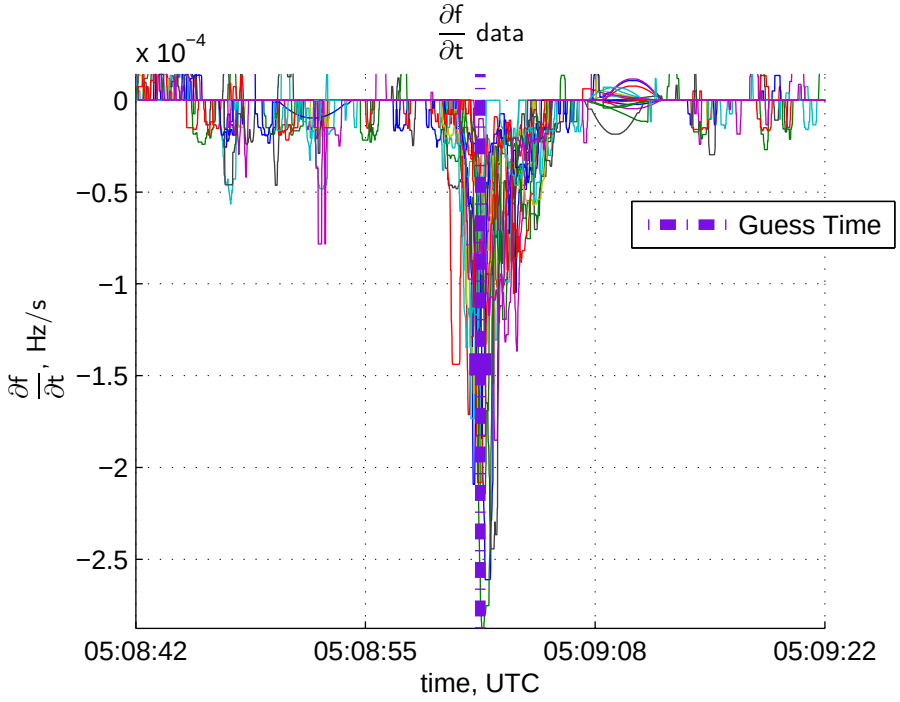
Figure D.67. Event location estimates: Belews Creek U1 (1135 MW, 36.3189°, –80.1484°) Trip on 06/12/2007 15:41:06

Table D.31. Ordering method comparison: Belews Creek U2 (1135 MW, 36.3189°, −80.1484°) Trip on 06/19/2007 05:09:02

	Old Ordering Method			New Ordering Method		
Mismatch estimate (MW)	693			677		
FDR Info	Number	Name	Distance (mi)	Number	Name	Distance (mi)
	6	ABB	90	11	Calvin	544.2
	42	FSU	473.1	41	Winnipeg	1259
	11	Calvin	544.2	13	MidwestISO	410.4
	503	Danbury	499.6	17	TVA4Jackson	487.5
	500	Chicago	550.7	6	ABB	90
	27	RPI	561.3	4	VT	65.02
	9	UFL	476.2	15	TVA3Nashville	369.9
	13	MidwestISO	410.4	27	RPI	561.3
	502	Toronto	525.8	40	MISOStPaul	904.5
	38	ISONE	570.3	42	FSU	473.1
	2	UMR	649.3	43	Bismarck	1284
	35	ISU	821.1	23	Duluth2	949.1
	40	MISOStPaul	904.5	35	ISU	821.1
	7	MISS	529.6	2	UMR	649.3
	17	TVA4Jackson	487.5	500	Chicago	550.7
	41	Winnipeg	1259	7	MISS	529.6
	43	Bismarck	1284	502	Toronto	525.8
	560	Duluth	949.1			
	15	TVA3Nashville	369.9			
	4	VT	65.02			
LS estimate	Latitude	Longitude	Distance (mi)	Latitude	Longitude	Distance (mi)
	34.8012°	−80.2775°	105.1	41.5236°	−83.1278°	393.6
	Q_{old} = 1.0000			Q_{old} = 0.2645		
	Q_{new} = 0.4886			Q_{new} = 1.0000		
Parzen windowing results	Q_{actual} = 0.8749			Q_{actual} = 0.4886		







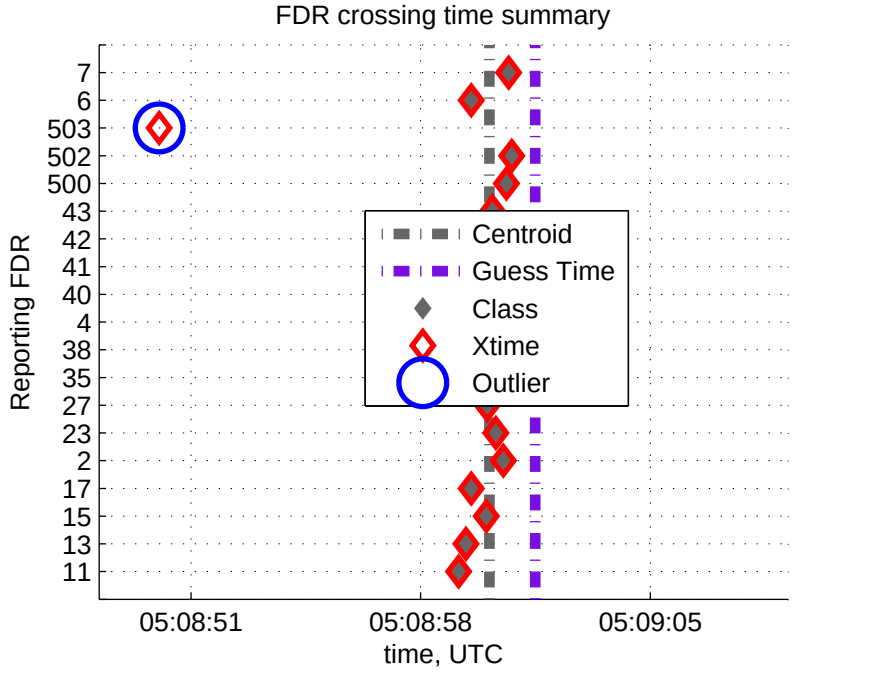
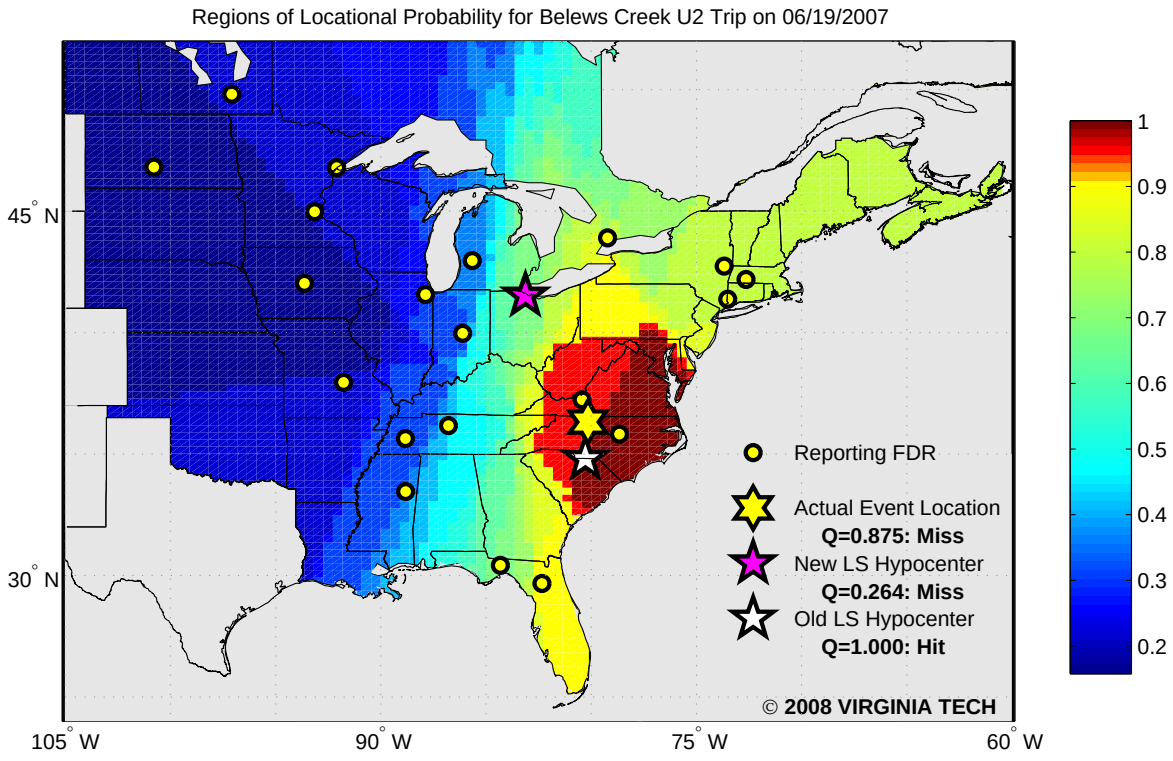
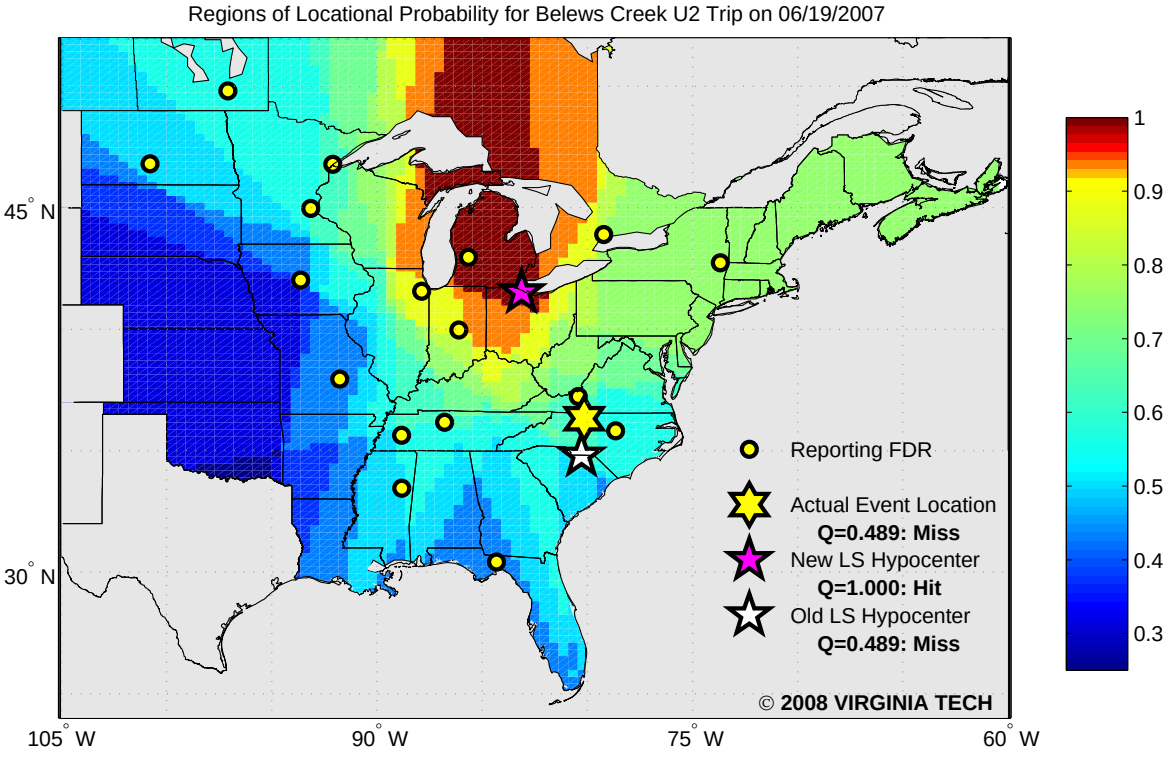


Figure D.68. Consolidated event ordering calculations: Belews Creek U2 (1135 MW, 36.3189°, −80.1484°) Trip on 06/19/2007 05:09:02



(a) Event location: old ordering method



(b) Event location: new ordering method

Figure D.69. Event location estimates: Belews Creek U2 (1135 MW, 36.3189°, –80.1484°) Trip on 06/19/2007 05:09:02

Table D.32. Ordering method comparison: Keystone (850 MW, 40.6388°, −79.3191°) Trip on 06/27/2007 08:50:09

	Old Ordering Method			New Ordering Method		
Mismatch estimate (MW)	774			735		
FDR Info	Number	Name	Distance (mi)	Number	Name	Distance (mi)
	503	Danbury	307.3	38	ISONE	362.2
	11	Calvin	363.6	4	VT	242.8
	4	VT	242.8	27	RPI	325.1
	27	RPI	325.1	516	LeRoy	192.2
	516	LeRoy	192.2	23	Duluth2	765.2
	38	ISONE	362.2	6	ABB	334.7
	6	ABB	334.7	11	Calvin	363.6
	500	Chicago	450	502	Toronto	225.1
	502	Toronto	225.1	41	Winnipeg	1067
	15	TVA3Nashville	508.3	17	TVA4Jackson	621.2
	35	ISU	747.5	35	ISU	747.5
	2	UMR	690.3	42	FSU	759.6
	13	MidwestISO	360.7	13	MidwestISO	360.7
	560	Duluth	765.2	15	TVA3Nashville	508.3
	43	Bismarck	1149	43	Bismarck	1149
	9	UFL	776.4	2	UMR	690.3
	41	Winnipeg	1067	40	MISOStPaul	761
	42	FSU	759.6	500	Chicago	450
	40	MISOStPaul	761			
	17	TVA4Jackson	621.2			
LS estimate	Latitude	Longitude	Distance (mi)	Latitude	Longitude	Distance (mi)
	41.7320°	−79.4519°	75.85	42.1859°	−72.6383°	362.2
	$Q_{old} = 0.2187$			$Q_{old} = 0.8893$		
	$Q_{new} = 0.1090$			$Q_{new} = 1.0000$		
Parzen windowing results	$Q_{actual} = 0.2984$			$Q_{actual} = 0.1090$		

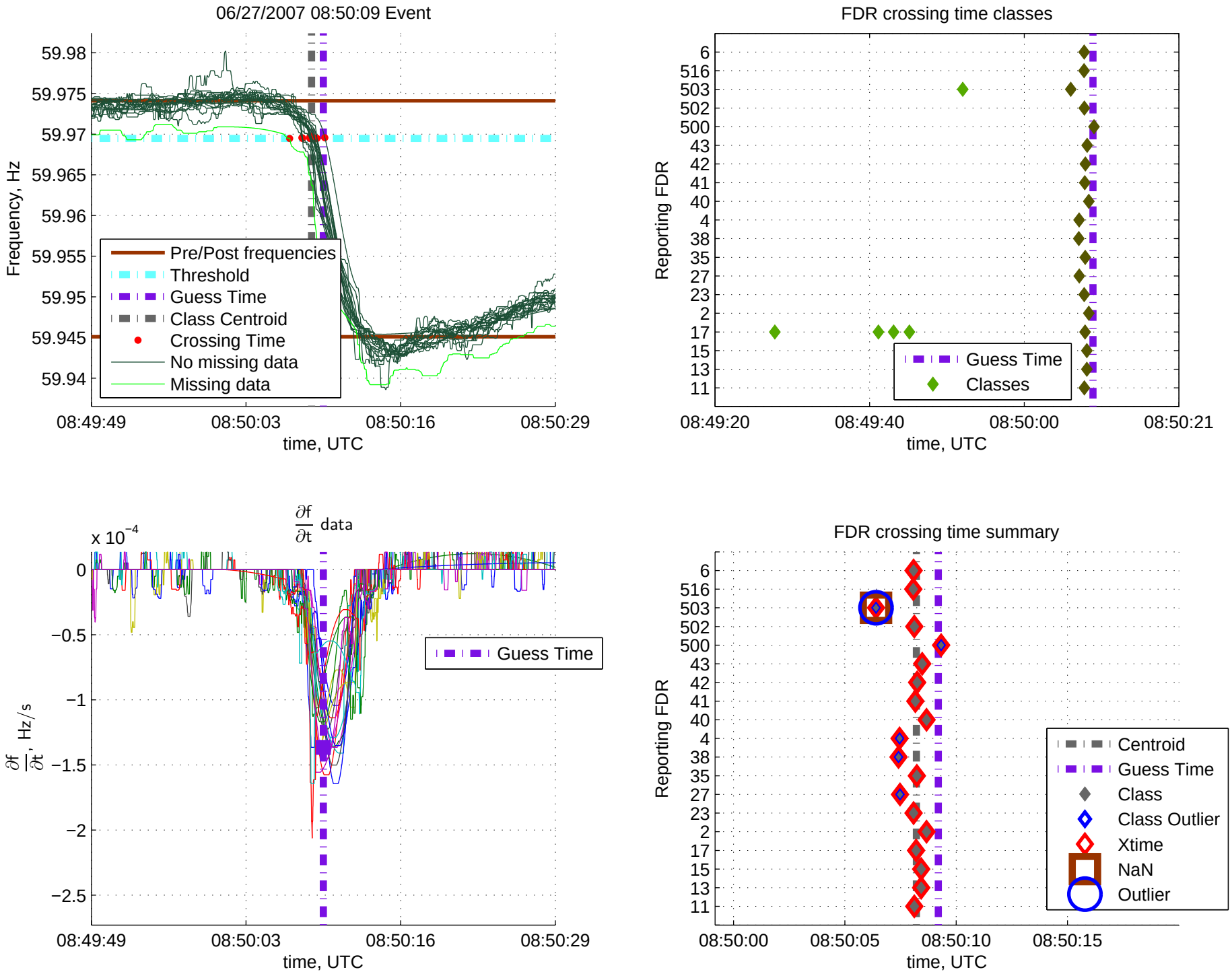
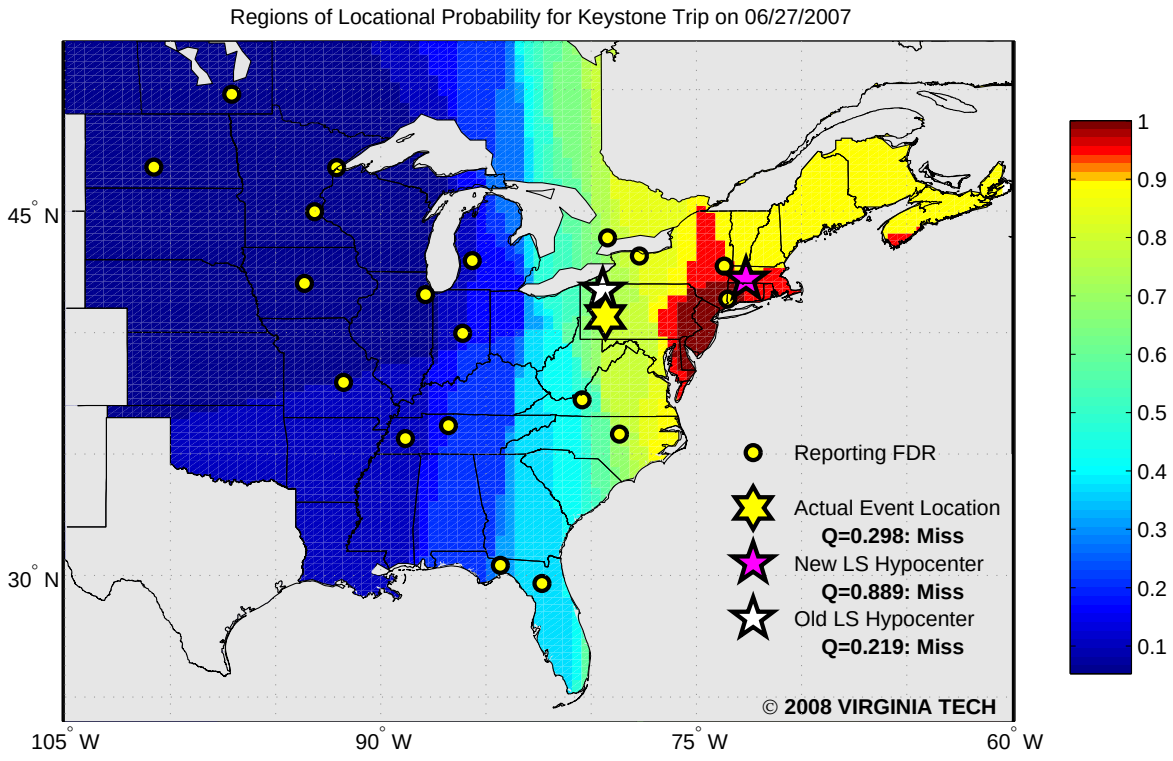
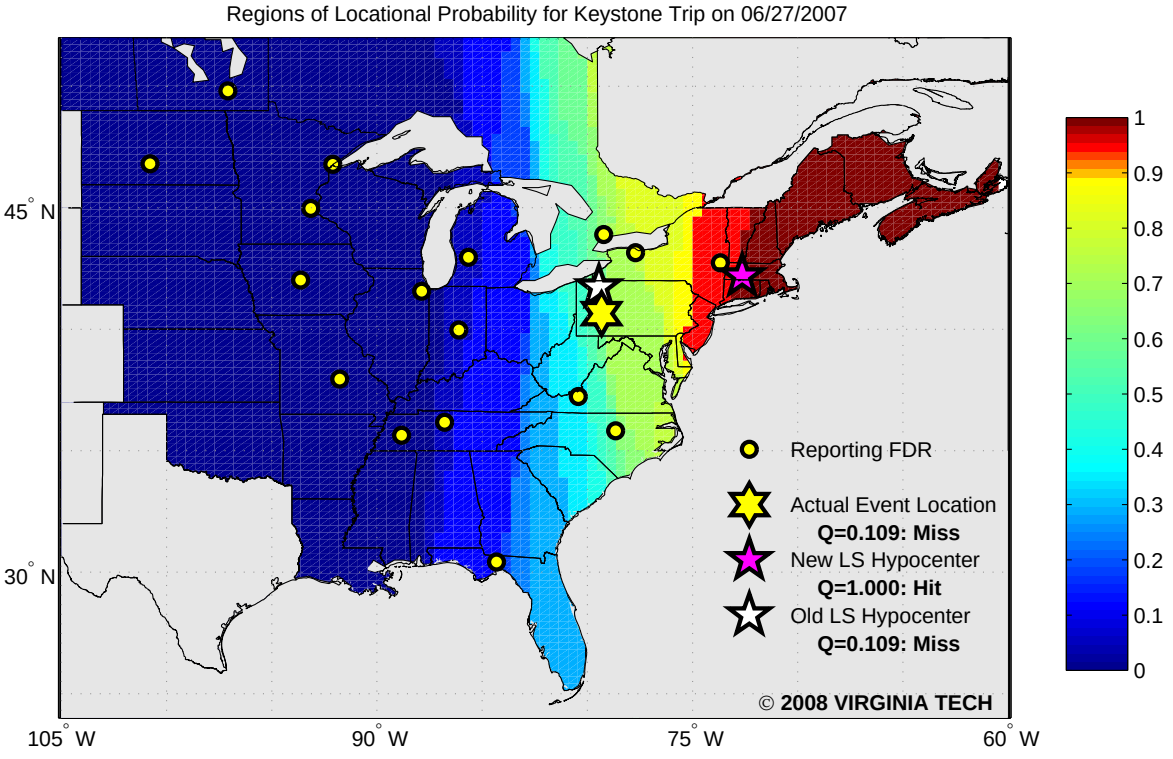


Figure D.70. Consolidated event ordering calculations: Keystone (850 MW, 40.6388°, −79.3191°) Trip on 06/27/2007 08:50:09



(a) Event location: old ordering method



(b) Event location: new ordering method

Figure D.71. Event location estimates: Keystone (850 MW, 40.6388°, −79.3191°) Trip on 06/27/2007 08:50:09

Table D.33. Ordering method comparison: Braidwood (1178 MW, 41.2288°, −88.2690°) Trip on 06/27/2007 14:21:15

	Old Ordering Method			New Ordering Method		
Mismatch estimate (MW)	875			896		
FDR Info	Number	Name	Distance (mi)	Number	Name	Distance (mi)
	13	MidwestISO	142.8	40	MISOStPaul	356.9
	11	Calvin	179.6	23	Duluth2	428.5
	35	ISU	282	4	VT	502
	2	UMR	293.2	41	Winnipeg	729.5
	560	Duluth	428.5	35	ISU	282
	4	VT	502	6	ABB	639.2
	508	ROA	521.4	11	Calvin	179.6
	41	Winnipeg	729.5	43	Bismarck	730.4
	43	Bismarck	730.4	13	MidwestISO	142.8
	6	ABB	639.2	2	UMR	293.2
	17	TVA4Jackson	387.8	17	TVA4Jackson	387.8
	502	Toronto	495.4	508	ROA	521.4
	27	RPI	755.8	502	Toronto	495.4
	516	LeRoy	556.1	42	FSU	778.7
	42	FSU	778.7	516	LeRoy	556.1
	503	Danbury	765.4			
	9	UFL	864.8			
LS estimate	Latitude	Longitude	Distance (mi)	Latitude	Longitude	Distance (mi)
	42.0513°	−88.4636°	57.71	45.4365°	−93.8410°	403.5
	$Q_{old} = 1.0000$			$Q_{old} = 0.6081$		
	$Q_{new} = 0.5153$			$Q_{new} = 1.0000$		
Parzen windowing results	$Q_{actual} = 1.0000$			$Q_{actual} = 0.3287$		

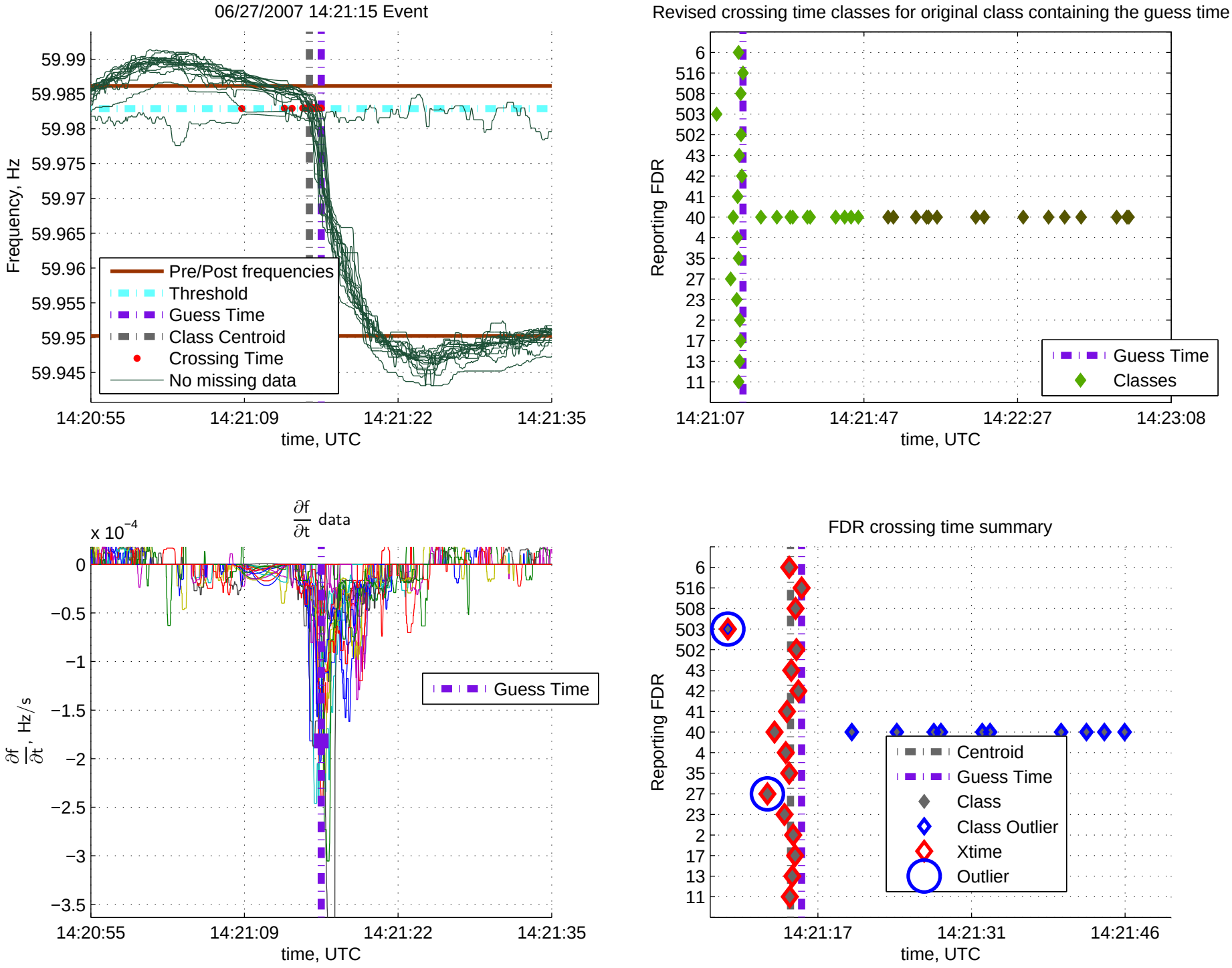
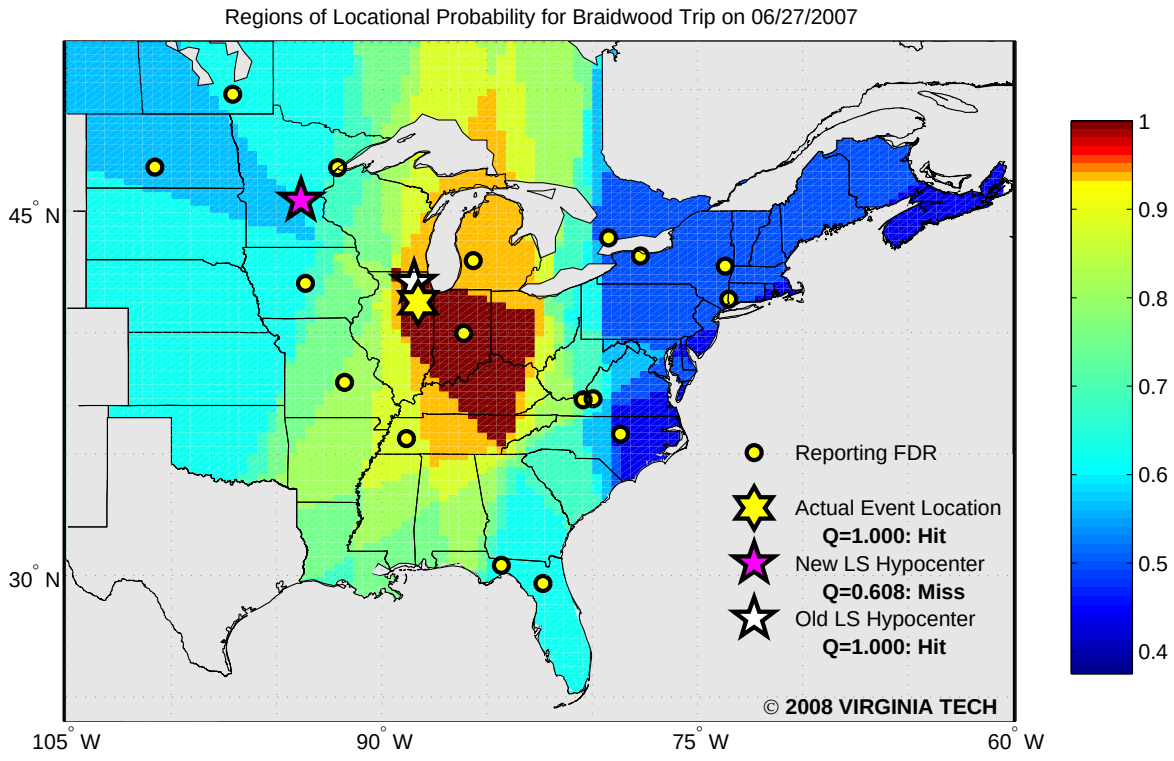
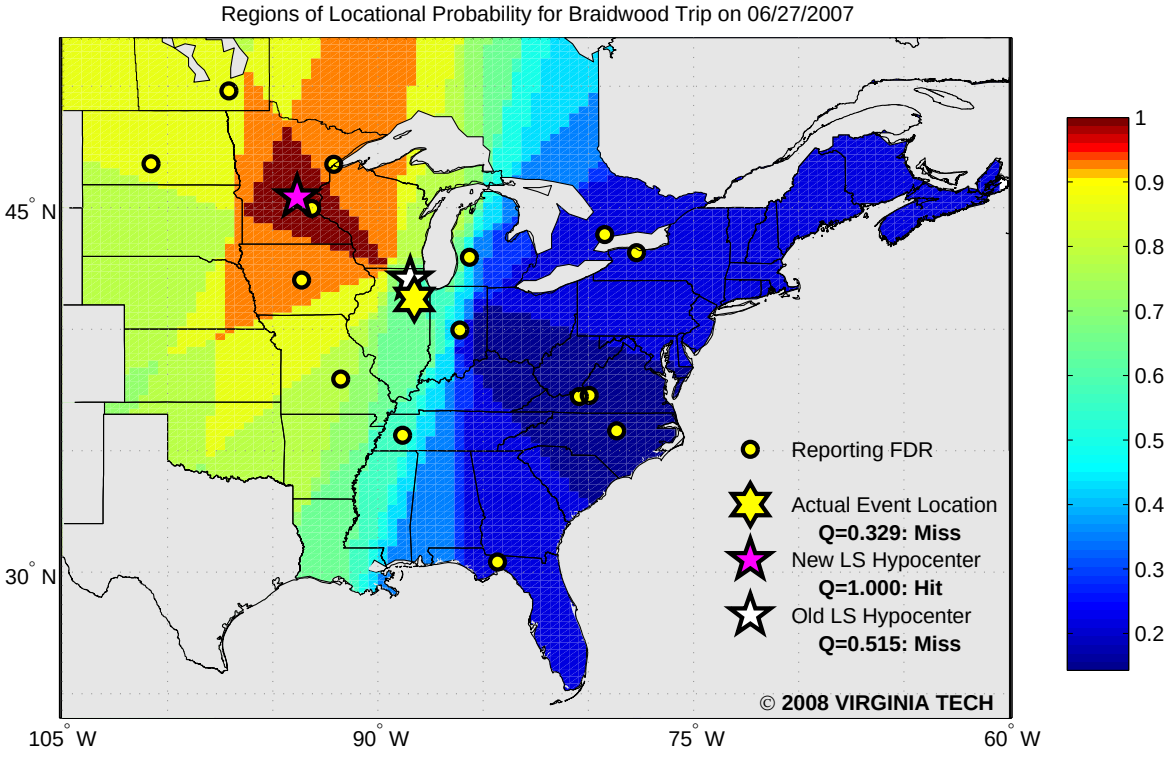


Figure D.72. Consolidated event ordering calculations: Braidwood (1178 MW, 41.2288°, −88.2690°) Trip on 06/27/2007 14:21:15



(a) Event location: old ordering method



(b) Event location: new ordering method

Figure D.73. Event location estimates: Braidwood (1178 MW, 41.2288°, −88.2690°) Trip on 06/27/2007 14:21:15

Table D.34. Ordering method comparison: North Anna2 (924 MW, 37.9986°, −77.8781°) Trip on 06/29/2007 21:53:58

	Old Ordering Method			New Ordering Method		
Mismatch estimate (MW)	864			834		
FDR Info	Number	Name	Distance (mi)	Number	Name	Distance (mi)
	6	ABB	156.5	4	VT	149.3
	508	ROA	124.2	6	ABB	156.5
	4	VT	149.3	27	RPI	394.9
	503	Danbury	329.3	38	ISONE	400.3
	27	RPI	394.9	11	Calvin	533.1
	13	MidwestISO	462.4	13	MidwestISO	462.4
	11	Calvin	533.1	23	Duluth2	943.6
	15	TVA3Nashville	506.7	516	LeRoy	356.1
	504	WayneState	407	502	Toronto	413.5
	38	ISONE	400.3	508	ROA	124.2
	9	UFL	629.3	42	FSU	639.6
	516	LeRoy	356.1	17	TVA4Jackson	626.9
	502	Toronto	413.5	15	TVA3Nashville	506.7
	42	FSU	639.6	35	ISU	877
	2	UMR	755.7	2	UMR	755.7
	40	MISOStPaul	923.3	40	MISOStPaul	923.3
	560	Duluth	943.6	43	Bismarck	1311
	35	ISU	877	41	Winnipeg	1251
	43	Bismarck	1311			
	41	Winnipeg	1251			
LS estimate	Latitude	Longitude	Distance (mi)	Latitude	Longitude	Distance (mi)
	37.3777°	−78.2819°	48.25	38.6023°	−77.3387°	50.94
	Q_{old} = 1.0000 Q_{new} = 0.9525			Q_{old} = 1.0000 Q_{new} = 0.9525		
Parzen windowing results	Q_{actual} = 1.0000			Q_{actual} = 0.9525		

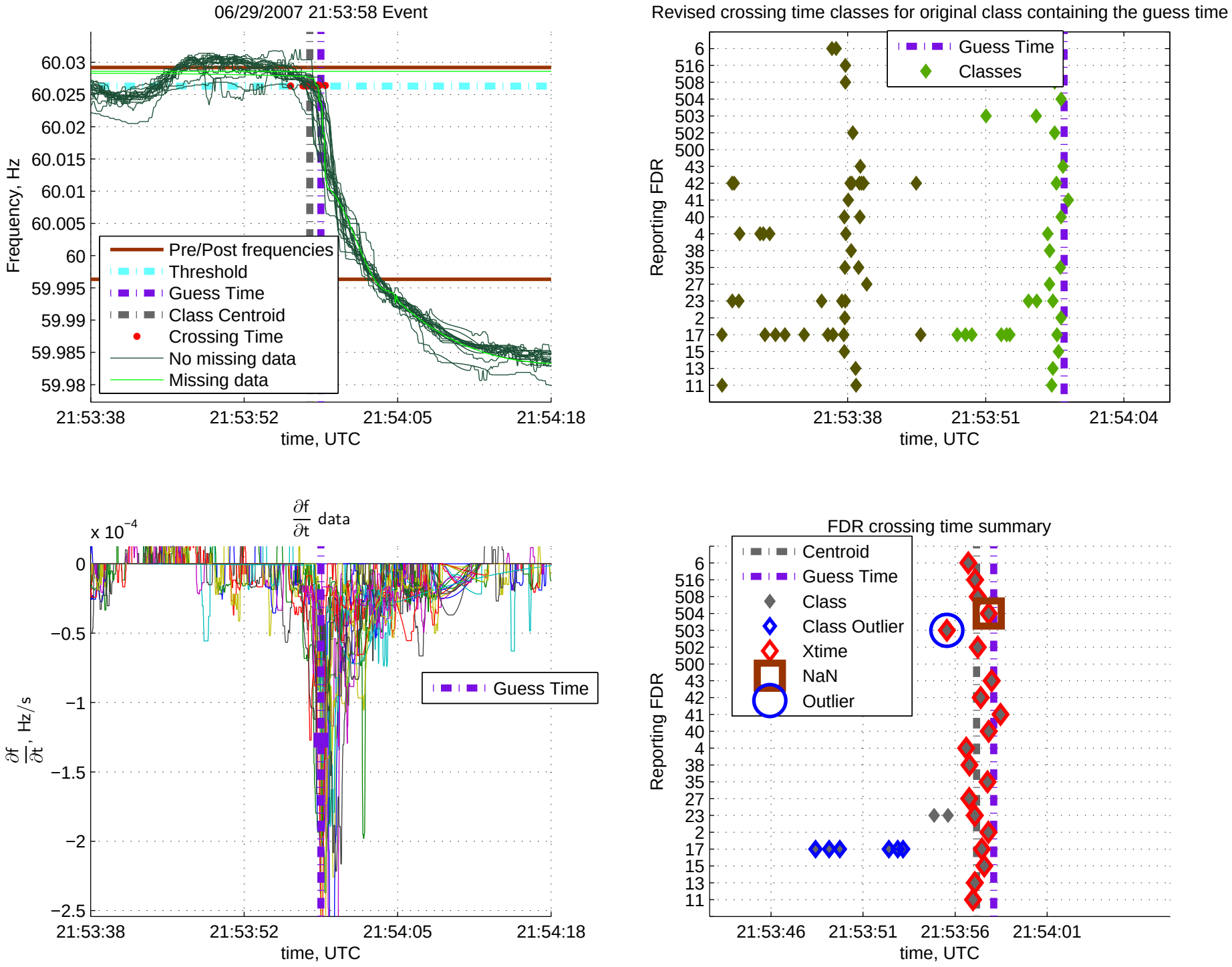
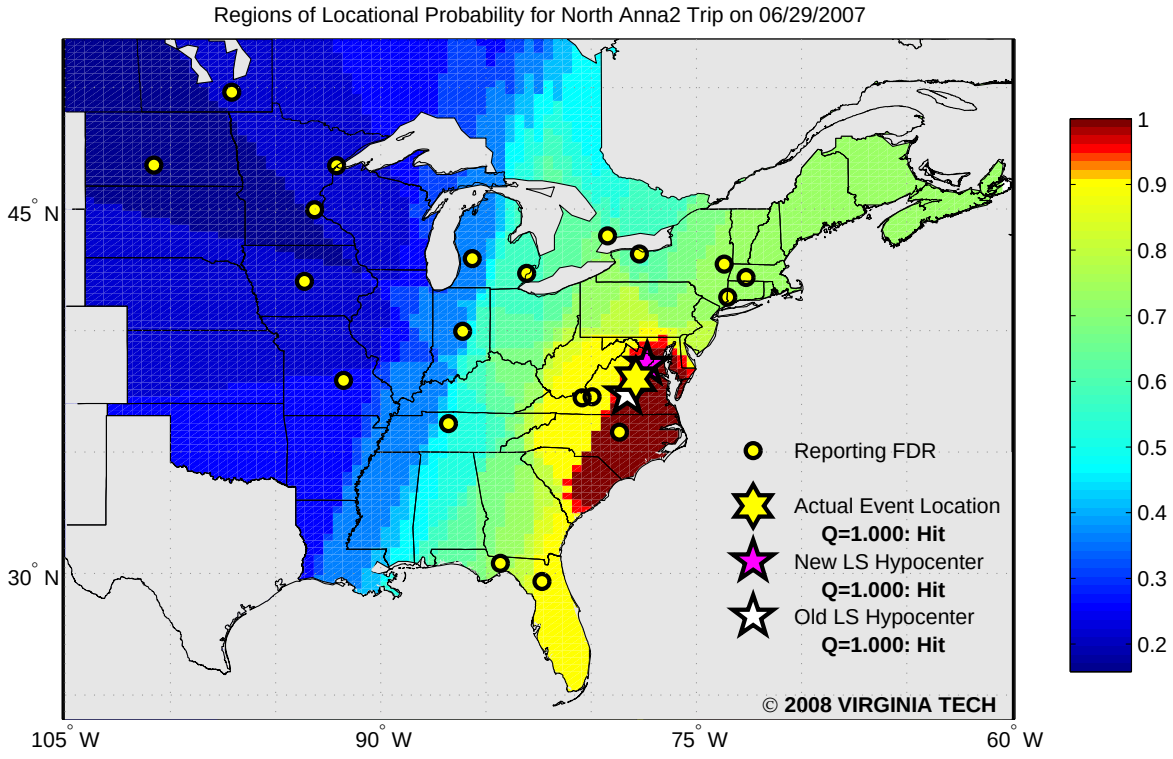
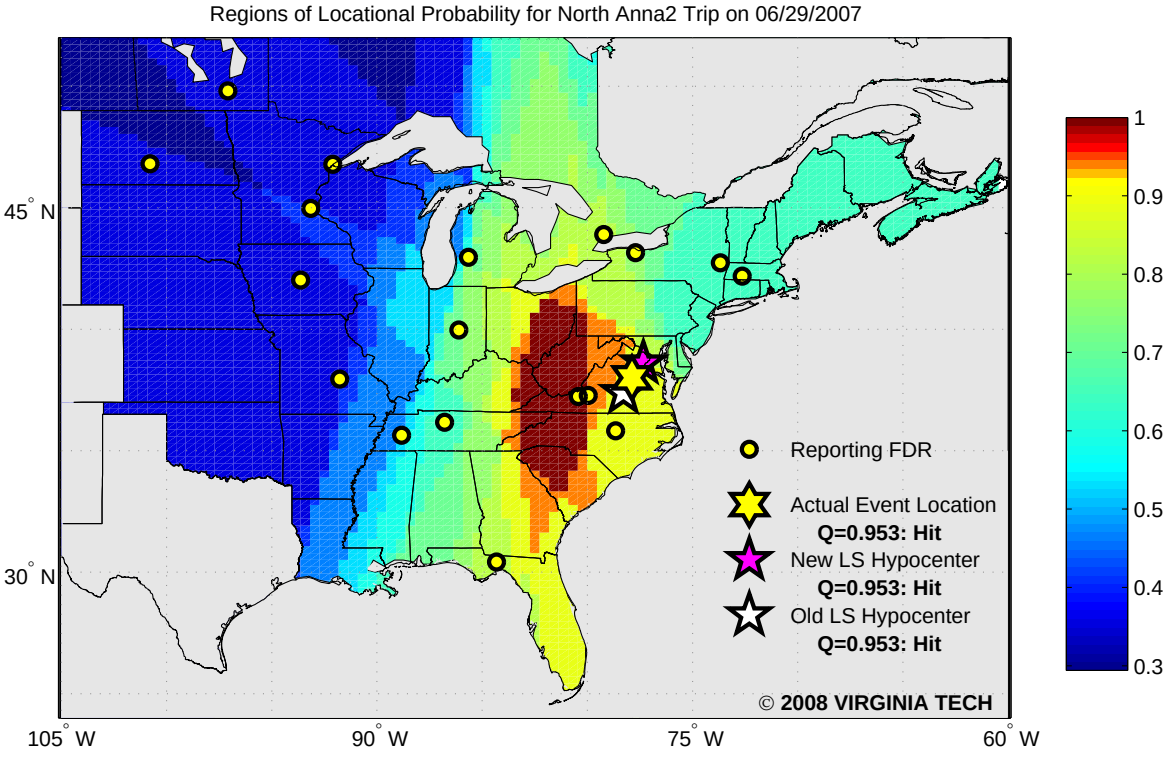


Figure D.74. Consolidated event ordering calculations: North Anna2 (924 MW, 37.9986°, −77.8781°) Trip on 06/29/2007 21:53:58



(a) Event location: old ordering method



(b) Event location: new ordering method

Figure D.75. Event location estimates: North Anna2 (924 MW, 37.9986°, −77.8781°) Trip on 06/29/2007 21:53:58

Table D.35. Ordering method comparison: Conemaugh (850 MW, 40.3823°, −79.0968°) Trip on 07/01/2007 23:34:17

	Old Ordering Method			New Ordering Method		
Mismatch estimate (MW)	756			651		
FDR Info	Number	Name	Distance (mi)	Number	Name	Distance (mi)
	27	RPI	323.9	6	ABB	316
	503	Danbury	300	4	VT	229.1
	6	ABB	316	27	RPI	323.9
	508	ROA	219.4	38	ISONE	357.6
	516	LeRoy	204.2	17	TVA4Jackson	622.6
	38	ISONE	357.6	508	ROA	219.4
	504	WayneState	247	504	WayneState	247
	11	Calvin	382.4	11	Calvin	382.4
	502	Toronto	242.9	502	Toronto	242.9
	4	VT	229.1	500	Chicago	465.1
	500	Chicago	465.1	516	LeRoy	204.2
	17	TVA4Jackson	622.6	40	MISOStPaul	779.6
	35	ISU	762.8	35	ISU	762.8
	42	FSU	748.1	2	UMR	698.5
	560	Duluth	785.4	42	FSU	748.1
	2	UMR	698.5	41	Winnipeg	1088
	40	MISOStPaul	779.6	23	Duluth2	785.4
	43	Bismarck	1168	43	Bismarck	1168
	41	Winnipeg	1088			
	9	UFL	762.1			
LS estimate	Latitude	Longitude	Distance (mi)	Latitude	Longitude	Distance (mi)
	38.7861°	−75.4686°	222.4	36.4059°	−78.9737°	274.8
	$Q_{old} = 0.9385$			$Q_{old} = 0.1756$		
	$Q_{new} = 0.7416$			$Q_{new} = 1.0000$		
Parzen windowing results	$Q_{actual} = 0.2548$			$Q_{actual} = 0.4779$		

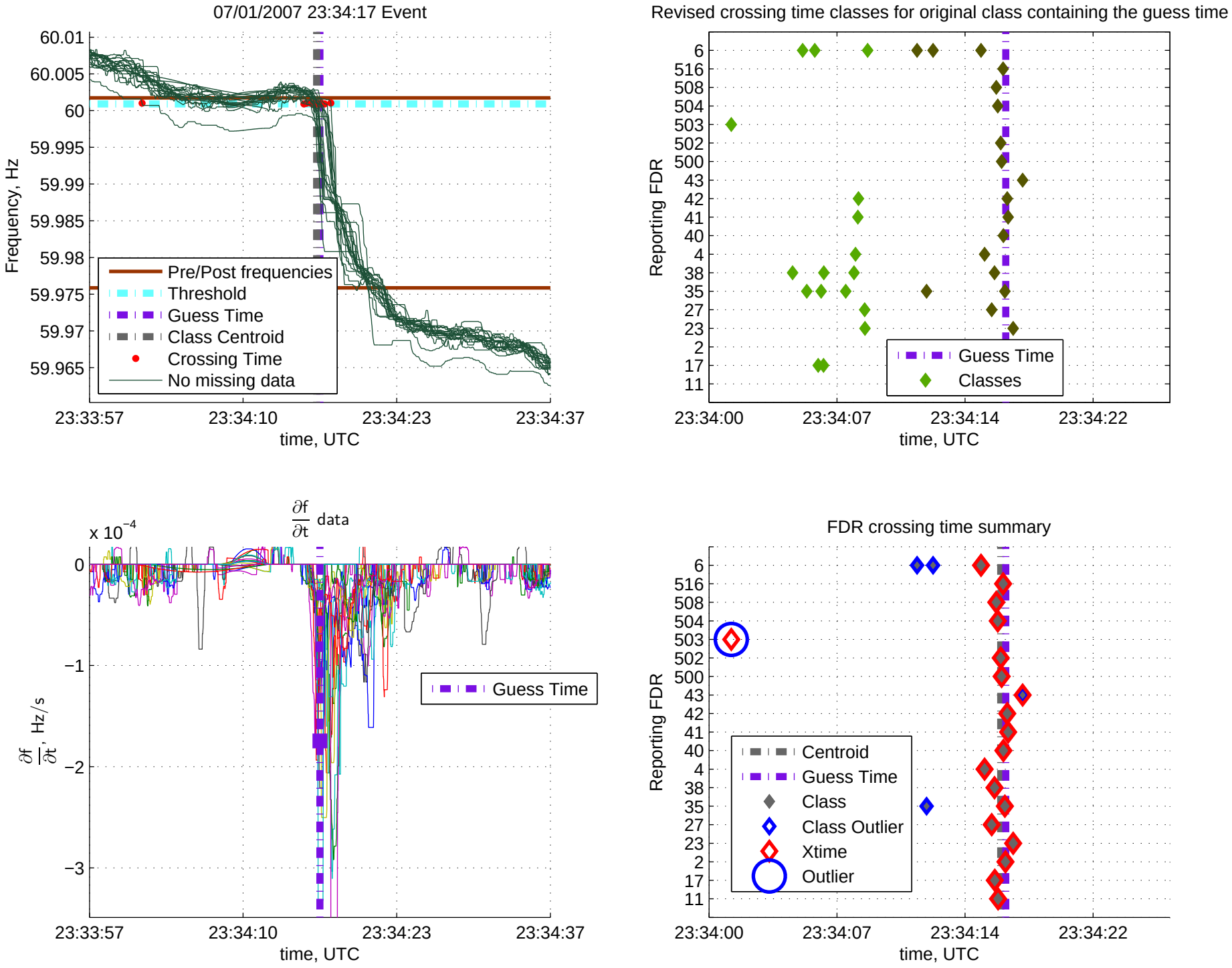
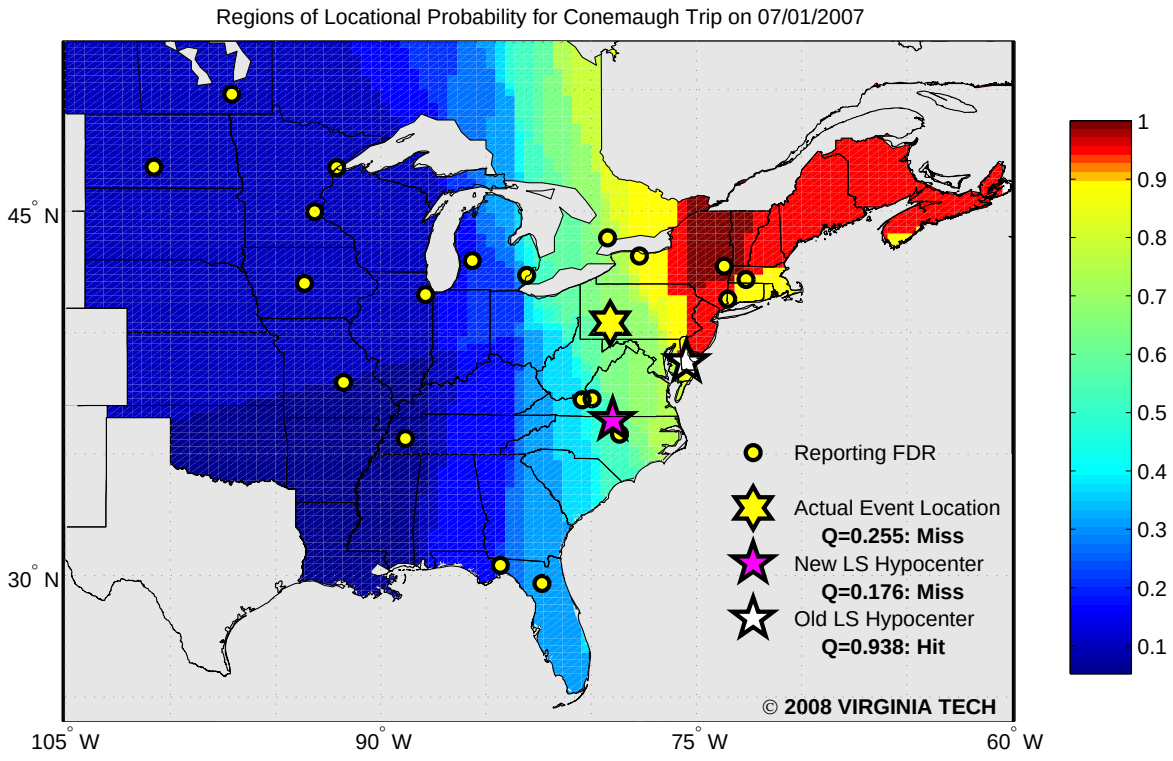
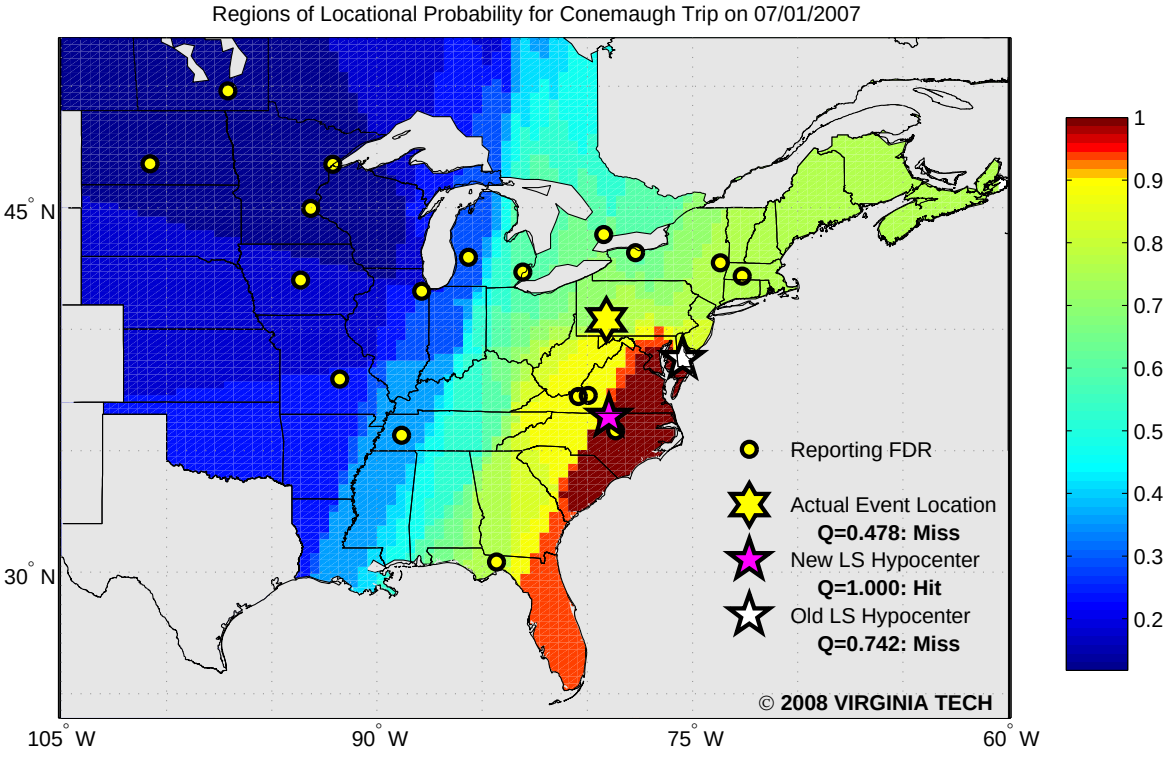


Figure D.76. Consolidated event ordering calculations: Conemaugh (850 MW, 40.3823°, −79.0968°) Trip on 07/01/2007 23:34:17



(a) Event location: old ordering method



(b) Event location: new ordering method

Figure D.77. Event location estimates: Conemaugh (850 MW, 40.3823°, −79.0968°) Trip on 07/01/2007 23:34:17

Table D.36. Ordering method comparison: Amos U3 (800 MW, 38.5072°, −81.8900°) Trip on 07/02/2007 16:49:46

	Old Ordering Method			New Ordering Method		
Mismatch estimate (MW)	1076			1106		
FDR Info	Number	Name	Distance (mi)	Number	Name	Distance (mi)
	4	VT	118.8	4	VT	118.8
	508	ROA	135.3	508	ROA	135.3
	11	Calvin	365.4	6	ABB	257
	6	ABB	257	11	Calvin	365.4
	500	Chicago	380.5	500	Chicago	380.5
	15	TVA3Nashville	313.5	15	TVA3Nashville	313.5
	2	UMR	537.2	17	TVA4Jackson	430.8
	17	TVA4Jackson	430.8	2	UMR	537.2
				503	Danbury	486.1
				502	Toronto	397.2
				516	LeRoy	388
				27	RPI	520.1
				42	FSU	575.5
				35	ISU	664
				38	ISONE	549.1
				40	MISOStPaul	731.2
				23	Duluth2	771
				43	Bismarck	1114
				41	Winnipeg	1081
LS estimate	Latitude	Longitude	Distance (mi)	Latitude	Longitude	Distance (mi)
	39.1575°	−82.4142°	53.06	38.9587°	−82.1235°	33.64
	Q_{old} = 1.0000			Q_{old} = 1.0000		
	Q_{new} = 1.0000			Q_{new} = 1.0000		
Parzen windowing results	Q_{actual} = 1.0000			Q_{actual} = 1.0000		

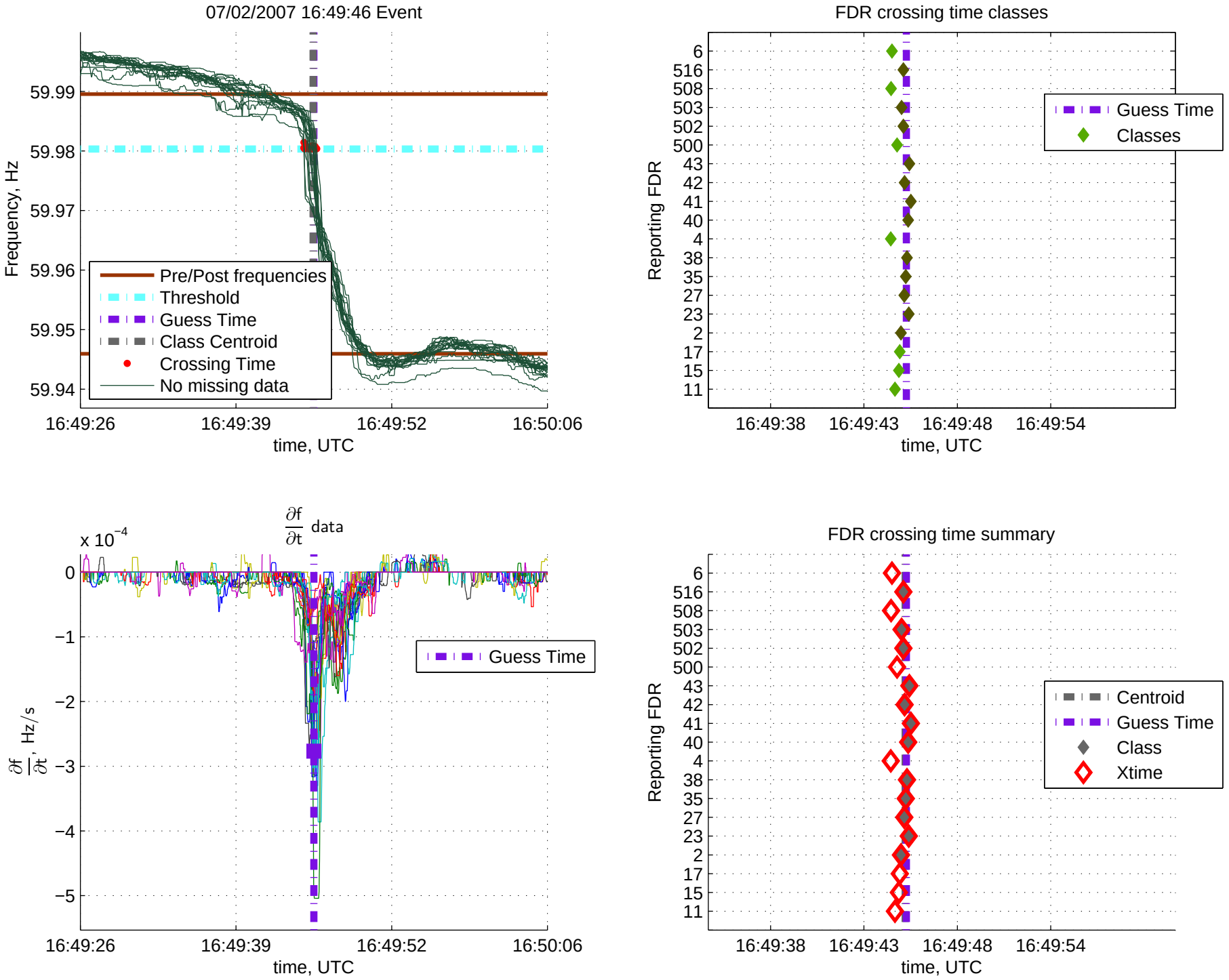
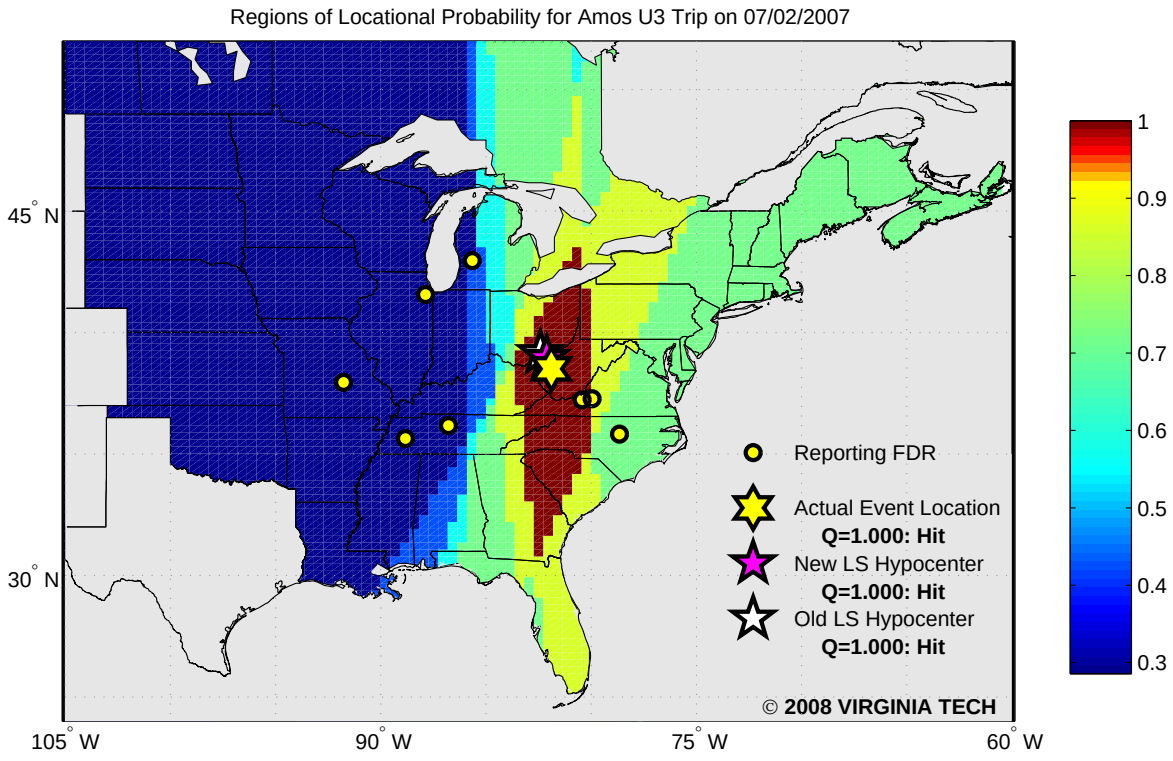
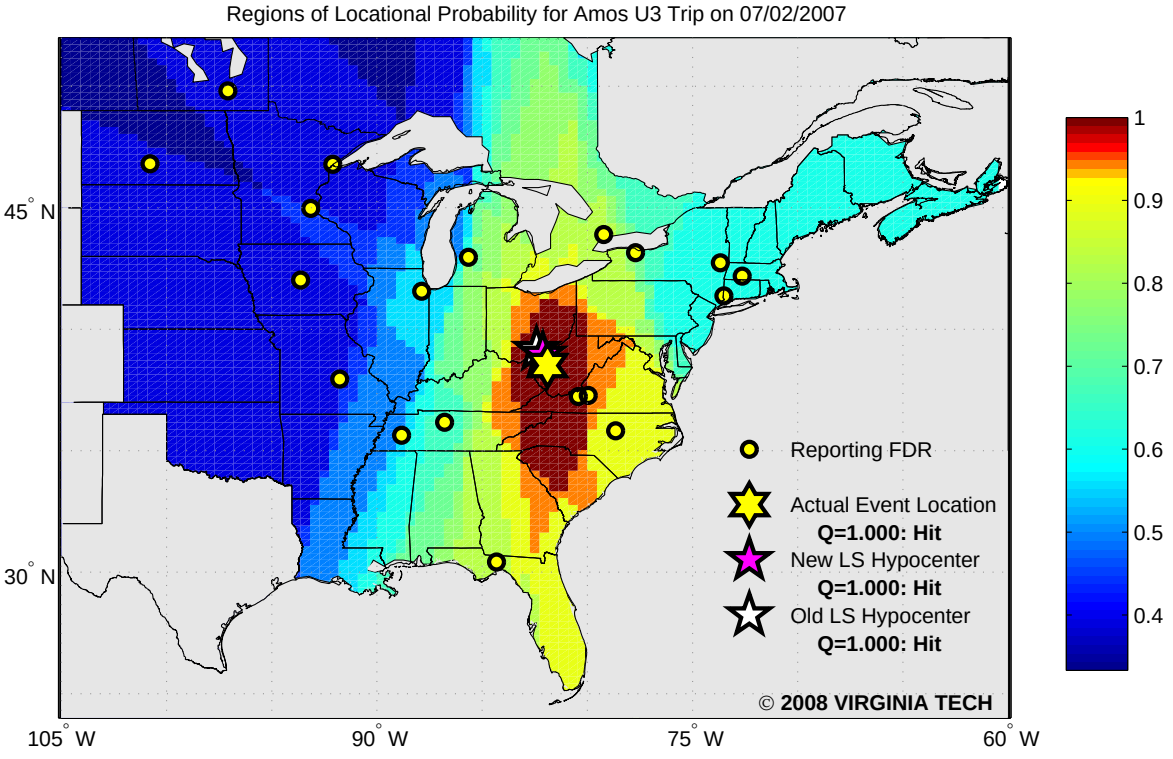


Figure D.78. Consolidated event ordering calculations: Amos U3 (800 MW, 38.5072°, −81.8900°) Trip on 07/02/2007 16:49:46



(a) Event location: old ordering method

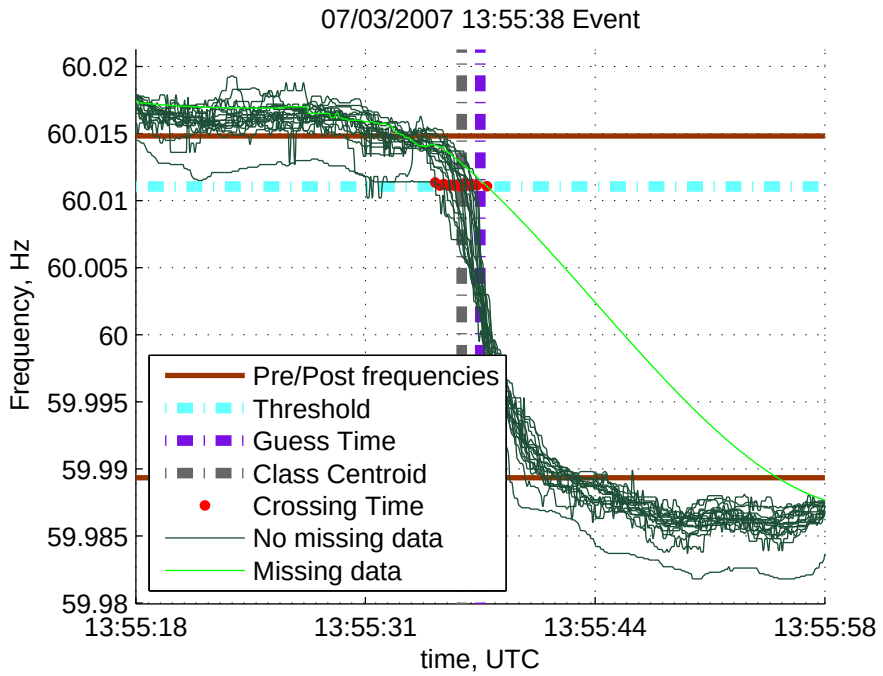


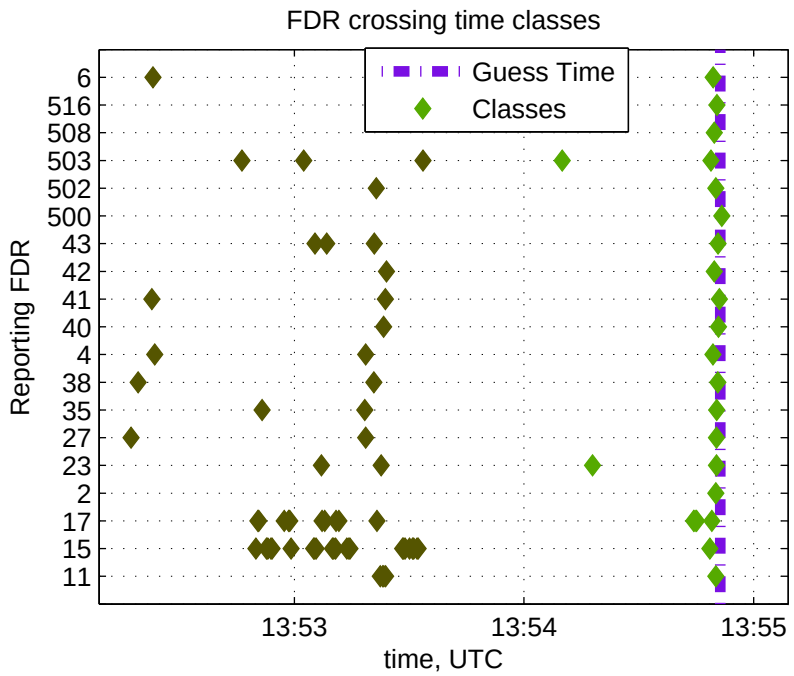
(b) Event location: new ordering method

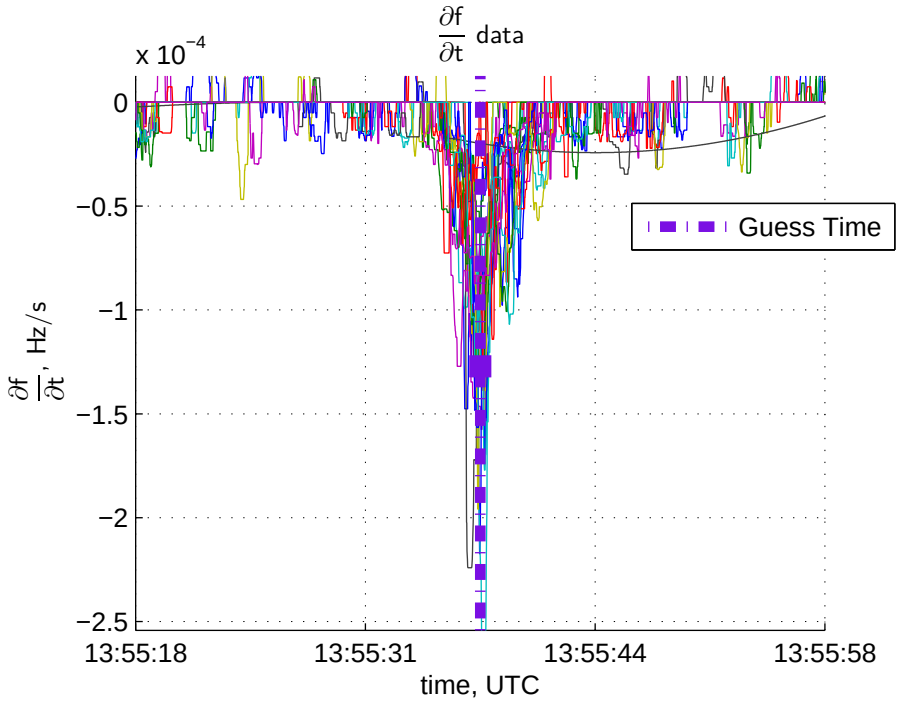
Figure D.79. Event location estimates: Amos U3 (800 MW, 38.5072°, −81.8900°) Trip on 07/02/2007 16:49:46

Table D.37. Ordering method comparison: Bull Run U1 (879 MW, 36.0188°, −84.1586°) Trip on 07/03/2007 13:55:38

	Old Ordering Method			New Ordering Method		
Mismatch estimate (MW)	663			640		
FDR Info	Number	Name	Distance (mi)	Number	Name	Distance (mi)
	500	Chicago	432.1	15	TVA3Nashville	147
	35	ISU	655.3	503	Danbury	682.6
	11	Calvin	486.2	17	TVA4Jackson	262.9
	9	UFL	450.9	4	VT	223.2
	503	Danbury	682.6	6	ABB	308
	27	RPI	726.2	42	FSU	386.9
	40	MISOStPaul	777.2	508	ROA	248.5
	17	TVA4Jackson	262.9	11	Calvin	486.2
	43	Bismarck	1135	502	Toronto	603.4
	42	FSU	386.9	2	UMR	440.4
	502	Toronto	603.4	27	RPI	726.2
	2	UMR	440.4	23	Duluth2	849.2
	560	Duluth	849.2	35	ISU	655.3
	38	ISONE	749.3	516	LeRoy	600.1
	41	Winnipeg	1152	38	ISONE	749.3
	4	VT	223.2	43	Bismarck	1135
	516	LeRoy	600.1	40	MISOStPaul	777.2
	508	ROA	248.5	41	Winnipeg	1152
	6	ABB	308			
	15	TVA3Nashville	147			
LS estimate	Latitude	Longitude	Distance (mi)	Latitude	Longitude	Distance (mi)
	38.5820°	−83.8531°	177.9	35.6046°	−84.7953°	45.74
	Q_{old} = 0.8087			Q_{old} = 0.7508		
	Q_{new} = 0.9659			Q_{new} = 1.0000		
Parzen windowing results	Q_{actual} = 0.4030			Q_{actual} = 1.0000		







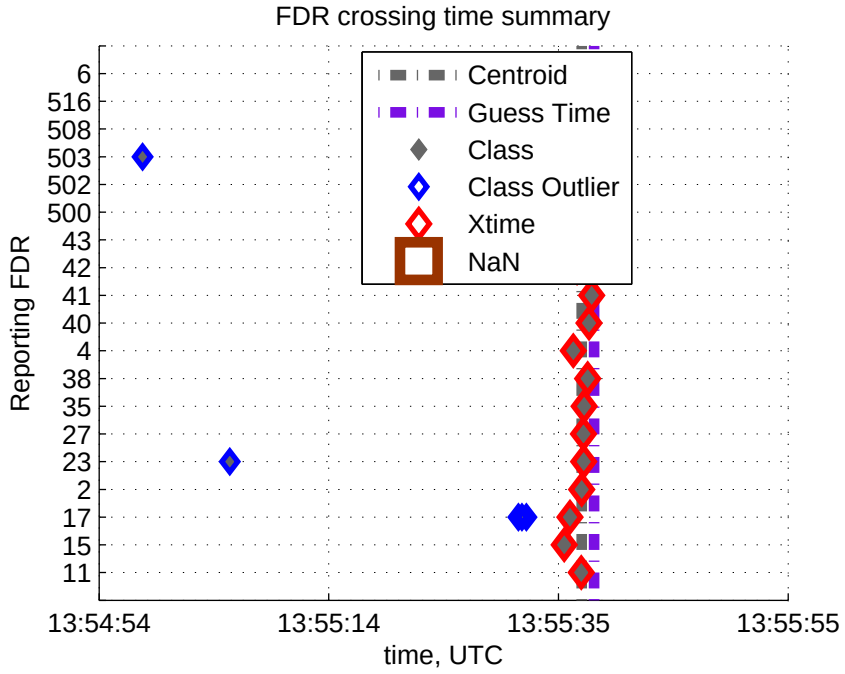
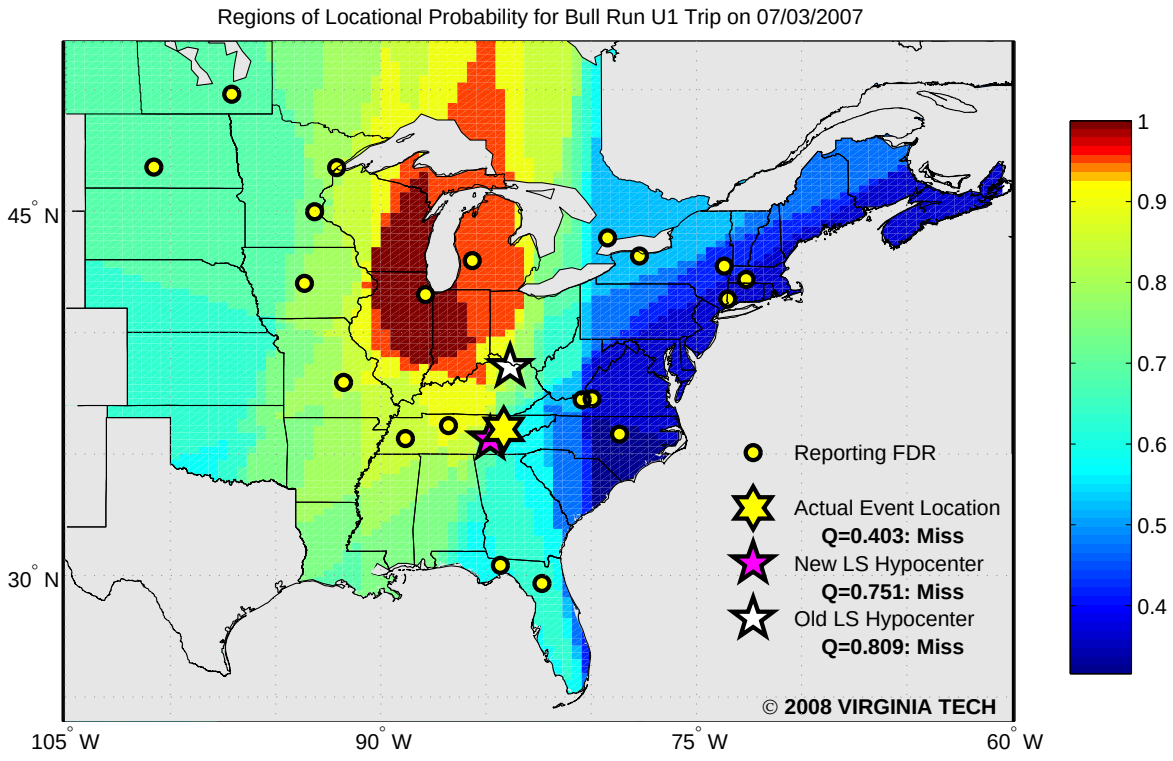
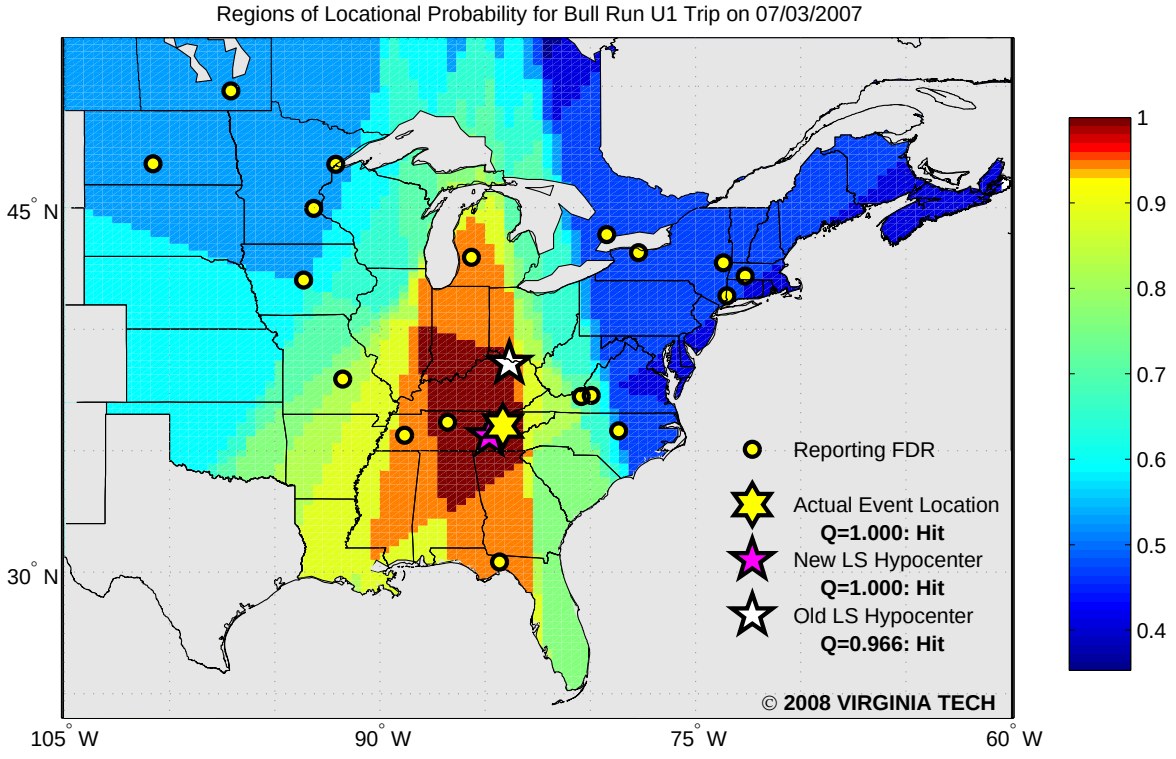


Figure D.80. Consolidated event ordering calculations: Bull Run U1 (879 MW, 36.0188°, −84.1586°) Trip on 07/03/2007 13:55:38



(a) Event location: old ordering method

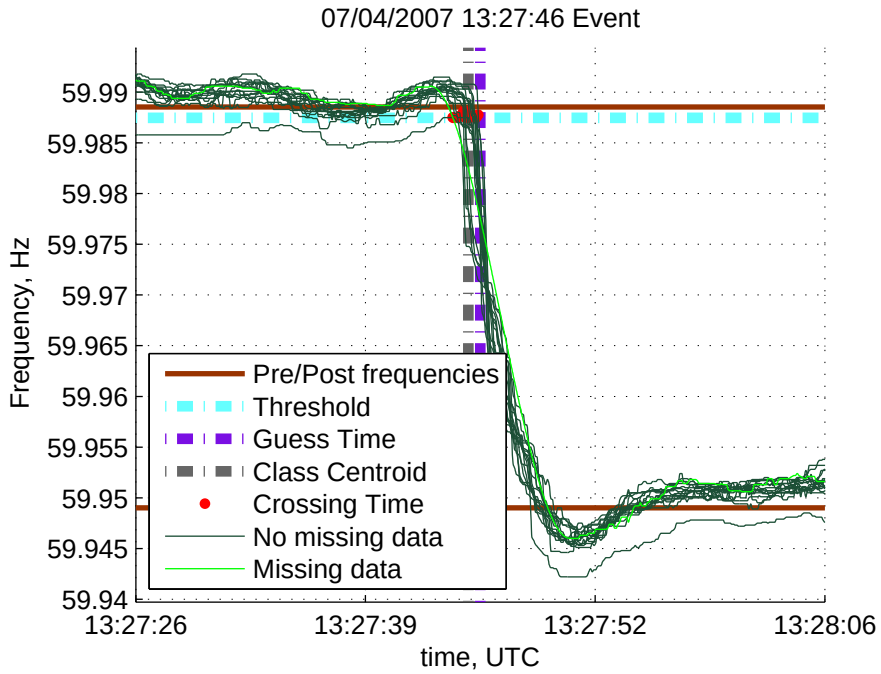


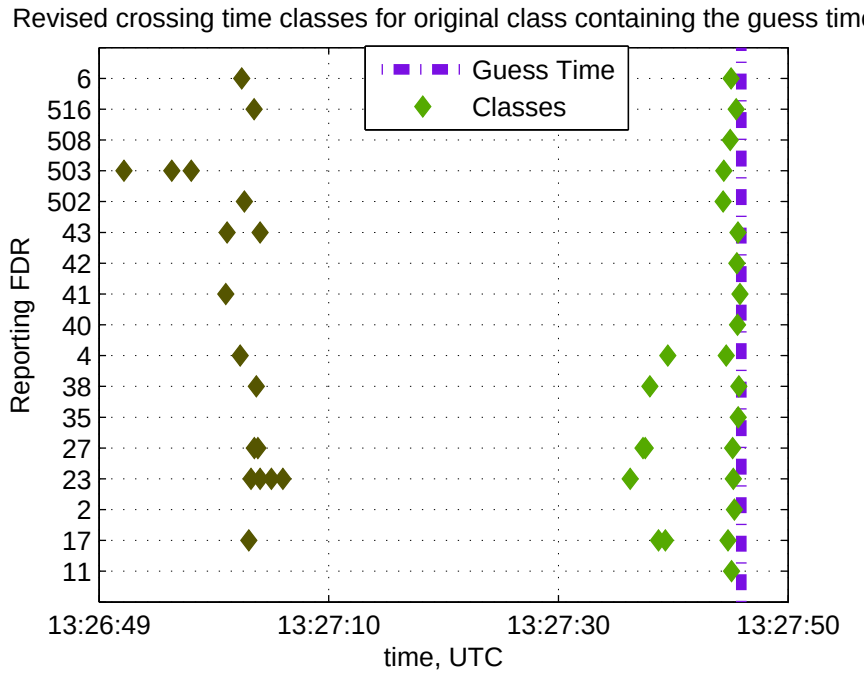
(b) Event location: new ordering method

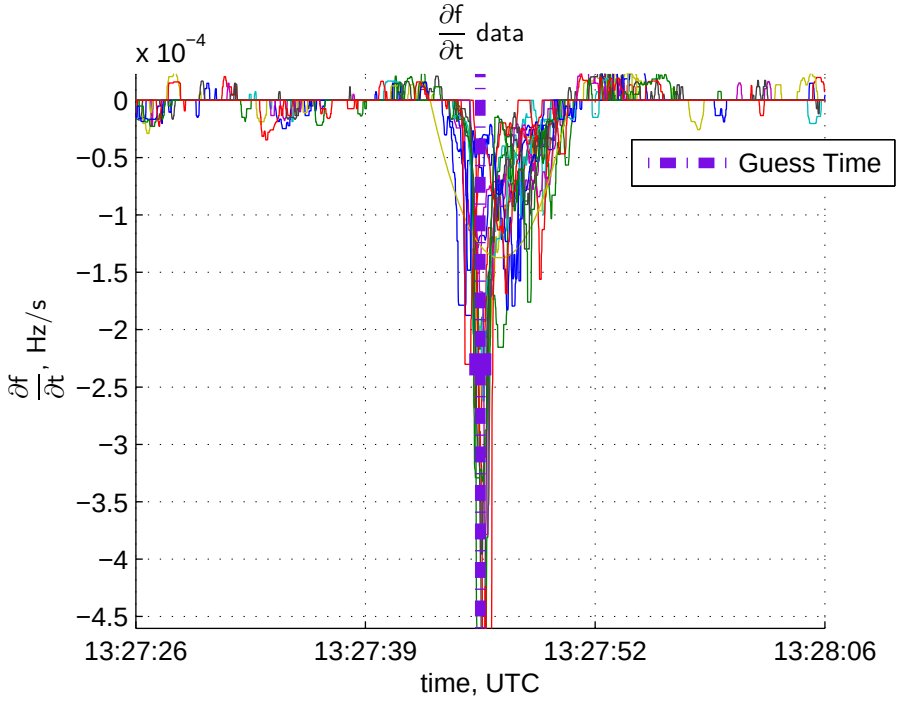
Figure D.81. Event location estimates: Bull Run U1 (879 MW, 36.0188°, −84.1586°) Trip on 07/03/2007 13:55:38

Table D.38. Ordering method comparison: Gavin U1 (1300 MW, 38.9587°, −82.1235°) Trip on 07/04/2007 13:27:46

	Old Ordering Method			New Ordering Method		
Mismatch estimate (MW)	1038			997		
FDR Info	Number	Name	Distance (mi)	Number	Name	Distance (mi)
	502	Toronto	372.7	503	Danbury	484.4
	4	VT	150.7	4	VT	150.7
	11	Calvin	332.3	17	TVA4Jackson	434.1
	6	ABB	288.3	508	ROA	165.3
	508	ROA	165.3	6	ABB	288.3
	27	RPI	512.5	11	Calvin	332.3
	503	Danbury	484.4	27	RPI	512.5
	17	TVA4Jackson	434.1	23	Duluth2	738.9
	2	UMR	526.1	2	UMR	526.1
	516	LeRoy	369.6	516	LeRoy	369.6
	9	UFL	641.6	42	FSU	602.9
	40	MISOStPaul	701.4	40	MISOStPaul	701.4
	35	ISU	639.8	43	Bismarck	1085
	42	FSU	602.9	35	ISU	639.8
	38	ISONE	545.1	38	ISONE	545.1
	43	Bismarck	1085	41	Winnipeg	1049
	41	Winnipeg	1049			
	560	Duluth	738.9			
LS estimate	Latitude	Longitude	Distance (mi)	Latitude	Longitude	Distance (mi)
	43.9634°	−78.3698°	396.6	41.0665°	−76.2443°	343.4
	$Q_{old} = 0.9203$			$Q_{old} = 0.8339$		
	$Q_{new} = 0.5730$			$Q_{new} = 0.8913$		
Parzen windowing results	$Q_{actual} = 0.8102$			$Q_{actual} = 0.1718$		







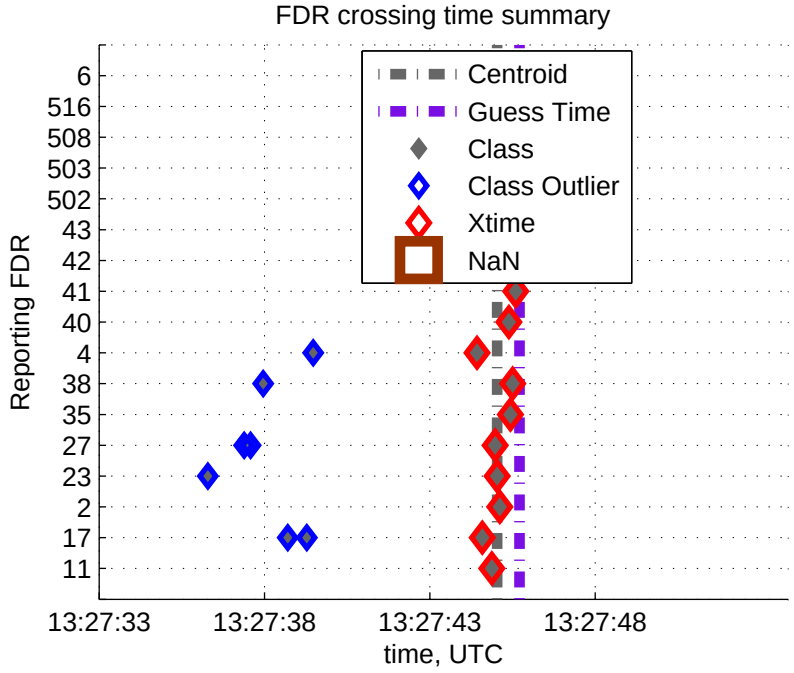
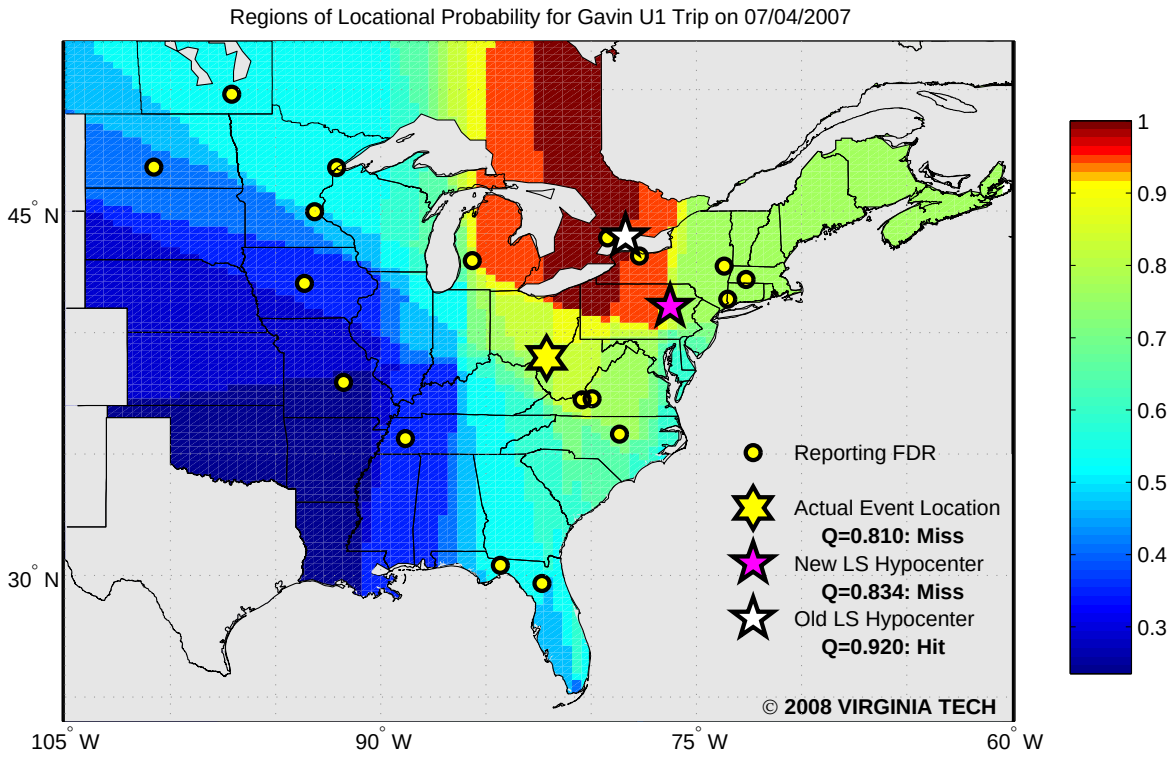
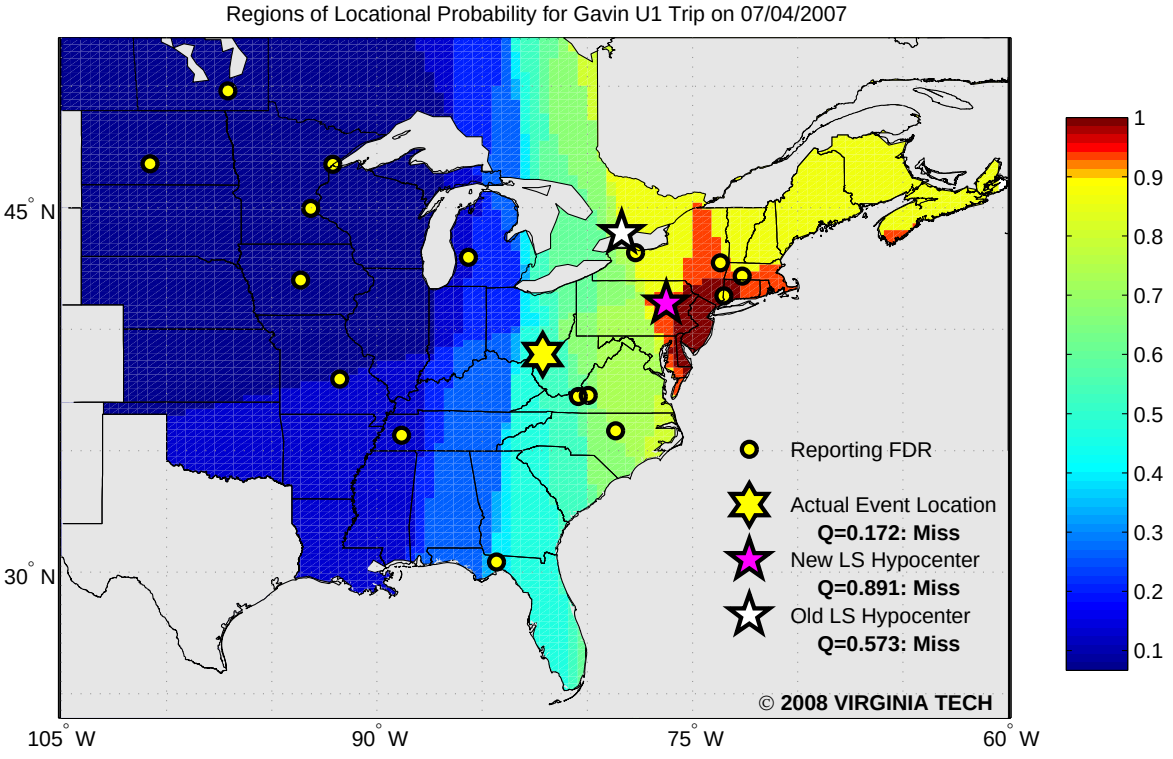


Figure D.82. Consolidated event ordering calculations: Gavin U1 (1300 MW, 38.9587°, −82.1235°) Trip on 07/04/2007 13:27:46



(a) Event location: old ordering method



(b) Event location: new ordering method

Figure D.83. Event location estimates: Gavin U1 (1300 MW, 38.9587°, −82.1235°) Trip on 07/04/2007 13:27:46

Table D.39. Ordering method comparison: Iatan (651 MW, 39.4453°, −94.9145°) Trip on 07/07/2007 20:37:56

	Old Ordering Method			New Ordering Method		
Mismatch estimate (MW)	570			551		
FDR Info	Number	Name	Distance (mi)	Number	Name	Distance (mi)
	35	ISU	190.5	23	Duluth2	526.7
	43	Bismarck	588.3	17	TVA4Jackson	424.7
	40	MISOStPaul	392.4	35	ISU	190.5
	41	Winnipeg	724	43	Bismarck	588.3
	560	Duluth	526.7	2	UMR	198.8
	17	TVA4Jackson	424.7	40	MISOStPaul	392.4
	6	ABB	922.6	41	Winnipeg	724
	508	ROA	823	11	Calvin	538.7
	4	VT	798.9	4	VT	798.9
	503	Danbury	1131	42	FSU	864.2
	42	FSU	864.2	6	ABB	922.6
	502	Toronto	864.5	508	ROA	823
	9	UFL	982	38	ISONE	1177
	11	Calvin	538.7	502	Toronto	864.5
	516	LeRoy	927	516	LeRoy	927
	38	ISONE	1177			
	2	UMR	198.8			
LS estimate	Latitude	Longitude	Distance (mi)	Latitude	Longitude	Distance (mi)
	43.4015°	−97.0531°	294.9	46.7872°	−92.0990°	526.7
	Q_{old} = 1.0000			Q_{old} = 0.7564		
	Q_{new} = 0.7460			Q_{new} = 1.0000		
Parzen windowing results	Q_{actual} = 1.0000			Q_{actual} = 0.8170		

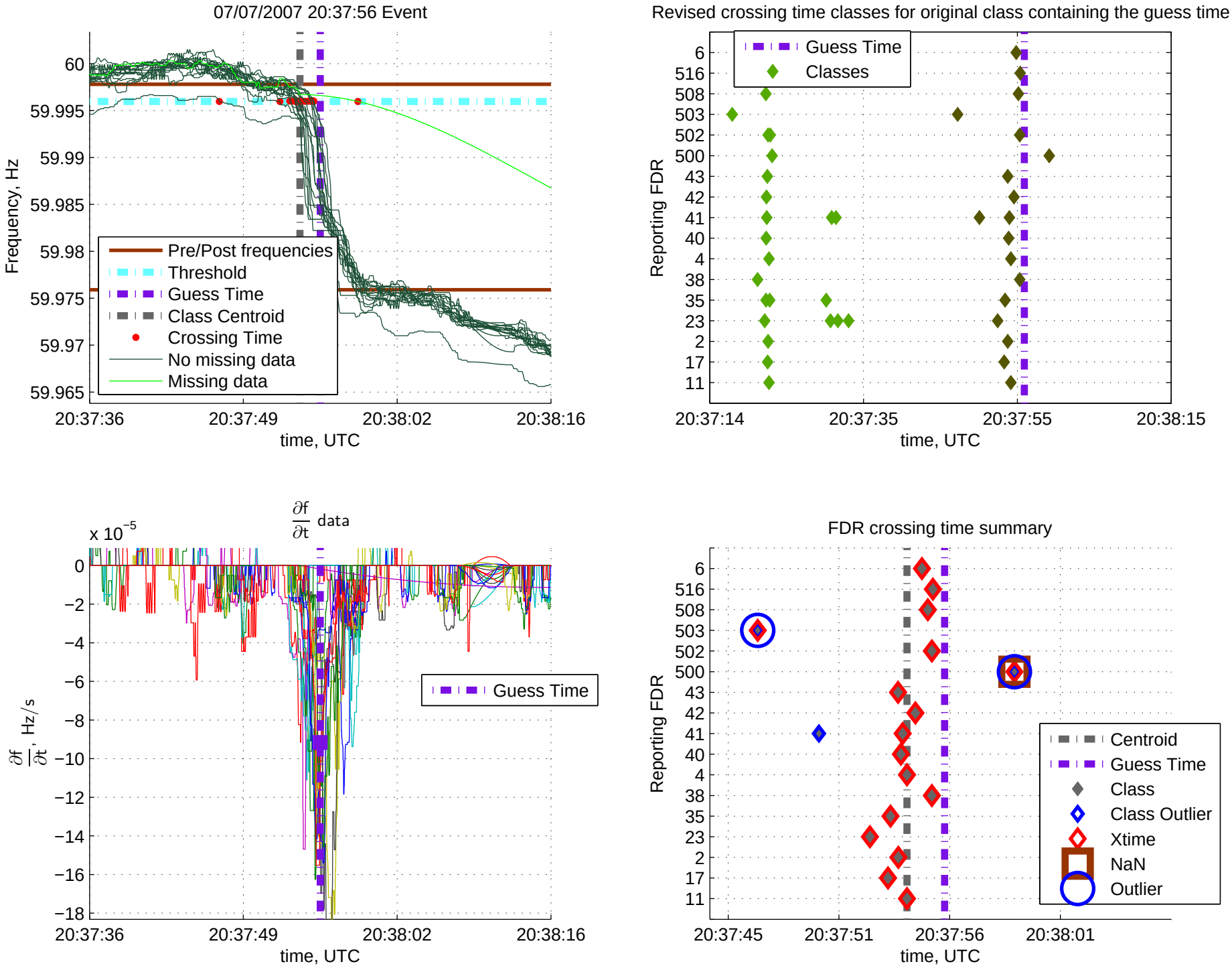
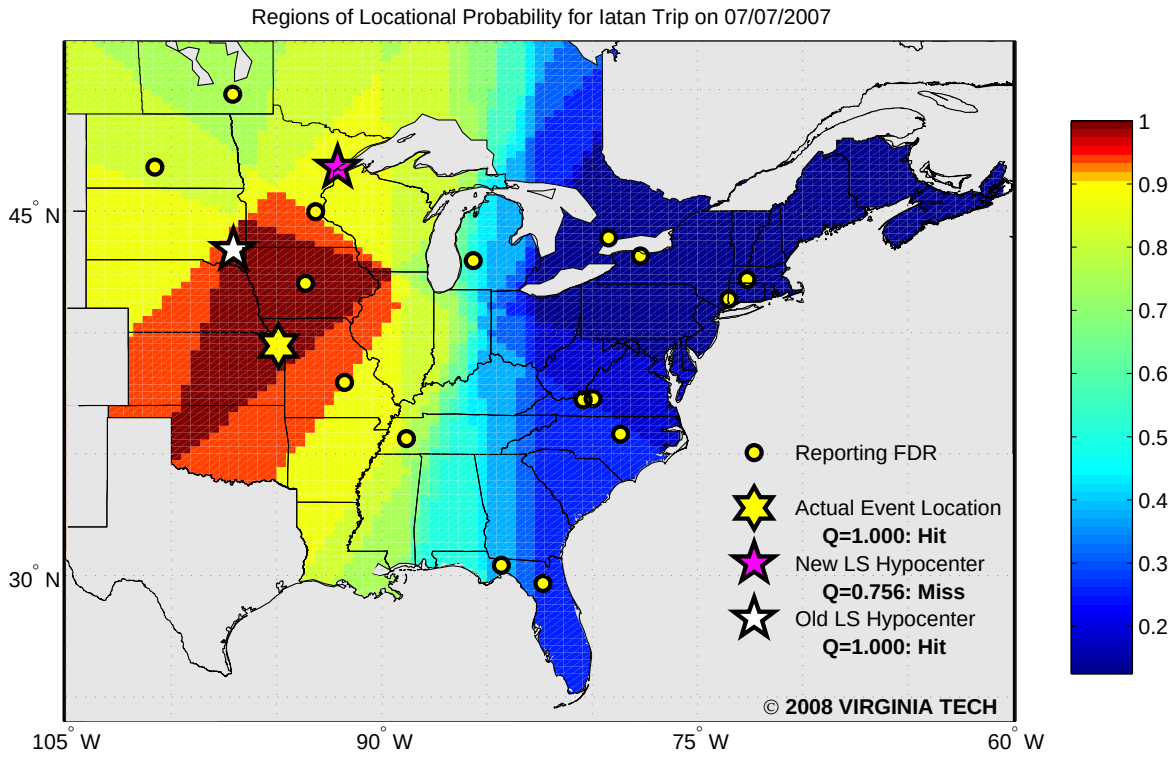
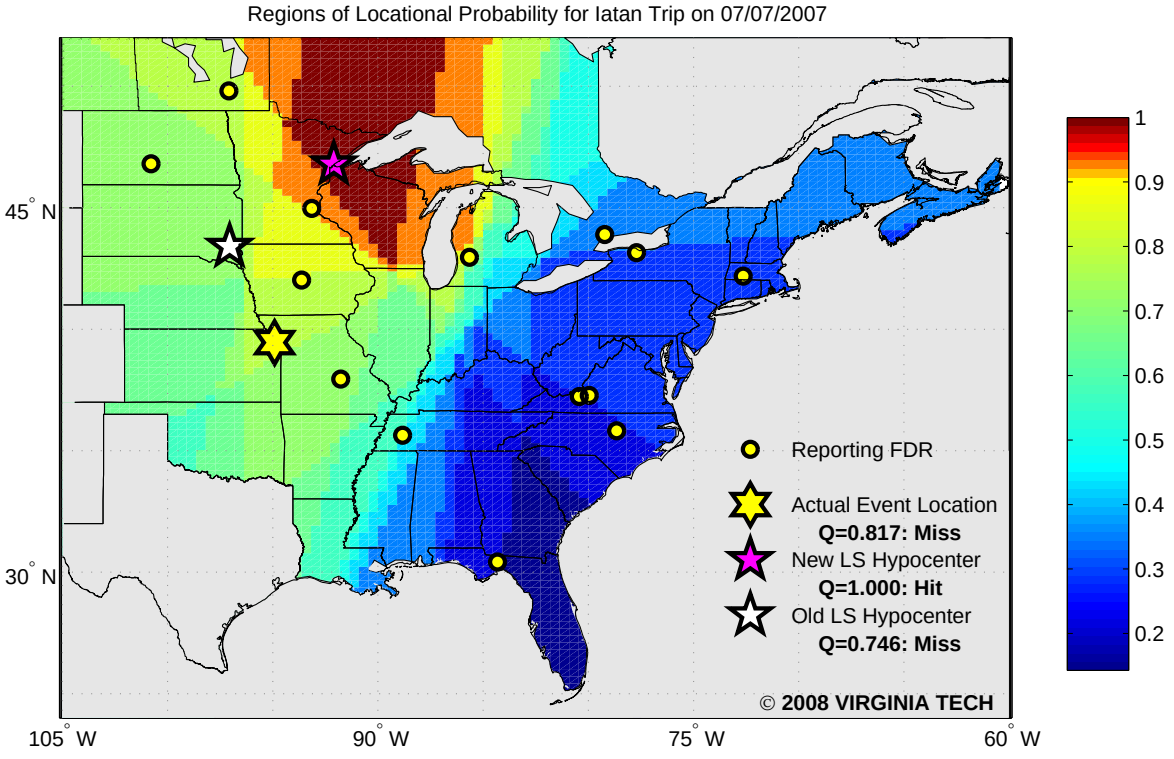


Figure D.84. Consolidated event ordering calculations: Iatan (651 MW, 39.4453°, −94.9145°) Trip on 07/07/2007 20:37:56



(a) Event location: old ordering method

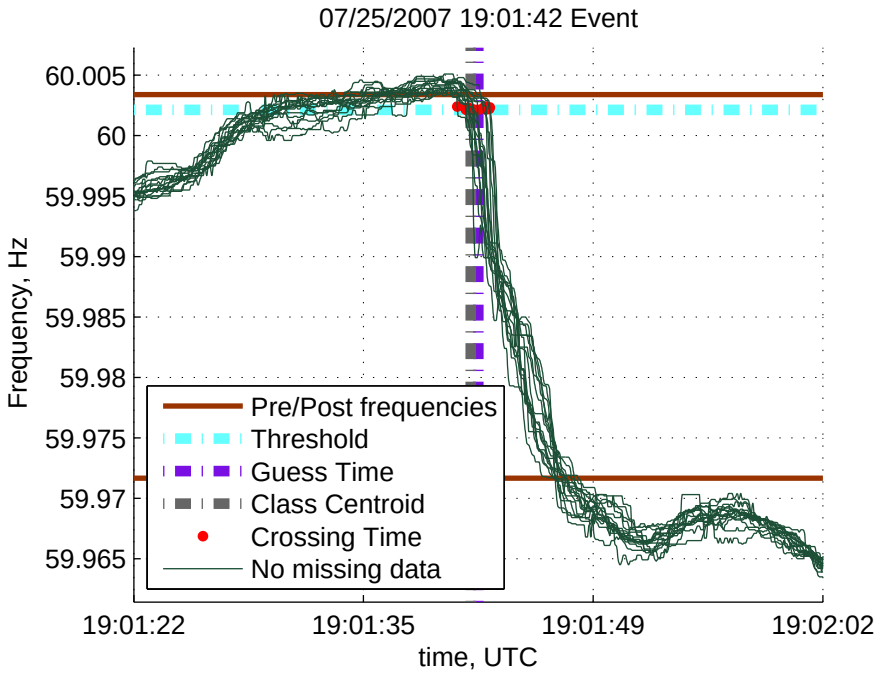


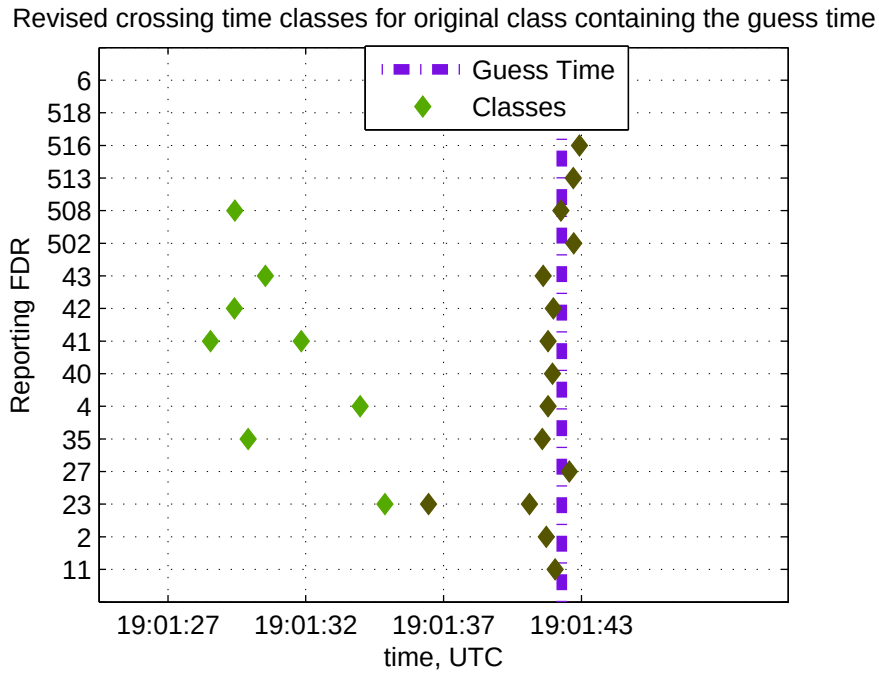
(b) Event location: new ordering method

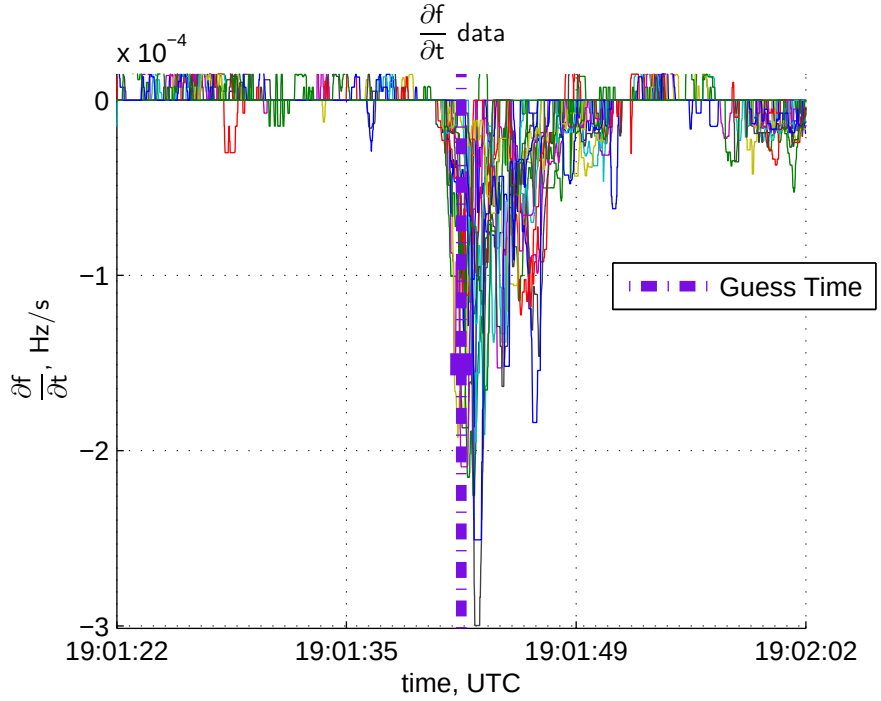
Figure D.85. Event location estimates: Iatan (651 MW, 39.4453°, –94.9145°) Trip on 07/07/2007 20:37:56

Table D.40. Ordering method comparison: Baldwin (595 MW, 38.1764°, −89.8265°) Trip on 07/25/2007 19:01:42

	Old Ordering Method			New Ordering Method		
Mismatch estimate (MW)	872			804		
FDR Info	Number	Name	Distance (mi)	Number	Name	Distance (mi)
	2	UMR	106.7	23	Duluth2	606
	35	ISU	333	35	ISU	333
	11	Calvin	396.4	6	ABB	636.9
	4	VT	517.6	43	Bismarck	815.5
	6	ABB	636.9	2	UMR	106.7
	40	MISOStPaul	499.8	4	VT	517.6
	560	Duluth	606	41	Winnipeg	880.1
	43	Bismarck	815.5	40	MISOStPaul	499.8
	42	FSU	621	42	FSU	621
	41	Winnipeg	880.1	11	Calvin	396.4
	508	ROA	542.6	508	ROA	542.6
	9	UFL	727.1	27	RPI	903.9
	502	Toronto	678.4	513	PSU	662.5
	513	PSU	662.5	502	Toronto	678.4
	518	NERC	823.4	518	NERC	823.4
	27	RPI	903.9	516	LeRoy	720.9
	516	LeRoy	720.9			
LS estimate	Latitude	Longitude	Distance (mi)	Latitude	Longitude	Distance (mi)
	34.9778°	−90.1490°	221.7	46.7872°	−92.0990°	606
	$Q_{old} = 1.0000$			$Q_{old} = 0.5421$		
	$Q_{new} = 0.5552$			$Q_{new} = 1.0000$		
Parzen windowing results	$Q_{actual} = 1.0000$			$Q_{actual} = 0.7115$		







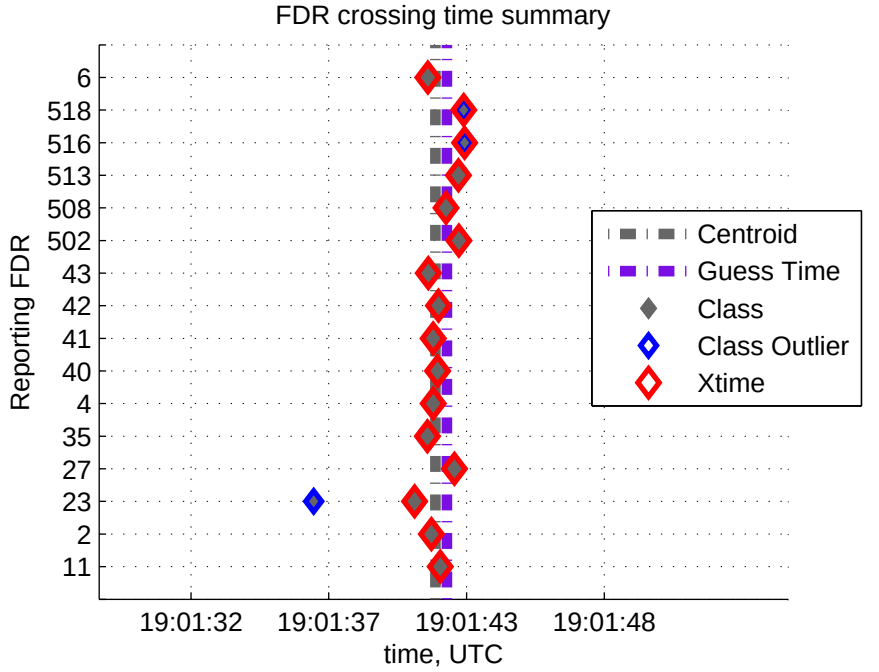
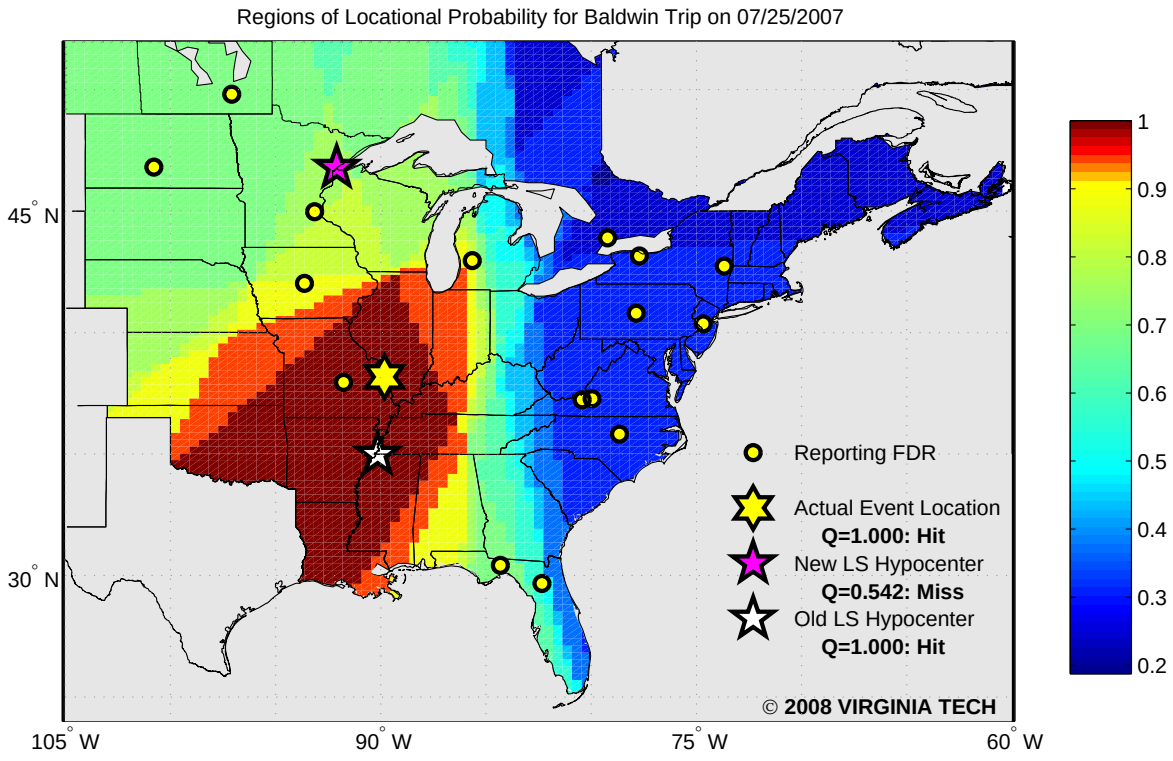
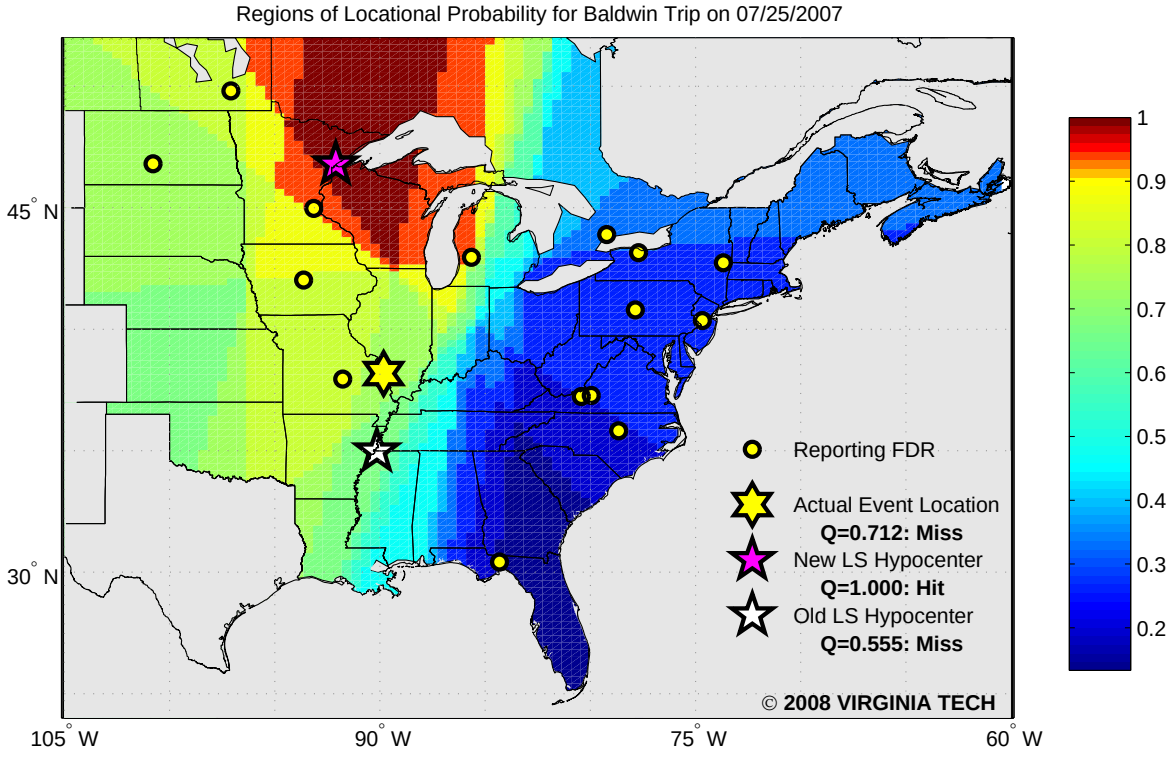


Figure D.86. Consolidated event ordering calculations: Baldwin (595 MW, 38.1764°, −89.8265°) Trip on 07/25/2007 19:01:42



(a) Event location: old ordering method



(b) Event location: new ordering method

Figure D.87. Event location estimates: Baldwin (595 MW, 38.1764°, −89.8265°) Trip on 07/25/2007 19:01:42

Table D.41. Ordering method comparison: Rockport (2600 MW, 37.8858°, −87.0770°) Trip on 08/04/2007 21:44:17

	Old Ordering Method			New Ordering Method		
Mismatch estimate (MW)	2387			2532		
FDR Info	Number	Name	Distance (mi)	Number	Name	Distance (mi)
	510	Blacksburg	369.7	4	VT	366.9
	508	ROA	391.9	510	Blacksburg	369.7
	4	VT	366.9	508	ROA	391.9
	500	Chicago	257.5	500	Chicago	257.5
	11	Calvin	358.5	20	TVA2Huntsville	221.1
	20	TVA2Huntsville	221.1	35	ISU	449.2
	35	ISU	449.2	11	Calvin	358.5
	40	MISOStPaul	581.5	513	PSU	531.4
	513	PSU	531.4	40	MISOStPaul	581.5
	6	ABB	486.6	6	ABB	486.6
	43	Bismarck	930.4	42	FSU	539.3
	42	FSU	539.3	43	Bismarck	930.4
	502	Toronto	583.1	518	NERC	685.8
	41	Winnipeg	961.1	502	Toronto	583.1
	516	LeRoy	611.1	27	RPI	780.3
	9	UFL	629.1	41	Winnipeg	961.1
	27	RPI	780.3	516	LeRoy	611.1
	518	NERC	685.8	38	ISONE	818.3
	38	ISONE	818.3			
LS estimate	Latitude	Longitude	Distance (mi)	Latitude	Longitude	Distance (mi)
	34.6454°	−80.2550°	440.9	37.2327°	−80.4284°	366.9
	Q_{old} = 0.9990			Q_{old} = 0.9990		
	Q_{new} = 0.9592			Q_{new} = 1.0000		
Parzen windowing results	Q_{actual} = 0.7570			Q_{actual} = 0.7833		

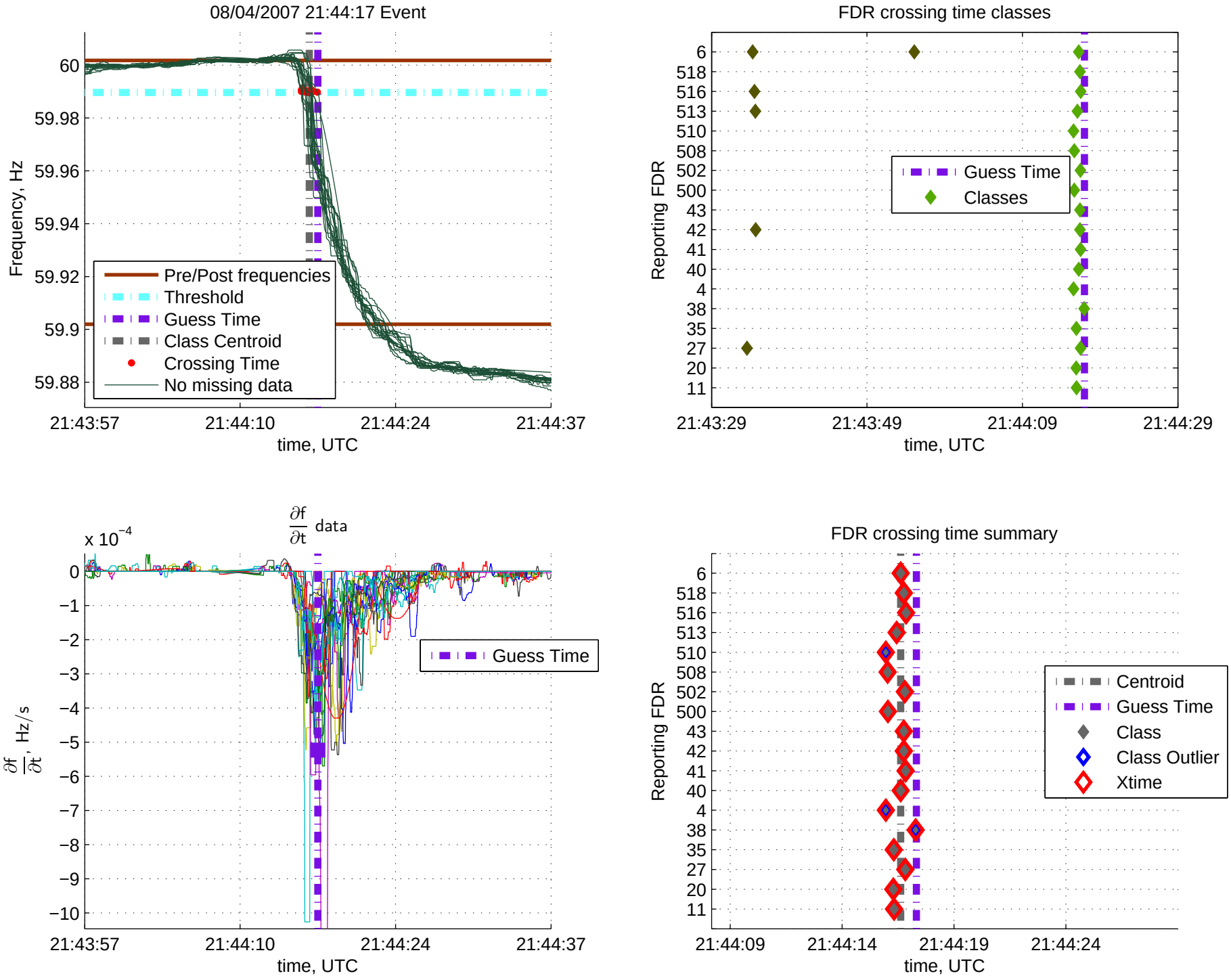
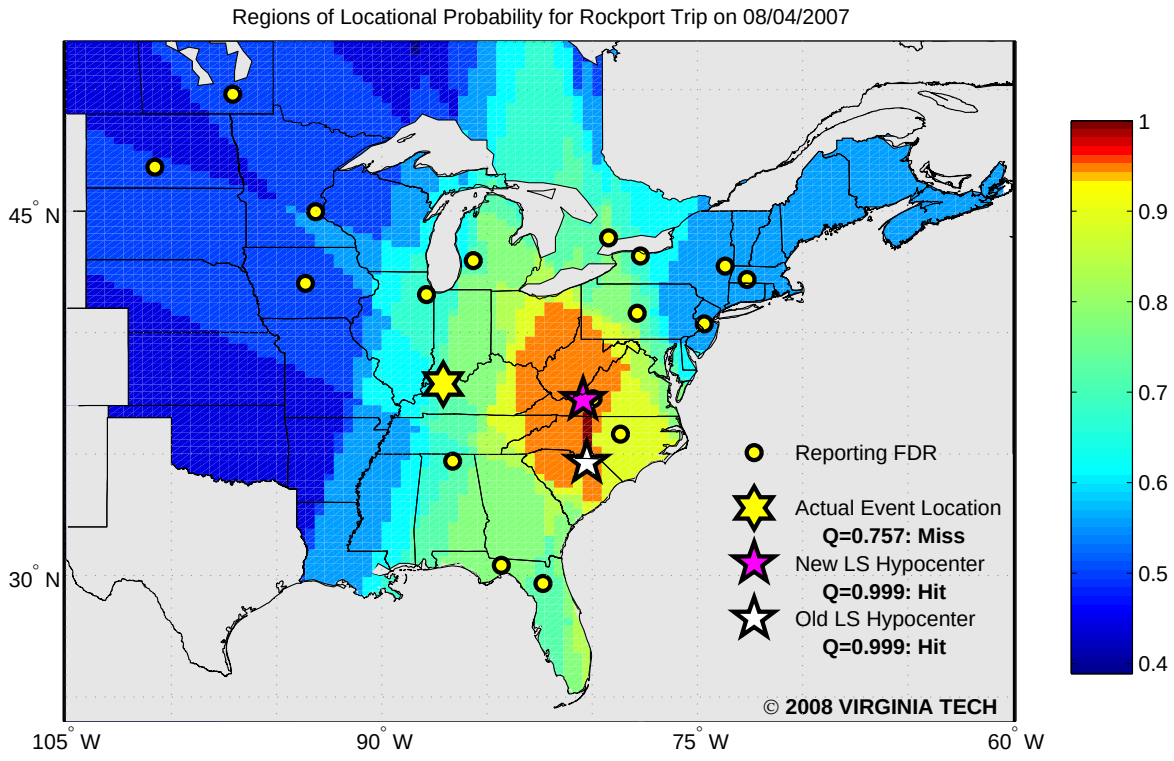
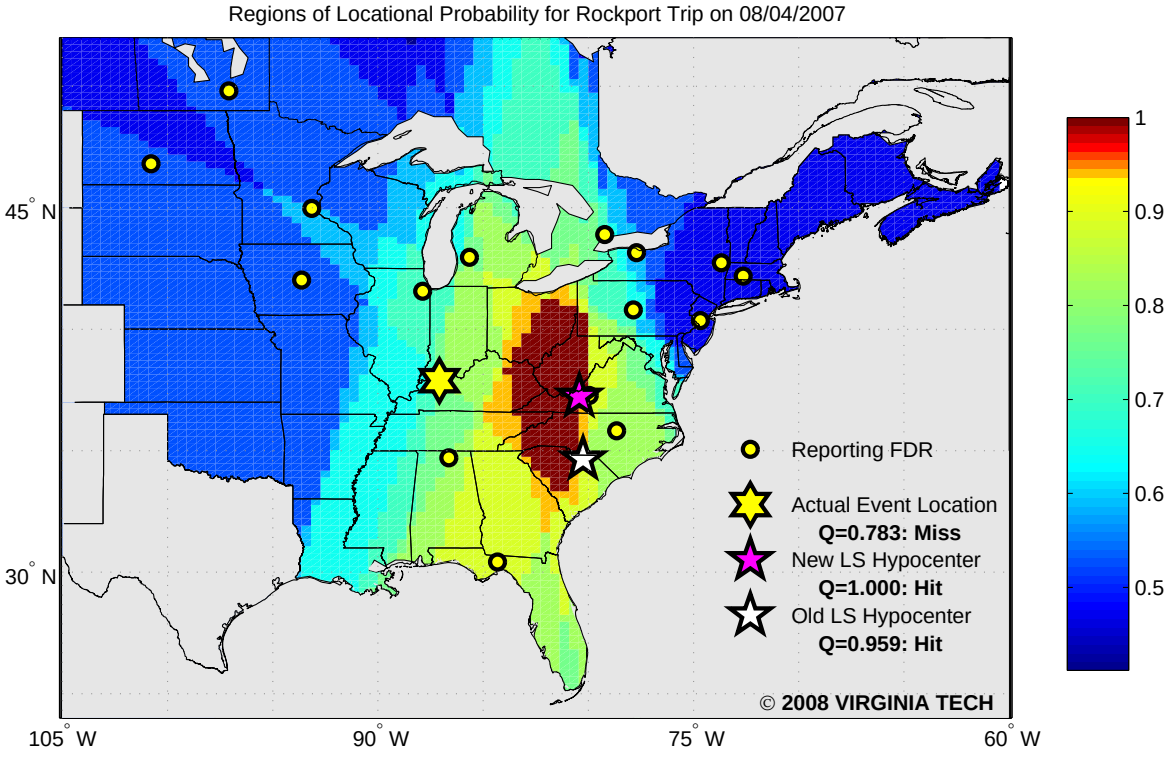


Figure D.88. Consolidated event ordering calculations: Rockport (2600 MW, 37.8858°, −87.0770°) Trip on 08/04/2007 21:44:17



(a) Event location: old ordering method



(b) Event location: new ordering method

Figure D.89. Event location estimates: Rockport (2600 MW, 37.8858°, −87.0770°) Trip on 08/04/2007 21:44:17

Table D.42. Ordering method comparison: Salem U2 (1130 MW, 39.4956°, −75.4733°) Trip on 08/06/2007 17:11:24

	Old Ordering Method			New Ordering Method		
Mismatch estimate (MW)	952			907		
FDR Info	Number	Name	Distance (mi)	Number	Name	Distance (mi)
	518	NERC	73	27	RPI	242.5
	513	PSU	154.9	518	NERC	73
	27	RPI	242.5	513	PSU	154.9
	4	VT	310.6	508	ROA	287.1
	510	Blacksburg	308.5	510	Blacksburg	308.5
	508	ROA	287.1	4	VT	310.6
	516	LeRoy	278	516	LeRoy	278
	6	ABB	307.8	11	Calvin	580.3
	502	Toronto	360.3	502	Toronto	360.3
	11	Calvin	580.3	514	FarrisSabrina	494.2
	514	FarrisSabrina	494.2	42	FSU	801.6
	20	TVA2Huntsville	697.3	20	TVA2Huntsville	697.3
	35	ISU	964	35	ISU	964
	9	UFL	782.3	40	MISOStPaul	977.5
	42	FSU	801.6	41	Winnipeg	1272
	43	Bismarck	1365	43	Bismarck	1365
	41	Winnipeg	1272			
	40	MISOStPaul	977.5			
LS estimate	Latitude	Longitude	Distance (mi)	Latitude	Longitude	Distance (mi)
	39.6950°	−75.6041°	15.44	43.8719°	−77.2786°	316.4
	Q_{old} = 1.0000			Q_{old} = 0.3221		
	Q_{new} = 0.2895			Q_{new} = 0.2213		
Parzen windowing results	Q_{actual} = 1.0000			Q_{actual} = 0.2895		

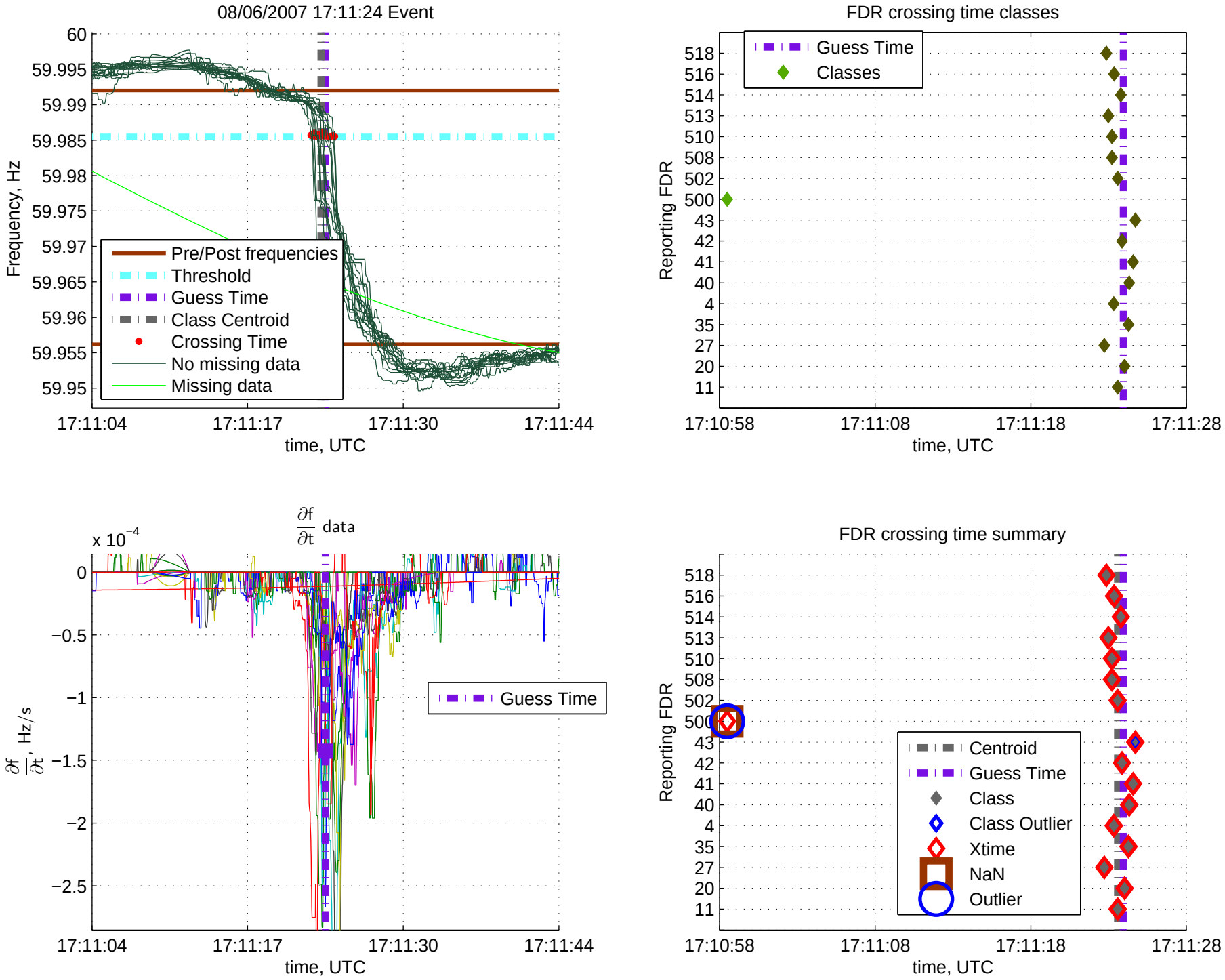
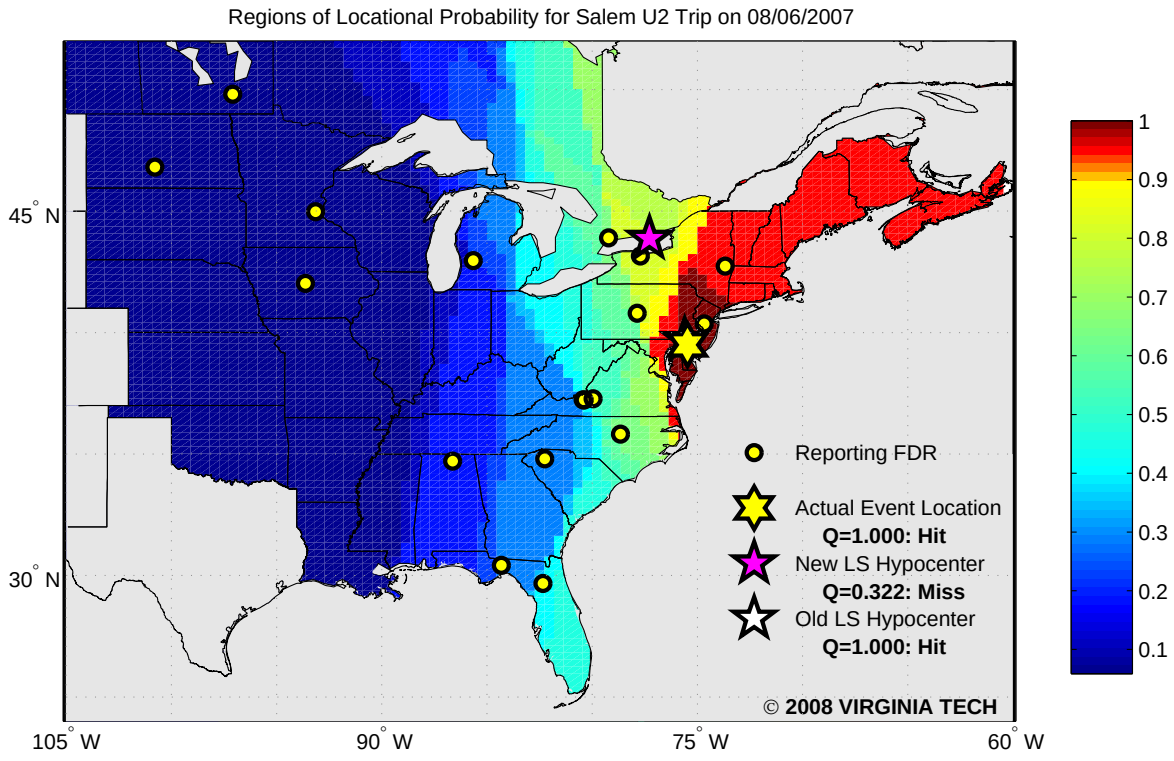
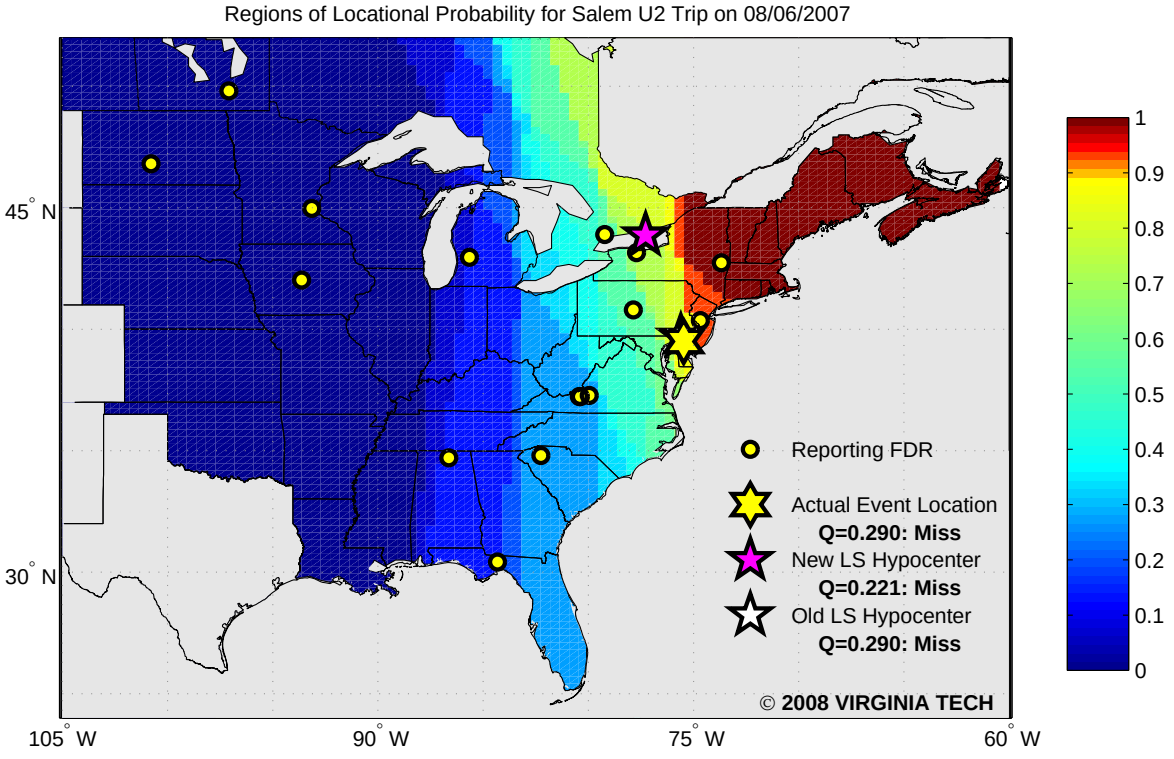


Figure D.90. Consolidated event ordering calculations: Salem U2 (1130 MW, 39.4956°, −75.4733°) Trip on 08/06/2007 17:11:24



(a) Event location: old ordering method

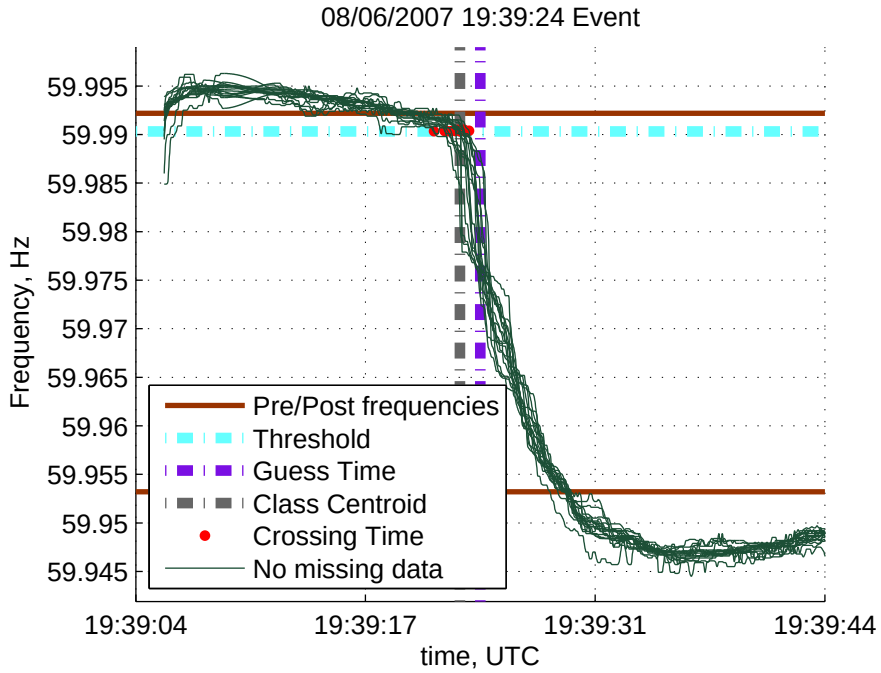


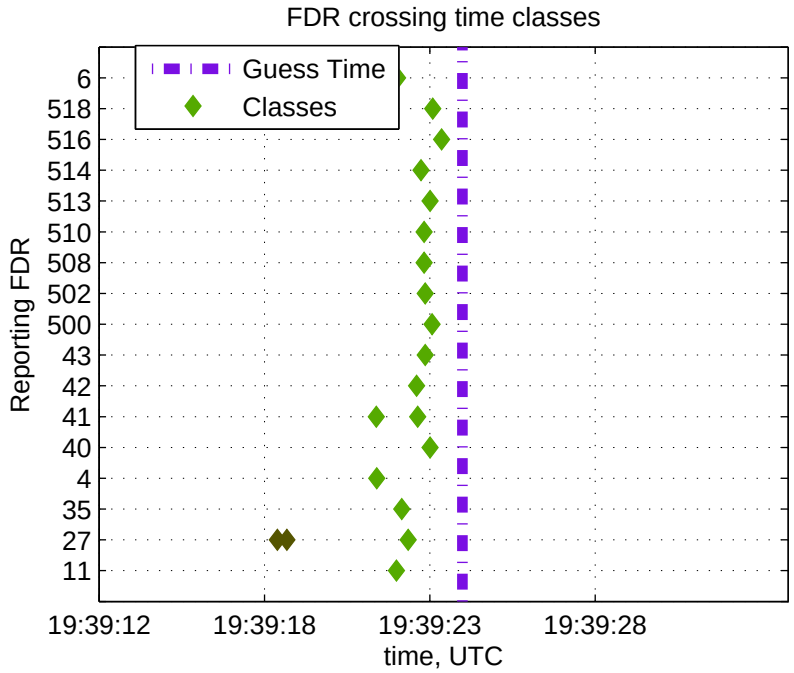
(b) Event location: new ordering method

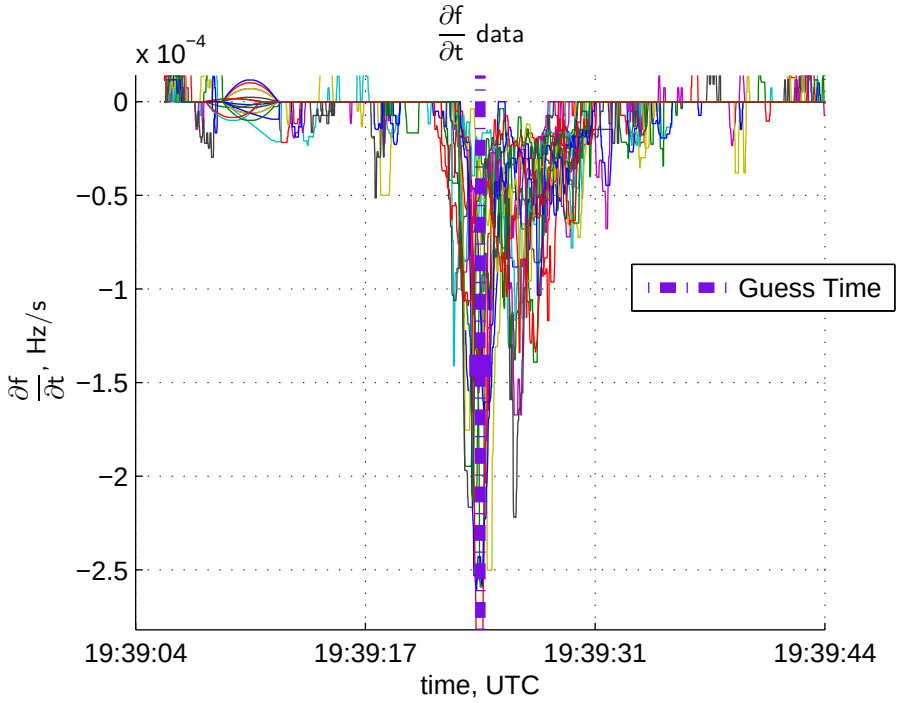
Figure D.91. Event location estimates: Salem U2 (1130 MW, 39.4956°, −75.4733°) Trip on 08/06/2007 17:11:24

Table D.43. Ordering method comparison: Amos U3 (1300MW capacity) (1300 MW, 38.5072°, −81.8900°) Trip on 08/06/2007 19:39:24

	Old Ordering Method			New Ordering Method		
Mismatch estimate (MW)	1037			984		
FDR Info	Number	Name	Distance (mi)	Number	Name	Distance (mi)
	4	VT	118.8	4	VT	118.8
	510	Blacksburg	121	11	Calvin	365.4
	508	ROA	135.3	6	ABB	257
	6	ABB	257	35	ISU	664
	11	Calvin	365.4	27	RPI	520.1
	500	Chicago	380.5	42	FSU	575.5
	513	PSU	266.1	41	Winnipeg	1081
	514	FarrisSabrina	256.6	514	FarrisSabrina	256.6
	518	NERC	405.6	508	ROA	135.3
	502	Toronto	397.2	510	Blacksburg	121
	42	FSU	575.5	43	Bismarck	1114
	27	RPI	520.1	502	Toronto	397.2
	516	LeRoy	388	40	MISOStPaul	731.2
	9	UFL	610.8	513	PSU	266.1
	40	MISOStPaul	731.2	500	Chicago	380.5
	35	ISU	664	518	NERC	405.6
	41	Winnipeg	1081	516	LeRoy	388
	43	Bismarck	1114			
LS estimate	Latitude	Longitude	Distance (mi)	Latitude	Longitude	Distance (mi)
	39.0454°	−81.8550°	37.24	38.9587°	−82.1235°	33.64
	Q_{old} = 1.0000			Q_{old} = 1.0000		
	Q_{new} = 1.0000			Q_{new} = 1.0000		
Parzen windowing results	Q_{actual} = 1.0000			Q_{actual} = 1.0000		







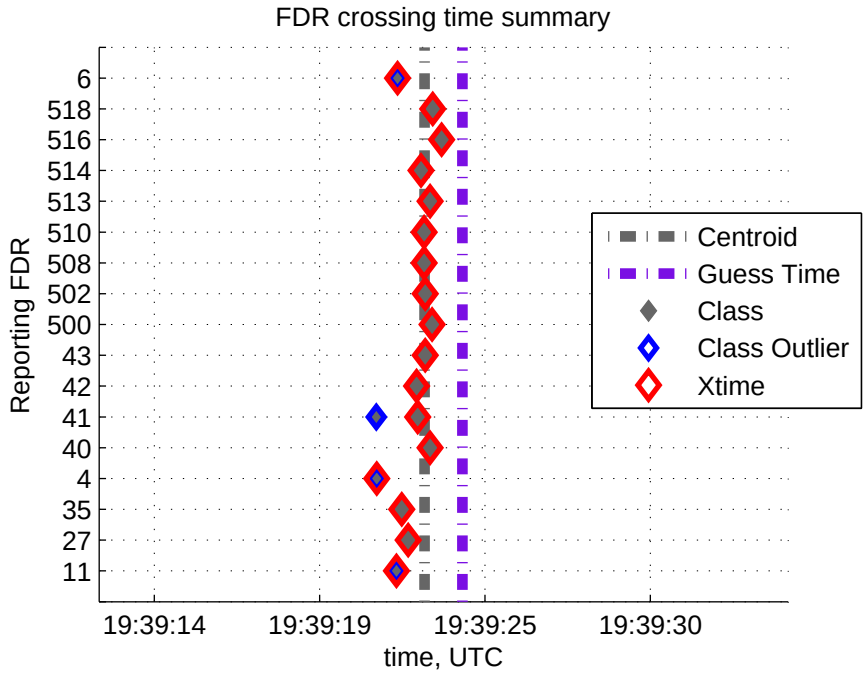
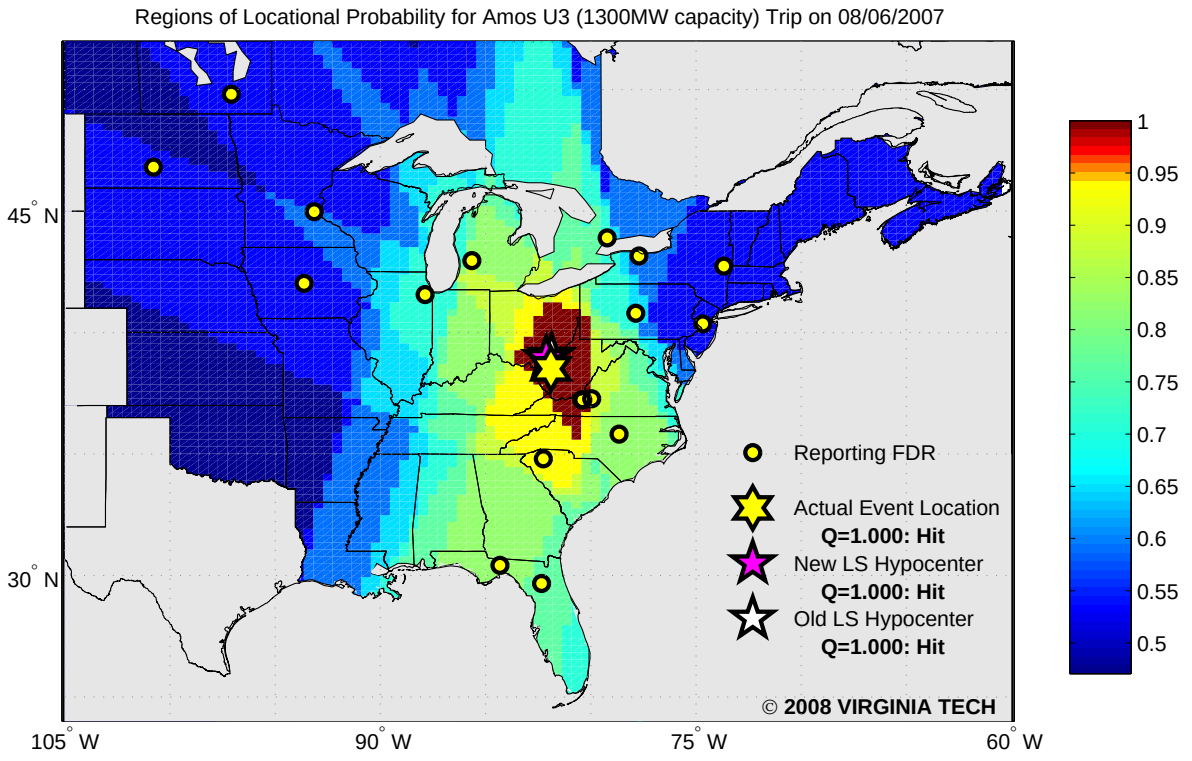
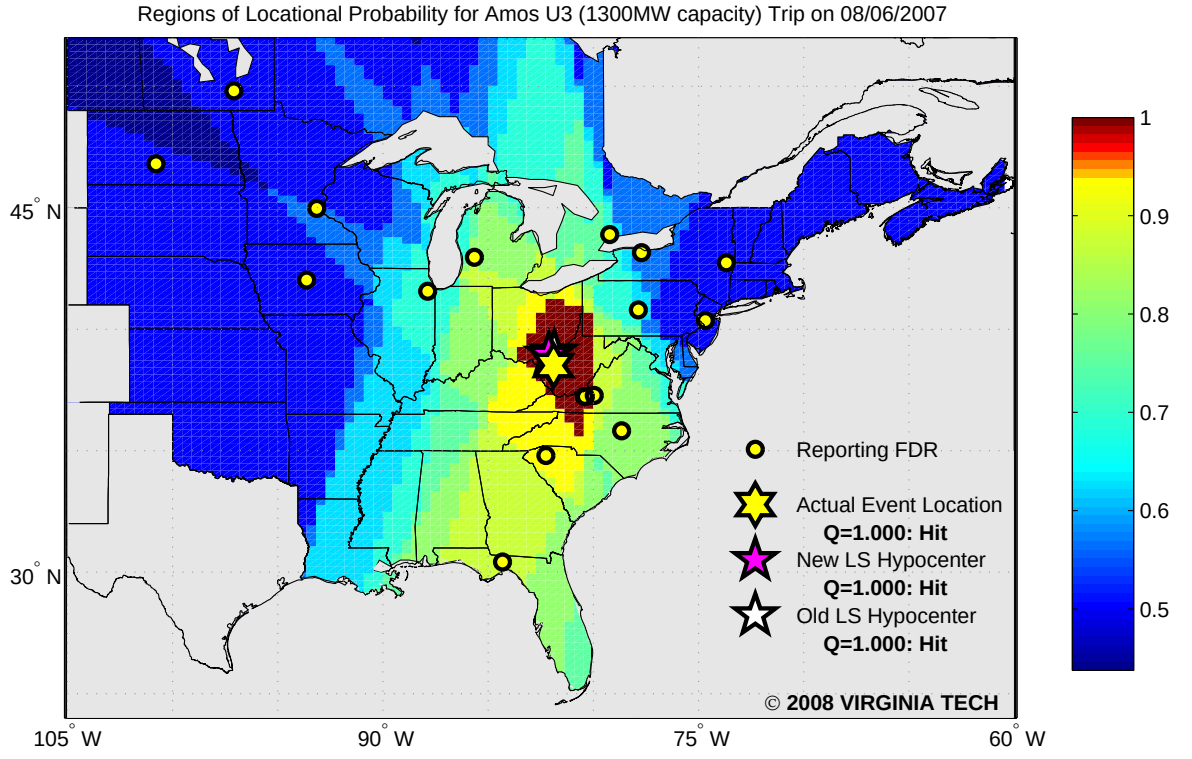


Figure D.92. Consolidated event ordering calculations: Amos U3 (1300MW capacity) (1300 MW, 38.5072°, –81.8900°) Trip on 08/06/2007 19:39:24



(a) Event location: old ordering method



(b) Event location: new ordering method

Figure D.93. Event location estimates: Amos U3 (1300MW capacity) (1300 MW, 38.5072°, −81.8900°) Trip on 08/06/2007 19:39:24

Table D.44. Ordering method comparison: Braidwood Nuclear (1178 MW, 41.2288°, −88.2690°) Trip on 08/18/2007 19:10:22

	Old Ordering Method			New Ordering Method		
Mismatch estimate (MW)	685			636		
FDR Info	Number	Name	Distance (mi)	Number	Name	Distance (mi)
	11	Calvin	179.6	4	VT	502
	35	ISU	282	11	Calvin	179.6
	508	ROA	521.4	20	TVA2Huntsville	459.4
	40	MISOStPaul	356.9	508	ROA	521.4
	43	Bismarck	730.4	41	Winnipeg	729.5
	502	Toronto	495.4	42	FSU	778.7
	6	ABB	639.2	40	MISOStPaul	356.9
	41	Winnipeg	729.5	27	RPI	755.8
	4	VT	502	35	ISU	282
	27	RPI	755.8	6	ABB	639.2
	20	TVA2Huntsville	459.4	43	Bismarck	730.4
	518	NERC	713	513	PSU	543
	514	FarrisSabrina	551.2	502	Toronto	495.4
	513	PSU	543	514	FarrisSabrina	551.2
	9	UFL	864.8	518	NERC	713
	42	FSU	778.7			
LS estimate	Latitude	Longitude	Distance (mi)	Latitude	Longitude	Distance (mi)
	41.2288°	−88.2690°	0.002335	37.9848°	−82.5857°	376.4
	$Q_{old} = 1.0000$			$Q_{old} = 0.5672$		
	$Q_{new} = 0.6385$			$Q_{new} = 1.0000$		
Parzen windowing results	$Q_{actual} = 1.0000$			$Q_{actual} = 0.6385$		

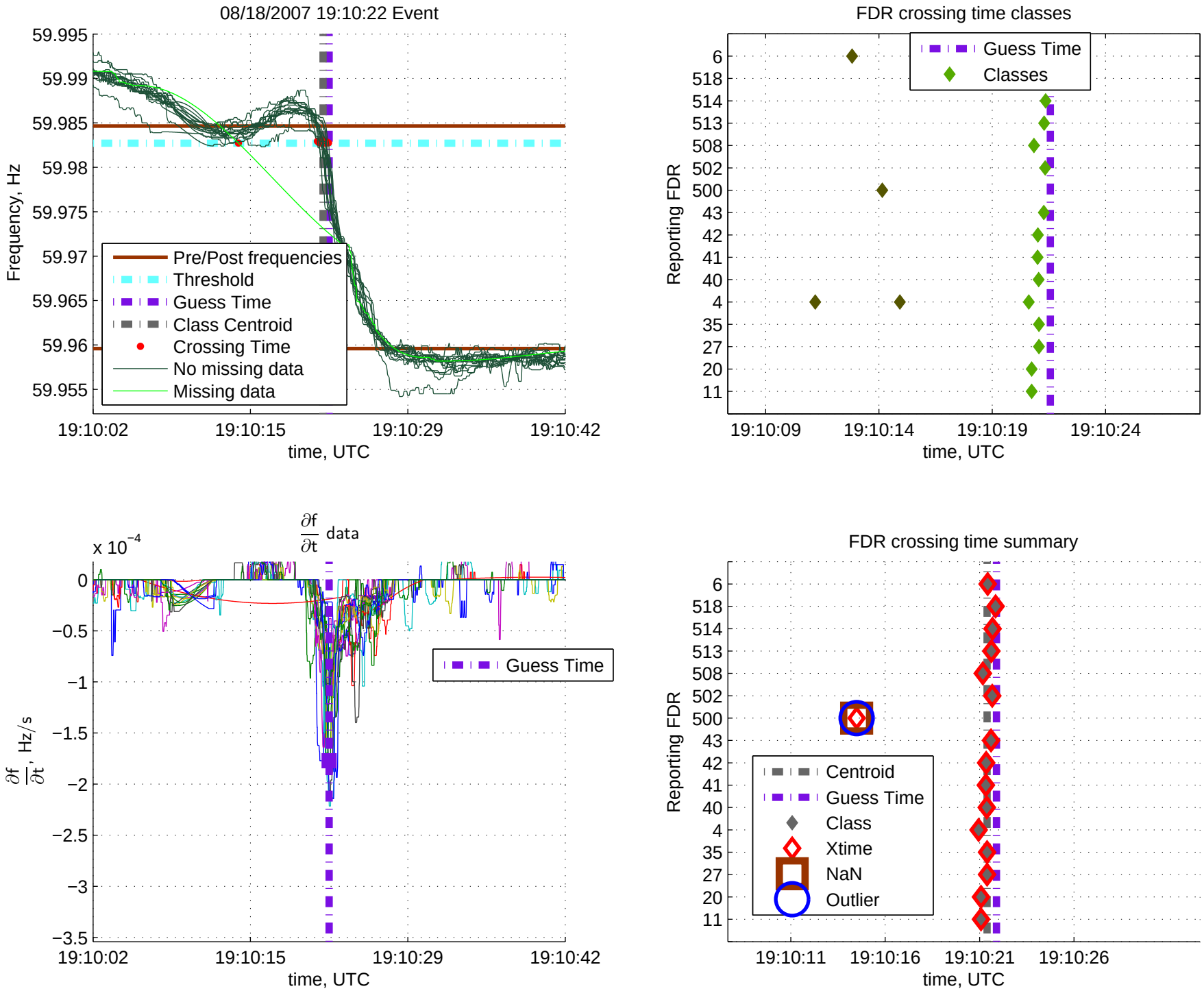
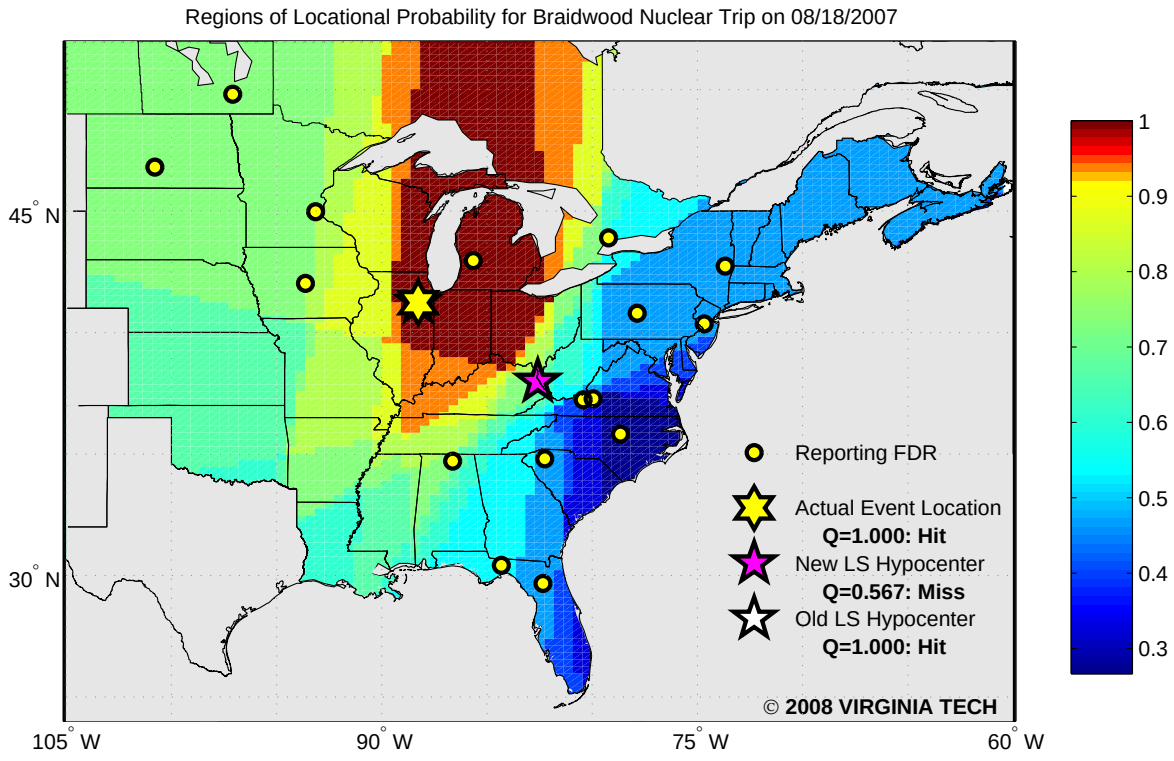
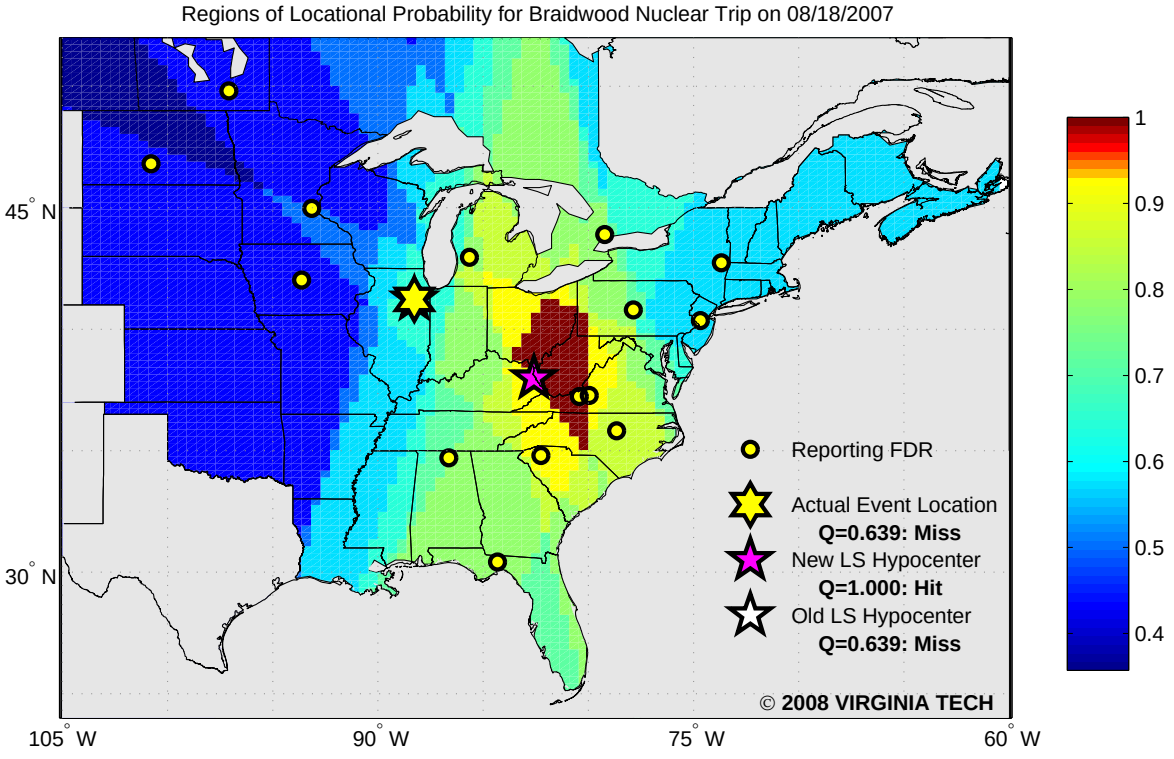


Figure D.94. Consolidated event ordering calculations: Braidwood Nuclear (1178 MW, 41.2288°, −88.2690°) Trip on 08/18/2007 19:10:22



(a) Event location: old ordering method



(b) Event location: new ordering method

Figure D.95. Event location estimates: Braidwood Nuclear (1178 MW, 41.2288°, −88.2690°) Trip on 08/18/2007 19:10:22

Table D.45. Ordering method comparison: Nine Mile Point Nuclear (621 MW, 29.9137°, −90.2078°) Trip on 08/20/2007 12:32:15

	Old Ordering Method			New Ordering Method		
Mismatch estimate (MW)	568			545		
FDR Info	Number	Name	Distance (mi)	Number	Name	Distance (mi)
	27	RPI	1273	40	MISOStPaul	1053
	502	Toronto	1138	20	TVA2Huntsville	391.6
	518	NERC	1133	11	Calvin	935.9
	513	PSU	1022	6	ABB	783.9
	6	ABB	783.9	4	VT	755.9
	508	ROA	778.1	502	Toronto	1138
	519	NewportNews	931.5	513	PSU	1022
	40	MISOStPaul	1053	41	Winnipeg	1421
	35	ISU	858	518	NERC	1133
	41	Winnipeg	1421	519	NewportNews	931.5
	11	Calvin	935.9	508	ROA	778.1
	514	FarrisSabrina	573.8	42	FSU	353.5
	42	FSU	353.5	500	Chicago	815.2
	500	Chicago	815.2	43	Bismarck	1298
	524	TTU	511	523	TTU3	546
	20	TVA2Huntsville	391.6	514	FarrisSabrina	573.8
	43	Bismarck	1298	35	ISU	858
	4	VT	755.9			
LS estimate	Latitude	Longitude	Distance (mi)	Latitude	Longitude	Distance (mi)
	43.5215°	−76.4041°	1208	44.9725°	−93.1470°	1053
	Q_{old} = 0.5456 Q_{new} = 0.1886			Q_{old} = 0.0000 Q_{new} = 1.0000		
Parzen windowing results	Q_{actual} = 0.0000			Q_{actual} = 0.2454		

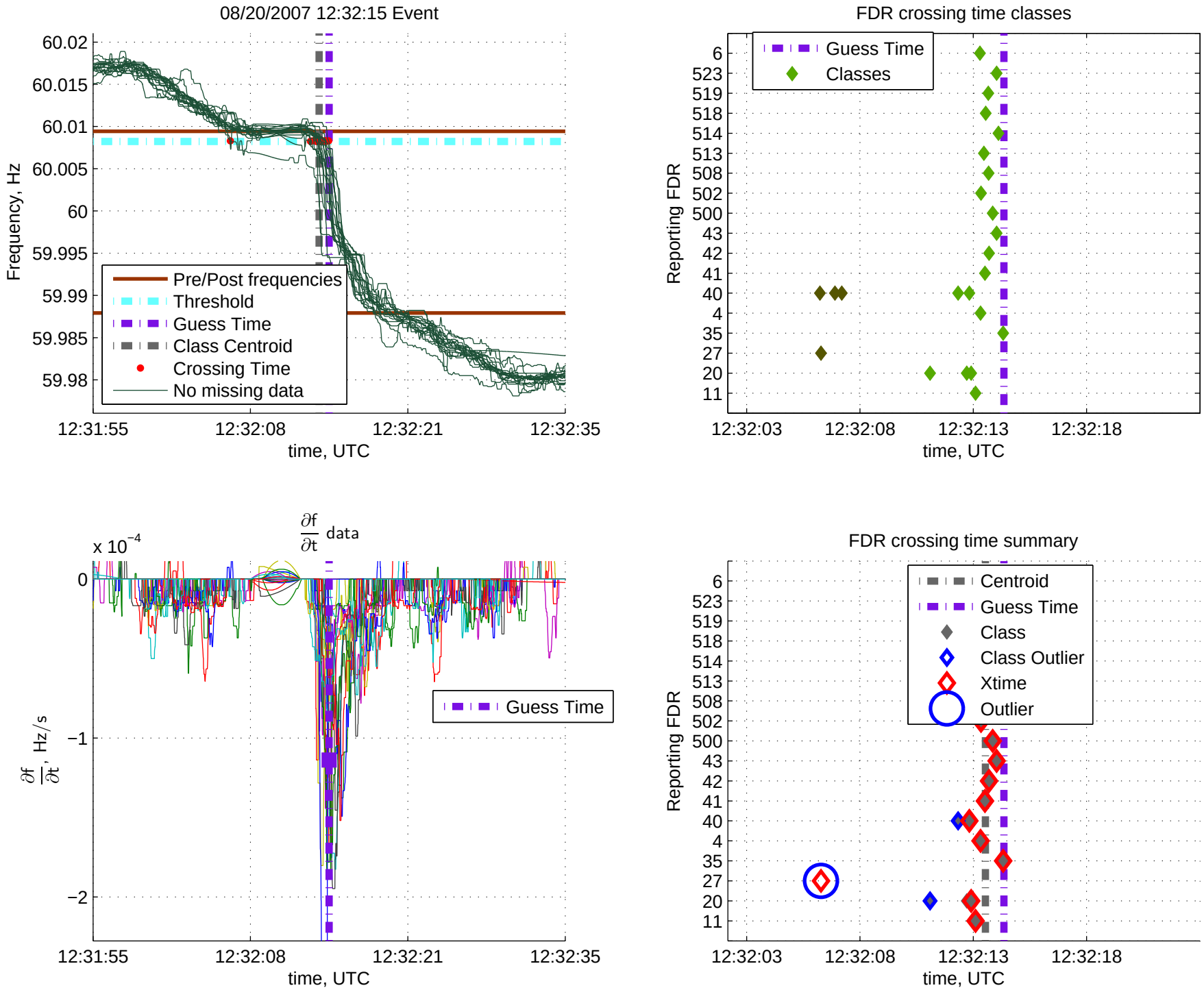
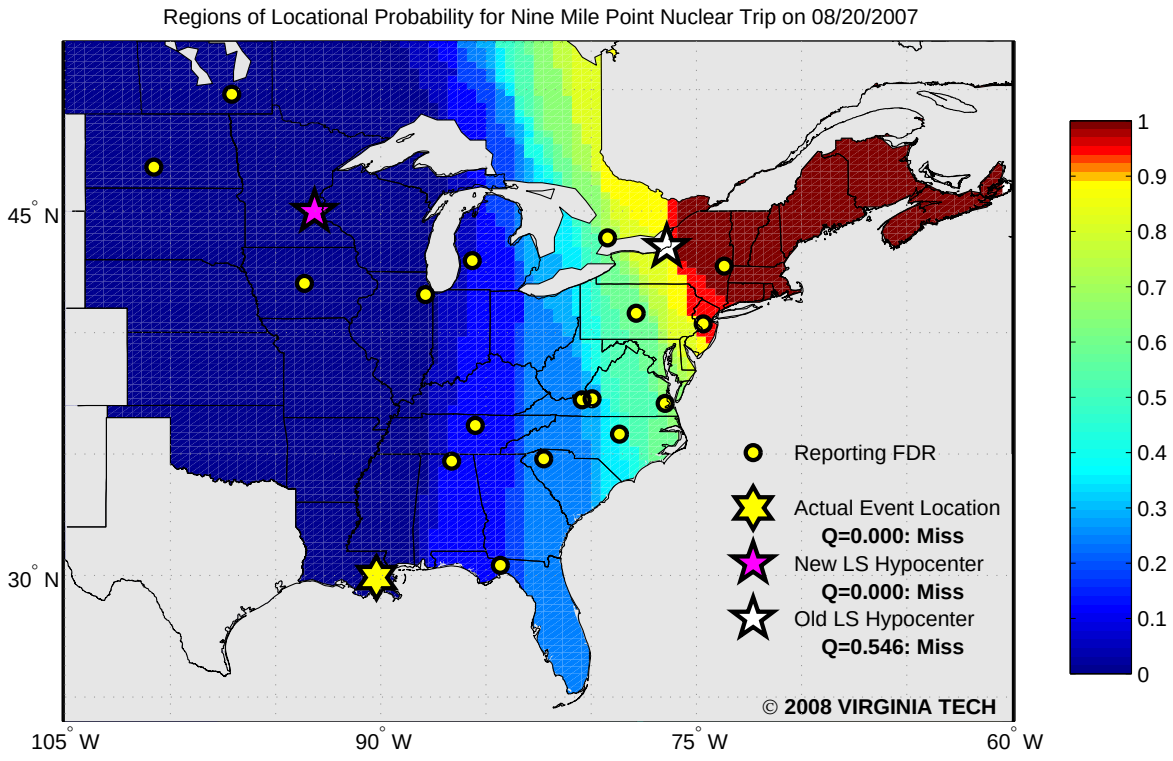
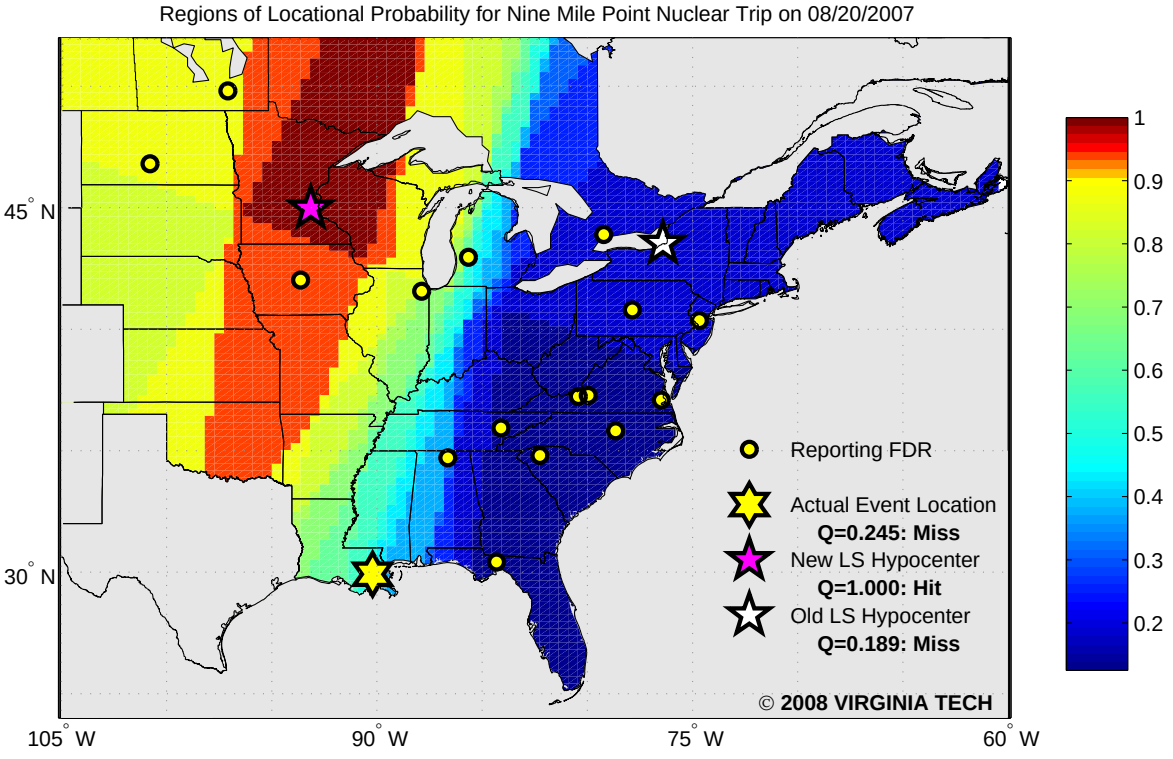


Figure D.96. Consolidated event ordering calculations: Nine Mile Point Nuclear (621 MW, 29.9137°, −90.2078°) Trip on 08/20/2007 12:32:15



(a) Event location: old ordering method



(b) Event location: new ordering method

Figure D.97. Event location estimates: Nine Mile Point Nuclear (621 MW, 29.9137°, −90.2078°) Trip on 08/20/2007 12:32:15

Table D.46. Ordering method comparison: Sequoyah (1150 MW, 35.2272°, −85.0943°) Trip on 08/24/2007 07:51:02

	Old Ordering Method			New Ordering Method		
Mismatch estimate (MW)	NaN			NaN		
FDR Info	Number	Name	Distance (mi)	Number	Name	Distance (mi)
				41	Winnipeg	1175
				35	ISU	657
				4	VT	294.6
				6	ABB	364.1
				500	Chicago	462.8
				11	Calvin	535.2
				508	ROA	319.3
				510	Blacksburg	296.9
				13	MidwestISO	332.3
				504	WayneState	504.4
				40	MISOStPaul	795.6
				519	NewportNews	496.9
				502	Toronto	675.2
				513	PSU	550
				27	RPI	801.9
				42	FSU	335.2
				518	NERC	669.6
				514	FarrisSabrina	163.3
				20	TVA2Huntsville	93.97
LS estimate	Latitude	Longitude	Distance (mi)	Latitude	Longitude	Distance (mi)
	$NaN°$	$NaN°$	NaN	$NaN°$	$NaN°$	NaN
	$Q_{old} = NaN$			$Q_{old} = NaN$		
	$Q_{new} = NaN$			$Q_{new} = NaN$		
Parzen windowing results	$Q_{actual} = NaN$			$Q_{actual} = 0.0000$		

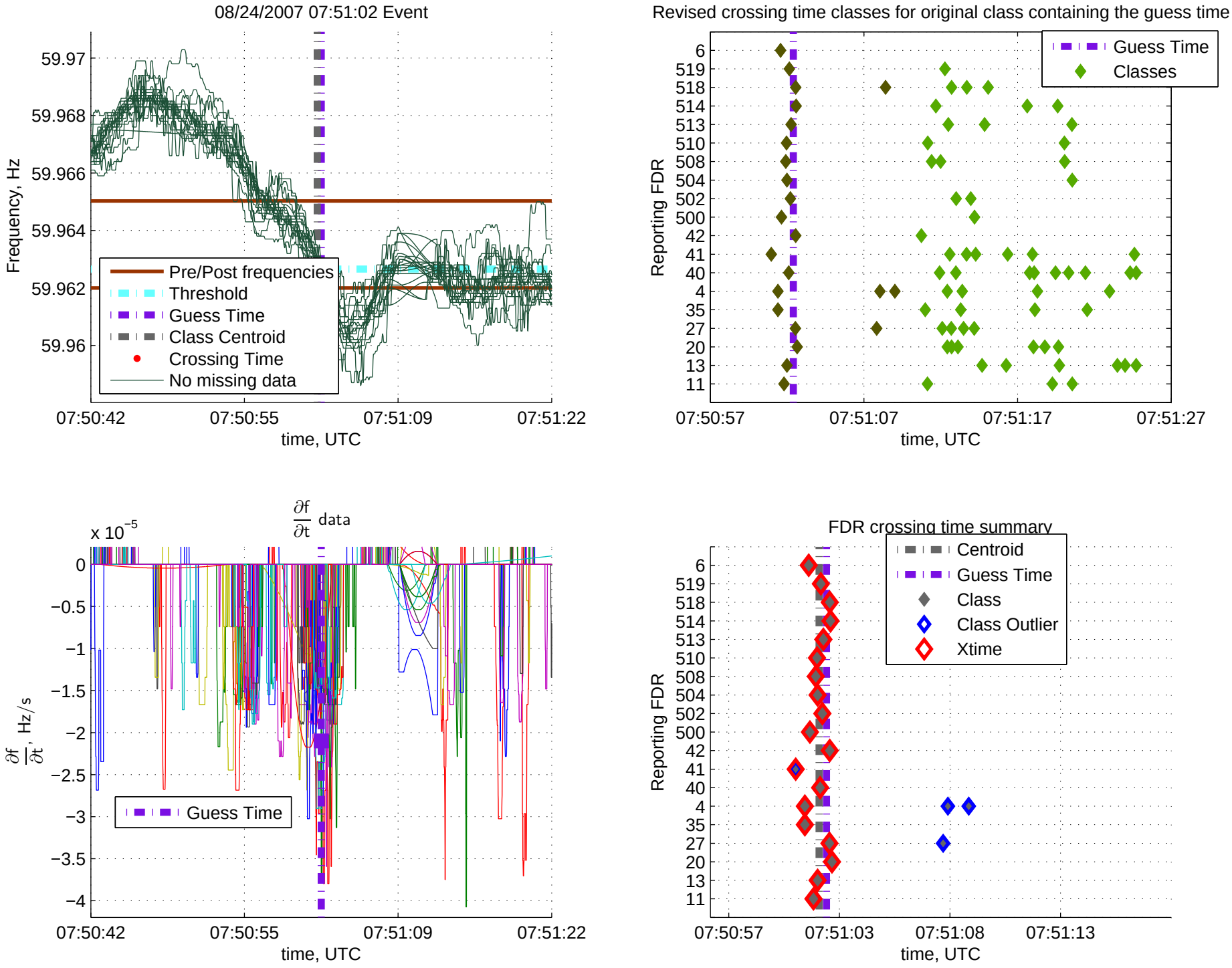


Figure D.98. Consolidated event ordering calculations: Sequoyah (1150 MW, 35.2272°, −85.0943°) Trip on 08/24/2007 07:51:02

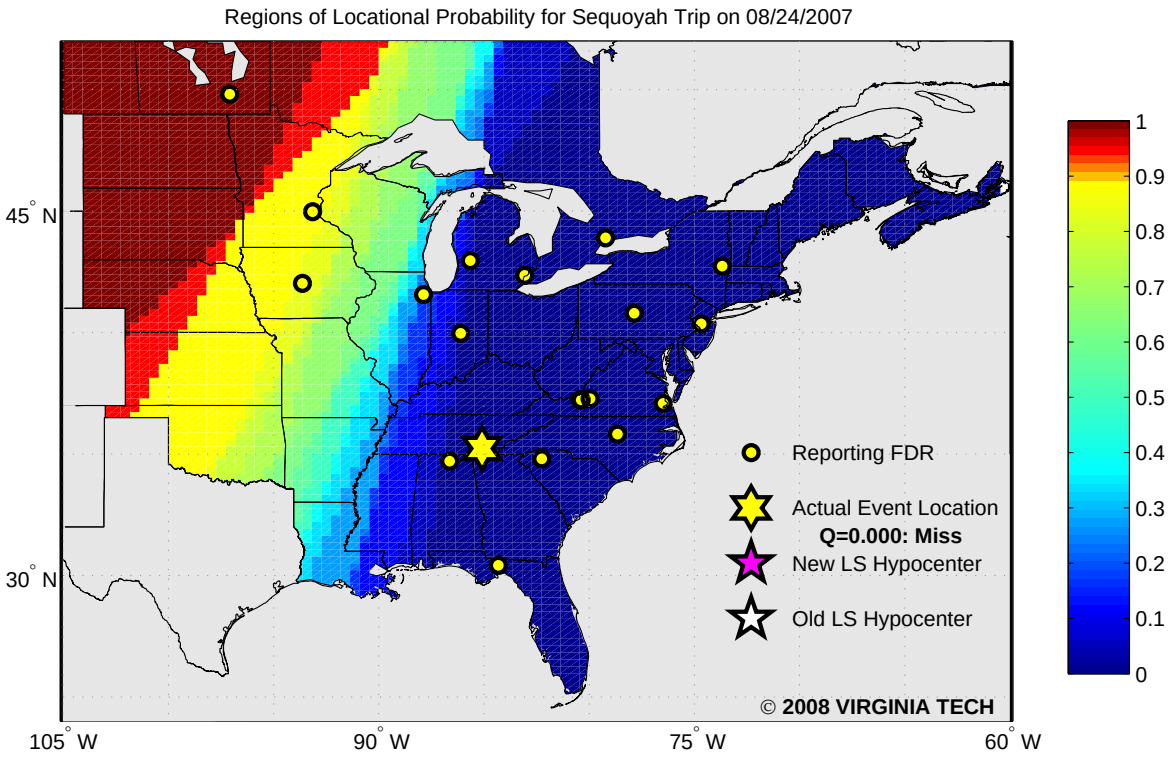
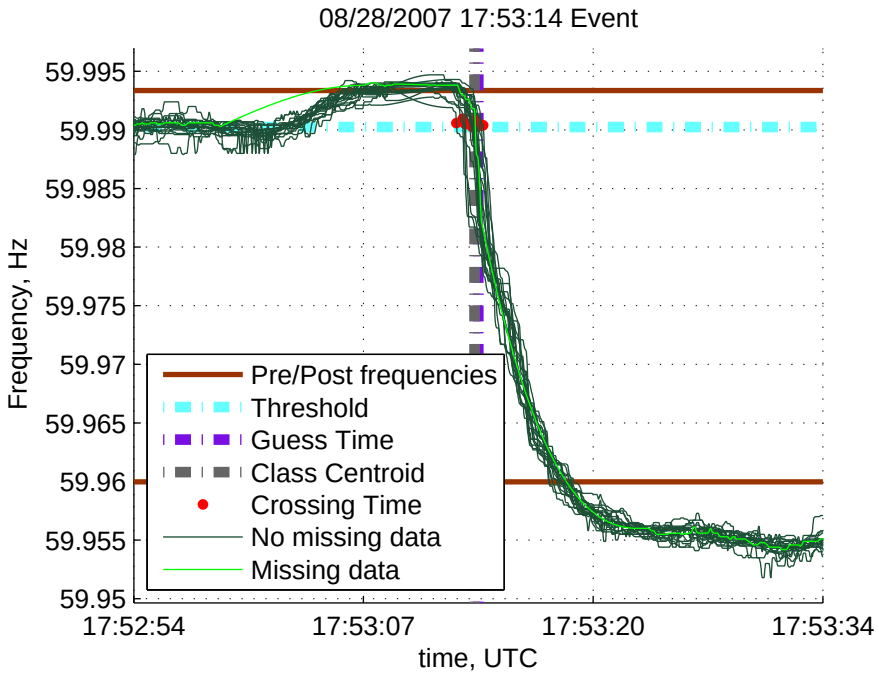
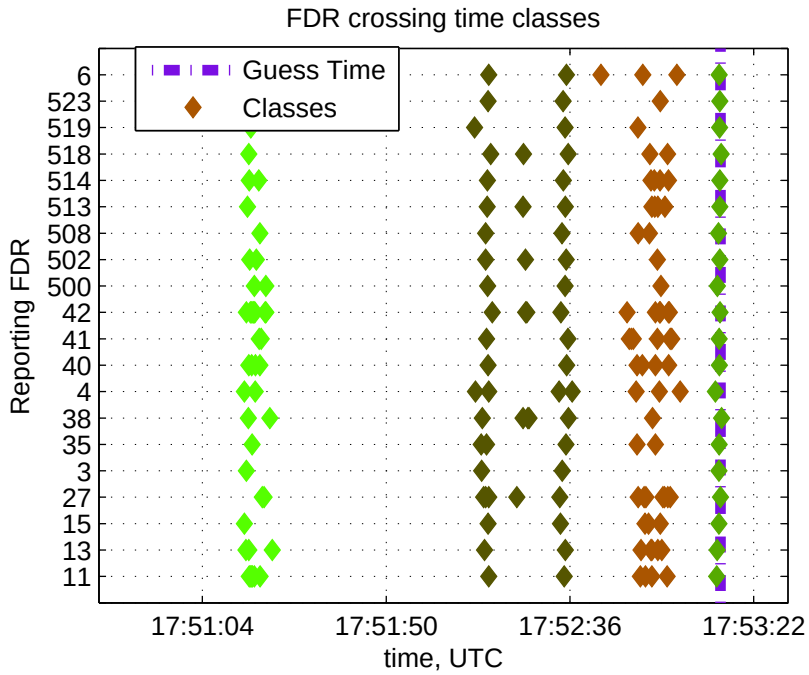


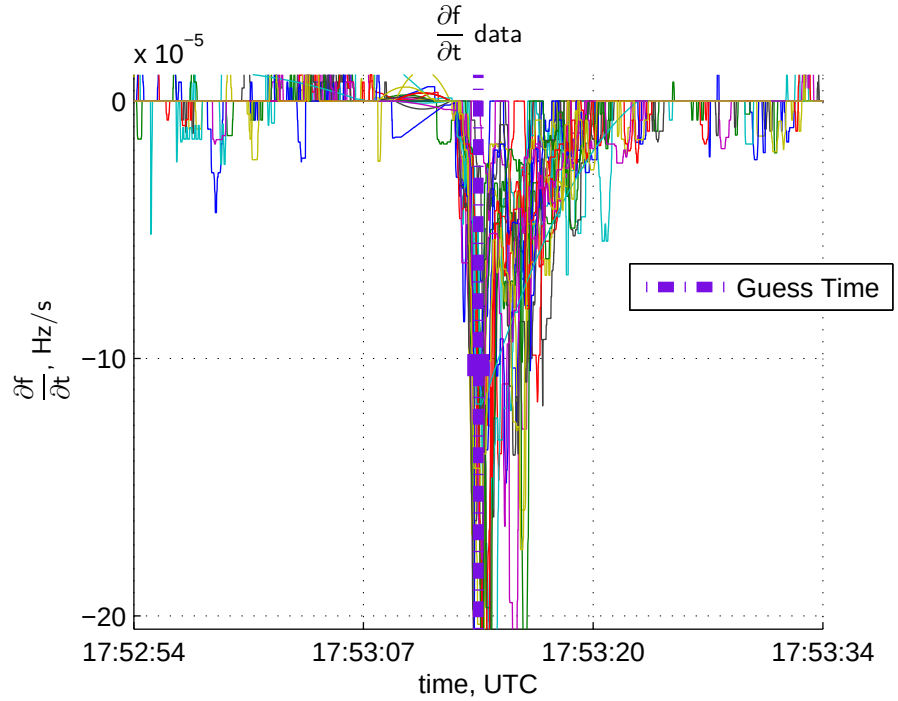
Figure D.99. Event location estimates (new ordering method): Sequoyah (1150 MW, 35.2272°, −85.0943°) Trip on 08/24/2007 07:51:02

Table D.47. Ordering method comparison: Donald C. Cook Unit 1 (1020 MW Capacity) (1029 MW, 41.9362°, −86.5543°) Trip on 08/28/2007 17:53:14

	Old Ordering Method			New Ordering Method		
Mismatch estimate (MW)	921			846		
FDR Info	Number	Name	Distance (mi)	Number	Name	Distance (mi)
	11	Calvin	84.35	4	VT	460.2
	13	MidwestISO	137.9	11	Calvin	84.35
	500	Chicago	72.97	13	MidwestISO	137.9
	35	ISU	363.1	500	Chicago	72.97
	508	ROA	476	508	ROA	476
	3	ARI	542.4	3	ARI	542.4
	40	MISOStPaul	391.4	15	TVA3Nashville	398.5
	502	Toronto	394.6	6	ABB	598.5
	519	NewportNews	632.3	35	ISU	363.1
	6	ABB	598.5	41	Winnipeg	742
	513	PSU	457.3	40	MISOStPaul	391.4
	4	VT	460.2	502	Toronto	394.6
	41	Winnipeg	742	513	PSU	457.3
	518	NERC	627.2	514	FarrisSabrina	544.8
	514	FarrisSabrina	544.8	523	TTU3	434.9
	42	FSU	805.3	42	FSU	805.3
	15	TVA3Nashville	398.5	27	RPI	659.4
	38	ISONE	713.3	518	NERC	627.2
	524	TTU	402	38	ISONE	713.3
	27	RPI	659.4			
LS estimate	Latitude	Longitude	Distance (mi)	Latitude	Longitude	Distance (mi)
	42.9384°	−86.1343°	72.48	37.2327°	−80.4284°	460.2
	Q_{old} = 1.0000			Q_{old} = 0.1369		
	Q_{new} = 0.7083			Q_{new} = 1.0000		
Parzen windowing results	Q_{actual} = 1.0000			Q_{actual} = 0.7083		







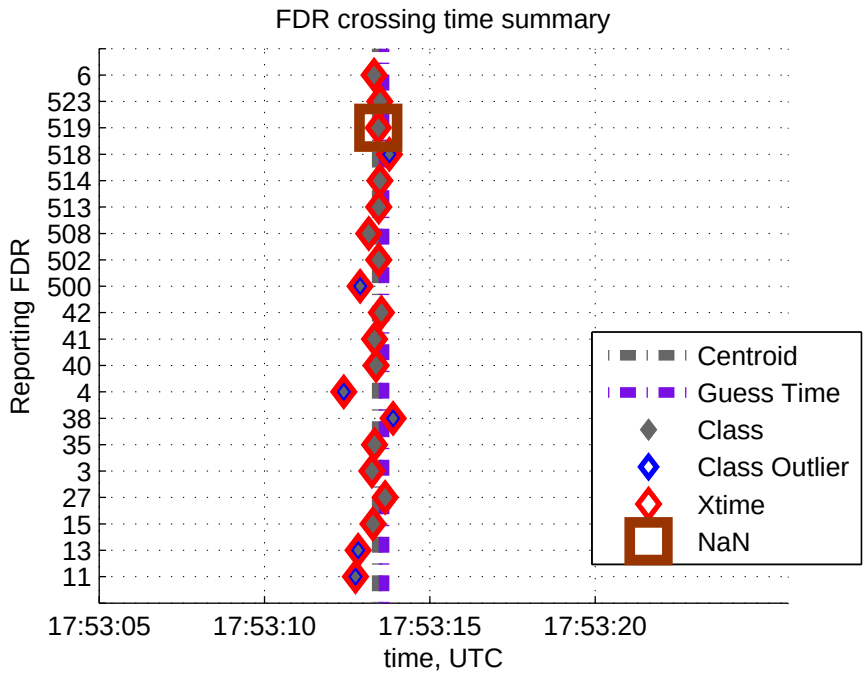
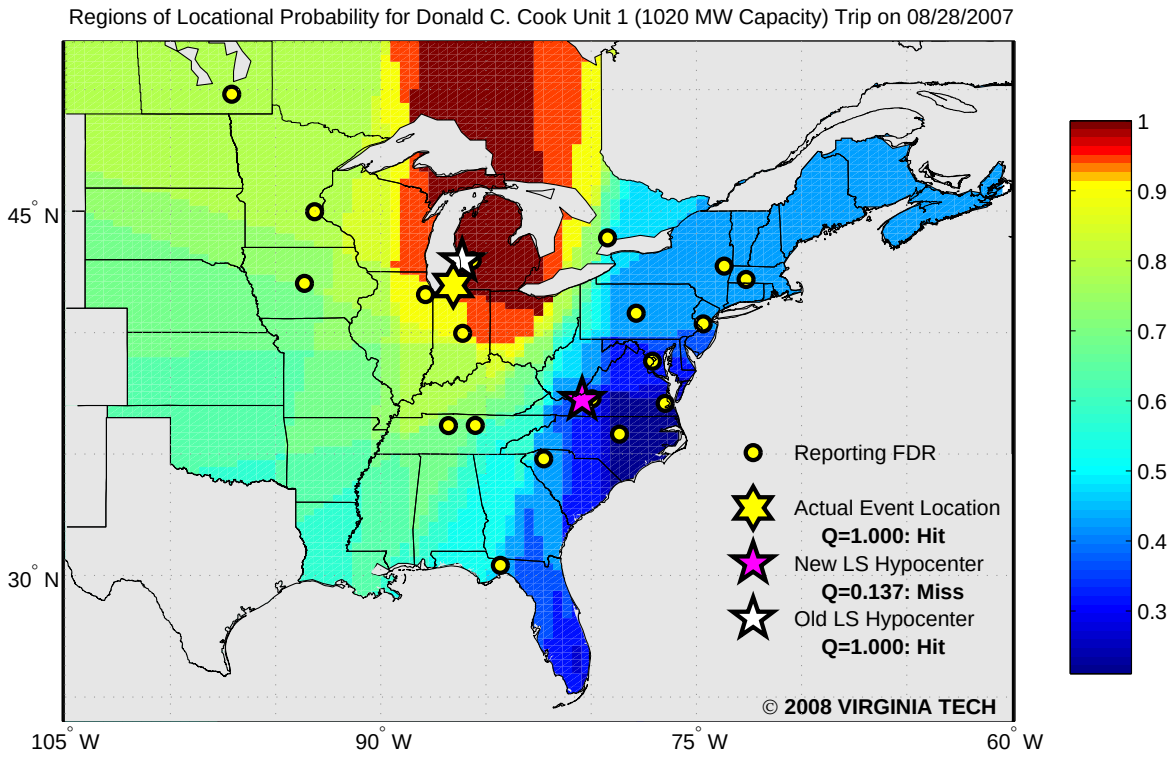
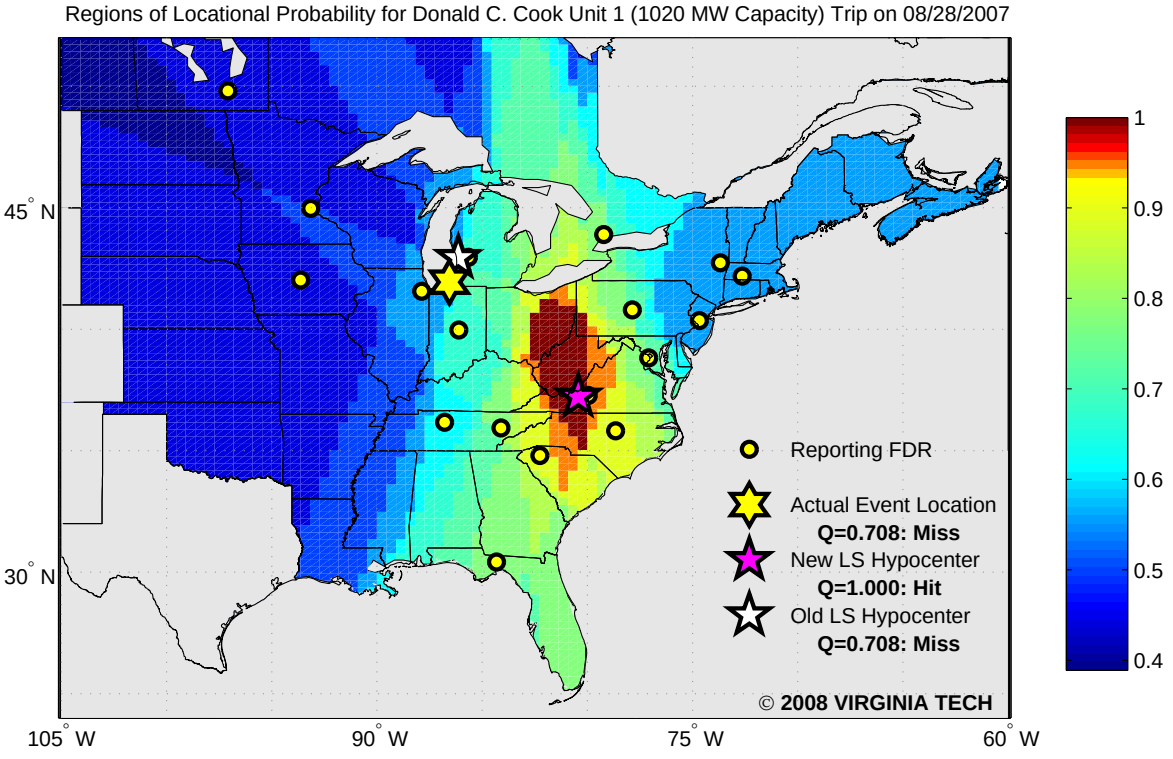


Figure D.100. Consolidated event ordering calculations: Donald C. Cook Unit 1 (1020 MW Capacity) (1029 MW, 41.9362°, −86.5543°) Trip on 08/28/2007 17:53:14



(a) Event location: old ordering method



(b) Event location: new ordering method

Figure D.101. Event location estimates: Donald C. Cook Unit 1 (1020 MW Capacity) (1029 MW, 41.9362°, −86.5543°) Trip on 08/28/2007 17:53:14

Table D.48. Ordering method comparison: Mountaineer U1 (1300 MW Capacity) (1300 MW, 38.7292°, −82.0223°) Trip on 09/01/2007 13:48:03

	Old Ordering Method			New Ordering Method		
Mismatch estimate (MW)	1089			1115		
FDR Info	Number	Name	Distance (mi)	Number	Name	Distance (mi)
	4	VT	135	4	VT	135
	510	Blacksburg	137.2	13	MidwestISO	234.6
	13	MidwestISO	234.6	6	ABB	273
	508	ROA	150.6	20	TVA2Huntsville	377.1
	3	ARI	265.9	11	Calvin	348.6
	11	Calvin	348.6	510	Blacksburg	137.2
	6	ABB	273	15	TVA3Nashville	315.3
	519	NewportNews	322.6	40	MISOStPaul	715.8
	513	PSU	262.9	508	ROA	150.6
	15	TVA3Nashville	315.3	27	RPI	516.9
	514	FarrisSabrina	271.4	3	ARI	265.9
	35	ISU	651.1	519	NewportNews	322.6
	518	NERC	407.3	513	PSU	262.9
	27	RPI	516.9	523	TTU3	224.4
	502	Toronto	385.3	42	FSU	588.7
	524	TTU	260.1	514	FarrisSabrina	271.4
	40	MISOStPaul	715.8	518	NERC	407.3
	20	TVA2Huntsville	377.1	502	Toronto	385.3
	42	FSU	588.7	35	ISU	651.1
				41	Winnipeg	1065
				38	ISONE	547.7
LS estimate	Latitude	Longitude	Distance (mi)	Latitude	Longitude	Distance (mi)
	38.9587°	−82.1235°	16.77	38.9587°	−82.1235°	16.77
	Q_{old} = 1.0000 Q_{new} = 1.0000			Q_{old} = 1.0000 Q_{new} = 1.0000		
Parzen windowing results	Q_{actual} = 1.0000			Q_{actual} = 1.0000		

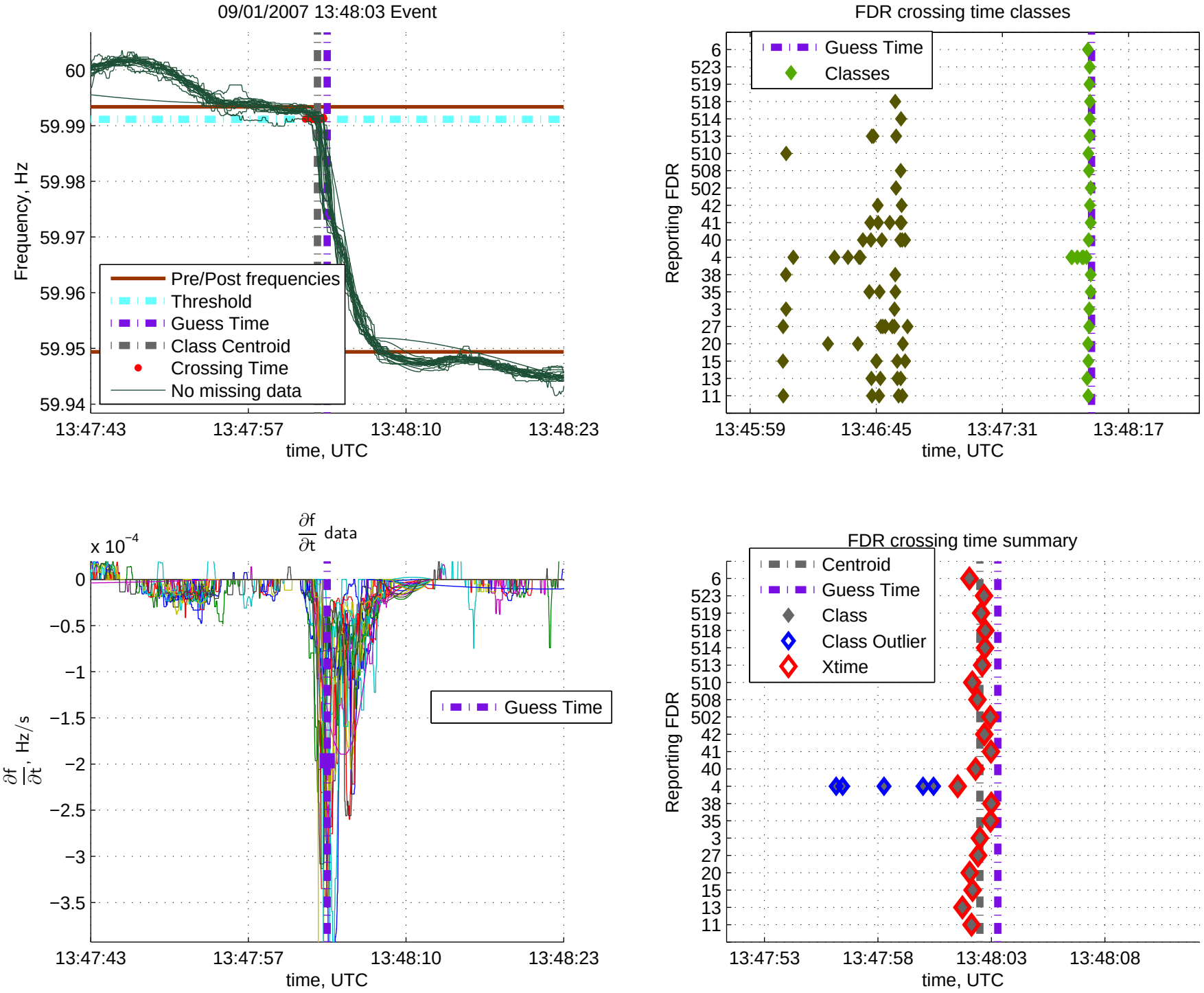
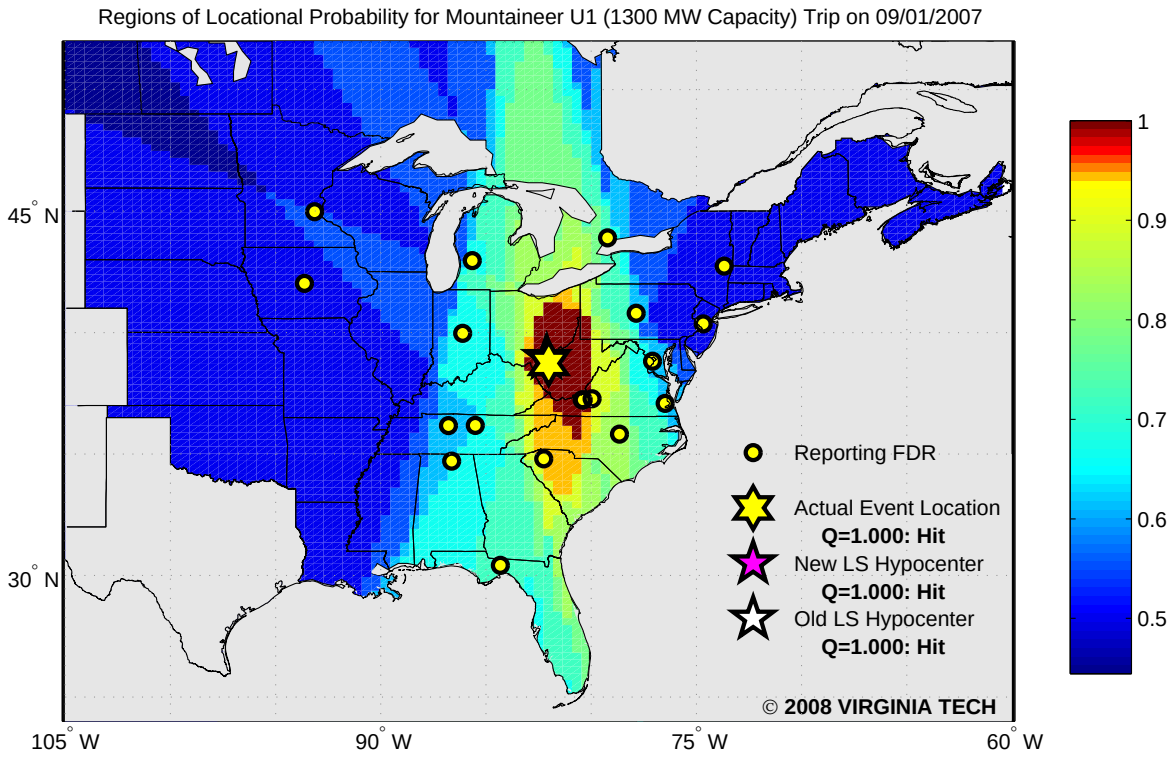
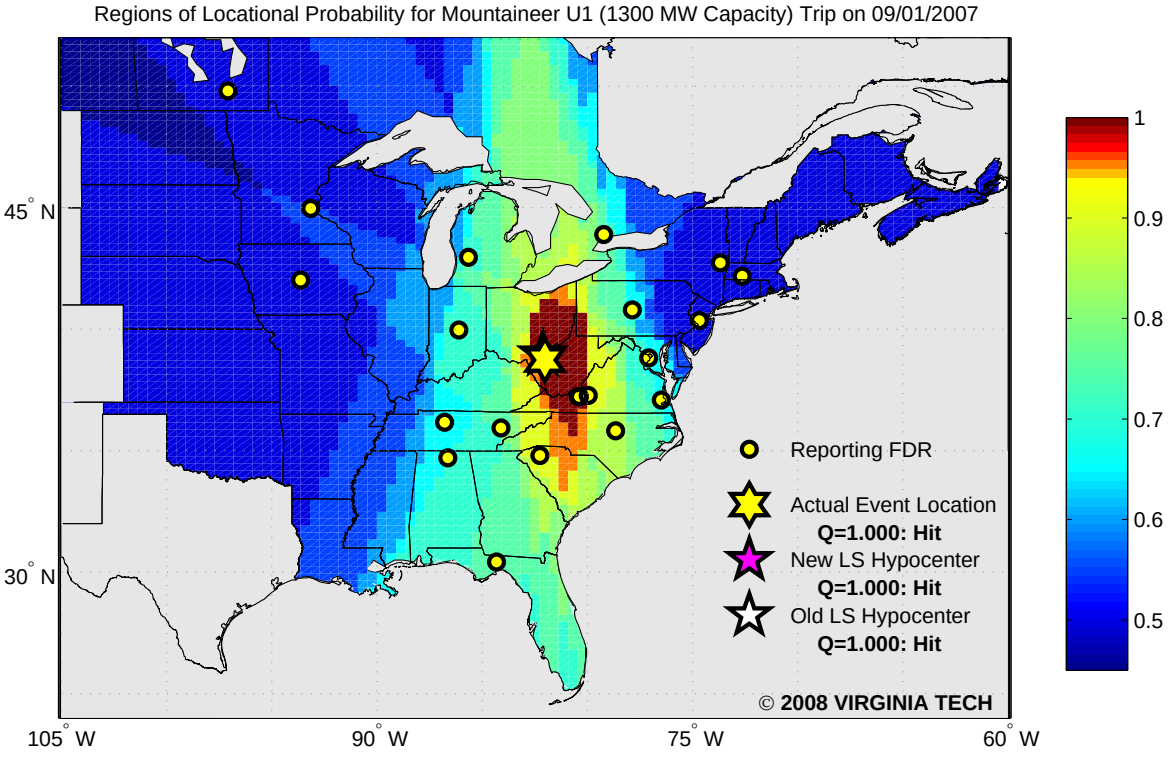


Figure D.102. Consolidated event ordering calculations: Mountaineer U1 (1300 MW Capacity) (1300 MW, 38.7292°, –82.0223°) Trip on 09/01/2007 13:48:03



(a) Event location: old ordering method



(b) Event location: new ordering method

Figure D.103. Event location estimates: Mountaineer U1 (1300 MW Capacity) (1300 MW, 38.7292°, −82.0223°) Trip on 09/01/2007 13:48:03

Table D.49. Ordering method comparison: Rockport Unit2 (1300 MW Capacity) (1300 MW, 37.8858°, −87.0770°) Trip on 09/04/2007 16:57:08

	Old Ordering Method			New Ordering Method		
Mismatch estimate (MW)	745			683		
FDR Info	Number	Name	Distance (mi)	Number	Name	Distance (mi)
	11	Calvin	358.5	13	MidwestISO	153.1
	500	Chicago	257.5	35	ISU	449.2
	510	Blacksburg	369.7	15	TVA3Nashville	119.5
	524	TTU	146.5	42	FSU	539.3
	3	ARI	544.9	20	TVA2Huntsville	221.1
	13	MidwestISO	153.1	41	Winnipeg	961.1
	35	ISU	449.2	11	Calvin	358.5
	40	MISOStPaul	581.5	523	TTU3	212.4
	508	ROA	391.9	4	VT	366.9
	514	FarrisSabrina	342.5	40	MISOStPaul	581.5
	513	PSU	531.4	500	Chicago	257.5
	27	RPI	780.3	508	ROA	391.9
	502	Toronto	583.1	3	ARI	544.9
	518	NERC	685.8	510	Blacksburg	369.7
	41	Winnipeg	961.1	514	FarrisSabrina	342.5
	42	FSU	539.3	27	RPI	780.3
	503	Danbury	760.4	38	ISONE	818.3
	38	ISONE	818.3	518	NERC	685.8
	15	TVA3Nashville	119.5	513	PSU	531.4
	20	TVA2Huntsville	221.1	502	Toronto	583.1
	9	UFL	629.1	503	Danbury	760.4
	4	VT	366.9			
LS estimate	Latitude	Longitude	Distance (mi)	Latitude	Longitude	Distance (mi)
	41.5236°	−83.1278°	327.4	41.9362°	−86.5543°	281.2
	$Q_{old} = 1.0000$ $Q_{new} = 0.9825$			$Q_{old} = 1.0000$ $Q_{new} = 0.9825$		
Parzen windowing results	$Q_{actual} = 0.6776$			$Q_{actual} = 0.9825$		

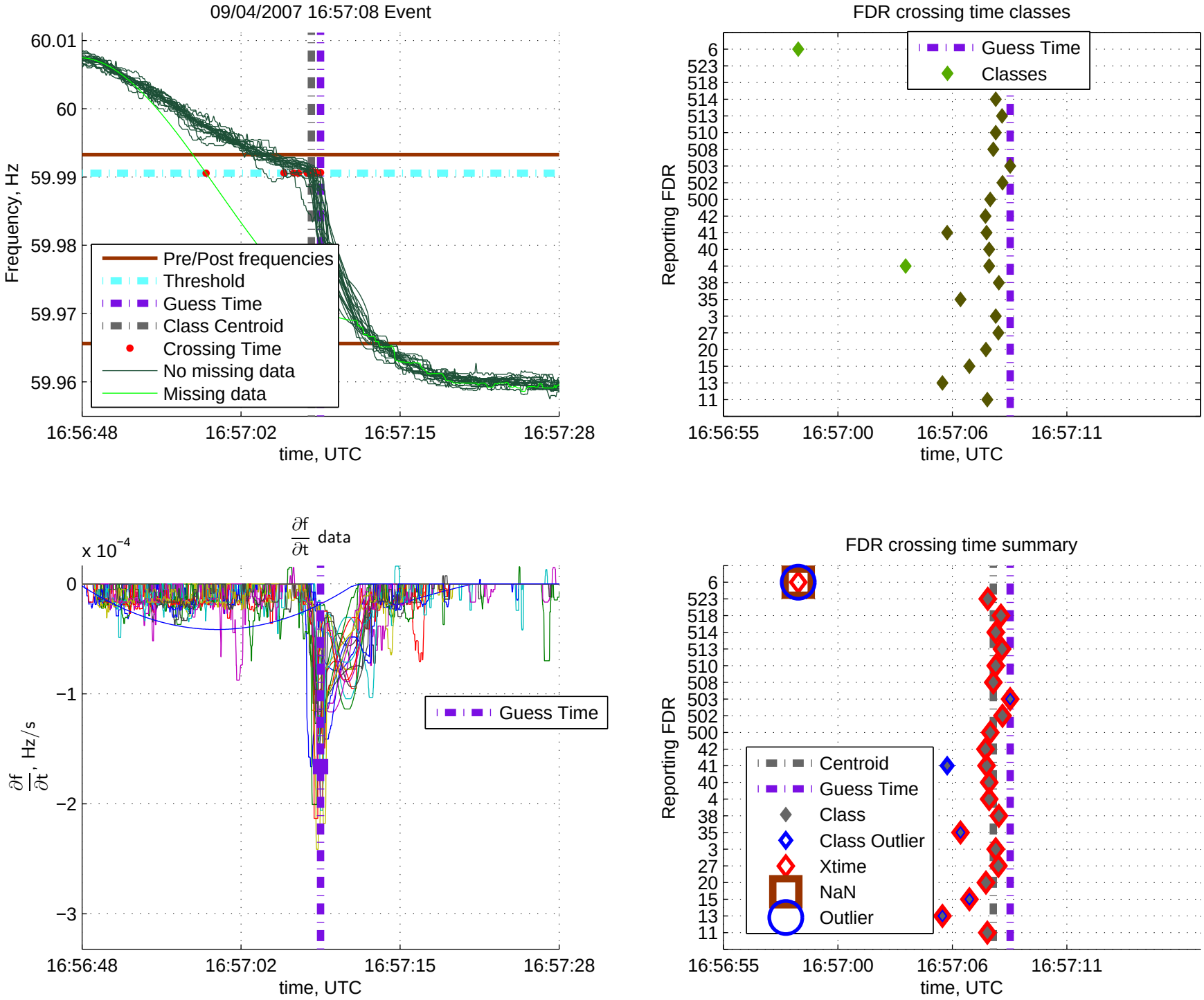
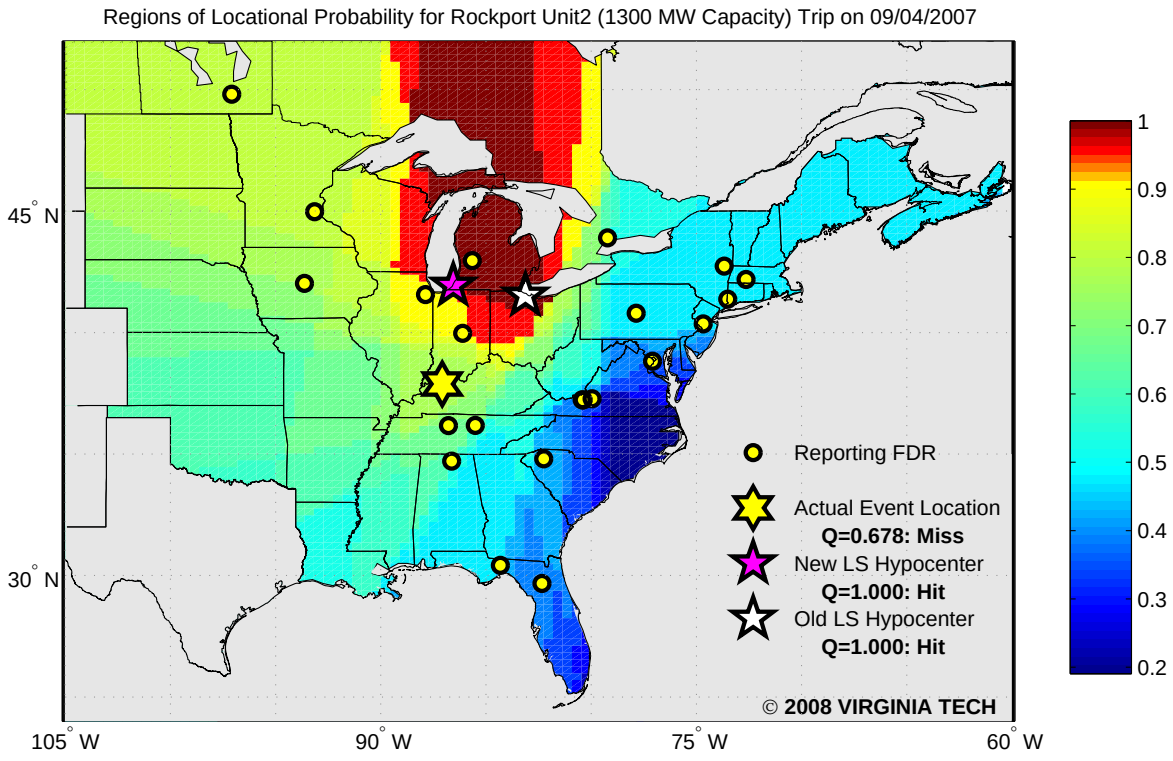
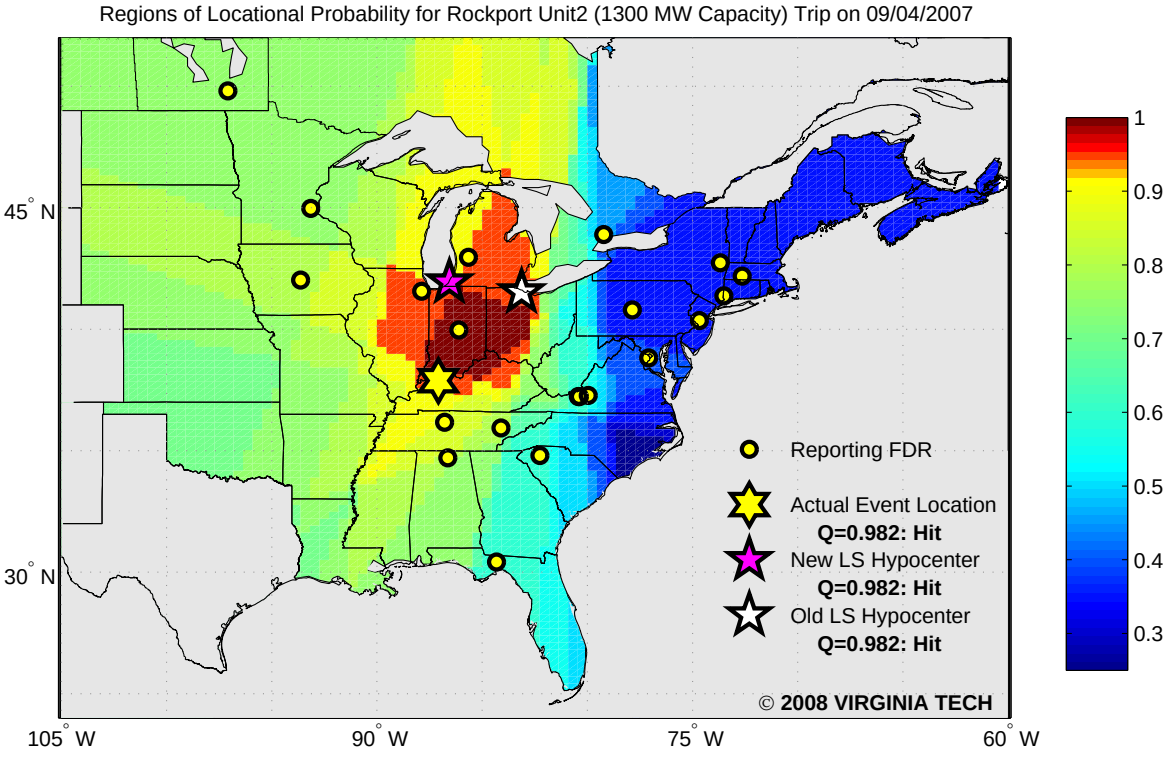


Figure D.104. Consolidated event ordering calculations: Rockport Unit2 (1300 MW Capacity) (1300 MW, 37.8858°, −87.0770°) Trip on 09/04/2007 16:57:08



(a) Event location: old ordering method



(b) Event location: new ordering method

Figure D.105. Event location estimates: Rockport Unit2 (1300 MW Capacity) (1300 MW, 37.8858°, −87.0770°) Trip on 09/04/2007 16:57:08

Table D.50. Ordering method comparison: Jeffrey Energy Center U3 (1474 MW, 39.1987°, −96.0683°) Trip on 10/03/2007 15:24:29

	Old Ordering Method			New Ordering Method		
Mismatch estimate (MW)	NaN			NaN		
FDR Info	Number	Name	Distance (mi)	Number	Name	Distance (mi)
				4	VT	858.7
				500	Chicago	460.7
				17	TVA4Jackson	467.2
				510	Blacksburg	861.5
				519	NewportNews	1072
				42	FSU	899.8
				523	TTU3	692.2
				514	FarrisSabrina	819.4
				20	TVA2Huntsville	606.2
				508	ROA	883.1
				40	MISOStPaul	426
				43	Bismarck	577.1
LS estimate	Latitude	Longitude	Distance (mi)	Latitude	Longitude	Distance (mi)
	$NaN°$	$NaN°$	NaN	$NaN°$	$NaN°$	NaN
	$Q_{old} = NaN$			$Q_{old} = NaN$		
	$Q_{new} = NaN$			$Q_{new} = NaN$		
Parzen windowing results	$Q_{actual} = NaN$			$Q_{actual} = 0.1130$		

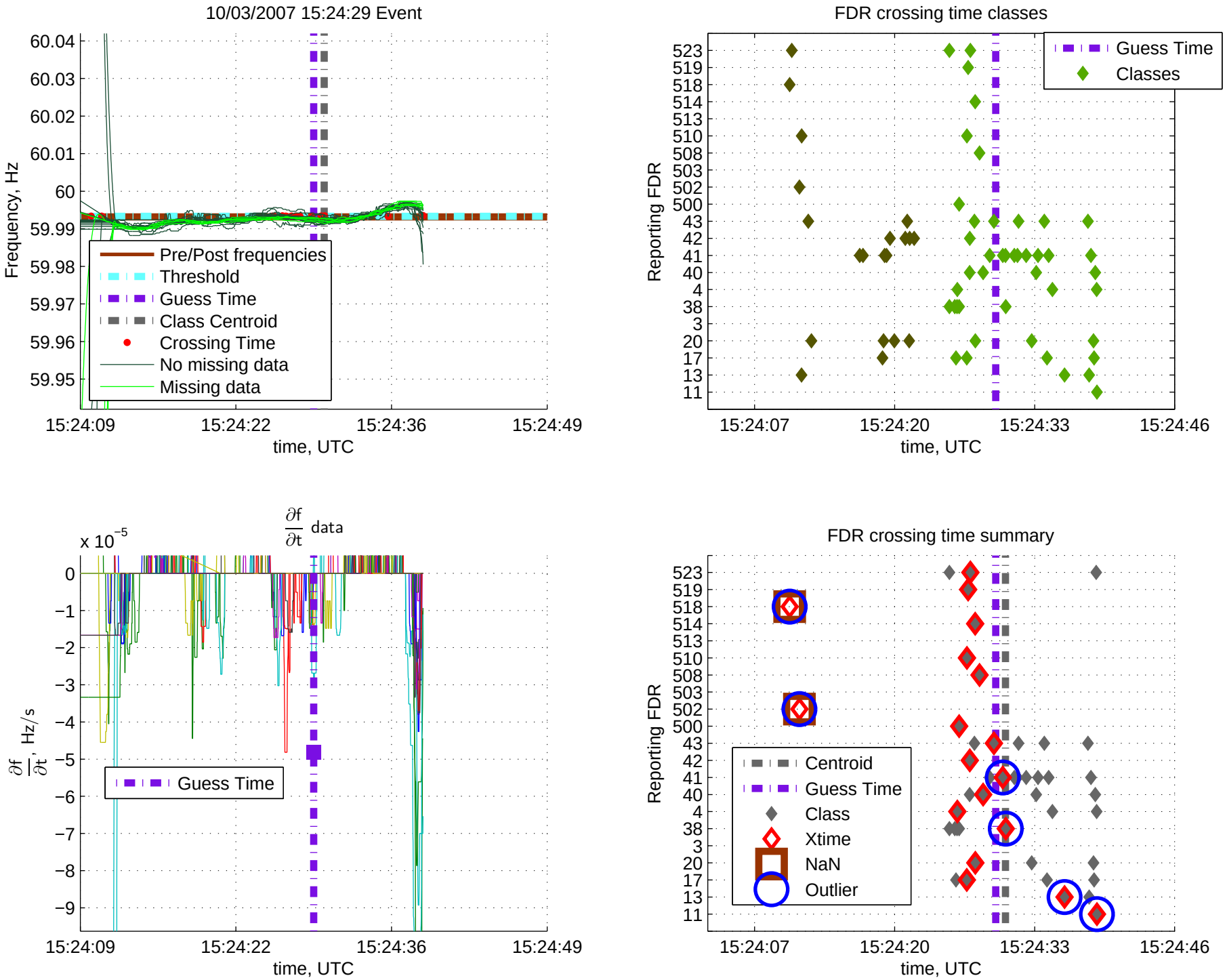


Figure D.106. Consolidated event ordering calculations: Jeffrey Energy Center U3 (1474 MW, 39.1987°, −96.0683°) Trip on 10/03/2007 15:24:29

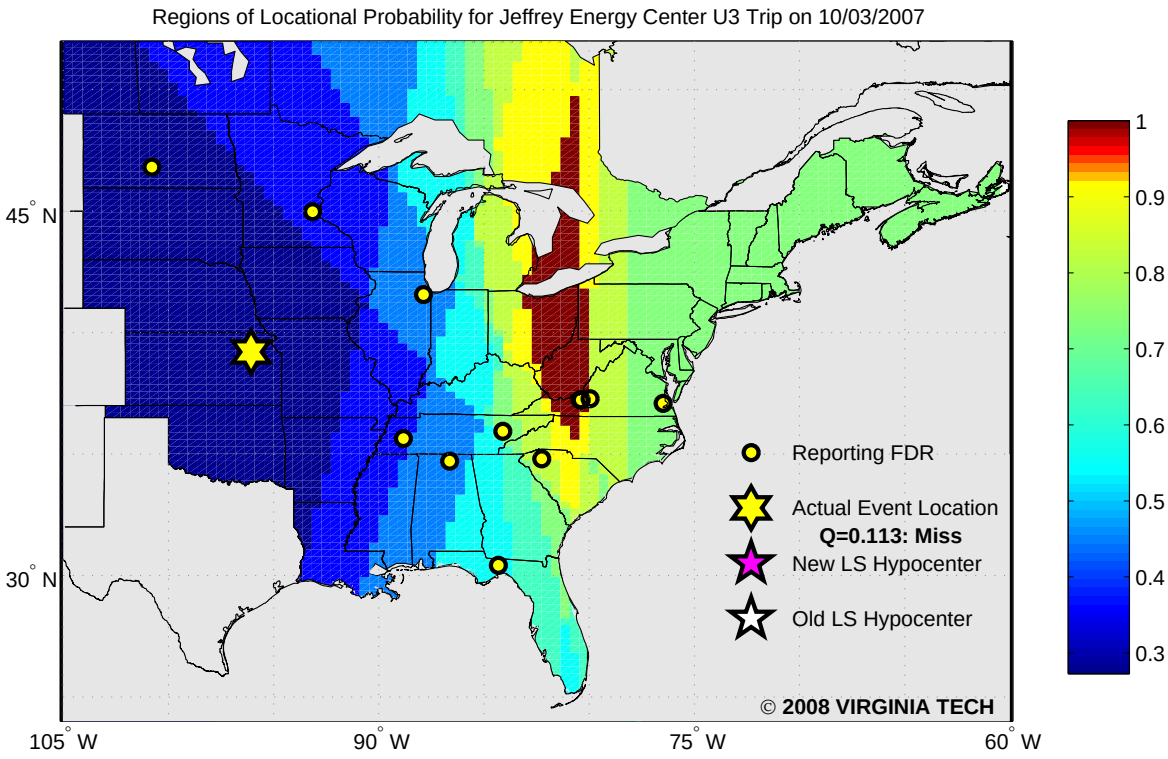


Figure D.107. Event location estimates (new ordering method): Jeffrey Energy Center U3 (1474 MW, 39.1987°, −96.0683°) Trip on 10/03/2007 15:24:29

Table D.51. Ordering method comparison: Farley Unit 2 (860 MW, 31.3352°, −85.1455°) Trip on 10/03/2007 19:10:13

	Old Ordering Method			New Ordering Method		
Mismatch estimate (MW)	726			696		
FDR Info	Number	Name	Distance (mi)	Number	Name	Distance (mi)
	42	FSU	80.02	514	FarrisSabrina	292.4
	17	TVA4Jackson	365	17	TVA4Jackson	365
	524	TTU	335.1	42	FSU	80.02
	514	FarrisSabrina	292.4	523	TTU3	323.4
	4	VT	488.3	4	VT	488.3
	508	ROA	506	510	Blacksburg	489.4
	510	Blacksburg	489.4	3	ARI	688.7
	3	ARI	688.7	11	Calvin	803.8
	500	Chicago	722.6	508	ROA	506
	513	PSU	769.1	43	Bismarck	1354
	518	NERC	854.6	13	MidwestISO	599
	40	MISOStPaul	1036	513	PSU	769.1
	502	Toronto	925.7	41	Winnipeg	1418
	43	Bismarck	1354	518	NERC	854.6
	503	Danbury	947.4	502	Toronto	925.7
	41	Winnipeg	1418	38	ISONE	1018
	38	ISONE	1018	40	MISOStPaul	1036
				503	Danbury	947.4
LS estimate	Latitude	Longitude	Distance (mi)	Latitude	Longitude	Distance (mi)
	31.3352°	−85.1455°	0.00252	33.1194°	−83.8235°	145.5
	Q_{old} = 1.0000			Q_{old} = 0.8149		
	Q_{new} = 0.8539			Q_{new} = 1.0000		
Parzen windowing results	Q_{actual} = 1.0000			Q_{actual} = 0.8539		

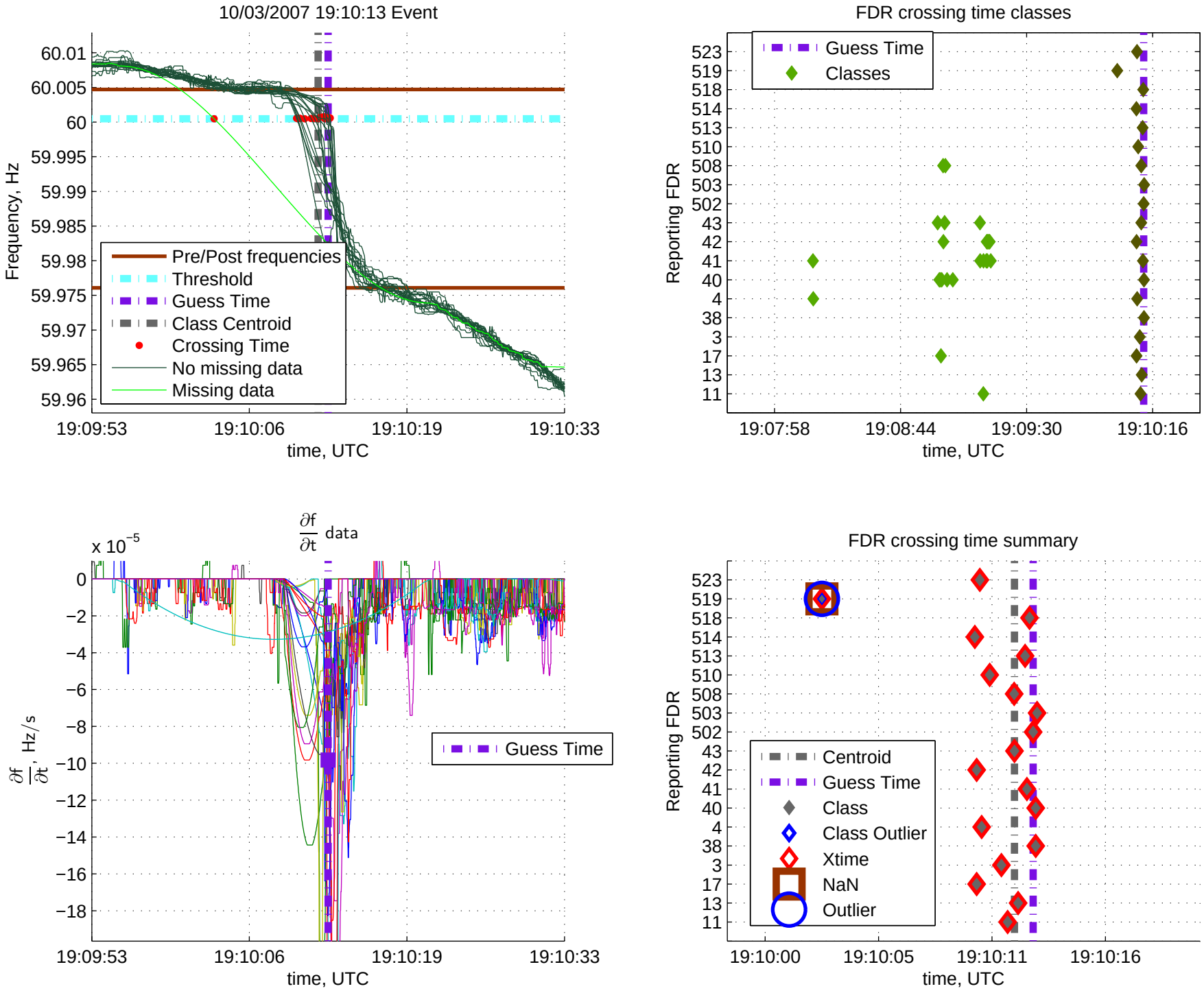
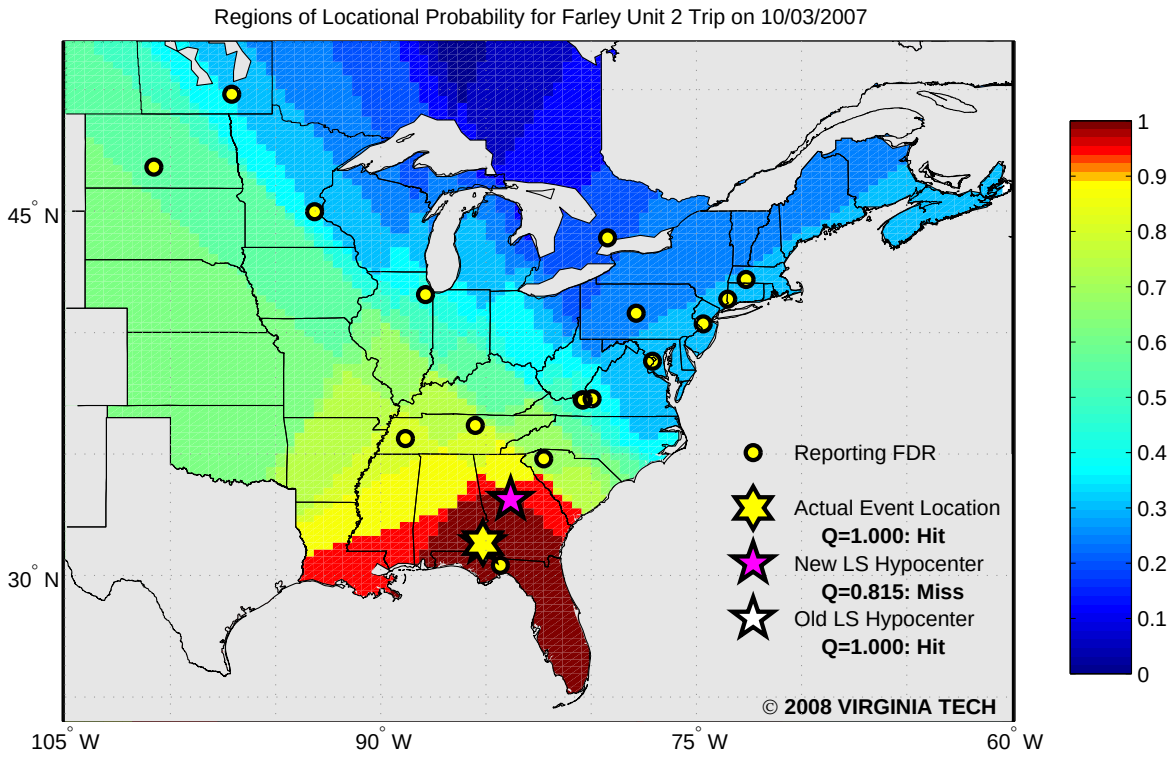
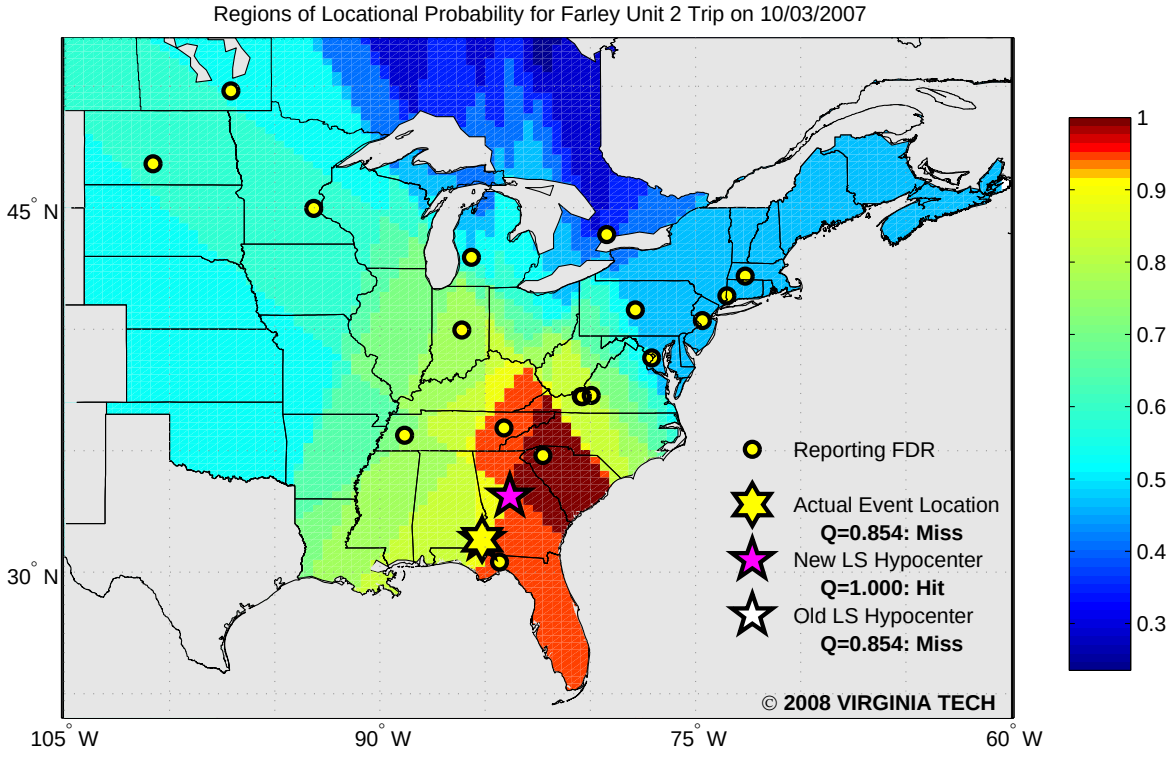


Figure D.108. Consolidated event ordering calculations: Farley Unit 2 (860 MW, 31.3352°, −85.1455°) Trip on 10/03/2007 19:10:13



(a) Event location: old ordering method



(b) Event location: new ordering method

Figure D.109. Event location estimates: Farley Unit 2 (860 MW, 31.3352°, −85.1455°) Trip on 10/03/2007 19:10:13

Table D.52. Ordering method comparison: Browns Ferry Unit 1 (1065 MW, 34.7055°, –87.1173°) Trip on 10/12/2007 13:02:37

	Old Ordering Method			New Ordering Method		
Mismatch estimate (MW)	NaN			767		
FDR Info	Number	Name	Distance (mi)	Number	Name	Distance (mi)
				15	TVA3Nashville	103
				17	TVA4Jackson	116
				4	VT	412.7
				523	TTU3	189.9
				42	FSU	337.9
				13	MidwestISO	367.9
				41	Winnipeg	1159
				35	ISU	616
				11	Calvin	575.8
				43	Bismarck	1097
				3	ARI	623.3
				519	NewportNews	617
				40	MISOStPaul	777.6
				500	Chicago	475.5
				504	WayneState	571.9
				513	PSU	657
				518	NERC	784.6
				502	Toronto	761.6
				38	ISONE	936.6
LS estimate	Latitude	Longitude	Distance (mi)	Latitude	Longitude	Distance (mi)
	$NaN°$	$NaN°$	NaN	35.2272°	−85.0943°	120.1
	$Q_{old} = NaN$			$Q_{old} = NaN$		
	$Q_{new} = NaN$			$Q_{new} = 0.9834$		
Parzen windowing results	$Q_{actual} = NaN$			$Q_{actual} = 1.0000$		

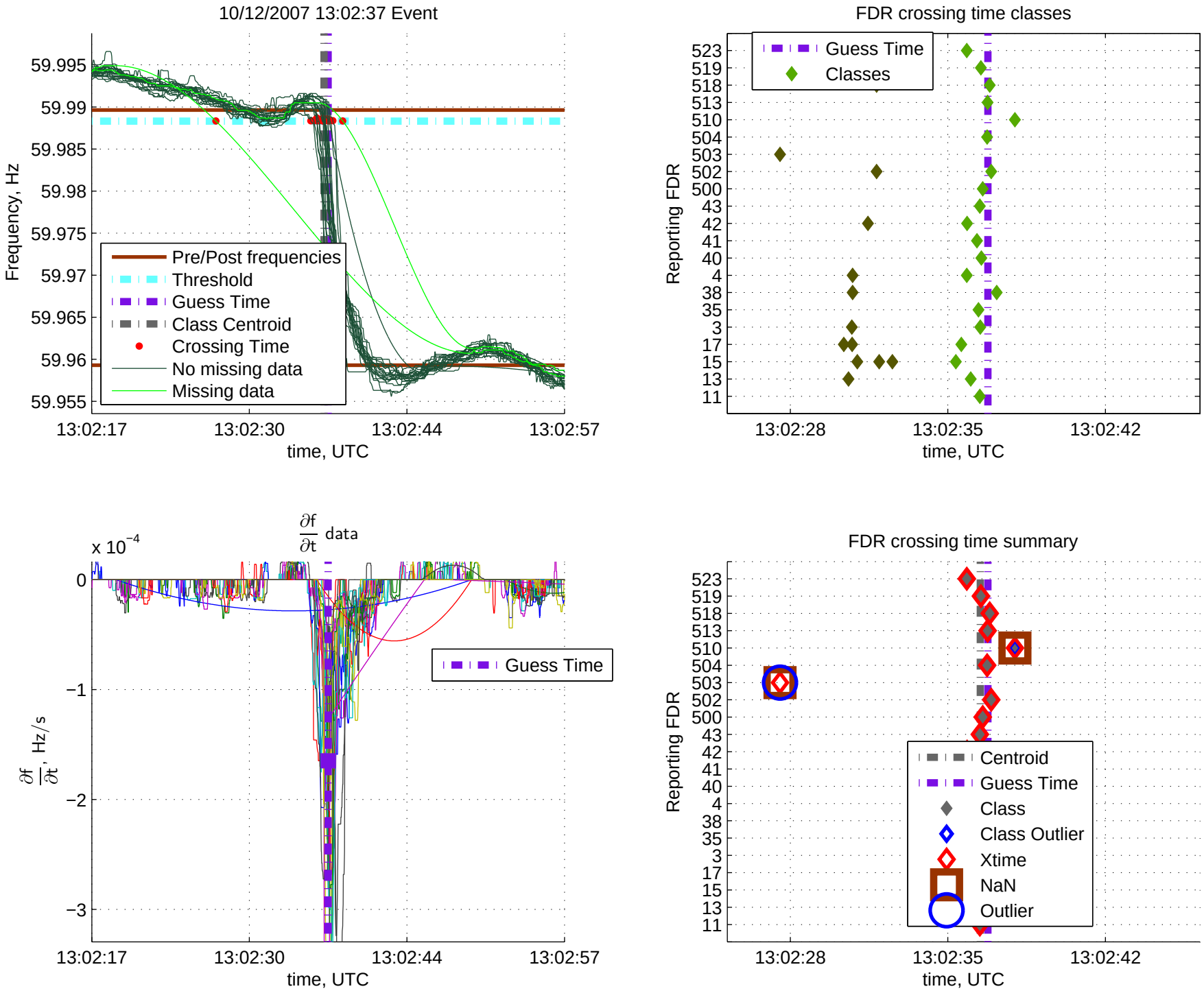


Figure D.110. Consolidated event ordering calculations: Browns Ferry Unit 1 (1065 MW, 34.7055°, −87.1173°) Trip on 10/12/2007 13:02:37

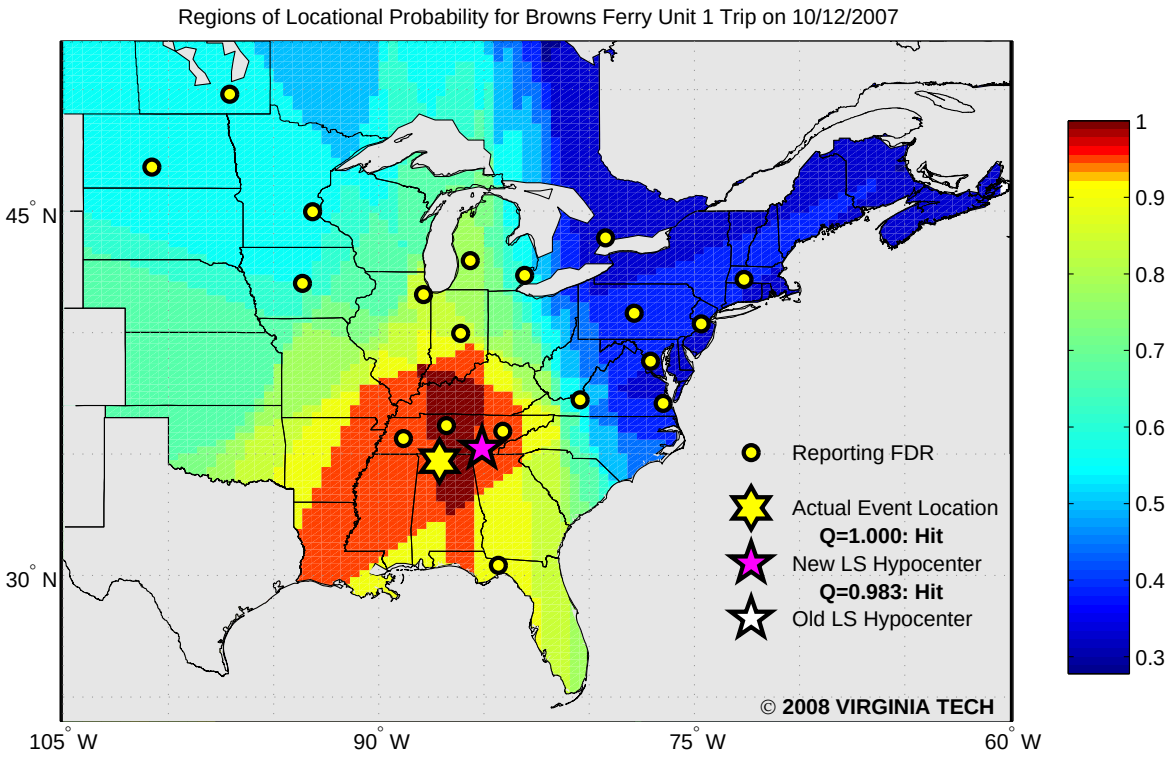


Figure D.111. Event location estimates (new ordering method): Browns Ferry Unit 1 (1065 MW, 34.7055°, −87.1173°) Trip on 10/12/2007 13:02:37

Table D.53. Ordering method comparison: Mitchell U2 (800 MW Capacity) (800 MW, 39.9148°, −80.7310°) Trip on 11/04/2007 09:26:36

	Old Ordering Method			New Ordering Method		
Mismatch estimate (MW)	634			591		
FDR Info	Number	Name	Distance (mi)	Number	Name	Distance (mi)
	3	ARI	208.8	508	ROA	186.9
	510	Blacksburg	186.8	13	MidwestISO	284.9
	11	Calvin	330.6	11	Calvin	330.6
	513	PSU	162.7	510	Blacksburg	186.8
	519	NewportNews	301.7	17	TVA4Jackson	531.7
	504	WayneState	208	519	NewportNews	301.7
	13	MidwestISO	284.9	3	ARI	208.8
	518	NERC	321.4	7	MISS	632
	502	Toronto	285.8	4	VT	186
	503	Danbury	391.9	15	TVA3Nashville	418.6
	38	ISONE	449.7	40	MISOStPaul	722
	514	FarrisSabrina	362.8	504	WayneState	208
	40	MISOStPaul	722	513	PSU	162.7
	42	FSU	686.4	502	Toronto	285.8
	35	ISU	687.6	35	ISU	687.6
	4	VT	186	42	FSU	686.4
	41	Winnipeg	1049	514	FarrisSabrina	362.8
	15	TVA3Nashville	418.6	518	NERC	321.4
	17	TVA4Jackson	531.7	38	ISONE	449.7
	7	MISS	632	503	Danbury	391.9
	508	ROA	186.9	41	Winnipeg	1049
LS estimate	Latitude	Longitude	Distance (mi)	Latitude	Longitude	Distance (mi)
	39.2867°	−80.3833°	47.18	38.9587°	−82.1235°	99.43
	$Q_{old} = 0.7675$			$Q_{old} = 0.2351$		
	$Q_{new} = 0.9680$			$Q_{new} = 0.9203$		
Parzen windowing results	$Q_{actual} = 0.3357$			$Q_{actual} = 0.9680$		

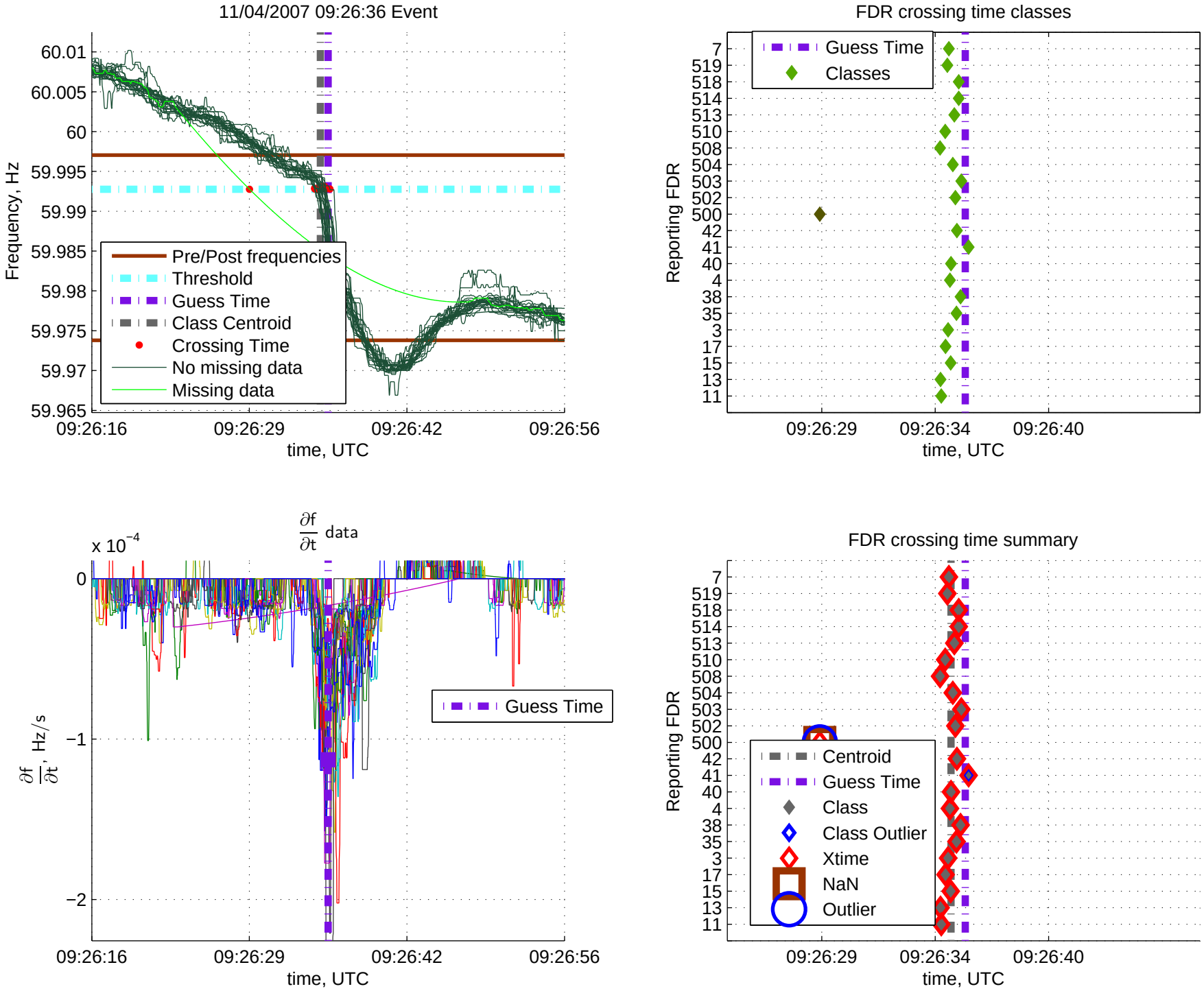
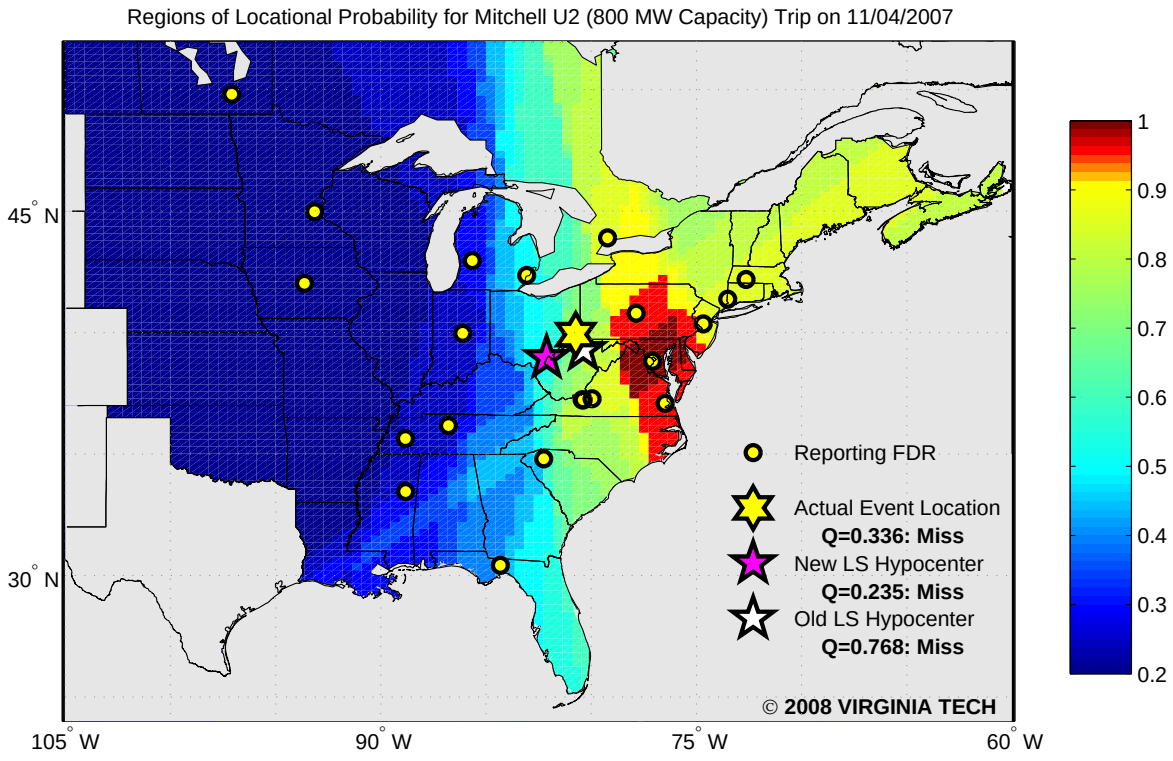
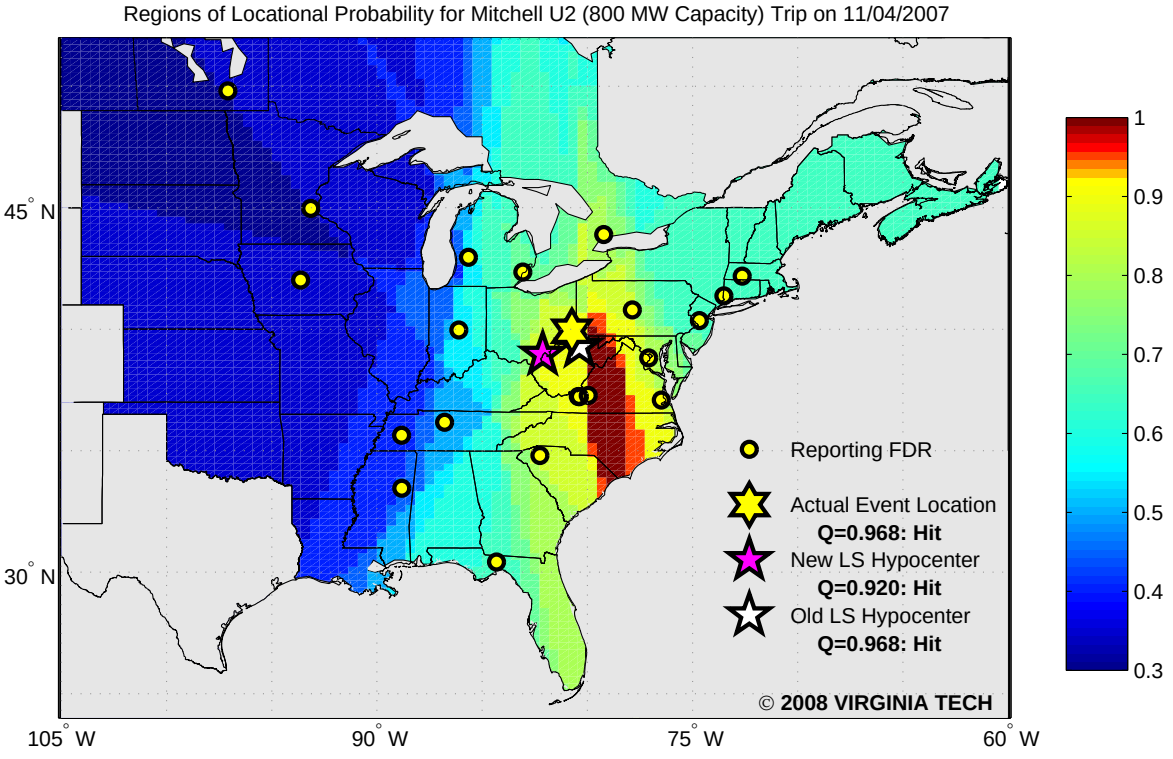


Figure D.112. Consolidated event ordering calculations: Mitchell U2 (800 MW Capacity) (800 MW, 39.9148°, –80.7310°) Trip on 11/04/2007 09:26:36



(a) Event location: old ordering method



(b) Event location: new ordering method

Figure D.113. Event location estimates: Mitchell U2 (800 MW Capacity) (800 MW, 39.9148°, −80.7310°) Trip on 11/04/2007 09:26:36

Table D.54. Ordering method comparison: Connesville U4 (780 MW Capacity) (780 MW, 40.1804°, −81.8951°) Trip on 11/04/2007 22:20:30

	Old Ordering Method			New Ordering Method		
Mismatch estimate (MW)	569			446		
FDR Info	Number	Name	Distance (mi)	Number	Name	Distance (mi)
	502	Toronto	291	17	TVA4Jackson	491.2
	504	WayneState	162.2	11	Calvin	273.3
	503	Danbury	446.5	13	MidwestISO	223.3
	11	Calvin	273.3	508	ROA	226
	4	VT	218.5	40	MISOStPaul	660.5
	513	PSU	216	41	Winnipeg	993.3
	519	NewportNews	362	7	MISS	601.8
	514	FarrisSabrina	371.9	510	Blacksburg	220
	42	FSU	688	504	WayneState	162.2
	7	MISS	601.8	500	Chicago	326.7
	15	TVA3Nashville	383.6	15	TVA3Nashville	383.6
	524	TTU	339.1	35	ISU	623.3
	35	ISU	623.3	519	NewportNews	362
	41	Winnipeg	993.3	513	PSU	216
	500	Chicago	326.7	514	FarrisSabrina	371.9
	13	MidwestISO	223.3	523	TTU3	317
	3	ARI	273	42	FSU	688
	508	ROA	226	502	Toronto	291
	510	Blacksburg	220	43	Bismarck	1048
	43	Bismarck	1048	503	Danbury	446.5
	40	MISOStPaul	660.5			
LS estimate	Latitude	Longitude	Distance (mi)	Latitude	Longitude	Distance (mi)
	43.3530°	−78.5963°	277.3	35.7118°	−91.4394°	604.3
	Q_{old} = 1.0000			Q_{old} = 0.0941		
	Q_{new} = 0.1791			Q_{new} = 1.0000		
Parzen windowing results	Q_{actual} = 0.7545			Q_{actual} = 0.2512		

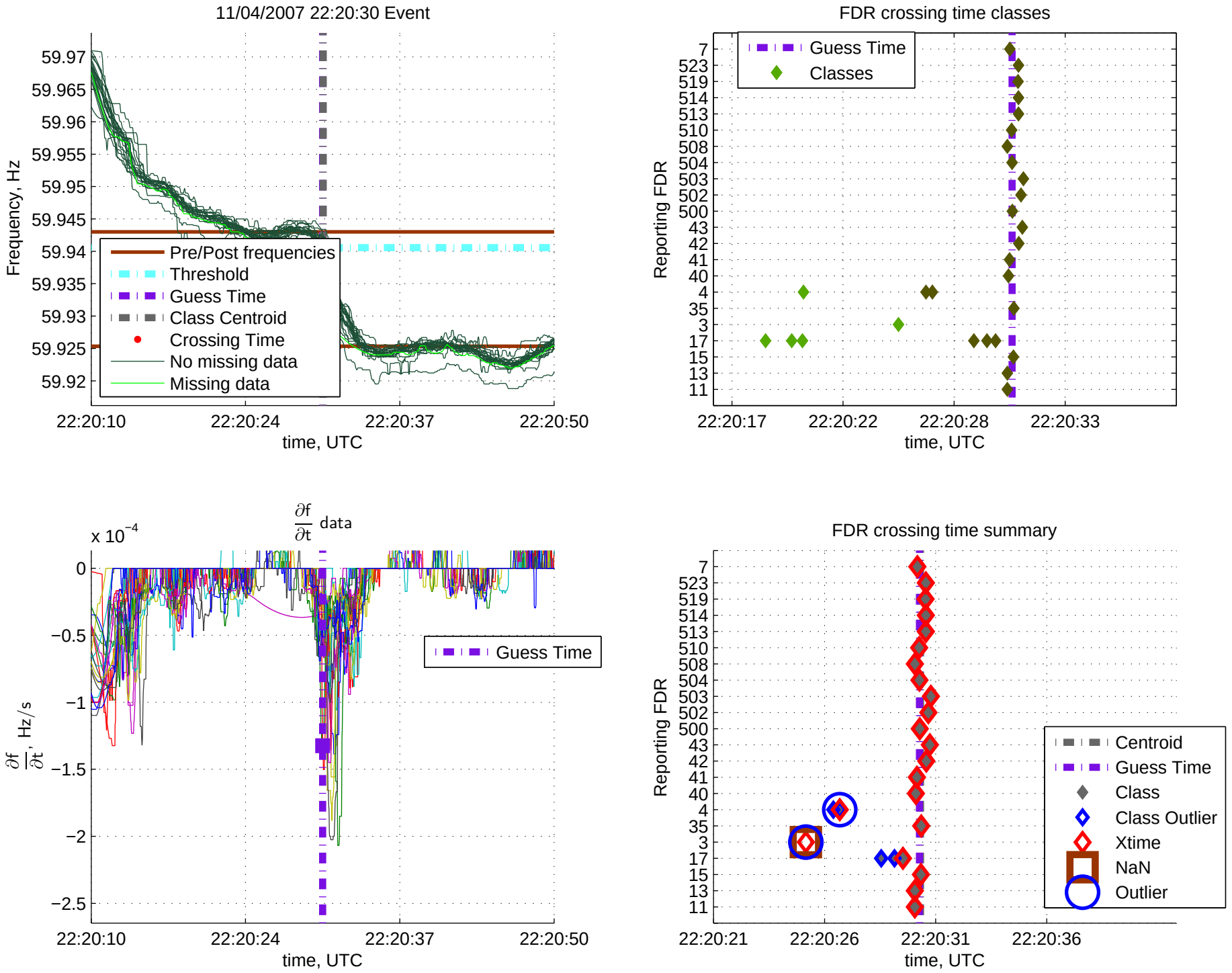
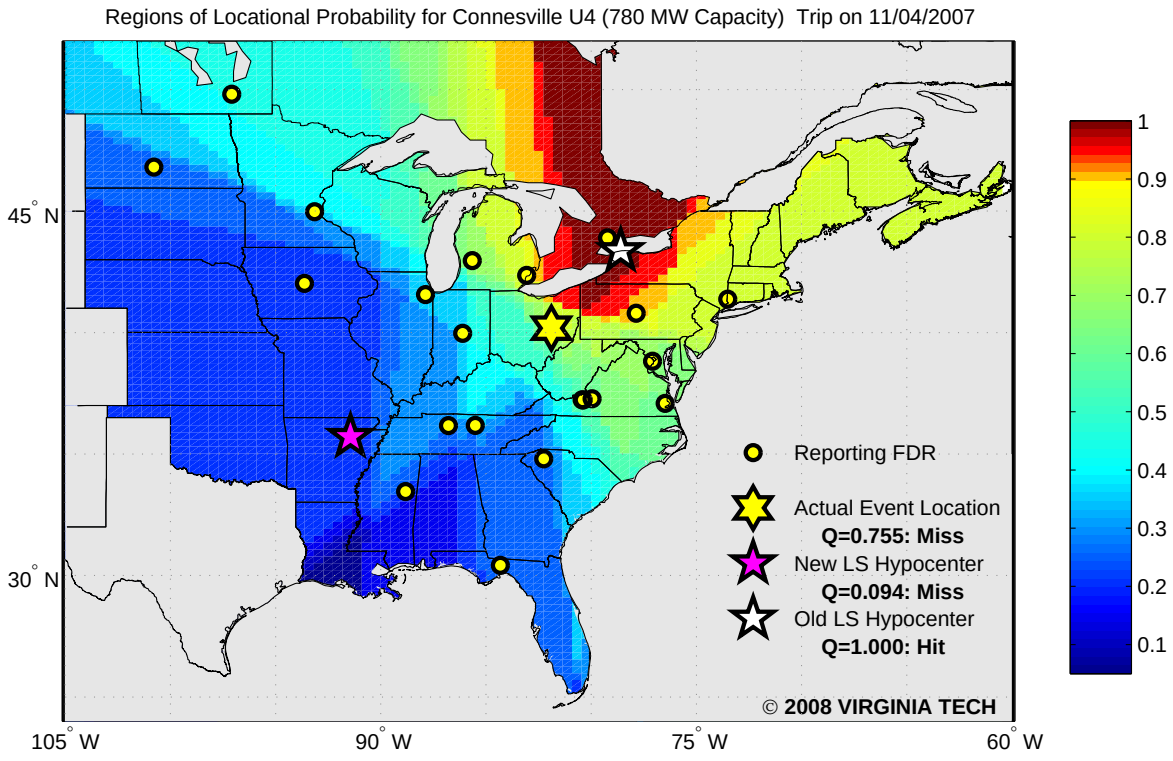
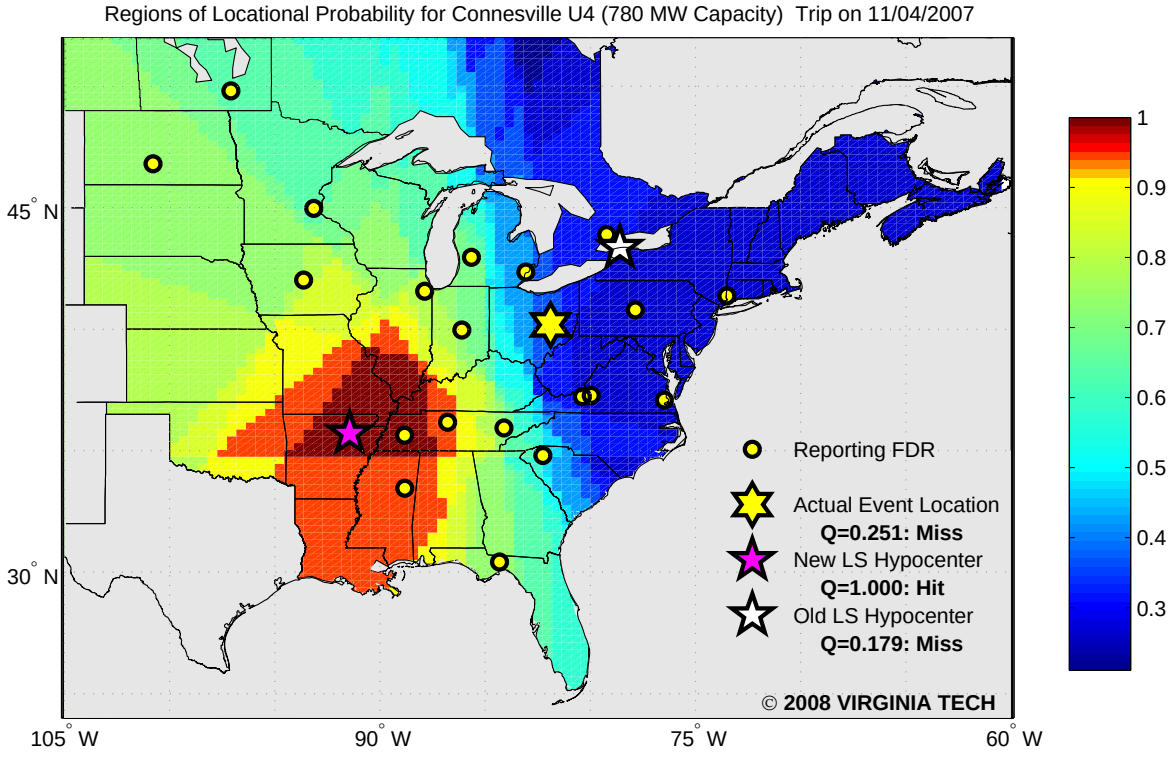


Figure D.114. Consolidated event ordering calculations: Connesville U4 (780 MW Capacity) (780 MW, 40.1804°, −81.8951°) Trip on 11/04/2007 22:20:30



(a) Event location: old ordering method



(b) Event location: new ordering method

Figure D.115. Event location estimates: Connesville U4 (780 MW Capacity) (780 MW, 40.1804°, −81.8951°) Trip on 11/04/2007 22:20:30

Table D.55. Ordering method comparison: Big Sandy U2 (800 MW, 37.9848°, −82.5857°) Trip on 11/09/2007 13:00:12

	Old Ordering Method			New Ordering Method		
Mismatch estimate (MW)	NaN			NaN		
FDR Info	Number	Name	Distance (mi)	Number	Name	Distance (mi)
				15	TVA3Nashville	263.2
				508	ROA	151.8
				504	WayneState	303.1
				40	MISOStPaul	728.3
				41	Winnipeg	1086
				43	Bismarck	1107
				500	Chicago	374.1
				35	ISU	646.8
				514	FarrisSabrina	220.5
LS estimate	Latitude	Longitude	Distance (mi)	Latitude	Longitude	Distance (mi)
	$NaN°$	$NaN°$	NaN	$NaN°$	$NaN°$	NaN
	$Q_{old} = NaN$			$Q_{old} = NaN$		
	$Q_{new} = NaN$			$Q_{new} = NaN$		
Parzen windowing results	$Q_{actual} = NaN$			$Q_{actual} = 0.6070$		

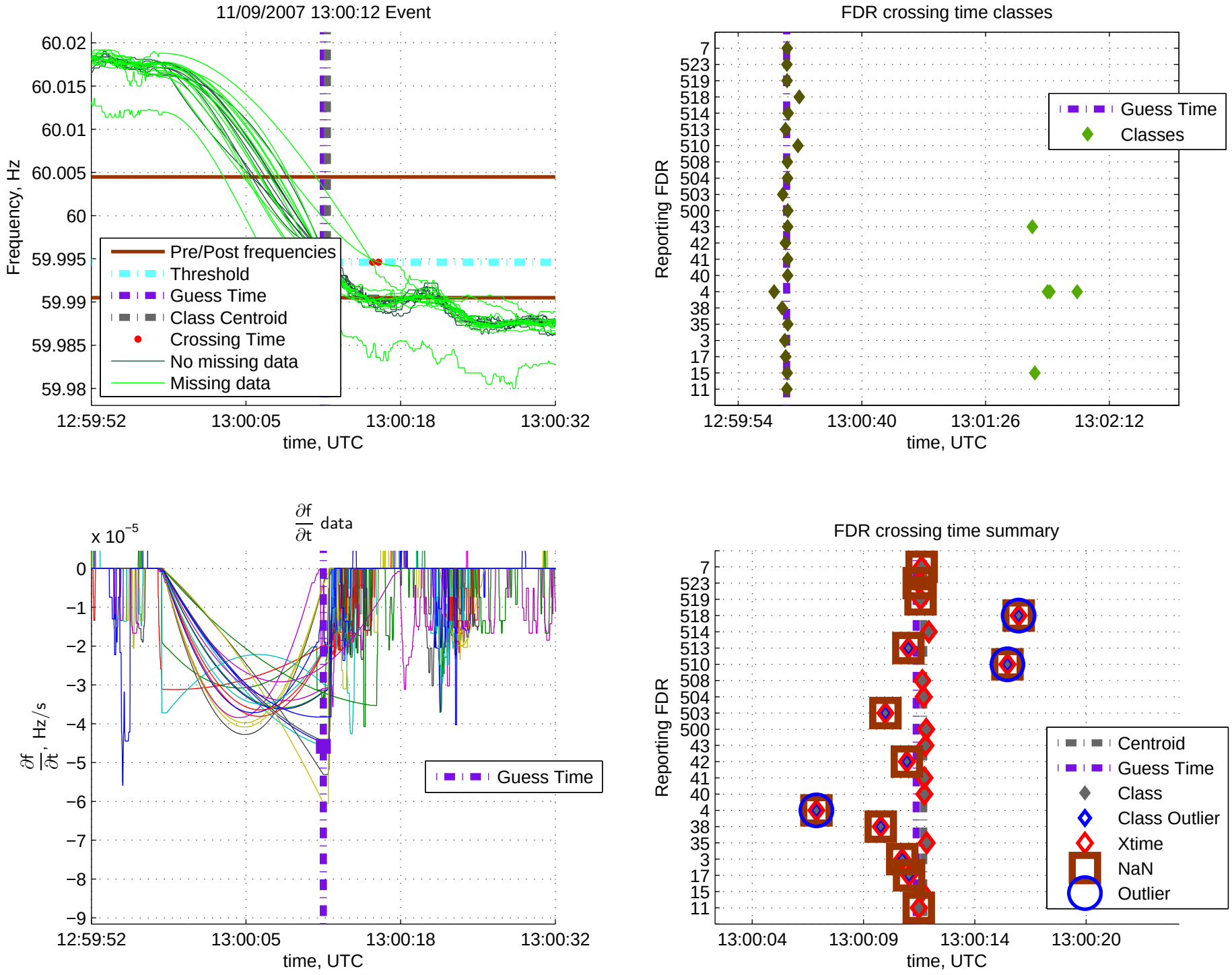


Figure D.116. Consolidated event ordering calculations: Big Sandy U2 (800 MW, 37.9848°, −82.5857°) Trip on 11/09/2007 13:00:12

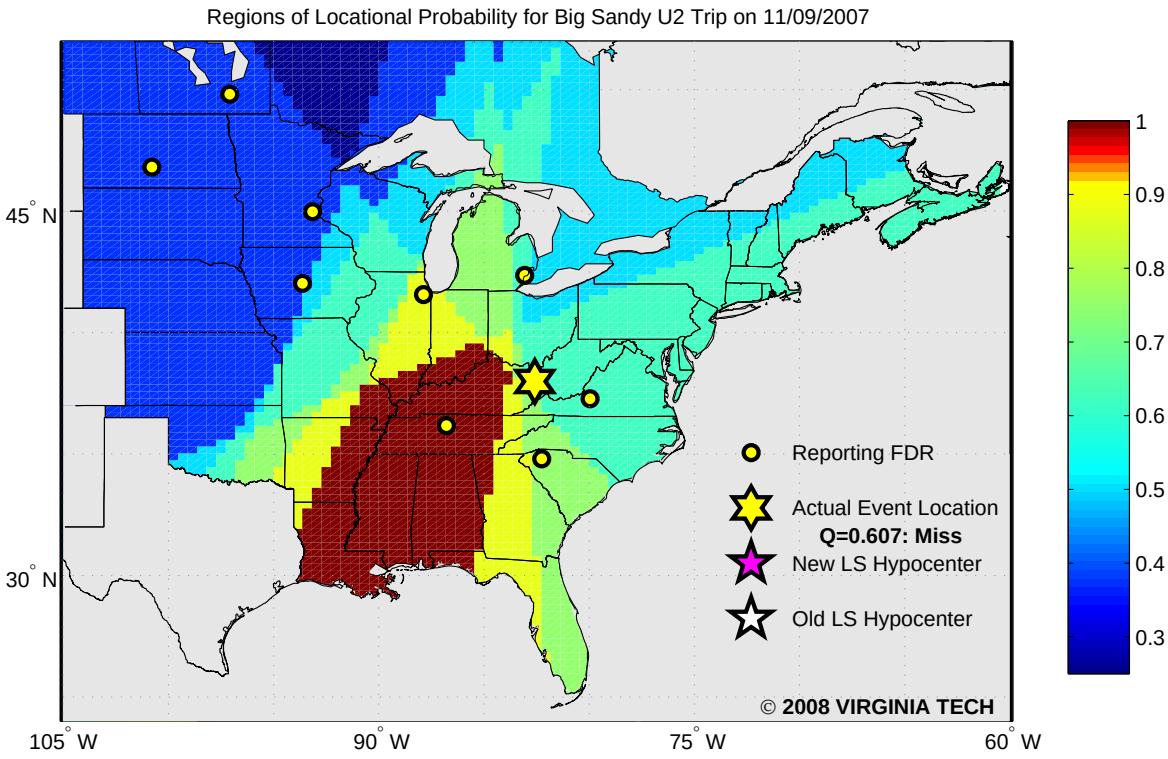


Figure D.117. Event location estimates (new ordering method): Big Sandy U2 (800 MW, 37.9848°, −82.5857°) Trip on 11/09/2007 13:00:12

Table D.56. Ordering method comparison: W H Zimmer (1300 MW, 39.0523°, −84.1505°) Trip on 11/14/2007 15:57:00

	Old Ordering Method			New Ordering Method		
Mismatch estimate (MW)	1295			1415		
FDR Info	Number	Name	Distance (mi)	Number	Name	Distance (mi)
	13	MidwestISO	122.1	4	VT	238.1
	510	Blacksburg	240.7	15	TVA3Nashville	245.8
	11	Calvin	281.2	11	Calvin	281.2
	4	VT	238.1	13	MidwestISO	122.1
	500	Chicago	261.9	510	Blacksburg	240.7
	3	ARI	379.9	17	TVA4Jackson	348.9
	15	TVA3Nashville	245.8	500	Chicago	261.9
	513	PSU	354.1	3	ARI	379.9
				7	MISS	465.9
				523	TTU3	215.4
				514	FarrisSabrina	311.6
				513	PSU	354.1
				42	FSU	596.5
				35	ISU	537.8
				40	MISOStPaul	616.3
				518	NERC	511.5
				38	ISONE	640.8
				503	Danbury	583.7
				43	Bismarck	994.6
LS estimate	Latitude	Longitude	Distance (mi)	Latitude	Longitude	Distance (mi)
	39.0523°	−84.1505°	0.003018	37.2327°	−80.4284°	238.1
	Q_{old} = 1.0000			Q_{old} = 0.2782		
	Q_{new} = 0.7620			Q_{new} = 1.0000		
Parzen windowing results	Q_{actual} = 1.0000			Q_{actual} = 0.7620		

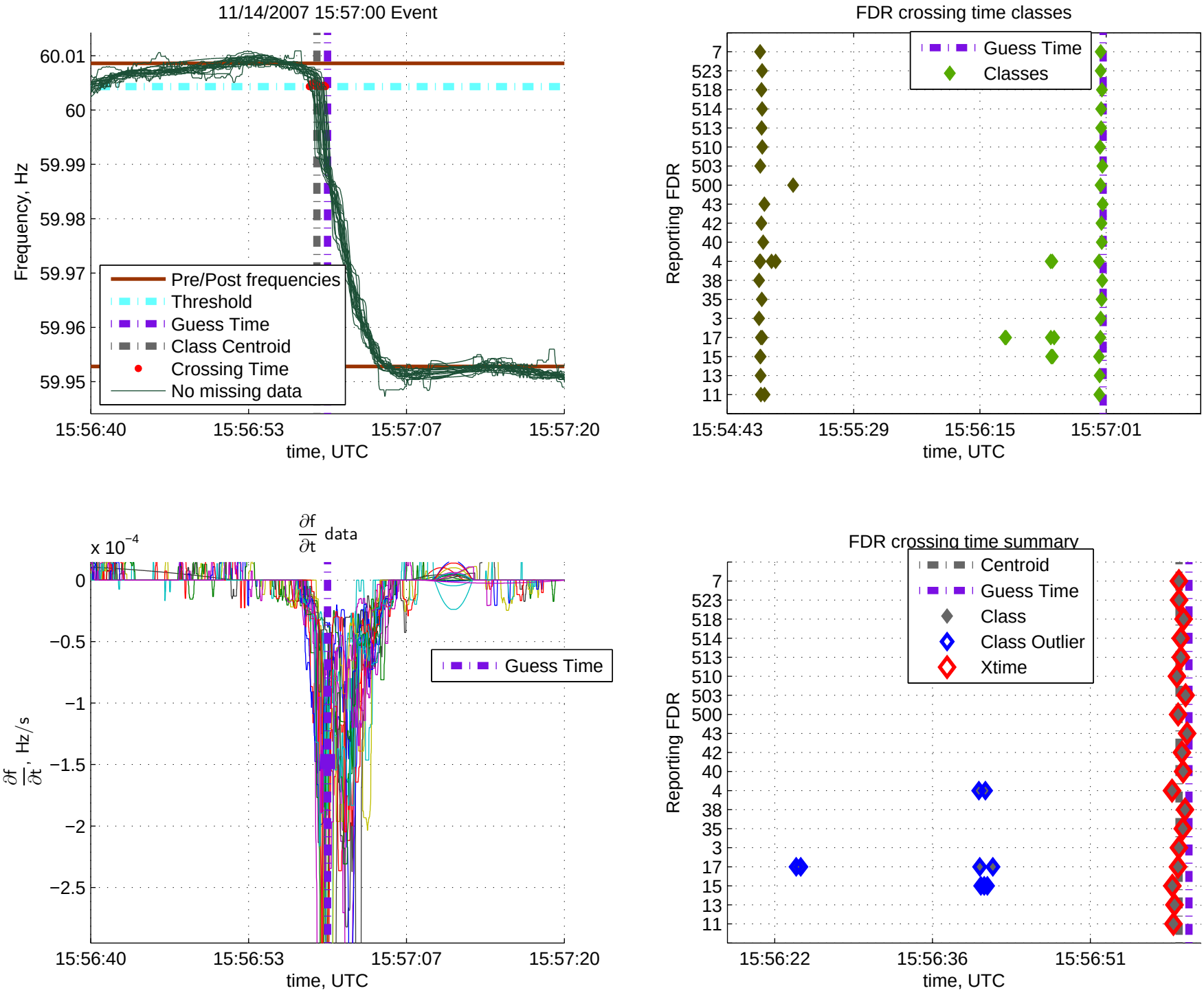
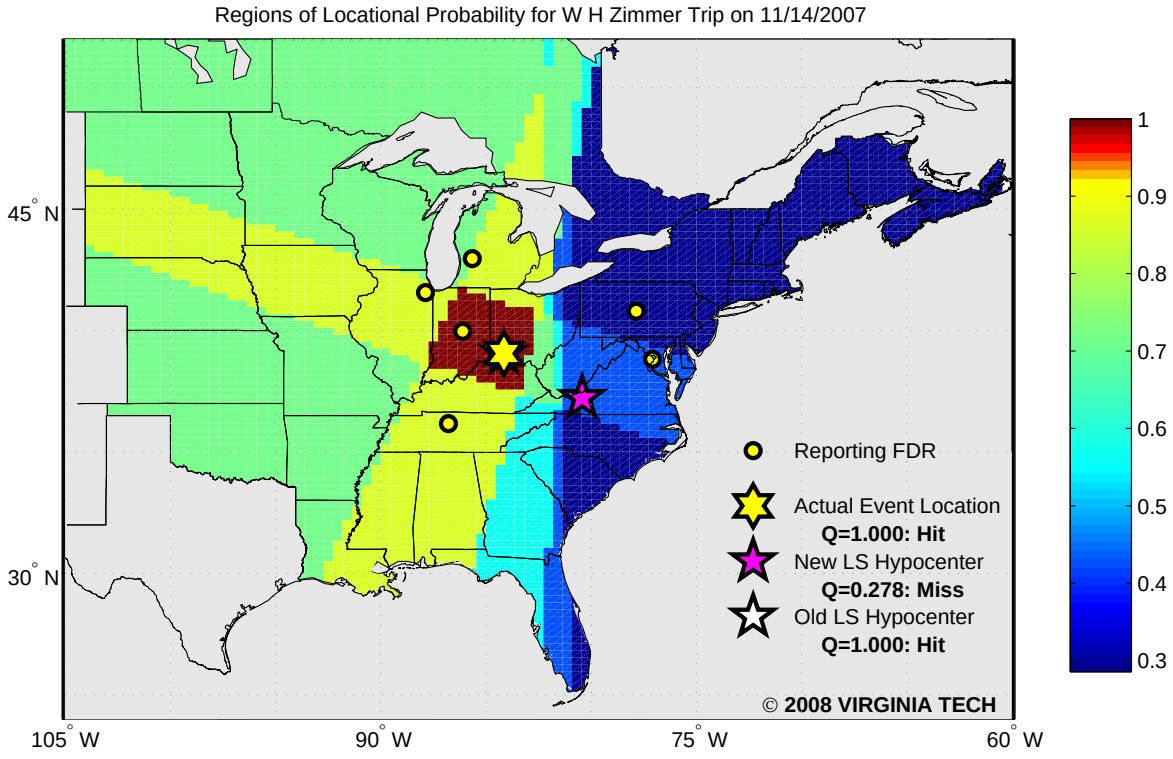
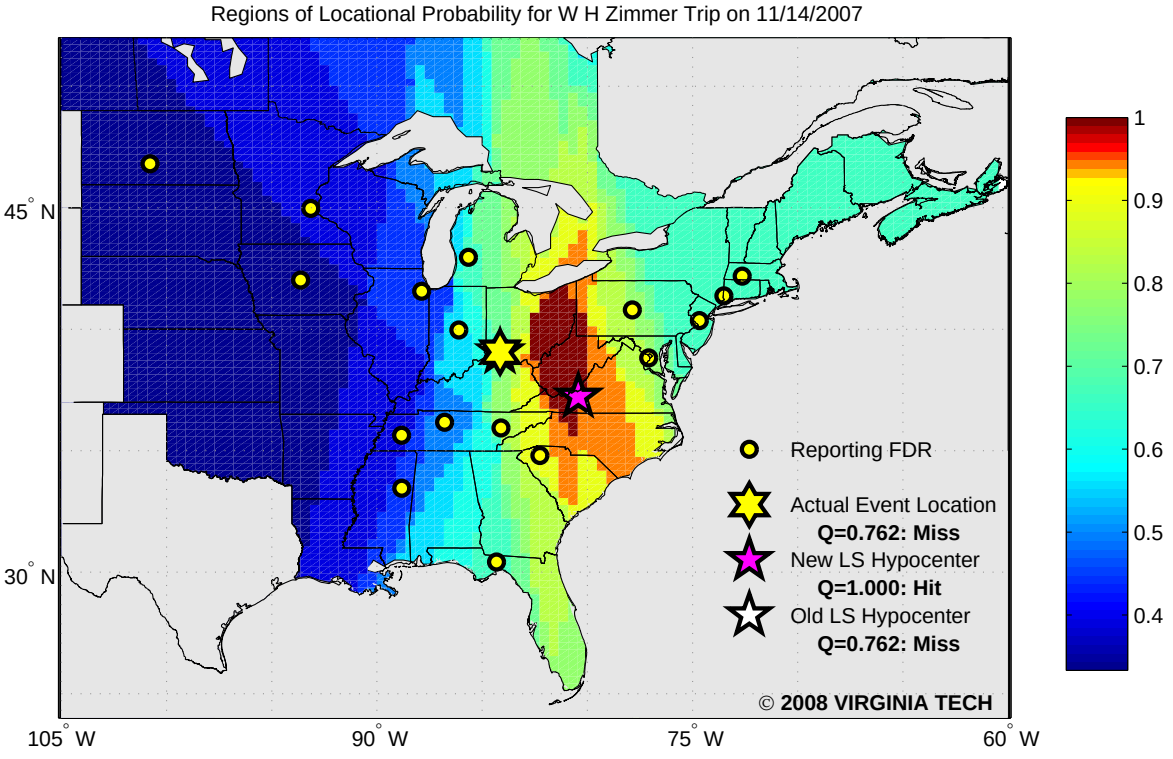


Figure D.118. Consolidated event ordering calculations: W H Zimmer (1300 MW, 39.0523°, −84.1505°) Trip on 11/14/2007 15:57:00



(a) Event location: old ordering method



(b) Event location: new ordering method

Figure D.119. Event location estimates: W H Zimmer (1300 MW, 39.0523°, −84.1505°) Trip on 11/14/2007 15:57:00

Appendix E

Two-area test system parameters

Table E.1. Simulated system parameters[6]

Base Quantities							
900 MVA				20/230 kV			
Transformer Parameters (p.u.)							
Z		0 + j0.15		off-nominal ratio		1.0	
Transmission Line Parameters (p.u./km)							
r	0.0001	x_L	0.001	b_C	0.00175		
Generator parameters (p.u. unless otherwise marked)							
X_d	1.8	X_q	1.7	X_l	0.2	K_D	0
$X_d^{'}$	0.3	$X_q^{'}$	0.55	R_a	0.0025	H (G1)	6.5 s
$X_d^{"}$	0.25	$X_q^{"}$	0.25	A_{sat}	0.015	H (G2)	6.5 s
$T_{d0}^{'}$	8.0 s	$T_{q0}^{'}$	0.4 s	B_{sat}	9.6	H (G3)	6.175 s
$T_{d0}^{"}$	0.03 s	$T_{q0}^{"}$	0.05 s	Ψ_{T1}	0.9	H (G4)	6.175 s

Generator loading			
	P (MW)	Q (MVAR)	E_t (p.u.)
G1	700	185	$1.03\angle 20.2°$
G2	700	235	$1.01\angle 10.5°$
G3	719	176	$1.03\angle -6.8°$
G4	700	202	$1.01\angle -17.0°$

Load parameters			
	Load		Shunt Capacitor
	P (MW)	Q (MVAR)	Q_C (MVAR)
A1	967	100	200
A2	1767	100	350